THE DESIGN OF A LATHE ATTACHMENT FOR GRINDING NON-CIRCULAR CROSS-SECTION SHAFTS SUITABLE FOR TORQUE TRANSMISSION

by

B. TAYLOR

A thesis submitted to the University of Newcastle upon Tyne for the Degree of Doctor of Philosophy.

APRIL, 1987

ACKNOWLEDGEMENTS

I wish particularly to express my gratitude to Mr. A.A. Fogarasy for his continued guidance and encouragement throughout this work. My thanks also go to Professor L. Maunder for permitting the work to be carried out in the Department of Mechanical Engineering and to the Northumbrian Universities Multiple Access Computer for the use of its facilities. Finally I wish to thank Mrs. S.M. Stone for her very efficient typing of this thesis.

DECLARATION

This thesis consists of the original work of the author except where specific reference is made to the work of others, and has not been previously submitted for any other degree or qualification.

B. Taylor

ABSTRACT

The principle concern of this work is the design of a lathe attachment for grinding non-circular 'polygonal' shaped workpieces suitable for use as torque transmitting machine elements. In the course of the work substantial attention is also given to the general theory and development of computer aided error analysis procedures for planar linkage mechanisms. A further smaller part of the work investigates the torsion of polygonal shafts.

The non-circular shapes considered here may be loosely defined as polygonal profiles. Their application is in torque transmitting couplings for which they represent an alternative to keyed and splined couplings, although, in comparison to keys and splines, their application has been limited, mainly due to the specialised nature of their manufacture. The main objective of this work is to investigate suitable profiles and the means for their production using an attachment which can be mounted on a conventional machine tool, such as a lathe or grinding machine.

The work progresses from initial consideration of shapes produced by various geometric generating methods and conception of an 'ideal' profile generating linkage mechanism, through to detailed design of a precision, polygonal profile grinding, lathe attachment, and final assessment of its feasibility based on a profile precision criterion.

In order to assess the precision of the attachment, computer-aided procedures are developed, after consideration of existing error analysis methods and their limitations for use in this case. These consider the various effects of tolerances, clearances, and deflections upon mechanism output.

As a coincidental investigation, the mechanical behaviour and strength of polygonal shaft-hub connections is reported. In particular, the torsion of a polygonal bar is theoretically analysed, using a stress function method, to determine maximum shear stresses.

CONTENTS

LATHE ATTACHMENT FOR GRINDING POLYGONAL PROFILES.

Engineering Drawings, Numbers 1 to 7
(see pocket inside back cover)

CHAPTER 1

INTRODUCTION

The work reported in this thesis principally concerns the design of a grinding attachment for producing non-circular or 'polygonal' shaped shafts and hubs suitable for use as engagement couplings or joints between torque transmitting machine elements. However, a major part of the work involves a general theoretical analysis of errors in function-generating linkage mechanisms and the development of computer aided procedures for predicting mechanism output error: these were specifically employed to predict the manufacturing precision and hence the technical feasibility of the profiling attachment.

A further area of work concerns the theoretical analysis of torsional shear stresses in polygonal shaped bars.

Although the profiles are not true polygons, being intermediate between circles and true polygons and having rounded corners and sides, they are subsequently simply referred to as polygonal profiles.

1.1 BACKGROUND

1.1.1 Application of polygonal profiles.

Polygonal couplings represent an alternative to the more commonly used, keyed and splined couplings for transmitting torque between shafts and the components they carry, e.g. gears etc.

Mentions of polygonal profiles in general texts are comparatively rare and usually brief, typically as by Dobrovolsky et al [1] who describe the benefits of using polygonal profiles as compared to keys and splines.

In keyed joints,Fig.1.1a, the mating elements are weakened by the considerable stress concentration caused by the slot for the key, and by the uneven load distribution which also makes it difficult to ensure concentric fits.

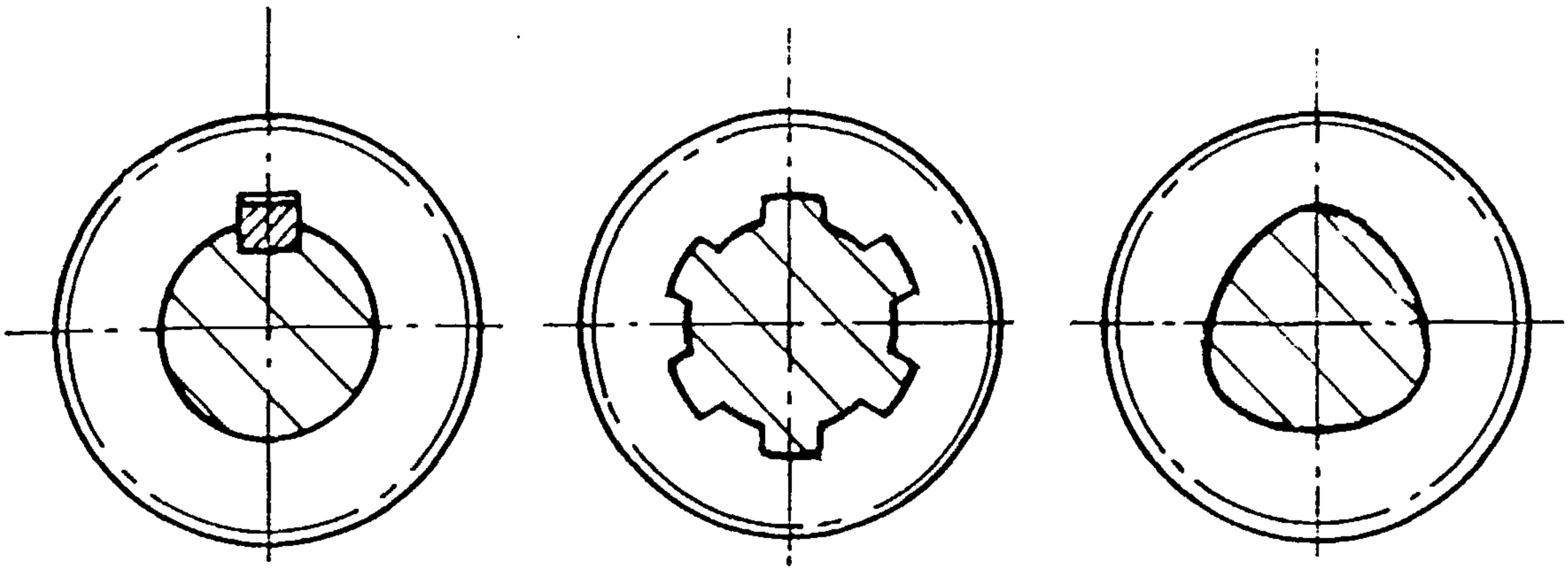

(a) Keyed (b) Splined (c) Shaped

Fig.1.1 Engagement Couplings

Splined couplings, Fig.1.1b, improve upon keyed couplings by distributing the load over a greater contact area and by offering better centring ability. However, their greater efficiency relies on much more accurate manufacture of the components and inevitably the load will not be equally shared amongst the splines; and stress concentrations, although less than in keyways, still arise at the roots of the splines.

In comparison, polygonal couplings, Fig.1.1c, offer even better centring of the mating elements and more equally distributed load, resulting in more precise, quieter running and also, because of the absence of stress raising features, greater endurance. Polygonal profiles manufactured by a continuous generation method in particular, are inherently more precise than splines produced generally by indexing methods; and their size, and thus the fit of mating elements is easier to control. Polygonal joints are generally more compact radially, and axially they do not require cutting-tool run outs as do splines.

1.1.2 Production methods.

Although their technical advantages have long been known polygonal couplings have been restricted in their application due to the difficulties and expense of their specialised manufacture, hence their limited mention in general texts.

A literature review revealed only one existing specialised means of producing precision polygon profiles. Musyl [2,3,4,5] describes mathematical principles governing the generation of polygon profiles and the basic construction of a profile grinding machine: essentially the method, based originally on cycloidal motions, involves moving the grinding wheel in an elliptical path as it machines a rotating workpiece. Grinding machines developed from this design and dedicated to polygon profile production are manufactured by a German company [6]. Musyl also reports investigations of the mechanical properties and behaviour of polygonal connections [7]. The specification of polygon profiles recently became the subject of two German (DIN) standards [8,9] which follow the work of Musyl. Importantly these standards note that existing patents cover only the construction of the profile grinding machine and not the profiles themselves which may be produced by other methods.

Other machines which might be used to produce polygon profiles include duplicating lathes and grinding machines, cam grinding machines, and numerically controlled machines. The ease and precision of polygon production by these methods will vary but none is likely to be economicall- suitable for single or small batch production. Particular difficulty might arise in the manufacture of profiled hubs, involving perhaps the manufacture of broaches for internal broaching. Furthermore none of these methods employs a generating method of production.

1.2 PRESENT WORK

The main objective of the present work is to investigate a means of producing non-circular shaped couplings, which is suitable for small batch production, utilising a suitable attachment mounted on conventional lathes or grinding machines and preferably based on an inherently precise generating method.

The initial stages of the work concern the investigation of various profiles and their geometric generation methods, in Chapter 2, and the conception of a planar linkage mechanism to implement the chosen hypocycloidal method, in Chapter 3.

The practical form that the mechanism should take is considered in Chapter 4 and is determined to be that of a grinding attachment for mounting on a lathe after the manner of a toolpost grinder. Precision requirements are considered and determined to be the most important criteria for assessing feasibility.

To assess the precision of the attachment, the effects of various sources of mechanism error such as tolerances, clearances, and deflections are investigated. First, in Chapter 5, existing methods of assessing errors in general linkage mechanisms are reviewed and some limitations discussed; and a computer aided error assessment procedure is developed which is more suitable for use in prototype design work. This includes a method of describing output path error by an 'output error characteristic' which registers 'real' error as opposed to 'mathematical' error; and account is also taken of non-linear sensitivities of output error to mechanism parameter errors.

The error analysis procedures are applied to the ideal polygon generating mechanism, in Chapter 6, producing various guidelines which are used to aid the design of a practical attachment, reported in Chapter 7. In the final design, presented here, the whole attachment is mounted on a single baseplate which in turn can be mounted on the cross slide of a suitable lathe. Profiles are produced by feeding the whole attachment towards the workpiece in the manner of normal lathe cutting tools.

A final error assessment is performed, the results of which are used to assess the technical feasibility, in Chapter 8.

Finally, in Chapter 9, some consideration is given to the mechanical behaviour and strength of polygonal shaft-hub connections. In particular,

the torsion of a polygonal bar is theoretically analysed, using stress function methods, and shear stresses are compared with those in equivalent cylindrical bars. The effect of the 'pressure angle' of the profiles upon behaviour is also considered.

CHAPTER 2

CHOICE OF PROFILE

2.1 CRITERIA OF SELECTION

Initially, suitable profiles were selected by comparing curves produced by various geometric generation methods. Several criteria were used in the comparisons.

The simplest criterion for suitability to transmit torque is that a profile should be non-circular. It is the degree of non-circularity that has to be decided upon.

A second criterion could be that the profile should be as close to circular as possible without losing its torque transmission capability. This last condition will depend upon the stiffness and strength, and manufacturing accuracy of the profiled components.

From a purely kinematic viewpoint, a polygon, with any number of sides, is ideal for torque transmission (see Fig.2.1.).

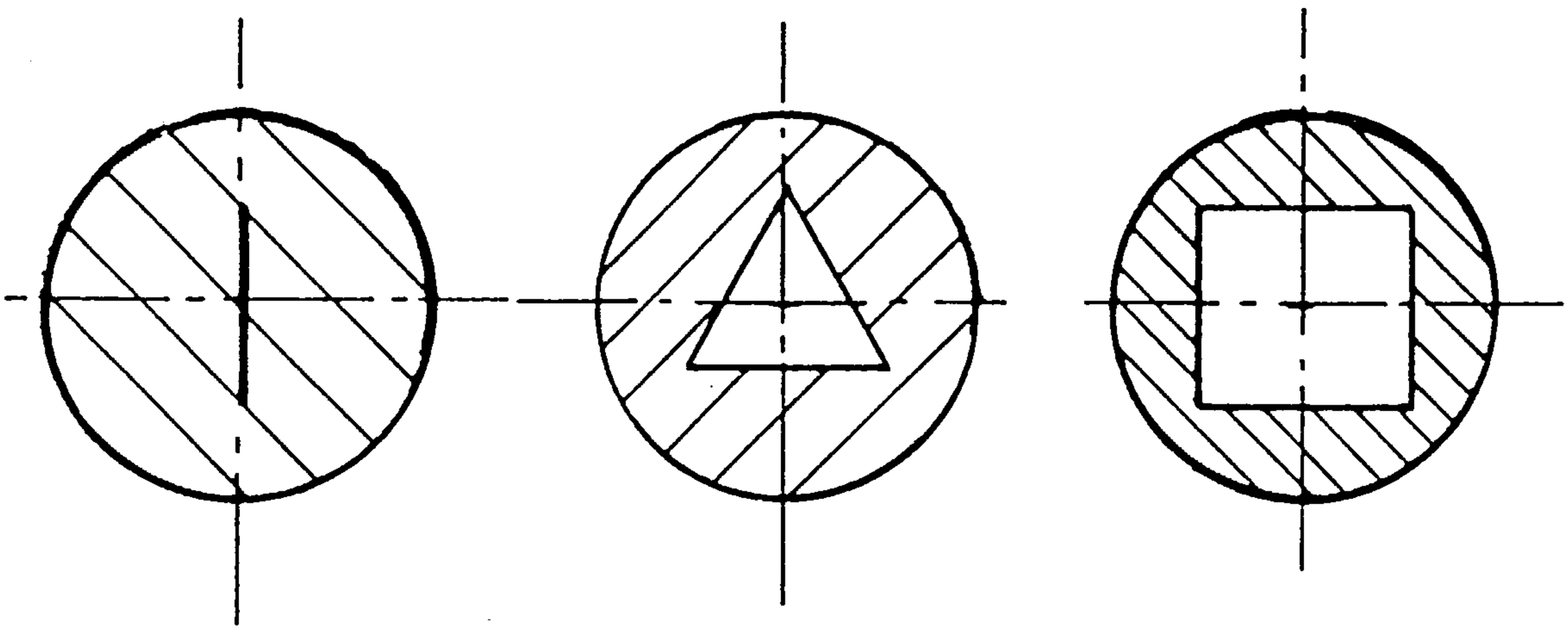

Fig. 2.1 Kinematically ideal polygon profiles

However when the resulting strength is considered, stress concentrations at the sharp corners of the true polygon should be avoided. A more suitable profile is a polygon with rounded corners, as in Fig.2.2.

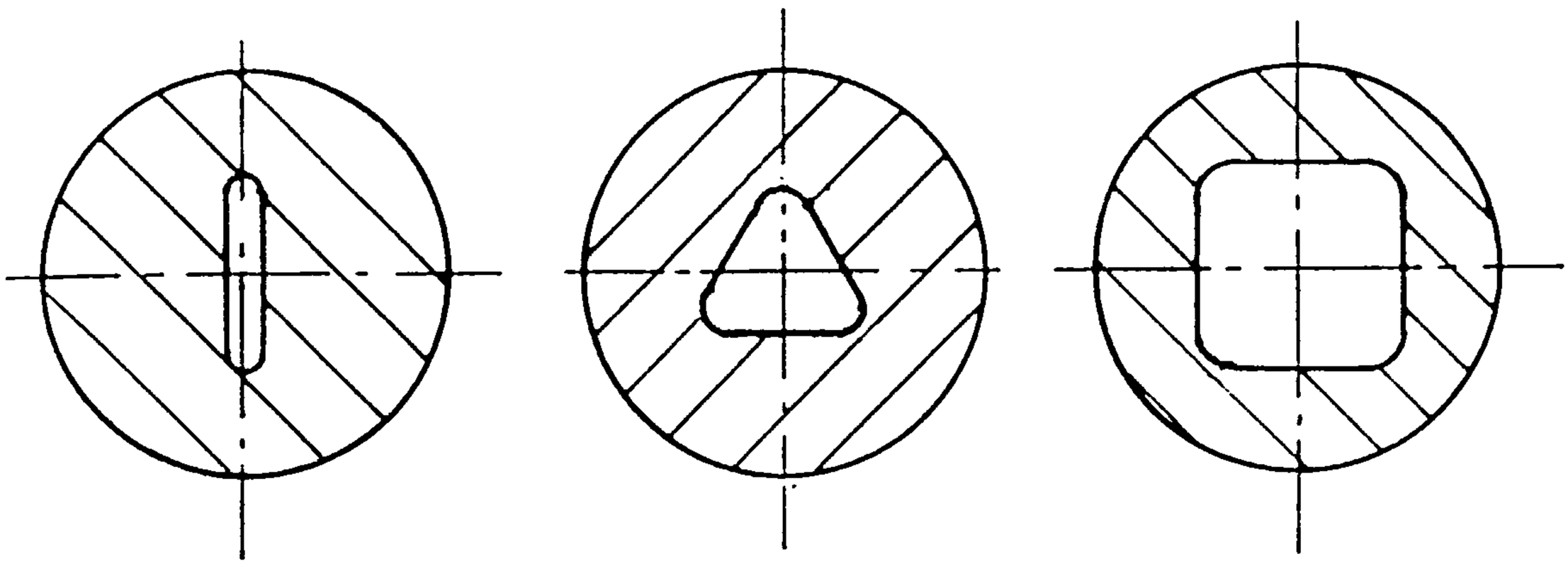

Fig.2.2. Polygons modified by strength criteria.

If manufacturing is now considered it is better still if the profile can be a continuously generated single curve,(Fig. 2.3) rather than be a composition of two separate curves for the corners and sides; especially when manufacturing holes. Thus only curves which could be produced by a single generation method were considered.

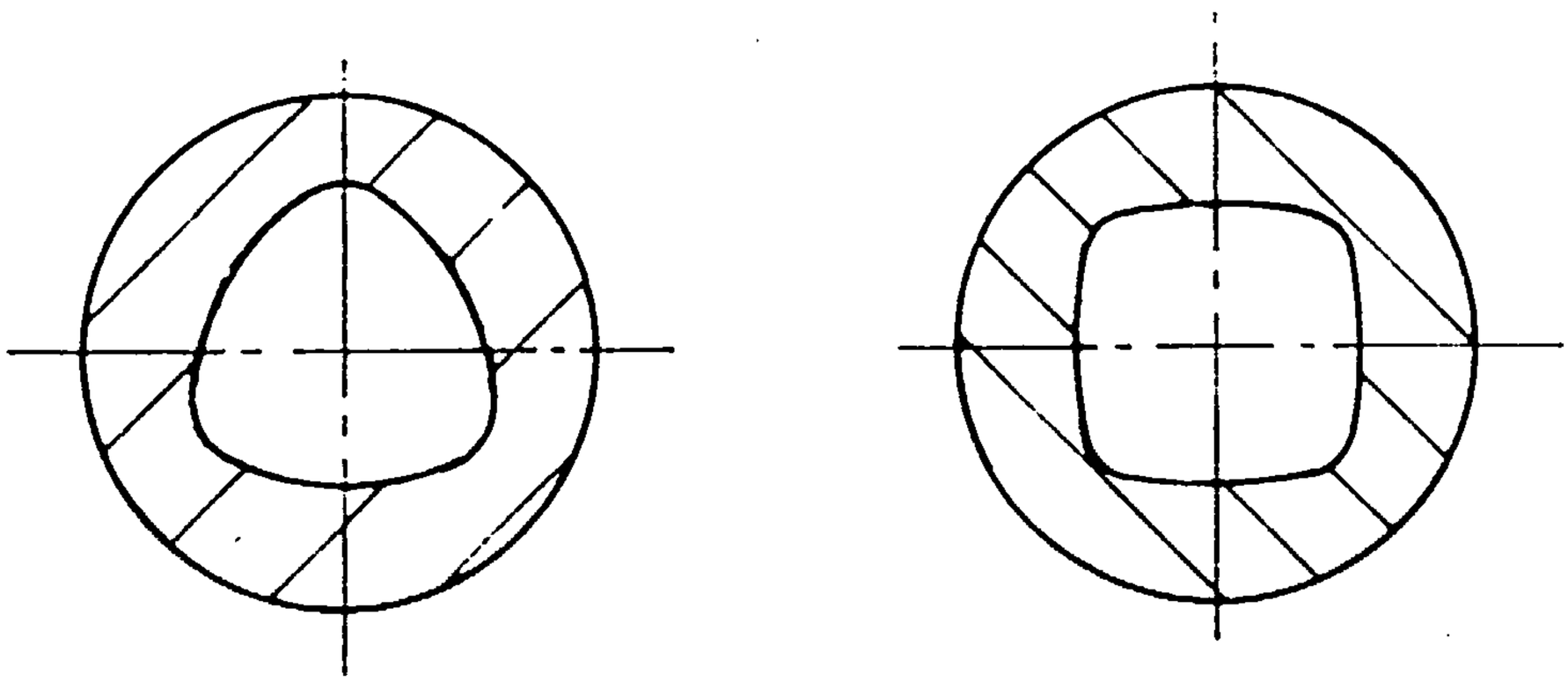

Fig.2.3. Polygons modified by manufacturing criteria.

The load distribution on, and location of, a shaft in a hub where there is a clearance fit is also important. For a profile with three corners the loads will tend to distribute equally and thus self-centre the shaft in the hub. One with more than three would lead to redundant corners not necessarily carrying any load. If less than three are used, then the loads acting on the corners will not be capable of completely locating the shaft in the centre. Therefore triangular-based profiles were primarily considered. In any case most of the arguments employed in the choice of a generation method apply also to profiles of other than triangular base.

2.2 THE ALTERNATIVES

Several geometrical methods were investigated. Profile shapes were plotted, using each method, for a range of eccentricities. Eccentricity, here, is being loosely defined as the maximum radial deviation of the profile from the mean radius.

The methods considered were;

1. Sinusoid
2. Hypocycloid
3. Epicycloid

a further curve used by Musyl, [5] , is also included;

4. Musyl ellipsoid

and a modification of this;

5. Cut-off ellipsoid.

2.3 SINUSOID PROFILE

This curve is that caused by superposing a sinusoidal waveform on a base circle. Three waves of the sine curve around the circumference produces a 'triangular' profile.

The curve is described algebraically, in polar, (r,α), coordinates, by;

$$r = R + e.\cos 3\alpha \qquad (2.1)$$

where R is the base circle radius, and e is the eccentricity.

This profile could be produced on a workpiece by rotating it at constant speed, as on a lathe, and moving the cutting tool in and out sinusoidally, three times per revolution of the workpiece, as in Fig.2.4

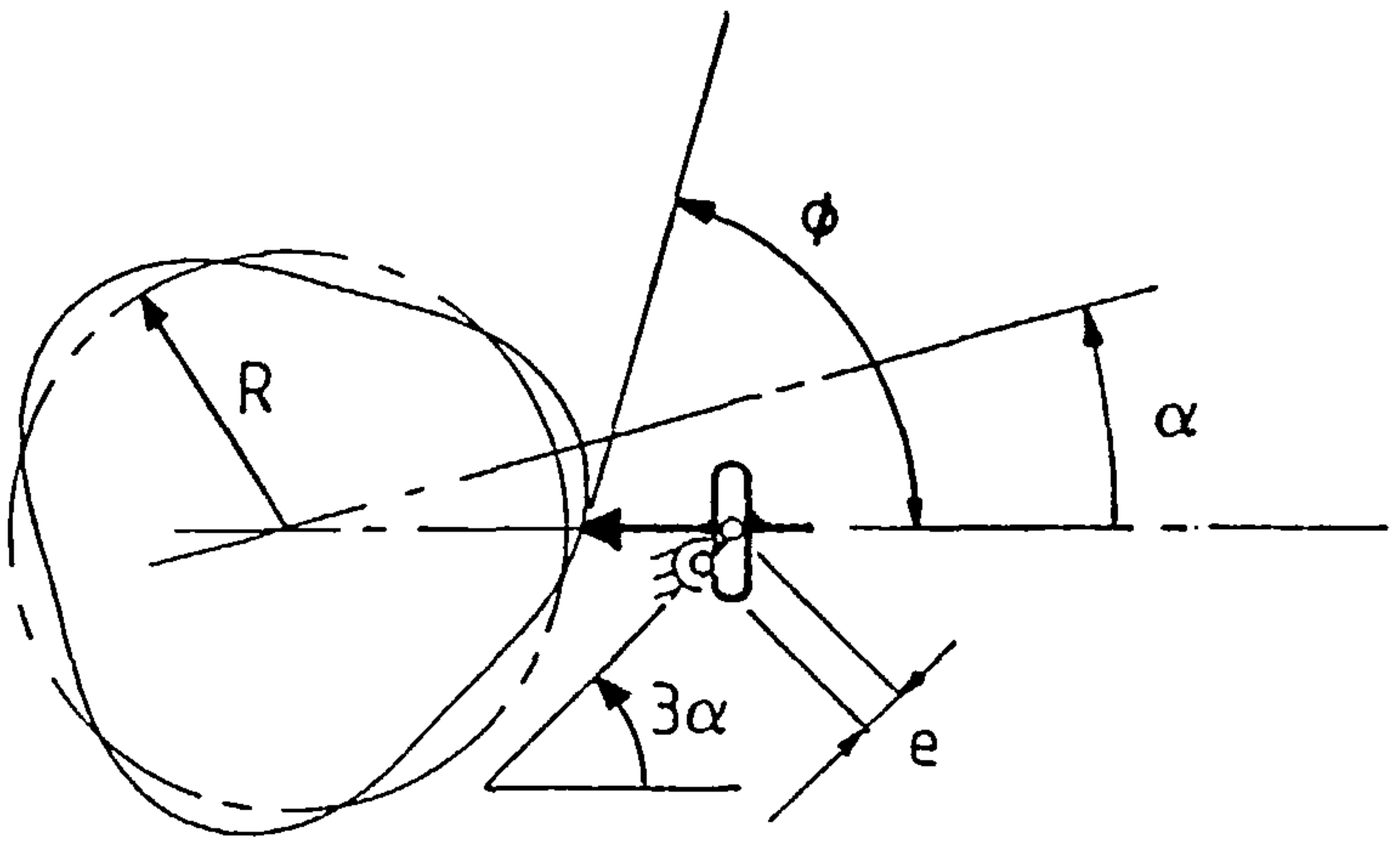

Fig.2.4. Sinusoid profile generation.

In practice it would not be as simple. If the cutting tool moved only as described then the rake angle of the tip, or cutting point in the case of a grinding wheel, to the work surface (ϕ in Fig.2.4) would be continuously changing. A means would need to be found to keep the cutting tool at a constant rake angle to ensure efficient cutting, surface finish, and accuracy. This is a problem to be overcome with any chosen profile.

Plots of this profile are shown in Fig.2.8.

2.4 HYPOCYCLOID PROFILE

2.4.1 Geometric Generation.

A hypocycloid, or hypotrochoid as it is sometimes known, [10,11], is the curve generated by a tracing point attached to a circle rolling inside a larger fixed circle.

The same curve can be produced by two different sets of circles, with the tracing point, P, inside and outside the rolling circles respectively, as in Figs.2.5(a) and (b). The curve is called a contracted or protracted

hypotrochoid depending on which method is used.

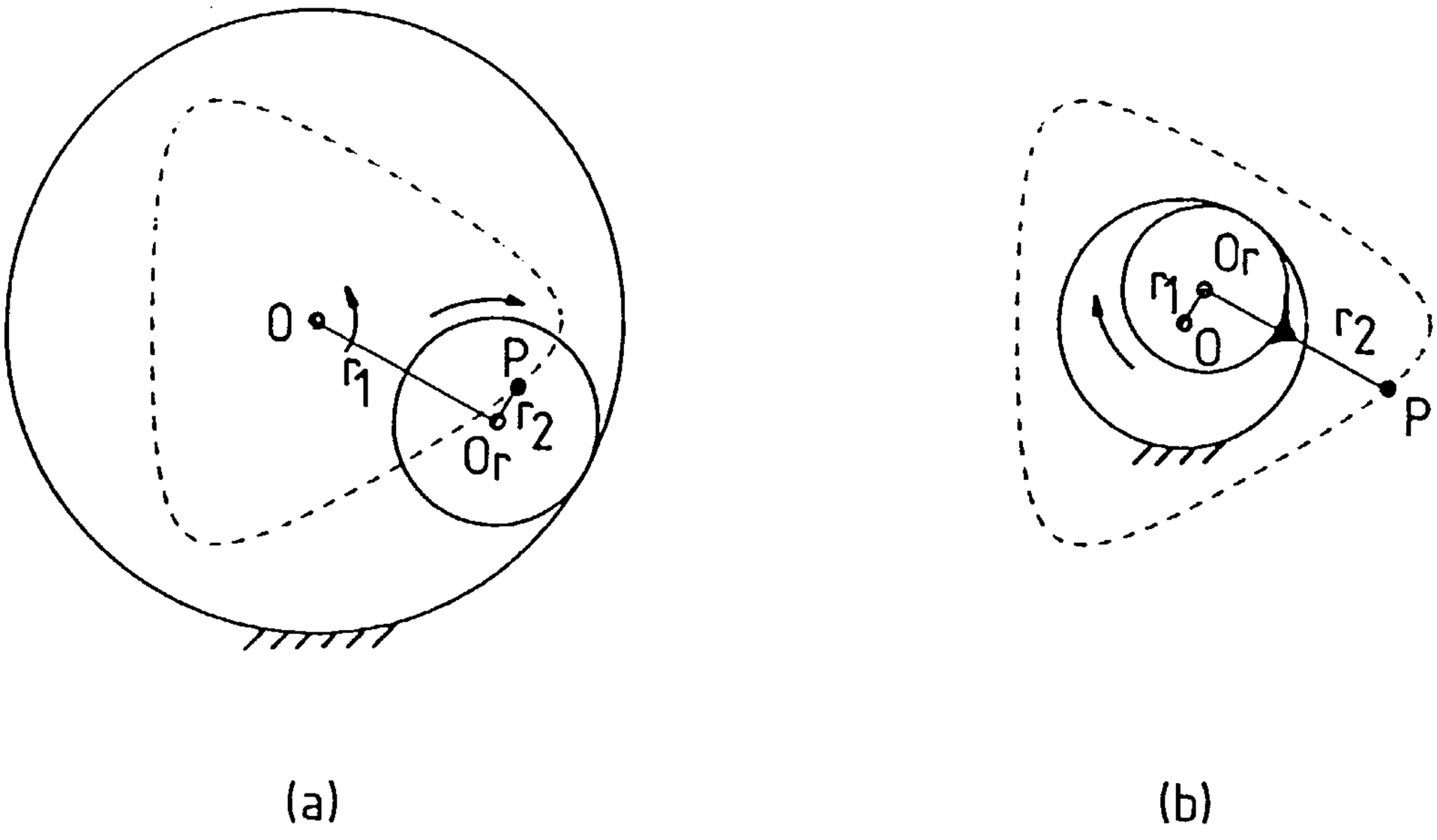

Fig.2.5(a) Contracted hypocycloid, and (b) Protracted hypocycloid, generation.

2.4.2 Derivation of Parametric Equations.

The hypocycloid curve can be described by parametric equations, derived from the two-bar linkage mechanism, shown in Fig.2.6, which is equivalent to the geometric constructions of Fig.2.5.

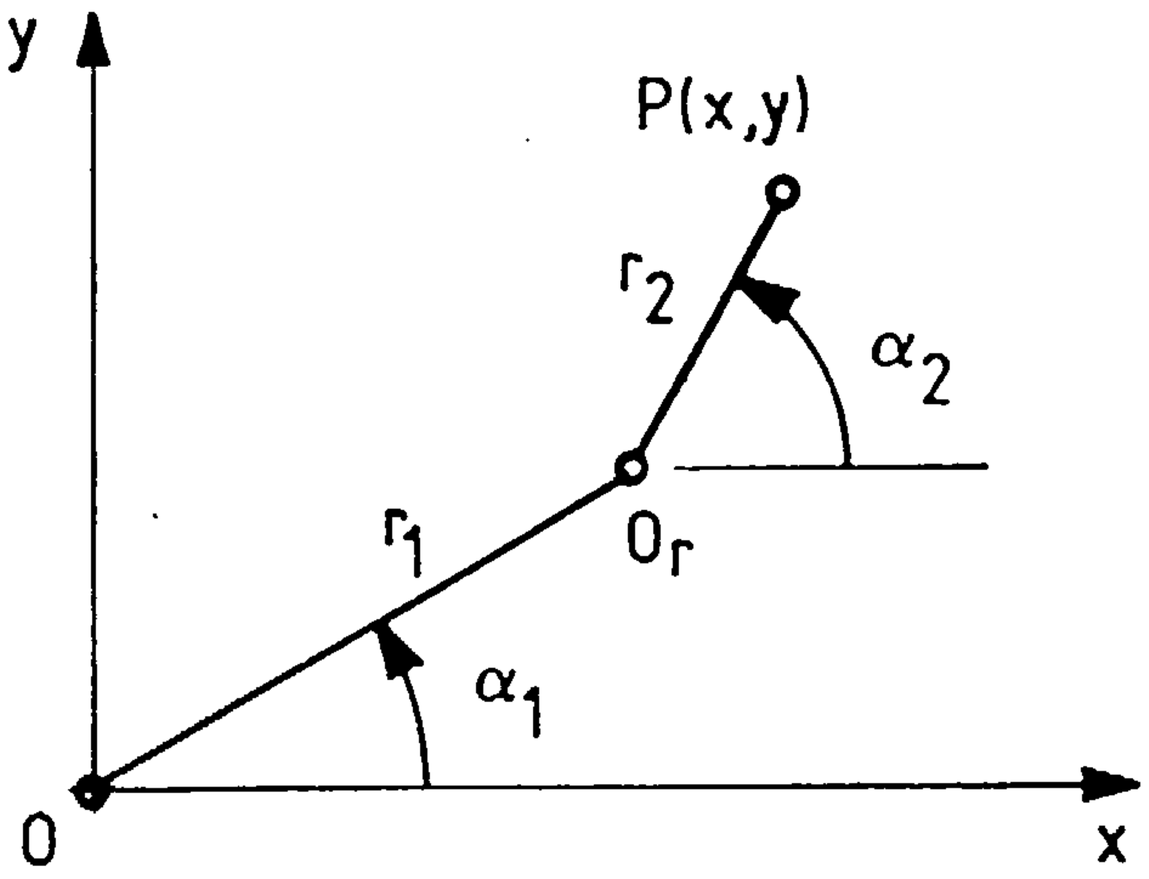

Fig.2.6. Equivalent linkage mechanisms to generate hypocycloid curve.

The coordinates (x,y) of point P can be written down directly;

$$y = r_1.\sin\alpha_1 + r_2.\sin\alpha_2 \qquad (a)$$

$$x = r_1.\cos\alpha_1 + r_2.\cos\alpha_2 \qquad (b)$$

Point P lies on a contracted hypocycloid if

$$\alpha_2 = -(n-1).\alpha_1. \qquad (c)$$

and $r_1 > r_2$

Note that in Fig.2.5(a), the direction of rotation of the rolling circle is opposite to that of its centre 0_r about 0. Hence the -ve sign above.

If eccentricity r_2/r_1 is denoted by e, and Eqn.(c) is substituted in Eqns.(a) and (b), then these become,

$$y = r_1\ (\sin\alpha_1 - e.\sin(n-1)\alpha_1) \qquad (d)$$

$$x = r_1.(\cos\alpha_1 + e.\cos(n-1)\alpha_1) \qquad (e)$$

(Note, from elementary trigonometry, sin(-a) = -sin(a), and cos(-a) = cos(a)).

Similarly for the protracted hypocycloid of Fig.2.5(b), where $r_1 < r_2$, $e = r_{1/r_2}$, and,

$$\alpha_2 = -\alpha_1/\ (n-1)$$

the equations become:

$$y = r_2.(-e.\sin(n-1)\alpha_2 + \sin\alpha_2) \qquad (f)$$

$$x = r_2.(e.\cos(n-1)\alpha_2 + \cos\alpha_2) \qquad (g)$$

which are of the same form as Eqns. (d) and (e).

Both cases can be represented by general equations for a hypocycloid:

$$y = R.(\sin\alpha - e.\sin(n-1)\alpha) \qquad (2.2)$$

$$x = R.(\cos\alpha + e.\cos(n-1)\alpha) \qquad (2.3)$$

Thus for a 'triangular' profile, n=3, and these become

$$y = R.(\sin \alpha - e.\sin 2.\alpha) \qquad (2.4)$$

$$x = R.(\cos \alpha + e.\cos 2.\alpha) \qquad (2.5)$$

Plots of these curves are shown in Fig.2.9.

2.5 EPICYCLOID PROFILE

The epicycloid, or epitrochoid , [10,11] curve is generated similarly to the hypocycloid curve except that in this case the rolling circle rolls on the outside of the fixed circle, as depicted in Figs. 2.7(a) and (b).

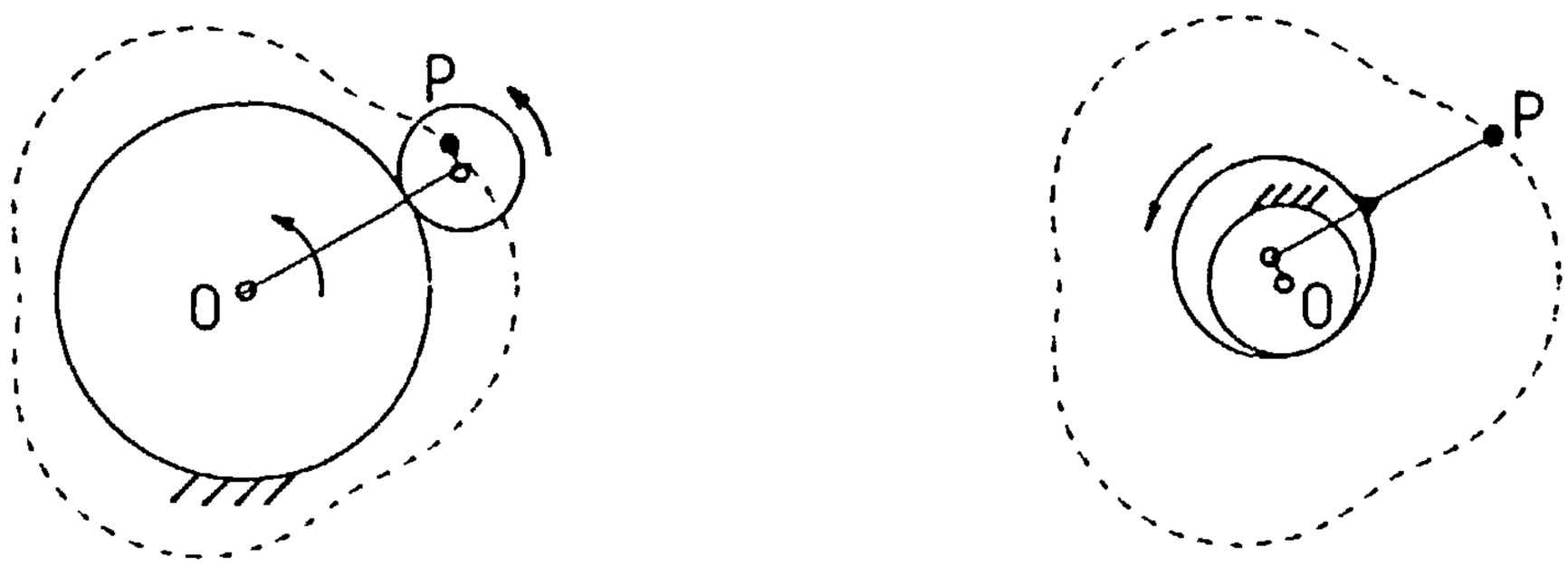

(a) (b)

Fig.2.7(a) Contracted epicycloid, (b) Protracted epicycloid generation.

The parametric equations describing an epicycloid are also derived similarly to those for the hypocycloid, in Section 2.4.2 giving:

$$y = R.(\sin \alpha + e.\sin(n+1)\ \alpha) \qquad (2.6)$$

$$x = R.(\cos \alpha + e.\cos(n+1)\ \alpha) \qquad (2.7)$$

and for the 'triangular' profile where n = 3

$$y = R.(\sin \alpha + e.\sin 4.\alpha) \qquad (2.8)$$

$$x = R.(\cos \alpha + e.\cos 4.\alpha) \qquad (2.9)$$

The application in manufacture is also similar.

Plots of this curve are shown in Fig.2.10.

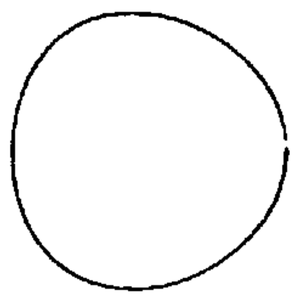

E= 0.030

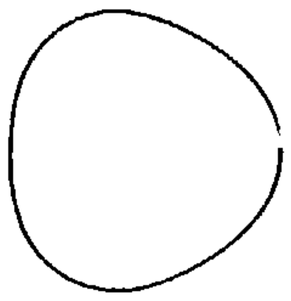

E= 0.060

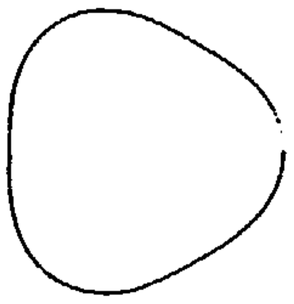

E= 0.090

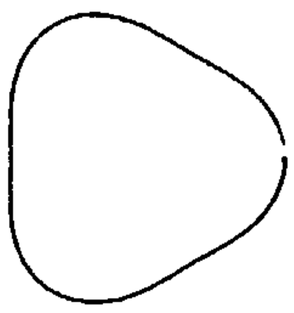

E= 0.120

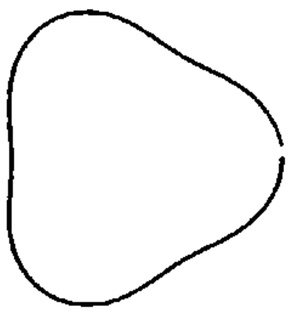

E= 0.150

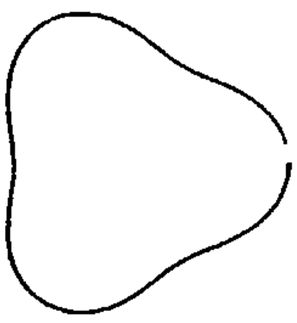

E= 0.180

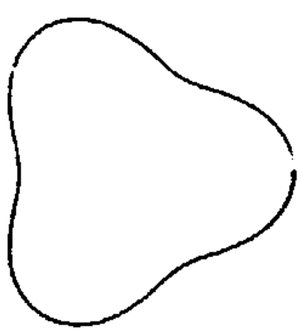

E= 0.210

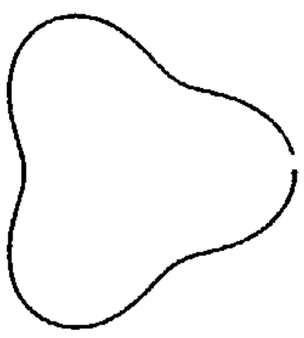

E= 0.240

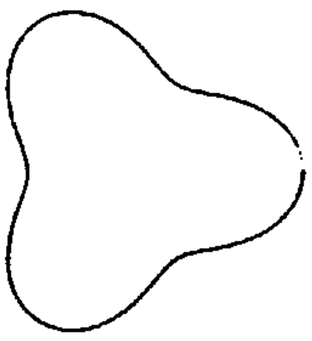

E= 0.270

Fig.2.8 Range of profiles produced by Sinusoid method

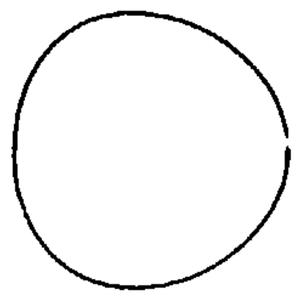

E= 0.030

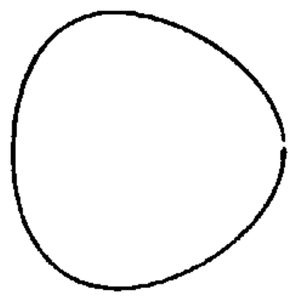

E= 0.060

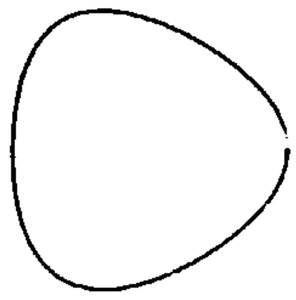

E= 0.090

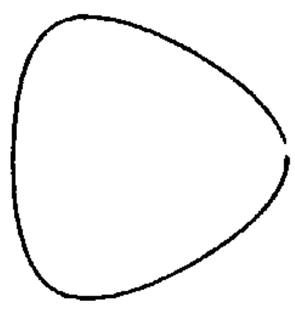

E= 0.120

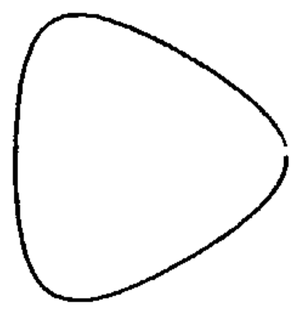

E= 0.150

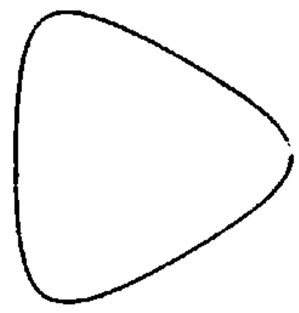

E= 0.180

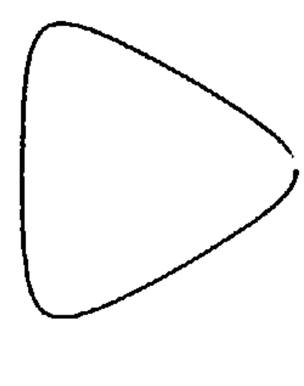

E= 0.210

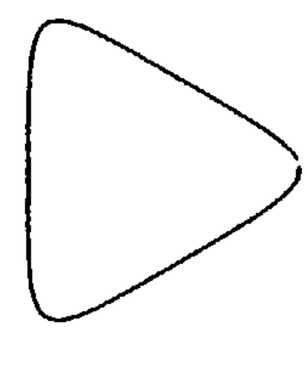

E= 0.240

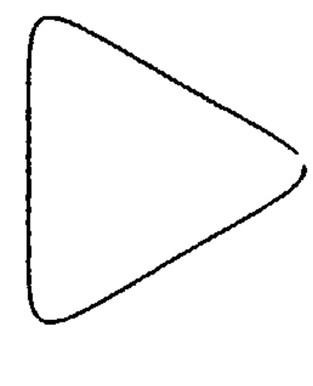

E= 0.270

Fig.2.9 Range of profiles produced by Hypocycloid method

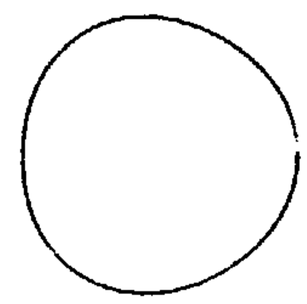

E= 0.030

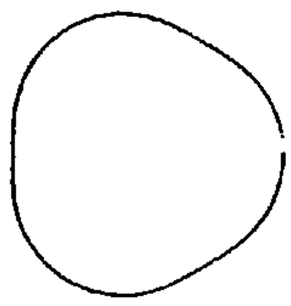

E= 0.060

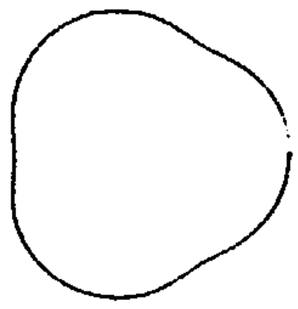

E= 0.090

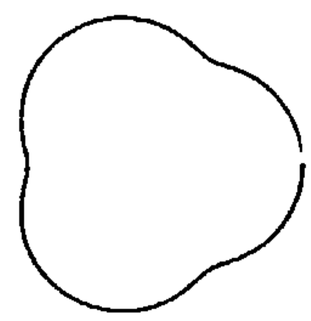

E= 0.120

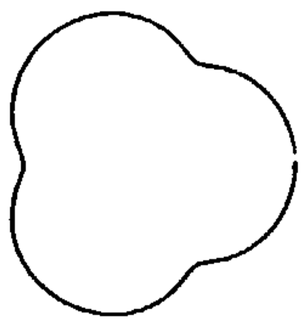

E= 0.150

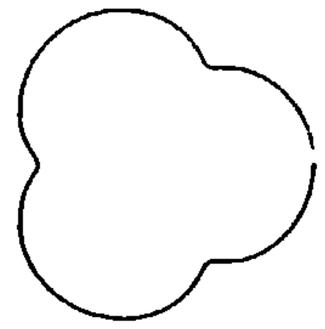

E= 0.180

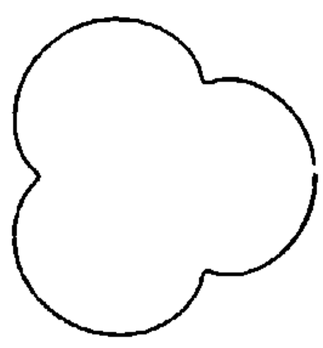

E= 0.210

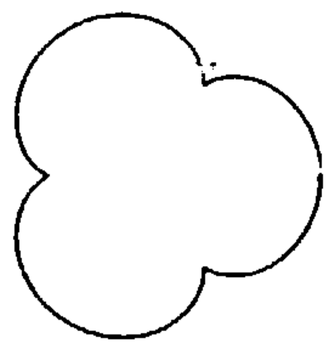

E= 0.240

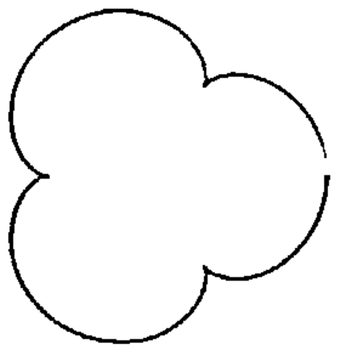

E= 0.270

Fig.2.10 Range of profiles produced by Epicycloid method.

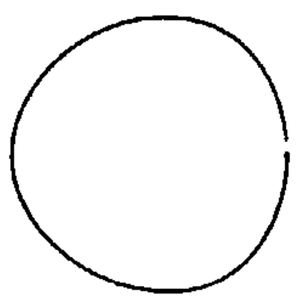

E= 0.030

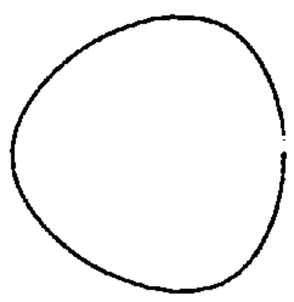

E= 0.060

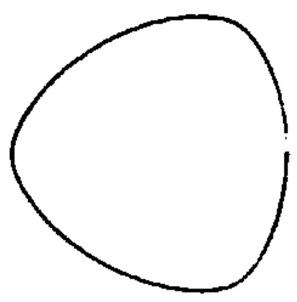

E= 0.090

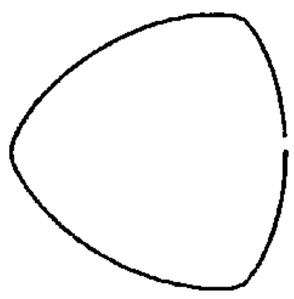

E= 0.120

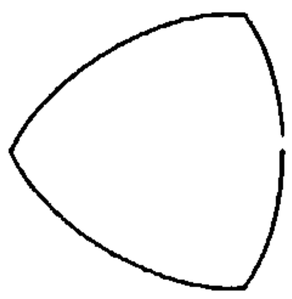

E= 0.150

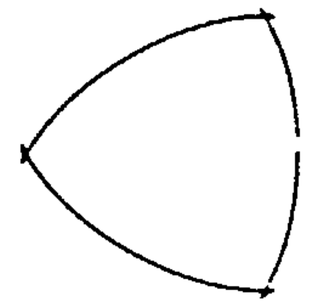

F= 0.180

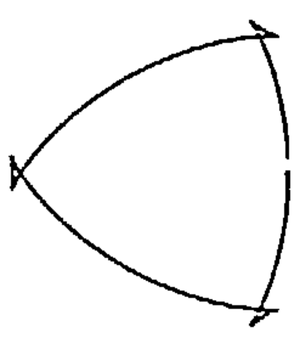

E= 0.210

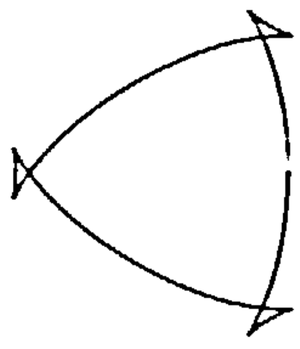

E= 0.240

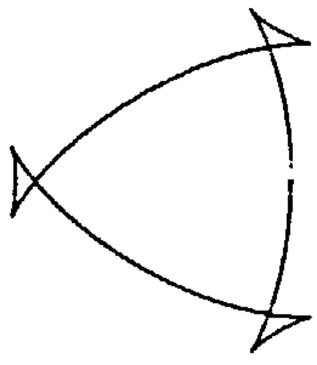

E= 0.270

Fig.2.11 Range of profiles produced by Musyl method.

2.6 MUSYL ELLIPSOID PROFILE

This profile was developed by Musyl,[4,5] who considered ways of producing polygonal profiles on shafts and in holes. His investigation led to a method whereby the profile is ground on the shaft by moving the grinding wheel in an elliptical path as the work rotates.

The curves are governed by the following parametric equations:

$$y = R(\cos\alpha - e\cos 3\alpha\cos\alpha - 3e \sin 3\alpha \sin\alpha) \quad (2.10)$$

$$x = R(\sin\alpha - e\cos 3\alpha\sin\alpha + 3e \sin 3\alpha \cos\alpha) \quad (2.11)$$

Plots of this curve are shown in Fig.2.11. They are also the subject of a DIN specification, [8].

2.7 CUT-OFF ELLIPSOID PROFILE

For profiles requiring relatively high eccentricities (to achieve greater contact pressure angles in a joint) Musyl describes a version of the previous profile, of Section 2.6, but with the corners machined off concentrically to limit the maximum size and the resultant sharp corners otherwise. Examples of these are shown in Fig. 2.12. These are also the subject of a DIN specification [9].

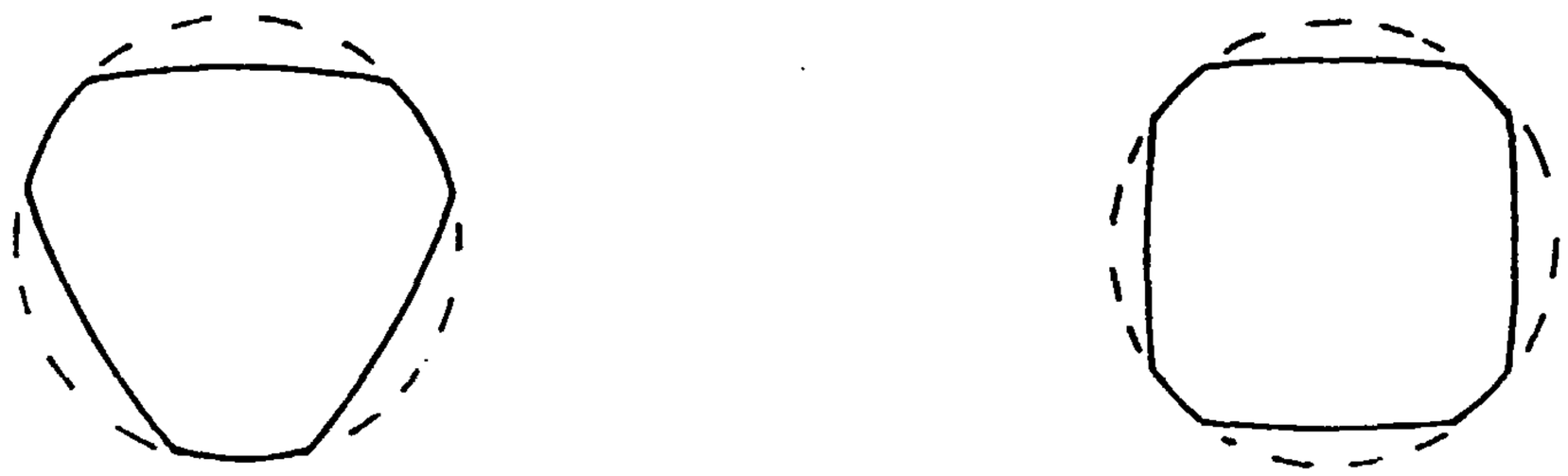

Fig.2.12. Ellipsoid profiles with sharp corners removed.

2.8 COMPARISON OF PROFILES

Each of the four basic profiles was plotted, by computer, for a range of values of eccentricity, e. R is set at unity in all the plots, which are shown in Figs. 2.8 to 2.11. In Fig.2.12 are depicted examples of cut-off profiles according to Musyl and DIN 32712.

The plots show that only the hypocycloid curve, Fig.2.9, can provide a complete range of profiles which progresses from circular through to virtually triangular, as the eccentricity increases.

Neither the sinusoid, Fig.2.8., nor the epicycloid, Fig.2.10, converge towards a triangular shape but rather to a lobed shape. As the eccentricity increases, the curvature of the corners does not change as much as the flatness of the sides, which rapidly become concave.

The range of shapes available by the sinusoid and the epicycloid which would appear to be useful and could be easily manufactured is limited to very small eccentricity values, less than 0.12 and 0.09 respectively. Beyond these their manufacture becomes more difficult as concave surfaces would need to be machined on shafts and convex surfaces in holes.

The Musyl curve, Fig.2.11, has the opposite tendency to the latter two, in that the corners become sharper as the eccentricity increases and the sides remain convex. However this also limits the useful range, as sharp corners giving rise to greater stress concentrations should be avoided. Indeed Musyl, [5], recommends an eccentricity of about 0.06.

The desired profile would be most useful if it could be used where clearance fits are required such as for hubs sliding on shafts.

The profiles limited to low eccentricities are disadvantaged by the fact that the more circular the shape, then the better must be the fit between a shaft and hub to avoid relative rotation under load and rounding-off of corners, thus limiting the torque. Rounding-off of corners is a familiar problem as for example when a badly fitting spanner is used on a nut or bolt head. These profiles would be best suited to low torque situations and non-sliding or interference fits, and also to more accurately fitted shafts and hub connections.

For applications involving high torques, relative translation of shafts and hubs, or sliding fits, the use of profiles with higher eccentricities, but with the corners cut off concentrically to limit the maximum size and remove the sharp corners that would have resulted otherwise, are recommended by Musyl [7] and DIN 32712 [9]. The higher eccentricity produces a better maximum contact pressure angle between the mating components, thus improving the torque capacity.

The disadvantages of this cut-off profile are the introduction of the discontinuities between the corners and sides which increase the machining difficulties, it is not possible to grind internal cut-off profiles. Also the lack of discontinuities is one of the original benefits compared to keyways and splines.

The hypocycloid offers the best prospects. A full range of shapes between circular and virtually triangular can be generated, theoretically, and high eccentricity profiles could be chosen for high torque, clearance fit situations, without resorting to cutting-off of corners although these also could be cut-off if this became desirable.

Another advantage of the hypocycloid is its relative insensitivity to changes of eccentricity compared to the other profiles; for a given change in shape a larger alteration of eccentricity is required. This would enable the accurate setting of the eccentricity in a machining device to be achieved more easily. Furthermore as will be shown in Chapter 3, a reasonably simple means of maintaining cutting tool orientation is possible when generating a hypocycloid.

CHAPTER 3

DEVELOPMENT OF A KINEMATIC ARRANGEMENT

In the previous chapter it was shown that a hypocycloid curve offered the most suitable profile range of those considered. This chapter deals with the kinematic development of a linkage mechanism to generate the profile on a workpiece by controlling the relative position of a grinding wheel.

3.1 DEVELOPMENT OF AN ELEMENTARY MECHANISM

3.1.1 Contracted Hypocycloid Method

Consider the arrangement for a contracted hypocycloid in Fig.3.1(a) with the inner circle rolling inside the outer fixed circle.

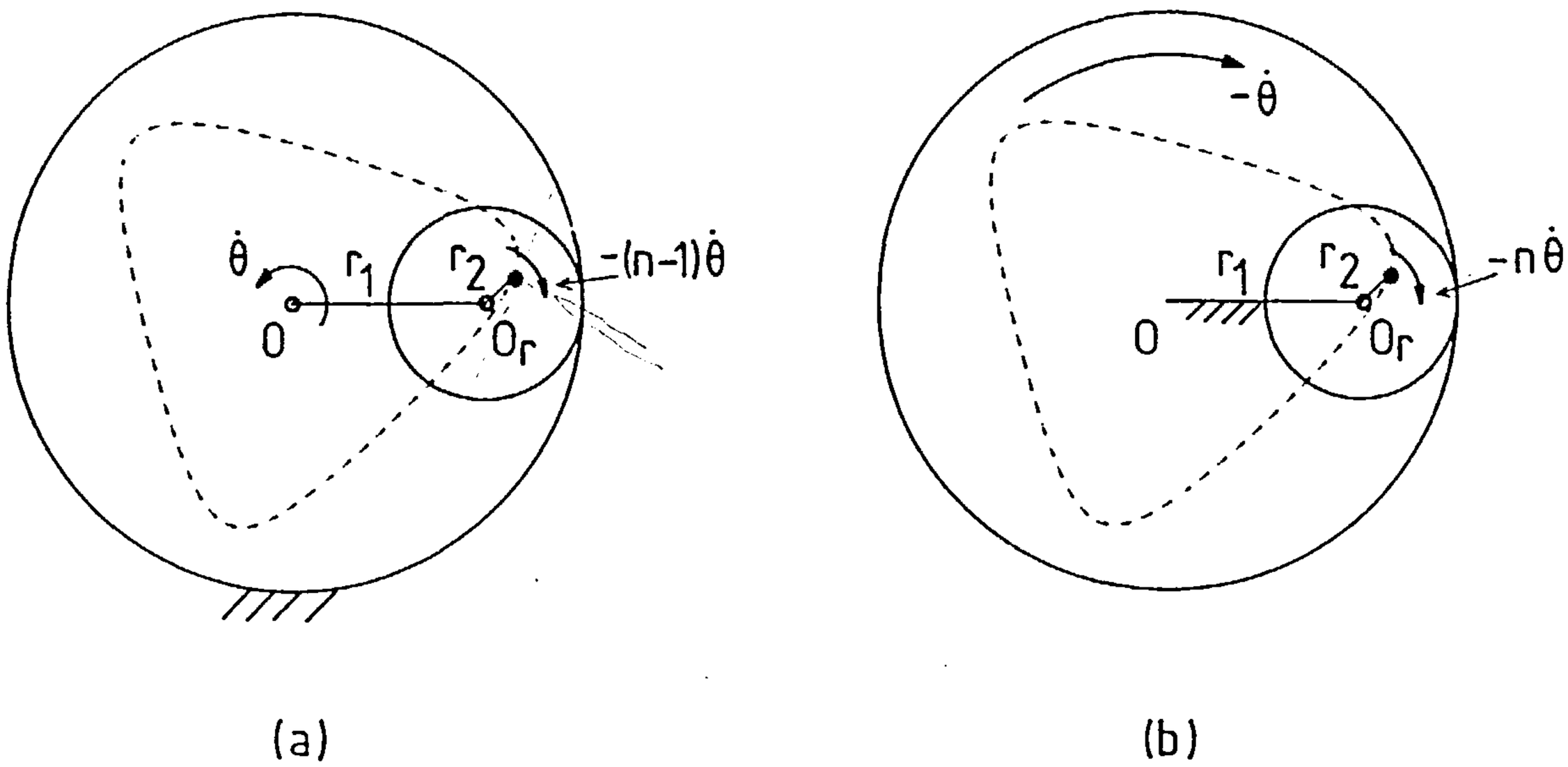

Fig. 3.1. Basic contracted hypocycloid generation with (a) outer circle fixed, (b) outer circle free to rotate.

If the angular velocity of the link r_1 is given as $\dot{\theta}$, then that of r_2 will be $-(n-1).\ \dot{\theta}$. It may be preferable to hold r_1, and thus O_r, stationary, in which case the outer circle must rotate with a velocity $-\dot{\theta}$. This in turn causes the velocity of r_2 to change to

$$-\dot{\theta} + (-(n-1)).\ \dot{\theta} = -n.\ \dot{\theta}.$$

This arrangement is shown in Fig. 3.1(b). The curve is still traced on the now rotating plane of the outer circle.

To produce the profile on a workpiece the geometric construction circles can be forgotten. All that is required is for the work to rotate at constant speed, and the cutting point to rotate in a circle of radius r_2, about a point at a distance r_1 from the work centre, and at an angular velocity of n times that of the workpiece. The mean radius, R, of the manufactured shaft would be equal to r_1 and the eccentricity, e, equal to r_2.

3.1.2 Protracted Hypocycloid Method

A similar method can be derived from the protracted hypocycloid geometry of Fig.2.5(b). However in this case the rotating radius r_2 of the cutting point is equal to the mean radius, R, of the profile and r_1 is equal to the eccentricity, e. Furthermore the rotational speed of the cutting point is equal to $+n/(n-1)$ times that of the workpiece. Fig.3.2 depicts the arrangement for a triangular profile.

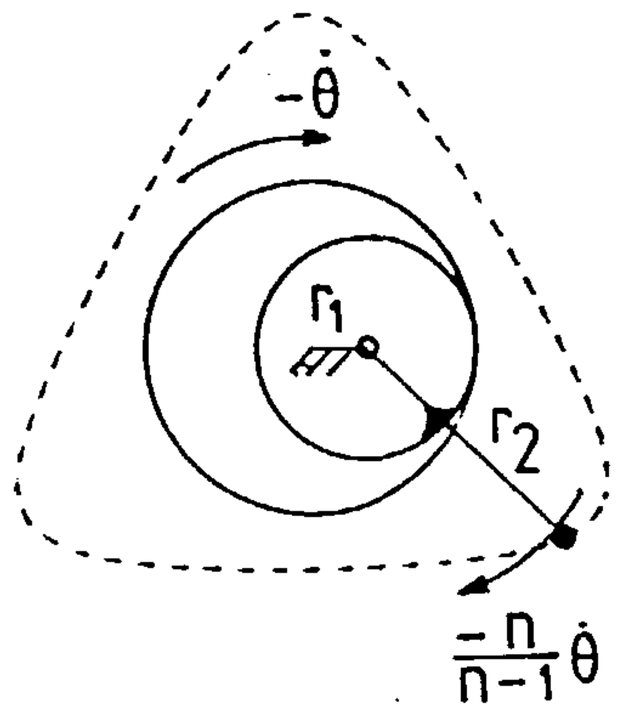

Fig.3.2 Protracted hypocycloid generating mechanism.

3.1.3 Comparison of Contracted and Protracted Based Methods

Comparing the two methods, that based on the contracted hypocycloid, in Fig.3.1(b), looks most promising as the cutting point travels in the smallest circle. Using the protracted method, not only the cutting point circle is much bigger, but also it encircles the workpiece completely. It would be impracticable for a cutting tool, especially a grinding wheel, to rotate around the workpiece.

3.2 ORIENTATION OF CUTTING TOOL

3.2.1 Effects of Orientation.

So far only generation by a single point has been considered. In practice it is insufficient simply to arrange for the tip of a tool or a grinding wheel to coincide with this point. In the case of a 'single-point tool', as commonly used on a lathe, the orientation with the surface is important to achieve the best cutting conditions.

Figure 3.3 depicts an arrangement in which the tool is kept horizontal and it is obvious that its rake angle, ϕ, changes considerably with the profile surface during each cycle. Notice that the problem cannot be overcome by simply aligning the tool with the link r_2 as this too changes orientation with the surface.

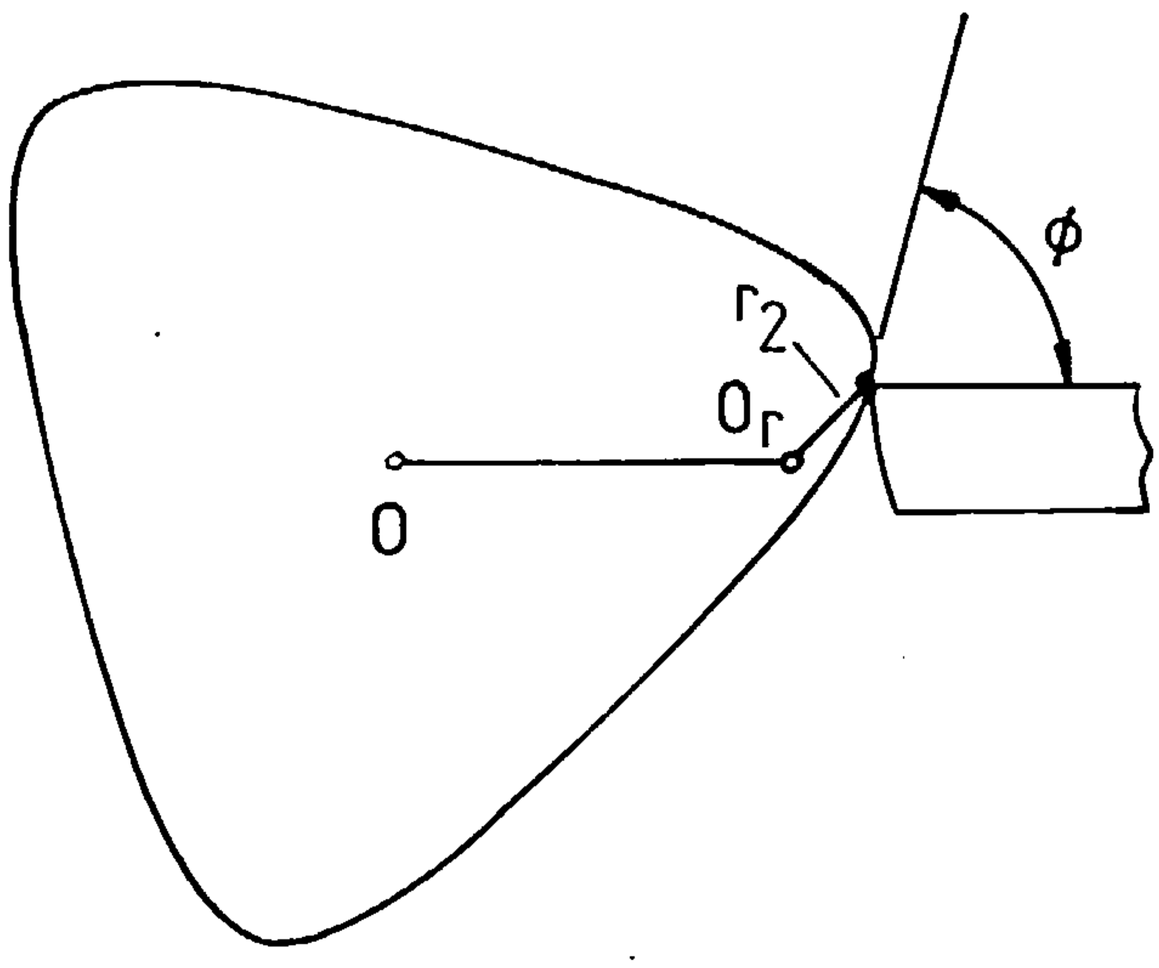

Fig. 3.3 Variation of cutting tool rake angle

The problems are even worse for a grinding wheel because it does not have a single well-defined cutting point. In this case the position of the effective cutting point on the wheel circumference is determined by its motion relative to the work, as seen in Fig. 3.4.

3.2.2 Solution to Orientation Problem.

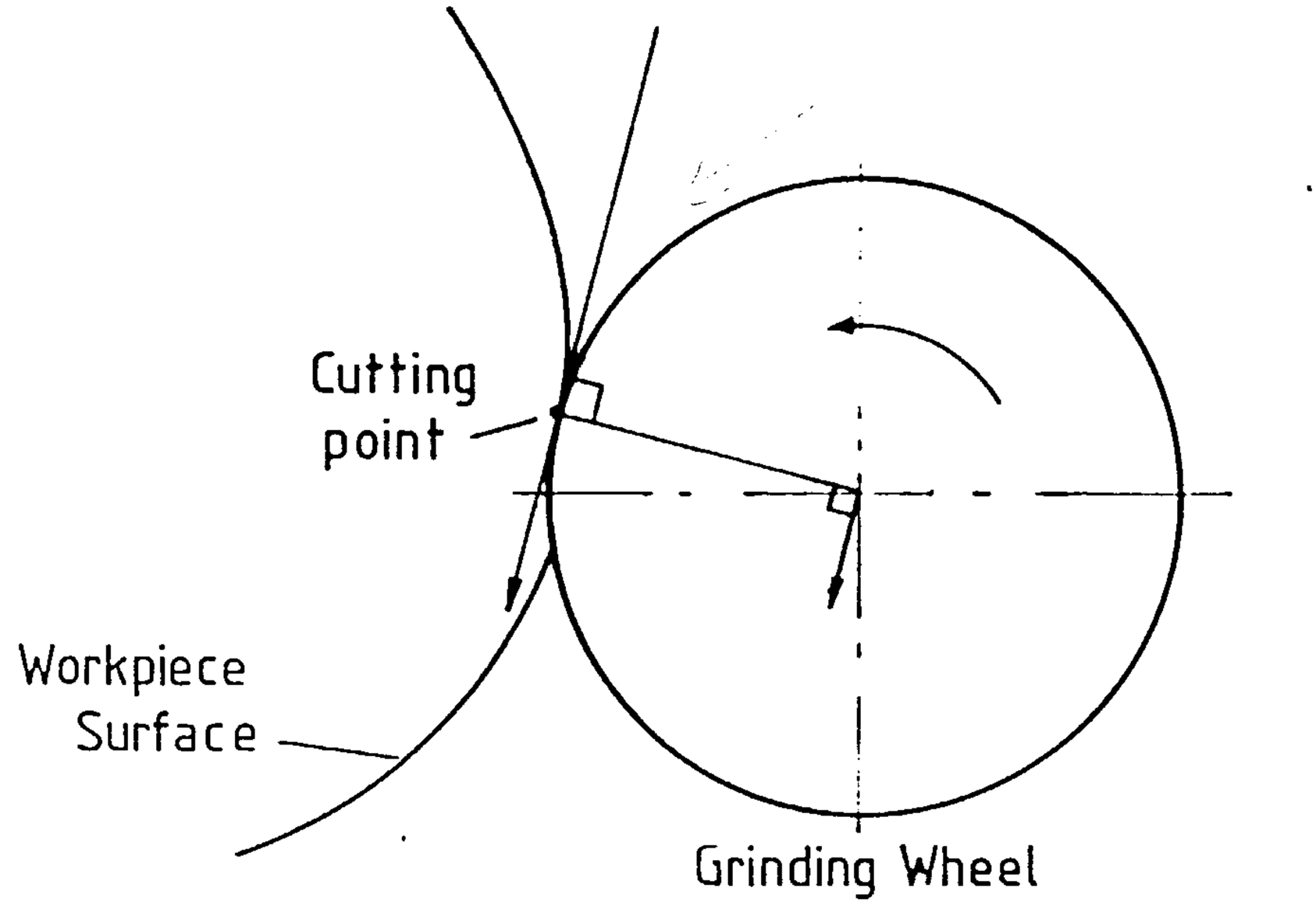

Fig.3.4 Grinding wheel cutting angle to work surface.

Consider the case of a grinding wheel. In Fig.3.4 the direction of relative motion of the cutting point to the surface is seen to be always along a common tangent to the cut surface and the grinding wheel at that point. This is also the direction of motion of the grinding wheel centre relative to the surface. Therefore the grinding wheel centre lies on a normal to the surface being cut, a fact that can be made use of to ensure correct positioning of the cutting point.

Consider again the original geometric configuration shown in Fig. 2.5(a).

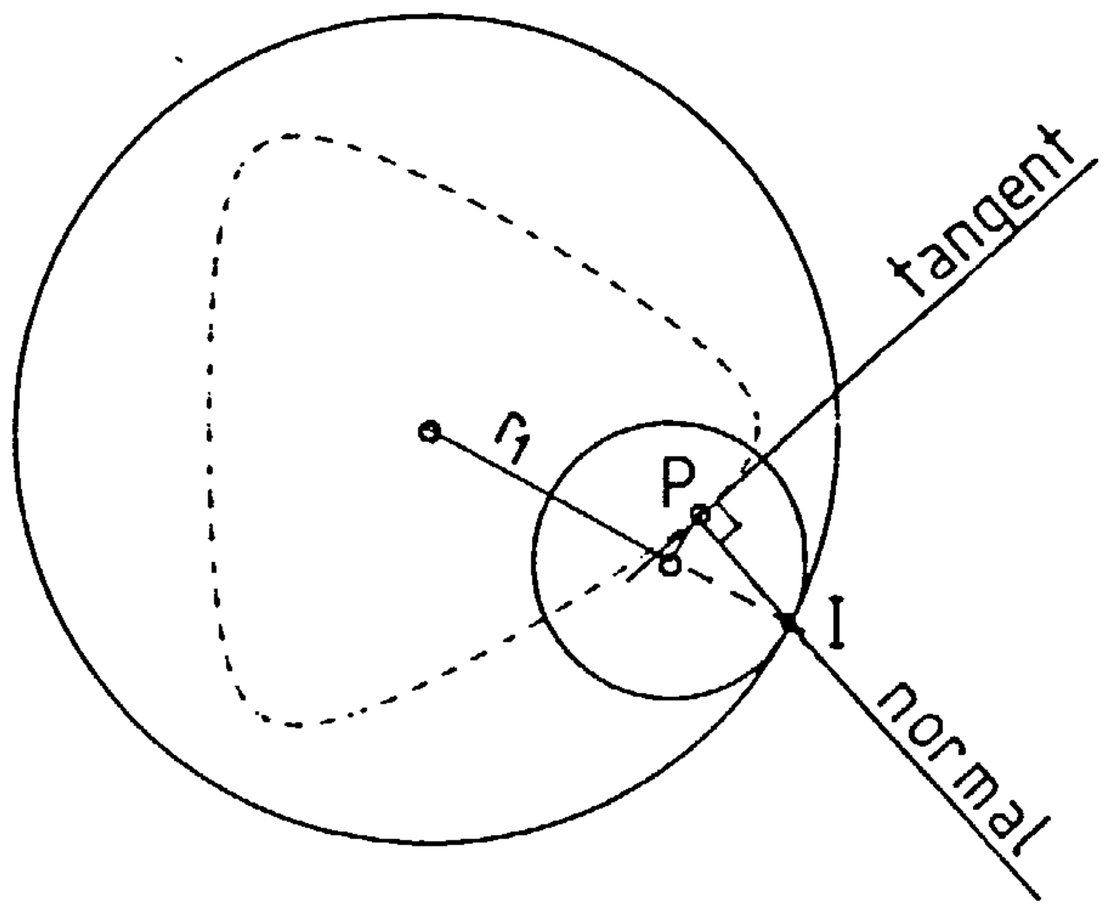

Fig. 3.5. Geometric solution of cutting tool orientation problem.

As the inner circle rolls, the point P traces the curve. At any instant the direction of motion of P is tangential to the curve.

Furthermore, any point attached to the rolling circle moves tangentially to a line through itself and the instantaneous centre of rotation, I, which is the point of contact between the two circles.

Consequently, at point P this line, IP, must be normal to the curve traced at that point.

The contact point, and instantaneous centre, is also where an extension of r_1 cuts the outer circle. And in the situation when the outer circle is rotating so that r_1 is stationary, then the locus of the instantaneous centre, I, of rotation of P relative to the profile also becomes a stationary point.

Therefore, in a generating mechanism, any link passing through the instantaneous centre and connected to point P, will provide a normal to the profile. If the grinding wheel centre, O_g, is located on this link at a distance from P equal to the wheel radius, it will always have the correct position and motion. The equivalent mechanism is shown in Fig.3.6. Note that the grinding wheel can be positioned for external or internal machining. However in most of the following discussions only the external positioning will be mentioned.

3.2.3 Alternative Mechanism Arrangements

3.2.3.1 Protracted hypocycloid mechanism.

The same arguments, when applied to the protracted method, result in the mechanism of Fig.3.7.

The grinding wheel must follow a large and impracticable path, completely circumnavigating the workpiece, and for this reason this mechanism is discarded.

3.2.3.2 Mechanism to give horizontal cutting point motion.

This is a rearrangement of the contracted mechanism of Fig.3.6 so that the cutting point is restricted to travel in a horizontal line as depicted in Fig.3.8.

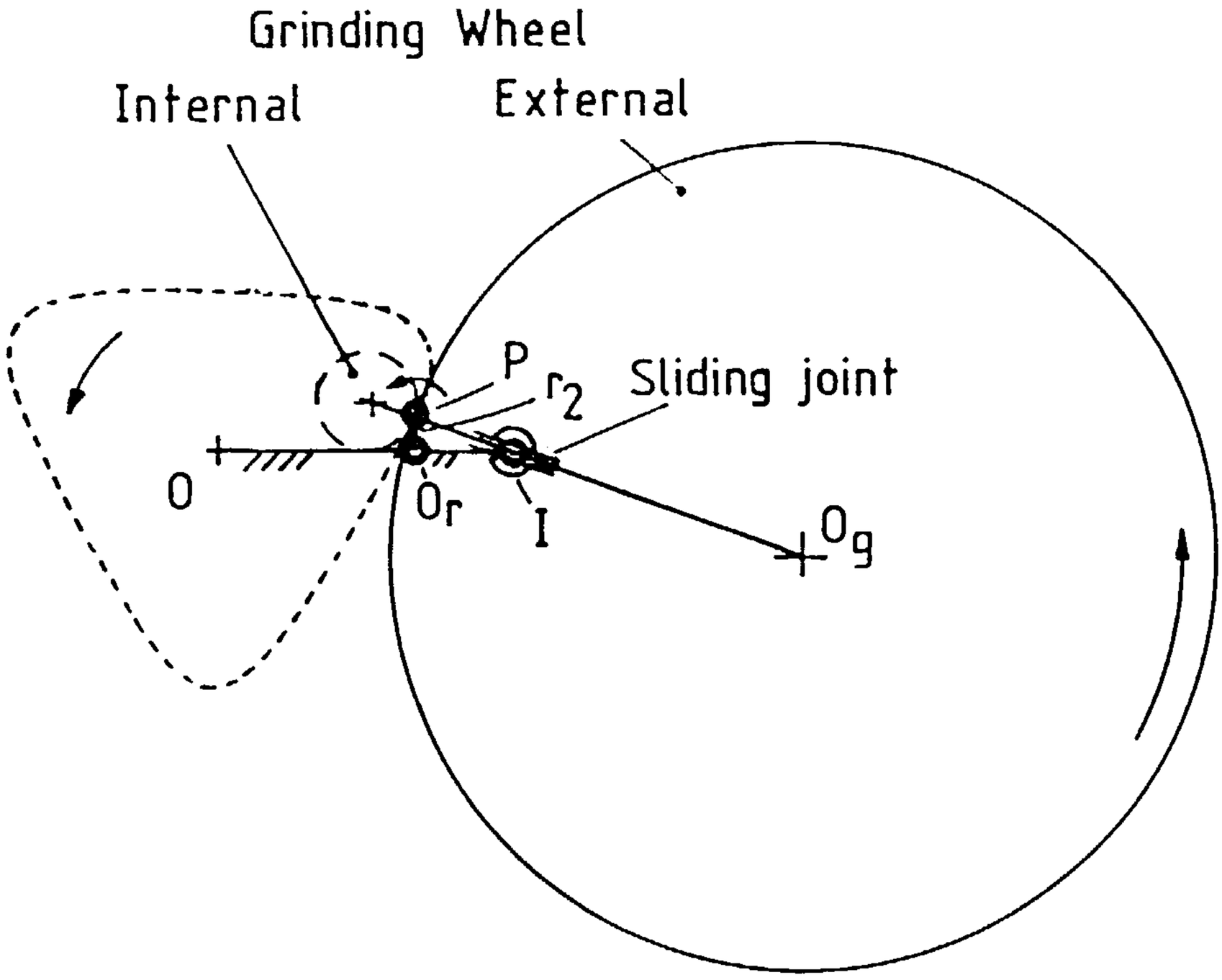

Fig. 3.6 Orientation of grinding wheel in contracted hypocycloid mechanism.

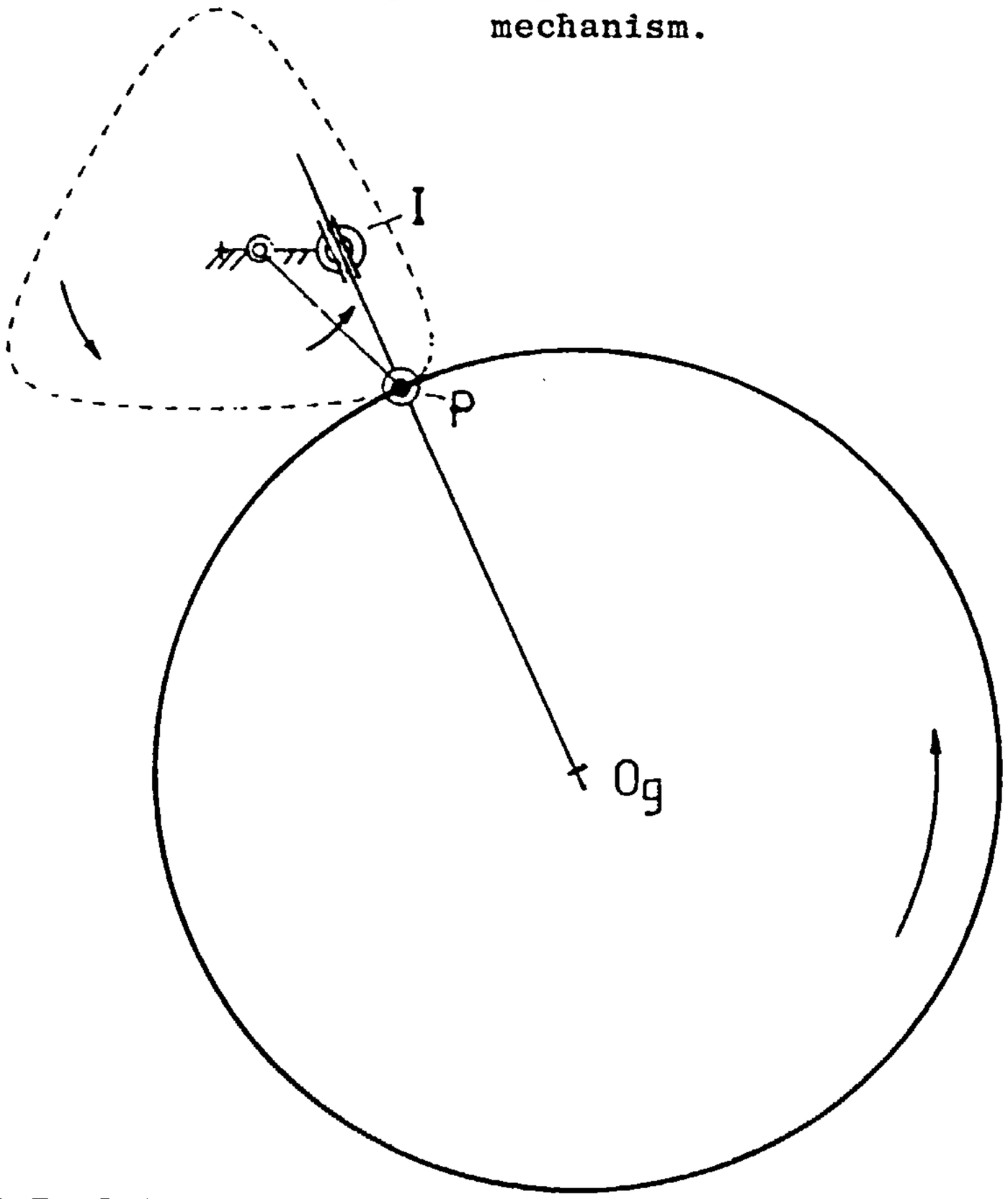

Fig. 3.7 Orientation of grinding wheel in protracted hypocycloid mechanism

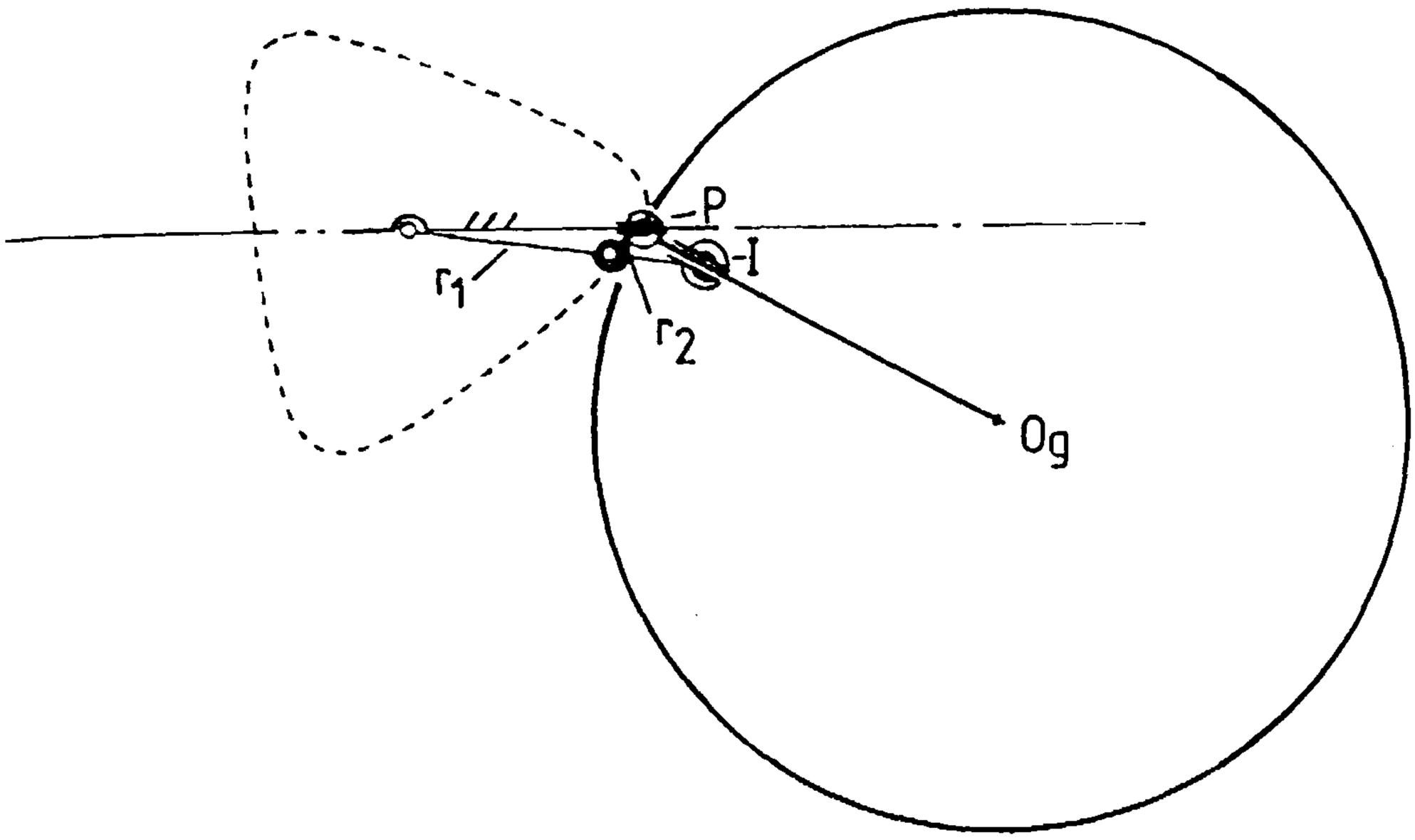

Fig. 3.8 Contracted hypocycloid mechanism giving horizontal cutting point motion

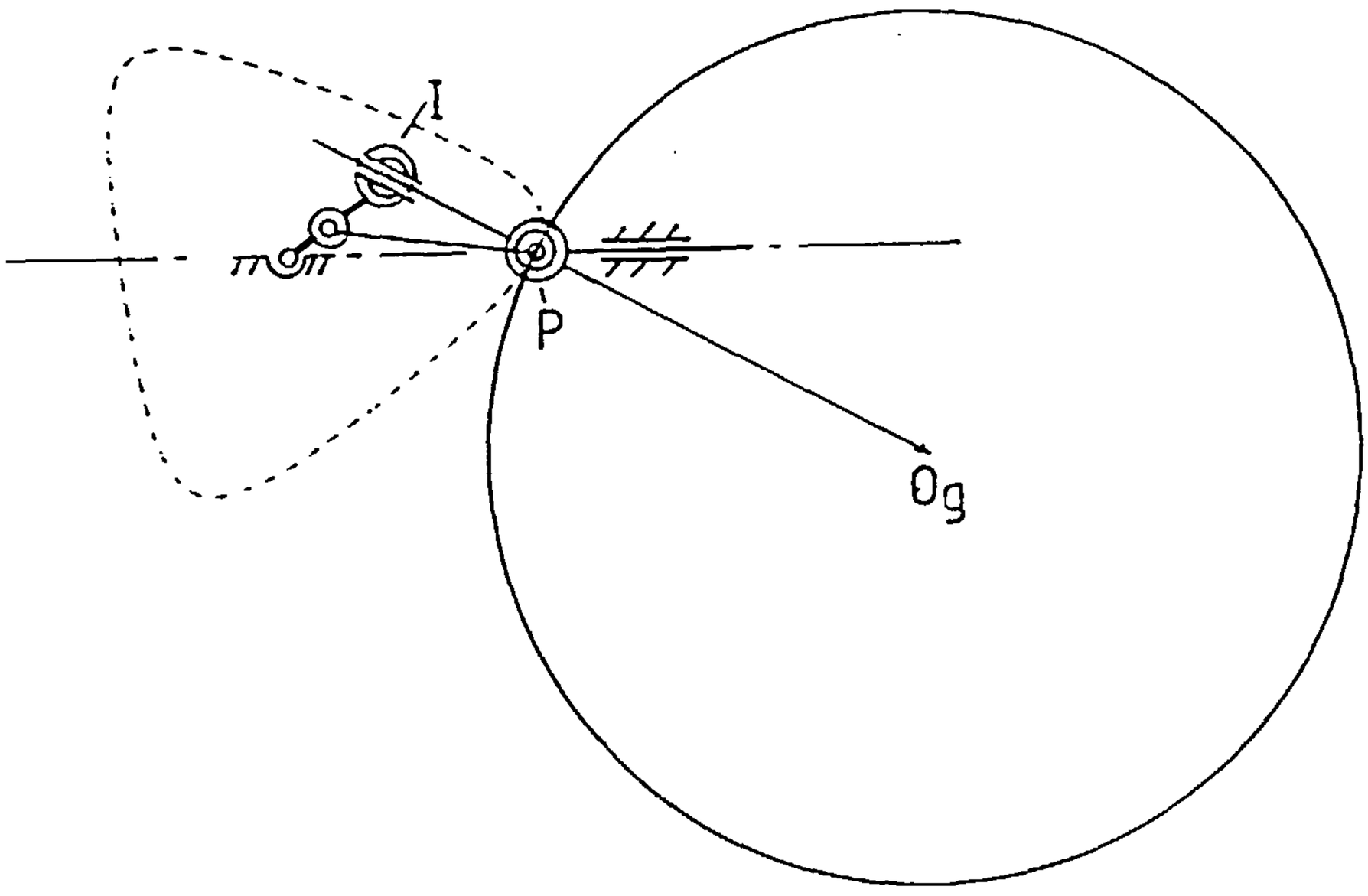

Fig.3.9 Protracted hypocycloid mechanism giving horizontal cutting point motion

For this to happen both the links r_1 and r_2 will move but not with constant speeds as before. Link r_2 will rotate about point P and r_1 will rock.

This mechanism does not appear to have any advantages over the original but obvious disadvantages because of the complexity of motions and the extra joints required.

There is another method of producing the same grinding wheel motions as above, but based on the protracted method as shown in Fig.3.9, and the same disadvantages apply. Both these mechanisms were therefore rejected.

3.3 PROBLEM OF POSITIONING THE MECHANISM

Consideration of the discussions above leads to the conclusion that the first mechanism, Fig.3.6, based on the contracted hypocycloid geometry should be used. This mechanism has the simplest linkage arrangement and produces the smallest motions of the grinding wheel.

However, practical implementation of this idealised mechanism gives rise to a further problem in the positioning of the mechanism relative to the workpiece.

In Fig.3.6 the generating mechanism configuration is such that the revolute joint at O_r and the link r_2 are seen to be inside the curve for part of the cycle. In practice the generating mechanism would have to be placed past the end of the workpiece so as not to foul it, as shown in Fig.3.10. This would obviously restrict the length of shaft that could be machined, and also hinder the use of a tail support centre for the work-piece, thereby further limiting the allowable cutting forces.

The mechanism must be developed further to allow the profile generating links to be removed from the vicinity of the work and still transmit the correct motions to the grinding wheel.

A commonly used device for just these purposes is the pantograph. This is a linkage mechanism with a parallelogram determining its movement. Points can be chosen on the pantograph which follow parallel paths, enabling

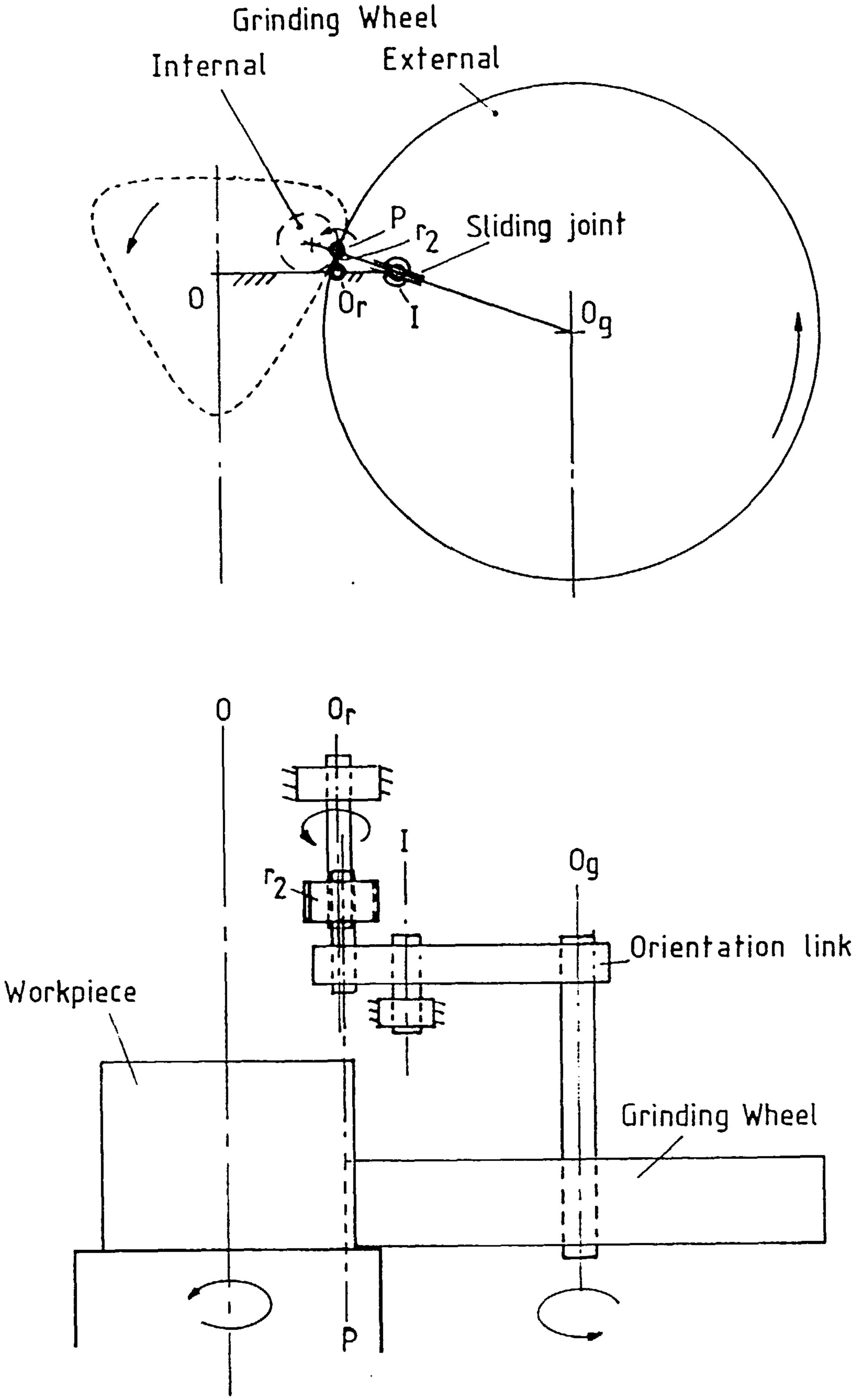

Fig.3.10 Problem of positioning the mechanism

motions to be copied. In this case, the grinding wheel motions could be produced by a generating mechanism placed well away from the work, and a pantograph used to transmit them to the grinding wheel, next to the work.

3.4 PANTOGRAPH DEVELOPMENT

3.4.1 Summary of Pantograph Properties and Types.

Several arrangements of pantographs are depicted in Fig.3.11. All of them contain at least one four-bar linkage mechanism with parallel sides, i.e. opposite sides of equal length.

Consider the configuration of Fig.3.11(a). If points A and B are chosen such that a line can be drawn through them and fixed joint O, then they will always follow parallel paths when moved. The sizes of the images traced by A and B will be in the ratio of OA:OB. Thus, as well as being able to copy motions, a pantograph can also reduce or magnify them.

In general

$$\frac{\text{Size of image traced by A}}{\text{Size of image traced by B}} = \frac{\text{Distance of A from fixed point O}}{\text{Distance of B from fixed point O}}$$

Notice that if the frame joint, O, is between A and B then the copied image will be inverted.

3.4.2 Choice of Pantograph

A conclusive choice could only be made after further consideration of the overall requirements, and more detailed development of layouts for an attachment design on a particular lathe.

However, a preliminary choice was made for use in the kinematic and dynamic analyses described in the next chapters.

Some considerations in the choice of a suitable pantograph are:

1. Should the reproduced motions be magnified, reduced or unchanged, and inverted, or not?
2. How many links and joints are required?
3. How easily will it fit in with rest of design?

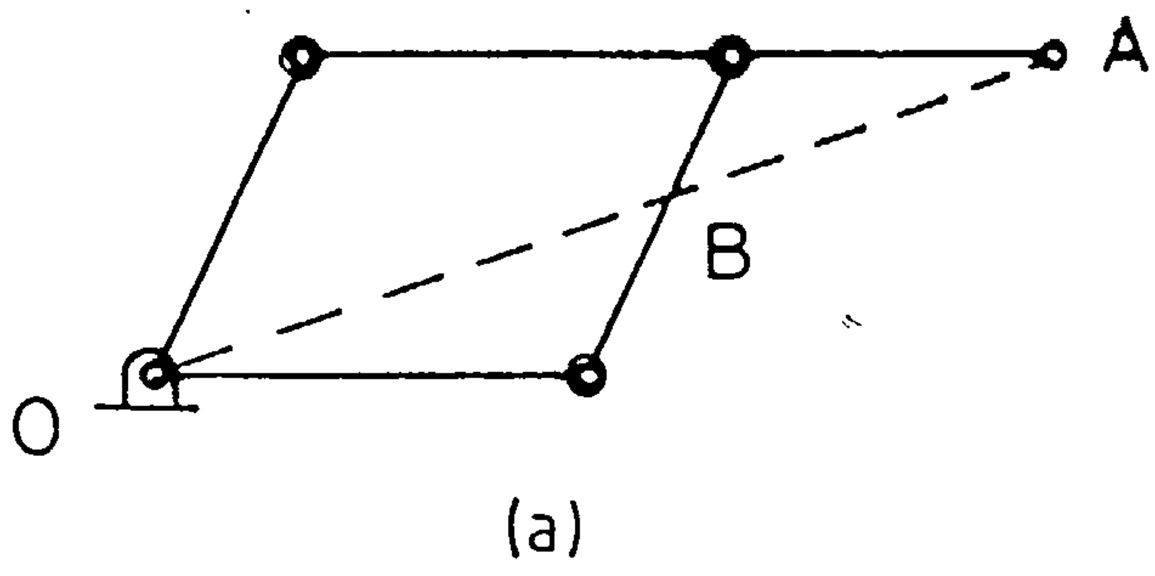

(a)

Image A > Image B

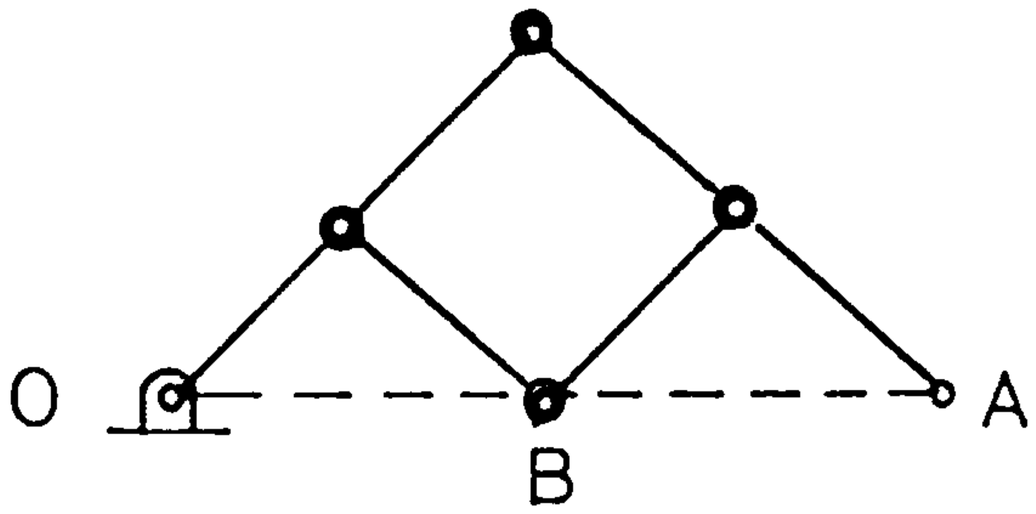

(b)

Image A > Image B

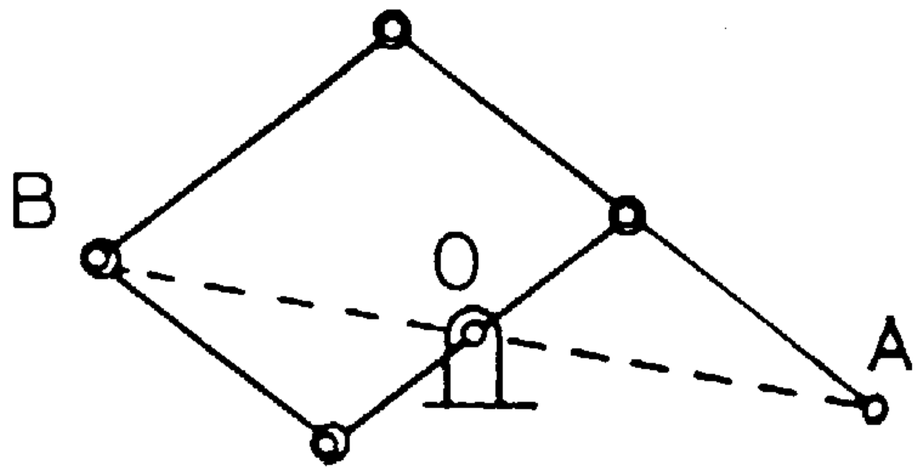

(c)

Image A > Image B

Image inverted

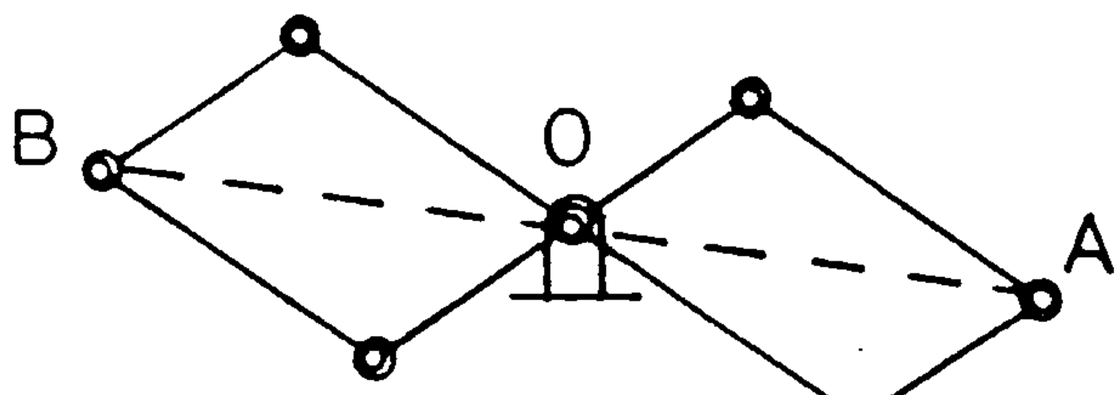

(d)

Image A > Image B

Image inverted

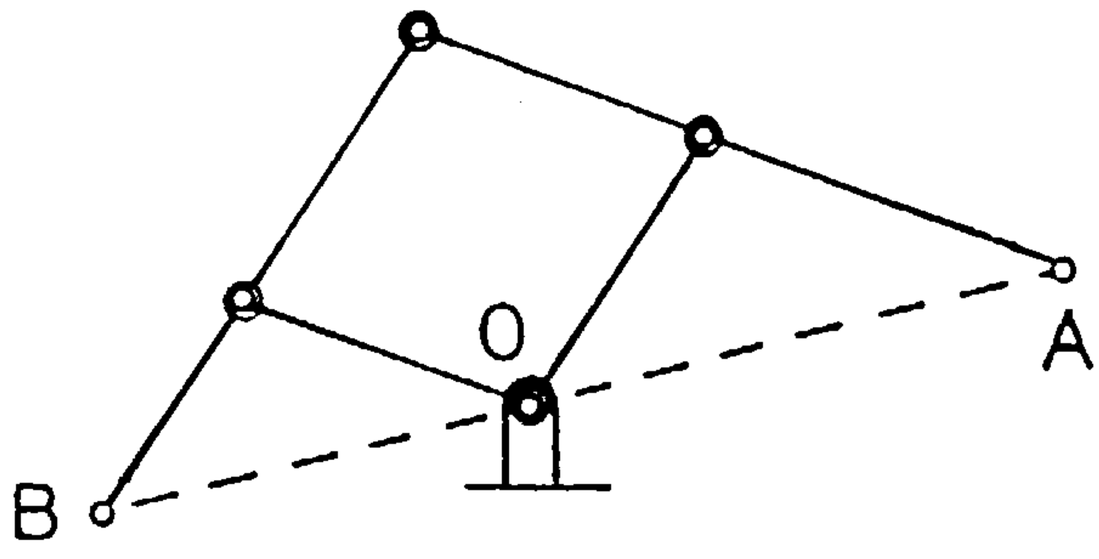

(e)

Image A > Image B

Image inverted

Fig. 3.11 Various pantograph configurations

For simplicity, as the pantograph is to be interposed between the generating mechanism and the grinding wheel, the input and output points, A and B, will most likely need to be either side of the fixed point, O. The inherent inversion this will cause should be irrelevant as the generating mechanism could be set up to input an inverted grinder motion.

Three of the arrangements in Fig.3.11 satisfy this criterion. They are kinematically equivalent and that of Fig. (e) is the simplest with the least number of joints and links.

The choice of pantograph magnification or reduction ratio, if any, is discussed in later chapters. This depends upon its effects on profile accuracy and upon the space available, etc.

Another point considered later, when necessary, is which orientation the pantograph should have. There are two possible configurations with the links above or below the line AOB. They are kinematically equivalent but will behave differently dynamically, and of course they occupy different spaces.

3.5 CONCLUSION

The final idealised kinematic linkage mechanism combines the generating mechanism of Fig.3.6 and the pantograph of Fig.3.11(e) and is shown in Fig.3.12. The alternative position of the pantograph is depicted by broken lines.

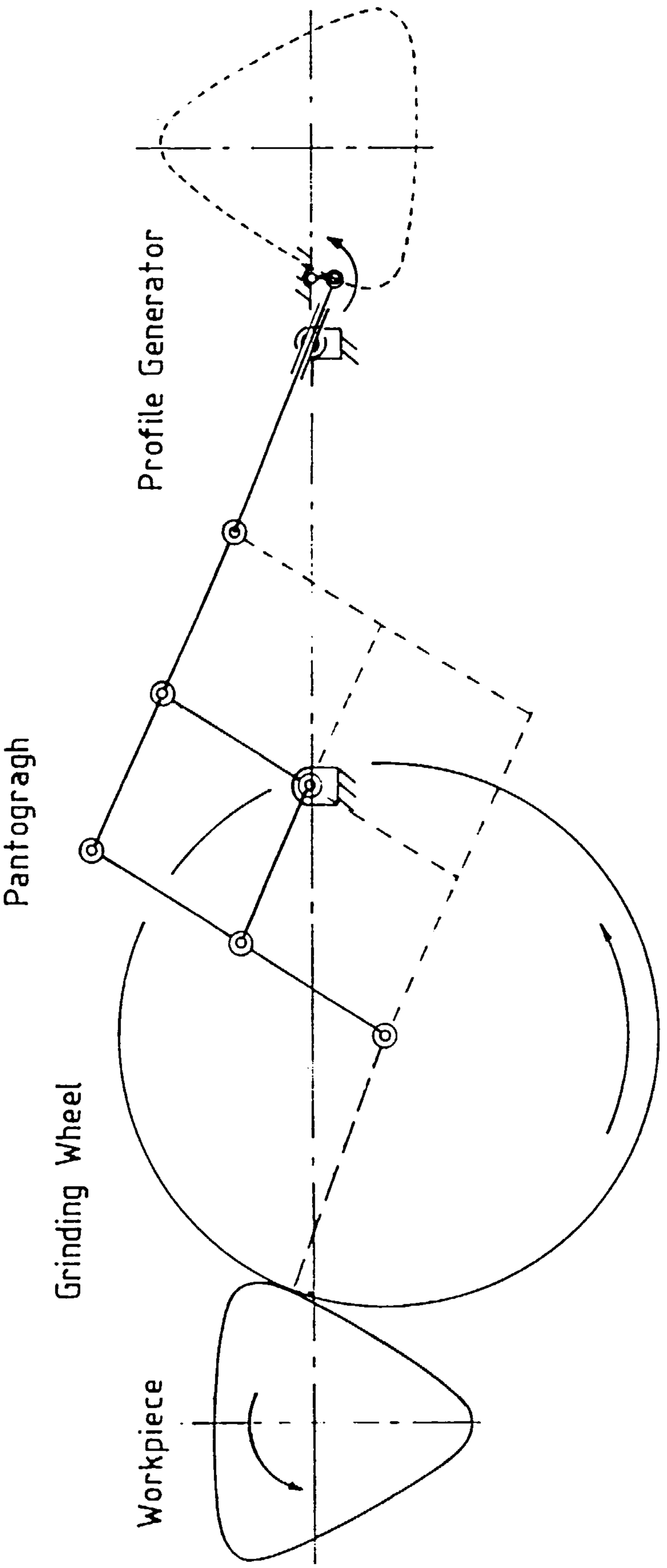

Fig.3.12 Final combined, profile generator and pantograph, idealised linkage mechanism

CHAPTER 4

SPECIFICATION OF PRACTICAL PROFILE MANUFACTURING DEVICE

4.1 INTRODUCTION

In the preceding chapters, the development of an idealised profile generating mechanism, as depicted in Fig.3.12, has been described and in the succeeding chapters its implementation as a practicable device for manufacturing polygonal profileson workpieces will be reported. This is an appropriate point to consider further the manufacturing process and to set down more detailed specifications, criteria,and requirements for the ensuing design analysis. Some important aspects of the design are also summarised.

4.2 MANUFACTURING METHOD AND RELATED MECHANISM SPECIFICATIONS

4.2.1 Form of the Mechanism

In Chapter 1 it has already been stated as an objective that the mechanism had to be implemented in the form of an attachment, to be mounted on a lathe or cylindrical grinding machine (or any other machine that could supply suitable rotation of a workpiece, and accommodation for the device).

To be of any use both external and internal profiles need to be machined on shafts and hubs respectively; the attachment had to be able to achieve this either directly,or indirectly by external machining of an appropriately formed internal cutting tool such as a broach.

4.2.2 Manufacture of External Profiles (Shafts)

Grinding seemed the most suitable choice of cutting method for several reasons. Compared to single point cutting tools or milling cutters,a grinding wheel generates smaller reaction forces between the workpiece and the machine; this will be particularly important in a mechanism which, by its nature, will provide less rigid support for its moving cutting tool than a fixed cutting tool would have. Furthermore grinding would, most likely, be desirable to achieve a satisfactory finish to the profile after rough machining by any other means and therefore might as well be used for the whole process. And generally, grinding is becoming more frequently used for main material removal as well as for finishing operations, [12].

Briefly, the manufacturing procedure would consist of mounting the profile grinding attachment on the tool post or slider of a lathe and feeding the whole attachment in towards the workpiece which would be mounted and rotating in the normal manner. The profiles could be ground onto cylindrical workpieces or preferably onto blanks which had been pre-forged or pre-formed to a rough polygon profile.

4.2.3 Manufacture of Internal Profiles (Hubs)

Kinematically, internal profiles can be generated as easily as external profiles; see Chapter 3. However from a practical point of view it is more problematic. Grinding wheels would be restricted in size, needing to be of considerably smaller radius than the minimum radius of curvature of the profile: this in turn would restrict productivity and increase costs.

A better method would be to broach internal hubs using broaches manufactured by the external profile grinding method as described in the previous section. Broaching costs will increase as batch size decreases therefore for small batch sizes or single jobs internal profile grinding might still be economical. Also for applications where a hardened internal surface is preferred, grinding would be necessary.

It was decided that, if possible, the attachment should have the capability to grind internal profiles, but that this should be of secondary importance to the external profile capability if it became difficult to achieve both in the same design.

4.2.4 Size and Power Specifications

For the workpieces, the range of sizes that the attachment should be able to machine was arbitrarily chosen to be from 10 mm to 100 mm for the mean profile diameters. This is similar to the range covered by German D.I.N. specifications for polygon profiles, [8,9].

Grinding wheel size and motor power were again chosen arbitrarily, after making reference to other types of machine tool attachments, such as 'tool post grinders', [13] and to the commercial availability of grinding spindles and wheels, [14, 15]. Most of the subsequent analysis is based on an 80 mm diameter grinding wheel powered by a

0.5 kW motor. No initial restrictions were made on overall attachment size, but during the design process reference was made to general lathe sizes and dimensions, [16], with the aim of making the attachment easily adaptable to as many as possible. However, particular reference was made to a Colchester 8½ in. Mascot Lathe, [17], which might eventually provide a test bed for a prototype attachment, as it is already available within the institution where the work of this thesis has been carried out.

4.3 SUBDIVISION OF THE DESIGN

The attachment design was split into three main design areas as follows:

(1) the linkage mechanism (sometimes sub-divided into generating mechanism and pantograph mechanism).

(2) the Drive system (mechanism drive and transmission).

(3) the Grinding system (grinding spindle, wheel, motor and transmission.

These are described in detail in Chapter 7, but the main problems are summarised below.

4.3.1 Linkage Mechanism Design

This work covered the detail design of the ideal kinematic chain of Fig. 3.12. Several factors complicated the design, especially when combined. Whereas the kinematic layout is two-dimensional, the real mechanism had to be laid out in three dimensions with the linkages operating in parallel planes interconnected at the joints by shafts normal to these planes, (commonly termed a co-planar mechanism as the links still only move in planes parallel to the ideal kinematic plane of motion). Another particular difficulty arose due to the fact that the bearings required for the joints needed to be much larger than some of the nominal link lengths.

For the operating mechanism several adjustments were required for setting it to machine different sizes of workpiece with various profile eccentricities, and also to compensate for changes in grinding wheel size either due to wear or replacement. These all needed to be accommodated with suitable space for access by an operator.

Further adjustments were initially considered (see Section 4.5 also) to compensate for mechanism assembly errors, in order to achieve suitable profile accuracy, although these were later proved to be unnecessary - see Chapter 6.

4.3.2 Mechanism Drive and Transmission

A suitable means was required to rotate the mechanism in synchronisation with the workpiece rotation but at an integral multiple of the workpiece speed. (3 x workpiece speed for a three-sided profile).

Originally it was intended to provide a gear box connecting the parent machine drive system to the mechanism. This would have required a flexible transmission geometry to cope with movement of the mechanism on the parent machine whilst feeding-in to the workpiece. Severe restraints would have been imposed on the overall mechanism layout and also on the adaptability to fit different host machines since it would have been necessary to have different transmissions for each attachment - lathe combination.

Eventually this idea was superceded by that of using an electrical-stepper-motor, to drive the mechanism, which is electronically synchronised to the parent machine and workpiece rotation but mechanically independent. This provided major advantages of much greater freedom of layout arrangement and of positioning on a host machine, and also of adaptability to different host machines.

4.3.3 Grinding System

The main problem arising in this area was the need for a variable-geometry transmission from a motor, fixed on the attachment frame or baseplate, to a grinding spindle supported in the variable, or moving, output position of the mechanism, thus making the transmission distance continuously variable. This was preferable to an integral spindle plus motor, which because of the increased moving mass, would have considerably increased the dynamic inertia forces and, as a consequence, the elastic deformations of the mechanism, resulting in loss of machining accuracy.

4.4 PROFILE MANUFACTURING ACCURACY SPECIFICATION

As discussed in the main Introduction, Chapter 1, the accuracy to which profiles could be manufactured would be most important in determining the attachment feasibility.

Dimensional accuracies, where 'good' fits are required are normally specified to IT 6/IT7 (using ISO tolerance system according to British Standard 4500) for shafts and IT7/IT8 for hubs. If the hubs are to be broached (see Section 4.2.3) then the dimensional accuracy required of the broaches needs to be 2 or 3 grades better than the required hub tolerance, that is IT4 to IT5.

Form, or geometric accuracies are normally expected to be higher than dimensional accuracies, perhaps to grades IT3 or IT4 for high precision components. For the polygon profiles covered by the German Standards DIN32711/2 [8,9], the dimensional tolerance is specified as IT6 for the mean diameter, and profile form tolerance is specified as IT4 (based on nominal size of mean diameter) for the eccentricity, 'e', where e is half the difference of the maximum and minimum radial size of the profile.

The attachment inaccuracies will affect form rather than dimensional profile accuracy. On a lathe, for instance, the basic size of a work-piece will be governed by in-feed and measurement accuracy much as normal (although the measurement will need to be more elaborate to observe the maximum and/or minimum points on the profile). The particular form error of functional significance affected by the attachment will be the profile shape governed by the eccentricity, e.

Some of the higher tolerance grades mentioned above would be difficult to achieve on a standard lathe (see next Section), even if the profile attachment itself was perfectly accurate; an attachment adapted for use on a grinding machine would be more suitable for such cases.

However, for a starting objective it was decided to aim for a profile accuracy of IT4. For the specified workpiece basic diameter range of 10mm to 100mm diameters (see Section 4.2.3), grade IT4 tolerances range from 4μm (1μm = 0.001mm) to 10 μm respectively. In other words, after discounting the mean size deviation the profile deviation should be within $\pm$ 2μm for a 10mm mean diameter workpiece.

4.5 SOURCES OF PROFILE ERROR

Inaccuracy of the manufactured profiles would be caused by many factors. To simplify the error assessment, these were divided into two groups; those that would normally be associated with the host machine operations, and those that would, in addition, be introduced by the profile generating attachment.

4.5.1 Host Machine Process Errors

The overall effects of this group would normally be known, either for a particular machine tool to be used as a host for the attachment, or from general data for machine tool types and processes, and specified as achievable tolerances.

For the types of machines upon which a profiling attachment might be used, the tolerance grades which are generally accepted as economically obtainable, [18], are IT7 to IT12 for turning operations on a basic lathe (IT6 to IT11 on a turret lathe), IT4 to IT7 for cylindrical grinding, and for broaching of internal profiles, IT5 to IT9.

4.5.2 Profile Generating Attachment Errors

The effects of this second group were unknown and needed to be determined. The various sources of error within the mechanism which needed to be assessed for their affect on profile accuracy were

(1) dimensional errors due to mechanism component manufacture and assembly tolerances,
(2) dimensional errors due to clearances in the mechanism,
(3) setting-up dimensional errors due to inaccurate adjustment (e.g. of eccentricity adjustment),
(4) dimensional errors due to deformation of mechanism components due to operating forces,
and (5) errors due to wear - these would manifest themselves as the other types 1 to 3.

4.5.3 Minimisation, or Compensation, of Mechanism Errors

The setting-up errors would be reduced by designing adjustments with suitable precision, and the deformation errors by increasing the stiffness of components.

However, reducing tolerances and clearances, to achieve the level of accuracy required in a mechanism of the complexity of the profiling attachment, at first sight appeared impossible using random assembly, or even selective assembly, of components which themselves could not be individually practicably manufactured to the required output tolerance specification of the whole mechanism. Initially, it was thought that it would be necessary to use compensating adjustments with which the mechanism's dimensional accuracy could be 'fine-tuned' after assembly.

4.5.4 Profile Accuracy Prediction

In order to assess all the various effects of tolerances, clearances, deflections, setting adjustments and compensating adjustments, a computer aided error analysis was carried out (the theory and development is described in the next Chapter). The techniques adopted were first used to generally establish the sensitivity of the profile accuracy to various mechanism parameters, then to check design decisions as the design developed, and finally to predict the operating accuracy of the final design for a range of operating conditions.

CHAPTER 5

ERROR ANALYSIS THEORY

5.1 INTRODUCTION

Overall profile manufacturing accuracy will depend upon many factors already mentioned in Chapter 4. In this chapter is described the development of an error analysis method to predict the particular effects of mechanism functional parameter deviations upon profile accuracy. Some general error analysis theory is presented and its application by other investigators reviewed; one or two limitations are identified and then the particular procedure employed in this present work is developed.

The adopted methods needed to be able to predict the effects of deviations from several sources which can be categorised as tolerances, clearances, deflections and adjustments: first of all the general characteristics of each deviation category are described.

5.2 CLASSIFICATION OF SOURCES OF ERROR

The deviations can be subdivided into four groups; 1) tolerances, 2) clearances, 3) deflections, 4) adjustments; classified as follows:

1) Tolerances are those parameter deviations which are due to the inaccuracies of mechanism component manufacture and assembly. They are probabilistic in nature since only the statistical distribution of possible deviation values can be predicted, via the tolerance specification. The actual errors that occur on components and thus the allocation to particular parameter deviations, will be constant, and unaffected by kinematic position or dynamic forces.

2) Clearances cause parameter deviations resulting from play, or backlash, between components at kinematic joints after assembly. They are also probabilistic in nature, being predicted either by a statistical clearance specification, (as for bearings) or by derivation from individual tolerance specifications of mating components. For particular joints the magnitude of clearance will normally be constant, but the direction of take-up will be variable and dependent upon mechanism position and dynamic loads, and thus allocation to parameter deviations should vary with kinematic position.

3) Deflections are those parameter deviations which are due to forces acting in the mechanism components, and are deterministic in nature, being derived from load-deflection formulae. Both the magnitudes and directions of deflections will vary depending on mechanism position and the dynamic loads. Thus allocation to specific parameter deviation will, in general, vary with mechanism position.

4) Adjustments are those constant parameter deviations that are specifically chosen to compensate for the effects upon profile accuracy of deviations, of any of the previous three types, to other parameters. They will be probabilistic in nature (although the desired compensating deviation may be deterministic, its achievement will be probabilistic due to the tolerance of its setting resolution). By definition they are allocated to specific parameter deviations.

5.3 GENERAL ERROR ANALYSIS THEORY

The required output position of a planar linkage mechanism can be defined by a single coordinate or by two coordinates, depending on whether the output angle of a link or the path described by a point on the link is required. The ensuing analysis is developed for a single output coordinate but is equally applicable to two output coordinates.

In general, the output of a mechanism as measured by coordinate, F, can be expressed as a function of n mechanism dimensional parameters, $q_{i=1,n}$, representing link lengths, and a mechanism input or position parameter, θ, giving

$$F = F\ (q_1, \ \ldots\ q_i\ \ldots\ q_n, \ \theta) \qquad (5.1)$$

For a small deviation, δq_i, of the parameter, q_i, where $\delta q_i \ll q_i$, the output deviation δF_i may be expressed by

$$\delta F_i = \frac{\partial F}{\partial q_i} \ . \ \delta q_i \qquad (5.2)$$

where $(\partial F/\partial q_i)$ is the first order partial derivative of the output with respect to the ith parameter calculated at its nominal value, q_i: it is commonly known as the 'sensitivity' of the output to a small deviation in that parameter.

For deviations which are deterministic, such as deflections, the total output deviation, F, due to all parameter deviations is given by

$$\delta F = \sum_{i=1}^{n} \delta F_i = \sum_{i=1}^{n} \frac{\partial F}{\partial q_i} \cdot \delta q_i \qquad (5.3)$$

For deviations which are probabilistic, such as tolerances and clearances, and are assumed to be random in nature, following a normal distribution whose mean value is the nominal value, the output deviation may be expressed probabilistically as

$$\delta F = \left(\sum_{i=1}^{n} \left(\frac{\partial F}{\partial q_i} \cdot \delta q_i\right)^2\right)^{\frac{1}{2}} = \left(\sum_{i=1}^{n} \delta F_i^{\,2}\right)^{\frac{1}{2}} \qquad (5.4)$$

Since the output distribution will also be normal, the output deviations can be assumed to fall within a tolerance, T, with the same probability as do parameter deviations within parameter tolerances, t_i, and the total output tolerance, T, may be expressed by

$$T = \left(\sum_{i=1}^{n} \left(\frac{\partial F}{\partial q_i} \cdot t_i\right)^2\right)^{\frac{1}{2}} = \left(\sum_{i=1}^{n} T_i^{\,2}\right)^{\frac{1}{2}} \qquad (5.5)$$

where T_i is the output tolerance separately associated with each of the individual parameter tolerances, t_i. Alternatively, T and t_i, may be replaced by σ_F and σ_i, the standard deviation of the output, F, and parameters q_i respectively.

For a normal distribution, 99.73% of values occur within $\pm 3\sigma$ of the mean values, which are also the nominal values, F and q_i in this case, and tolerances, are normally specified as $6\sigma < t < 8\sigma$. The partial derivatives in eqns.(5.2),(5.3),(5.4)and(5.5)may be derived analytically, or for complex mechanisms computed numerically using difference methods as given by

$$\frac{\partial F}{\partial q_i} = \frac{F(q_1, q_2, \ldots, q_i + h, \ldots, q_n, \theta) - F(q_1, q_i, .., q_i - h, .., q_n, \theta)}{2h} \qquad (5.6)$$

where $h \ll q_i$.

5.4 REVIEW OF ERROR ANALYSIS APPLICATIONS BY OTHER INVESTIGATORS

Relatively few investigations of mechanism 'mechanical error' have been conducted; more have considered the 'structural errors' occurring in mechanisms synthesised by approximate methods.

To produce the desired output in this case, the mechanism sysnthesis is exact (see Chapters 2 and 3) and the structural error is zero and not considered. For much of the work selectively reviewed here, the theory of section 5.3 forms a basis.

Various methods of applying eqns.(5.1) to(5.5)have been used to predict the effects of linkage tolerances and clearances, as extensively reviewed by Sharfi and Smith [19]. The simplest methods estimate the maximum possible output error by simple addition, according to eqn.(5.3), of the deviations due to individual maximum possible, parameter deviations within individual tolerances [21]. More realistic methods [19,20,22,23] considered the probabilistic nature of tolerances and clearances and used statistical summation according to eqns.(5.4) or (5.5).

Optimisation techniques have been reported, utilising eqn.(5.4) to minimise the output error by appropriate allocation of tolerances and clearances to parameters. [19, 22, 23]. In particular, Sharfi and Smith [19] developed a procedure to allocate tolerances and clearances, irrespective of manufacturing costs, such that each parameter contributes equally to total output deviation, i.e. all $\delta F_1 = \delta F_2 =, \ldots, = \delta F_n$ etc. In this way those parameters that least affect output error, (smallest $\partial F/\partial q_i$, s) can be allocated the largest tolerances and conversely the most sensitive parameters, the tightest tolerances.

Since sensitivities vary with mechanism position, the maximum sensitivities to each parameter are used. Sharfi [20] reviewed optimisation methods which take account of the manufacturing costs, which vary with specified tolerances, and introduced simple tolerance-cost relationships into the aforementioned optimisation procedure for allocating tolerances and clearances.

5.5 INITIAL APPLICATION OF BASIC ERROR THEORY TO PROFILE GENERATING MECHANISM AND ITS LIMITATIONS

The application of the preceding optimisation techniques is of limited use in prototype mechanism design, as in this present work: the design can change drastically as it proceeds, and manufacturing cost data, if known, would be difficult to formulate into sufficiently simple relationships. Each functional parameter tolerance may, for example, be a compilation of several tolerances on the components composing that parameter. These techniques seem more appropriately applied to the optimisation and further development of established designs for which manufacturing costs may be more readily available.

A more suitable procedure for prototype design work, is to investigate the effects of individual parameters upon output accuracy and make design decisions based on experience or design intuition, and to compute total output deviations as a final check for satisfactory accuracy or necessity for re-design as required. This is especially true if the effects of compensating adjustments on profile error due to individual parameter deviations are required to be assessed as in this present work.

For these reasons an analysis was originally formulated to calculate sensitivities $\partial F/\partial q_i$ for each parameter using eqn.(5.6), which could then be taken into account during the detail design process. Using trial and error methods the effects upon sensitivities of varying parameters, such as increasing pantograph dimensions, could be observed. Also the effectiveness of any adjustments could be assessed. However this procedure was discarded for several reasons. First of all the nominal dimensions of the mechanism were eventually determined by space constraints, not by the assessment of the effects of dimensons on sensitivities, which thus became redundant and which in any case were intuitively obvious (e.g. increasing pantograph size will reduce output error).

More seriously, the procedure was limited by the basic assumptions underlying the theory of Section 5.3, namely that the parameter deviations are much smaller than the nominal parameter dimensions ($\delta q_i << q_i$) and also that the output deviation is determined solely by the first order derivatives, $\partial F/\partial q_i$. For the present application both these assumptions are, at times, invalid:

(i) For some parameters, at particular mechanism settings, deviations may be considered which are of the same order of magnitude as some nominal dimensions, i.e. $\partial q_i > 0.1\ q_k$ where $1 \leq k \leq n$.

(ii) For certain parameters, $\partial F/\partial q_i = 0$ for all positions of the mechanism, in which case the sensitivity is taken as zero. This implies, using eqn.(5.2) and the method of Sharfi and Smith, that infinite deviation of that parameter is allowable. In reality, the sensitivity is not zero, but very small and to establish practical limits to deviations, this very small sensitivity must be determined.

5.6 FURTHER DEVELOPMENT OF ERROR ANALYSIS THEORY.

The limitations of the basic assumptions, (i) and (ii) in Section 5.5 can be accounted for by reformulating the general theory of Section 5.3, with the inclusion of higher order derivatives.

A more accurate expression for the output deviation is given by reformulating eqn.(5.3) using both the first and second order terms of a Taylor series, giving

$$\delta F = \sum_{i=1}^{n} \frac{\partial F}{\partial q_i} . \delta q_i + \frac{1}{2} \sum_{i=1}^{n} \sum_{j=1}^{n} \frac{\partial^2 F}{\partial q_i \partial q_j} \cdot \delta q_i \cdot \delta q_j \qquad (5.7)$$

In the case where the more accurately defined 'first order sensitivity', $\partial F/\partial q_i = 0$, the output deviation δF_i due to that individual parameter q_i, will be given by

$$\delta F_i = \frac{1}{2} \frac{\partial^2 F}{\partial q_i^2} \cdot \delta q_i^2 \qquad (5.8)$$

and the 'second order sensitivity' can be defined by $(\frac{1}{2} \frac{\partial^2 F}{\partial q_i^2} . \delta q_i)$, which is not constant, but depends on the deviation.

Sharfi [20] recognised the problems induced by the second limitation, (ii) in Section 5.5, without acknowledging the effects of higher order derivatives. Instead he replaced the 'central difference' computation of $\partial F/\partial q_i$ by eqn.(5.6), by averaging the moduli of forward- and backward-

differences to give

$$\frac{\partial F^*}{\partial q_i} = \Big(\Big|F(q_1, \ldots, q_i+h, \ldots, q_n, \Theta) - F(q_1, \ldots, q_i, \ldots, q_n, \Theta)\Big| + \Big|F(q_1, \ldots, q_i, \ldots, q_n, \Theta) - F(q_1, \ldots, q_i-h, \ldots, q_n, \Theta)\Big|\Big)/2h$$

and by always choosing, through iterations, $h \approx \delta q_i$.

In effect the $\partial F^*/\partial q$ was made dependent upon δ_i, and although perhaps satisfactory for the particular procedure in which it was used, may not be generally so. For instance, it is doubtful if it can be correctly applied in statistical summations according to eqn.(5.4), which assumes the $\partial F/\partial q_i$'s are independent of the deviations.

The inclusion of second order terms considerably complicates the analysis of probabilistic deviations. The determination of output tolerances, T_i, due to individual parameter tolerances, t_i considering only first order terms can be re-stated in more detail than before,(see Section 5.3).

For a normal distribution the tolerances, t_i, are assumed to be centred about the nominal dimension and the maximum deviations are now specified as $\delta q_i^+ = + t_i/2$ and $\delta q_i^- = -t_i/2$ and the output deviations as ${}_1\delta F_i^{\mp} = \frac{\partial F}{\partial q_i} .(+t_i/2)$ and ${}_1\delta F_i^- = \frac{\partial F}{\partial q_i} .(-t_i/2)$.

Therefore ${}_1\delta F_i^+ = -{}_1\delta F_i^-$ and the output tolerance $T_i = \pm \delta F_i$ also centred about the nominal output and $T = (\Sigma T_i^2)^{\frac{1}{2}}$ as before in eqn.(5.5).

Similarly for output deviations due to solely second order terms

$$ {}_2\delta F_i^+ = \frac{1}{2}\frac{\partial^2 F}{\partial q_i^2} \cdot (+t_i/2)^2, \quad {}_2\delta F_i^- = \frac{1}{2}\frac{\partial^2 F}{\partial q_i^2} (-t_i/2)^2 \qquad (5.9)$$

Therefore ${}_2\delta F_i^+ = {}_2\delta F_i^-$, and in this case the output deviations are now distributed completely to one side or the other of the nominal output. This is no longer a normal distribution and in fact the distribution appears to be exponential. The limits within which certain probabilities of deviation will occur can still be determined from eqns.(5.9). If it is assumed that 99.73% of parameter deviations occur within $\pm t_i/2$ (i.e. $\pm 3\sigma$), then 99.73% of second-order-derived output deviations will occur between zero (the nominal value) and ${}_2\delta F_i$ or zero and $-{}_2\delta F_i$. A tolerance zone, T_i, within which 99.73%

of deviations occur can still be specified, with a fundamental deviation from the nominal of $T_i/2$, however this is not the mean of this distribution and more deviation will occur on the nominal dimension side of the fundamental deviation. The total statistical variation can no longer be calculated by eqn.(5.5) especially if first and second order deviations are to be superimposed. Inclusion of second order mixed derivatives, $\partial^2 F/\partial q_i \partial q_j$, would further complicate matters.

Sufficient insight had been acquired for this present work, and these arguments were pursued no further although they may be a suitable topic for future study. Some of the problems raised in this and the previous section can simply be avoided by ignoring the partial derivatives and directly computing output deviations due to parameter deviations using

$$\delta F_i = (F(q_1,\ldots,q_i + \delta q_i,\ldots q_n,\theta) - F(q_1,\ldots,q_i,\ldots q_n,\theta) \qquad (5.10)$$

The foregoing theory still provides valuable insight when eqn.(5.10) is applied to the individual parameters and decisions on allocating allowable deviations have to be made

5.7 ERROR ANALYSIS OF PATH GENERATING MECHANISM (TWO-COORDINATE OUTPUT)

The foregoing error analysis, described in this Chapter, has all been developed for a 'single-function generating' mechanism, that is one for which the output can be defined by a single coordinate, F in eqn(5.1). For a 'path-generating' mechanism, such as the polygonal profile generating mechanism, the output for a planar mechanism must be defined by two coordinates; say (R_o,θ_o) if a polar coordinate system is adopted.

Consequently, any deviation of the output can be defined by deviations $(\delta R_o, \delta\theta_o)$ of (R_o,θ_o), and which can each be applied in similar expressions to eqns.(5.1) to(5.10). Thus the output deviations resulting from a deviation of a single parameter, q_i are

$$\delta R_{oi} = R_o(q_1,..,q_i + \delta q_i,.....,q_n,\theta) - \bar{R}_o(q_1,\ldots,q_i,..,q_n,\theta) \qquad (5.11)$$

and $$\delta\theta_{oi} = \theta_o(q_1,..,q_i + \delta q_i,.....,q_n,\theta) - \bar{\theta}_o(q_1,\ldots,q_i,..,q_n,\theta) \qquad (5.12)$$

(the $\bar{(\ )}$'s over coordinates indicate nominal or desired outputs) and the total

output deviations from all parameter deviations are:

$$\delta R_o = R_o(q_1 + \delta q_1,\ldots,q_i + \delta q_i,..,q_n + \delta q_n,\theta) - R_o(q_1,\ldots,q_i,..,q_n,\theta) \quad (5.13)$$

$$\text{and} \quad \delta\theta_o = \theta_o(q_1 + \delta q_1,\ldots,q_i + \delta q_i,..,q_n + \delta q_n,\theta) - \theta_o(q_1,\ldots,q_i,..,q_n,\theta) \quad (5.14$$

$$\text{or} \quad \delta R_o = \sum_{i=1}^{n} \delta R_{oi} \quad , \quad (5.15$$

$$\text{and} \quad \delta\theta_o = \sum_{i=1}^{n} \delta\theta_{oi}, \quad (5.16)$$

if 2nd order mixed derivatives can be ignored, see Section 5.6.

The output deviations determined by eqns.(5.11) to(5.16) could be plotted against input position coordinate, θ, to give two 'profile characteristics', δR_{oi} (or δR_o) vs. θ and $\delta\theta_{oi}$ (or $\delta\theta_o$) vs. θ. These could then be used to compare parameter deviations of various types; for example, to assess the effectiveness of any adjustment deviation to compensate for a tolerance, clearance, or deflection, deviation.

However there are two distinct disadvantages to using the error analysis as it stands:

(i) it is conceptually difficult to assess and compare parameter deviations when the profile sensitivity is expressed by two characteristics, for δR_o and $\delta\theta_o$,

(ii) perhaps more important, δR_o and $\delta\theta_o$ are the true mathematical deviations and do <u>not discriminate real, effective deviations from absolute deviations</u>.

This last situation is illustrated in Fig. 5.1 where the absolute error δR_o, $\delta\theta_o$, happens to lie further along the desired path, from its nominal position $\bar{R}_o$, $\bar{\theta}_o$. Although this may be a significant absolute or mathematical deviation, it may in many cases be inconsequential and thus the effective error is zero.

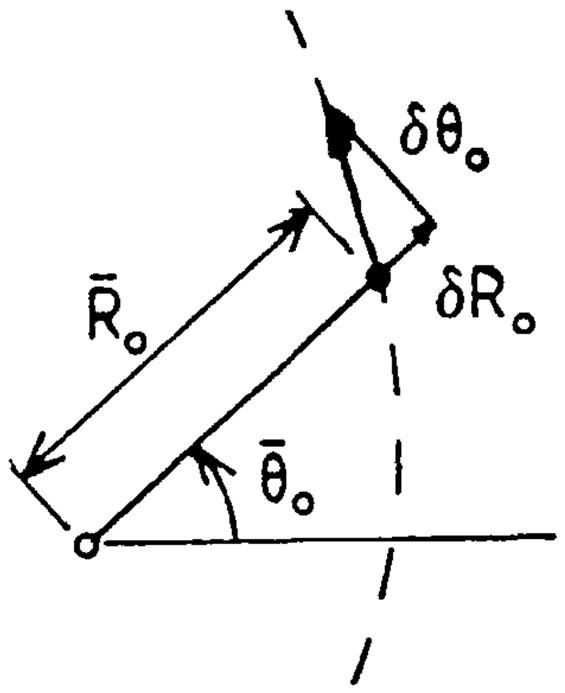

Deviated output point ($R_o + \delta R_o$, $\theta_o + \delta\theta_o$) is on desired path. Thus real error is zero.

Fig.5.1 Comparison of absolute and effective errors.

These disadvantages have led to an important modification that reduces the output deviation to description by a single 'effective' output coordinate, described in the next section.

5.8 PATH DEVIATIONS DESCRIBED BY A SINGLE OUTPUT COORDINATE

The development of the single-output-deviation modification is best explained by reference to Fig.5.2.

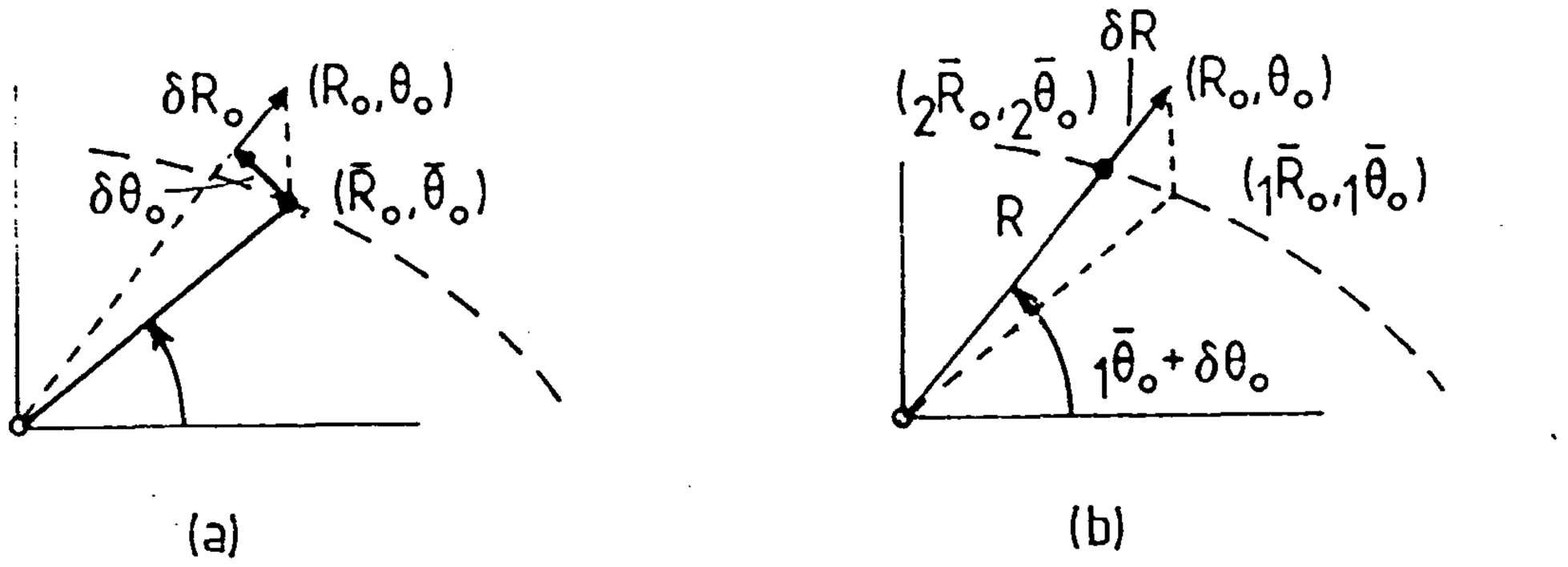

Fig. 5.2 Reduction of (a)'two-output', to (b)'one-output' coordinate.

In Fig.5.2(a) the deviation is expressed conventionally by δR_o and $\delta\theta_o$. These could be reduced to a single deviation by taking the resultant $(\delta R_o^2 + \bar{R}_o^2.\delta\theta_o^2)^{\frac{1}{2}}$, however, in doing so, all directional information is lost and also effective and absolute deviations could not be discriminated from each other.

Now consider Fig.5.2(b) where the same deviation is expressed by δR, on a radial coordinate R, noting that δR and R do not necessarily equal the

original (indicated by suffix, 1) $_1\delta R_o$ and $_1R_o$ respectively, but R is equal to $_2\bar{R}_o$ calculated at $\theta_o = (_1\bar{\theta}_o + _1\delta\theta_o)$. In other words R is the nominal radial coordinate, $_2\bar{R}_o$, at nominal $_2\bar{\theta}_o = (_1\bar{\theta}_o + _1\delta\theta_o)$, and the actual deviation relative to point $(_2\bar{R}_o, _2\bar{\theta}_o)$ is expressed by a radial deviation

$$\delta R = R_o - _2\bar{R}_o = (_1\bar{R}_o + _1\delta R_o) - _2\bar{R}_o \qquad (5.17)$$

and an angular deviation

$$\delta\theta^* = (_1\bar{\theta}_o + _1\delta\theta_o) - _2\bar{\theta}_o = 0 \text{ by definition.} \qquad (5.18)$$

In this way $\delta\theta^*$ can always be reduced to zero and a single effective output error δR be determined.

This δR can now be plotted against the input position coordinate $_2\theta$ that would produce the nominal point $(_2\bar{R}_o, _2\bar{\theta}_o)$, and which can be computed iteratively. The calculation of δR and $_2\theta$ can be summarised as follows.

Step (i) Calculate $_1\bar{R}_o$, $_1\bar{\theta}_o$, δR_o and $\delta\theta_o$ at nominal input $_1\bar{\theta}$

(ii) Put $_2\bar{\theta} = _1\bar{\theta} - k\,\delta\theta_o$, (where k is an appropriate convergence factor approximating the relationship $\theta_o = \theta_o(\theta)$) and calculate $_2\bar{R}_o$, $_2\bar{\theta}_o$,

(iii) Recalculate $\delta\theta_o = (_1\bar{\theta}_o + _1\delta\theta_o) - _2\bar{\theta}_o$,

(iv) Repeat (ii) and (iii) until $\delta\theta_o \sim 0$ then,

(v) Calculate $\delta R = _1\bar{R}_o + _1\delta R_o - _2\bar{R}_o$,

(vi) Plot δR vs. $_2\bar{\theta} \equiv \underline{\delta R \text{ vs. } \theta}$

As well as overcoming the disadvantages expressed in section 5.7, there is a further advantage as far as the polygon profiles are concerned, which is that the single effective radial deviation is also the most direct measurement of deviation that can be made on a polygonal workpiece!

The plots of δR against input, θ, can now provide a single 'profile-deviation sensitivity - characteristic' for each individual or combination of parameter deviations, which can easily be used for assessment of tolerances, clearances, deflections and adjustments.

This single output approach could be applicable generally for many output path error analyses. However it should be noted that actual deviations, not 1st order partial-derivative-sensitivities, should be used, since generally δR is not directly proportional to $\partial R_o/\partial q_i$.

5.9 SPECIFICATION OF MECHANISM PARAMETERS

Determination of the basic mechanism input-output relationship expressed in general form by eqns.(5.1), requires the specification of the mechanism by suitable parameters. For a mechanism such as the profile generator, whose nominal configuration is shown in Fig. 3.12, the most obvious allocation is to identify each link by a single parameter, q_i, equal to its length. In practice more parameters are generally used, either through necessity or for convenience, in carrying out the subsequent kinematic analysis.

For a simple 'binary' link with only two joints, one parameter, $q_i (\equiv \text{length } r_i)$, is sufficient, as shown in Fig. 5.3(a).

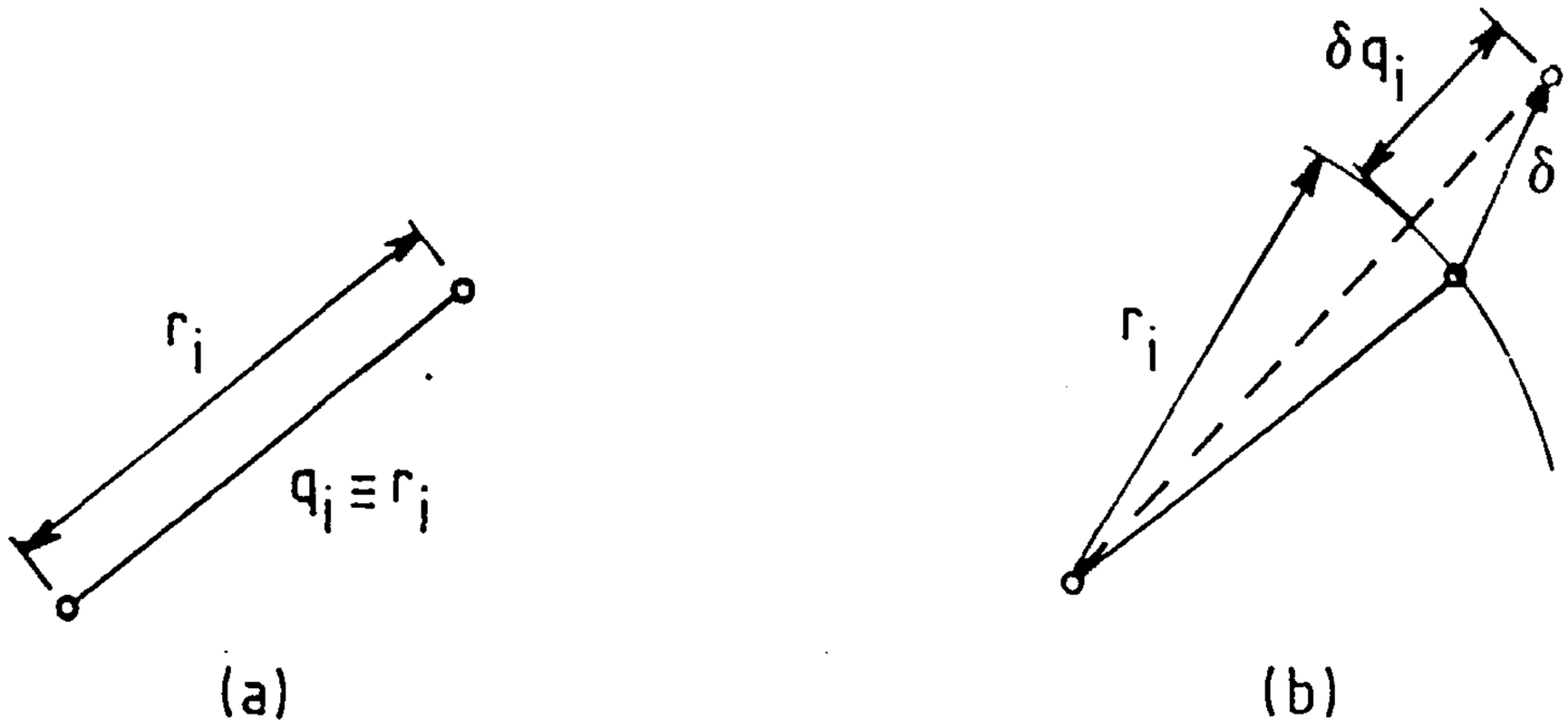

5.3 Parameter specification of binary links.

Any deviation of this link as shown in Fig. 5.3(b) can be described by a deviation δq_i of q_i, even if the actual deviation is not in-line with the original link centre-line since it is the distance between the joints which is the functional dimension.

However, now consider a 'ternary' link which contains three joints which initially are considered co-linear, as depicted by Fig. 5.4(a).

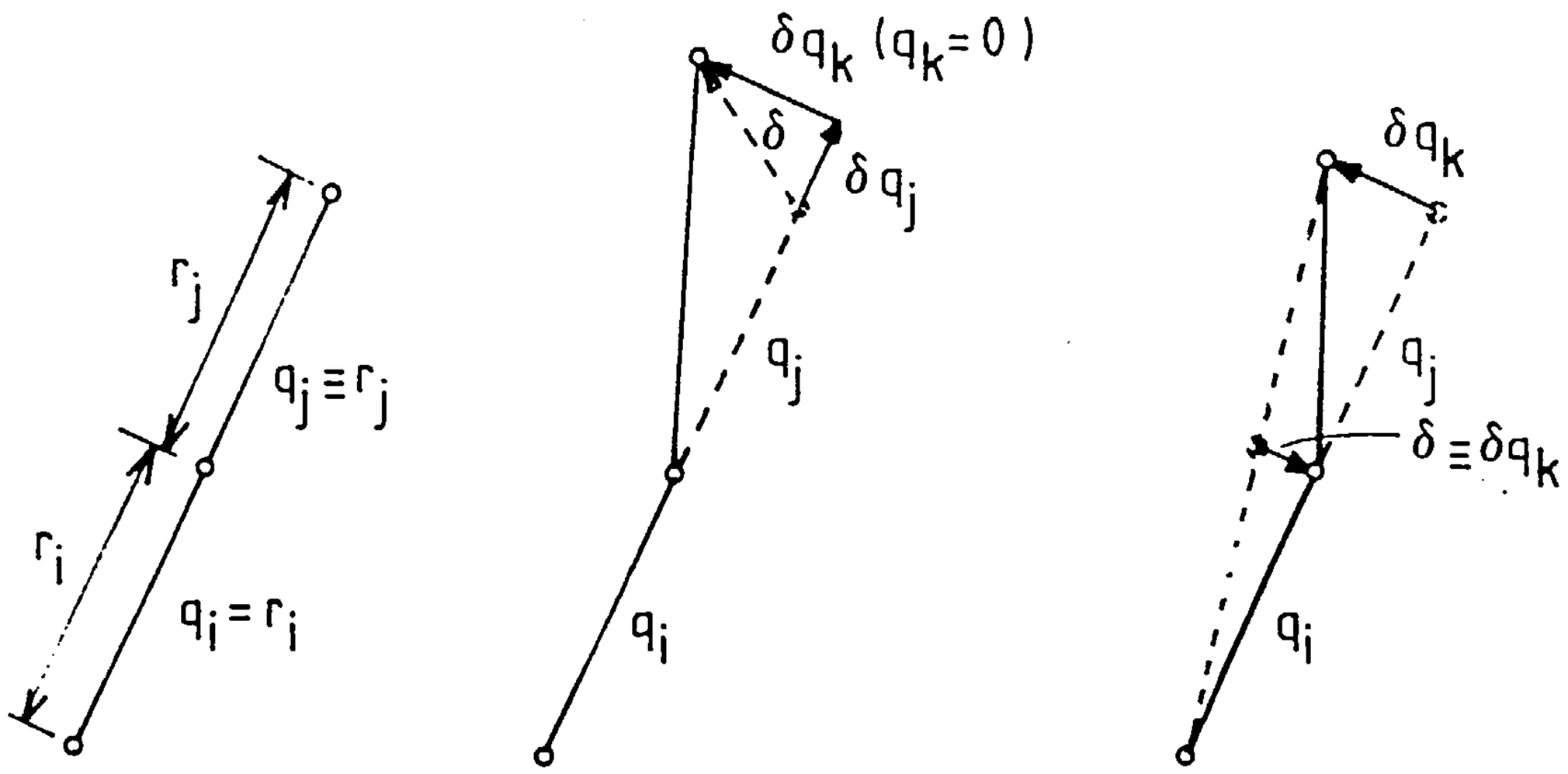

(a) (b) (c)

Fig.5.4 Parameter specification of ternary links.

For convenience two 'axial' parameters q_i, q_j may be used which denote the distances between the joints r_i, r_j. If in addition a deviation is considered which has a component normal to the link centre-line, as in Fig. 5.4(b), then a third 'lateral' parameter q_k can be introduced whose nominal value, $\bar{q}_k = 0$, and the actual deviation, δ, can be resolved into components, δq_j and δq_k. For general ternary links $\bar{q}_k$ may not be zero if the joints are not co-linear: however all the profile generating mechanism links are nominally co-linear. These three parameters are sufficient to describe other link deviations in addition to that shown in Fig. 5.4(b).

In Fig.5.4(c) is shown a deviation δ to the centre joint which has an identical effect to that of an equivalent deviation, δq_k, as before, where in this case $\delta q_k = \delta . (q_i + q_j)/q_i$.

To summarise: all actual deviations of links can be resolved into components orthogonal to the nominal link axes, by specifying axial and lateral parameters for each link. The allocation of the types of mechanism deviations, due to tolerances, clearances, deflections and adjustments, to parameter deviation depends on their nature and the particular assessment procedure for each type.

5.10 TOLERANCE ASSESSMENT PROCEDURE

5.10.1 Individual Tolerance Assessment

The effects of individual parameter tolerances can be assessed by setting the parameter deviation equal to the extreme value of the tolerance

zone, and determining the output deviation characteristic according to Section 5.8. This can then be used to determine the maximum parameter tolerance, which may be allowed without exceeding a specified output deviation limit, either directly or after using a compensating adjustment. The choice of, and effectiveness of, a possible compensating adjustment is determined by comparing its characteristic with that of the parameter to be compensated for and then superposing the characteristics in such a way as to cancel each other out; that is by trying to arrange

$$\delta R_i = R(q_1,.,q_i+\delta q_i,q_j-\delta q_j,..,q_n,\Theta)-\bar{R}(q_1,..,q_i,q_j,..,q_n,\Theta)\simeq 0 \qquad (5.19)$$

where δq_i is the parameter extreme tolerance, and δq_j may be the compensating adjustment. It is assumed that any degree of compensation that can be achieved for the maximum possible parameter deviation could also be achieved for any lesser deviation of that particular parameter which may occur.

5.10.2 Total Tolerance Assessment

The assessment of a total output tolerance may be estimated by summation of the remaining output deviations, δR_i in eqn.(5.19), after individual tolerance assessment by the preceding methods of Section 5.10.1, but bearing in mind the restrictions on combining tolerances expressed in Section 5.6. Although statistical summation, $(\Sigma\ \delta R_i^2)^{\frac{1}{2}}$, may be inaccurate since not all output deviations will be normally distributed, this should still be acceptable as it gives a conservative estimate.

Note that a total output tolerance cannot be determined from individual tolerances and then compared with compensating adjustments: although a total output deviation characteristic could be obtained by addition of individual worst-case deviations this would be of no practical use since, unlike individual characteristics, the total characteristic is probabilistic and indeterminate for lesser deviations and any compensation could not be assumed to apply to all possible combinations of deviations.

The only exception would be if several parameters all produced similar output error characteristics, identical in form, but not necessarily in magnitude; in which case their combined output characteristics would also

be of the same form and therefore determinate, and its magnitude could be estimated, by statistical summation, prior to comparison with compensating adjustments.

5.10.3 Tolerances in Profile Generating Mechanism

In practice the tolerances in the profile generating mechanism could be divided into two groups for assessment: those on parameters with first order sensitivities (see Section 5.6) could all be effectively cancelled by compensating adjustments,while those on parameters with second order sensitivities could be allowed large tolerances since they had very small effects on the output which, in some cases, could be further reduced by adjustments.

5.11 CLEARANCE ASSESSMENT PROCEDURE

5.11.1 General Problem

The analysis of clearance effects is potentially the most complex. They are similar to tolerances in their probabilistic nature and the procedures set out for tolerances can be applied to clearances, once the allocation of the clearances to particular parameter deviations is determined. However, it is this last condition which creates the extra difficulties. Unlike for tolerances, the deviations in parameters due to clearances may change throughout the mechanism motion. As the mechanism configuration and the forces on it change, the effective dimensions of links, connected by joints with clearance, will also change. This is illustrated in Figs. 5.5(a),(b), which show the same joint clearance between two links, but taken up in different directions and so changing the effective link lengths.

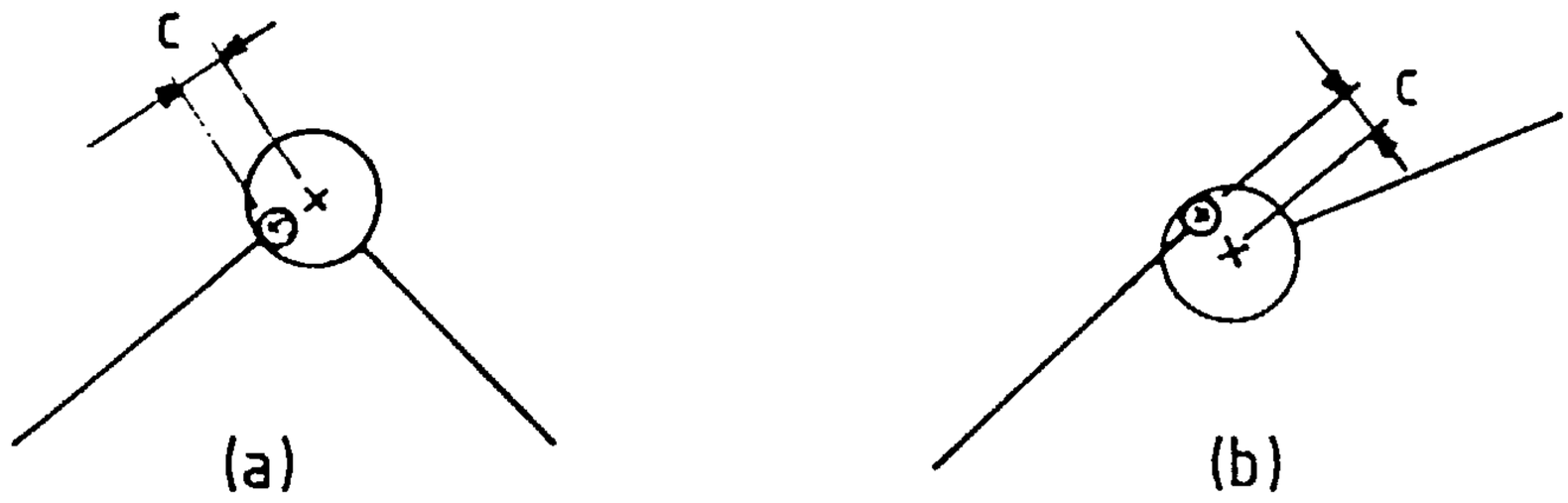

Fig.5.5 Variation of clearance take-up directions.

5.11.2 Parameter Allocation

At any instant, if the direction of take-up is known, the clearance could be allocated to parameter deviations on either or both links by resolving into orthogonal, lateral and axial, components as proposed in Section 5.9. Two possibilities are shown in Fig. 5.6 where the clearance 'c' is allocated totally to one of either of the links shown.

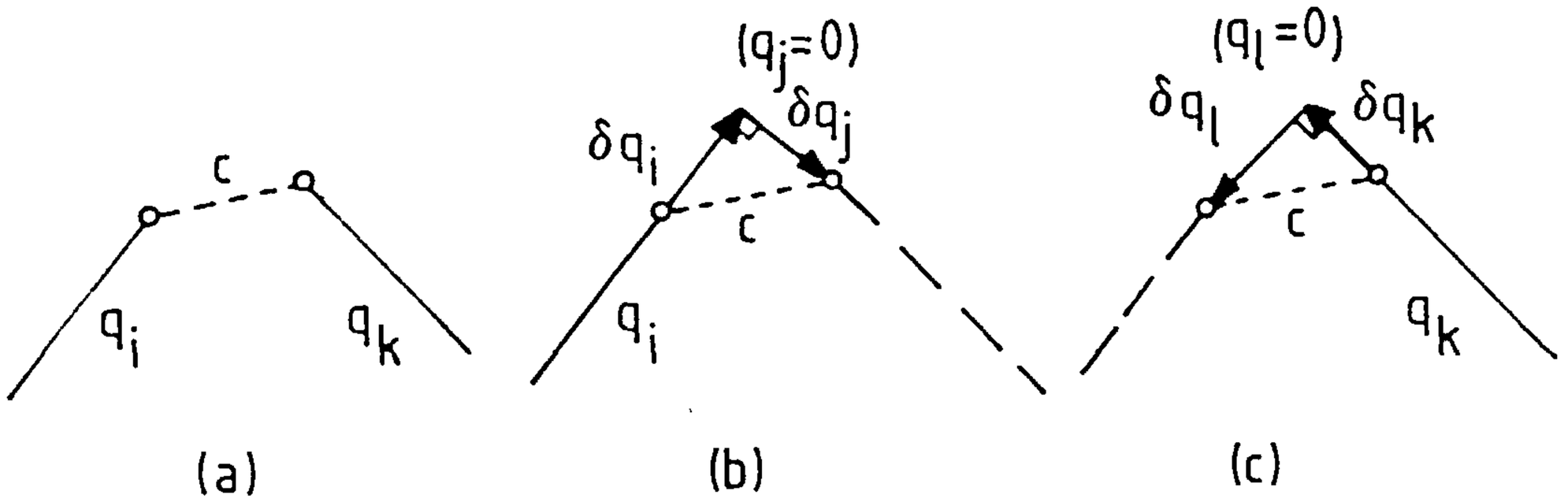

Fig. 5.6 Equivalent allocations of clearances to parameters.

There is one other alternative, which is to specify the clearance as an extra 'imaginary' or 'effective' link (c, in Fig. 5.6(a)) between the actual links. However, this might increase the complexity of the mechanism kinematic analysis, and is not used for the profile mechanism.

5.11.3 Dynamic Considerations

The greatest difficulties arise when trying to determine the direction of take-up, which is governed by the dynamic behaviour of the mechanism. Investigations of the behaviour of clearances have been reviewed by Haines [24], and can be very complex, especially when vibrations are present, or directions of loads (load vector), applied across a clearance, change rapidly so that contact between links is sometimes lost, with subsequent further impact and vibration when it is regained.

Even if the load vector changes sufficiently slowly for contact to be maintained, it may still change faster than the joint can respond so that the clearance take-up direction lags behind the load direction. Thus it cannot necessarily be assumed that clearance take-up is always aligned with the load vector.

5.11.4 Three-dimensional Effects

The preceding arguments all apply to a two-dimensional planar mechanism: in practice forces and moments acting out-of-plane may cause relative rotations, or tilting, of links with clearances, thus further complicating any assessment.

5.11.5 Clearances in Profile Generating Mechanism

Fortunately, the analysis of clearances in the profile generating mechanism could be greatly simplified, for several reasons:

(i) the operating speed of the mechanism is, relatively, very slow compared to natural vibration periods of the mechanism; and clearance take-ups were assumed to be in line with loads;

(ii) in many joints the load directions change very little;

and (iii) most joints were preloaded to avoid clearances.

5.12 DEFLECTION ASSESSMENT PROCEDURE

5.12.1 Basic Procedure

Because deflections are, theoretically, completely deterministic, the resulting output deviation is also determinate, either for individual or any combination of parameter deviations, and can be compared with any adjustment characteristic. Therefore, once deflections are determined the analysis is straightforward. Any complexities arise from the determination of the deflections and their allocation to parameters.

5.12.2 Parameter Allocation

The obvious way to allocate deflections is to resolve them into lateral and axial components and allocate them to the parameters defining the links on which they occur. However, they could alternatively be allocated to other link parameters in the same way that clearances could be allocated to either link shown in Fig. 5.6.

5.12.3 Dynamic Considerations

Provided that the mechanism operates at sufficiently low speeds, so that resonances in links are not excited and can be ignored, then the instantaneous deflections can be calculated as static deflections due to loads determined by a rigid-body dynamic analysis.

5.12.4 Deflection Calculations

The greatest difficulty in analysing the effects of mechanism deflections, arises from the calculation of the deflections themselves; mainly because actual mechanisms are co-planar and out-of-plane forces, moments and deflections,must be considered.

The out-of-plane forces and couples can be estimated from the two-dimensional forces determined for a basic planar mechanism.

However, many different load-deflection relationships must be employed, to take account of, for instance, bending, shear, and torsion of links, and contact deflections in bearings, etc., which increase the analysis complexity. Any out-of-plane deflections then need to be resolved into components acting in the operating plane of the mechanism before further consideration in the error analyses.

5.12.5 Deflections in the Profile Generating Mechanism

Although the calculation of deflections was complex, by making suitable approximations a simplified allocation could be made to only a few parameters which were most significant.

5.13 ADJUSTMENT ASSESSMENT PROCEDURE

The assessment of compensating adjustments is dealt with by implication in the assessment of the tolerances, clearances and deflections (see Sections 5.10 to 5.12).

The setting-up adjustments that are particularly required in the profile generating mechanism, could simply be checked for output sensitivities and the required adjustment resolutions estimated and checked.

In practice, almost all compensating adjustment could be achieved using the setting-up adjustments for profile eccentricity and size (by mechanism in-feed) etc.

CHAPTER 6

ERROR ANALYSIS OF THE PROFILE GENERATING MECHANISM

6.1 INTRODUCTION

This chapter considers the application of the error analysis theory, developed in Chapter 5, to the profile generating mechanism depicted earlier in Fig.3.12. The mechanism analyses required to assessthe various deviation types are described together with the computer programs which performed the analyses. Results produced by the programs are summarised and their implications for the mechanism design discussed.

The extent of the analyses depended on the nature of the particular type of deviation being assessed; on whether it was constant or variable, and, deterministic or probabilistic, as stated in section 5.2. In all cases a kinematic analysis was required to provide the fundamental mechanism input-output relationship, as expressed generally by Eqn(5.1),and to perform the subsequent error analysis procedures. Additionally a dynamic analysis, to calculate mechanism forces, was required for determination of mechanism deflections and their allocation, and also clearances allocation, to particular parameter deviations. Also the dynamic analysis of forces was useful for other general design purposes. Two main computer programs, MECHKIN and MECHDYN, were written, using the FORTRAN programming language, for the kinematic and dynamic analyses respectively.

Before further discussion a suitable notation system is introduced.

6.2 GENERAL NOTATION

6.2.1 Discussion

When deriving the kinematic and dynamic relationships, the mechanism was treated as three smaller sub-mechanisms, and various 'local' notations were adopted for convenience, and these are introduced when appropriate. Furthermore, upon writing the computer programs, different notations yet again were required because of the restrictions of the FORTRAN language. Therefore, for ease of general assessment and discussion, a general reference notation is adopted for the whole mechanism; this is depicted in Figs.6.1, 6.2 and 6.3: Fig. 6.1 shows the notation for the ideal mechanism for

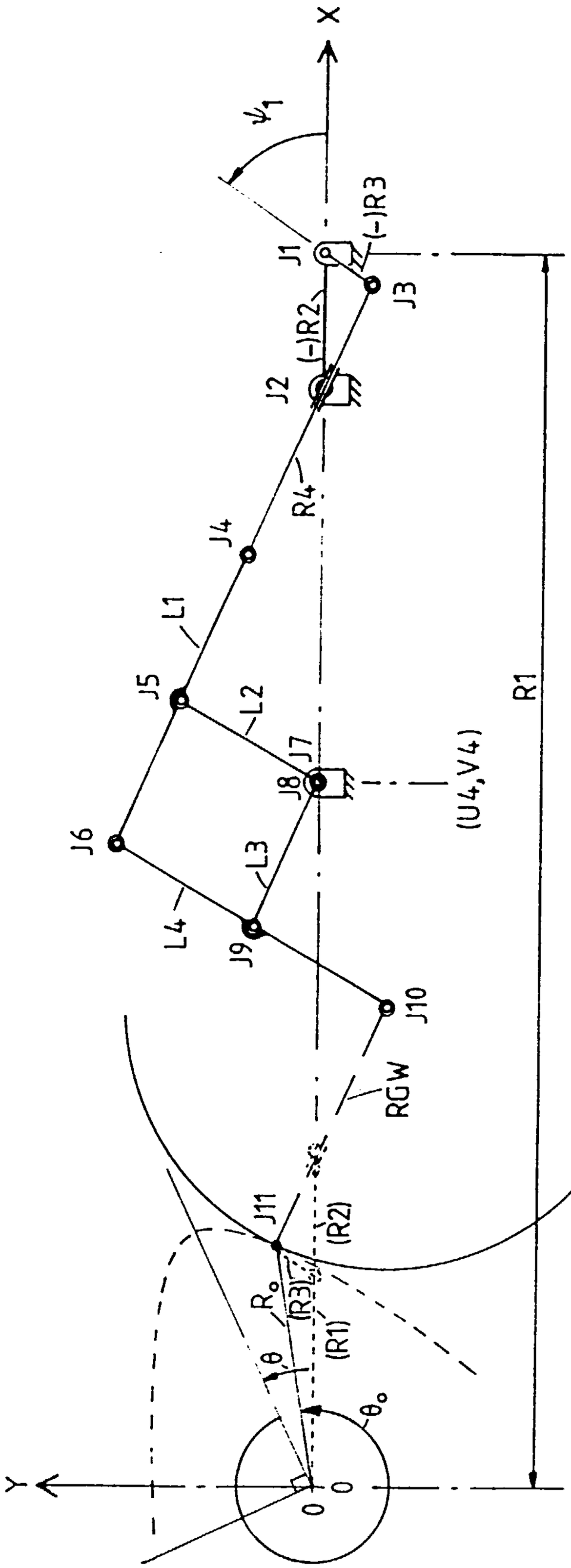

Fig. 6.1 General reference notation for the 'nominal' mechanism.

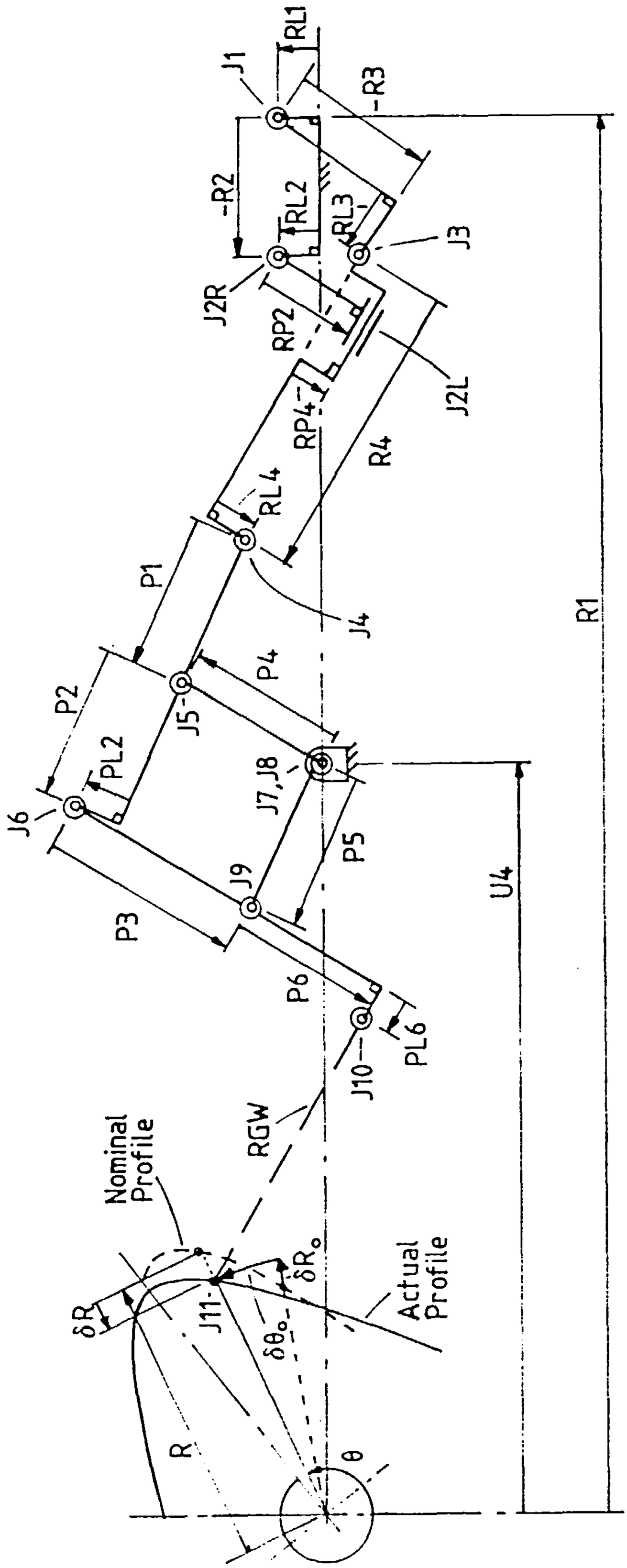

Fig. 6.2 Additional kinematic notation (to that of Fig.6.1) for error analysis of the mechanism.

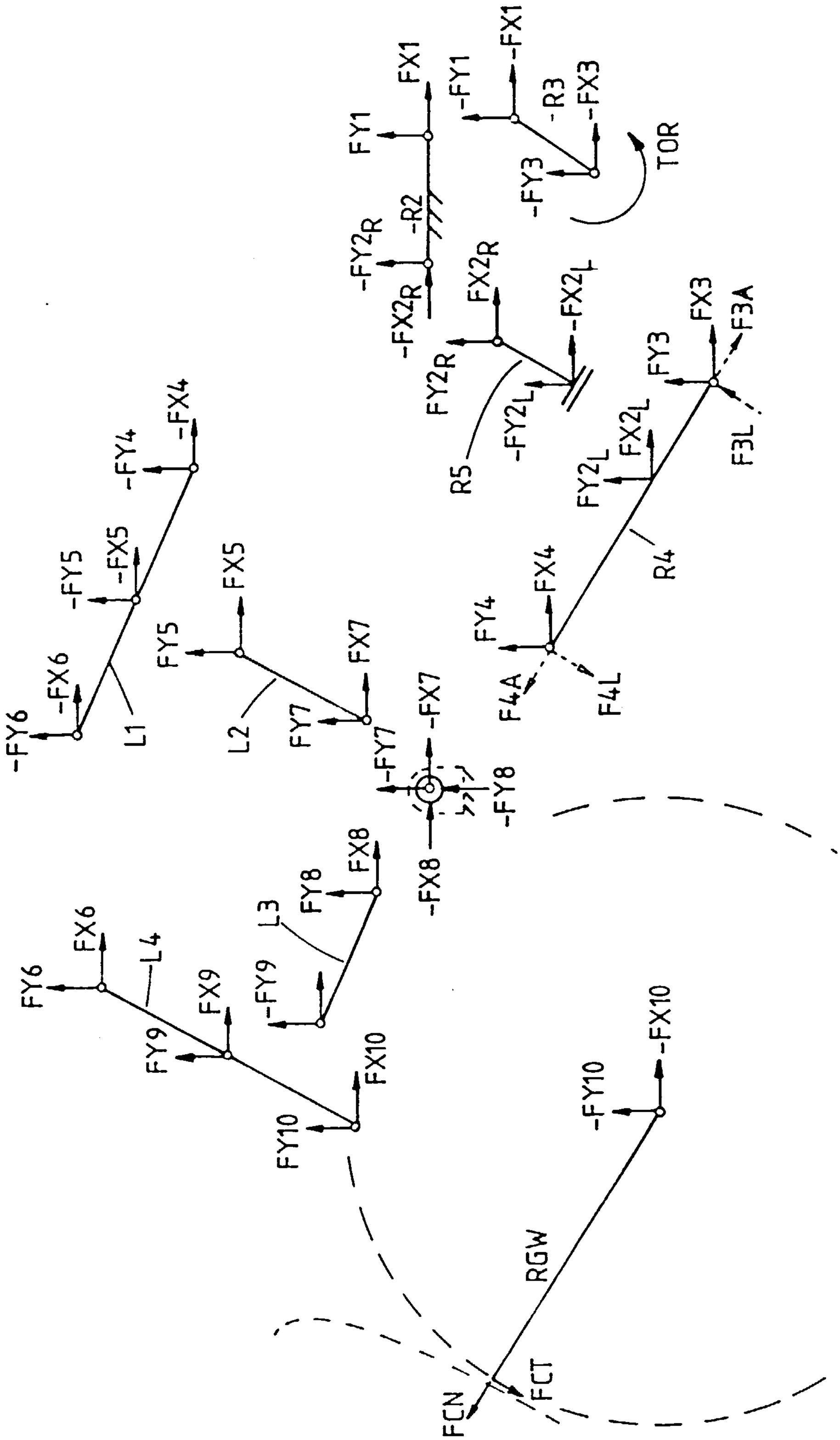

Fig. 6.3 Additional notation (to that of Fig.6.1) for dynamic analysis of the mechanism.

general discussion purposes; Fig.6.2 introduces the extra parameters required for the error analysis; and Fig.6.3 depicts notation for forces and torques on the links.

6.2.2 Basic mechanism notation

With reference to Fig.6.1:

J1 to J11	joints of mechanism (J2 includes a rotary joint, $J2_R$, and a linear joint, $J2_L$, and J11 is the cutting point).
R1	'apparent' frame link connecting J1 and the workpiece centre, O. (originally ='mean radius of profile' as depicted by (R1)).
(-)R2	frame link = 0.5 x 'mean profile radius' ((-) indicates inversion from original position (R2)).
(-)R3	input crank = eccentricity link (R3=e, see Chap.3) ((-) indicates inversion from original position (R3)).
R4	profile-normal link = grinding wheel radius.
RGW	equivalent link representing grinding wheel = R4.
L1,L2,L3,L4	pantograph links.
U_4,V_4	position of pantograph support in X-Y reference frame centred at O.
θ	workpiece angular displacement position.
ψ_1	R3 angular rotation = 3 x θ.
R_o,θ_o	polar coordinates of cutting point in reference frame rotating with workpiece.

6.2.3 Error analysis notation

In addition to section 6.2.2 and with reference to Fig.6.2:

RL1	lateral deviation of J1 on R1
RL2	" " " $J2_R$ on R2
RP2	" " " $J2_L$ from $J2_R$
RL3	" " " J3 on R3
RP4	" " " $J2_L$ on R4
RL4	" " " J4 on R4

P1 linear separation of J4 and J5 on L1

P2 " " " J5 and J6 on L1

P3 " " " J6 and J9 on L4

P6 " " " J9 and J10 on L4

P4 ≡ L2

P5 ≡ L3

PL2 lateral deviation of J6 on P2(L1)

PL6 " " " J10 on P6(L4)

$\delta R_o, \delta\theta_o$ output profile deviation of R_o, θ_o (conventional definition).

δR " " " " R (single effective output definition).

6.2.4 Dynamic analysis notation

In addition to section 6.2.2 and with reference to Fig.6.3:

R5 apparent link connecting $J2_R$ and $J2_L$

FX1 to FX10 forces on joints J1 to J10 respectively in X direction,

and FY1 to FY10 " " " " " " " " Y direction,

of stationary Cartesian reference frame.

FCT,FCN cutting forces tangential and normal, respectively, to grinding wheel and RGW.

F4A,F4L orthogonal forces on joint J4 in reference frame fixed to link R4.

F3A,F3L " " " J3 " " " " " " R4.

TOR external torque required to drive link R3.

6.3 KINEMATIC ANALYSIS - PROGRAM MECHKIN

6.3.1 Kinematic equations.

The kinematic equations defining the mechanism output (profile coordinates) in terms of the input position and mechanism parameters are derived in Appendices A1 to A4. For convenience of analysis and subsequent computer programming the mechanism was sub-divided into: the profile generator, the pantograph and the grinding system. Each of these was treated separately, adopting local notations as shown in Figs. A1.1, A2.1, A2.2 and A3.1.

6.3.2 Computer programming

The equations for each part of the mechanism were programmed in separate subroutines GEN, PANTO and GRIND which were brought together to analyse the complete mechanism in the main program MECHKIN. A flowchart for MECHKIN

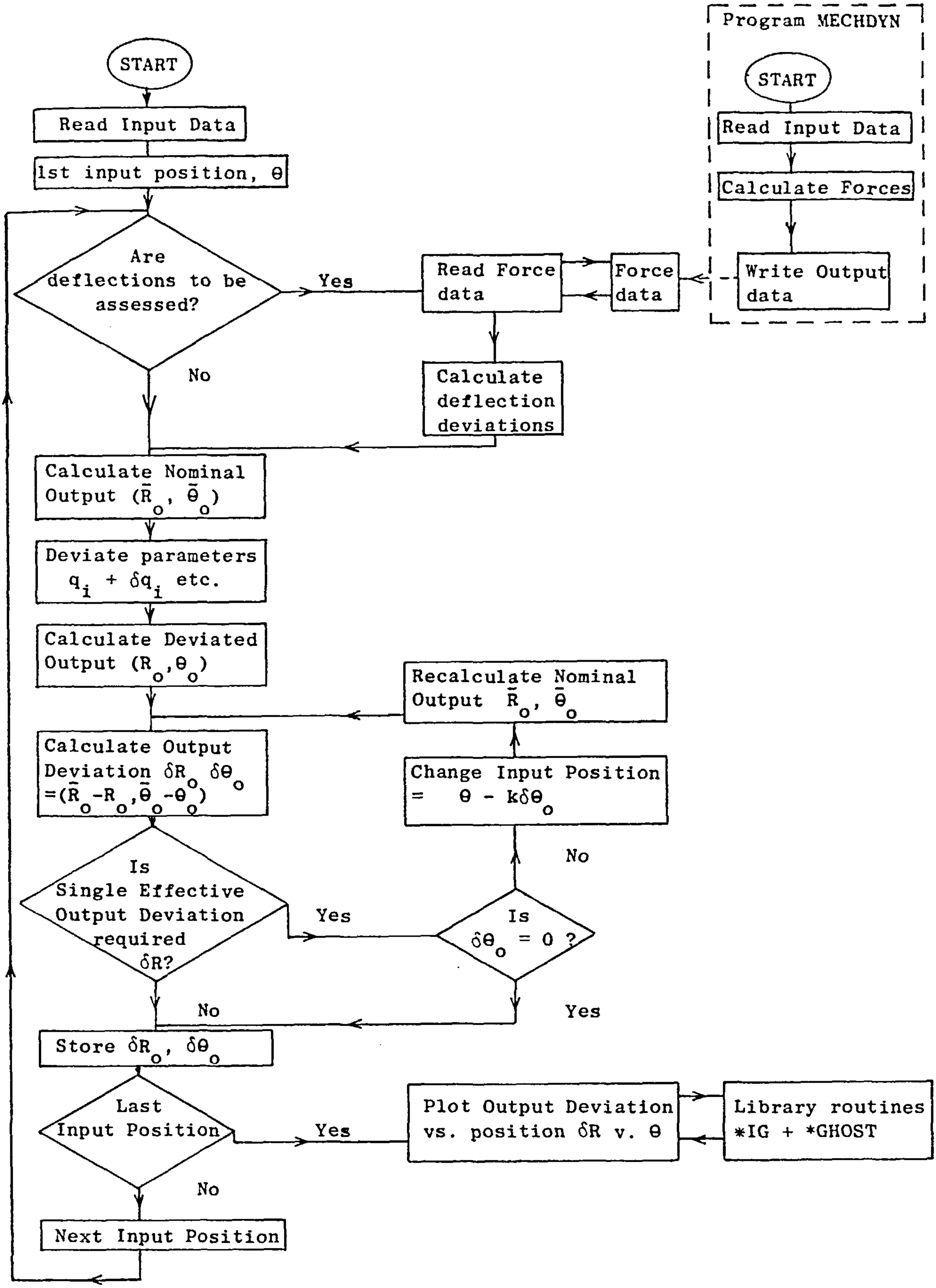

Fig.6.4 Flowchart of computer program MECHKIN

is given in Fig.6.4: the program performs the calculations and procedures developed in Chapter 5, necessary to assess profile error due to various parameter deviations.

Constant deviations are specified as external data read by MECHKIN. Deflections are calculated by deflection-force equations included in MECHKIN upon supply of force data which is previously calculated by the dynamic analysis program, MECHDYN.

MECHKIN is listed in App.A6 with typical input data (but not including force data).

6.3.3 Computer output - profile error plots.

The results are produced by MECHKIN as plots of profile error versus angular rotation of the profile (≡ workpiece rotation, θ). (Although the mechanism input is seen as ψ_1 in Fig.6.1, ψ_1 is geared to θ in the ratio 3:1, and thus θ is the true mechanism input. The transmission system errors will cause deviations of ψ_1, relative to θ, which were treated by inclusion as RL3 deviations, as these are equivalent to angular ψ_1 deviations for small values. See also Secs. 6.5.1 and 6.8.2).

Plots can be produced defining profile error either conventionally by two coordinate deviations (δR_o, $\delta\theta_o$) or by the single 'effective' deviation δR as described in Section 5.8: the latter method was found most useful. These plots represent the 'profile error characteristics'. Typical characteristics of profile error for deviation of each individual parameter are shown in App.A7: their significance is discussed later in this Chapter.

The interpretation of the plots is aided by also including in each plot, a line representing the profile shape (by plotting R ÷ 100 vs. θ), enabling, for instance, the quick realisation of the position of maximum errors relative to maximum profile radius (a corner).

6.4 DYNAMIC ANALYSIS - PROGRAM MECHDYN

6.4.1 Dynamic equations

The dynamic equations for determining mechanism internal forces in terms of input position, and external and inertia forces are derived in Appendices B1 to B3. Again, as for the kinematic analysis, the mechanism

is similarly subdivided and local notation systems adopted as given by Figs. B1.1, B2.1 and B3.1.

6.4.2 Computer programming

The dynamic equations are solved by subroutines GENDYN, PANDYN and GRIDYN called up by the main program MECHDYN, which must also call upon simplified (no deviation parameters) versions of subroutines GEN, PANTO and GRIND to provide kinematic information for the dynamic analysis. The procedure of MECHDYN is straightforward: mechanism specifications, including link masses and inertia moments, are supplied as input data, inserted directly in equations, and forces calculated. MECHDYN is listed in App.B4 with typical input data.

6.4.3 Computer output - mechanism force plots

MECHDYN produces two types of plots, for forces and torques. Forces are given by plotting orthogonal components against each other (e.g. FY1 vs. FX1) for one revolution of the mechanism. The plotted curve is therefore the locus of the resultant force. The curves are annotated at intervals with mechanism angular displacement, ψ_1. ($\psi_1 = 0$ to 360^o, is one revolution of the mechanism).

Torques are given by plotting torque vs. angular displacement (ψ_1 replacing X, torque replacing Y).

On each plot, as well as the total force, or torque, the components due to cutting forces alone, and inertial forces alone, are also plotted.

Typical plots are given in Appendix B5.

Also, when required, forces are tabulated, for increments of mechanism position, ready for use by MECHKIN to calculate mechanism deflection deviations.

6.5 SUMMARY OF ERROR ANALYSIS RESULTS

6.5.1 General classification of profile errors.

Profile error characteristics computed and plotted by program MECHKIN are shown in Figs. A7.1 to A7.21 of Appendix A7 for arbitrary constant deviations (chosen solely to demonstrate sensitivity) of each individual parameter of the mechanism kinematic model shown in Fig.6.2.

For all these plots the nominal parameter dimensions were those of the final detail design (described in Chap. 7) set up to manufacture profiles of mean diameter 10mm and eccentricity $\pm$0.75mm (R=5mm, R3= -0.75mm). The input data for program MECHKIN is listed in Appendix A6.

The mechanism parameters as defined in Fig.6.2 can be categorised according to the magnitude and nature of the profile error which their respective deviations create. The magnitude of the profile error depends on whether the profile sensitivity is predominantly either

(i) 1st Order (see Sec.5.6) where the profile error is approximately linearly related to, and of the same order of magnitude as, the parameter deviation;

or (ii) 2nd Order (see Sec.5.6) where the profile error is proportional to the square of, and of much lower magnitude than, the parameter deviation.

The nature of the profile error depends on the relative contribution of three general types of error:

(i) Size error, where the mean diameter or radius is incorrect. Fig. A7.1 demonstrates the predominantly size error caused by R1 deviation.

(ii) Shape error, where the profile shape is distorted: Fig.A7.7 shows that R3 deviation causes shape error alone (as expected since R3 represents eccentricity which governs profile shape).

and (iii) Rotation error, where the profile is rotated through a constant angle from its nominal position, but is otherwise perfect. The profile error characteristic for RL3 deviation (Fig.A7.8) demonstrates almost pure rotational error. (A small lateral deviation of RL3 on link R3 is approximately equivalent to an angular deviation of the link position, ψ_1. This, in turn, is equivalent to an angular deviation of the profile position, θ, relative to which it is defined ($\psi_1 = 3\theta$). Thus a constant deviation of RL3 effectively produces rotation of the profile. The accuracy of this assumption is discussed in Sec.6.8.2 and see also Sec.6.3.3).

6.5.2 Profile error due to individual parameter deviations

The parameters can be sorted into groups producing similar profile error characteristics and summarised in terms of the preceding definitions as follows:

1) R1, R4(RGW), and U4 deviations (see Figs. A7.1,.9,& .20 resp.) cause predominantly 1st order, size errors. Note that R4 deviation also represents RGW deviation, since nominally R4=RGW and thus, by definition, R4 deviation is the relative difference between R4 and RGW dimensions.

2) RL1, RL3 and V4 deviations (see Figs.A7.2,.8,and .21) all cause predominantly 1st order, rotational errors.

3) P1, P2, PL2, P3, P4, P5, P6 and PL6 deviations (see Figs. A7.12 to A7.19 resp.) all cause profile errors composed of both 1st order, size and rotation, errors; they are grouped together even though the combinations of each type of error may vary. Also, P4 and P5 cause twice the error of the others by virtue of the nature of the pantograph.

4) R3 deviation (Fig.A7.7) causes 1st order, shape error by changing the eccentricity.

5) R2 deviation (Figs.A7.3 and .4) causes 2nd order, size and shape error (size error = 0.5 maximum error). The two plots verify the 2nd order square law (see Sec.5.6) since the maximum profile error increases from 0.5 μm to 2.0 μm when R2 deviation increases from 100 μm to 200 μm.

6) RL2, RP2 and RP4 deviations (Figs. A7.5, .6, and .10) cause 2nd order size and shape errors. The size is always smaller and the shape is always more eccentric whatever the parameter deviation polarity.

7) RL4 deviation (Fig.A.7.11) causes 2nd order, size and shape errors. The size is always larger and the shape always more eccentric whatever the parameter deviation polarity.

6.5.3 Explanation of parameter effects

The effects of the various parameters can be explained briefly by reference to Fig.6.2. It can be seen that the parameters to which the profile is most (1st order) sensitive are those that influence directly the position of the cutting point J11, or joint J3, the equivalent mirror image position in the profile generator by virtue of the pantograph inversion.

The parameters to which the profile is least (2nd order) sensitive are generally those that affect the orientation of link R4, without affecting the position of joint J3, the equivalent cutting point. This might be expected to produce a similar change of orientation of the equivalent grinding wheel link, RGW, without deviating the cutting point, J11: however, since RGW is defined by the relative motion of the grinding wheel and workpiece and not vice-versa, the actual cutting point, J11, will deviate slightly, thus producing the low sensitivity errors.

6.5.4 Effect of profile size on errors

The plots in Figs.A7.1 to .21, for R=5mm, R3=0.75mm represent, in general, the worst case. For manufacture of larger profiles or profiles with less eccentricity, the sensitivity of the profile to parameter deviations, tends to remain unchanged or decrease. The 2nd order sensitivities, above diminish significantly for any other mechanism settings considered later.

Higher order sensitivities to pantograph parameters (group 3) do increase slightly for the largest profiles because of the greater distortion of the pantograph geometry, however these effects are negligible especially when compared to the increased error allowance for larger profiles.

6.6 SUMMARY OF DYNAMIC ANALYSIS RESULTS

The forces on each joint and the input torque computed by program MECHDYN are shown in Figs.B5.1 to B5.15 of Appendix B5. These were all obtained for the mechanism dynamic model of Fig.6.3:the nominal parameter dimensions,and mass and inertia data, were those of the final detail design (described in Chapter 7) set up to manufacture profiles of mean diameter 10mm and eccentricity $\pm$0.75mm and using an 80mm diameter grinding wheel and workpiece velocity of 30rpm. The input data for MECHDYN is listed in App.B4.

It can be seen that the forces are lowest at the grinding wheel 'joints' J11, J10, and highest at the input shaft joint J1. The increase is gradual through the pantograph, but dramatic at link R4 because of the leverage exerted about joint J2, for which the maximum leverage ratio in this case is approximately 22:1. Between joints J4 and J3, cutting and gravitational forces increase in proportion to the leverage ratio, and inertia forces increase in proportion to the square of the leverage ratio.

It can also be seen that cutting forces generally act opposite to the other forces, thus reducing the total force: for design purposes the maximum forces were assumed to be those occurring when cutting forces are negligible (FCT, FCN = 0), such as during final grinding operations when the greatest precision is required.

These results of Figs. B5.1 to B5.15represent the worst case considered: for other settings of the mechanism the forces are lower, especially in the profile generator links, and joints J1, J2 and J3, as the leverage on link R4 reduces substantially, as shown in Figs. B5.17 to .19 This is discussed further in the final assessment of Chapter 8.

6.7 PROFILE ERROR COMPENSATION

6.7.1 Definition of compensating adjustments.

Reduction of profile errors, by compensating for the effects of parameter deviation, may be achieved by 'intrinsic' and 'extrinsic' adjustment of the mechanism. These two types of adjustment may be defined as follows:

Intrinsic adjustments: are those that occur naturally during the normal operation of the mechanism, and affect size and rotation error. During the manufacture of each workpiece the grinding attachment, as a whole, would be fed towards the workpiece until the correct size was achieved thus providing intrinsic adjustment of size error (within the limits of measurement and feed accuracy). Although there is, nominally, only one correct position of the mechanism relative to the workpiece, deviation from this still causes predominantly size error as indicated by R1 deviation in Fig.A7.1.

In general the angular position of the profile on the workpiece is not expected to be particularly important and would not need to be specified to the same order of precision as profile size and shape; in which case rotation errors can generally be ignored. Deduction of the rotational component of profile error may be considered as, effectively, an intrinsic adjustment.

Extrinsic adjustments: are those that are required to compensate for any errors remaining after intrinsic compensation, and need to be deliberately applied either during operation or during initial assembly of the mechanism.

Links R2, R3 and R4 would, in normal operation, need to be adjusted for setting up purposes and further adjustment of these might be used to compensate for profile errors. This could be done before each operation by anticipation of errors which would occur, or during each operation after detection of errors by measurement.

Any errors still remaining might have to be adjusted for, during initial assembly of the mechanism or by redesign of the mechanism to eliminate or nullify the source of the error.

6.7.2 Compensation procedure.

The effectiveness of compensating for any parameter deviation can be assessed by reference to their profile error characteristics computed before and after introduction of the adjustment parameter deviation. First of all, possible intrinsic adjustments should be checked: rotation errors can be eliminated by superposition of appropriate RL3 deviation, and size errors by superposition of appropriate, equal deviations of both R1 and U4 (represented on the computer plots by FEED, where positive FEED indicates displacement towards the profile so as to reduce size, thus FEED ≡ - R1, and - U4 deviation).

For any remaining profile error, extrinsic adjustments can then be checked by further superposition of appropriate parameter deviations.

6.8 PRELIMINARY ASSESSMENT OF PROFILE ERROR DUE TO TOLERANCES

6.8.1 General

Since the actual deviations that might occur in a mechanism due to manufacturing tolerances would be constant, considerable preliminary assessment of their effects could be made prior to consideration of the detail-design of the mechanism. General guidelines for later tolerance specification could be established, based on the profile error sensitivity to constant parameter deviations and the effectiveness of possible compensating adjustments, the assessment of which is reported next.

6.8.2 Compensation of constant parameter deviations

The effectiveness of compensating adjustments and the extent of their requirement was assessed by attempting to compensate for constant parameter deviations which were arbitrarily chosen, depending on the circumstance.

The application of the methods described in Section 6.7 is reported below for parameters, grouped as in Section 6.5.2. The nominal dimensions of the parameters are, as before, those for the final detail-design arranged to manufacture profiles of 10mm mean diameter and $\pm$ 0.75 mm eccentricity, generally the worst case arrangement. Appendix A8 contains plots used to demonstrate (tolerance) compensation. Refer to Fig. 6.2 for notation below.

Group 1) R1, R4 and U4 deviations

By definition (see Section 6.7.1) R1 and U4 deviations would be intrinsically adjusted and the remaining profile size error would depend on the accuracy of the mechanism in-feed and of workpiece measurement, as normal. (See also Section 4.4). Operational adjustment of R4 would be needed to compensate for grinding wheel wear and this is discussed further in Chapters 7 and 8 as part of the assessment of operational accuracy. However, it can be seen from Fig.A8.1 that profile error due to R4 deviation (100 μm) can be significantly reduced by intrinsic FEED adjustment. (100 μm → $\pm$ 2 μm).

Group 2) RL1, RL3 and V4 deviations

Small RL3 deviation is (in Section 6.5.1) considered equivalent to rotation error and thus, by definition, intrinsically compensated. However, this has an effective limit, determined by the error in the assumption of

'small' deviation, which may be calculated with reference to Fig. 6.5.

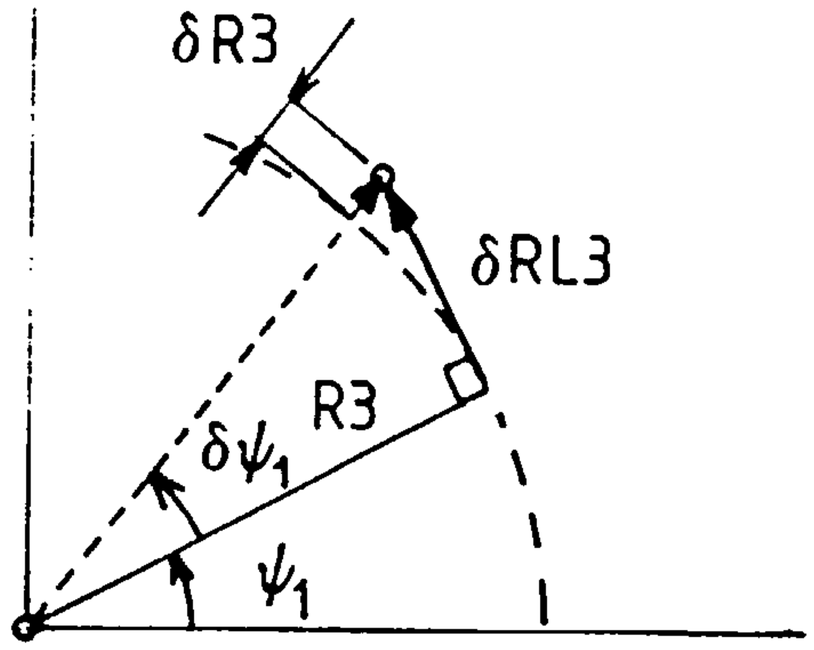

Fig.6.5 Lateral deviation δRL3 of link R3

It can be seen that lateral deviation δRL3 is equivalent to angular deviation $\delta\psi_1$ plus axial deviation δR3 where δR3 << δRL3. Thus the limit of compensation by intrinsic rotation alone, is reached when δR3 becomes significant. For this case, when link R3 = 0.75mm, the limit for, say, δR3 = 1μm, occurs when RL3 deviation,

$$\delta RL3 = (751^2 - 750^2)^{\frac{1}{2}} = 39\mu m.$$

Thus for larger RL3 deviations, additional extrinsic (eccentricity) adjustment would be needed to compensate for the remaining error.

This limit also indicates the accuracy with which RL3 profile error characteristics can assess rotational compensation of other parameters, such as RL1 which is considered next.

A RL1 deviation (50μm) can first be intrinsically compensated by RL3 deviation (-15μm) to deduct rotational error, the remaining error, as shown in Fig.A8.2, is seen to be 2nd order, size and shape error similar to that caused by RL2, RP2 and RP4 deviations. (see Figs. A7.5,A7.6 and A7.10 respectively).

This can be further compensated intrinsically by FEED (2μm) to reduce size error and extrinsically by R3 adjustment (1.5μm) to reduce the shape error to that shown in Fig.A8.3. For larger RL1 deviation

(100 μm) the effectiveness of the compensation diminishes as indicated in Fig.A8.4.

Alternatively the 2nd order error can be compensated more effectively by extrinsic adjustment of RP2 (or RL2 or RP4) (50 μm) as demonstrated by Fig.A8.5. Since these are not operational adjustments this compensation would need to be done during mechanism assembly (see Section 7. 3. 5) or by inclusion of an additional adjustment device. However, the latter adjustment would require much lower resolution than the R3 adjustment because of their respective profile sensitivities.

Yet another alternative compensation of the 2nd order error could be achieved by adjustment of RL4 deviation and FEED as shown in Fig. A8.6 (for RL1 = 100 μm). This also would require special assembly or design for adjustment.

V4 deviation (50 μm) can be compensated almost completely by intrinsic adjustments as demonstrated in Fig.A8.7; although a small 2nd order eccentricity error is also present.

Group 3) P1, P2, PL2, P3, P4, P5, P6 and PL6 deviations

A similar compensation procedure can be applied to all of these and is demonstrated for P1 deviation (50 μm) in Fig.A8.8. The error is reduced first by FEED adjustment (35 μm) to that of Fig.A8.9, and then by RL3 adjustment (14 μm) to deduct rotation error and leave the negligible error shown in Fig.A8.10. This demonstrates that constant deviations of the pantograph parameters cause almost entirely, size and rotation error of the profile, and can thus be compensated by the intrinsic adjustments alone. Fig. A8.11 indicates the slightly reduced effectiveness for a larger P1 deviation (100 μm).

Because of their similarities the profile error due to all of the pantograph deviations combined, can be adequately assessed by simply adding their tolerances statistically and considering them as a single P1 deviation. In fact the actual error is likely to be less than that predicted since, because of the varying combinations of size and rotation polarities, some internal compensation must take place. For instance combining equal P2 (Fig.A7.13) and P3 (Fig.A7.15) deviations, although adding rotation error, would cancel out size errors. (Fig.A9.1).

Group 4) R3 deviation.

This represents eccentricity and is adjustable and thus by definition is the primary adjustment for shape errors and accuracy will depend on the resolution of the adjustment.

Group 5) R2 deviation.

This could be compensated by FEED, however R2 is itself adjustable since it must be set to R2 = 0.5 x R (mean profile radius). Because of the low sensitivity of the profile, the accuracy or resolution of this adjustment can be relatively low.

Group 6) RL2, RP2 and RP4 deviations.

All these deviations can be compensated in the same way as the 2nd order component of RL1 error above by FEED and R3 adjustment as demonstrated by Fig.A8.3. It is fairly obvious, from Fig.6.2, that RP2 and RP4 can compensate each other and they can each also compensate RL2 deviation very effectively as in Fig.A8.12, despite slight differences in individual profile error characteristics (due to the fact that the component of RL2 deviation acting perpendicular to link R4 and parallel to RP2 varies with position): because the resulting lateral deviation of link R4 due to the discrepancy between RL2 and RP2 is small, the profile sensitivity is negligible.This emphasizes the importance of superposing 2nd order sensitivity deviations prior to calculation of the resulting profile error and not simply superposing the individual parameter profile errors which would have indicated some remaining profile error in the case of RP2 and RL2.

Alternatively, RL4 deviation together with FEED can extrinsically compensate RL2, RP2, RP4 as shown previously for RL1 2nd order error Fig. A8.6.

Group 7) RL4 deviation.

This can be compensated by the converse procedures of those involving RL4, described above for RL1, RL2, RP2 and RP4 deviations. FEED is also required since only the shape error is the same for all these deviations and RL4 deviation.

6.8.3 Design implications of tolerance compensation.

The most important implication of the preceding analysis is that most profile errors due to tolerances are likely to be easily compensated or be relatively small and are thus not likely to have asgreat an influence on the design as was anticipated. In particular the pantograph deviations, within reasonable tolerances, will cause only size and rotation error which can be intrinsically compensated.

Another implication, due to the non-linearity of 2nd order errors generally affecting orientation of link R4, is that the parameters concerned should not be treated independently.

6.9 PRELIMINARY ASSESSMENT OF PROFILE ERROR DUE TO CLEARANCES

Since assessment depends on other assumptions of the detailed design work, such as specification of preloading, in the joints, to eliminate clearances, most discussion is left till later (in Chapters 7 and 8). However, it was stated earlier that clearances could be potentially very difficult to assess unless the direction of loads acting at clearances, change relatively little during motion in which case they may be treated as constant deviations. With reference to the results of MECHDYN in Appendix B5, this is seen to be generally the case for the profile generating mechanism loads.

The variations in magnitude and direction are worst for joints J1, J2 and J3 where the load direction actually reverses, however even this only occurred for the worst case arrangement (R=5mm, R3=0.75) for most other cases the magnitude variation of these loads is greatly reduced such that they are always uni-directional.

An example of the simplified assessment of clearance effects is given by reference to joint J6 in Fig.6.2. The direction of load shown in Fig.B5.10 is such that any clearance at joint J6 will tend to align itself parallel to a line through joints J4 and J10 of the pantograph. Such a clearance deviation, C, can be approximately simulated by an appropriate combination of P2 and P3 deviations as shown in Fig.6.6.

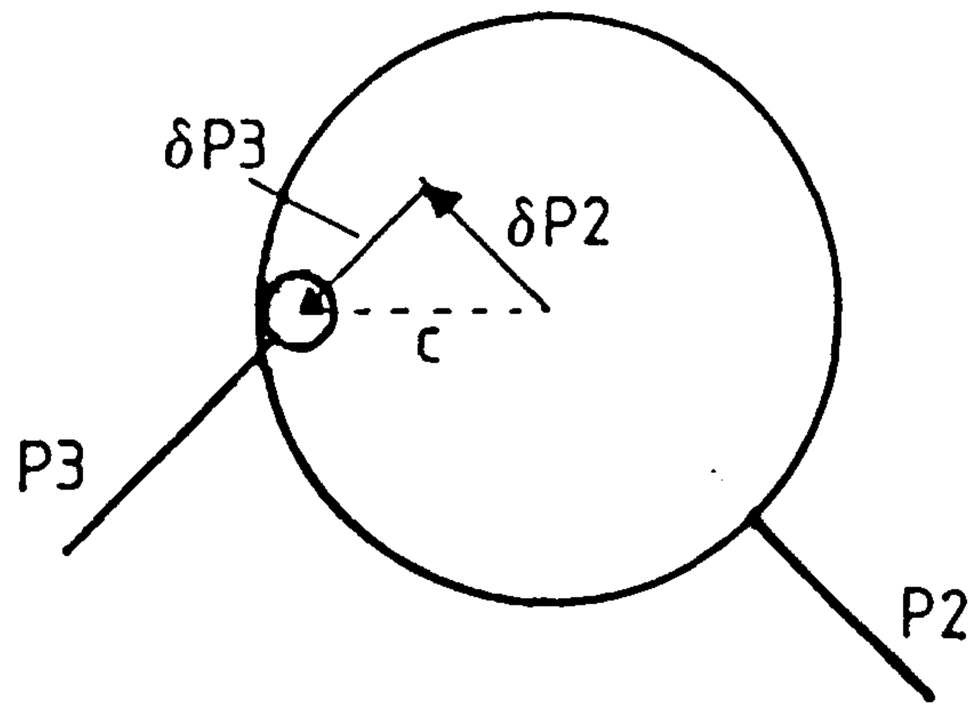

Fig.6.6 Simulation of clearance deviation.

The result of this can be seen in Fig.A9.1 of Appendix A9 for P2 and P3 deviations of 50 μm each, which simulate a clearance deviation of 71μm. The profile error is predominantly rotation error which can be intrinsically compensated by an RL3 deviation (-30μm) as shown in Fig.A9.2.

6.10 PRELIMINARY ASSESSMENT OF PROFILE ERROR DUE TO DEFLECTIONS.

Little preliminary assessment of the profile errors caused by deflections can be made since deflections depend so much on the detail design of the mechanism: they are therefore more easily discussed in Chapters 7 and 8 after introduction of the detail design.

What may be mentioned at this stage is the significance of the largest forces, and their directions; which occur in the profile generator at joints J1, J2 and J3 (see Appendix B5). The force at joint J3 on link R4 is plotted in Fig.B5.6 in component directions which are orthogonal to the axis of R4, and it can be seen that the largest force always acts perpendicular to link R4; this is also true for forces at J1 and J2 and happens because the direction is that in which leverage is exerted by R4 pivoting about joint J2 to produce these large forces. It also happens to be the direction for which the profile is least sensitive to deviations! This has an important implication for the detail design, because the relatively large deflections which may occur in the maximum-load direction will not

produce the severe profile errors that might be anticipated at first sight. It also has an important implication for the error analysis of deflections,by facilitating the simplification of the analysis, through allocation of deflections to only a few parameters (see Appendix C3 .10).

Various profile error characteristics, due to deflections, are shown in Appendix A10. The individual characteristics due to each of the parameter deflections which were used to analyse the total error are shown in Figs.A10.1 to A10.8 for the worst mechanism operating condition and for which the total profile error is shown in Fig.A10.9 The total error characteristic for a range of other operating conditions is shown in Figs. A10.11 to A10.23 which also show that some intrinsic compensation for size and rotation errors can be applied.

6.11 *CONCLUSIONS*

The application of error analysis theory to the profile generating mechanism and preliminary results (mainly for the worst operating conditions) have been reported and several design implications raised. In practice the computer analyses using programs MECHKIN and MECHDYN were repeatedly referred to as the need arose during the detailed design work when various options had to be considered and compared. The final assessment of results and the conclusions reached are discussed in Chapter 8.

CHAPTER 7

DESIGN OF PROFILE GRINDING ATTACHMENT

7.1 INTRODUCTION

The main concern of this chapter is to present the conceptual layout, for a practical polygon profile grinding attachment, which represents the end-product of this work. The design layout is shown in drawing Nos. 1 to 7 (inside the back cover), It provides the basis for detailed design of an experimental prototype and ultimately the possible development of a commercial production attachment.

Design is essentially an iterative process and the final layout has evolved from several earlier stages of layout, variation and refinement. To report all these stages of the process would be very laborious and this chapter is mainly restricted to a straightforward functional description of the final design.

A general description of the overall design and its basic mode of operation is given, followed by more detailed explanations of the main features of the design. The general specifications and the main problems have already been presented in Chapter 4.

The influence of the error analysis upon the design is mentioned occasionally in this chapter, but most discussion of it is reserved for Chapter 8.

For the sake of clarity when referring to the drawings, the general notation previously adopted in Chapter 6 (Figs.6.1, .2, and .3) is used wherever possible, together with a supplementary, simple numbering notation which is introduced as appropriate; where views in particular drawings are recommended, the Drawing Numbers, in parentheses, are appended to the notation (in the text, not the drawings), e.g. stepper motor 2(1,2) - item 2 in Drawing Nos. 1 and 2.

The major design analyses and calculations are contained in Appendix C. These are restricted to those calculations that are most important for determining the design feasibility; many of the more routine calculations are omitted; for example, bolt design calculations are not presented.

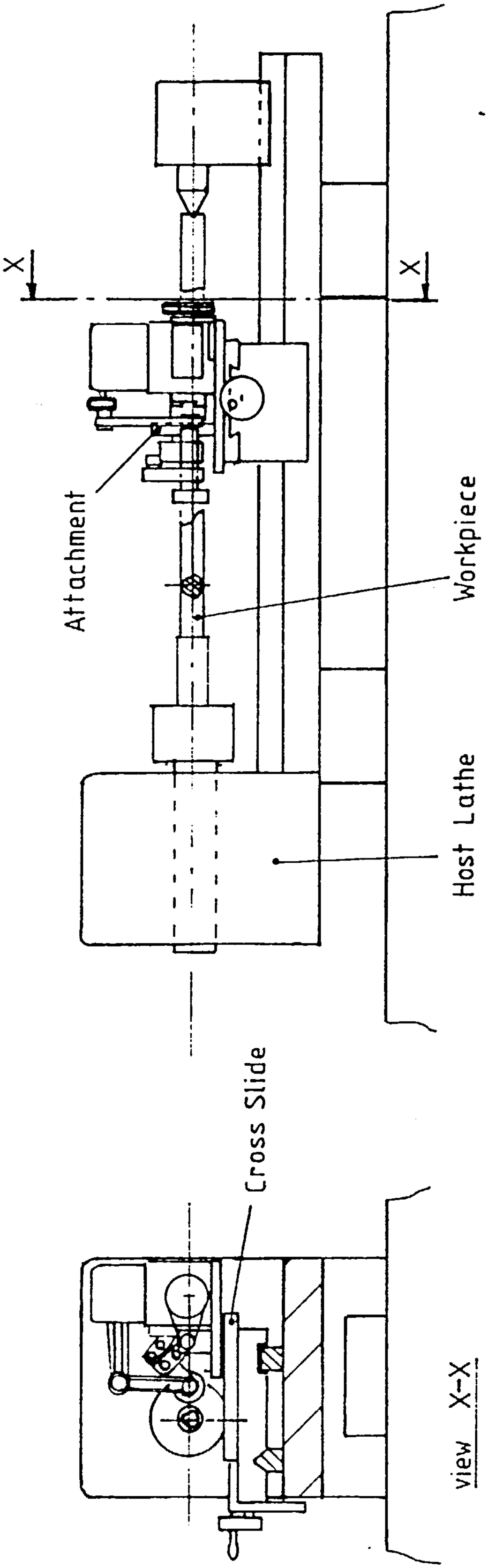

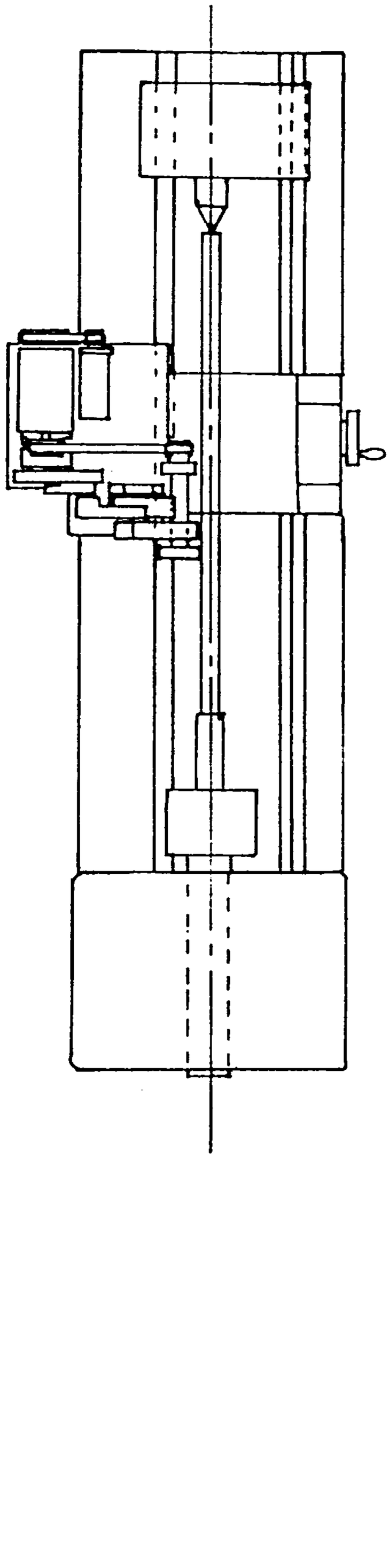

Fig. 7.1 Location of the profile grinding attachment on a host lathe

7.2 GENERAL DESCRIPTION OF THE PROFILING ATTACHMENT

The three main orthogonal views of the design are depicted in Drawings 1, 2 and 3 and further, selected views of certain features of the design are shown in Drawings 4, 5, 6 and 7.

The attachment is designed for mounting at the rear of the host lathe cross slide, on the opposite side of the work to the normal operator position, as shown schematically in Fig.7.1. Because of its size this seemed preferable to mounting it in the normal toolpost position, and on some lathes this may avoid any need to remove the toolpost, possibly allowing it to remain operational. This position also means that the grinding swarf will be directed downwards when the workpiece rotates in the normal forward direction.

Although designed specifically with a Colchester lathe in mind (see Section 4.2.3) which has a 5½" workpiece centre-height above the cross slide, it can easily be adapted for other centre-heights. For smaller centre-heights the pantograph fulcrum height (V4) could be altered to a position midway between the heights of the workpiece and of the profile generator (joints J1 and J2) respectively.

The whole assembly (except for electrical controls and power supplies which are housed separately, and not shown in the drawings) is mounted on a single baseplate, 1, which will be bolted to the cross slide of the host lathe. The cross slide will feed the whole attachment towards the workpiece during profile grinding.

The input link, R3, of the mechanism is composed of the bearing shafts of joints J1(1) and J3(1) which are connected by a dovetail sliding joint 4(1) and it effectively form a single main drive shaft. Link R3 is driven by a stepper motor 2 (2,3) through a timing belt and pulley transmission 3. The correct gearing with the workpiece is achieved electronically: the work rotation is detected by an optical, or magnetic, encoder (shown not in the drawings, but, schematically only, in Fig. 7.2), whose signal is converted by an electronic controller which drives the motor and the mechanism at three times the speed of the workpiece.

Joints J1(1) and J3(1) both contain pairs of taper roller bearings which are each mounted back to back and preloaded for high rigidity. The functional dimension R3 which determines profile eccentricity is set by adjusting the dovetail slides 4(1) using the dial and screw mechanism 5(2). (Note: the drawings show R3 set at zero, the assembly position - see Section 7.3.5).

The housing of joint J3(1) forms part of link R4(1,2) which is mounted on a linear ball bearing J2L(1,2) and translates on a shaft which, in turn, is mounted on the inside of the annular shaft of a rotary bearing J2R(1,2). The latter, J2R, consists of a large needle roller bearing which encompasses the whole assembly constituting joint J2. The housing of J2R is clamped to a bearing pad on the bedplate by two bolts 6(1,2). These are loosened when the displacement (in the kinematic plane) of J2 relative to J1 is adjusted, using the screw and dial assembly 7(2), to set up the kinematic dimension R2 (also shown at R2=0, in the drawings). The dimension R4(2) also needs to be adjustable and the bearing shaft, connecting R4 to the pantograph link L1 at joint J4(1,2,5), is mounted on a parallel slide which is adjusted by another screw and dial assembly 8(2,5). (R4 is set at 40 mm in the drawings).

The mechanism motion is transmitted through the pantograph links L1, L2, L3 and L4 (1,2,6) to the grinding spindle 9(2,6) which is clamped at J10(2,6) in link L4.

The power required for grinding is provided by a 0.55kw electric motor 10, which is mounted on top of the bearing housing of joint J1, and is transmitted to the grinding spindle via two flat belt pulley drives 11(3) and 12(3) carried on a jointed linkage to allow for the spindle movement.

The grinding wheel speed can be adjusted by electrical control of the motor and/or selection of appropriate pulley diameters.

7.3 PROFILE GENERATOR DESIGN

7.3.1 Design of bearings for joints J1 and J3

The final arrangement of the mechanism is such that the joints at J1(1) and J3(1) must carry the highest operating loads (see Sec. 6.10) as overhang, or cantilever loads. Taper roller bearings A and B, and C and D, in J1 and J3 respectively, were chosen because they offer high rigidity and resistance to overhang loads when arranged in 'back to back' pairs (see Refs [25, 26]), and they can be easily preloaded against each other, which serves two purposes in this mechanism:

(1) preloading increases bearing contact stiffness and thus reduces bearing deflections,

(2) preloading produces a friction torque in the bearings which can be used to control backlash in the stepper motor drive system (see also Sec.7.5).

To satisfy both these requirements the preload has to be controlled accurately at a suitable compromise value. An analysis of bearing friction and preloading is given in Appendix C5.2.

The bearing arrangements are best seen in Drawing No.1. The simplest method of preloading each bearing pair would be to separate the outer races with spacers 13, 14, and then to adjust the separation of the inner races using a locknut 15, 16, and lock washers, as shown in the drawing. However, when analysed, (see Appendix C5.2.5) it became apparent that it might be difficult to set the preload with sufficient accuracy, firstly because the preloading deflection would be too small to measure accurately and secondly because the resolution of the locking method is not small enough as the lockwasher can only set the preload in increments, determined by the locknut thread pitch, which would be too large.

These problems could possibly be overcome by using locknuts with finer pitch, or dispensing with the lockwashers and using two locknuts in each joint which would provide infinite locking resolution, and by measuring the static, or starting, friction torque directly. The disadvantage would be the extra space required especially in joint J3 which would increase deflections of the main shaft assembly.

Various other locking methods might also be tried, however a better alternative would be to use disc springs placed between the outer races in each bearing pair. These have a low effective stiffness at the design point and thus are relatively insensitive to the locknut adjustment accuracy. The method is analysed in Appendix C5.2.2 and, since it only requires replacement of the outer ring spacers, by the disc springs and an inner ring spacer, and no redesign of other parts, it can easily be compared experimentally with the original method.

The housing for joint J1 is bolted to the bedplate, and also supports the grinding spindle motor. The housing for joint J3 is bolted to a flange 17(1,2) on link R4: this facilitates assembly of the bearings and also provides a mean for compensation of component errors, during assembly, as explained later in Section 7.3.5.

7.3.2. Eccentricity (link R3) adjusting mechanism

This is best seen in Drawing Nos. 1,2, and, especially, 4. A dovetail joint 4(1,4) is used in the adjustment for eccentricity of link R3 because of its ability to provide a rigid and backlash-free joint in a small space and because it can be simply set up and locked using reasonably accessible set screws. The optimum clearance required between the slideways to ensure accuracy of travel during eccentricity adjustment can be achieved accurately and periodically re-adjusted for wear, using three set screws 18 acting via hardened pins on the parallel gib 19(1,4). Similarly after each eccentricity adjustment by the screw mechanism, the dovetail joint can be locked in position by tightening the two larger set screws 20(2,4) via pins against the gib, thus eliminating backlash.

The load exerted by the set screws must produce sufficient friction between the mating surfaces to resist transverse loads, when they align with the direction of slideways travel, and adequate axial preloading in the joint to resist bending moments. Resistance to bending is improved by countersinking one of the vertical mating surfaces 21(1) so that the contact area is reduced to increase the axial clamping pressure and also to concentrate it in an annular zone near the outer circumference where the maximum tensile bending stresses will occur which tend to open up the joint.

The slideways do not contain any means of adjustment for lateral deviation, RL3, of the centreline of the shaft of J3 with that of J1: such errors can be compensated intrinsically as rotation and by eccentricity R3 adjustment; and the RL3 deviation will be determined solely by the production accuracy of the components.

The screw feed mechanism provides a coarse and a fine adjustment of the eccentricity link R3, using the principle of a differential screw: such a screw, connecting the components requiring relative adjustment, has a different thread pitch in each component so that one turn of the screw produces a relative displacement of the two components equal to the difference in pitches. Referring to Drawing No.4, it can be seen that one end of the adjusting screw 22, which has a 0.50mm thread pitch, screws into a tapped hole in the male dovetail slideway 23 (on the J3 side of the joint), and the other end, which has a 0.45mm thread pitch, screws into a tapped bush 24 in the mounting plate 25 attached to the female slideway 21(J1 side of joint). A graduated dial 26 is locked on the outside end of the screw, and the flange of the bush 24 is also graduated as a dial. Because of the small size of the dials (imposed because they must rotate with the main drive shaft R3 during operation), they can be adjusted using a two pronged, or forked, key (not shown) locating in the two holes in each dial. Both dials together or the outer dial alone can be turned to provide coarse and fine adjustments respectively.

When both dials are turned together, say, in the anticlockwise direction the male slide and joint J3 will move to the right (in Drawing 4) 0.50 mm for each full turn. However when only the outer dial is turned anticlockwise and the inner bush is held stationary, the screw will also move 0.45mm to the left and thus the male slide will now move only 0.5-0.45 = 0.05mm to the right. A preloaded spring 27 in the mechanism is used to keep the bush axially in contact with the mounting plate. Although the axial load between the mating threads of the bush and screw will be the same as that between the bush flange and mounting plate, the friction torque resisting rotation will be greater between the latter two because of the larger radius, and thus the bush should not turn when only the outer dial and screw is turned.

The outer dial 26 has 50 graduations of approximately 1mm separation: for fine adjustment each represents 0.001 mm eccentricity travel and for rough adjustment each represents 0.010mm. A further graduated scale 28 is positioned on the male slide outer circumference next to the set screws, to indicate approximately the overall eccentricity setting.

Although it may be possible to manufacture and calibrate the eccentricity adjuster with sufficient precision to adjust and measure the absolute dimension of R3, a more likely and cheaper method would probably be to use a separate, displacement, dial gauge, measuring against the housing of J3 or a specimen profiled workpiece, to determine the absolute eccentricity and only use the screw and dial as a high resolution incremental adjuster, whose absolute accuracy over the whole range of adjustment becomes irrelevant. This is also discussed in more depth in Section 8.5.2.

7.3.3. Linear and rotary bearing assembly of joint J2.

This is only shown in Drawn Nos. 1 and 2. A Rotolin [27] ball bearing 29 is used for the sliding joint J2L, which supports link R4, because of its simplicity and low space requirements. The bearing consists of balls, retained in several rows not in grooves, running between an outer sleeve and the shaft 30 allowing rotary as well as linear motion. The outer sleeve is press fitted in link R4, which slightly preloads the balls on the shaft (as recommended by the manufacturer). The shaft is supported at each end in a ring 31 on which the rotary bearing J2R is mounted.

A needle roller bearing 32 is used for the rotary bearing J2R; also because of its relatively low space requirements and simple construction. The size of the bearing is governed by the size and travel required of the linear bearing and is thus considerably overdesigned for the loads carried. Because of the bearing's size, relative to the kinematic dimensions of the linkage, the friction torque arising could be significant and this is analysed in Appendix C5.1. The analysis indicates that, with suitable choice of lubricants, the additional loads incurred can be considered negligible, although this should be investigated experimentally. The bearing should run with a reduced clearance and not be preloaded by interference fit since with such a stiff bearing, this could not be controlled adequately and could give rise to excessive load-dependent friction torque which would be significant.

This clearance will generally take up position perpendicular to parameter R4 which is the least sensitive direction. Reversal of the direction only takes place for the worst operating case, see Sections 6.9 and 8.3. A 'reduced clearance fit' following manufacturers instructions [28] will result in an internal clearance between 30μm and 60 μm, which may reduce further depending on the operating conditions and relative heat expansion of the rings and housing.

This can be compensated for during assembly along with other deviations as explained in Section 7.3.5.

7.3.4 Adjusting mechanisms for R2 and R4 dimensions

The mechanism error analysis showed that the profile accuracy is relatively insensitive to deviations in the kinematic dimensions R2 and R4 (see Section 6.8.2) and therefore the precision required of the adjusting mechanisms is relatively low. Apart from their mounting plates 33(5), 34(2), identical screw and dial mechanisms 7,8(2) are used for both R2 and R4 adjustment. That for R4 is shown in more detail in Drawing No.5.

The dial 35 has 50 graduations (of approx. 1mm separation) and a full turn imparts 0.5mm travel, via a 0.5mm pitch screw 36,to the slider 37 supporting the shaft 38 of joint J4; thus each graduation represents 0.010 mm travel.

The slider travels between parallel slideways adjusted by two gibs; the lower gib 39 may be adjusted by shims for compensation of RL4 deviation during assembly, as explained in Section 7.3.5, and the upper gib 40 by set screws for locking and releasing the slider. The R4 slideways are designed for a total travel of 50mm, giving R4 settings from -10mm (for internal grinding) to +40mm as drawn. The total operational travel of the R2 adjustment is from 0 mm to 25 mm and is limited by the travel of the linear bearing J2L(2) inside the rotary bearing J2R(2), the housing 41(1,2) of which is displaced by the dial and screw 7(2) relative to joint J1 to determine R2(2). The J2 housing is mounted on a flat bearing pad and relies on the bearings of J1, J3 and J2 to maintain the correct alignment.

The dial and screw mechanism 7 for R2 adjustment is mounted on the attachment bedplate 1 adjacent to the housing 41 of the J2 needle roller bearing to which a mating nut 42(2) is bolted.

The R4 adjustment will take place more frequently than that of R2. The latter is only adjusted each time the workpiece finished size is changed, whereas R4 needs to be adjusted as the grinding wheel size reduces due to wear and, in particular, dressing of the wheel which may take place as often as for each workpiece being ground. This is discussed further in Section 8.5.3.

7.3.5. Tolerance compensation during assembly.

The preliminary assessment of Chapter 6 shows that profile errors caused by constant deviations, such as those due to component tolerances, can be effectively eliminated. Most 1st order errors will be intrinsically compensated (as size and rotation error) and the remaining 2nd order errors either will be insignificant or can be substantially further compensated by extrinsic adjustment of the eccentricity, R3. Even so, for the last case there will be a significant error (>1μm) if the deviations exceed a certain limit (100μm for the worst case; see Section 6.8.2).

The deviations concerned (to RL1, RL2, RP2, RP4, RL4 in Fig.6.2) must be considered cumulatively and the relatively large number of component dimensions involved in the tolerance chain will make it difficult and expensive to keep within this limiting value by restricting tolerances. Furthermore for ease of setting up, it would be preferable if use of the R3 adjustment for this purpose could be avoided. Therefore an alternative and more effective compensating adjustment is performed during assembly of the mechanism.

7.3.5.1 Assembly compensation principle.

The housing 43 of joint J3 is attached to sliding link R4 by a flat flange 17(1) enabling the deviation to parameter RP4, of J3 relative to R4 and joints J2 and J4, to be adjusted and this can be used to compensate the other 2nd order deviations as described in Section 6.8.2.

The adjustment procedure takes advantage of the fact that the centrelines of the joints J1, J2, J3 and J4 should nominally coincide if the

kinematic dimensions R3, R2 and R4 are all set to zero: in this position, dial gauges can easily detect any deviations of these centrelines by measuring the radial 'run-out' of components as they rotate. Adjustment can be made using the centreline of joint J1 as a reference centre-height. The deviation of the J1 centre-height from that of the workpiece (because of the J1 bearing housing, bedplate,and lathe centre-height, tolerances) is considered later, however it will not affect the compensation of 2nd order errors which are due to the relative height deviations of joints J1, J2, J3 and J4.

7.3.5.2 Assembly compensation procedure

The compensation proceeds in stages as follows. (Reference should be made to layout Drawings Nos.1 and 2, and Fig.6.2).

1) Main shaft, link R3, including the eccentricity slides and adjustment, and the bearings and housing of joint J3, is assembled and mounted in joint J1, the housing of which is bolted firmly to the bedplate.

2) Slider link R4 is assembled on the linear and revolute bearings, of joint J2, of which the housing 41 is mounted loosely on the bedplate.

3) Eccentricity, dimension R3, is set to zero: this can be achieved accurately by using a dial gauge, locating against the stationary housing 43 of J3, and rotating the shaft. Ideally there should be no displacement registered, however there may be some run-out in a direction perpendicular to the eccentricity slides 4(1) which is caused by allowable RL3 deviation. By minimising run-out in-line with the slides (R3=0) and aligning the slides vertically, the centre height of joint J3 is established equal to that of J1.

4) The inner ring of the needle roller bearing 32 of joint J2 should be positioned, and held, with the linear bearing 29 horizontal (parallel with the bedplate). This can be checked by restraining the horizontal movement of link R4 and sliding the J2 bearing housing 41 on the bedplate: there should be no vertical movement of link R4 as indicated by a dial gauge. The clearance in the needle roller bearing should also be held in the position of operational take-up (that is at the top of the bearing) for it to be compensated correctly.

5) The housing of joint J2 is next clamped to the bedplate and the flange 17 on R4 offered up to the housing 43 of joint J3 and bolted securely to it. In this way any deviations of the revolute bearing centre height RL2 and the linear bearing centreline, RP2 are compensated by equal RP4 deviation; i.e. the centreline of R4, which by definition (see Fig.6.2) intersects the centreline of joint J3 and is parallel with that of linear bearing J2L, now must also correctly intersect the centre line of J1.

6) Finally the lateral deviation of joint J4 with link R4 (which may be increased by the preceding procedure) can be checked and adjusted, although this may not be necessary because of its very small effect on profile error. This is done by setting dimensions R2(2) and R4(2) both to zero, which ideally should allow link R4, and the shaft 38 of joint J4 to rotate freely about the reference centreline (of J1 & J2). In practice, any deviation between the centre-heights of J1 and the revolute bearing of J2L, will restrict rotation, but this would be overcome by sliding the housing 41 (after freeing it from the bedplate) off the needle roller bearing 32, thus freeing the inner bearing race to rotate fully.

The correct centre-height of joint J4 is, here again, checked using a dial gauge while link R4 rotates to detect the run-out of the shaft 38 of J4 which is mounted on the parallel slideway in link R4. Adjustment could be made by using shims between the lower gib 39(1) and the bottom slideway.

7.3.5.3 Summary

This procedure should limit the effective cumulative deviation to much less than 100μm depending on the skill with which it is carried out. However even if it only limited the cumulative deviation to 100 μm, further compensation with eccentricity will still limit profile error to 1μm in the worst case! In general it will be assumed that the compensation is completely effective and profile errors due to these 2nd order tolerance deviations are insignificant.

7.4 PANTOGRAPH DESIGN

The principle of pantograph operation was explained in Section 3.4 and various configurations illustrated. In the final layout the configuration shown in Fig.3.11e is used with the links above the line through the input and output joints, and giving a 1:1 input:output ratio. Additional views of the pantograph are given in Drawing No.6, and main reference should be made to this.

The pantograph is mounted on a bracket 44 which is clamped to a flat bearing pad on the bedplate, using bolts 45 running through slots in the bedplate: this allows the position of the pantograph to be adjusted, depending on the mechanism setting, in order to maintain adequate operating clearances between the pantograph links. The flat pad allows the alignment to be determined by the pantograph bearings.

The fulcrum shaft 46 supports links L2 and L3 through joints J7 and J8 and is fixed to the bracket at one end only. One reason for this is to facilitate the incorporation of any height adjustment of the shaft which might be needed (see Section 8.2.5). This could be performed by making the fixed end of the shaft eccentric with the part supporting the bearings and rotating it in the bracket. (No eccentricity is shown in the drawings). The pantograph links are arranged so that the line of action of the input and output forces, from the generator and grinding system respectively, is close to the fixed end of the fulcrum shaft.

The grinding spindle 9(2,6) is clamped in the split housing at joint J10 of link L4, near to the grinding wheel RGW(2). To provide the spindle with as much rigidity as possible, especially to forces and couples not acting in the kinematic plane of motion, the nearest joints J9 and J8, in link L3,are fitted with taper roller bearings mounted in preloaded back-to-back pairs 48, 49. Thus out of plane loads will be resisted by the fulcrum support bracket and the bedplate close to their source. The in-plane grinding rigidity will be determined by the stiffnesses of all the components,of the mechanism and stepper motor drive system,which determine its kinematic position.

The other pantograph joints, J4, J5, J6,and J7, are all fitted with pre-sealed needle roller bearings. These were chosen in preference to other types such as plain bearings in order to minimise clearances and possibly eliminate them altogether by using interference fits to preload

the bearings. However, this last practice is not generally recommended and would have to be checked experimentally. The preliminary analysis of clearances, in Section 6. 9, suggests that they can be compensated. However, if all the bearings in links L1 and L2 have clearance, the links will tilt due to the out of plane couples and the 'effective' deviations due to clearances will be much greater than the actual clearances themselves, as explained in Section 8.3

Notice that the needle roller bearing 50 of joint J7 is mounted on a sleeve 51 and not directly on the shaft: the sleeve is used to preload the inner rings of the taper roller bearings 48 in the adjacent joint J8 by tightening the locknut 52 on the other side of joint J7.

7.5 DRIVE SYSTEM

7.5.1 General application of stepper motors.

The characteristic feature of a stepper (or stepping) motor is its step by step rotation in response to an applied electrical pulse train. A full rotation of the motor is composed of a specific number of accurately defined steps, and the motor rotates through a fixed step angle in response to each pulse.

Position and speed control is relatively simple, since digital signals are converted directly into mechanical motion normally avoiding the need for feedback. Position error is non-cumulative since the motor, operating under correct conditions, is locked in synchronisation with the reference signal, and speed depends directly on the frequency of the control pulses - the 'step rate'.

If the reference signal is generated by the rotation of a machine tool spindle, using a suitable digital speed detection device, or 'encoder,' then the stepper motor can be driven at any fixed ratio of the spindle speed. The number of encoder pulses produced per revolution of the reference spindle need not necessarily equal the number of steps per revolution of the stepper motor: control circuitry can multiply or divide the encoder pulse rate to produce a slower or faster motor step rate.

Such a system effectively operates as an electronic gear-box, and is ideally suited to application in the profile generating mechanism.

The main advantage is the resulting mechanical independence of the attachment from the transmission system of the host machine, as explained in Section 4.3.2.

There are a great variety of stepper motors commercially available and even more methods of controlling them. The complete detailed design and specification of a stepper motor and its control system has not been attempted because there was insufficient time available to carry out the work involved and also because this would require considerable consultation with stepper motor suppliers, whose cooperation can justifiably only be sought once a firm decision to develop and build an attachment has been made. However, in order to complete the attachment mechanical layout and feasibility assessment, and also form the basis of a future detailed specification, a suitable motor and timing belt drive has been selected (see Appendix C6) and several basic control schemes of varying complexity are proposed and compared. The technical feasibility of the schemes was checked by reference to various trade publications (manufacturers catalogues and application notes) [29, 30, 31] and a useful recent textbook by Kenjo [32] in which up-to-date theory and application,of stepper motors and their control,is reviewed and illustrated by practical examples.

7.5.2 Selection of stepper motor and timing belt drive system.

The selection procedure for a stepper motor 2(2,3) and timing belt 3(1,2,3) and pulleys is presented in Appendix C6. A motor manufactured by Berger Lahr GmbH has been chosen, because it appears to offer smoother and more precise operation than in general: according to the manufacturer this is chiefly because of its unique 5-phase construction providing 500 steps per revolution, and a correspondingly small step angle of 0.72^{o}. (A more common 'standard' is 200 steps/rev.). The motor will run at 3 x the speed of the profiling mechanism and at 9 x the speed of the workpiece on the host lathe. Therefore, for each full rotation of the workpiece 4500 pulses need to be applied to the motor control circuits, and each step will correspond to a workpiece rotation of 0.08^{o}.

Ignoring friction, the torque required to maintain constant mechanism speed alternates such that the motor has sometimes to assist and at other times to resist the motion of the mechanism, and so will tend to cause backlash in the drive system. This can be reduced, to some extent, by adjusting the timing belt tension; however, a better method is to utilise

the friction torque which will arise in the bearings of joints J1 and J3, as explained in Section 7.3.1. The bearing friction can be controlled, by adjusting the bearing preload, to ensure that the drive system is always required to assist the mechanism motion and is subjected only to varying, not alternating, torque.

7.5.3 Control system

The basic requirement of the control system is to achieve and maintain the correct speed ratio and synchronisation between the workpiece and the mechanism during profile grinding.

The two basic elements of the control system are the workpiece rotation sensor, or 'encoder', and the electronic input controller of the motor drive circuits. There are various options in each case and although the choice of each is not entirely independent they are discussed separately.

7.5.3.1 Speed sensor.

Although many types of sensor, employing various principles based on various optical, magnetic, mechanical, and other effects, are capable of generating a digital signal to indicate rotation of an element, they may not all achieve sufficient precision economically.

Possibly the most common sensor used for this type of precision application is the optical encoder. It basically consists of a transparent disc, with accurately spaced, regular line markings, which is coupled to the shaft being monitored. As the disc rotates with the shaft, the markings interrupt a photo-electric beam and as a consequence, for each interruption, an electrical pulse is generated. There are two fundamental encoder types; 'incremental' and 'absolute'.

In an incremental encoder, the simplest, each line is marked identically, except perhaps for a single individually identifiable zero datum line, and position is known only by recording the sequence of increments from a definite starting position; whereas, in an absolute encoder each line has an individual pattern or code which can identify the absolute position directly.

The number of lines and thus the angular resolution and pulse rate can be varied to suit the application: in this case this depends mainly on the stability of workpiece speed and on the controller sophistication.

At first sight the most obvious choice is to use an incremental encoder directly coupled to the work spindle and producing the exact number of pulses required to drive the motor at the correct ratio: that is 4500 pulses for each full workpiece revolution, which will rotate the 500 step Berger Lahr motor through 9 revolutions. In this case the motor would follow very closely any variation in workpiece speed. If the workpiece speed is sufficiently stable the encoder resolution (number of lines) could be reduced and the input controller used to interpret and generate the correct motor step rate. In the limit the encoder could be reduced to 1 line per revolution, in which case, angular resolution is large (360^{o}) but exact, this would significantly simplify the type of encoder required, with any simple, optical, or perhaps magnetic or even mechanical sensor becoming suitable. However, the motor would now only respond to speed variations occurring over several revolutions. The principal determining criterion is, in essence, that; any variation of the workpiece speed between successive encoder lines should not exceed that which would cause unacceptable profile error, due to the temporary synchronisation error and the consequent angular deviation between the mechanism and workpiece.

The final choice of encoder will also depend on the input controller and may be a compromise between the sophistication of each.

7.5.3.2 Input controller-alternatives

The maintenance of synchronisation at speed is relatively easy; it is the initial attainment of synchronisation which is the most difficult control task and which will primarily determine the input controller design. As well as at start-up this will also have to be performed after any interruption to the profiling operation, perhaps for workpiece measurement or grinding wheel dressing purposes, during which synchronisation may be disrupted.

Many possible control schemes may be envisaged, and four basic categories may be summarised as follows, in increasing order of complexity:

(i) Workpiece and mechanism synchronisation is physically set-up by the lathe operator prior to both lathe and mechanism motors being switched on.

(ii) With the workpiece stationary, the mechanism is synchronised by the operator by electrically stepping the motor into position.

(iii) After both workpiece and mechanism are running at the correct speed the operator can manually adjust the phase of the motor and the workpiece by modifying the pulse rate to the motor. The phase can be indicated by counting the number of steps separating an encoder reference pulse and a motor reference step which should coincide for position synchronisation.

(iv) Similarly to scheme (iii) except that the synchronisation by phase adjustment is performed automatically by a microprocessor using simple logic.

Although the first scheme requires the simplest electronic input controller, especially if the encoder produces the exact pulse rate for the motor, it will also be the most cumbersome and time consuming for the operator to employ. This is improved in scheme (ii) by using a relatively simple electrical step by step motor drive circuit under operator control.

However, both these schemes risk loss of synchronisation, during start-up, if at any stage the acceleration of the workpiece exceeds the maximum acceleration capability of the stepper motor: there is a maximum step rate at which the motor torque can accelerate its load and it will not keep up with any reference pulse rate above this.

In Appendix C6.5, it is estimated that the chosen Berger Lahr motor will be able to accelerate up to operating speed in under 72 degrees of mechanism input shaft rotation; the workpiece acceleration will depend on the power of the lathe and on the workpiece size. From general, casual observation, it seems unlikely that the workpiece will reach full speed before the stepper motor (i.e. in under 24 degrees of workpiece rotation). However, this is uncertain and needs to be investigated further; especially at the moment when the lathe motor is switched on in case a starting kick occurs just as the stepper motor has to overcome

starting friction.

If this problem does arise, it could be overcome although perhaps not economically, by choosing a more powerful stepper motor and/or increasing the timing belt drive ratio. An alternative solution would be to use an electronic 'pulse buffer' in the input controller.

If the reference pulse rate exceeds the maximum step rate of the motor, during acceleration, the pulse buffer delays the transmission of pulses to the motor, thereby effectively storing incoming pulses and releasing them at a suitable rate for the motor. As workpiece acceleration eventually reduces and it reaches operating speed, the buffer continues the lower acceleration of the motor, until the motor step rate slightly exceeds the reference rate and speed of the workpiece so that the stored pulses are used up, at which point synchronisation is re-established and the reference and stepping rates are equalised again. Depending on the severity of the problem the pulse buffer may be achieved by an electric circuit which may even be commercially available, or a microprocessor.

The problem of initial acceleration rates is avoided completely using the remaining two schemes (iii) and (iv) above, by performing position synchronisation after speed synchronisation. Of these, the last (iv) is more sophisticated, but the extra cost of using a microprocessor, if any, is probably more than adequately offset by the operator time saving achieved. Furthermore, a microprocessor allows greater flexibility in the selection of an encoder.

7.5.3.3 Control system summary

Based on the preceding arguments, the most likely control system to be implemented, would consist of an incremental optical encoder with sufficient resolution to detect any significant workpiece speed fluctuations and a microprocessor-based input controller to direct the electric drive circuits of the stepper motor.

The electronics would all be housed in a control box, independent of the attachment and host lathe. The encoder would be mounted on the lathe and coupled to the main spindle, as most convenient; this may require customised encoder design. A basic control system is shown schematically in Fig.7.2.

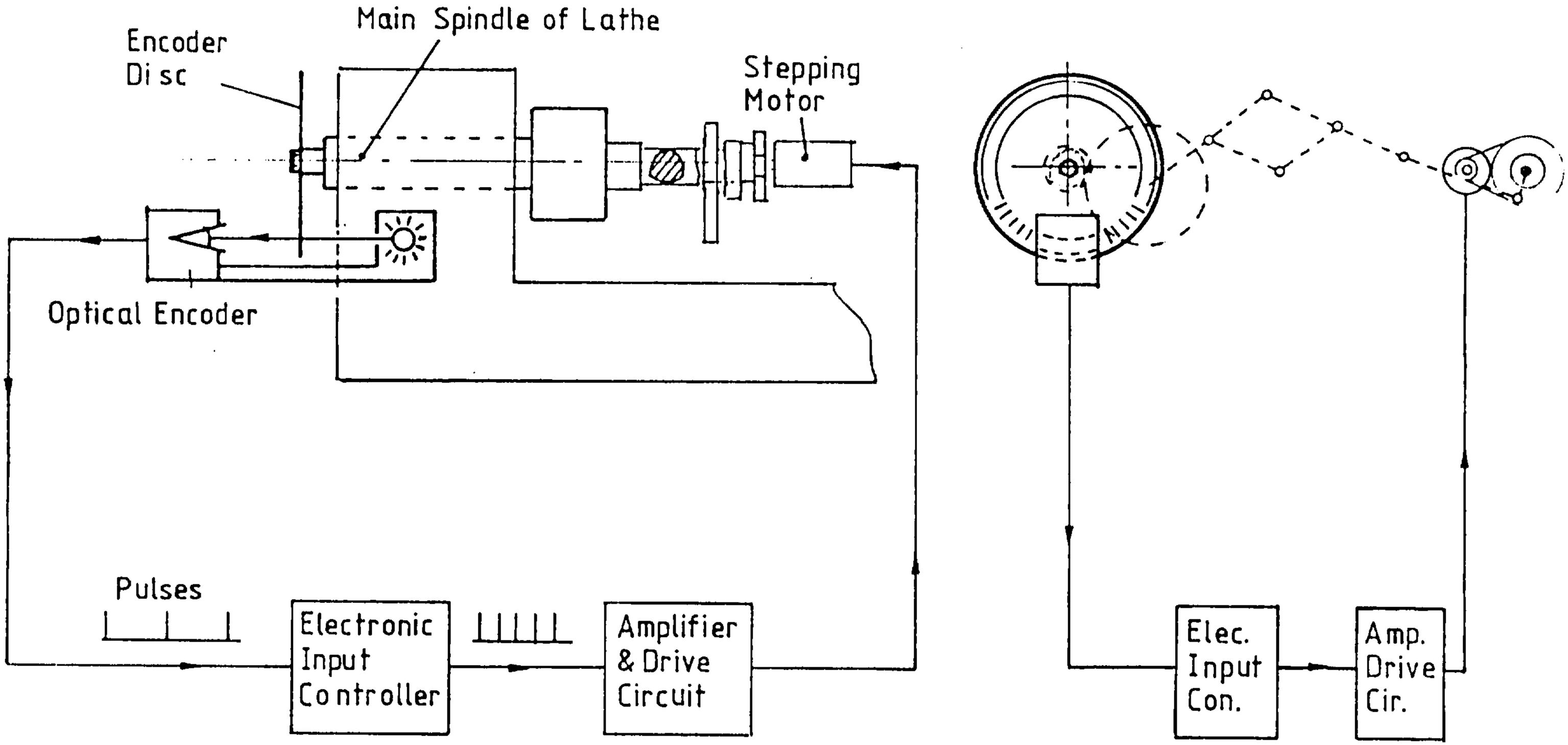

Fig. 7.2 Basic control scheme for stepper motor.

7.6 GRINDING SYSTEM

The general specification of the grinding system was given in Section 4.2.3, and the system is shown in most detail in Drawing No.7.

The grinding spindle 9(2,7) is based on commercially available designs [14, 15]. The spindle dimensions shown in the drawings are representative of those for various types of spindles which may be used specifically for internal, external or universal grinding according to their internal design. The actual choices of spindle will depend on the intended usage.

The electric motor 10 is also representative of various suitable motors, which may use a similar frame size (in this case Frame 5, according to BS.4999, [33]), such as a 0.55 Kw 3 phase A.C., drip proof, totally enclosed, NECO motor.

During profile grinding,the grinding spindle is subjected to continuous motion by the profile generating mechanism and the power drive from the motor must have a continuously variable geometry. To achieve this, power is transmitted through two flat belt pulley drives 11,12 interconnected by a common twin pulley 53 whose bearings also serve as the joint connecting the two supporting links. A horizontal link 54 carries the first belt 11 from a pulley 55 at the motor to the twin pulley and a vertical link 56 carries the second belt 12 from the twin pulley to the grinding spindle pulley 57.

Both links contain a structural bolted joint with which to adjust the belt tensions and also enable them to be fitted.

The lower end of the vertical link is supported on a plain bearing 58 mounted on the outside of the grinding spindle housing, the upper end carries a bearing shaft 59 to support one side of the twin pulley. A pair of angular contact ball bearings 60 are mounted back to back to resist the vertical belt tension and the overhanging load (weight and dynamic load) of the horizontal belt drive. A similar arrangement supports the horizontal link at the other side of the twin pulley.

A more elaborate arrangement is used to support the horizontal link and the pulley at the motor. An extension shaft 61 is fitted to the motor output shaft 62 using a Trantorque mounting device 63.

(The Trantorque device consists of a tapered inner collet-like element and a matching outer sleeve. A controlling nut expands the device in the hub and contracts it on the shaft therefore providing space saving locking of hub and shaft, [34]). Another Trantorque device 64 locks the pulley on to the end of the extension shaft. The horizontal link is supported by bearings 65 on the extension shaft, between the pulley and the motor.

Three deep groove ball bearings are used, one separated from the other two, to resist the force and couple exerted on the link by the belt tension.

The speed of the grinding wheel can be set by appropriate selection of pulley diameters at the motor and grinding spindles, and also by electronic speed control of the motor.

7.7. OTHER DESIGN FEATURES

Although not shown in the drawings, any attachment built should be furnished with suitable covers and seals both for operator safety and dirt exclusion.

Safety covers should as far as possible, without restricting operations, prevent access to any of the moving parts unless the grinding and mechanism motors are switched off, when they should allow easy access to adjustment mechanisms for setting up purposes. The R4 adjustment in particular may need frequent access.

Separate covers for various parts of the attachment may be most appropriate, e.g. the grinding wheel drive belts.

The grinding wheel is shown with a safety guard 66, which should conform to safety regulations [35].

Grinding swarf and fluids should be excluded from working parts, especially bearings and slideways. To help in this, grinding debris should be directed and guided away from the mechanism and operator. A vacuum device would be most suitable.

Simple space-efficient sealing arrangements for the bearings are shown in the drawings.

The taper roller bearings are all sealed by felt contact seals, and the smaller needle roller bearings are supplied with contacting lip seals. The large needle roller bearing of joint J2 is simply fitted

with rings to provide non-contact narrow gap sealing. This method is also used in the grinding pulley bearings.

In all cases grease is intended to be used, because of its greater sealing ability than oil.

The most difficult to protect is the linear bearing shaft 32; covers 67(1) are fitted which have slots to allow link R4 to traverse.

CHAPTER 8

FEASIBILITY OF THE DESIGN

8.1 INTRODUCTION

Considerable preliminary assessment of the design was described in Chapter 6 and now that the detail design layout has been presented in Chapter 7, a final assessment can be made. First the influence of various sources of errors are considered separately; in addition to the mechanism tolerances, clearances, and deflections, the other factors considered are the accuracies of the mechanism mounting on a host machine, of the various setting adjustments and their mode of operation, and of the grinding process itself.

The cumulative influence from all sources is then assessed. Proposals for further developments are also discussed and their effect on profile accuracy considered. The Chapter concludes with a final assessment of the technical feasibility of the design to meet the original objectives specified in Chapter 4.

The notation of Figs.6.1, 6.2 and 6.3 is again used throughout this Chapter.

8.2 INFLUENCE OF MECHANISM TOLERANCES ON PROFILE ERROR.

8.2.1 General

The principal conclusion of the error analysis of tolerance - derived deviations is that, despite the high precision specified for the mechanism's kinematic accuracy (see Sec. 4.4), much lower precision may be specified for its components because of the considerable profile error compensation that can be achieved. The various means of compentation have been discussed for the ideal mechanism, in Sec.6.8; and their implementation in the practical design is relatively straightforward and effective, thus removing most of the kinematic constraints upon tolerance specifications. In fact, the main constraints on tolerance specification are those which would normally be imposed to facilitate assembly and efficient smooth running of the mechanism, and concern, in particular, form errors such as parallelism and perpendicularity in order to avoid misalignment of bearings.

The constraints on tolerances for the main areas of the design are summarised below.

8.2.2 Profile generator mechanism.

The tolerances which directly affect parameter deviations are those of position and parallelism of bearing housing bores and shafts, and the radial run-outs of the bearings themselves. Any misalignments of shafts due to parallelism errors (in planes, perpendicular to the kinematic co-planes of motion) are assumed to cause constant deviations (in an appropriately chosen kinematic reference plane) which can be allocated to parameter deviations, in the same way as positional deviations, and be compensated just as effectively.

The radial run out of a bearing inner or outer ring is the total radial displacement measured by a fixed indicator locating against the outer ring, as one ring rotates through a full revolution while the other ring is held stationary. The outer ring (or race) is rotated in order to indicate outer ring run-out, and the inner ring rotated in order to indicate inner race run-out. The run-out of the outer race will contribute to the parameter deviations of the link containing the bearing housing, and that of the inner race, if one is used, will contribute to the parameter deviations of the link containing the bearing shaft; the deviation being equal to half the run-out. It is assumed that the radial run-out is principally composed of concentricity error, and that roundness errors are insignificant. This seems reasonable since the load in a bearing is supported by many elements (rollers) on a large proportion of the circumference (all of it, if preloaded) which should average out the effect of such errors. Furthermore, the specified run-outs which are presented in Appendix C4 are those measured in the unloaded state and these normally reduce when the bearing is loaded

The parameter deviations caused by these tolerances can all be compensated by adjustment either intrinsically during operation (R1, RL1, RL3) or extrinsically during setting-up (R2, R3, R4) and assembly (RL1, RL2, RP2, RP4, RL4), thus, effectively removing all kinematic constraints on the tolerance specifications.

Therefore bearings of normal precision (Class 0) and their associated shaft and housing tolerances as specified by bearing manufacturers should be adequate. And even some of these tolerances concerning parallelism and perpendicularity may not need to be as strict as recommended since the design of the attachment is such that it is relatively insensitive to misalignment. In the horizontal plane, the flat bearing pads on the bed-plate allow the housings, and thus the centrelines of joints J1, J2 and J3

to self-align during setting up. In the vertical plane, perpendicular to the kinematic plane, although there is no adjustment, the effects of misalignments are mitigated by the linear bearing of joint J2L: this can also rotate and thus does not resist any misalignment in a plane perpendicular to its axis and since it is always orientated close to the horizontal (the maximum angle of R4 with the horizontal $\simeq 17^{o}$ for an eccentricity ratio of e = 0.15) it effectively de-couples the vertical plane alignments of joints J1 and J2. The linear bearing J2L also alleviates, in similar fashion, the effects of misalignments caused by perpendicularity errors between the housing bore of joint J3 in link R4 and the linear bearing J2L and between the latter and the inner ring of the rotary bearing J2R. However, it cannot alleviate the effects of any misalignment between the shafts, of joints J1 and J3 on link R3, the main drive shaft: this rotates completely and thus, twice per revolution the plane of misalignment will be parallel with the axis of the linear bearing at which time the full effect of the misalignment will be passed on to the linear and rotary bearings J2L and J2R. Therefore the strictest tolerances should be on parallelism of the shafts of J1 and J3 and possibly, by implication, on their respective perpendicularities with the dovetail slides of the R3 eccentricity adjustment, depending on the method of manufacture; ie.the slides could be assembled and locked before finishing the shafts as an integral component.

8.2.3 Pantograph tolerances

The profile errors due to pantograph tolerances can be significantly, intrinsically compensated, as size and rotation errors, within limits as explained in Sec.6.8.2. Various combinations of joint centre-distance tolerances and bearing precision classes are considered in Appendix C4.2 and their equivalent allocation to a single parameter P1 estimated. Comparing these,with reference to Table C4.1,it can be seen that the remaining profile error can be limited to $\pm$ 1μm, using IT8 position tolerances and normal (Class 0) precision bearings, or to much less with higher precision grades, all reasonably attainable.

Therefore, here again, it is assumed that negligible profile errors due to pantograph tolerances can be achieved.

Adequate parallelism tolerances to avoid bearing misalignments within the pantograph should be readily achieved during manufacture because of the simple design of the components. And the flat bearing pad

on the bedplate allows the whole pantograph to align horizontally with the generating mechanism, as determined by the needle roller bearing of joint J4 as shown in Drawing No.6. However, this bearing may have to be replaced by a self-aligning bearing to allow for vertical misalignment between the pantograph and generating mechanism, in which case, the automatic horizontal alignment would be lost and would then have to be set by mounting the pantograph on pre-aligned slideways or, less efficiently, by guidance from the grinding system transmission. Otherwise the tolerances on parallelism in the vertical plane, for both pantograph and generating mechanism may need to be restricted (this is discussed further in Sec. 8.2.5). The pantograph bearings should be able to tolerate misalignments larger than the recommended allowable misalignments because the bearing loads are relatively very low (since the bearings were primarily selected for high stiffness) and the equivalent operating speeds (given by [28] : oscillation frequency (=90 r.p.m.) x oscillation amplitude ($\simeq 15^{o}$) $\div 180^{o} \simeq 7.5$ r.p.m. for eccentricity R3 = 0.75 mm) are also very low. Kinematically, the profile should be insensitive to any misalignment of the whole pantograph because of inherent compensation due to the basic nature of its operation: that is, any input deviation due to misalignment will be compensated by equal and opposite output deviation. Any resulting misalignment of the grinding wheel would be corrected by truing and dressing operations (see Sec. 8.5.3.1).

8.2.4 Stepper motor drive tolerances.

The kinematic accuracy of the stepper motor and timing belt drive is analysed in Appendix C6.6. Any errors will cause a loss of synchronisation between the mechanism and the workpiece; i.e. an angular deviation which may be represented as an equivalent deviation of parameter RL3. But, unlike other mechanism tolerances, these will cause varying deviations due to the changing alignment of drive components during rotation.

One source of error not included in the analysis is that to do with workpiece speed measurements and electrical pulse generation by the optical encoder and electronic stepper motor control. These are assumed to be capable of sufficiently greater precision than the other

components to be considered relatively insignificant, e.g. pulse generation accuracies of $\pm$ 0.3'(min. of arc) are possible for Gaebridge [31] incremental encoders compared to $\pm$ 3.0' for the motor step accuracy.

The equivalent RL3 deviations resulting from the cumulative tolerance of the drive system components when in the worst possible alignment are presented in Table C6.6.4 (of Appendix C6.6) for various mechanism settings. The maximum profile error will equal these RL3 values if they happen to occur at a mechanism position when the profile is most sensitive to them. Such errors would obviously be significant as most of them actually exceed the IT4 tolerance specified in Sec. 4.4 for the whole mechanism. However, such an extreme set of circumstances should be rare and although a more accurate analysis could be attempted to establish more realistic values this seems unnecessarily cumbersome for the present requirements. Several factors indicate that actual tolerances should be much less than those tabulated, such as:

(a) even assuming the worst alignment occurs the probability of a combination of components giving rise to the maximum deviation in Table C6.6.4 is only 0.27% (if a tolerance zone of $\pm 3\sigma$ and normal distribution is assumed).

(b) the most probable non-alignment of components in extreme positions,

(c) the most probable non-alignment of the maximum deviation with maximum sensitivity of profile,

(d) as some of the alignments vary during motion, the extreme deviation is not likely to repeat very often (i.e. within a few revolutions); thus only profile errors which are undersize are likely to remain since oversize errors would most likely be removed during a subsequent revolution of the workpiece, and associated pass of the grinding wheel, when the deviation is smaller.

Furthermore, several improvements could be made, if necessary, to encourage the occurrence of the preceding factors.

(i) Those components which are in fixed alignment with each other could be deliberately assembled to minimise errors, e.g. the eccentricity of a pulley could be aligned opposite to that of

its locking bush on the shaft. Also any eccentricity of the pulley on the large shaft could be aligned to minimise profile sensitivity (maximum eccentricity aligned with R3 direction, taking account of a 90^{o} phase shift of angular error with pulley eccentricity).

(ii) More selective assembly and rejection of components with extreme dimensions.

(iii) The transmission ratio could be changed to ensure non-repetition of extreme alignments at the same position on successive cycles of the mechanism.

(iv) Finally, the assessment above was based on the use of standard precision components as commonly supplied by manufacturers; higher precision components could be used if necessary.

Thus a qualitative assessment suggests that although transmission errors may be significant, they will be much less than those tabulated in Table C6.6.4, except in very exceptional circumstances. If it were necessary there is considerable scope for improvement by reasonable measures, some of which can easily be checked by experiment. For consideration in later arguments, assume error can be restricted to < 25% of IT4 tolerance grade.

8.2.5 Attachment mounting tolerances on host machine.

Mounting of the attachment on the host machine with sufficient accuracy is not expected to present major difficulties. Ideally (see Fig. 6.1) the centrelines of the fixed, or frame, joints, J1 and J2 in the generating mechanism, and J7 and J8 of the pantograph pivot, all should be parallel with, and lie in, the same horizontal plane as the workpiece centreline. However this may be modified without incurring any profile error, to allow J1 and J2 to lie in a different parallel plane to that of the workpiece as long as the pantograph pivot lies in another parallel plane mid-way between them.

Errors in centre height will be due to the deviation of the bedplate thickness and of the centre height of the workpiece above the cross-slide on the host machine, as well as of the centre heights of generator joints J1 and J2 and the pantograph pivot above the bedplate. There is no need to impose strict tolerances upon these.

Internal adjustment during assembly, as described in Sec.7.3.5, compensates for the 2nd order errors which are due to relative height deviations of the J1 and J2 bearing assemblies, and the common height deviation (within reason) of the attachment with the workpiece will cause only 1st order errors of size and rotation which will be compensated intrinsically during operation. However it is still advisable to adjust height reasonably accurately using shims or by adjusting the pantograph pivot height perhaps by using an eccentric mounting shaft as described in Sec. 7.4.

Any misalignment in the kinematic vertical plane (causing rotation about an axis parallel with workpiece) will cause similar errors to centre height deviation, although a slight second order error may be introduced due to the induced height deviation of J2 relative to J1. However these can all be compensated in the same way as, and together with, any height adjustment as described above.

Misalignments in the horizontal plane (rotation about a vertical axis) will effectively foreshorten the eccentricity in the horizontal direction but not in the vertical direction so that the cutting point will follow an elliptical path rather than a circular path. The maximum error will occur at the maximum and minimum radii of the profile thus causing profile error, similar to an eccentricity form error, together with a size error which should both be capable of substantial compensation. Again, however, the mechanism should be aligned as accurately as possible by adjusting bedplate positions on the cross-slide. Alignment could be checked by grinding specimen profiles. For R3=0.75mm it would take 3^{o} misalignment error to cause 1 μm maximum profile form error without any compensation (for R3=7.5, 1 μm caused by 1^{o} error).

Misalignment in the non-kinematic vertical plane (rotation about an axis perpendicular to the workpiece axis) will present the greatest difficulty as with internal mechanism vertical alignments.

The eccentricity will again be foreshortened, but in the vertical direction, causing the cutting point to follow an elliptical path. In this case the maximum error will occur near the position of maximum slope,

or pressure angle, of the profile, in between the maximum and minimum radii which themselves will be unaffected. This will cause errors similar to those of R4 deviation after FEED compensation or similar, but opposite, to those of R2 deviation, thus suggesting possible compensation methods. (see Sec.6.8.2).

There is no direct adjustment of this alignment, except by differing shim heights at each side of the mounting surface between the bedplate and cross slide. The bedplate could be mounted on adjustable feet, probably the best method, but this will reduce the overall rigidity of the mechanism and the grinding wheel. The effects of this could be determined experimentally.

Alternatively, in view of the vertical alignments also required within the mechanism (see Secs. 8.2.2 and -.3) it may be preferable to restrict their tolerances. The necessity for this may be judged by estimating the effect of misalignment as follows:

The maximum profile error $\simeq$ (the 'eccentricity foreshortening') x sin ψ_2,

where ψ_2 is the orientation angle of R4 with horizontal ($\simeq$ 16.7 degrees) when R3 is in a vertical position, and 'eccentricity foreshortening' = eccentricity R3 x (1- cos (misalignment angle))

Thus a maximum profile error of say 1 µm would be caused by a vertical misalignment of 5.5^{o} . or 1.7^{o} . for eccentricities R3 of 0.75 mm or 7.5 mm respectively.

This is very large compared to general machine tool accuracies and it should be possible to achieve much lower misalignments without resorting to special adjustments or particularly high precision, machining tolerances. The geometric accuracy of grinding or milling machines, for instance, may be of the order of 1000 x better than required above (angularity errors within 0.01/100(=0.006^{o}) to 0.001/100(=0.0006^{o}) may be achieved).

It is therefore concluded that mounting tolerances should not add significantly to profile errors and can be assumed to have negligible effect.

8.2.6 Final conclusion of tolerance analysis.

The preceding analysis indicates that the influence upon profile accuracy of most tolerances concerned with the production, the assembly and the mounting of the attachment, can be considered negligible without resorting to very high precision grades. The main area of doubt concerns the stepper motor drive system. However, there is ample scope for improvement, if found necessary, in practice.

8.3 INFLUENCE OF CLEARANCES UPON PROFILE ERROR

In the final design there are likely to be few clearances. The bearings of joints J1, J2L, J3, J8 and J9 will be preloaded, thus eliminating internal clearance. The needle roller bearings of joints J4, J5, J6 and J7, although originally intended to be preloaded, as explained in Sec.7.4, may run with small internal operating clearances. The loads on all these joints (J4-J7) are virtually uni-directional and therefore the clearances will effectively cause constant parameter deviations and can be compensated as such (see Sec.6.9). It should be noted, however, that the effective displacement may be greater than the internal clearance if the bearing load is an overhang load and tilting occurs. For instance, referring to Fig.8.1, if the needle rollers are 11mm long, the internal clearance is 10 μm, and the load is applied at 55 mm from the centre of the bearing, then the effective displacement at the load point is 50μm.

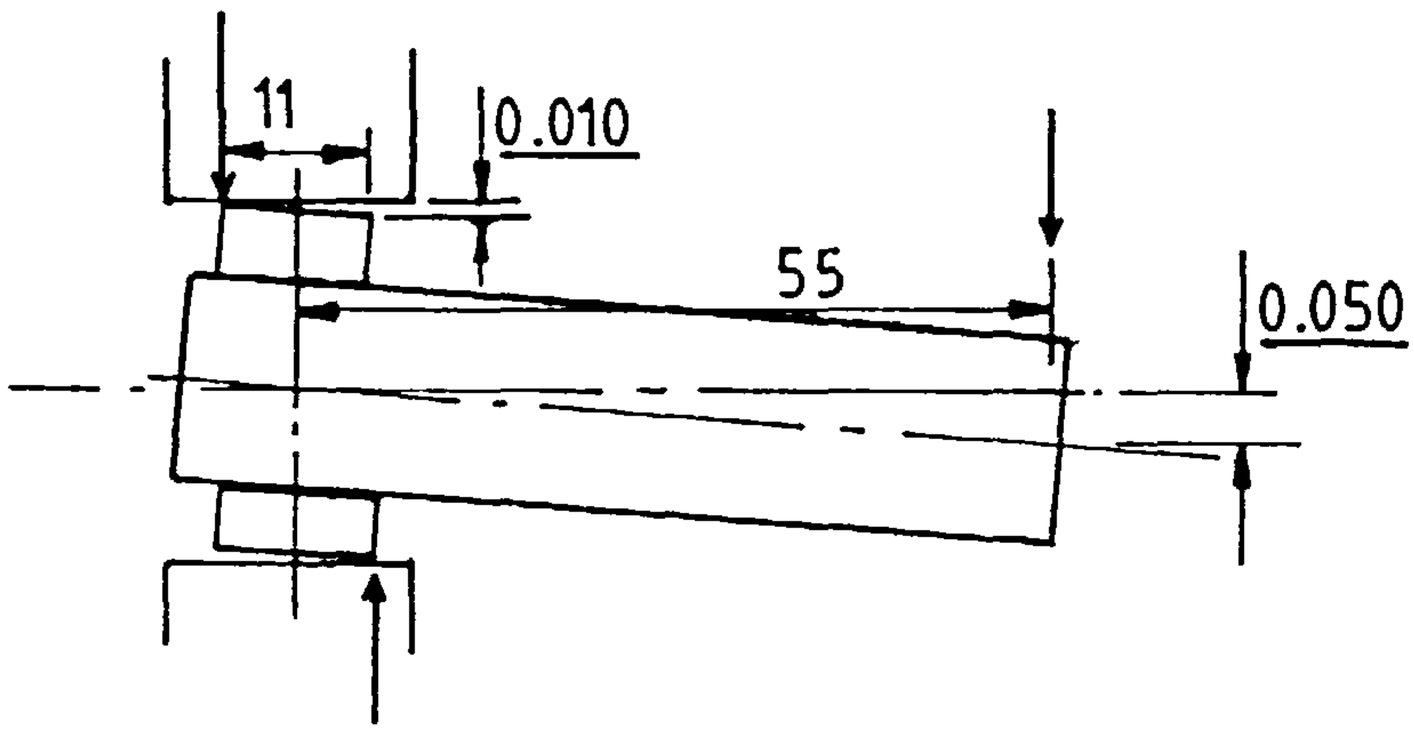

Fig.8.1 Tilting take-up of clearance in a joint.

Tilting of each link will be resisted by several bearings and the amount of overturning of the links will be determined primarily by the bearing with the smallest clearance, although relative stiffnesses will also be involved. This also poses a problem in the deflection analysis (see Appendix C3.13) when determining the couples acting at each joint, as the problem is statically indeterminate. To avoid this tilting, it would be preferable if at least one bearing on each link was preloaded or designed to resist overturn moments.

The only other bearing with clearance (between 30 μm and 60 μm in unloaded condition; less when loaded and running) is the needle roller of J2R for reasons given in Sec.7.3.3. Since the loads at this joint are uni-directional in all cases except the very worst (see Table 8.1 in Sec.8.4) the clearance can again generally be treated as constant. It occurs in the relatively insensitive RP2 direction, and will be compensated along with tolerances by the procedure employed during assembly as described in Sec.7.3.5. In the worst cases when the clearance may reverse direction, the resulting profile error will still be small (50μm RP2 deviation causes approximately 1 μm profile error, in the mechanism position when the reversed load occurs) and since it occurs at a point in the operating cycle when RP2 deflections (see Sec.8.4) are very small there will be no increase due to the cumulative effect (of 2nd order errors, see Sec.6.8.2).

There are no other clearances which directly effect kinematic accuracy and the general conclusion is that profile errors due to clearances will be negligible.

8.4 INFLUENCE OF DEFLECTIONS UPON PROFILE ERROR

8.4.1 General

The basis of the deflection error analysis and a brief preliminary assessment were presented in Secs. 5.12 and 6.10 respectively where it was predicted that the analysis could be much simplified because of the manner of mechanism loading and behaviour of various kinematic parameters.

The derivations of load-deflection formulae for the final mechanism layout shown in Drawing Nos. 1 to 7 are given in Appendix C3. Initially these were used individually during the iterative design process, as well as cumulatively in the computer performed deflection error analysis.

8.4.2 Simplification of deflection analysis.

The simplified cumulative assessment used relatively few of the mechanism loads and deviation parameters in its computer calculation because of assumptions, explained below, about the behaviour of various elements of the design.

8.4.2.1 Profile Generator.

Many of the components of the profile generator are symmetric about the axis of the main shaft (link R3) through joint J1, and variations from symmetry at different mechanism settings are small compared to the size of the components; and therefore their combined stiffness (to transverse loadings) is considered constant in all directions, and whatever the orientation of the loads, the deflections are assumed to align with them. Several other components, although not axi-symmetric, remain aligned with loads in any case, e.g. the linear bearing assembly J2L, by definition, only sustains loads normal to its axis of travel. The deflections of these can thus be allocated to deviations of parameters RP2, R4, RP4 and RL4 as explained in Appendix C3.10. Other components such as the bedplate are much stiffer in the horizontal than the vertical direction, and therefore will tend to deflect vertically whatever the resultant load direction and these deflections are allocated to RL1 deviation.

8.4.2.2 Pantograph

The greatest simplification is the allocation of all the deflections of the pantograph (including the grinding spindle) to deviations of only two parameters, P4 and P5, which can be calculated using only two load components. This is based on the following assumptions:

(i) Because of the relatively small input and output motion compared to the pantograph size, the distortion of the panto-graph geometry is sufficiently small to assume that its links remain mutually orthogonal.

(ii) The forces on binary links L2 and L3 always act axially and parallel to them and therefore, based on assumption (i), are assumed to act perpendicular to the axes of links L1 and L4.

(iii) The forces on links L1 and L4 can be resolved into components parallel and perpendicular to the links and thus can be expressed in terms of the forces on links L2 and L3 based on assumption (ii) and on the further assumption that the discrepancies due to the inertial forces of the links will be small.

(iv) Finally the deflections can also be derived in two component directions orthogonal to the link axes and since the profile errors due to all the parameter deviations in each of these directions are similar, they can be allocated to axial P4 and P5 deviations of the two mutually perpendicular links L2 and L3, and calculated using only the forces on these links.

The component formulae with their allocations to equivalent P4 or P5 error are given in Appendices C3.13 to -.20.

8.4.2.3 Stepper motor drive

The stepper motor and timing belt drive components will deflect under the action of the torque required to drive link R3 and cause angular synchronisation error, between the mechanism and workpiece, which can be allocated to equivalent RL3 deviation. The formula relating these deviations to mechanism torque is derived in Appendix C6.7.

Only the varying non-friction torque, as calculated by the dynamic analysis program MECHDYN (see Sec.6.4) is used in the calculation: the friction torque component (see Sec.7.5.2) is assumed to cause a constant angular deflection component causing only profile rotation which can be ignored.

8.4.3 Profile error due to individual deflection components.

The simplified deflection formulae and their parameter allocations are summarised in Appendix C3.21; all other deviations to parameters were considered as equivalent deviations to these, or as negligible and ignored.

The profile error due to each of these deviations occuring individually are shown in Figs. A10.1 to -.8 for the worst case operating conditions previously used in the preliminary analysis of Sec . 6.6. It can be seen immediately from Figs. A10.2 and A10.4 that deviations to RP4 and RL4 are also negligible and could have been ignored.

Comparing Fig.A10.1 with Fig.A10.3, demonstrates the difference in profile sensitivity to the deflections of the axi-symmetric components causing RP2 deviations and those of the more vertically deflecting components causing RL1 deviations: although the latter components have more than ten times greater stiffness they cause maximum profile errors of about half those caused by the former, for similar loading. The non-linear 2nd order (see Sec.6.5.2) profile error due to RP2 deflection reduces dramatically as the loads decrease (see Fig.8.2 and Table 8.1) for other settings of the mechanism; the linear 1st order error due to RL1 deviations will also reduce, but more gradually.

The error caused by the R4 deflection shown in Fig.A10.5 is significant despite the fact that the load in the R4 direction (see Fig. B5.8)is very much smaller than that normal to it (see Fig.B5.6)which causes the RP2 and RL1 deflections. The shape of the error characteristic for R4 deflections, indicates that it consists mostly of size and rotation error, which will be intrinsically compensated.

The error characteristics due to P4 and P5 deflections shown in Figs.A10.6 and A10.7 respectively, are fairly similar except in direction to those for constant P4 and P5 deviations shown in Figs.A7.16 and A7.17 respectively, reflecting the generally small variation in pantograph loads, and indicating their potential for intrinsic compensation similar to the constant deviations.

The profile errors due to R4, P4 and P5 deflections reduce significantly for smaller eccentricity, R3, settings, but not so much for other variations in settings.

Fig.A10.8 shows the profile error caused by RL3 deflection to be smaller than those caused by RP2 and RL1 deviation. But whereas the latter two decrease for larger profile sizes, the RL3 error increases (as shown by Fig.A10.24) because the torque on the stepper motor drive system increases as the eccentricity actual size increases for larger profiles, as indicated in Fig.8.2 and Table 8.1 (after Sec.8.4.7).

8.4.4 Assessment of total profile error due to deflections.

The total profile error characteristics caused by deflections are shown in Figs.A10.9 to A10.23 for a variety of mechanism operating conditions. The error variations, after compensation, are summarised

in Table 8.1 and Fig.8.2 which also indicate for comparison, the torque and force (on J2) variation, and the appropriate IT4 and IT5 tolerance limits.

The error due to the cumulative effects of the preceding individual deviations for the worst case (Sec. 8.4.2.4) is seen in Fig.A10.9 and again in Fig.A10.10 after size compensation, by FEED, where the remaining error varies by approximately 6 μm: this is outside the IT4 tolerance limit, and actually takes up all the IT5 limit. However if the operating speed is reduced (workpiece speed from 30 r.p.m. to 15 r.p.m.) the reduction in inertia loads reduces the error by over 50% as shown in Fig.A10.12 after size and rotation compensation (size compensation alone is shown in Fig.A10.11).

Alternatively if the grinding wheel radius and the dimension R4 are halved (from 40mm to 20mm) thus reducing the leverage exerted by link R4 about joint J2, the error is reduced by about 40% as seen in Fig.A 10.13.

For profiles of smaller eccentricity ratio e(= R3/R), the errors are much smaller. For the worst case, just considered above, but with eccentricity R3 reduced from 0.75 mm (e = 0.15) to 0.3 mm (e=0.06), the error is only 0.9 μm peak to peak. As before this also can be reduced further by operating at a lower speed or using a smaller grinding wheel, or both, as demonstrated in Figs.A10.14 to A10.17.

Figs.A10.18 to A10.23 show the profile errors, after size and rotation compensation (by FEED and RL3 deviation), for profile nominal sizes of 20mm, 50mm and 100mm mean diameters (R=10, 25 and 50 respectively) each with eccentricity ratios of e= 0.06 and e = 0.15.

It can be seen that profile errors are lower for the intermediate sizes but higher again for the largest sizes, so that for 100 mm diameter workpieces, Figs.A10.22 and A10.23 show that error variations of 15 μm and 2.4 μm occur for e = 0.15 and 0.06 respectively. This is almost entirely due to the influence of the increased torque on the drive system, the component errors due to RP2 and RL1 deviations having decayed enormously and those due to R4, P4 and P5 deviations being effectively compensated. This is illustrated by comparing the total error characteristics in Figs.A10.22 and A10.23 with those in Figs.A10.24 and A10.25

for their respective RL3 component errors only (note that the total characteristics have been distorted slightly during compensation). This influence could be reduced substantially by increasing the drive ratio with the stepper motor, whose deflection is proportional to $1/(\text{Ratio})^2$. Therefore a change from 3:1 to 4:1 would give approximately 44% reduction in RL3 deflection. This could be tried out during prototype trials, if found necessary or desirable.

8.4.5 Summary of deflection assessment.

The influence of deflections upon profile accuracy may be assessed with reference to Table 8.1 and Fig.8.2 (after Sec.8.4.7).

For all profile sizes with eccentricity ratio of e = 0.06 the profile form error is well within the limits of an IT4 tolerance grade. However for the largest eccentricity ratio considered of e = 0.15, only the intermediate sizes will have profile errors within IT4 limits, and then only just, unless the operating speed or grinding wheel size is reduced, as shown for a 10 mm diameter profile.

For the smaller sizes, when the generating mechanism loads and the profile sensitivity are greatest, the RP2 and RL1 deflections are most prominent, but at the largest sizes, when driving torque is greatest, the angular deflection RL3 due to the drive system dominates.

The deflections of R4, P4 and P5, vary little with changes in size and since they may be effectively, intrinsically compensated, they have little influence on actual profile error.

8.4.6 Accuracy of deflection analysis.

The results of the deflection analysis are less certain than most other parts of the assessment due to the large number of calculations involved, each containing various approximations and assumptions. However, the vast majority of these err on the safe side, therefore it is assumed that both the results for forces and deflections will represent over-estimates and there is no need to introduce a further safety factor. Furthermore, the majority of the errors should be systematic and therefore the general trends indicated by the results will be more accurate than the actual values.

Finally as stated in Chapter 6, all 2nd order sensitivity parameter deviations should be considered cumulatively, not in isolation and therefore the profile error due to the deflections of parameters RP2 and RL1 would be increased by the presence of similar deviations due to tolerances or clearances. However it is assumed here that compensation of the latter during assembly should restrict these to sufficiently low magnitude that the effect will be small, e.g. if other sources of RP2 deviations are 10% of the RP2 deflection deviations, the profile error will be 1.21 ($=1.1^2$)x that due to the deflection alone. In any case these will only affect the total profile error in the most adverse operating conditions for the smallest profile sizes.

8.4.7 Final conclusion of deflection analysis.

Mechanism deflections will have a significant influence upon profile error, especially for profiles with the larger eccentricity ratios, but which can be reduced by suitable choice of mechanism operational parameters, i.e. by reducing mechanism speed or grinding wheel size.

Figure	Mean Dia	Mechanism Set-up R1 mm	R3 mm	R4/RGW mm	Operating Speed ψ rad.s^{-1}	Profile error** µm	ISO Tolerances IT4 µm	IT5 µm	Torque Peak to Peak Nm	Force at J2 max / min N	variation N
A10.10	10.0	5.0	0.75	40.0	10.0	6.2	4(5)*	6(8)*	2.66	2940 - 50	2990
.12	"	"	"	"	5.0	2.7	"	"	2.15	2020 750	1270
.13	"	"	"	20.0	10.0	3.7	"	"	1.63	1890 390	1500
.14	"	"	0.3	40.0	10.0	0.9	"	"	0.79	1650 780	870
.15	"	"	"	"	5.0	0.4	"	"	0.75	1400 980	420
.16	"	"	"	20.0	10.0	0.4	"	"	0.43	910 340	570
.17	"	"	"	"	5.0	0.3	"	"	0.41	720 500	220
.18	20.0	10.0	1.5	40.0	10.0	4.7	6	9	2.84	1500 - 50	1550
.19	"	"	0.6	"	10.0	0.7	"	"	0.83	820 420	400
.20	50.0	25.0	3.75	"	10.0	7.7	7(8)*	11(13)*	3.2	590 30	560
.21	"	"	1.5	"	10.0	1.0	"	"	1.01	440 190	250

Table 8.1 (continued on next page)

(continued from previous page)

.22	100.0	50.0	7.5	"	10.0	15.1	10	15	3.85	300 40 — 260
.23	"	"	3.0	"	10.0	2.4	"	"	1.31	180 120 — 60

* The ISO IT values in parentheses are those for the next IT range of sizes where the nominal size lies at the upper limit of its IT size range:

e.g. for R = 5.0, nominal size = 10

ISO tolerance tables give { for sizes; over 6 to 10, IT4 = 4 μm
for sizes; over 10 to 18, IT4 = 5 μm

Thus sizes = 10; IT4 specified as 4(5), above. 5 μm is the more realistic value for a range of sizes starting at R $\geqslant$ 5 mm.

** Profile size error = maximum variation after intrinsic size and rotation compensation.

Table 8.1 Summary of profile error due to dynamic deflections for various operating conditions.

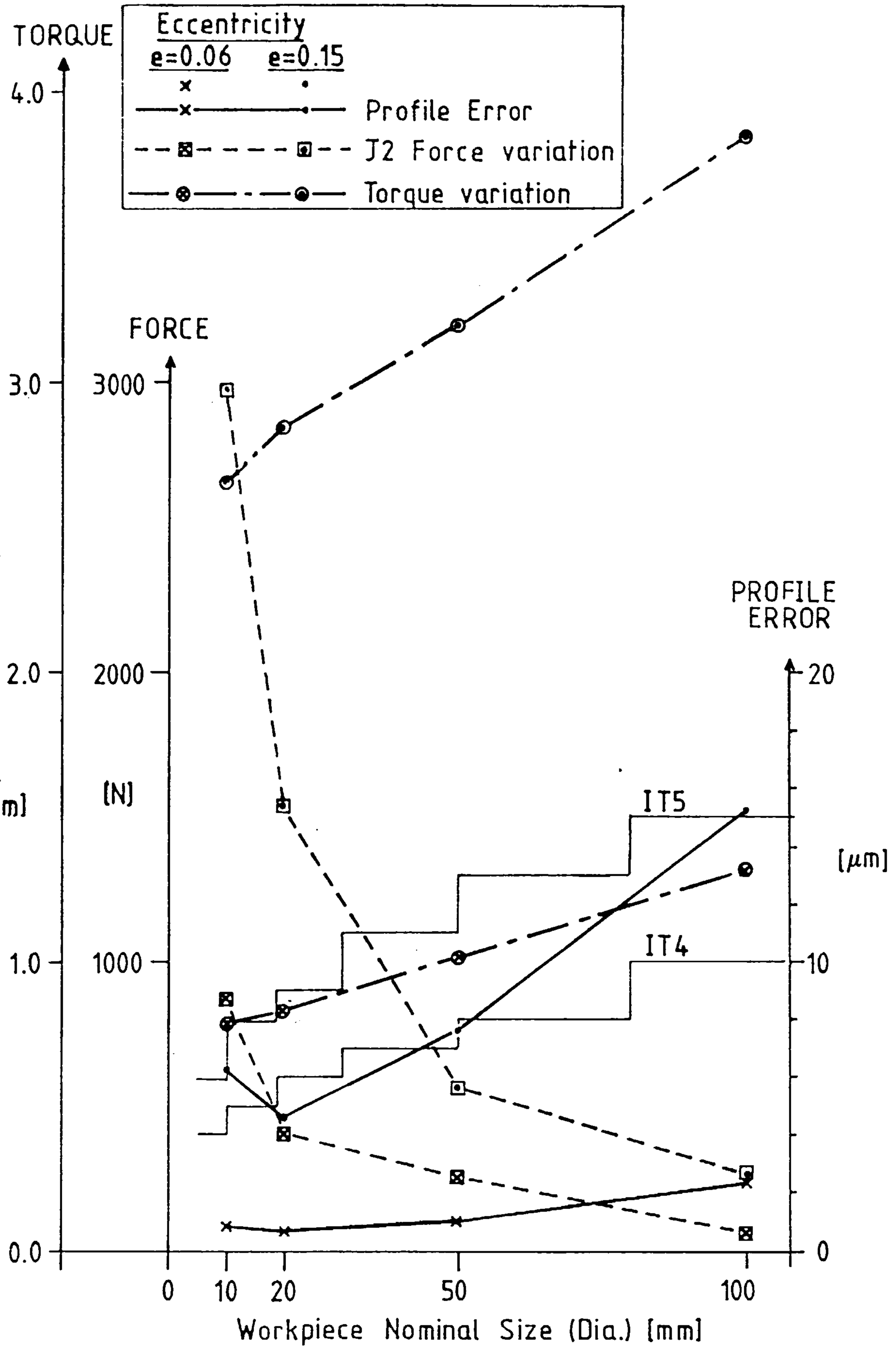

Fig.8.2 Profile error (due to deflections), torque, and force (on J2) vs. profile size and eccentricity. (RGW = 40mm and $\dot{\psi}_1$ = 10 rad.s^{-1} are constant).

8.5 INFLUENCE OF SETTING ACCURACY UPON PROFILE ERROR.

8.5.1 R2 adjustment (position of pivot J2 of orientation link R4).

The profile has such low sensitivity to parameter R2 as explained in Sec.6.5.2 that there should be no difficulty in setting it up. A simple scale (suitably fixed on the bedplate and read by means of a pointer fixed to the housing of J2, or vice versa) when used together with the adjusting screw (see Sec.7.3.4) will provide adequate precision. The screw dial has a resolution of 10μm per graduation interval; and a scale, with the precision of an engineers steel rule (to B.S. 4372 specification), will be accurate to within ± 0.1 mm over a 300 mm range [36]: and the range of R2 is only 25 mm. Fig. A7.3 shows that even for the worst mechanism settings, an R2 deviation of ± 0.1 mm will only cause profile errors of ± 0.13 μm (between 0.0 and -0.25 μm).

Thus the error due to R2 adjustment can be considered insignificant.

8.5.2 Eccentricity, link R3, adjustment.

8.5.2.1 General

The adjustment of R3 requires the greatest precision since it directly defines the eccentricity of the profile, whose form error is consequently 100% sensitive to setting errors.

Although the screw and dial setting mechanism (see Sec.7.3.2) has a fine incremental adjustment resolution of 1μm, its absolute accuracy over the full range of adjustment (0 to 7.5mm) will be much less precise (unless components to micrometer standards of precision are used) and it is only intended for setting R3 with reference to an independent, more precise, absolute measurement of eccentricity. Thus the overall accuracy of the setting will be determined by that of the independent measurement method, for which several alternatives are proposed and considered below. Only limited comment is made concerning their implementation using specific instrumentation.

The method adopted in practice will depend on the general precision required, and may even vary according to the specific precision required of individual workpieces.

8.5.2.2 Eccentricity measurement methods.

Three basic methods are proposed, as follows, in order of increasing precision:

(i) Direct measurement of mechanism eccentricity.

(ii) Direct measurement of a specimen profile in situ on the host machine, by either in-process or post-process gauging.

(iii) Direct measurement of a specimen profile removed from the host machine, to a separate inspection facility.

The first method (i) would involve the measurement of the total displacement or run out of a suitable mechanism component such as the housing of joint J3 during a full revolution of link R3 (the main shaft) which will be equal to twice the eccentricity.

The second method would involve similar measurement of the total run-out of a specimen profile determined by its maximum and minimum radii as shown in Fig.8.3.

The third method (iii) is all embracing of other methods since use may be made of whatever method and instrumentation is necessary to achieve the desired precision. Other errors of form could also be detected, not just that of eccentricity.

Whatever the instrumentation used, comparing the basic methods; method (i) is least precise because it only measures the actual setting of the link R3, and therefore will not detect any further eccentricity errors emanating in the mechanism between joint J3 and the profile, or from deflections in any part of the mechanism.

Method (ii) will intrinsically detect all eccentricity profile errors due to the mechanism, and thus eccentricity compensation becomes intrinsic rather than extrinsic as defined in Sec.6.7.1.

Method (iii) offers the highest precision of all since in addition to method (ii) it will also detect other errors introduced during manufacture, such as host machine work-centre running errors.

8.5.2.3 Measurement instrumentation.

The instrumentation used in any of these methods will again depend on the precision required. The simplest instruments to employ, as shown in Fig.8.3(a) for method (ii), would be standard dial indicator gauges (to BS907 precision standards) which can have an accuracy to $\pm$ 0.001μm, although this would only be achieved if used as a comparator with reference to suitable precision gauge blocks: the accuracy deteriorates, as the range

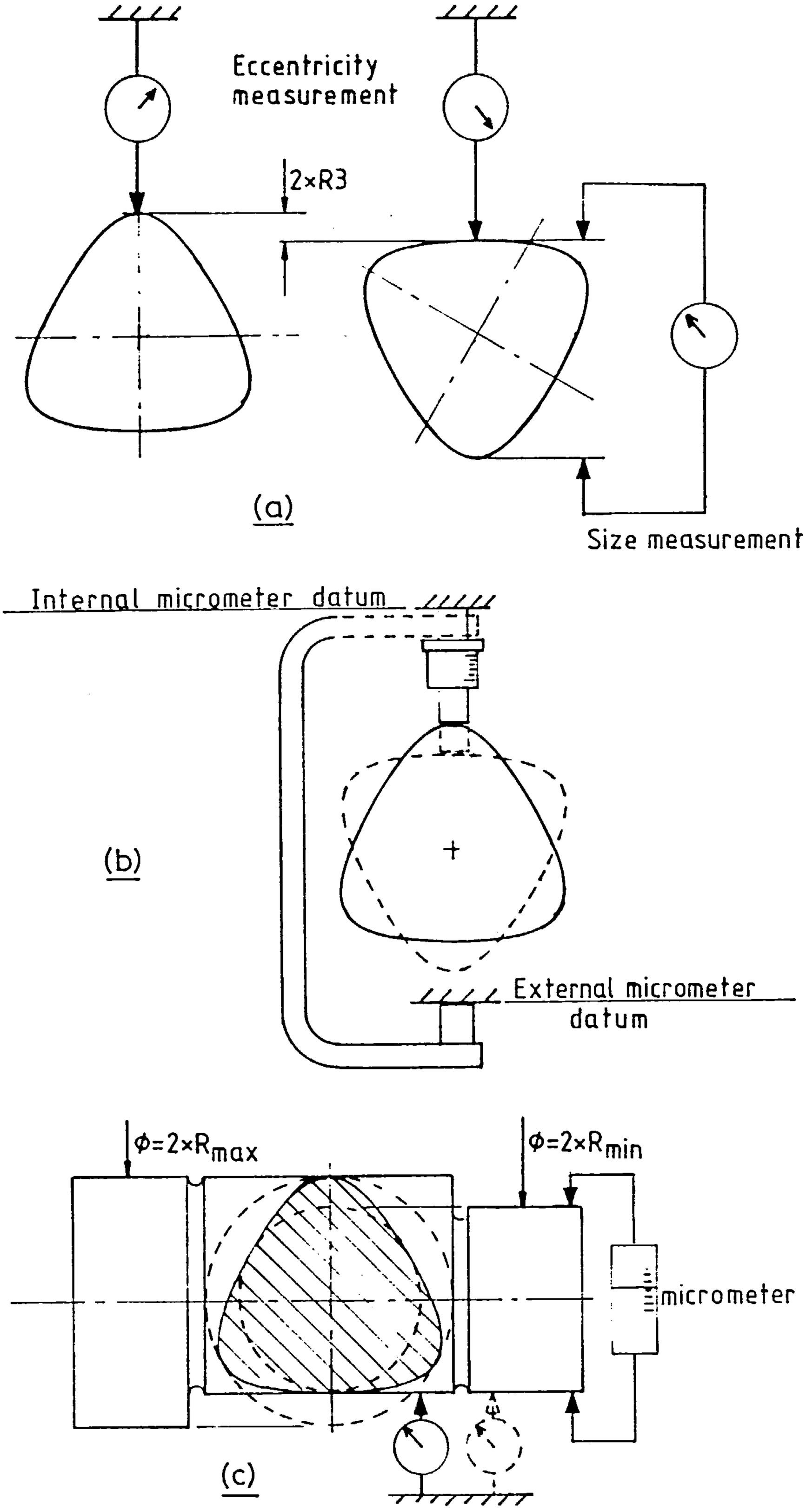

Fig. 8.3 Measurement of specimen profiles for setting purposes.

of measurement increases, to perhaps ± 20 μm for the full travel of the gauge. Micrometers could be used for more accurate measurement of the total run-out (= 2 x R3) (to within 3 μm over the full travel of micrometer according to BS870); these would require a suitably fixed datum to measure against, as illustrated schematically in Fig.8.3(b) for method (ii).

In the second method precision could be improved, perhaps, by locking the mechanism in each of its extreme positions and grinding on a specimen two cylindrical sections with diameters equal to those of the inscribed and escribed circles respectively, of the profile as shown in Fig.8.3(c): these diameters could then be measured accurately using a micrometer (perhaps in comparison with block gauges); the eccentricity being equal to a quarter of the difference in diameters.

An even better method may be to machine, by any means, two cylindrical sections nominally equal to the minimum and maximum profile radii, these could be measured accurately using a micrometer and then used as references for comparative measurements on an adjacent profiled section using a dial gauge utilising its high accuracy over a limited range.

For the most precise measurements purpose built comparators, of which there are many types, could be used.

8.5.2.4 Conclusion

The eccentricity adjustment can be set to virtually any desired precision; this will depend primarily on the accuracy of the independent measurement method and instrumentation which will ultimately be determined on the cost criteria.

For general purposes the most practically feasible setting method may be to combine methods (i) and (ii): initial setting can be made by method (i) and checked by method (ii) both methods using dial gauges. More accurate instrumentation may only be necessary in certain circumstances, e.g. when machining broaches.

8.5.3 Adjustment for grinding wheel size, R4 setting.

The dimension R4 must nominally be set equal to the grinding wheel radius, and therefore will need to be frequently readjusted to compensate for reduction of the grinding wheel size due to wear and the process of wheel dressing.

8.5.3.1 Grinding wheel dressing.

Dressing is the process by which the optimum texture of the grinding wheel cutting surface is maintained for efficient grinding. It involves traversing a dressing tool, commonly consisting of single or multiple diamond cutting points, across the grinding wheel cutting surface, as the wheel rotates, in such a way as to breakdown the crystal structure and remove the surface layer of the wheel to expose fresh cutting points.

The speed and depth of this traverse determine the surface texture and this can be varied to suit particular grinding operations, i.e. different surfaces are generally suited to rough, fine, and finish grinding. The depth of the cut, and thus wheel radius reduction, usually varies from 0.010 mm to 0.025 mm and the frequency of dressing will depend on the grinding operations required; it may be greater than once per workpiece ground.

8.5.3.2 Adjustment sensitivity

Since R4 deviations can be compensated substantially by in feed (see Sec.6.8.2) the effective sensitivity of the profile to the adjustment is relatively low. The sensitivity is affected by profile eccentricity, but not its size, although of course for larger sizes the constant sensitivity will effectively be smaller compared to the increased limits for a given tolerance grade.

For several eccentricity ratios, Table 8.2 shows, in column 2, the allowable R4 deviation for profile form error not to exceed 2 μm and conversely, in column 3, the profile error that would be caused by 100 μm R4 deviation. There is some ambiguity about the interpretation of this error. The 2 μm total variation, shown in Fig.A11.1 for e=0.1(R3=0.5mm) and for a deviation of +100 μm, could be interpreted as $\pm$ 1 μm about the mean size, including peak error at maximum and minimum radii positions: for a -100 μm R4 deviation the curve would be inverted and still be

considered as ± 1 μm error so that an R4 deviation of ± 100 μm produces ± 1 μm profile error. However, if the profile size is gauged by measuring only at the positions of the maximum and minimum radii, it will compensate for the R4 error in such a way as to produce zero error at these positions, leaving a profile error as shown in Fig.A11.2 ranging from 0 to +2 μm; for a negative deviation the error will range from 0 to -2 μm, thus the error for ± 100 μm R4 deviation would be ± 2 μm, double the previous interpretation. In view of the proposals of Sec. 8.5.2, this last interpretation should be used.

1 Eccentricity Ratio, e	2 R4 deviation to cause ± 2μm error	3 Profile error caused by 100 μm R4 deviation
0.06	± 250 μm	± 0.72 μm
0.08	± 150	± 1.3
0.10	± 100	± 2.1
0.12	± 70	± 3.1
0.15	± 43	± 5.1

Table 8.2 Profile error due to grinding wheel size adjustment.

8.5.3.3 Adjustment accuracy.

For the smaller eccentricity ratios, the resolution and accuracy of the adjusting mechanism should be adequate to set R4, to a known grinding wheel size, with sufficient accuracy to limit profile errors to almost insignificant proportions, much less than ± 1 μm. For the higher eccentricities, this precision could be achieved, if necessary, by using a micrometer or block gauges to measure the displacement of the slider of joint J4 relative to the slideway and screw mechanism; the zero datum having been previously measured or set during the assembly procedure outlined in Sec. 7.3.5.

The major restriction on accuracy will be the determination of grinding wheel size which will generally be unknown. Its initial size, after mounting and truing by the dressing tool to correct for concentricity, squareness and roundness error, can be measured with sufficient accuracy using a micrometer, however, it would be very inconvenient to do this repeatedly and as often as the size reduces and needs to be adjusted for.

Two more practical methods of keeping track of wheel reductions are proposed. The initial few stages in each procedure are identical; they only diverge at the last stages. The various stages are as follows:

1) The profile generating mechanism should be held stationary in a reference position using either the stepper motor or preferably a locking device (as yet to be designed) near to the grinding spindle.
2) Using the cross and traverse feeds of the host machine the grinding wheel can be dressed and initially trued by moving the whole attachment on the cross slide relative to a dressing tool fixed to the host machine bed.
3) The in feed will control the depth of dressing cut, and its position for the final cut can be marked on the feed indicating dial and this together with the fixed dressing tool will provide zero reference datums for the rest of the procedure.
4) The grinding wheel initial size can be measured accurately using a micrometer.
5) The initial dimension of R4 can be set.

There are two alternatives for the last stages;

6) After subsequent grinding operations, the wheel can again be dressed by repeating stages (1) and (2) and the reduction in grinding wheel radius can be determined by the deviation of the feed from its initial datum established in stage (3).
7) The dimension R4 can be readjusted to compensate for wheel reduction if it exceeds the allowable R4 deviation. Note: adjustment should return the attachment to the original feed datum when the wheel touches the dressing tool.

As an alternative to stages (6) and (7) the following may be adopted:

(8) After subsequent grinding operations the wheel can again be dressed by repeating stage (1) and then repositioning the attachment at the feed reference position established in stage (3). The depth of the dressing cut in this case can be set by reducing the R4 dimension: this will advance the grinding wheel towards the dressing tool by virtue of the pantograph action. Thus the grinding wheel size is automatically adjusted to the R4 dimension by the dressing tool, rather than vice versa as in stage (7).

The last method offers the best accuracy since the wheel size is governed directly by the R4 setting adjustment. The errors due to each successive adjustment will be non-cumulative and total error will depend mainly on the accuracy of the initial wheel measurement and R4 setting.

The first method may be preferable where lower eccentricities are concerned, since R4 may require adjustment less often than the dressing operations to remain within allowable limits.

In both cases wear of the dressing tool will change its datum accuracy, however this should be insignificant over the life of a grinding wheel.

8.5.3.4 Conclusion

The influence of grinding wheel size adjustment upon profile error could, at first appearance, be very significant but by following the proposed setting procedure it should be restricted to an acceptable level.

8.6 GRINDING PROCESS

So far only the effects of the mechanism design and mode of operation, upon profile accuracy, have been considered. However, the grinding process itself will also influence accuracy. This has not been examined in depth because of the vastness of the subject. Many factors with complex interrelationships are involved, making it difficult to predict the grinding efficiency and this is best determined by experimental investigation of a prototype attachment.

The purpose of this section is simply to point out the main differences between the profile grinding process and a comparable conventional cylindrical grinding process, which might give rise to adverse effects additional to those normally encountered, and to discuss their significances.

The main influences upon general grinding efficiency are the machine structure and grinding operating conditions. The grinding machine structure should preferably be light, well damped, and rigid to minimise deflections and, especially, vibration and chatter [12]. The workpiece stiffness will also be a contributory factor.

There are many variables concerning the operating conditions such as the choice of

(1) wheel abrasive and its dressing technique,

(2) workpiece and wheel surface speeds,

and (3) work material removal rates, governed by depth of cut and traverse rate.

The most obvious difference between the profile and a conventional grinding machine is the continuous motion of the grinding spindle; this in itself should not be significant since the motion is too slow to introduce major adverse dynamic effects; although it will cause a variation in effective work surface speed but this is relatively small (see App.C.1).

The structure of the mechanism is, of course, restricted and its stiffness will be less than that of a comparable rigid structure, especially in the plane of motion where it is determined by the stiffness of many components including the stepper motor transmission. Although this may make it more susceptible to vibration, this might possibly be alleviated by the lighter structure and perhaps greater damping (due to the many joints in the attachment). The vibrational response of the mechanism can be determined by experiment and there should be scope for improvement, if found necessary. Since vibration is also related to the production rate, the adverse effects may be realised as a loss in production efficiency rather than in profile accuracy.

Finally, the mechanism speed is restricted, to minimise deflections due to inertia forces, and consequently, so too is the workpiece surface speed. The ideal speeds usually range from 2m/min in fine grinding to 15 m/min in rough grinding and for the design work speed of 30 r.p.m. (the minimum on some smaller lathes) and the range of sizes from 10 to 100 mm diameter, the work surface speeds will range from ~ 1 m/min to ~10m/min. In general, higher mechanism speeds would be preferable therefore it may not be possible always to achieve the optimum speeds, but this might be compensated by varying other conditions such as wheel abrasive, dressing, and surface speeds, and the material removal rate.

In conclusion:

It is not expected that the profile grinding attachment will be able to match the performance of a comparable, conventional grinding machine, or attachment. However, the discrepancy in performance is likely to be realised as a loss in production rate or efficiency, rather than in precision, which can only be assessed satisfactorily by experiment.

8.7 FINAL ERROR ASSESSMENT

8.7.1 Original specification

The criterion specified in Sec.4.4 for assessing feasibility was that the component of profile error introduced by the attachment, in addition to that normally associated with a comparable conventional grinding process, should not exceed IT4 tolerance grade. The effects of individual sources of error have been assessed both for a range of mechanism settings which represent the expected limits of operation and in the case of eccentricity settings of e = 0.06, which can be compared with DIN 32711, [8], which specifies IT4 tolerances for approximately equivalent profiles.

8.7.2 Separate assessments; summary

The individual influences of the main sources of error may be summarized as follows

(a) Tolerances.

Even for the worst conditions that were considered (R=5mm, R3=0.75mm etc.) the profile error that will be caused by most tolerances can be considered negligible due to the considerable compensation capability. The exceptions are the tolerances of the stepper motor drive system which may cause significant profile error (up to 25% of IT4) which varies in direct proportion to the actual eccentricity size; only in rare cases might these cause excessive errors, in which case remedial measures can be taken.

(b) Clearances

The few clearances that may occur will cause negligible error.

(c) Deflection

For small eccentricity ratios (e=0.06) the deflection will cause significant but acceptable profile error (<1μm); for large

eccentricity ratios (e=0.15) the deflection will be excessive for the operating conditions considered, but they could be reduced to acceptable limits by moderating the operating conditions (i.e. by reducing grinding wheel size or operating speed).

d) Setting adjustments

The R2 adjustment will easily be set with relatively low precision to give negligible error because of the extremely low profile sensitivity to it. The R4 grinding wheel size adjustment may cause significant error for large eccentricity settings, although this could be restricted to <1μm if due care is taken; at low eccentricity ratios the profile is much less sensitive and profile error is less significant.

The R3 eccentricity adjustment, due to the 100% profile sensitivity, directly determines profile shape and its precision will depend only on that of the measurement method and instrumentation used in its setting-up process and therefore it could be set with very high precision if necessary.

e) Grinding process

Although this has not been analysed, the profile error caused by the grinding process is most likely to be related to the stock removal rate and it is assumed that reducing the latter will improve precision to any acceptable level desired.

8.7.3 Cumulative assessment

The preceding individual assessments of this Chapter show that the profile is effectively insensitive to many sources of error and therefore the final assessment of their cumulative influence is reduced to consideration of relatively few sources, these being,

(i) stepper motor drive system component tolerances,
(ii) eccentricity adjustment error,
(iii) grinding wheel size adjustment error,
(iv) deflections generally,
and (v) grinding process errors.

The cumulative effect of these is difficult to quantify since it depends on a combination of probabilistic and deterministic components many of which can be varied by assorted means: therefore only a qualitative assessment is made.

Bearing in mind their individual influences and that the errors of (i), (ii), (iii), and perhaps (v), should be statistically summed and that the errors of (iv) and (v) are dependent on operating conditions, it is concluded that the original aim of IT4 form precision is generally achievable especially for profiles of small eccentricity (e=0.06). To achieve this precision in the case of profiles with large eccentricities, the grinding wheel size or mechanism speed may need to be reduced compared to those used for profiles of small eccentricity. However a lower precision may be acceptable for the more eccentric profiles because errors of form are likely to have less effect on their functional efficiency.

The best precision should be achieved over the intermediate size range: the profile is generally most sensitive to tolerances and deflections of the mechanism at the smallest sizes and of the stepper motor and drive at the largest sizes.

And, there is one final mitigating factor, not as yet considered, of the effects of the profile errors that do occur, which is their cyclic nature. Once the mechanism is set up and operating, most of the errors (from (ii) to (v) above) will systematically repeat with each successive cycle of the mechanism, and therefore be identical on each 'side' of the profile. Such errors are likely to have less adverse effects on profile functional efficiency than purely random error, e.g. the self-centring ability and the symmetry of load distribution will be unaffected.

8.7.4 Internal profile grinding assessment

The analysis has concentrated on the accuracy of grinding external profiles, but most of the preceding arguments apply equally to internal profile grinding. In fact, for internal grinding much smaller grinding wheels will be used in any case and therefore the loads and deflections will also be much lower and consequently the profile error due to them.

In general, it is assumed that internal profile grinding will be at least as accurate as external profile grinding, if not more so, and there is no need to analyse it in depth.

8.7.5 'Square' profile grinding.

So far only 3-fold 'triangular' profiles have been considered. However, the mechanism can easily be set up to grind 4-fold 'square' profiles (or even 2-fold elliptic profiles) by changing the mechanism: workpiece drive ratio from 3:1 to 4:1 (or 2:1). For 'square' profile grinding, since the mechanism speed would be relatively higher than for triangular profiles grinding, the inertia loads and deflections would cause larger errors. Conversely, the effect of some errors on the profile will be less due to the increased gearing.

It may be concluded that high accuracy can also be achieved for profiles of other than 3-fold but perhaps not at the same production rate, which might be higher or lower!

8.8 FUTURE DEVELOPMENT

Although it culminates from several preliminary layouts, the design presented in Drawings Nos. 1 to 7 still represents the first workable layout achieved, and most areas of it would benefit from further, more specialised attention. Generally, the design should be reviewed from a production engineering viewpoint and its compliance with any relevant safety standards should be ensured. Specifically, some areas needing further development have already been identified during the preceding assessments, and these are summarised as follows, without further discussion:

1) Bearings a) preloading - see Secs. 7.3.1 and 7.4.
   b) alternative types - see Secs. 8.2.3 and 8.3

2) Stepper motor drive system
   a) final detail design of control system - Sec.7.5.3
   b) precision of components - Sec. 8.2.4
   c) stiffness of system - Sec. 8.4.4

3) Profile setting measurements - see Secs. 8.5.2 and 8.5.3
   a) methods
   b) instrumentation

4) Experimental investigation of the grinding process - Sec. 8.6.

And other specific areas for future development are suggested as follows:

5) Reduction of deflections

   (a) Optimisation of existing design

   Further general optimisation of the existing arrangement would yield greater efficiency by reducing loads and deflections.

Particular attention should be focused on the main drive shaft and bearing assemblies. The stiffness analysis of App. C3.10 shows that the linear bearing J2L is the weakest element, taking full advantage of the insensitivity of the profile to its deflections (RP2 deviation): reduction of these and also, if possible, reducing the overhang length of the main shaft from joint J1 to J2 would improve performance during grinding of the smaller profiles (see Sec.8.4.5).

The performance of the system would also be improved by reducing the size of joint J3, whose housing inertia contributes significantly to the torque variation, and thus RL3 deviation as it oscillates.

b) Rearrangement of design

A more substantial rearrangement of joints J1, J3 and eccentricity adjustor might provide greatest dividends; perhaps by mounting joint J3 within the inner ring of joint J1 so that they operate in the same plane. This also implies complete redesign of the eccentricity adjustor to adjust J3 within J1.

c) Counterbalancing

A significant development would be to include counterbalancing to reduce variations in the mechanism forces. Balancing of static forces, due to the weight of components alone, would reduce the torque variation seen by the stepper motor. A verticallyacting spring could be simply implemented to support the weight of the grinding system, and also a spring acting between joints J4 and J10 could resist the pantograph weight.

More elaborate counterbalancing might be employed to balance the oscillating loads at the linear bearing J2L and sliding link R4 assembly.

An indication of the error reduction which could be gained is given by Fig.A12.1 where static force balancing is simulated approximately by excluding gravitational forces from the calculation of the profile error for the largest profile (R=50mm, R3=7.5mm) originally shown in Fig.A10.22.

6) Improvement of setting adjustments

In general these can be improved, possibly by incorporation of commercially available adjusting mechanisms. In particular, the R3 eccentricity adjustment may require further development, especially of its anti-backlash spring arrangement and also the friction locking of the slider. A possible alternative to the set screws shown currently, might be a single much larger tie-bolt running axially in a bore through the length of the shafts joined by the slideways; this would be tightened by a single nut at the exposed end of the shaft, (outside of the pulley mounted at joint J1) thus providing direct and substantial axial compressive preloading of the slideways.

An alternative setting method, instead of the screw mechanism, might be to employ precision block gauges to provide direct and absolute setting of the eccentricity without recourse to external measurements. These could be positioned between suitable locating surfaces, one on each of the mating slideways, to directly determine their separation, and thus eccentricity, and would remain locked in position during mechanism operation. Development 5(b) above would also require a re-design of the R3 adjustment, perhaps using eccentric cams.

7) Provision of locking device

This would be used to lock the mechanism in a particular position, mainly to be used as a reference position but also to increase general rigidity during dressing of the grinding wheel, rather than rely on the stepper motor to hold position. It could best be implemented as a clamp on the grinding spindle itself, however it should be detachable during mechanism operation. Such a device would be beneficial if the attachment were also to be used for conventional cylindrical grinding.

8.9 FEASIBILITY CONCLUSIONS

8.9.1 Technical Feasibility

The principal conclusion of the error assessment is that the profile is generally insensitive to most sources of error due to the substantial error compensation that can be achieved, particularly of errors of the production, assembly, and mounting of the attachment. The actual precision achieved in practice will depend primarily on the eccentricity setting precision and on the production rate (as determined by the operating conditions).

Furthermore, there is considerable potential for improvement through further development and experimental investigation of a prototype.

It is therefore concluded that the design presented in Drawings 1 to 7 is technically feasible especially as a prototype.

8.9.2 Economic feasibility

The overall feasibility as a production attachment must include its economic feasibility which has not been analysed and perhaps can only be accurately gauged after testing of a prototype. However, the following considerations are pertinent.

The initial cost of an attachment is minimised by the general avoidance of relatively high and expensive mechanism tolerances and will depend predominantly on the cost of the stepper motor control and instrumentation (an optical encoder will be, perhaps, the single most expensive item).

The running costs will depend on setting up times and production rates which can only be established accurately in experimental prototype trials.

A further consideration which improves its economic feasibility would be the additional use of the attachment, once mounted on a host machine, for conventional cylindrical grinding (after locking of the grinding spindle - see Sec. 8.8).

8.9.3 Comparison with existing profile machine tools

The attachment design presented here is primarily intended as a relatively inexpensive means of converting conventional machine tools, such as lathes, for one-off or small batch production of profiles. Therefore direct economic comparisons cannot easily be drawn with the mass production capabilities of existing large capacity, dedicated profile grinding machines based on the methods of Musyl and developed over many years.

In principle, the only technical disadvantage of the profile generation method used in the design presented here, compared to that of Musyl, is the kinematic and dynamic dependence of the profile on

the grinding wheel size and the consequent adjustment for wear and dressing (see Sec.8.5.3). In the method of Musyl the profile is kinematically independent of grinding wheel diameter therefore requiring no regular adjustment and allowing any size of wheel to be used. In the present method the kinematic disadvantage is alleviated by incorporating automatic grinding wheel size adjustment in the regular wheel dressing procedure, as explained in Sec.8.5.3.3. The size restriction, to limit dynamic deflections (see Sec.8.4.7), depends on general mechanism size and stiffness: however, adequate wheel sizes can be used to suit the size of the attachment as specified in Sec.4.2.3.

CHAPTER 9

STRENGTH OF POLYGONAL CONNECTIONS

9.1 INTRODUCTION

The work reported in this Chapter was originally instigated as part of the procedure for selecting a suitable profile. The intention was to study the general stress behaviour of polygonal joints in order to decide upon the profile with a particular eccentricity which was most suitable. This became largely irrelevant when it was decided to design an attachment which could produce profiles with a range of eccentricities. It also quickly became apparent that this subject area was too large to explore within the bounds of this project and work on it was discontinued, and effort concentrated on the attachment design. Prior to this a theoretical study of shear stress distribution, due to torsion, in bars of hypocycloidal section (see Sec.2.2) was conducted, and is presented here.

The analysis, based on the general theory of elasticity, is basically reduced to the determination of a suitable stress function; the work follows the method of Timoshenko [37] who presents a solution for torsion of an equilaterally triangular section bar. However in this case only an approximately suitable stress function is found analytically and a computer performed 'fitting' procedure is derived to produce an accurate stress function. The final calculation also requires a numerical integration by computer. The results of the analysis are presented in comparison with those of cylindrical bars in torsion, in the form of suitable stress concentration factors.

Later in the chapter the general conditions in polygonal joints are discussed and the influence of the 'pressure angle' of the profiles considered. A formula for calculating pressure angles is presented and those for various profile eccentricities tabulated.

9.2 TORSIONAL STRESS ANALYSIS

9.2.1 Notation

ψ	stress function
G	modulus of rigidity
θ	angle of twist per unit length along z axis
M	torque
x,y,z	rectangular coordinates
τ_{xz}, τ_{yz}	shear stress components in plane normal to z axis

Various notation is also given in Fig.9.1

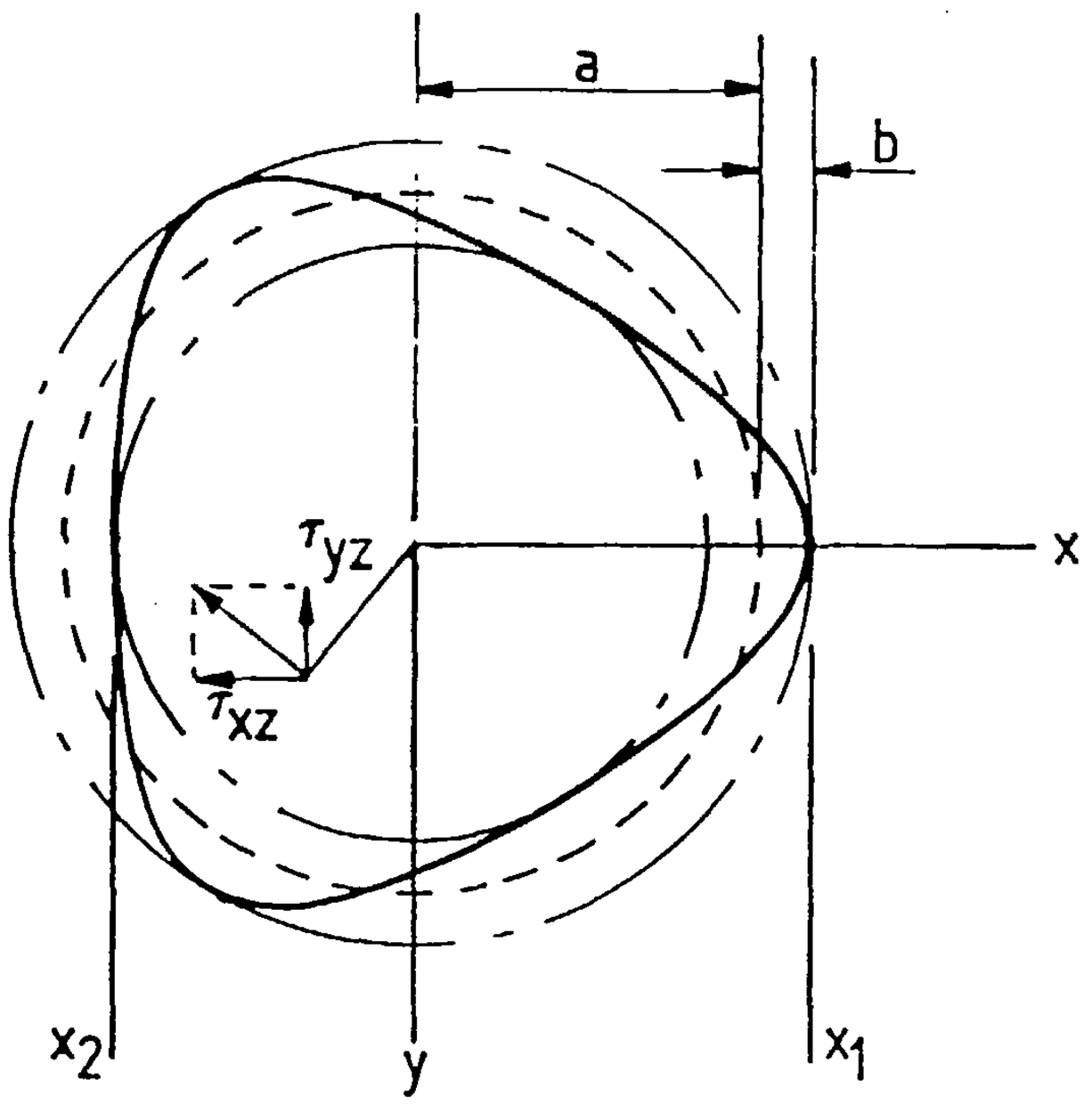

Fig. 9.1 Stress analysis notation

9.2.2 General theory

From the theory of elasticity [37] the stress distribution over the cross section of a bar in torsion may be determined by finding a 'stress function' ψ which satisfies the following equations

$$\frac{\partial^2\psi}{\partial x^2} + \frac{\partial^2\psi}{\partial y^2} = -2G\theta \qquad (9.1)$$

and

$$\frac{d\psi}{ds} = 0, \quad \text{where s is a perimeter coordinate} \qquad (9.2)$$

Equation (9.2) implies that the function ψ must be constant along the boundary of the cross section, and in the case of solid bars may be satisfied by a function that is zero at the boundary.

The shear stress may be derived from the stress function and expressed by:

$$\tau_{xz} = \frac{\partial \psi}{\partial y} \tag{9.3}$$

$$\tau_{yz} = \frac{-\partial \psi}{\partial x} \tag{9.4}$$

which relate shear stress directly to the angle of twist, θ.

The torque M applied at the ends of the bar may also be derived from the stress function by:

$$M = 2 \iint \psi \; dx \quad dy \tag{9.5}$$

which will eventually relate torque directly to the angle of twist θ.

Equations(9 .3), (9.4) and (9.5) may be used, ultimately, to relate shear stress directly to the torque.

9.2.3 Specific Theory

9.2.3.1 Stress function

The boundary of the bar is described by the parametric equations

$$x = a \cos\alpha + b \cos 2\alpha \tag{9.6}$$

$$y = a \sin\alpha - b \sin 2\alpha \tag{9.7}$$

By combining eqns.(9.6) and (9.7) and eliminating α, a single boundary equation is found.

$$(a^4 + a^2b^2 - 2b^4)(x^2+y^2) + b^2(x^2+y^2)^2 - 2a^2b(x^3-3xy^2)$$
$$- (a^6 - 3a^4b^2 + 3a^2b^4 - b^6) = 0 \tag{9.8}$$

The left-hand side of eqn.(9.8) could form the basis of a function that would satisfy the condition implied by eqn.(9.2). But it would not satisfy eqn.(9.1) and therefore will not be a suitable stress function.

However, a stress function may be found from eqn.(9.8) by neglecting the second term, $b^2(x^2+y^2)^2$, since the remaining terms do provide a function which satisfies eqn.(9.1); this is expressed, in a suitable form, by

$$\psi = -2G\Theta\left(\frac{1}{2}(x^2+y^2) + a_1(x^3-3xy^2) + a_2\right) \tag{9.9}$$

where $$a_1 = \frac{-a^2b}{(a^4+a^2b^2-2b^4)} \tag{9.10}$$

and $$a_2 = \frac{-(a^6-3a^4b^2+3a^2b^4-b^6)}{2(a^4+a^2b^2-2b^4)} \tag{9.11}$$

Therefore the stress distribution can be solved <u>exactly</u> for a bar whose boundary is described by

$$\tfrac{1}{2}(x^2+y^2) + a_1(x^3-3xy^2) + a_2 = 0 \tag{9.12}$$

and <u>approximately</u> for the hypocycloid bar of interest as described by eqn.(9.8). Although the approximation is good for small eccentricity ratios of b/a when the neglected term is relatively small, it gradually deteriorates as b/a increases. Therefore a method of improving the approximation was devised. If the values of the coefficients a and b used to calculate a_1 and a_2 in eqn.(9.12) are deviated from the nominal values used in eqn.(9.8), the approximate boundary described by eqn.(9.12) can be made to fit very closely the nominal boundary as described by eqn.(9.8). Therefore, using the modified coefficients a and b in eqn. (9.9), provides a stress function that can more accurately be applied to the hypocycloidal bar.

The adjustment of the approximate boundary to the nominal boundary was performed iteratively by a computer program, and when the two plotted curves were superposed the fit was so good over a range of eccentricities that they were indistinguishable by eye. It was therefore concluded that the results determined using the approximate stress function could be considered 'exact' for the purposes of this analysis.

The coefficient adjustment procedure is shown in the flowchart of Fig.D1.1 in App. D1. The fit of the approximate and nominal cross-sections is demonstrated in Fig.9.2, where the approximate boundary calculated by eqn. (9.12) using the nominal coefficients (a=1.0, b=0.21) is shown by the broken curve and using the modified coefficients (to a=0.962 , b=0.177) by the full curve. It is seen that the exact hypocycloid boundary determined by eqn.(9.3) with coefficients (a=1.0, b=0.21), and depicted by a broken curve is virtually hidden by the modified approximate boundary.

RAVE	ECC.	TAU	SCFAVE	SCFMIN	SCFMAX	REQUIV	SRATIO
1.000	0.030	0.672	1.056	0.964	1.154	0.982	1.049
1.000	0.060	0.715	1.123	0.933	1.338	0.962	1.102
1.000	0.090	0.765	1.201	0.906	1.552	0.941	1.159
1.000	0.120	0.817	1.283	0.876	1.802	0.920	1.217
1.000	0.150	0.878	1.379	0.848	2.097	0.898	1.280
1.000	0.180	0.948	1.489	0.820	2.442	0.876	1.347
1.000	0.210	1.032	1.622	0.800	2.864	0.851	1.422
1.000	0.240	1.133	1.780	0.780	3.367	0.825	1.503
1.000	0.270	1.256	1.974	0.766	3.990	0.797	1.593
1.000	0.300	1.411	2.216	0.758	4.715	0.767	1.695

Table 9.1 Results of stress analysis by computer program STRESS

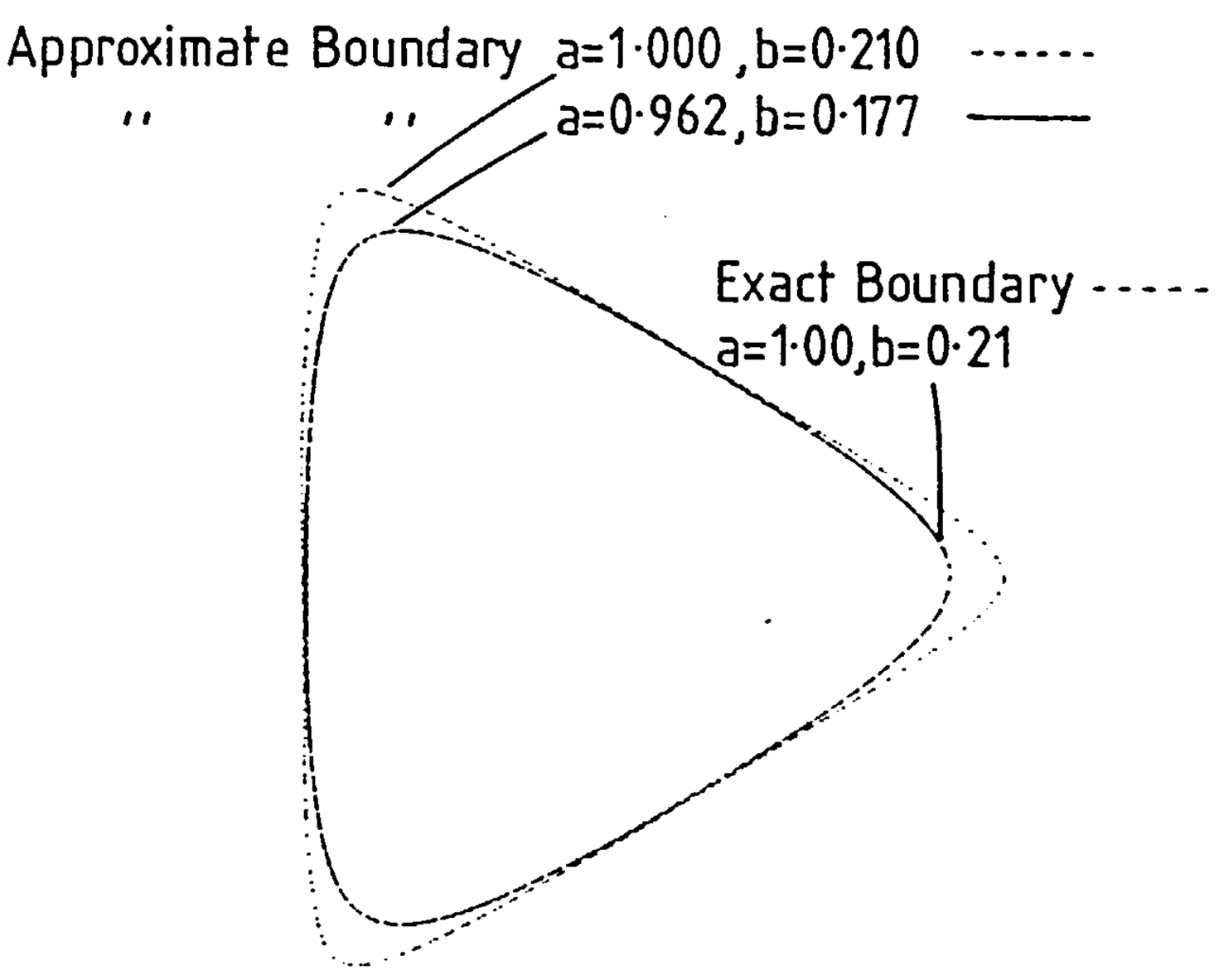

Fig.9.2 Fit of approximate curve to exact boundary curve.

The analysis involves both analytical and numerical methods. First, using eqn.(9.5), an analytical expression for the angle of twist θ is found in terms of the torque M, which then requires a numerical integration by computer for its solution. This is then used to determine the shear stresses in terms of the torque by substituting for θ in eqns. (9.3) and (9.4) and solving.

9.2.3.2 Torque relationship

Substitution of stress function ψ, eqn.(9.9), into eqn.(9.5) gives

$$M = -2G\theta \int_{x_2}^{x_1} \int_{y_2=f_2(x)}^{y_1=f_1(x)} (\tfrac{1}{2}(x^2+y^2) + a_1(x^3-3xy^2) + a_2)\,dy\,dx \qquad (9.13)$$

This expression can be integrated analytically, with respect to y. The limits y_1 and y_2 are given by the boundary of the cross section above and below the x-axis, and can be found from eqn.(9.12) which can be rearranged to give $y = \pm f(x)$ as follows

$$y = \pm \frac{(2a_1x^3 + x^2 + 2a_2)^{\frac{1}{2}}}{(6a_1x - 1)^{\frac{1}{2}}} \qquad (9.14)$$

Thus the limits are given by $y_1 = +f(x)$ and $y_2 = -f(x)$.

Integrating eqn.(9.13) with respect to y, and substituting the limits y_1 and y_2, results in the following expression for M in terms of x:

$$M = -\frac{4}{3} G\theta \int_{x_2}^{x_1} \frac{(2a_1x^3 + x^2 + 2a_2)^{3/2}}{(6a_1x - 1)^{\frac{1}{2}}}\,dx \qquad (9.15)$$

The limits x_1 and x_2 are the points at which the curve cuts the x-axis and therefore $x_1 = a + b$ and $x_2 = b - a$ (where a and b equal their nominal values).

Eqn.(9.15) may be rewritten as

$$M = -G\theta S$$

where S = 4/3 x(integral in eqn.(9.15))

and rearranged to give

$$\theta = \frac{-M}{GS} \qquad (9.16)$$

The integral S may be solved numerically using the 'trapezoidal' or 'corrected trapezoidal' rule [38]. Both methods were performed (as a crosscheck) by

computer program STRESS (see App. D2).

9.2.3.3 Shear stresses

The shear stresses can be found from eqns.(9.3) and (9.4) by differentiating eqn.(9.9), giving

$$\tau_{xz} = G\theta\, y(6a_1 x - 1) \tag{9.17}$$

$$\tau_{yz} = G\theta\, (x + 3a_1(x^2 - y^2)) \tag{9.18}$$

More useful expressions are given by substituting for θ, from eqn.(9.16) in eqns. (9.17) and (9.18) giving stress directly related to torque by

$$\tau_{xz} = -\frac{M}{S}\, y\, (6a_1 x - 1) \tag{9.19}$$

$$\tau_{yz} = -\frac{M}{S}\, (x + 3a_1(x^2 - y^2)) \tag{9.20}$$

9.2.4 Stress Distribution Solution

Since $\tau_{xz} = 0$, when $y = 0$, the stress distribution along the x-axis is given by τ_{yz} from eqn.(9.20) alone, after normalising against M/S, i.e. putting M/S = 1.

9.2.5 Maximum Shear Stress Solution

The largest shear stress occurs on the boundary at the middle of the sides of the profile (this is true for an equilateral triangle as found by Timoshenko [37] and there is no reason to assume otherwise here) and this also can be determined from eqn.(9.20) putting $y = 0$ and $x = x_1 = b - a$ (nominal values of a and b).

The maximum shear stress is best interpreted by comparison with that in a cylindrical bar.

The maximum shear stress $\hat{\tau}_c$ in a cylindrical bar of radius r is given by

$$\hat{\tau}_c = \frac{2M}{\pi r^3} \tag{9.21}$$

if the maximum stress of a polygonal profile calculated from eqn.(9.20) is denoted by $\hat{\tau}_p$, the equivalent radius of a circular bar with the same maximum stress is given by

$$r_{equiv.} = \left(\frac{2M}{\pi\hat{\tau}_p}\right)^{1/3} \qquad (9.22)$$

A more useful comparison may be the size ratio of the escribed circle of the profile, of radius r_{max} (=a+b), to the equivalent bar of radius $r_{equiv.}$

i.e. $$SRATIO = \frac{a+b}{r_{equiv.}} \qquad (9.23)$$

Stress concentration factors SCFAVE, SCFMIN and SCFMAX are also determined which relate the maximum shear stress τ_p of the profile to that , τ_c, in cylindrical bars of diameters equal to those of the average inscribed and escribed circles, respectively of the profile (by using r = a, r = a-b, or r = a+b respectively in eqn.(9.21)).

The calculation of the maximum shear stress and the stress concentration factors was performed using the computer program STRESS which is listed in Appendix D2. A basic flowchart for the program is shown in Fig. D1.1.

9.2.6 Results

A typical example of the stress distribution along the x-axis is shown in Fig.9.3 for a profile of eccentricity ratio (see Sec.2.2.2) e=0.15, i.e. for a=1.0, b=0.15 in eqns.(9.6) and (9.7). The largest stress, as expected, is at the middle of a side where the boundary is closest to the centre of the section. The stress at a corner furthest from the centre is much smaller. (In the case of a proper equilateral triangle section, it would be zero).

The variation of the maximum shear stress with the eccentricity of the profile is shown by the results tabulated in Table 9.1.

The real maximum shear stress may be obtained by multiplying the value TAU, given in Column 3, by (M/a^3) as both M and a were taken as unity in the calculations. The variously defined stress concentration factors calculated from eqn.(9.21) and the equivalent radius from eqn. (9.22) are also given. However perhaps the most useful comparison may be the size ratio from eqn.(9.23) since it is an indication of the

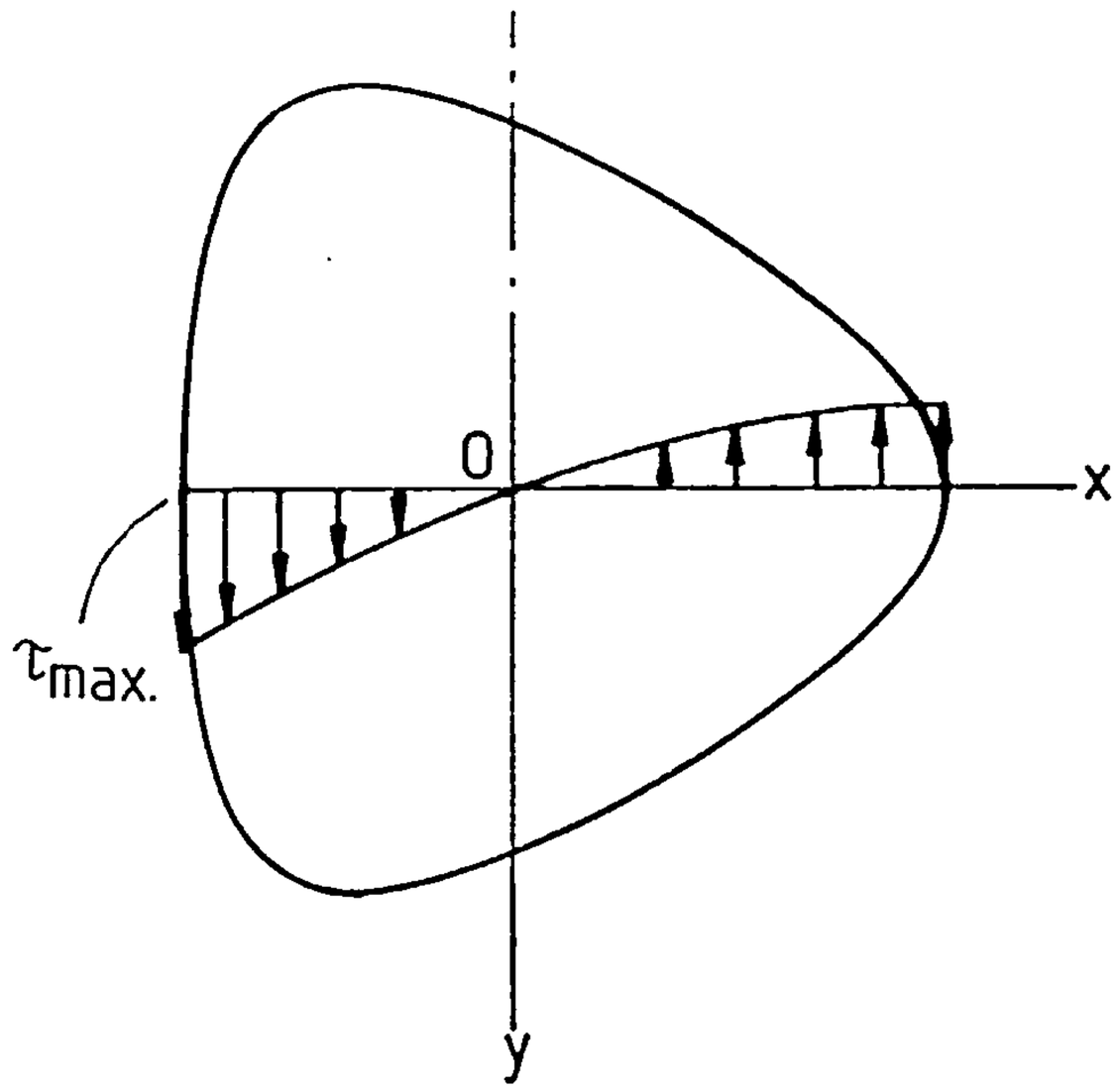

Fig. 9.3 Shear stress distribution

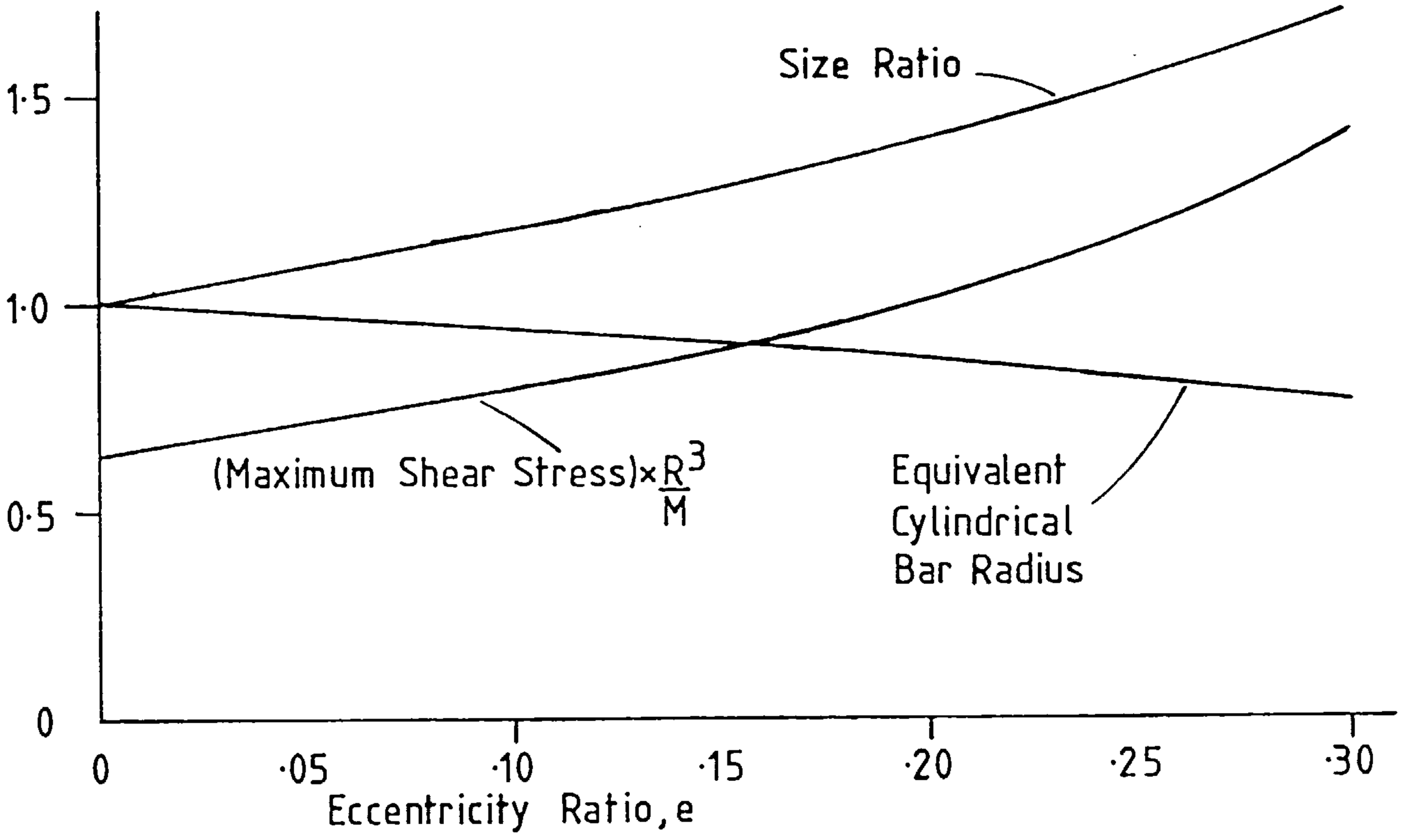

Fig. 9.4 Maximum shear stress vs. eccentricity ratio

extra space required by the profile to achieve the same shear strength as a cylindrical bar. Fig. 9.4 shows plots of maximum shear stress, equivalent bar radius and size ratio, against eccentricity ratio, e.

9.3 GENERAL BEHAVIOUR OF POLYGONAL JOINTS

9.3.1 Pressure angle of polygonal joints.

The results presented in Sec.9.2.6 strictly, only apply in a bar away from end effects, although they still give useful comparative data. Another critical problem in determining the strength of polygonal joints concerns the stresses within the shaft hub connection. Polygonal profiles have a low pressure angle compared to keyed and splined connections and this produces relatively large contact pressures and radial loads in the joint. This is demonstrated in Fig.9.5 where the distributed loads are approximated by concentrated loads acting at the position of the maximum pressure angle $\hat{\phi}$.

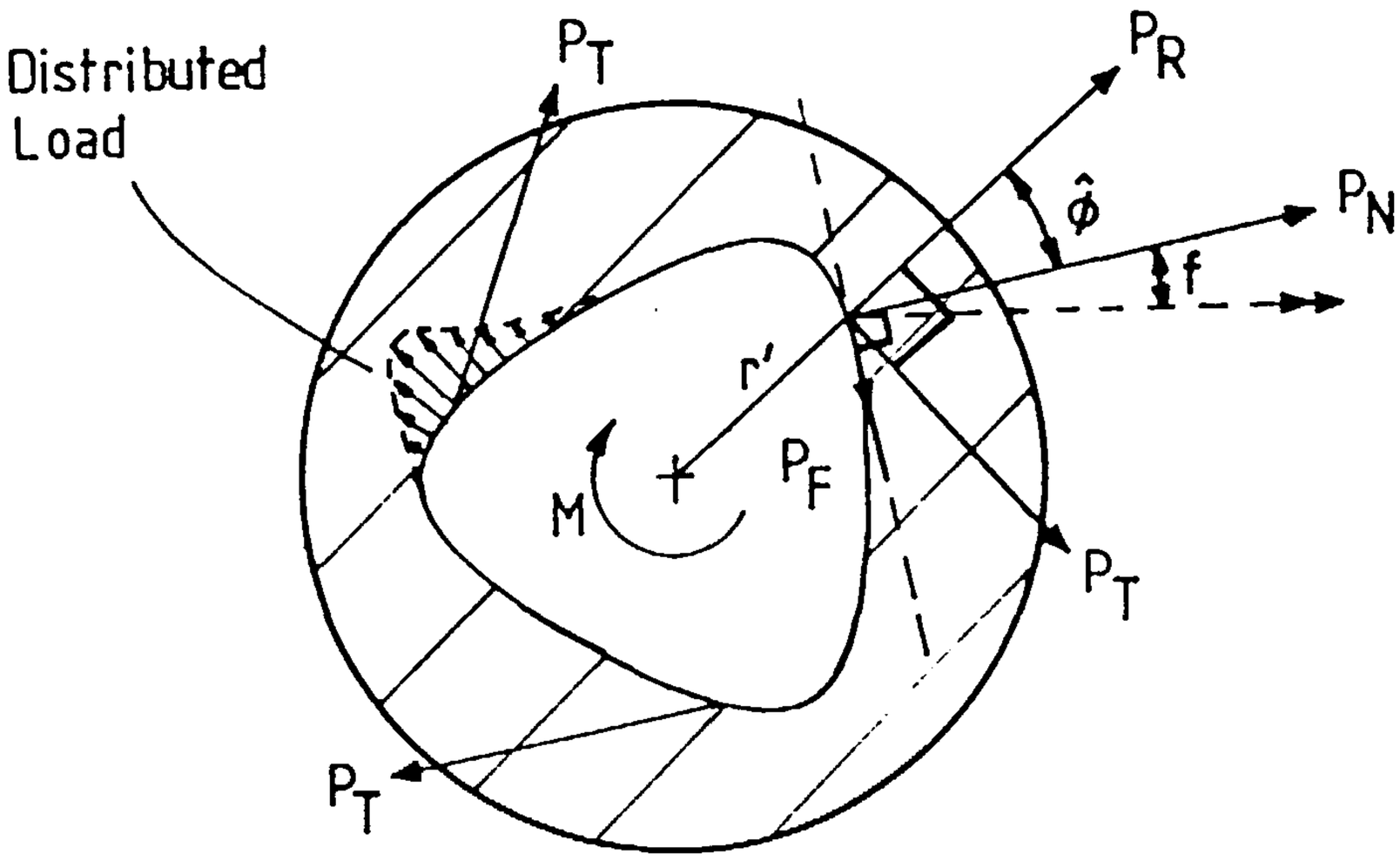

Fig. 9.5 Forces in polygonal joints.

The radial load P_R is given by

$$P_R = \frac{P_T}{\tan(\phi+f)} \qquad (9.24)$$

where f is the friction angle = $\tan^{-1}(\mu$, the coefficient of friction) and the tangential load P_T is related to torque M, assuming symmetric distribution at each side, by

$$P_T = \frac{M}{nr'}$$

where n = number of load points
= 3, for a triangular profile

and r' is the profile radial dimension at the position of $\hat{\phi}$. Thus for a given torque M, the radial force is related to the number of sides n and the pressure angle by

$$P_R \quad \alpha \quad \frac{1}{nr'\tan(\phi+f)} \qquad (9.25)$$

Therefore the strength of a joint will depend substantially on the maximum pressure angle $\hat{\phi}$; this can be related to the eccentricity of the profile by

$$\tan\hat{\phi} = \frac{ne}{(1+(n-1)^2e^4 - (n^2-2n+2)e^2)^{\frac{1}{2}}} \qquad (9.26)$$

and for small eccentricities e by

$$\tan\hat{\phi} \simeq ne \qquad (9.27)$$

The derivation of eqn.(9.26) is given in Appendix D3.

It can be seen that the greatest radial force reduction is achieved by increasing the number of sides of the polygonal profile, although this assumes the equal distribution of loads is maintained at a greater number of points on the profile.

The maximum pressure angles for triangular and square hypocycloid profiles are given in Table D3.1, App.D3.

9.3.2 Strength of polygonal hubs

The element determining the strength and efficiency of the joint may well be the hub, especially if it consists of a narrow annular section.

The high radial loads will tend to expand the hub which would lead to deterioration of the kinematic function of the joint and even tensile failure of the hub section. These problems will be offset by the much better general stress conditions due to the absence of stress raising fillets and the more equal load distribution, compared to keyed and splined joints, as explained in Sec.1.1.

An investigation of the deformations and stresses within various polygonal hubs is reported by Musyl [7] : after preliminary experiments a theoretical analysis is conducted which is simplified by treating the hub as a simple annular ring of constant section, subjected to concentrated loads acting at the positions of maximum contact angle. Deformations and stresses are determined by bending theory using energy methods (Castigliano's Theorem), and extensive results are produced for variations of profile type, size, and eccentricity. As stated earlier, in Sec.1.1.2, these form the basis of design data currently specified in German standards (DIN32711 and DIN32712) and the design manual of the polygon grinding machine manufacturer, Fortuna-Werke [6]. These results should also apply to approximately equivalent hypocycloid polygonal profiles.

A stress analysis of a similar problem, that of true-polygon sockets, is reported by Guenther, Chiang and Langdon [39] and although the results are not directly applicable to the profiled hubs concerned in this work, the theories could be (as an alternative to the method of Musyl): these were based on stress function analyses similar to that used here for torsion of the polygonal shaft.

Finally, as a matter of related interest, the stresses in a splined shaft, including, uncommonly, bending and contact stresses as well as torsional stresses, are discussed by Volfson [40] .

9.3.3 Friction in polygonal joints.

It can be seen from eqn.(9.25) that the radial forces are reduced if friction is increased. Therefore in fixed connections friction may be a favourable factor. In sliding connections, of course, friction would not be favourable, particularly if the joint is not to seize, or jam, and is to slide freely.

Basically, to avoid jamming of the profile and ensure free sliding, the pressure angle must be greater than the friction angle or else an external reverse torque would be required to free the joint. This is seen by the example of a wedge shown in Fig.9.6.

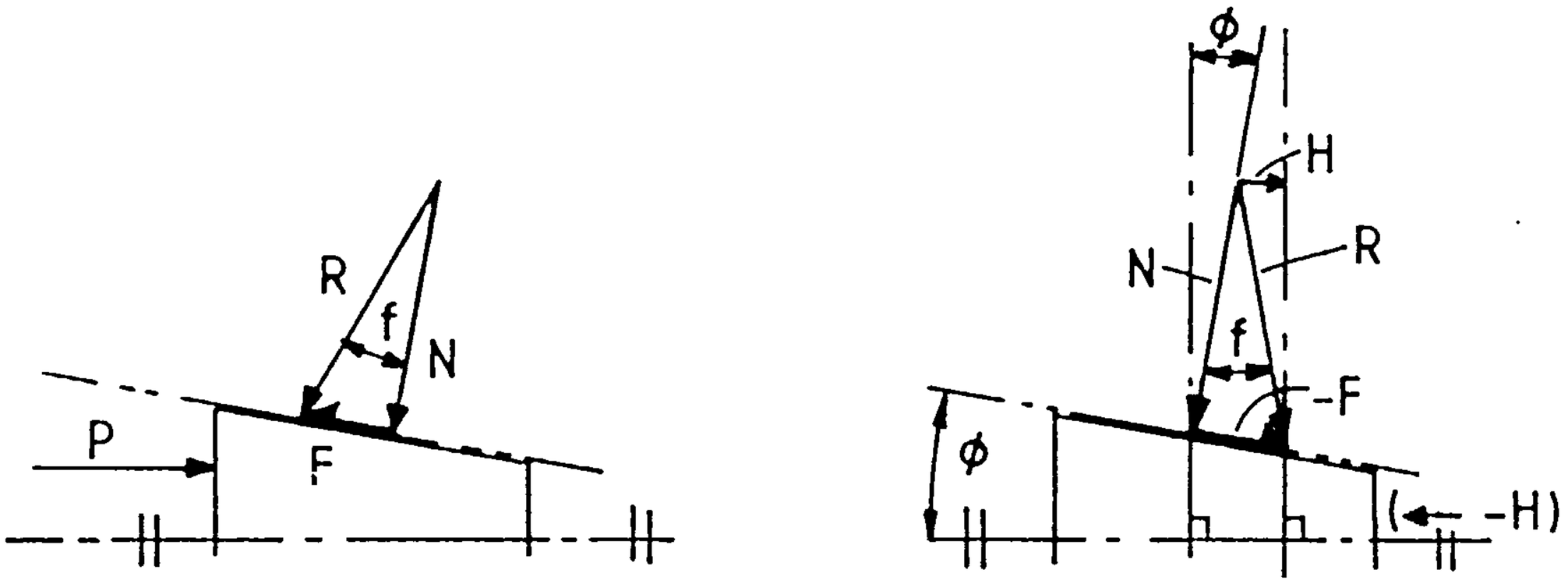

(a) (b)

Fig. 9.6 Effect of friction in jamming a joint

The driving load, P, in Fig.9.6a simulates the torque in a polygonal joint which is resisted by normal force N and friction force F; when the driving load is removed the friction force F reverses direction, Fig.9.6b to resist release of the wedge. If the friction force is ' sufficiently large that the residual horizontal component of force, H, does not act to the left to release the wedge, then the joint can be considered jammed and requires an external releasing force $\geq$ - H acting to the left. This condition implies that the resultant R must act to the left of the vertical and that$(\phi - f) > 0$.

This qualification applies to the pressure angle of the polygonal profile, e.g. for a friction coefficient of 0.2, say, for steel on steel, the friction angle $f = 11.3^{o}$, therefore ϕ should be greater than 11.3^{o}.

Maximum pressure angles are given in Table D3.1 for various eccentricities of profile and most are seen to be greater than 11.3^{o}. In actual effect though, the load is not concentrated but distributed about the maximum pressure angle in the zones either side where the pressure angle decreases. Therefore the actual resultant force might not be aligned with that of the concentrated forces and might be more likely to cause jamming. In this case, even higher maximum pressure

angles and thus more eccentric profiles would be required. The situation would change yet again if the corners of the profiles were concentrically machined-off, thus removing a zone of decreasing pressure angle (and replacing it by an abrupt change to zero angle) and increasing the load concentration at a higher pressure angle.

CHAPTER 10

CLOSING COMMENTS

10.1 REVIEW OF WORK

The major part of the work reported in this thesis concerned the conception, detail design,and precision assessment of a polygon profile grinding attachment to be used on a host machine tool such as a lathe or cylindrical grinding machine. The precision assessment work involved the investigation of general mechanism error analysis theories and the development of a computer-aided assessment procedure.

In a minor way the general mechanical behaviour of a polygonal coupling was considered; in particular, the torsion problem for polygonal bars was theoretically analysed.

10.1.1 Design conception

The initial task was to select a suitable profile, and a hypocycloid curve was chosen, in Chapter 2, after comparison with various others including that used by the sole existing (to this author's knowledge) manufacturer of polygon grinding machines [6,8,9] . One of the main advantages of the hypocycloid was considered to be the large family of profiles which could be generated, ranging from a circle to a virtual true-triangle. It was noted that these profiles were less sensitive to changes in the eccentricity parameter governing their generation method.

The second task, considered in Chapter 3, was the synthesis of an ideal linkage mechanism to produce the hypocycloid profile. The two major problems were to maintain a moving cutting tool in a constant orientation (rake angle) with the work surface and to distance the mechanism out of fouling reach of the workpiece; the first problem was solved by using a suitably pivoted sliding link which maintains a constant orientation, normal to the profile boundary,and the second, by using a pantograph mechanism.

The general requirements of a practical profile manufacturing device were considered in Chapter 4. It was decided that the ideal mechanism should be implemented in the form of a grinding attachment capable of producing profiles with a range of eccentricities, both externally on shafts and internally in hubs. Furthermore, it was decided that the main criterion for determining technical feasibility should be the precision, of form in particular, of the manufactured profile, and that the various sources of error within the mechanism should be investigated in order to predict precision.

10.1.2 Error Analysis

10.1.2.1 Theory

The precision assessment initially, in Chapter 5, involved the development of a general mechanism output error analysis procedure, incorporating several original ideas (to the author's best knowledge), which could be implemented by computer. The function of the procedure was to predict the output error, caused by mechanism parameter deviations from various sources, and the effectiveness of any compensating adjustments which might be employed to improve precision.

Commonly in mechanisms, the components of output error are taken to be in direct proportion to each causal parameter deviation, and the constants of proportionality, or sensitivity, to be the 'first-order partial derivatives' of the output function with respect to each parameter because of linearity the total error is obtained from the component errors, calculated individually, by simple addition (or by Pythagorean addition if only statistical distributions are known). Limitations of this method were discussed and the effects of 'second order partial derivatives', previously neglected, were considered, and it was concluded that, where very high precision, and thus very small errors, are being assessed, the latter should not be ignored, and furthermore their effects are non-linear and therefore should not be considered in isolation from other similar errors.

In view of this, the procedure developed here directly calculates the output error due to deviations and bypasses the intermediate stage of calculating sensitivities.

10.1.2.2 Implementation

To assess the effects of parameter deviations and combinations of deviations, the output error is produced in the form of 'output error characteristics' by plotting error against mechanism position. The effectiveness of any compensating adjustments can be assessed from the characteristic after superposing adjustments and other deviations (before calculation, to account for non-linear effects). These give a more realistic assessment than methods often based on comparing only the largest errors from each source regardless of where they occur in the mechanism cycle. Another and perhaps the most significant development in the error analysis procedure was the adoption of an 'effective, single, output-path-error, coordinate' as compared to the normal two which define the error in each of the two coordinates describing the output path. This has two distinct and general advantages, (i) real error is diagnosed as opposed to mathematical error, and (ii) output characteristics, now composed of single curves, are conceptually much easier to use, than ones composed of two curves, when comparing the effects of different deviations. There is also a third advantage, specific to the polygon profiles, in that (iii) the single output coordinate happens to correspond to the most easily measured, radial dimension of the profile.

10.1.2.3 Application

In Chapter 6 the specific application of the error assessment procedure to the profile generating mechanism was considered. The natures of the various sources of mechanism deviations, such as tolerances, clearances, and deflections, were categorised. For implementation of the procedures, both kinematic and dynamic equations of the mechanism motion were derived and solved by computer programs.

A preliminary analysis of the ideal mechanism produced guidelines, used during the detailed design of an attachment.

10.1.3 Design and feasibility assessment of a practical attachment.

The detailed design of an attachment was described in Chapter 7. Although the attachment was principally designed for mounting on a lathe, it could be adapted to suit other machine tools, such as cylindrical grinding machines which generally have less space than a lathe to accommodate it. A feature of the design is the use of a stepper motor,

to drive the mechanism which is, consequently, geared electrically rather than mechanically to the host machine thus making it largely independent of the host machine design.

The attachment is set up for various profile sizes and eccentricities by adjustment of dial and screw mechanisms with reference to independent measuring instrumentation. Profiles are ground by simple feed of the whole attachment towards the normally mounted workpiece.

The main conclusion of the error assessment, completed in Chapter 8, is that the profile is relatively insensitive to most sources of mechanism errors, especially those which are independent of operating conditions (e.g. tolerances): those sources which are dependent on operating conditions (e.g. deflections) are generally expected only to limit the production rate as a compromise with precision. Profile precision will primarily be determined by that of the measurements involved in setting the mechanism.

It was therefore concluded that the attachment is technically feasible. Whether it is economically feasible can only be accurately assessed after future testing and development of a prototype, in particular to assess the grinding efficiency. However, the initial costs of the mechanism are minimised by the avoidance of restrictive tolerances to achieve the desired precision.

In comparison with existing polygon grinding machines the attachment should be considerably cheaper to build but it will not achieve the same production rates. However it was not intended to compete with mass production methods but to be more suitable for single and small batch production.

10.1.4 Behaviour of polygon joints.

Only the problem of torsion of a bar of hypocycloidal section was theoretically analysed, and solved numerically with the aid of a computer although the effects of the profile 'pressure angle' upon the mechanical behaviour of polygonal joints were discussed and formulae for calculating it derived.

The torsion analysis involved curve fitting, to the exact hypocycloid boundary curve, an approximate curve for which a suitable stress function could be analytically derived, upon which to base the analysis: the interative curve fitting and a subsequent numerical integration to solve

the stress problem were performed by computer. The results and the subsequent comparison between the maximum shear stresses in the polygonal bar with those in a cylindrical bar, indicate the full extent of any strength disparity since no stress concentrations, as arise in splines and keyways, need be considered.

The'pressure angle' which varies with profile eccentricity (and number of sides) is low compared to splines and keyways and gives rise to high radial loads within polygonal connections. The effects of this, particularly upon the hub, and also the influence of friction were discussed qualitatively but not analysed. Pressure angles for 'triangular' and 'square' profiles of various eccentricities are tabulated.

10.2 CONCLUSIONS

The principal product of the work is the detail design for a practical, precision,polygon profile grinding,attachment which forms a suitable basis for future prototype construction and for further development.

A major side product is an error analysis procedure which may be of general applicability in precision mechanism design. The method fits in well with the normal iterative design process as found in its application here; although in this case it was complicated by the large range of mechanism settings (in effect many mechanisms were studied) and the vast data which it produced; however its general application to mechanisms of fixed parameters should be straightforward.

A torsional stress analysis and other qualitative assessments of polygonal joint behaviour produced comparative data to assist the design selection of the profiles themselves.

10.3 FUTURE DEVELOPMENTS

Various suggestions for future work concerning the testing and development of a prototype attachment were proposed in Chapter 8.

The behaviour of polygonal joints and comparisons with keyed and splined joints could also be explored further, both analytically and experimentally.

Of more general application to mechanism error analysis, it was suggested, in Chapter 5, that the statistical assessment of mechanism output error due to second order effects could be investigated further. And the implementation of the 'profile error characteristic' methods in general mechanism analysis computer programs and in optimisation procedures might be useful subjects for study.

REFERENCES

1. V. Dobrovolsky, K. Zablonsky, S. Mak, A.Radchick and L. Erlikh, Machine Elements MIR Publishers, Moscow, 1977.

2. R. Musyl, Das K-Profil eine zyklische Kurve Maschinebau und Wärmewirtschaft, Vienna, 1946, H3/4 pp.59-63.

3. R. Musyl, Die Anwendung der K-Profilverbindung Maschinebau und Wärmewirtschaft, Vienna, 1946, H5/6 pp.100-103.

4. R. Musyl, Das Wälzstossen von Polygonprofilen Maschinebau und Wärmewirtschaft, 1955, Vol.10, pp.17-22.

5. R. Musyl, Die Kinematische Entwicklung der Polygonkurve aus dem K-Profil. Maschinebau und Wärmewirtschaft, 1955, Vol.10, pp.33-36.

6. Fortuna Polygon System, Catalogue 1091e Fortuna-Werke Maschinenfabrik GmbH, Stuttgart-Bad Cannstatt.

7. R. Musyl Die Polygon-Verbindungen und ihre Nabenberechnung. Konstruktion 1962, Vol.14, Part 2, pp-2.3-218.

8. DIN 32711 Polygonprofile P3G DIN (Deutsches Institut für Normung) Mar. 1979.

9. DIN 32712 Polygonprofile P4C DIN, Mar. 1979.

10. E.A. Dijksman Motion Geometry of Mechanisms. Cambridge University Press, 1976.

11. B. Paul Kinematics and Dynamics of Planar Machinery. Prentice Hall, Inc., U.S.A. 1979.

12. H. Challis and C. Stanton. Grinding:Research on the problems of Grinding Technology. Science and Engineering Research Council, 1982.

13. Duplex Precision Tool-Post Grinders and Grinding Spindles. Duplex Electric Tools Ltd., 1983, Kenley, U.K.

14. GMN Grinding Spindles Catalogue 2010 George Müller Kugellagerfabrik KG, Nürnberg, Fed.Rep. of Germany.

15. SFJ High Efficiency Grinding Spindles
E. Fischer AG, 1982, Herzogenbuchsee, Switzerland.

16. Capstan and Turret Lathes
H.W. Ward & Co., Worcester, England.

17. Manual for Colchester 8½" Mascot Lathe.
Colchester Lathe Co. Ltd., Colchester, England.

18. A. Davidson,
Handbook of Precision Engineering: Vol.1 Fundamentals
MacMillan & Co. Ltd., G.B. 1970.

19. O.M.A. Sharfi and M.R. Smith,
A Simple Method for the Allocation of Appropriate Tolerances and Clearances in Linkage Mechanisms.
Mechanism and Machine Theory, Vol.18, No.2, 1983, pp.123-129.

20. O.M.A. Sharfi,
A Study of the Optimal Allocation of Tolerances and Clearances in Planar Linkage Mechanisms.
Ph.D. Thesis, University of Newcastle upon Tyne, July 1982.

21. L.F. Knappe,
A Technique for Analysing Mechanism Tolerances.
Machine Design, Vol.35, 1963, pp.155-157.

22. S.S. Rao and C.P. Reddy,
Mechanism Design by Chance Constrained Programming Techniques.
Mechanism and Machine Theory, Vol.14, 1979, pp 413-424.

23. M. Choubey and A.C. Rao,
Synthesising Linkages with Minimal Structural and Mechanical Error Based upon Tolerance Allocation.
Mechanism and Machine Theory, Vol.17, No.2, 1982, pp.91-97.

24. R.S. Haines,
Survey: 2-Dimensional Motion and Impact at Revolute Joints.
Mechanism and Machine Theory, Vol.15, 1980, pp.361-370.

25. P.S. Houghton,
Ball and Roller Bearings.
Applied Science Publishers Ltd., London, 1976.

26. SKF Precision Bearings.
Catalogue 3055E/GB 680.
SKF(UK) Ltd., Luton, U.K. 1978.

27. Rotolin Bearings.
Lloyd Coley Ltd., Solihull, U.K., July 1981.

28. INA Catalogue 304 GB
INA Bearing Co. Ltd., Sutton Coldfield, U.K., April 1982.

29. 5-Phase Stepping Motor System.
Catalogue No.250/3, April 1982.
Berger Lahr GmbH, (Berger Lahr U.K, Langley, Berks).

30. Stepping Motors : Application Considerations.
Motion Control Division
Sigma Instruments Inc., U.S.A.

31. Incremental Optical Shaft Encoders.
Gaebridge Ltd., Essex, U.K.

32. T. Kenjo,
Stepping motors and their microprocessor controls.
Clarendon Press, Oxford, 1984.

33. NECO Powerdrives,
Normand Electrical Co. Ltd., Aylesbury, England, Aug. 1983.

34. Trantorque
Manheim Manufacturing & Belting Co., Manheim, U.S.A. 1981,
(distributed by Wraxall Engineering Products Ltd., Rugby, U.K.)

35. Safety in the Use of Abrasive Wheels.
Health and Safety Series Booklet HS(G)17
Her Majesty's Stationery Office, London, 1984.

36. K. Brooker,
Manual of British Standards in Engineering Metrology.
British Standards Institution 1984.
Hutchinson & Co. (Publishers) Ltd.

37. S.P. TImoshenko and J.N. Goodier,
Theory of Elasticity, 3rd Edition.
McGraw-Hill Kogakusha Ltd., 1970.

38. S.D. Conte and C. de Boor,
Elementary Numerical Analysis: an algorithmic approach. 3rd Ed.
McGraw-Hill, New York, 1980.

39. D.A. Guenther, H.H. Chiang, and R.C. Langdon,
Design Analysis of the Torsional Properties of Sockets.
Trans. ASME, J.Mech.Des. Vol.104, July 1982, pp.565-571.

40. B.P. Volfson,
Stress Sources and Critical Stress Combinations for Splined Shaft.
Trans. ASME, J.Mech.Des., Vol.104, July 1982, pp.551-556.

41. R.J. Roark and W.C. Young,
Formulas for Stress and Strain 5th Ed.
McGraw-Hill Book Co. 1975.

42. SKF General Catalogue.
Catalogue 3000 11 E/GB 66611, July 1978.
SKF (UK) Ltd., Luton, U.K.

43. Disc Springs for Ball Bearings.
Bauer Springs Ltd., Worcs., U.K.

44. Power Grip Timing Belt Engineering Guide.
Uniroyal Ltd., London.

APPENDIX A

KINEMATIC ANALYSIS OF MECHANISM

A1. PROFILE GENERATING LINKS

Equations for position, velocity and acceleration are derived for the mechanism shown in Fig.A1.1(b).

A1.1 Position

Resolving and equating displacements in the x and y directions gives

$$x_1 = r_1 + r_3.\cos\psi_1 - r_{\ell 3} \sin \psi_1 \quad \text{(A1.1)}$$

$$y_1 = r_3 \sin\psi_1 + r_{\ell 3} \cos\psi_1 + r_{\ell 2} \quad \text{(A1.2)}$$

$$x_2 = r_4 \cos\psi_2 - r_{\ell 4} \sin\psi_2 + x_1 \quad \text{(A1.3)}$$

$$y_2 = r_4 \sin\psi_2 + r_{\ell 4} \cos\psi_2 + y_1 \quad \text{(A1.4)}$$

where

$$\cos\psi_2 = \frac{C2U}{C2L} \quad \text{(A1.5)}$$

$$\sin\psi_2 = \frac{S2U}{C2L} \quad \text{(A1.6)}$$

in notation suitable for programming in FORTRAN computer language

and where

$$C2U = r_2 - r_3 \cos\psi_1 + r_{\ell 3} \sin\psi_1 - (r_{p2}-r_{p4}) \sin\psi_2 \quad \text{(A1.7)}$$

$$S2U = -r_3\sin\psi_1 - r_{\ell 3}\cos\psi_1 - r_{\ell 1} + r_{\ell 2} + (r_{p2} - r_{p4}) \cos\psi_2 \quad \text{(A1.8)}$$

$$C2L = (C2U^2 + S2U^2)^{\frac{1}{2}} \quad \text{(A1.9)}$$

Eqns. (A1.5) to (A1.9) do not give ψ_2 explicitly, since it appears in the last term of both eqns. (A1.7) and (A1.9). However, these terms are relatively small (r_{p2} and r_{p4} only have values of deviations) and by setting $(r_{p2} - r_{p4}) = 0$, for a first iteration only, a good approximation can be obtained for the values of $\sin\psi_2$ and $\cos\psi_2$ which can then be used

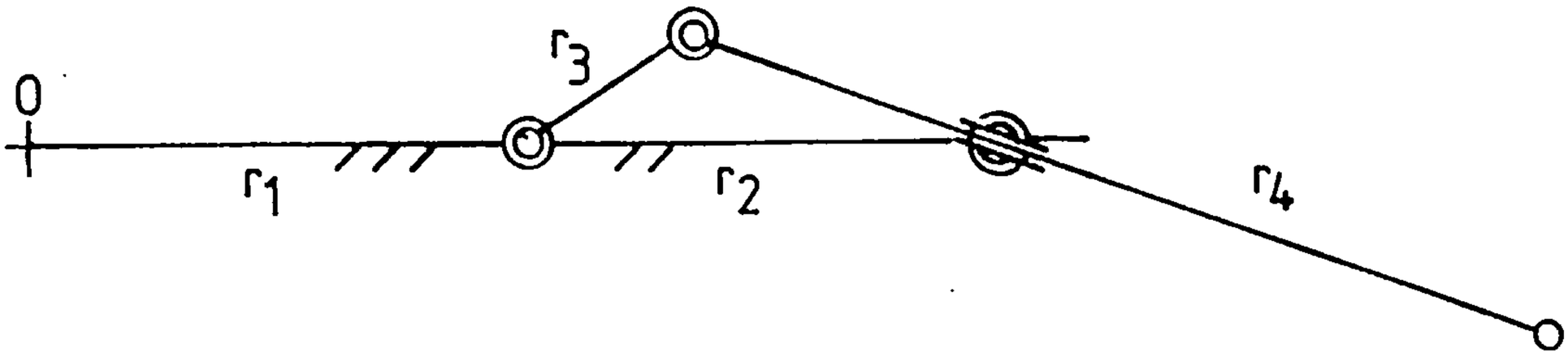

(a)

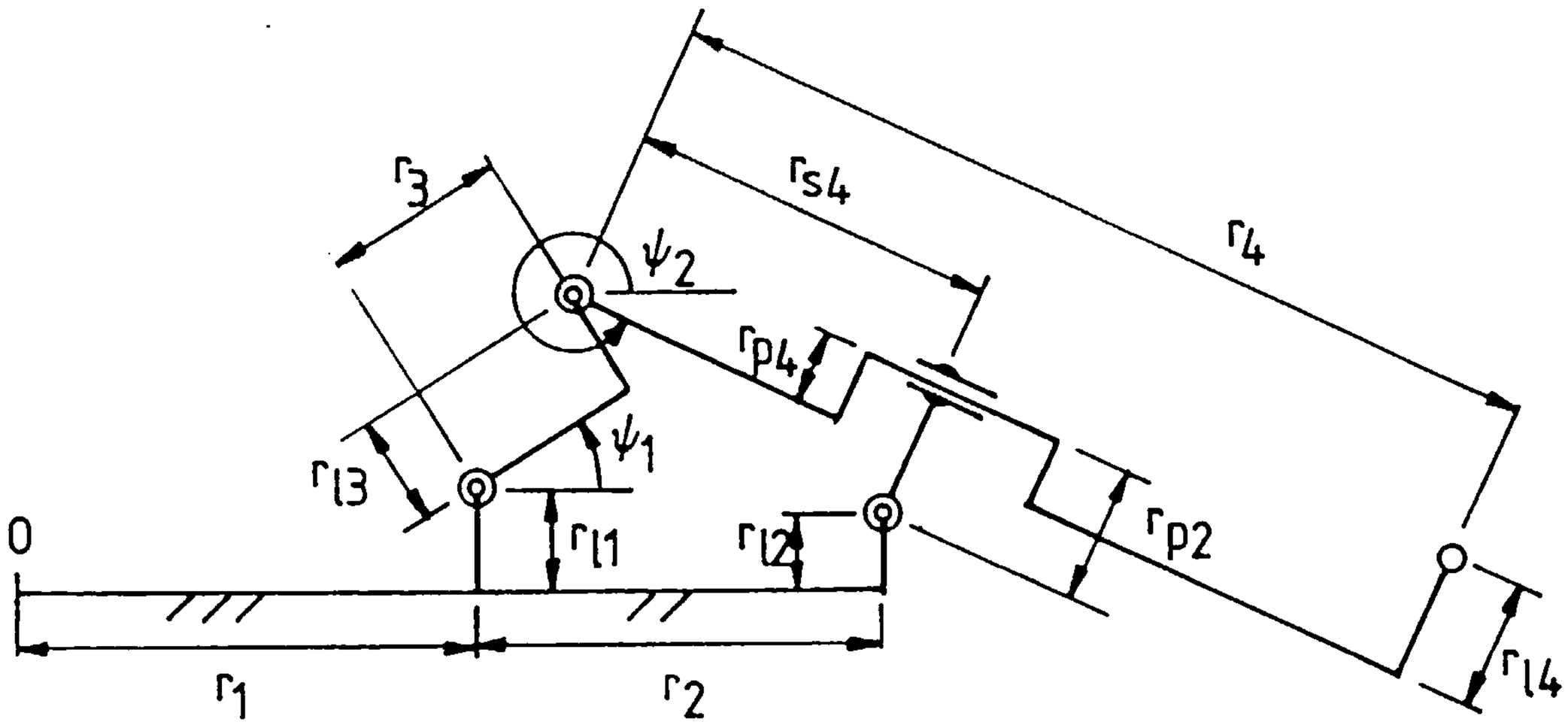

(b)

Fig. A1.1 Profile generator - kinematic notation for mechanism
(a) basic parameters (b) with additional lateral deviation parameters.

in a more accurate 2nd calculation of eqns. (A1.7) and (A1.8). The iterations could be repeated, but in practice this was found to be unnecessary.

For the nominal mechanism, shown in Fig. A1.1(a) the lateral parameters $r_{\ell 1}$, $r_{\ell 2}$, $r_{\ell 3}$, $r_{\ell 4}$, r_{p2}, r_{p4} can be ignored, leaving much simpler expressions, especially

$$\cos\psi_2 = \frac{r_2 - r_3 \cos\psi_1}{(r_2^2 + r_3^2 - 2\ell_2\ell_3\cos\psi_1)^{\frac{1}{2}}} \qquad \text{(A1.10)}$$

$$\sin\psi_2 = \frac{-r_3 \sin\psi_1}{(r_2^2 + r_3^2 - 2r_2r_3 \cos\psi_1)^{\frac{1}{2}}} \qquad \text{(A1.11)}$$

A1.2 Velocity

Differentiating eqns. (A1.1) to (A1.4) with respect to (w.r.t) time gives

$$\dot{x}_1 = -r_3\dot{\psi}_1 \sin\psi_1 - r_{\ell 3}\dot{\psi}_1 \cos\psi_1 \qquad \text{(A1.12)}$$

$$\dot{y}_1 = r_3\dot{\psi}_1 \cos\psi_1 - r_{\ell 3}\dot{\psi}_1 \sin\psi_1 \qquad \text{(A1.13)}$$

$$\dot{x}_2 = -r_4\dot{\psi}_2 \sin\psi_2 - r_{\ell 4}\dot{\psi}_2 \cos\psi_2 + \dot{x}_1 \qquad \text{(A1.14)}$$

$$\dot{y}_2 = r_4\dot{\psi}_2 \cos\psi_2 - r_{\ell 4}\dot{\psi}_2 \sin\psi_2 + \dot{y}_1 \qquad \text{(A1.15)}$$

and differentiating eqns. (A1.6) to (A1.9)

$$\frac{d}{dt}\sin\psi_2 = \frac{1}{C2L}\frac{d}{dt}\,S2U - \frac{S2U}{C2L^2}\,\frac{d}{dt}\,C2L \qquad \text{(A1.16)}$$

$$\frac{d}{dt}\,C2U = r_3\dot{\psi}_1 \sin\psi_1 + r_{\ell 3}\dot{\psi}_1 \cos\psi_1 - (r_{p2}-r_{p4})\dot{\psi}_2 \cos\psi_2 \qquad \text{(A1.17)}$$

$$\frac{d}{dt}\,S2U = -r_3\dot{\psi}_1 \cos\psi_1 - r_{\ell 3}\dot{\psi}_1\sin\psi_1 - (r_{p2}-r_{p4})\dot{\psi}_2 \sin\psi_2 \qquad \text{(A1.18)}$$

$$\frac{d}{dt}\,C2L = \left(C2U\,\frac{d}{dt}\,C2U + S2U\,\frac{d}{dt}\,S2U\right)\frac{1}{C2L} \qquad \text{(A1.19)}$$

furthermore

$$\frac{d}{dt} \sin\psi_2 = \dot{\psi}_2 \cdot \cos\psi_2$$

therefore

$$\dot{\psi}_2 = \frac{1}{\cos\psi_2} \frac{d}{dt} \sin\psi_2 \qquad \text{(A1.20)}$$

Thus $\dot{\psi}_2$ can be determined from eqns. (A1.5) and (A1.15) to (A1.20), although an iteration similar to that for eqns. (A1.7) and (A1.9) is again necessary because $\dot{\psi}_2$ occurs on the right-hand side of eqns. (A1.17) and (A1.18).

For the simplified nominal case, ignoring lateral parameters, a single expression can be derived to give

$$\dot{\psi}_2 = \dot{\psi}_1 \cdot (1 - r_2\cos\psi_2 (r_2^2 + r_3^2 - 2r_2r_3 \cos\psi_1)^{-\frac{1}{2}}) \qquad \text{(A1.21)}$$

A1.3 Accelerations

Accelerations are not required for the error analysis and are only derived for the basic mechanism (for use in the dynamic analysis).

Therefore ignoring lateral parameters, and differentiating eqns. (A1.12) to (A1.15) w.r.t. time gives

$$\ddot{x}_1 = -r_3\ddot{\psi}_1 \sin\psi_1 - r_3\dot{\psi}_1^2 \cos\psi_1 \qquad \text{(A1.22)}$$

$$\ddot{y}_1 = r_3\ddot{\psi}_1 \cos\psi_1 - r_3\dot{\psi}_1^2 \sin\psi_1 \qquad \text{(A1.23)}$$

$$\ddot{x}_2 = -r_4\ddot{\psi}_2 \sin\psi_2 - r_4\dot{\psi}_2^2 \cos\psi_2 + \ddot{x}_1 \qquad \text{(A1.24)}$$

$$\ddot{y}_2 = r_4\ddot{\psi}_2 \cos\psi_2 - r_4\dot{\psi}_2^2 \sin\psi_2 + \ddot{y}_1 \qquad \text{(A1.25)}$$

and differentiating eqn. (A1.21) and rearranging with substitution from eqn. (A1.21) gives

$$\ddot{\psi}_2 = \frac{\dot{\psi}_2}{\dot{\psi}_1} \cdot \ddot{\psi}_1 + r_2 \sin\psi_2 (r_2^2 + r_3^2 - 2r_2r_3 \cos\psi_1)^{-\frac{1}{2}} \dot{\psi}_2\dot{\psi}_1 - r_2^2 \cos\psi_2 \sin\psi_2 (r_2^2 + r_3^2 - 2r_2r_3 \cos\psi_1)^{-1} \dot{\psi}_1^2 \qquad \text{(A1.26)}$$

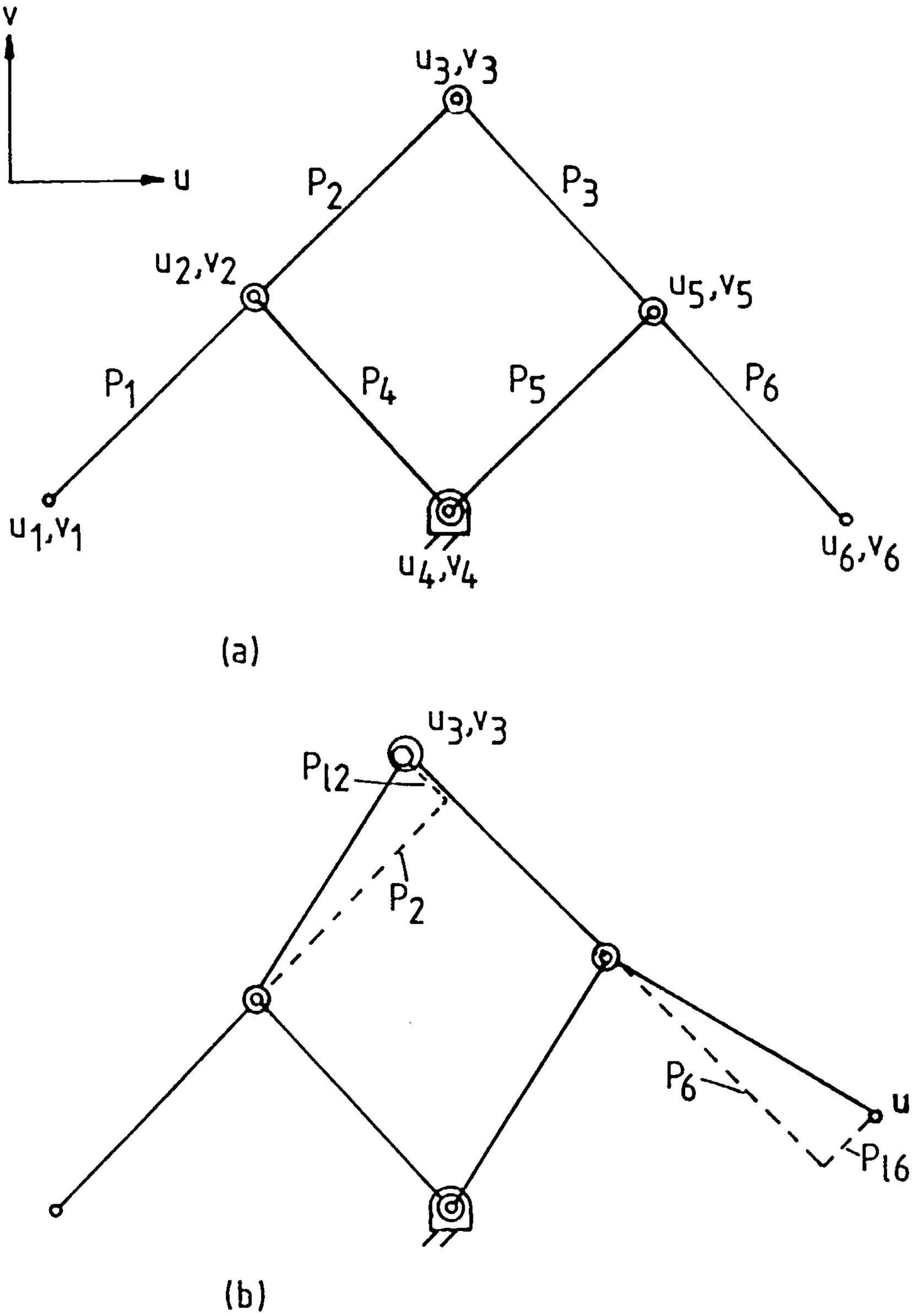

Fig. A2.1 Pantograph - kinematic notation for
(a) ideal mechanism parameters only
(b) including additional lateral parameters.

A1.4 Computer Program

Equations (A1.1) to (A1.26) are incorporated in Subroutine GEN in programs MECHKIN and MECHDYN.

A2. PANTOGRAPH

Equations for position, velocity, and accelerations are derived for the mechanism shown in Fig.A2.1(b); those for the mechanism of Fig.A2.1(a) are given by omitting the lateral link parameters $P_{\ell 2}$ and $P_{\ell 6}$ from the ensuing equations.

The positions, velocities and accelerations are assumed to be known for coordinates (u_1, v_1), which are equivalent to generating mechanism coordinates (x_2, y_2), and for coordinates (u_4, v_4) the fixed pivot of the pantograph.

A2.1 Position

A2.1.1 General solution

First consider generally the solution for a combination of two links as shown in Fig.A2.2 where the unknown cartesian coordinates (u_a, v_a) are required to be found in terms of known coordinates (u_b, v_b) and $u_c, v_c)$ and the link lengths P_b and P_c

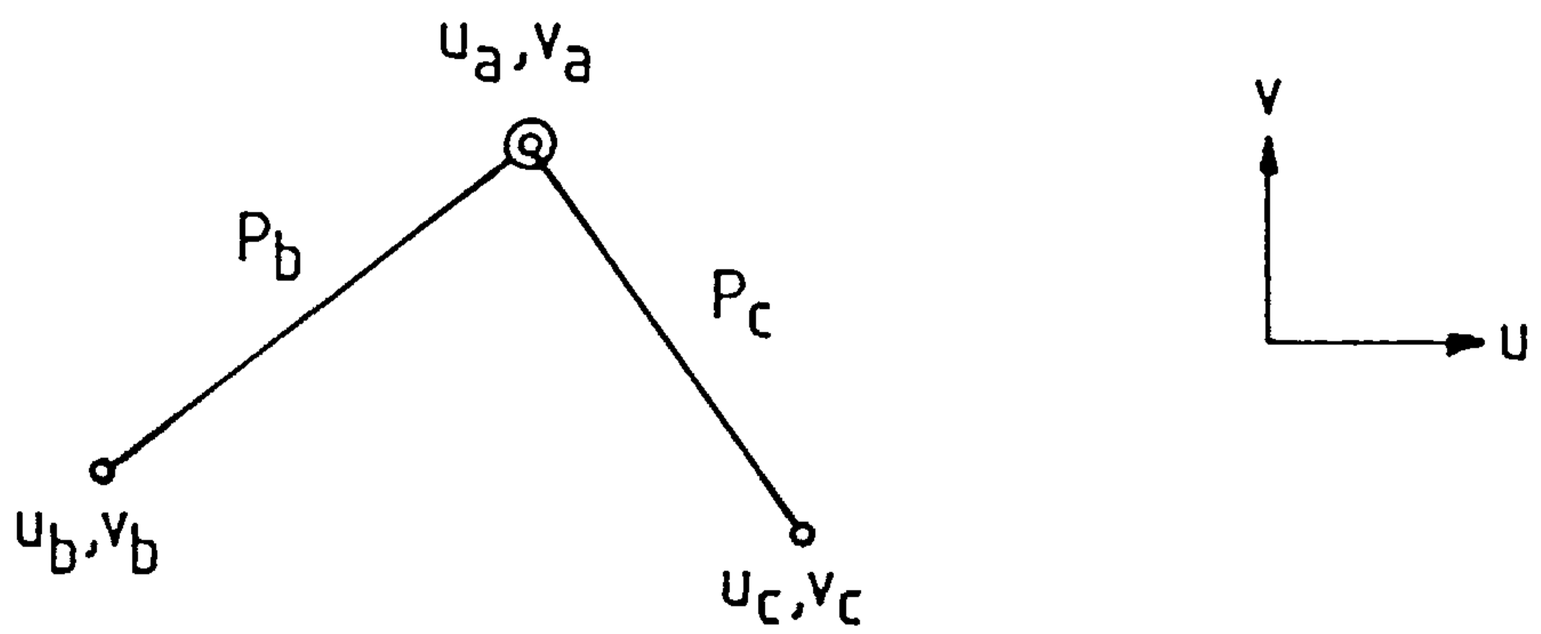

Fig.A2.2 Two link combination

Two equations of constraint may be written, giving

$$(u_a-u_b)^2 + (v_a-v_b)^2 - P_b^2 = 0 \qquad \text{(A2.1)}$$

$$(u_a-u_c)^2 + (v_a-v_c)^2 - P_c^2 = 0 \qquad \text{(A2.2)}$$

After multiplying out the brackets and combining eqns. (A2.1) and (2.2), the u_a^2 and v_a^2 terms can be eliminated and after rearrangement u_a is given in terms of v_a;

$$u_a = C_1 v_a + C_2 \qquad \text{(A2.3)}$$

where $$C_1 = \frac{u_b - v_c}{u_c - u_b} \qquad \text{(A2.4)}$$

and $$C_2 = \frac{u_c^2 - u_b^2 + v_c^2 - v_b^2 + P_b^2 - P_c^2}{2(u_c - u_b)} \qquad \text{(A2.5)}$$

Substitution of eqn.(A2.3) in (A2.1) leaves a quadratic equation in v_a;

$$C_a v_a^2 + C_b v_a + C_c = 0$$

where $$C_a = 1 + C_1^2 \qquad \text{(A2.6)}$$

$$C_b = 2(C_1 C_2 - C_1 u_c - v_c) \qquad \text{(A2.7)}$$

$$C_c = C_2^2 - 2C_2 u_c + v_c^2 + u_c^2 - P_c^2 \qquad \text{(A2.8)}$$

and the solution of the quadratic equation is

$$v_a = \frac{-C_b \pm (C_b^2 - 4C_a C_c)^{\frac{1}{2}}}{2C_a} \qquad \text{(A2.9)}$$

Equation (A2.9) can be substituted in eqn. (A2.3) to find, u_a.

A2.1.2 Pantograph solution

Referring to Fig. A2.1(a) and (b), the coordinates (u_2,v_2) are found using eqns. (A2.1 - 2.9) by substituting

$$(u_a,v_a) = (u_2,v_2),\ (u_b,v_b) = (u_1,v_1),\ (u_c,v_c) = (u_4,v_4)$$

$$P_b = P_1, \quad \text{and } P_c = P_4.$$

NOTE: There are two possible configurations of links P_1 and P_4 and the correct solution, of the two given by eqns. (A2.9) and (A2.3), must be chosen.

NOTE: Coordinates (u_3,v_3) are found by the 'similar triangles rule' which gives

$$u_3 = u_2 + \frac{P_2}{P_1}(u_2-u_1) - \frac{P_{\ell 2}}{P_1}(v_2-v_1) \qquad \text{(A2.10)}$$

$$v_3 = v_2 + \frac{P_2}{P_1}(v_2-v_1) + \frac{P_{\ell 2}}{P_1}(u_2-u_1) \qquad \text{(A2.11)}$$

Coordinates (u_5,v_5) are found by again using eqns. (A2.1 - 2.9), this time putting

$$u_a = v_5,\ v_a = -u_5\ *$$

$$u_b = v_3,\ v_b = -u_3$$

$$u_c = v_4,\ v_c = -u_4$$

$$P_b = P_3,\ P_c = P_5$$

* Notice the change in orientation of coordinate system. This was done to achieve a consistent solution as point (u_3,v_3) changes quadrants during motion.

Coordinates (u_6,v_6) are then found by the 'similar triangles rule' giving

$$u_6 = u_5 + \frac{P_6}{P_3}(u_5-u_3) - \frac{P_{\ell 6}}{P_3}(v_5-v_3) \qquad \text{(A2.12)}$$

$$v_6 = v_5 + \frac{P_6}{P_3}(v_5-v_3) + \frac{P_{\ell 6}}{P_3}(u_5-u_3) \qquad \text{(A2.13)}$$

A2.2 Velocities

A2.2.1 General solution

Referring to Fig. A2.2, the velocities at point (u_a,v_a) are obtained by differentiating eqns. (A2.1) and (A2.2) w.r.t. time and solving the

resulting simultaneous equations for $\dot{u}_a, \dot{v}_a$.

$$\dot{v}_a = \left[(u_a-u_b)\dot{u}_b + (v_a-v_b)\dot{v}_b - (u_a-u_b)\dot{u}_c - \frac{(u_a-u_b)(v_c-v_a)}{(u_c-u_a)}\dot{v}_c\right] \times \left[(v_a-v_b) - \frac{(u_a-u_b)(v_c-v_a)}{(u_c-u_a)}\right]^{-1} \quad \text{(A2.14)}$$

$$\dot{u}_a = \dot{u}_c - \frac{(v_c-v_a)}{(u_c-u_a)}(\dot{v}_a-\dot{v}_c)$$

A2.2.2 Pantograph solution

Equations (A2.14) and (A2.15) can be used to calculate $\dot{u}_2$, $\dot{v}_2$ in similar fashion as (u_2,v_2) are determined.

Velocities at $(\dot{u}_3,\dot{v}_3)$ are given by differentiating eqns. (A2.10) and (A2.11)

$$\dot{u}_3 = \dot{u}_2 + \frac{P_2}{P_1}(\dot{u}_2 - \dot{u}_1) - \frac{P_{\ell 2}}{P_1}(\dot{v}_2 - \dot{v}_1) \quad \text{(A2.16)}$$

$$\dot{v}_3 = \dot{v}_2 + \frac{P_2}{P_1}(\dot{v}_2 - \dot{v}_1) - \frac{P_{\ell 2}}{P_1}(\dot{u}_2 - \dot{u}_1) \quad \text{(A2.17)}$$

Velocities at (u_5,v_5) $\dot{u}_5$ and $\dot{v}_5$ are again calculated using eqns. (A2.14) and (A2.15) with suitable substitutions.

Velocities at (u_6,v_6) are given by differentiating eqns. (A2.12) and (A2.13),

$$\dot{u}_6 = \dot{u}_5 + \frac{P_6}{P_3}(\dot{u}_5 - \dot{u}_3) - \frac{P_{\ell 6}}{P_3}(\dot{v}_5 - \dot{v}_3) \quad \text{(A2.18)}$$

$$\dot{v}_6 = \dot{v}_5 + \frac{P_6}{P_3}(\dot{v}_5-\dot{v}_3) - \frac{P_{\ell 6}}{P_3}(\dot{u}_5 - \dot{u}_3) \quad \text{(A2.19)}$$

A2.3 Accelerations

All accelerations are obtained by direct differentiation w.r.t. time of the velocity eqns. (A2.14) to (A2.19). The resulting acceleration equations are applied in similar fashion to the velocity equations and are not given here.

A2.4 Computer Program

Equations (A2.1) to (A2.19) and the acceleration equations are incorporated in SUBROUTINE PANTO within the main programs MECHKIN and MECHDYN.

The equations relating to Fig.A2.1 are implemented in SUBROUTINES CALCUV, VELUV and ACCUV, called within SUBROUTINE PANTO for positions, velocities, and accelerations respectively.

A3. GRINDING WHEEL CUTTING-POINT

A3.1 Position

Referring to Fig.A3.1 the coordinates of the final cutting point of the grinding wheel are given by

$$x_{cp} = R_{gw} \cos\psi_3 + x_{gw} \qquad \text{(A3.1)}$$

$$y_{cp} = R_{gw} \sin\psi_3 + y_{gw} \qquad \text{(A3.2)}$$

The motion of the grinding wheel centre x_{gw}, y_{gw} (= u_b,v_6) is predetermined from the pantograph analysis and the angle, ψ_3, of the grinding wheel equivalent link, R_{gw}, is determined by the motion of the grinding wheel relative to the workpiece: the relative velocity vector of the grinding wheel to the workpiece must always be tangential to both workpiece and grinding wheel at point (x_{cp},y_{cp}). Since equivalent link R_{gw} is always normal to the grinding wheel surface, it must also be normal to the relative velocity vector; this is shown in Fig.A3.1.

If the direction of the relative velocity is denoted by ψ_v, then

$$\psi_3 = \psi_v - 90^o \qquad \text{(A3.3)}$$

From basic trigonometry

$$\cos\psi_3 = \cos\ (\psi_v - 90^o) = \sin\psi_v$$

$$\sin\psi_3 = \sin\ (\psi_v - 90^o) = -\cos\psi_v$$

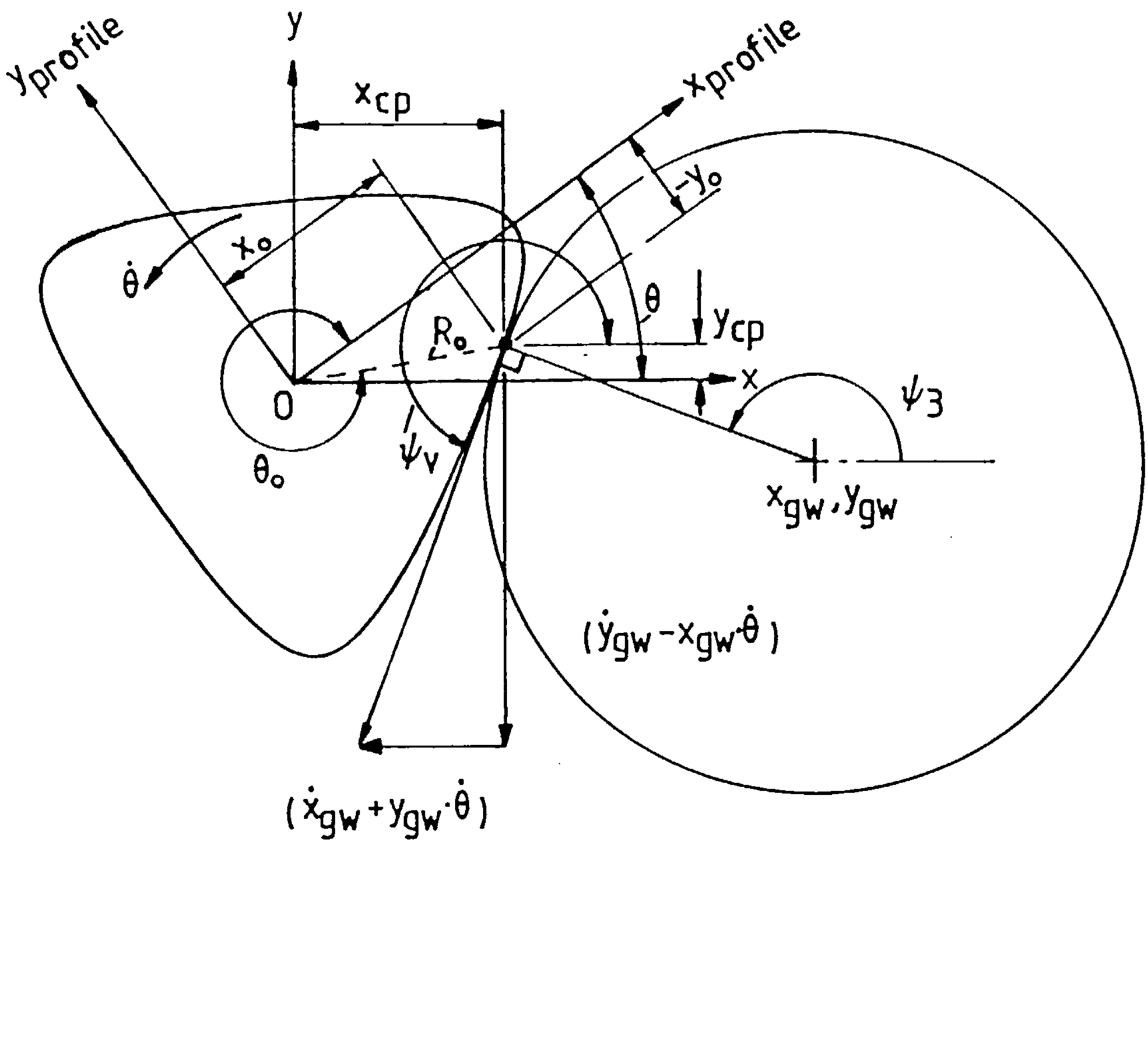

Fig. A3.1 Relative motion of grinding wheel and workpiece.

The relative velocity of x_{gw} to x_{cp} is $\dot{x}_{gw} + y_{gw}\ \dot{\theta}$

and the " " " y_{gw} to y_{cp} is $\dot{y}_{gw} - x_{gw}\ \dot{\theta}$

and therefore

$$\cos\psi_3 = \sin\psi_v = \frac{\dot{y}_{gw} - x_{gw}\ \dot{\theta}}{((\dot{y}_{gw}-x_{gw}\ \dot{\theta})^2 + (\dot{x}_{gw}+y_{gw}\ \dot{\theta})^2)^{\frac{1}{2}}} \qquad \text{(A3.4)}$$

$$\sin\psi_3 = -\cos\psi_v = \frac{\dot{x}_{gw} + \dot{y}_{gw}\ \dot{\theta}}{((\dot{y}_{gw}-x_{gw}\ \dot{\theta})^2 + (\dot{x}_{gw}+y_{gw}\ \dot{\theta})^2)^{\frac{1}{2}}} \qquad \text{(A3.5)}$$

Thus x_{cp}, y_{cp} can be determined by substitution of eqns. (A3.4) and (A3.5) in eqns. (A3.1) and (A3.2).

Only the position of the cutting point is required, not velocity or acceleration.

A3.2 Computer Program

Equans (A3.1) to (A3.5) are incorporated in SUBROUTINE GRIND which is called from main programs MECHKIN and MECHDYN.

A4. PROFILE COORDINATES

The mechanism output position, denoted by coordinates (x_{cp},y_{cp}), as derived in section A3, is more usefully expressed by profile cartesian, or polar, coordinates (x_o,y_o), or (R_o,θ_o), respectively, in a coordinate system fixed relative to the workpiece. The latter are given by transformation of the coordinates x_{cp}, y_{cp} as follows; referring to Fig.A3.1

$$x_o = x_{cp}\cos\theta + y_{cp}\sin\theta$$

$$y_o = y_{cp}\cos\theta - x_{cp}\sin\theta$$

$$R_o = (x_o^2 + y_o^2)^{\frac{1}{2}} \qquad \text{(A4.1)}$$

$$\theta_o = \arctan\left(\frac{y_o}{x_o}\right) \qquad \text{(A4.2)}$$

A5. DEFLECTION CALCULATIONS

When the output deviations due to deflections of mechanism parameters are considered, new deviations will be required for every mechanism input position. These are calculated within computer program MECHKIN, using the deflection-force relationships derived in Appendices C3 and C6.7, after reading the force data which must be previously calculated by the dynamic analysis within program MECHDYN, given in Appendix B.

A6. LISTING OF PROGRAM MECHKIN

At the end of MECHKIN a sample data file, KINDATA, is listed.

A 'flowchart' of MECHKIN is given in Fig.6.4, Chap.6.

Listing of MECHKIN at 20:32:25 on APR 4, 1987 for CCid=MCBO

```
      C
      C          MECHKIN
      C          *******
      C
      C       This program calculates the effects of mechanism
      C    deviations on profile accuracy
      C
      C       Plots of profile errors v.s.individual mechanism
      C    deviations or combinations of deviations can be produced.
      C
      C        The plots can show profile errors as radial &angular errors
      C       of the theoretical profile, or as radial errors only (after
      C      adjusting for angular errors - 'single output error'.
      C
      C  To run; concatenate compiled version with +*IG+*GHOST (plotting library)
            IMPLICIT REAL*8(A-H,O-Y)
            COMMON/G1/R1,R2,R3,R4,VP1,AP1,RL1,RL2,RL3,RL4,RP2,RP4
            COMMON /P1/P1,P2,P3,P4,P5,P6,U4,V4,PL2,PL6
            DIMENSION X(101),Y(101),FX(101),FY(101),DX(101),DY(101),PSI(101),
           /R(101),DR(101),FR(101),TG(12),TP(10),DTHETA(101),
           /DRDT(101,22),DTOTAL(101),TOL(22),DTHEDT(101,22)  ,
           /RDEV1(101),RDEV2(101),TDEV1(101),TDEV2(101)
            REAL ZRDEV1(101),ZRDEV2(101),ZTDEV1(101),ZTDEV2(101),
           /ZR(101),ZPSI(101)
            EQUIVALENCE (R1,TG(1)),(P1,TP(1))
            RL1=0.0
            RL2=0.0
            RL3=0.0
            RL4=0.0
            PL2=0.0
            PL6=0.0
            RP2=0.0
            RP4=0.0
      C
      C  Read input data - nominal kinematic parameters etc.
      C
            READ(5,40)R1,R2,R3,R4,RGW,VP1,AP1
        40  FORMAT(F8.4,6(/F8.4))
            READ(5,41)P1,P2,P3,P4,P5,P6,U4,V4,H,EFFDR,TSCALE
         41 FORMAT(F7.3,8(/F7.3),2(/F7.3))
      C
      C  Read constant deviations to parameters
      C
            READ(5,42)TOL,FEED
        42 FORMAT(F7.3,22(/F7.3))
            TOL(1)=TOL(1)-FEED
            TOL(19)=TOL(19)-FEED
      C
      C  For deflection analysis only ; read nominal mech. settings
      C  as supplied by MECHDYN (to over-ride those above)
            READ(7,1010)R1,R2,R3,R4,RGW,VP1
         1010  FORMAT(6(F10.6))
            R1=R1*1.0D03
            R2=R2*1.0D03
            R3=R3*1.0D03
            R4=R4*1.0D03
            RGW=RGW*1.0D03
      C
```

Listing of MECHKIN at 20:32:25 on APR 4, 1987 for CCid=MCBO

```
      R1D=R1
      R2D=R2
      R3D=R3
      R4D=R4
      NPLOT=0
      U4=R1D+R4D+(P5*P5+P6*P6)**0.5
      V4=0.0
      R1=U4*2.0 -R1
      R2=-R2
      R3=-R3
      PI=4.0*DATAN(0.1D1)
C
C  Set input position
          DO 11 I=1,101
C
C For DEFLECTION analysis ONLY; read force data supplied by MECHDYN
C
          READ (7,1001)FY2,FY4,F5,F9,TOR,F4A,F4L,F3L
 1001   FORMAT(8(F9.2))
C
C  Calculate deflection deviations
C
          RP2DYN=-(35.97*F3L+6.89*(F3L/DABS(F3L))*(DABS(F3L)**0.9)
     / +80.0*(F3L/DABS(F3L))*(DABS(F3L)**0.67))
C
          RP4DYN=+11.84*F4L+8.15*(F4L/DABS(F4L))*(DABS(F4L)**0.9)
C
          RL1DYN=3.3*FY2+5.14*FY4
C
          RL4DYN=18.27*F4L+4.24*(F4L/DABS(F4L))*(DABS(F4L)**0.9)
     / +4.93*F3L+2.66*(F3L/DABS(F3L))*(DABS(F3L)**0.9)
C
          R4DYN=22.13*F4A+4.24*(F4A/DABS(F4A))*(DABS(F4A)**0.9)
C
          P4DYN=-29.0*F5-22.71*(F5/DABS(F5))*(DABS(F5)**0.9)
C
          P5DYN=-3.31*F9-20.87*(F9/DABS(F9))*(DABS(F9)**0.9)
C
          RL3DYN=-921.0*R3*TOR
C
          RP2DYN=RP2DYN*1.D-06
          RP4DYN=RP4DYN*1.D-06
          RL1DYN=RL1DYN*1.D-06
          RL4DYN=RL4DYN*1.D-06
          R4DYN=R4DYN*1.D-06
          P4DYN=P4DYN*1.D-06
          P5DYN=P5DYN*1.D-06
          RL3DYN=RL3DYN*1.D-06
C
C Remove C's from following statements to isolate individual deflection
C  deviations (i.e. set all others to zero
C       RP2DYN=0.0D0
C       RP4DYN=0.0D0
C       RL1DYN=0.0D0
C       RL4DYN=0.0D0
C       R4DYN=0.0D0
C       P4DYN=0.0D0
C       P5DYN=0.0D0
```

Listing of MECHKIN at 20:32:25 on APR 4, 1987 for CCid=MCBO

```
      C       RL3DYN=0.0D0
      C
      C  Allocate deflections to parameter deviations
            TOL(11)=TOL(11)+RP2DYN
            TOL(12)=TOL(12)+RP4DYN
            TOL(7)=TOL(7)+RL1DYN
            TOL(10)=TOL(10)+RL4DYN
            TOL(4)=TOL(4)+R4DYN
            TOL(16)=TOL(16)+P4DYN
            TOL(17)=TOL(17)+P5DYN
            TOL(9)=TOL(9)+RL3DYN
      C
      C  Calculate nominal output position
            THETA=2.0*PI*(I-1)/100.0
            PSI1=3.0*THETA
            CALL GEN(X2,Y2,VX2,VY2,AX2,AY2,PSI1)
            CALL PANTO(X2,Y2,VX2,VY2,AX2,AY2,U6,V6,VU6,VV6,AU6,AV6)
            CALL GRIND(XCP,YCP,U6,V6,VU6,VV6,RGW,VP1/3.0)
            X(I)=XCP*DCOS(THETA)+YCP*DSIN(THETA)
            Y(I)=YCP*DCOS(THETA)-XCP*DSIN(THETA)
            R(I)=(X(I)*X(I)+Y(I)*Y(I))**0.5
            THETCP=DATAN2(Y(I),X(I))
      C  Deviate parameters
             DO 31 NTOL=1,22
            IF(NTOL.GT.12) GO TO 21
            TG(NTOL)=TG(NTOL)+TOL(NTOL)
            GO TO 31
         21 TP(NTOL-12)=TP(NTOL-12)+TOL(NTOL)
         31  CONTINUE
      C
      C  Calculate deviated output position
         22 CALL GEN(X2,Y2,VX2,VY2,AX2,AY2,PSI1)
            CALL PANTO(X2,Y2,VX2,VY2,AX2,AY2,U6,V6,VU6,VV6,AU6,AV6)
            CALL GRIND(XCP,YCP,U6,V6,VU6,VV6,RGW,VP1/3.0)
            FX1=XCP*DCOS(THETA)+YCP*DSIN(THETA)
            FY1=YCP*DCOS(THETA)-XCP*DSIN(THETA)
            FR1=(FX1*FX1+FY1*FY1)**0.5
            THET1=DATAN2(FY1,FX1)
            DTHET=THET1-THETCP
      C     CORRECTION FOR THET1 &THETCP BEING IN DIFFERENT QUADRANTS
            IF((DTHET-PI).GT.0.0) DTHET=DTHET-PI*2.0
            IF((DTHET+PI).LT.0.0) DTHET=DTHET+PI*2.0
      C  Reset nominal parameters
             DO 24 NTOL=1,22
            IF(NTOL.GT.12) GO TO 23
            TG(NTOL)=TG(NTOL)-TOL(NTOL)
            GO TO 24
         23 TP(NTOL-12)=TP(NTOL-12)-TOL(NTOL)
         24 CONTINUE
            DR(I)=FR1-R(I)
      C  Is Single Effective Output Desired?
            IF(EFFDR.LT.1.0) GO TO 81
      C
      C Change input position & Recalculate nominal output position.
         80  THETA=THETA-DTHET
            PSI1=3.0*THETA
            CALL GEN(X2,Y2,VX2,VY2,AX2,AY2,PSI1)
            CALL PANTO(X2,Y2,VX2,VY2,AX2,AY2,U6,V6,VU6,VV6,AU6,AV6)
```

Listing of MECHKIN at 20:32:25 on APR 4, 1987 for CCid=MCBO

```
175            CALL GRIND(XCP,YCP,U6,V6,VU6,VV6,RGW,VP1/3.0)
176            FX2=XCP*DCOS(THETA)+YCP*DSIN(THETA)
177            FY2=YCP*DCOS(THETA)-XCP*DSIN(THETA)
178            FR2=(FX2*FX2+FY2*FY2)**0.5
179            THET2=DATAN2(FY2,FX2)
180       C
181       C  recalculate output position
182            DR(I)=(FR1-FR2)
183            DTHET=THET1-THET2
184       C    CORRECTION FOR THET1 &THET2 BEING IN DIFFERENT QUADRANTS
185            IF((DTHET-PI).GT.0.0) DTHET=DTHET-PI*2.0
186            IF((DTHET+PI).LT.0.0) DTHET=DTHET+PI*2.0
187       C  If Angular error= 0, store single output Radial error
188            IF(DABS(DTHET).GT.0.00001) GO TO 80
189          81 CONTINUE
190            DTHETA(I)=DTHET
191            R(I)=R(I)/(R1D*100.0)
192            PSI(I)=THETA*180.0/PI
193          35 CONTINUE
194       C
195       C  Reset deflection deviations before next position
196             TOL(11)=TOL(11)-RP2DYN
197             TOL(12)=TOL(12)-RP4DYN
198             TOL(7)=TOL(7)-RL1DYN
199             TOL(10)=TOL(10)-RL4DYN
200             TOL(4)=TOL(4)-R4DYN
201             TOL(16)=TOL(16)-P4DYN
202             TOL(17)=TOL(17)-P5DYN
203             TOL(9)=TOL(9)-RL3DYN
204       C
205          11 CONTINUE
206       C
207       C    GRAPH PLOTTING
208       C
209             DO 32 I=1,101
210              ZTDEV1(I)=DTHETA(I)
211              ZRDEV1(I)=DR(I)
212            ZR(I)=R(I)
213            ZPSI(I)=PSI(I)
214          32 CONTINUE
215            NPLOT=NPLOT+1
216            CALL PAPER(1)
217            CALL MAP(-20.0,400.0,-TSCALE,TSCALE)
218            CALL POSITN(300.0,(TSCALE-NPLOT*TSCALE*0.05))
219            CALL LINE(50.0,0.0)
220            CALL CTRMAG(15)
221            CALL TYPECS('  DR',4)
222            CALL CURVED(ZPSI,ZRDEV1,1,101)
223            CALL BROKEN(7,7,7,7)
224            NPLOT=NPLOT+1
225            CALL POSITN(300.0,(TSCALE-NPLOT*TSCALE*0.05))
226            CALL LINE(50.0,0.0)
227            CALL CTRMAG(15)
228            CALL TYPECS('  DTHETA',8)
229            CALL CURVED(ZPSI,ZTDEV1,1,101)
230            CALL BROKEN(10,10,10,10)
231            NPLOT=NPLOT+1
232            CALL POSITN(300.0,(TSCALE-NPLOT*TSCALE*0.05))
```

Listing of MECHKIN at 20:32:25 on APR 4, 1987 for CCid=MCBO

```
      CALL LINE(50.0,0.0)
      CALL CTRMAG(15)
      CALL TYPECS('  R/100',7)
      CALL CURVED(ZPSI,ZR,1,101)
      CALL FULL
      CALL FULL
      CALL AXES
      CALL PLACE(53,43)
      IP=0
      DO 57 NTOL=1,20
      IF(DABS(TOL(NTOL)).LT.0.0001) GO TO 57
      IP=IP+1
      CALL TYPECS('TOL',3)
      CALL TYPENI(NTOL)
      CALL TYPECS('=',1)
      CALL TYPENF(TOL(NTOL),3)
      CALL TYPECS(' MM',3)
      CALL PLACE(53,(43-IP))
   57 CONTINUE
      CALL PLACE(20,43)
      CALL TYPECS('R1=',3)
      CALL TYPENF(R1D,3)
      CALL TYPECS(' MM',3)
      CALL PLACE(37,43)
      CALL TYPECS('R3=',3)
      CALL TYPENF(R3,3)
      CALL TYPECS(' MM',3)
      CALL CTRMAG(15)
      CALL PLACE(15,1)
      CALL TYPECS('PLOT OF PROFILE ERRORS V.S. ANGULAR POSITION',44)
      CALL PLACE(16,2)
      CALL TYPECS('FOR GIVEN MECHANISM TOLERANCES',30)
      CALL PLACE(69,22)
      CALL TYPECS('ANGULAR',7)
      CALL PLACE(69,24)
      CALL TYPECS('POSITION',8)
      CALL PLACE(38,25)
      CALL TYPECS('(DEGS)',6)
      CALL CTRORI(1.0)
      CALL PLACE(45,2)
      CALL TYPECS('PROFILE ERROR',13)
      CALL CTRORI(0.0)
      CALL GREND
C  END OF PLOTTING
      STOP
      END
C
C  End of MAIN program
C
C
C Calculation of positions, velocities, & accel.s in generating mech.
C
      SUBROUTINE GEN(X2,Y2,VX2,VY2,AX2,AY2,PSI1)
      IMPLICIT REAL*8(A-H,O-Z)
      COMMON/G1/R1,R2,R3,R4,VP1,AP1,RL1,RL2,RL3,RL4,RP2,RP4
      C1=DCOS(PSI1)
      S1=DSIN(PSI1)
      X1=R3*C1+R1-RL3*S1
```

Listing of MECHKIN at 20:32:25 on APR 4, 1987 for CCid=MCBO

```
      Y1=R3*S1+RL3*C1+RL1
C
      S2=0.0
      C2=0.0
      DO 1 I2=1,2
      C2U=R2-R3*C1+RL3*S1 -(RP2-RP4)*S2
      S2U=-R3*S1-RL3*C1-RL1+RL2 +(RP2-RP4)*C2
      C2L=(C2U*C2U+S2U*S2U)**0.5
      C2=C2U/C2L
      S2=S2U/C2L
    1 CONTINUE
C
      X2=R4*C2+X1-RL4*S2
      Y2=R4*S2+Y1+RL4*C2
      VX1=-R3*S1*VP1-RL3*C1*VP1
      VY1=R3*C1*VP1-RL3*S1*VP1
C
      AX1=-R3*S1*AP1-R3*C1*VP1*VP1
      AY1=R3*C1*AP1-R3*S1*VP1*VP1
C
      VP2=0.0
      DO 2 J2=1,2
      DC2U=(R3*S1+RL3*C1)*VP1-(RP2-RP4)*C2*VP2
      DS2U=(-R3*C1+RL3*S1)*VP1-(RP2-RP4)*S2*VP2
      DC2L=(C2U*DC2U+S2U*DS2U)/C2L
      DS2=DS2U/C2L-S2U*DC2L/C2L**2.0
      VP2=DS2/C2
    2 CONTINUE
      AP2=(VP2/VP1)*AP1+R2*(S2/C2L)*VP2*VP1+R2*R2*R3*C2*(S1/C2L**3.0)
     +*VP1*VP1
      VX2=-R4*S2*VP2+VX1-RL4*C2*VP2
      VY2=R4*C2*VP2+VY1-RL4*S2*VP2
C
      AX2=-R4*S2*AP2-R4*C2*VP2*VP2+AX1
      AY2=R4*C2*AP2-R4*S2*VP2*VP2+AY1
      RETURN
      END
C
C  Calculation of grinding cutting coordinates
C
      SUBROUTINE GRIND(XCP,YCP,XGW,YGW,VXGW,VYGW,RGW,DTHETA)
      IMPLICIT REAL*8(A-H,O-Z)
      SU=-VXGW-YGW*DTHETA
      CU=VYGW-XGW*DTHETA
      SCL=(SU*SU+CU*CU)**0.5
      S=SU/SCL
      C=CU/SCL
      XCP=RGW*C+XGW
      YCP=RGW*S+YGW
      RETURN
      END
C
C Calculation of pantograph positions,velocities,& accelerations
C
      SUBROUTINE PANTO(U1,V1,VU1,VV1,AU1,AV1,U6,V6,VU6,VV6,AU6,AV6)
      IMPLICIT REAL*8(A-H,O-Z)
      COMMON /P1/P1,P2,P3,P4,P5,P6,U4,V4,PL2,PL6
      CALL CALCUV(U2,V2,U1,V1,U4,V4,P1,P4)
```

Listing of MECHKIN at 20:32:25 on APR 4, 1987 for CCid=MCBO

```
      U3=(P2/P1)*(U2-U1)+U2-(PL2/P1)*(V2-V1)
      V3=(P2/P1)*(V2-V1)+V2+(PL2/P1)*(U2-U1)
      CALL CALCUV(V5,U5,V3,-U3,V4,-U4,P3,P5)
       U5=-U5
C     LAST LINE AS CANNOT ASSIGN TO -VE ARG'S
      U6=(P6/P3)*(U5-U3)+U5-(PL6/P3)*(V5-V3)
      V6=(P6/P3)*(V5-V3)+V5+(PL6/P3)*(U5-U3)
C
C     PANTOGRAPH VELOCITIES
C
      CALL VELUV(U2,V2,U1,V1,U4,V4,VU2,VV2,VU1,VV1,0.0D0,0.0D0)
      VU3=(P2/P1)*(VU2-VU1)+VU2-(PL2/P1)*(VV2-VV1)
      VV3=(P2/P1)*(VV2-VV1)+VV2+(PL2/P1)*(VU2-VU1)
      CALL VELUV(U5,V5,U3,V3,U4,V4,VU5,VV5,VU3,VV3,0.0D0,0.0D0)
      VU6=(P6/P3)*(VU5-VU3)+VU5-(PL6/P3)*(VV5-VV3)
      VV6=(P6/P3)*(VV5-VV3)+VV5+(PL6/P3)*(VU5-VU3)
C
C
C  ACCELERATIONS
C
      CALL ACCUV(U2,V2,U1,V1,U4,V4,VU2,VV2,VU1,VV1,0.0D0,0.0D0,
     /AU2,AV2,AU1,AV1,0.0D0,0.0D0)
      AU3=(P2/P1)*(AU2-AU1)+AU2
      AV3=(P2/P1)*(AV2-AV1)+AV2
      CALL ACCUV(U5,V5,U3,V3,U4,V4,VU5,VV5,VU3,VV3,0.0D0,0.0D0,
     /AU5,AV5,AU3,AV3,0.0D0,0.0D0)
      AU6=(P6/P3)*(AU5-AU3)+AU5
      AV6=(P6/P3)*(AV5-AV3)+AV5
      RETURN
      END
C
C
C Solution of simple linkage pair
C
      SUBROUTINE CALCUV(UA,VA,UB,VB,UC,VC,PB,PC)
      IMPLICIT REAL*8(A-H,O-Z)
      C1=(VB-VC)/(UC-UB)
      C2=0.5*(UC*UC-UB*UB+VC*VC-VB*VB+PB*PB-PC*PC)/(UC-UB)
      CA=1.0+C1*C1
      CB=2.0*(C1*C2-C1*UC-VC)
      CC=C2*C2-2.0*C2*UC+VC*VC+UC*UC-PC*PC
      VA=(-CB+(CB*CB-4.0*CA*CC)**0.5)/(2.0*CA)
C
C NOTE:- IS THIS NECESSARY SOL OF QUADRATIC (CB+/-)?
C
      UA=C1*VA+C2
      RETURN
      END
C
      SUBROUTINE VELUV(UA,VA,UB,VB,UC,VC,VUA,VVA,VUB,VVB,VUC,VVC)
      IMPLICIT REAL*8(A-H,O-Z)
       UAB=UA-UB
       VAB=VA-VB
       UCA=UC-UA
       VCA=VC-VA
C
        VVA1=+UAB*VUB+VAB*VVB-UAB*VUC
        VVA2=-UAB*VCA*VVC/UCA
```

Listing of MECHKIN at 20:32:25 on APR 4, 1987 for CCid=MCBO

```
      VVA3=VAB-UAB*VCA/UCA
     VVA=(VVA1+VVA2)/VVA3
     VUA=-VCA*VVA/UCA+VUC+VCA*VVC/UCA
     RETURN
     END
C
C
     SUBROUTINE ACCUV(UA,VA,UB,VB,UC,VC,VUA,VVA,VUB,VVB,VUC,VVC,
    /AUA,AVA,AUB,AVB,AUC,AVC)
     IMPLICIT REAL*8(A-H,O-Z)
     UAB=UA-UB
     VAB=VA-VB
     UCA=UC-UA
     VCA=VC-VA
C
     DUAB=VUA-VUB
     DVAB=VVA-VVB
     DUCA=VUC-VUA
     DVCA=VVC-VVA
C
     VVA3=VAB-UAB*VCA/UCA
C
    AVA1=DUAB*VUB+UAB*AUB+DVAB*VVB+VAB*AVB-DUAB*VUC-UAB*AUC
    AVA2=DUAB*VCA*VVC/UCA+UAB*DVCA*VVC/UCA
    AVA3=UAB*VCA*AVC/UCA-UAB*VCA*VVC*DUCA/(UCA*UCA)
    AVA4=DVAB-DUAB*VCA/UCA-UAB*DVCA/UCA+UAB*VCA*DUCA/(UCA*UCA)
   AVA=(AVA1-AVA2-AVA3)/VVA3-VVA*AVA4/VVA3
C
      AUA1=(-DVCA*VVA-VCA*AVA+VCA*VVA*DUCA/UCA)/UCA
      AUA2=(+UCA*AUC+DVCA*VVC+VCA*AVC-VCA*VVC*DUCA/UCA)/UCA
   AUA=AUA1+AUA2
   RETURN
   END
#
```

Listing of KINDATA at 21:00:30 on APR 4, 1987 for CCid=MCBO

1	5.0	R1 Nominal dimensions
2	2.5	R2
3	0.75	R3
4	40.0	R4
5	40.0	RGW
6	10.0	VP1
7	0.0	AP1
8	75.0	P1
9	75.0	P2
10	75.0	P3
11	75.0	P4
12	75.0	P5
13	75.0	P6
14	107.0	U4
15	0.0	V4
16	0.1	H Redundant data - NOT used
17	2.0	EFFDR If normal twin coord. output desired, put this <1.0 .
18	0.020	TSCALE Sets scale of plots
19	0.00	R1 Deviations (constant) to parameters
20	0.0	R2
21	0.00	R3
22	0.00	R4
23	0.0	VP1
24	0.0	AP1
25	0.0	RL1
26	0.00	RL2
27	0.0	RL3
28	0.0	RL4
29	0.0	RP2
30	0.0	RP4
31	0.0	P1
32	0.0	P2
33	-0.0	P3
34	0.0	P4
35	0.00	P5
36	0.00	P6
37	0.0	U4
38	0.0	V4
39	0.00	PL2
40	0.0	PL6
41	-0.00	FEED

##
##

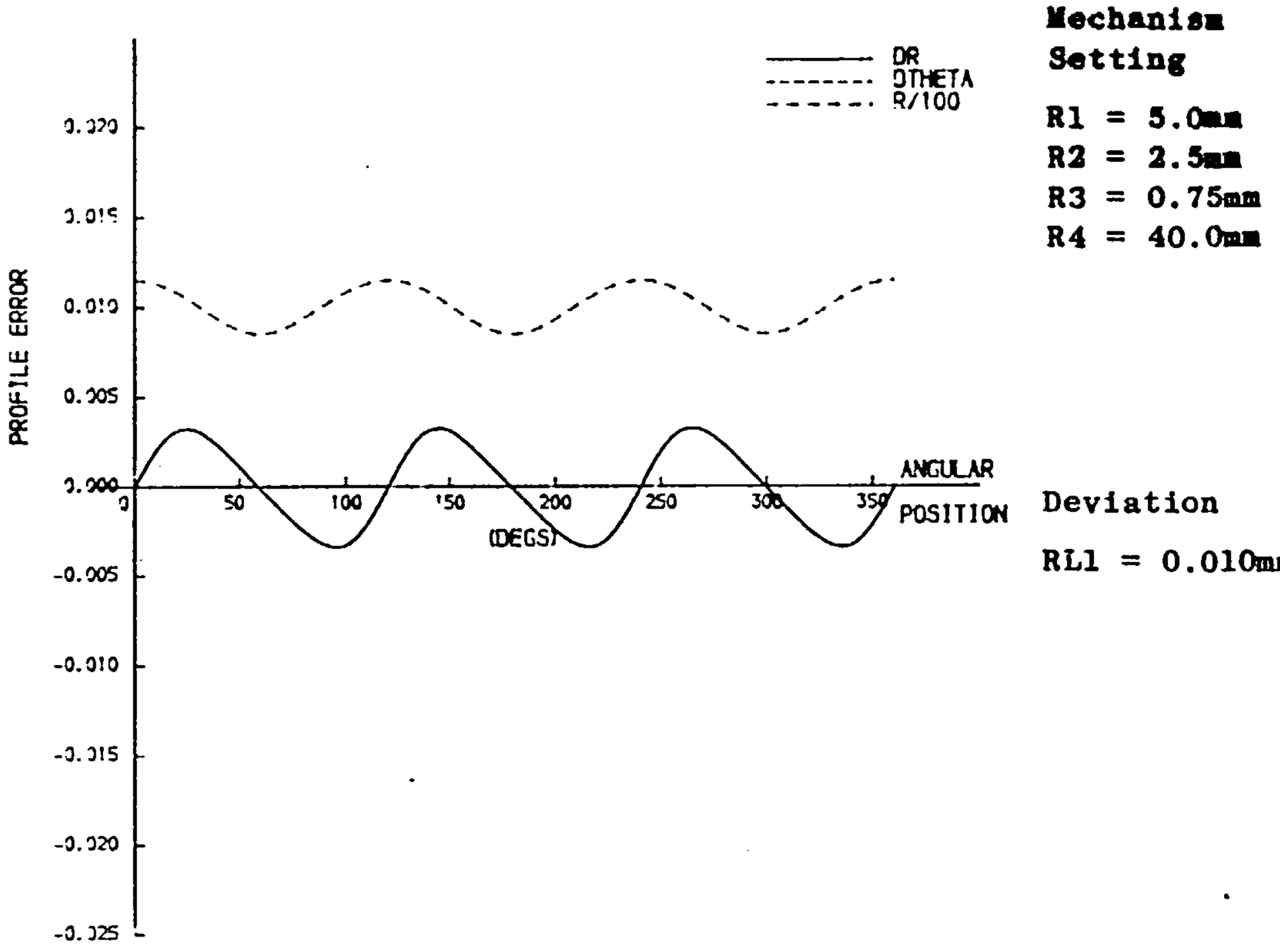

Profile error caused by constant deviations of individual parameters (notation of Fig.6.2)

Fig.A7.2 RL1 deviation

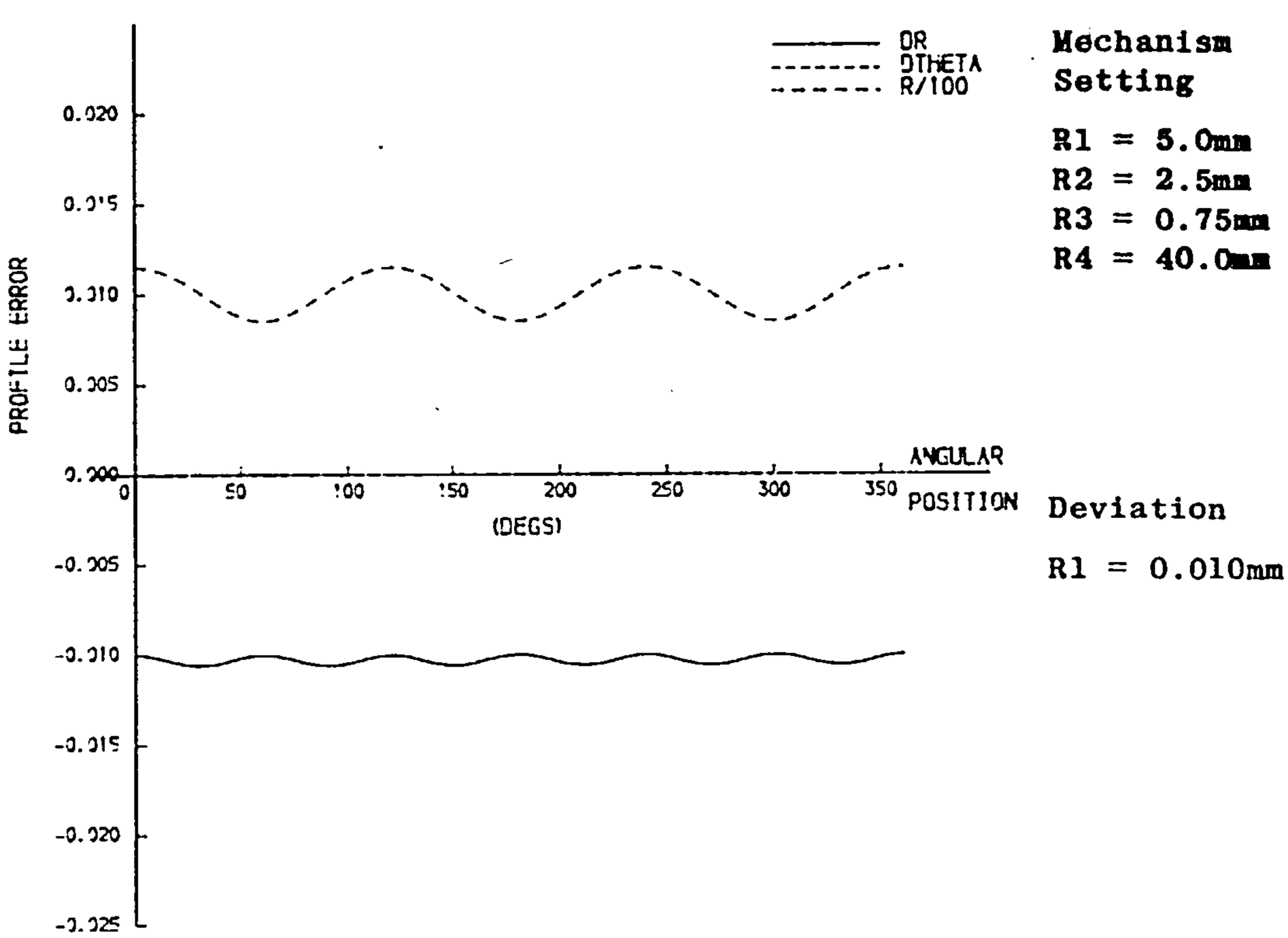

Profile error caused by constant deviations of individual parameters (notation of Fig.6.2)

Fig. A7.1 R1 deviation

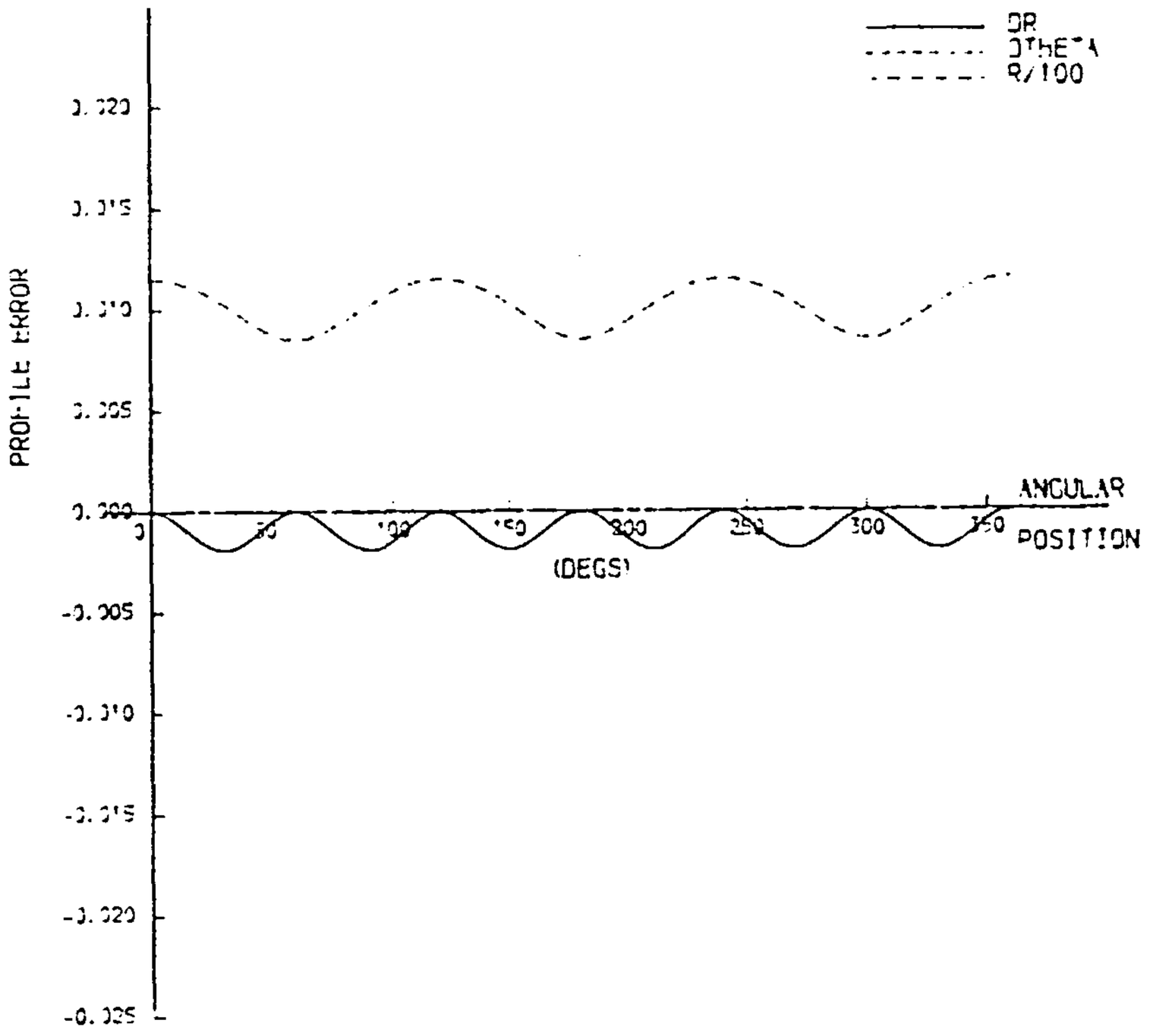

Profile error caused by constant deviations of individual parameters (notation of Fig.6.2)

Fig. A7.4 R2 deviation

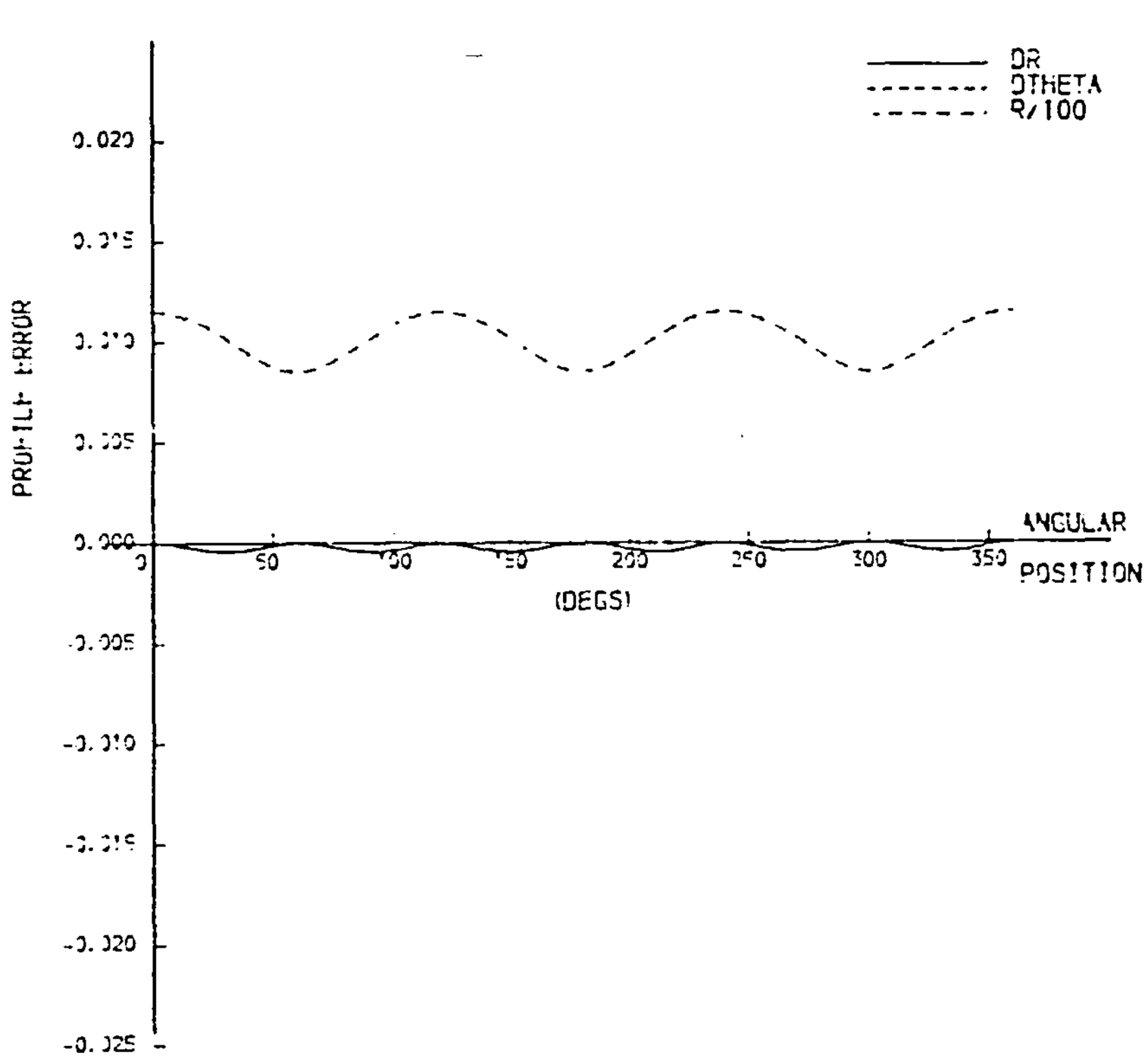

Profile error caused by constant deviations of individual parameters (Notation of Fig.6.2)

Fig. A7.3 R2 deviation

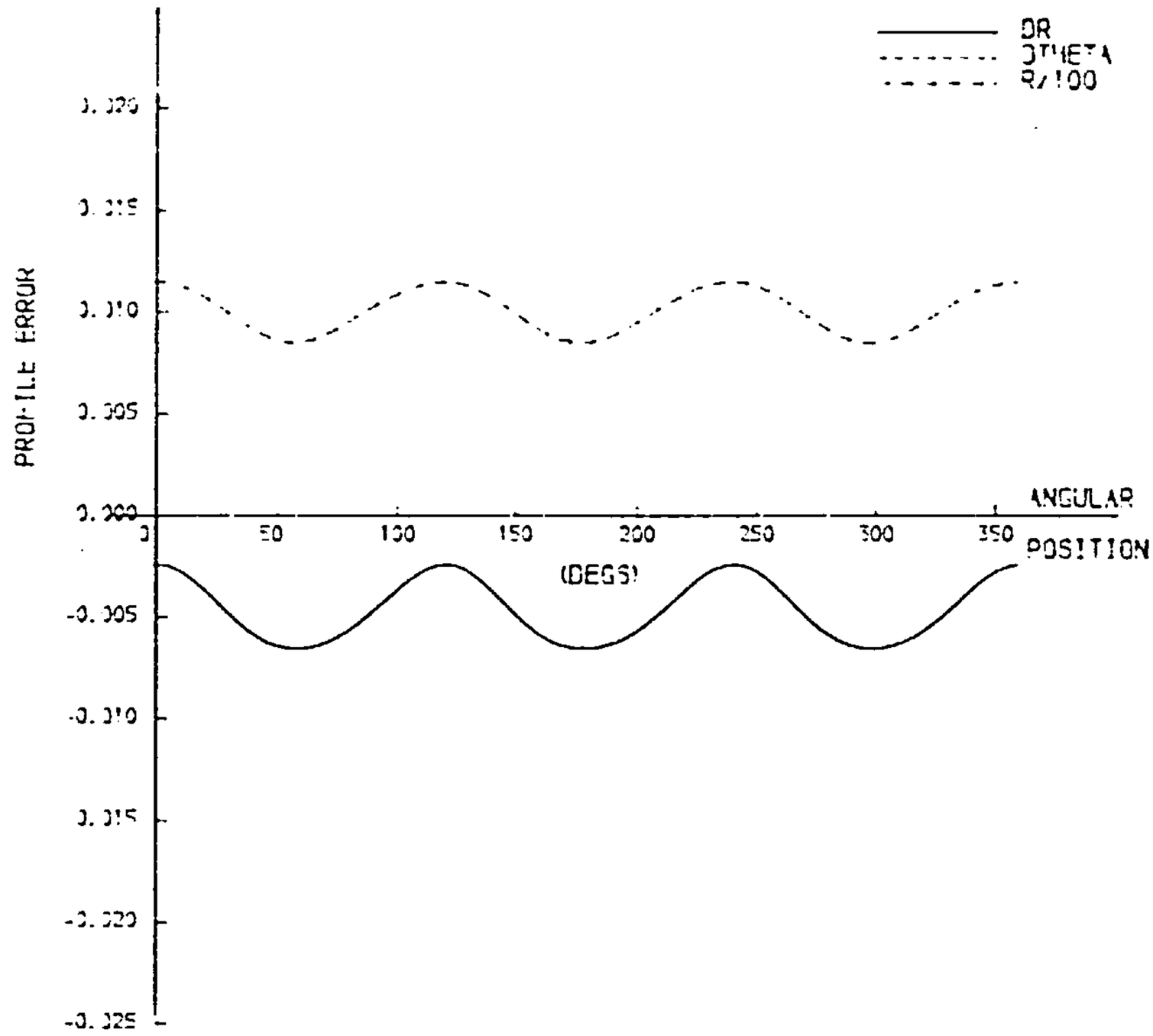

Mechanism Setting

R1 = 5.0mm
R2 = 2.5mm
R3 = 0.75mm
R4 = 40.0mm

Deviation

RP2 = 0.100mm

Profile error caused by constant deviations of individual parameters (notation of Fig.6.2)

Fig. A7.6 RP2 deviation

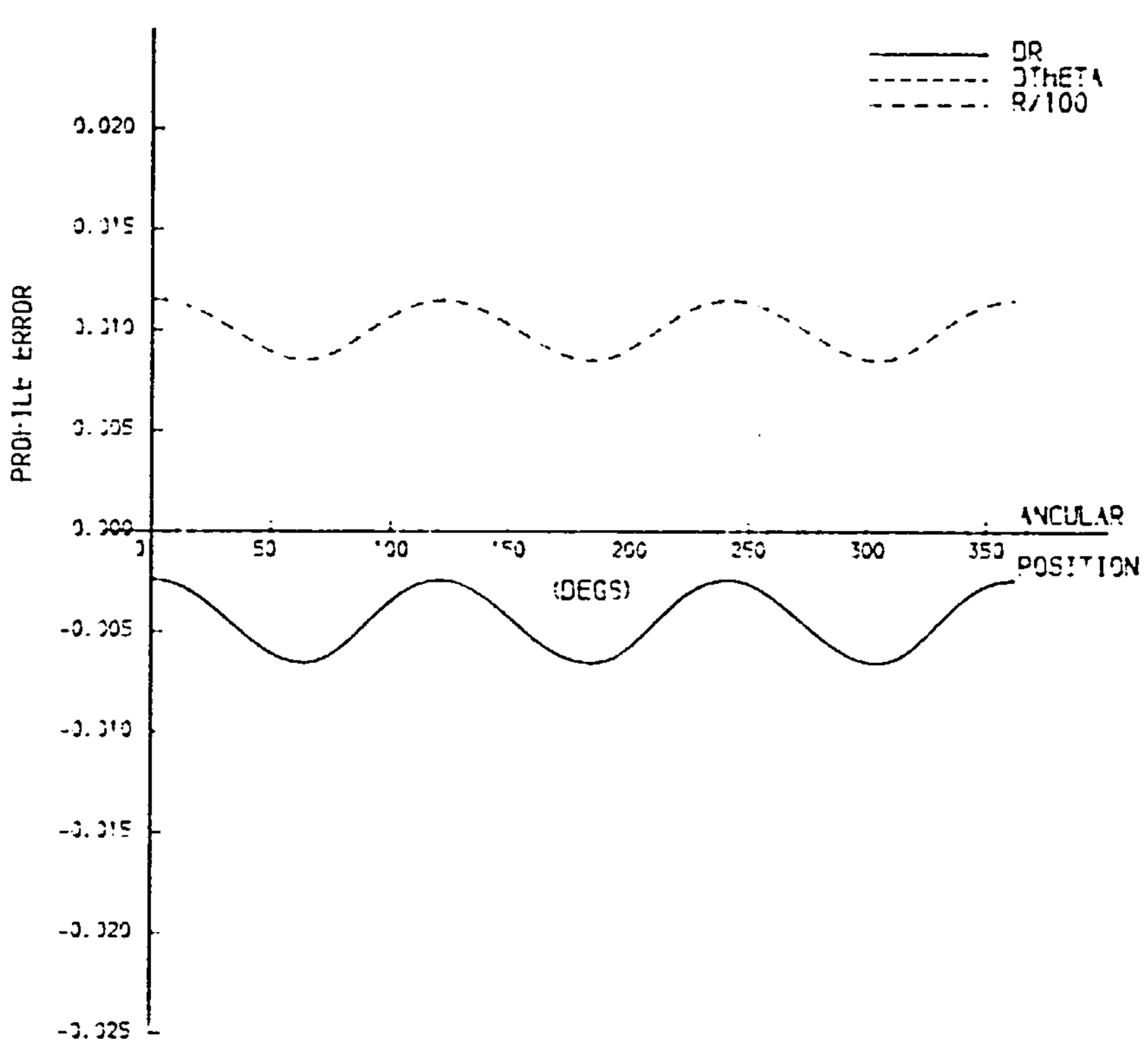

Mechanism Setting

R1 = 5.0mm
R2 = 2.5mm
R3 = 0.75mm
R4 = 40.0mm

Deviation

RL2 = 0.100mm

Profile error caused by constant deviations of individual parameters (notation of Fig.6.2)

Fig. A7.5 RL2 deviation

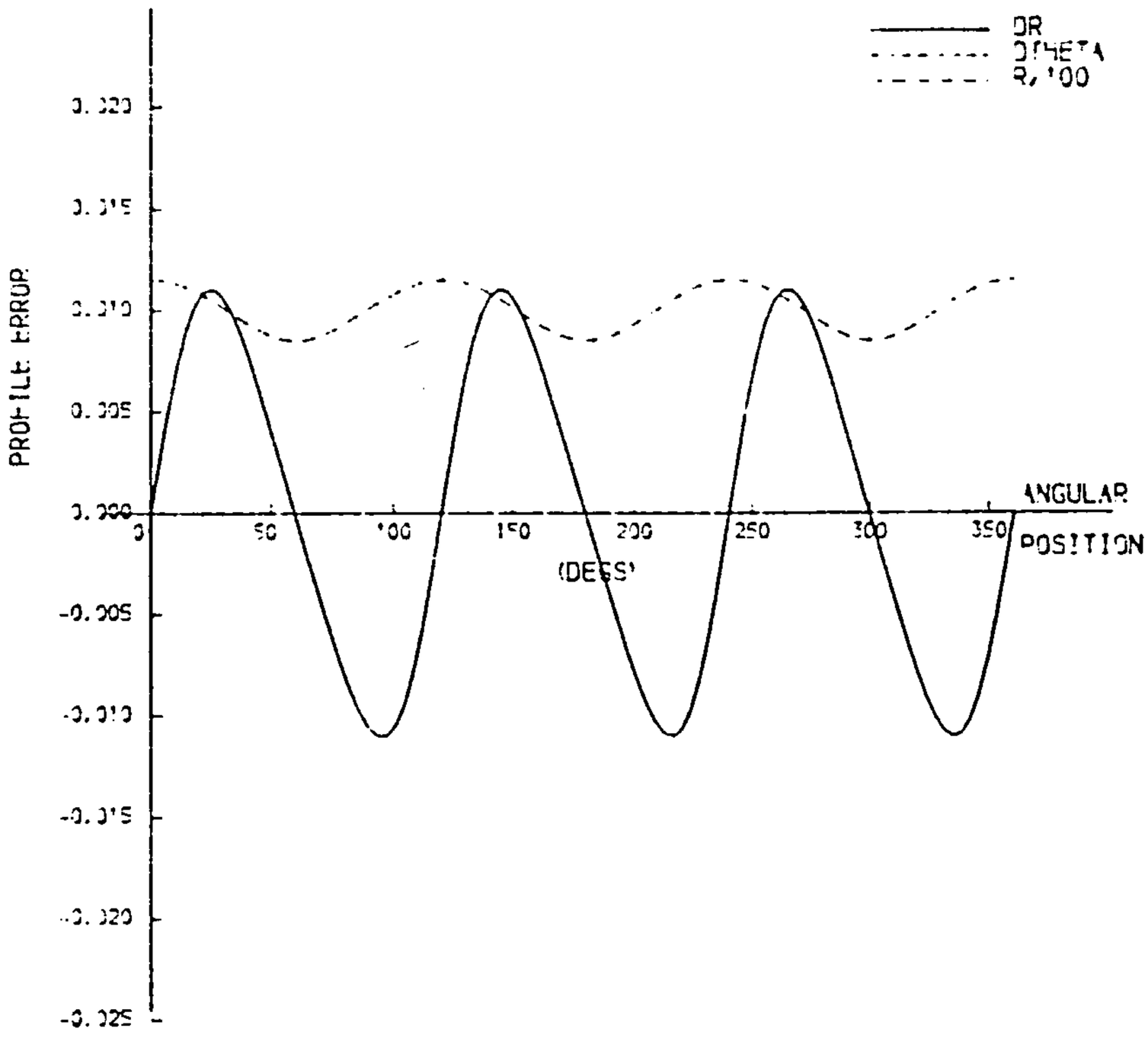

Profile error caused by constant deviations of individual parameters (notation of Fig.6.2)

Fig.A7.8 RL3 Deviation

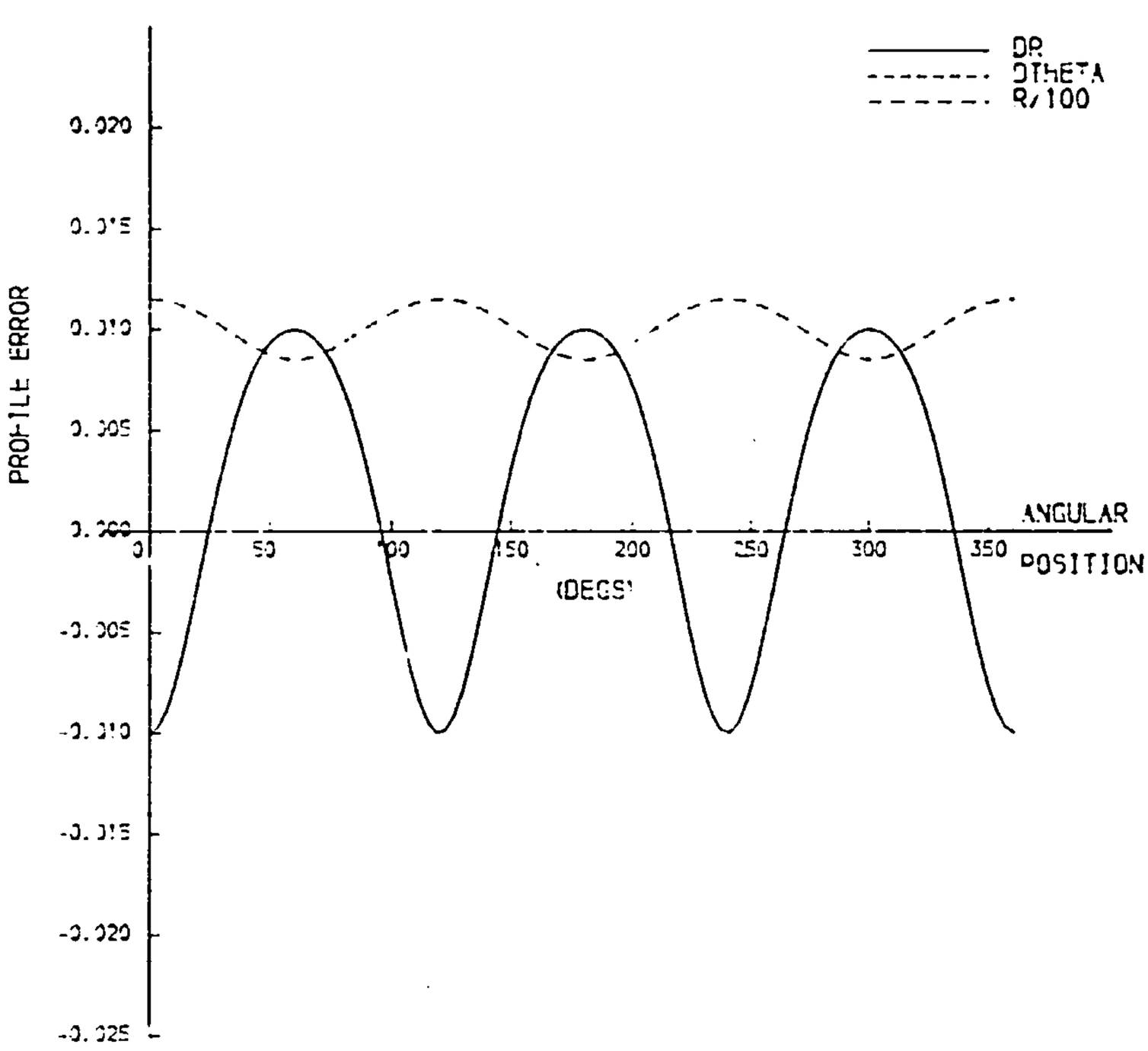

Profile error caused by constant deviations of individual parameters (notation of Fig.6.2)

Fig. A7.7 R3 Deviation

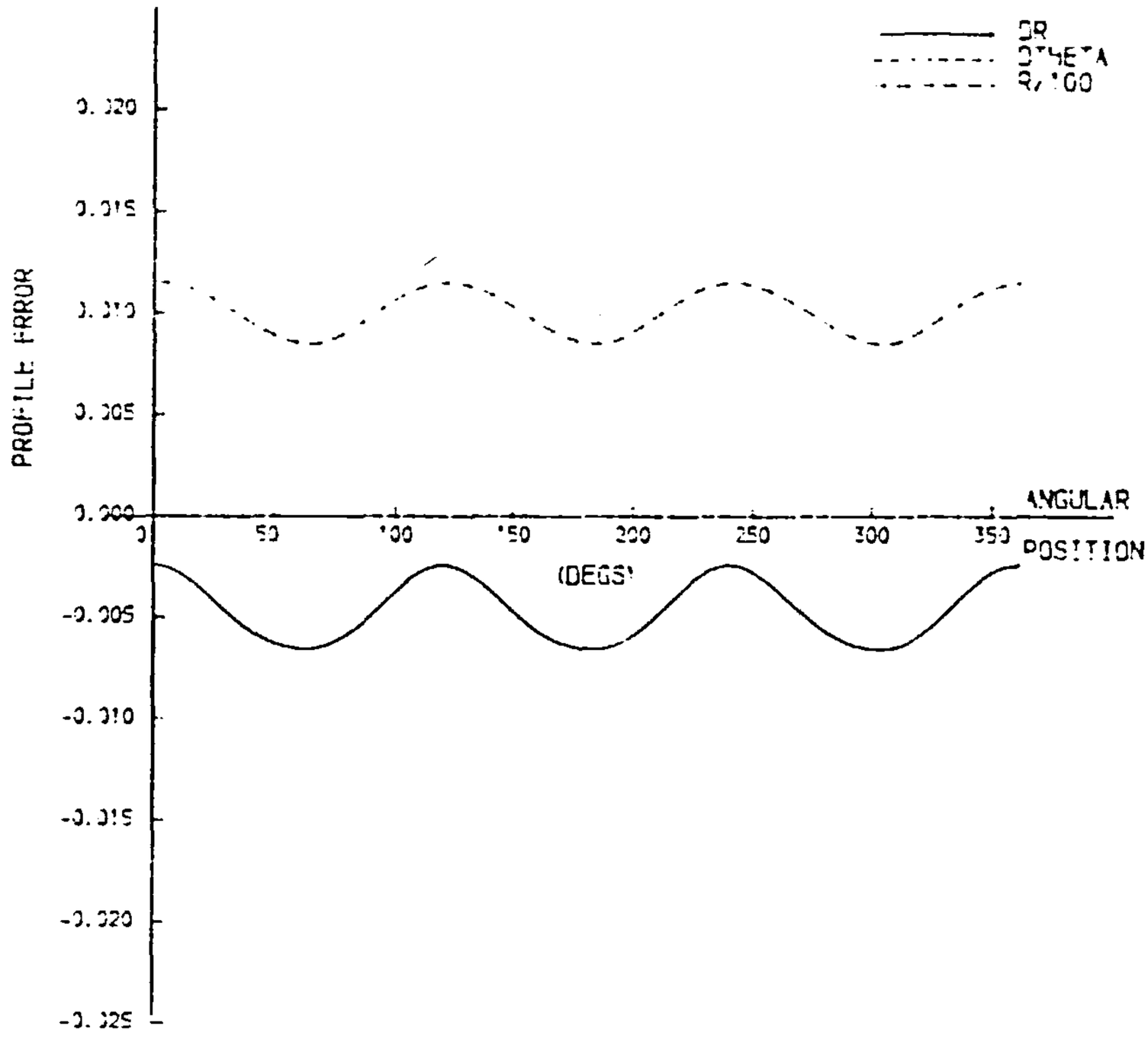

Mechanism Setting

R1 = 5.0mm
R2 = 2.5mm
R3 = 0.75mm
R4 = 40.0mm

Deviation

RP4 = 0.100mm

Profile error caused by constant deviations of individual parameters (notation of Fig.6.2)

Fig. A7.10 RP4 deviation

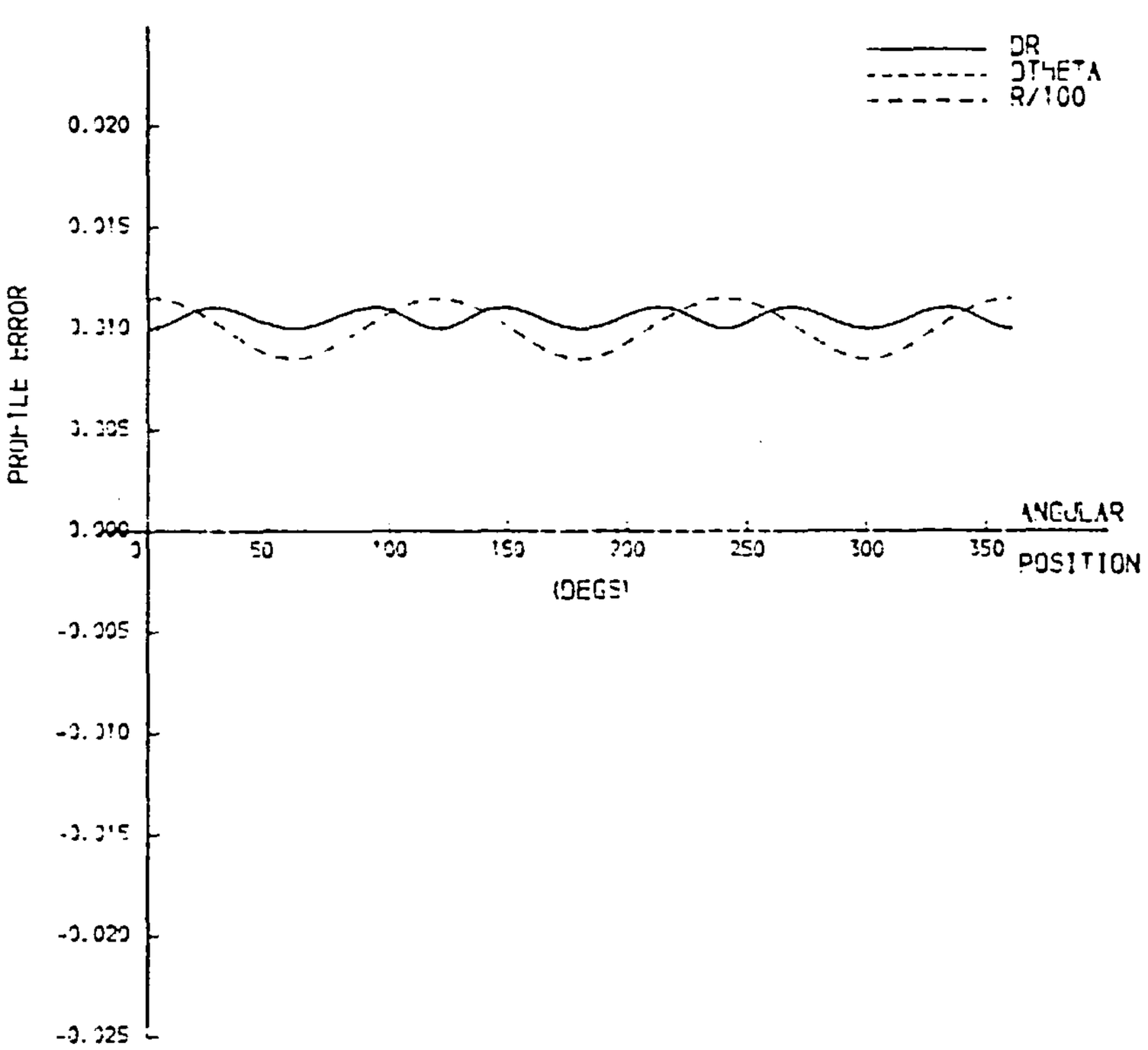

Mechanism Setting

R1 = 5.0mm
R2 = 2.5mm
R3 = 0.75mm
R4 = 40.0mm

Deviation

R4 = 0.010mm

Profile error caused by constant deviations of individual parameters (notation of Fig.6.2)

Fig. A7.9 R4 deviation

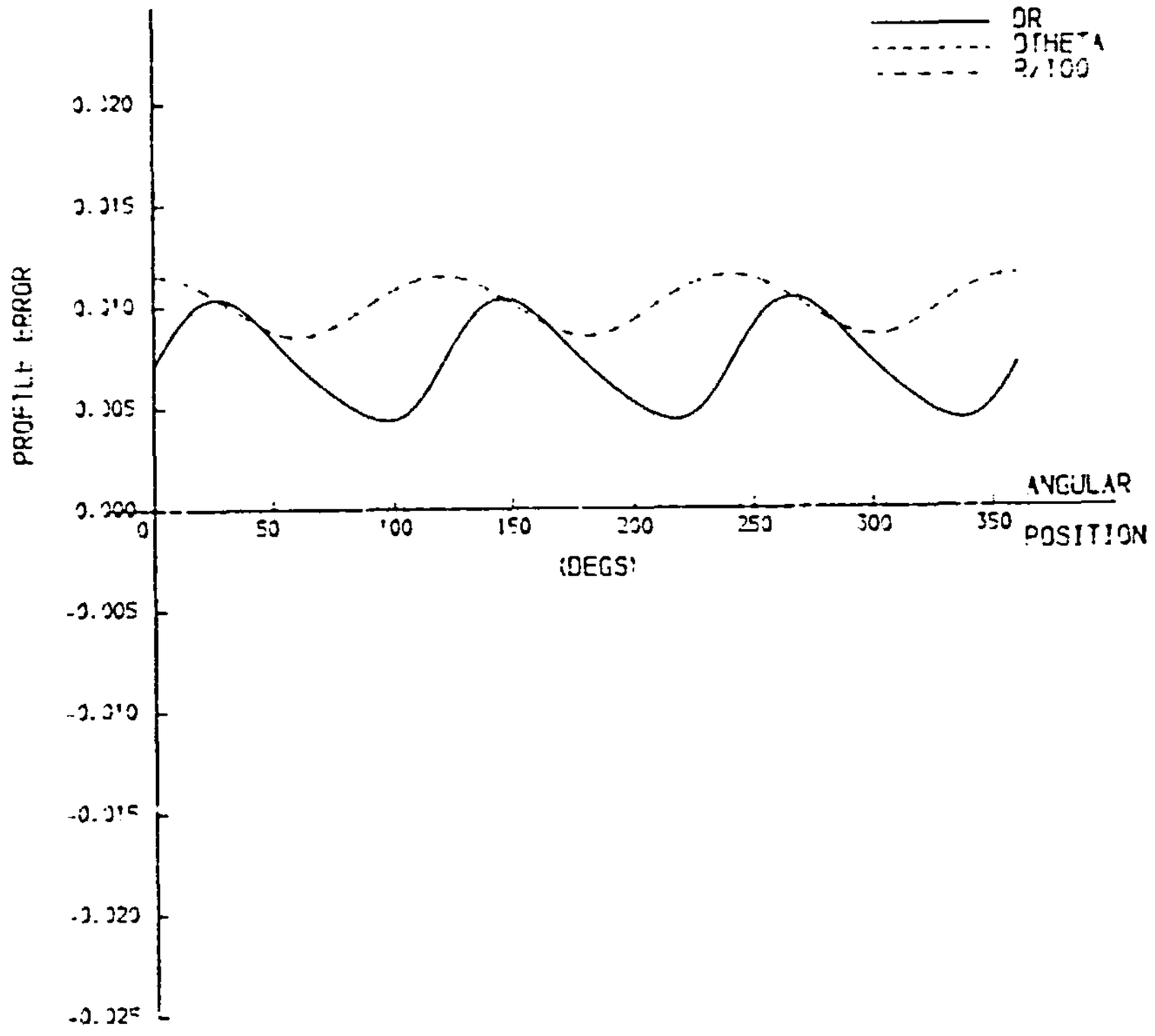

Mechanism Setting

R1 = 5.0mm
R2 = 2.5mm
R3 = 0.75mm
R4 = 40.0mm

Deviation

P1 = 0.010mm

Profile error caused by constant deviations of individual parameters (notation of Fig.6.2)

Fig. A7.12 P1 deviation

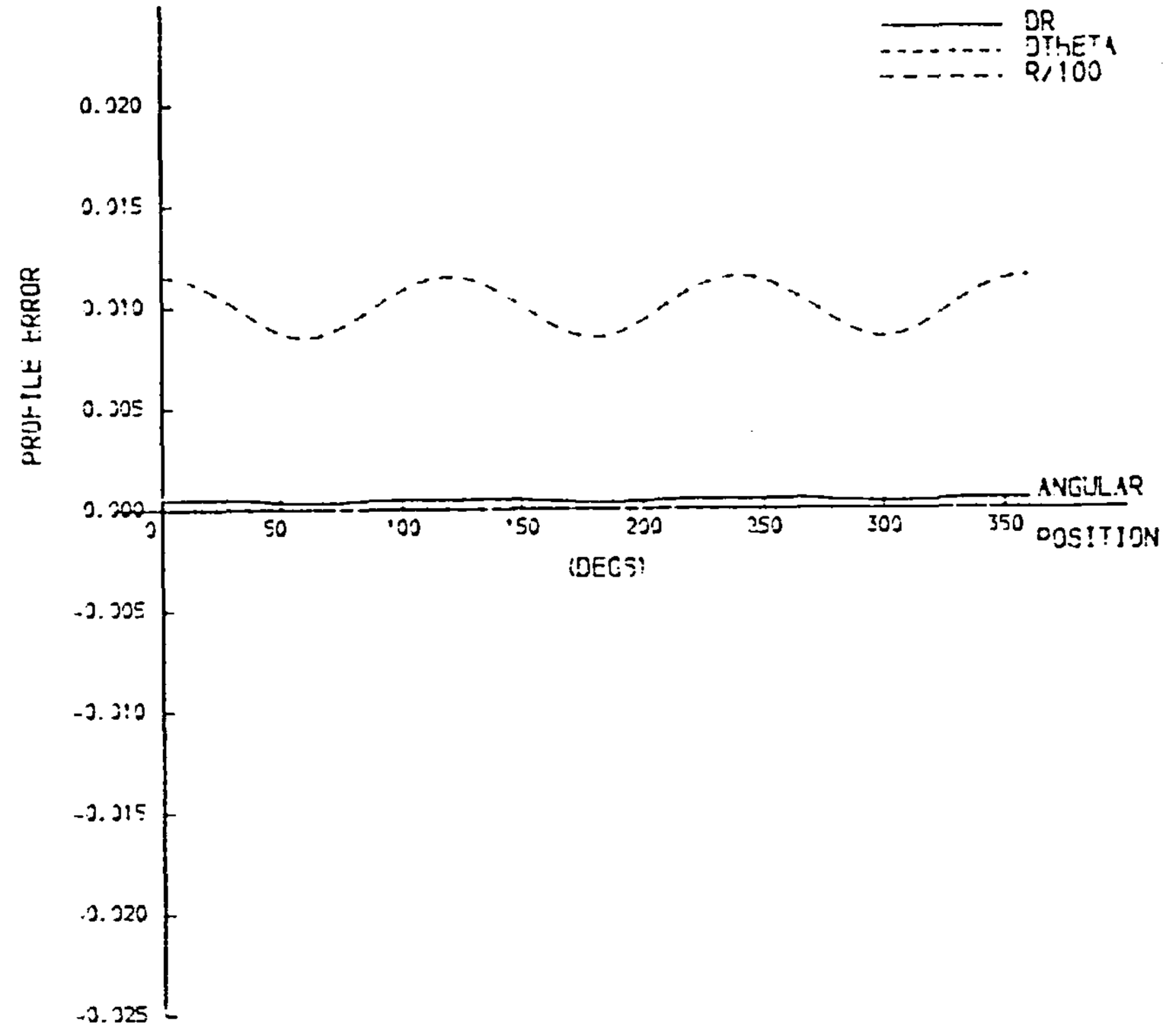

Mechanism Setting

R1 = 5.0mm
R2 = 2.5mm
R3 = 0.75mm
R4 = 40.0mm

Deviation

RL4 = 0.200mm

Profile error caused by constant deviations of individual parameters (notation of Fig.6.2)

Fig. A7.11 RL4 deviation

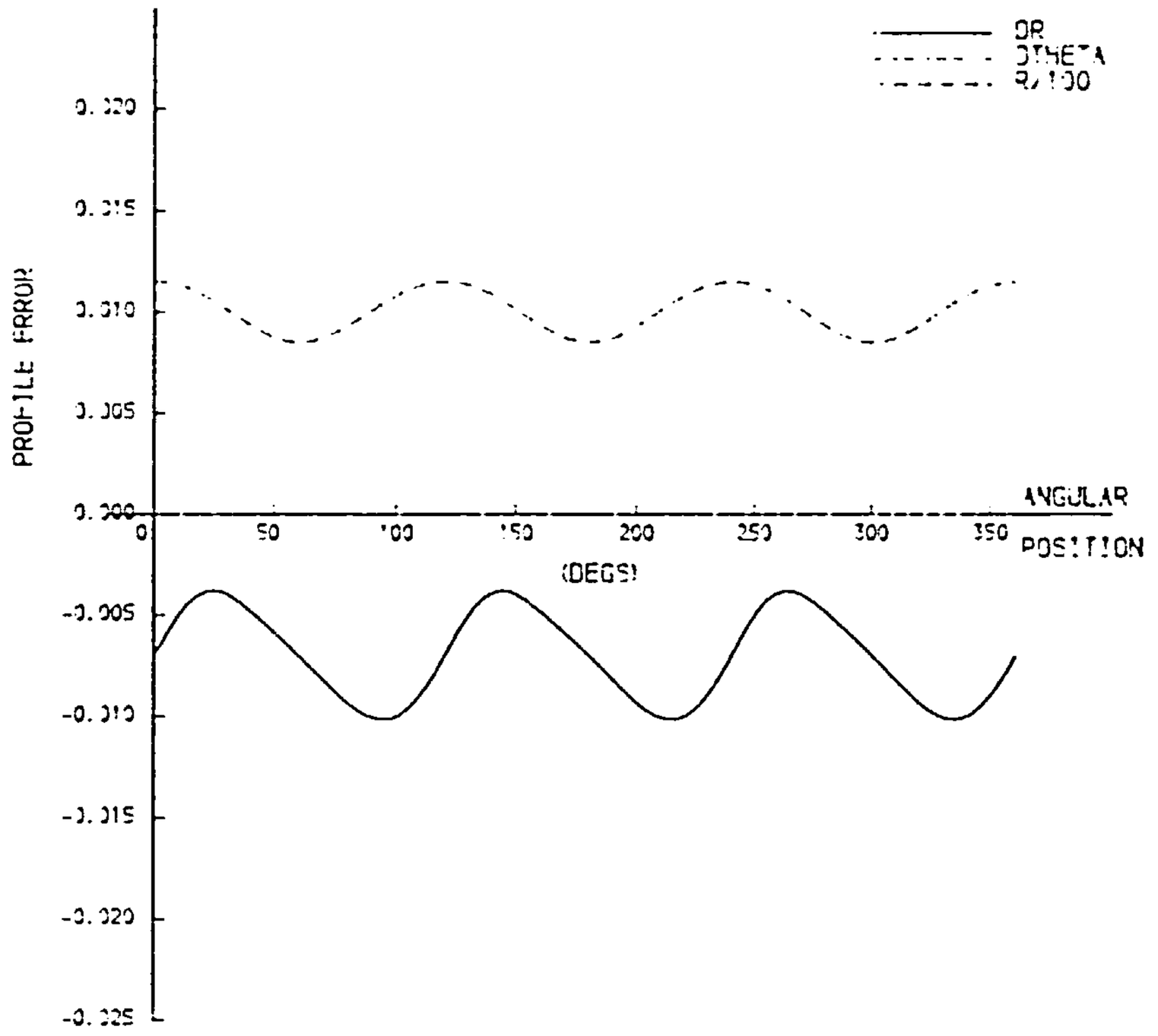

Profile error caused by constant deviations of individual parameters (notation of Fig.6.2)

Fig. A7.14 PL2 deviation

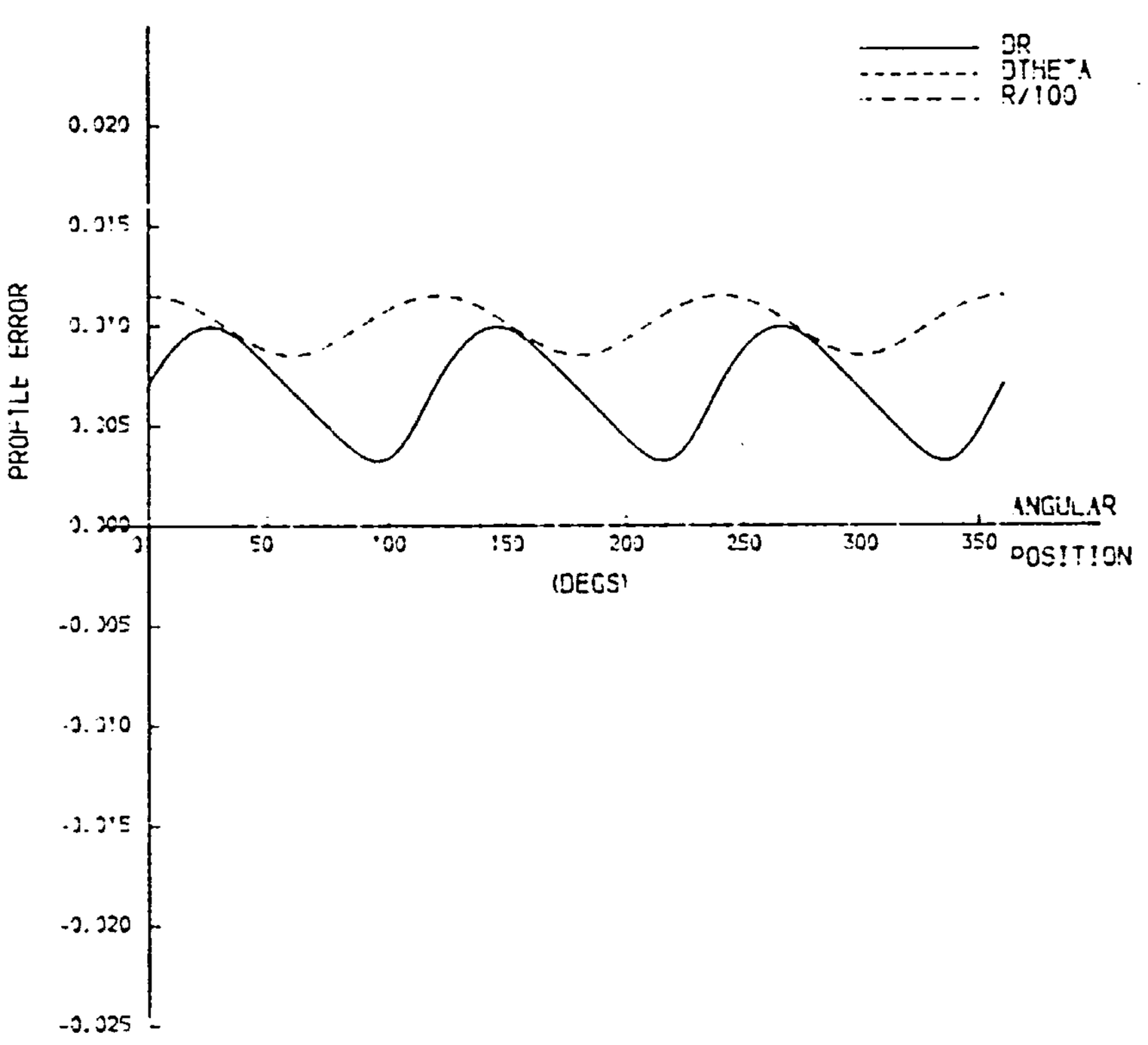

Profile error caused by constant deviations of individual parameters (notation of Fig.6.2)

Fig. A7.13 P2 deviation

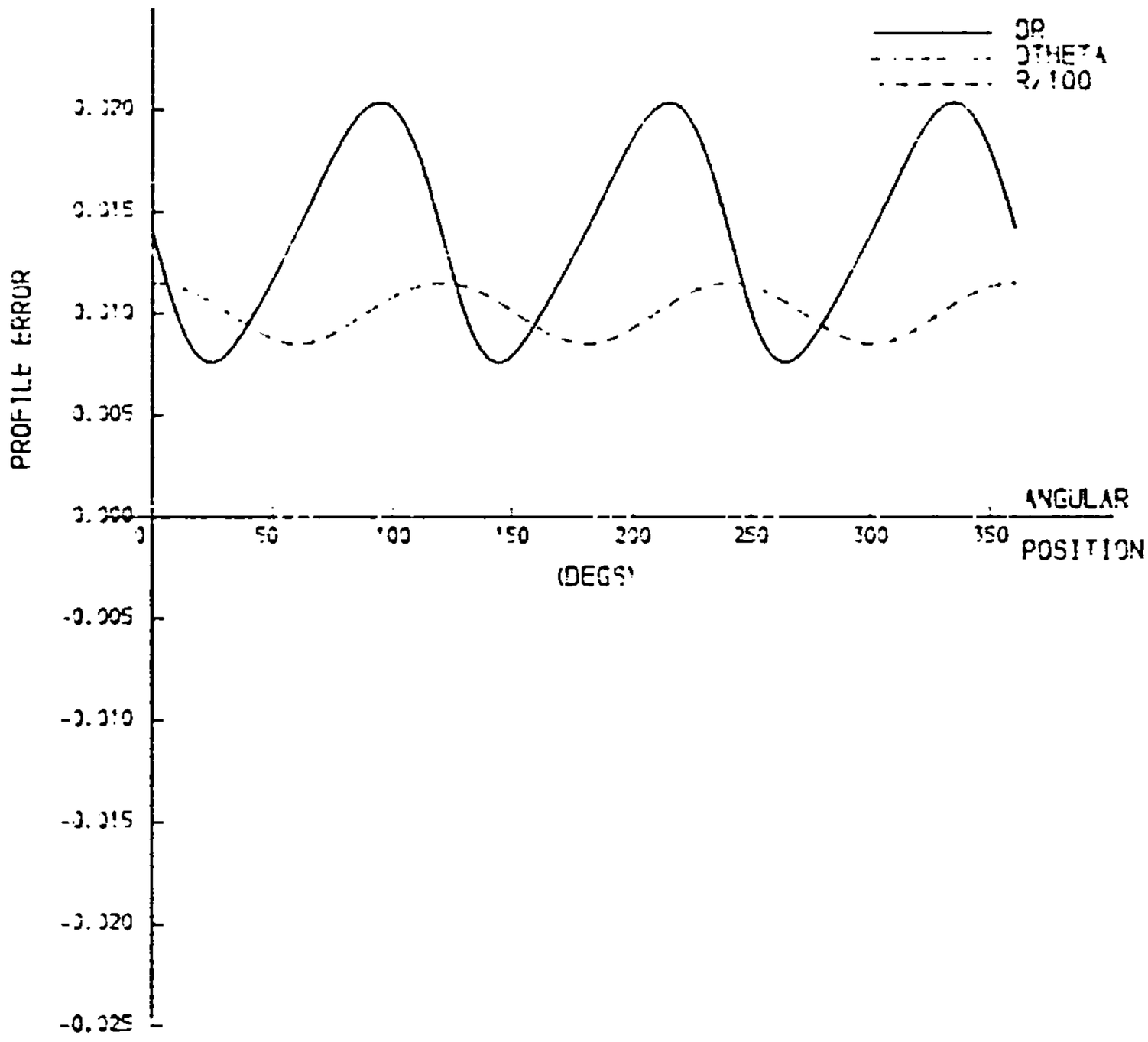

Mechanism Setting

R1 = 5.0mm
R2 = 2.5mm
R3 = 0.75mm
R4 = 40.0mm

Deviation

P4 = 0.010mm

Profile error caused by constant deviations of individual parameters (notation of Fig.6.2)

Fig. A7.16 P4 deviation

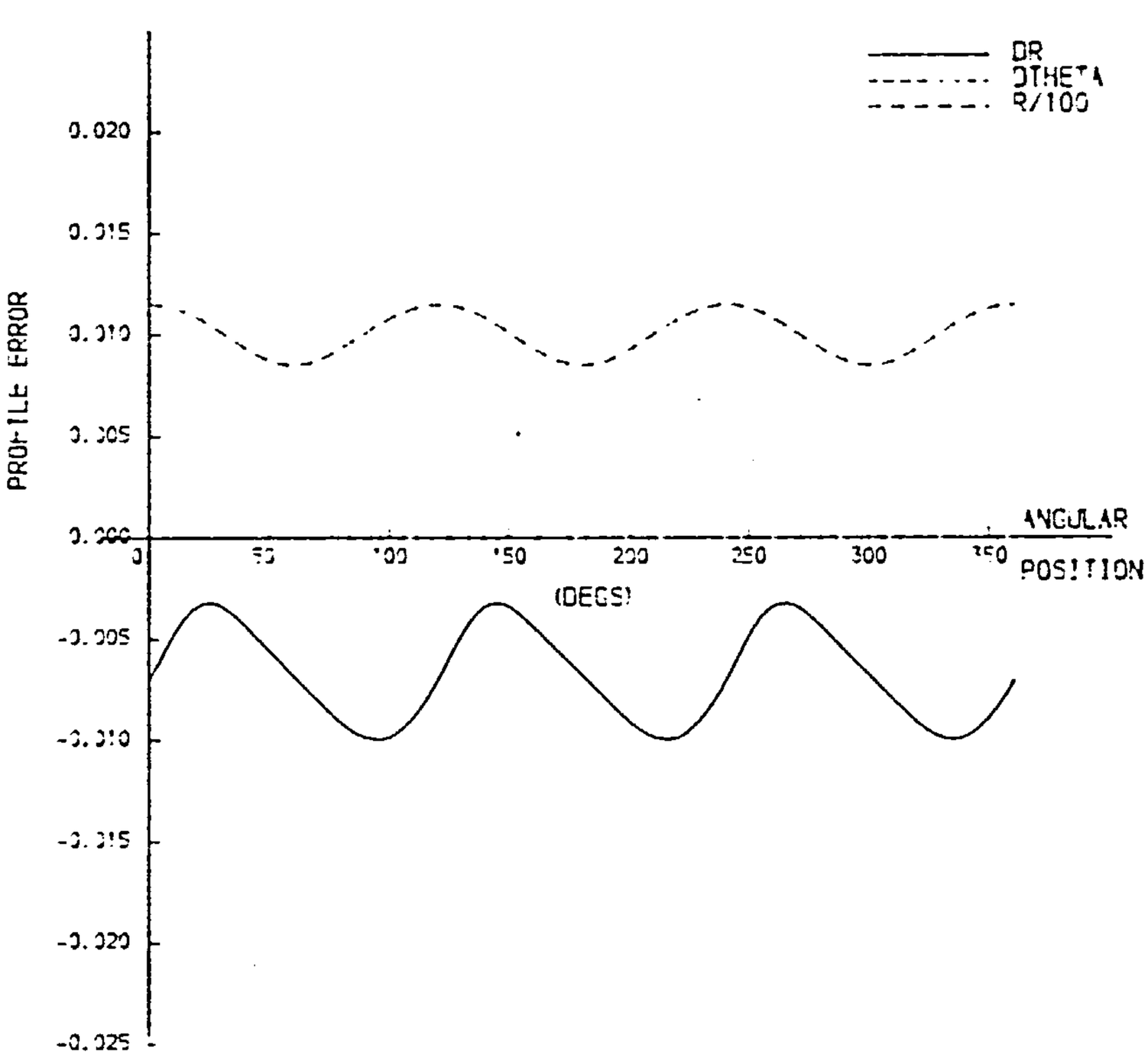

Mechanism Setting

R1 = 5.0mm
R2 = 2.5mm
R3 = 0.75mm
R4 = 40.0mm

Deviation

P3 = 0.010mm

Profile error caused by constant deviations of individual parameters (notation of Fig.6.2)

Fig. A7.15 P3 deviation

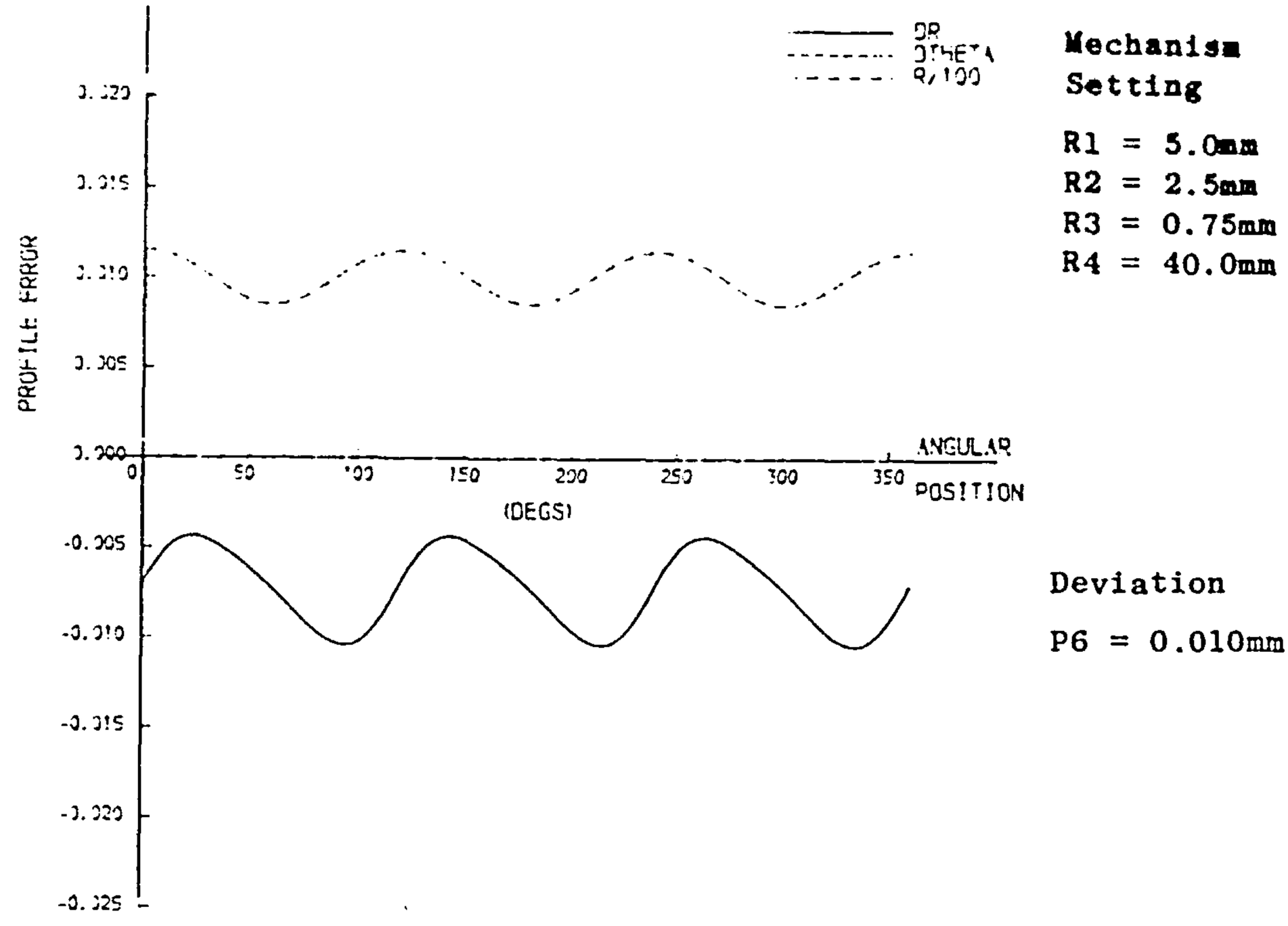

Profile error caused by constant deviations of individual parameters (notation of Fig.6.2)

Fig. A7.18 P6 deviation

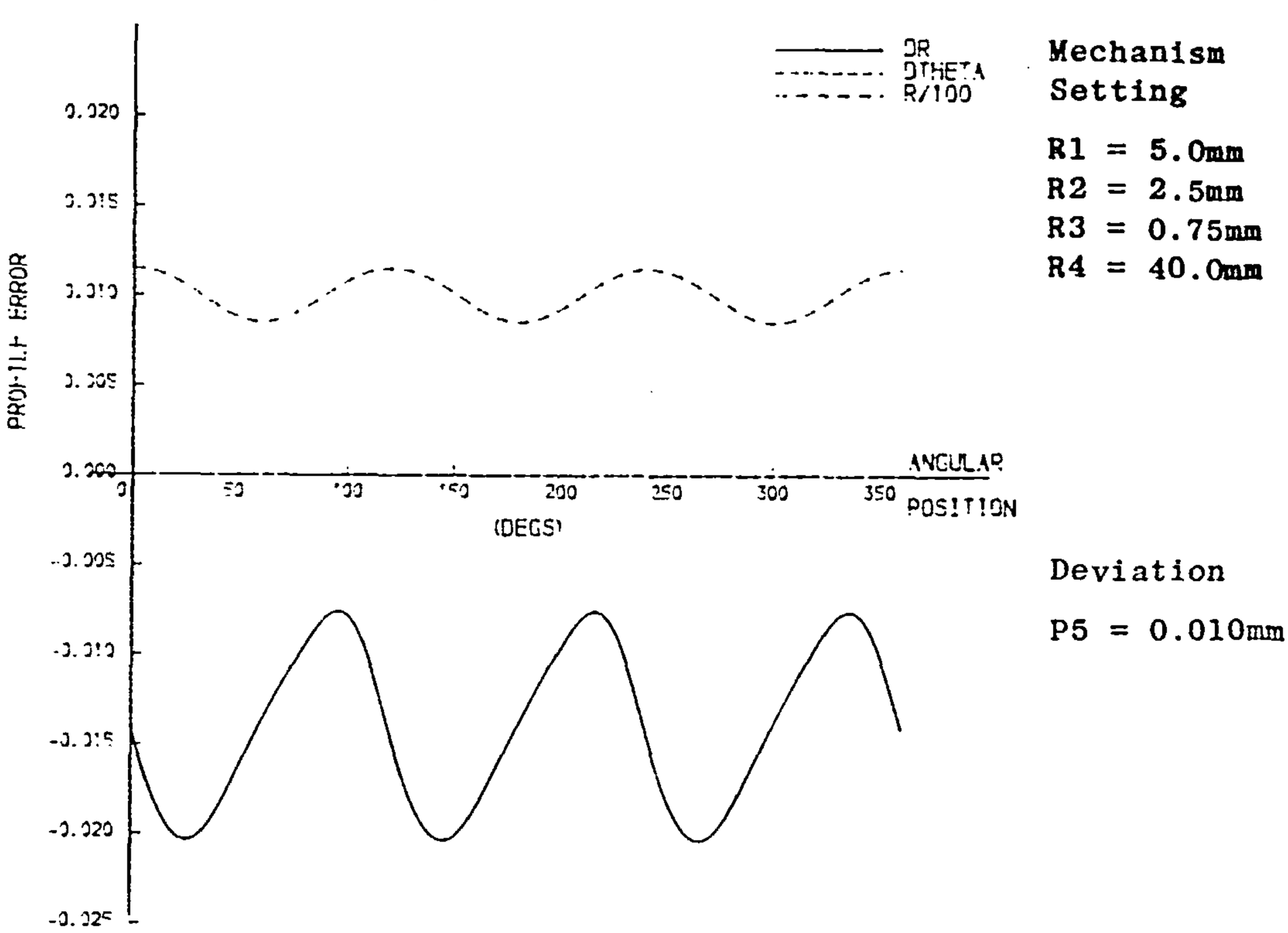

Profile error caused by constant deviations of individual parameters (notation of Fig.6.2)

Fig. A7.17 P5 deviation

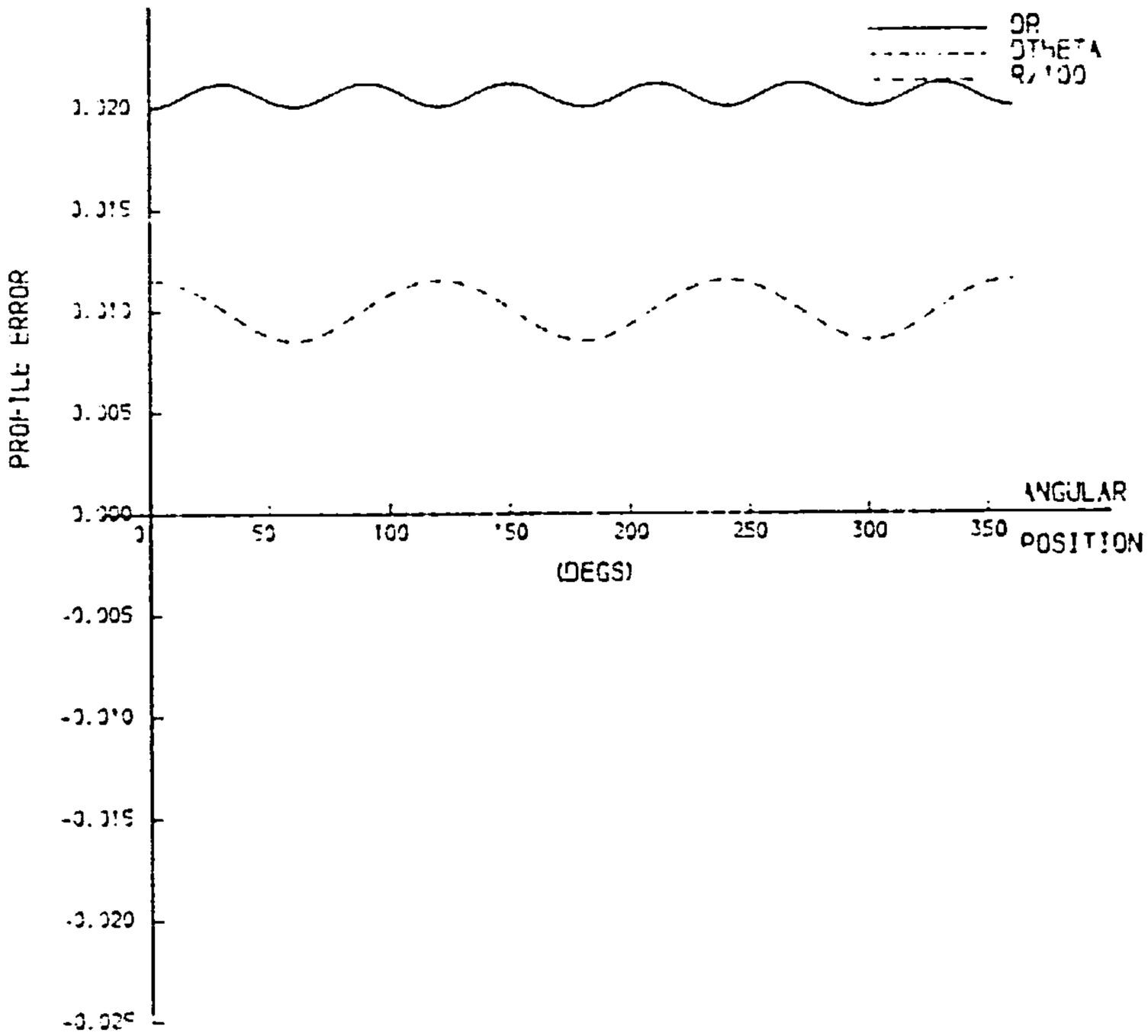

Mechanism Setting

R1 = 5.0mm
R2 = 2.5mm
R3 = 0.75mm
R4 = 40.0mm

Deviation

U4 = 0.010mm

Profile error caused by constant deviations of individual parameters (notation of Fig.6.2)

Fig.A7.20 U4 deviation

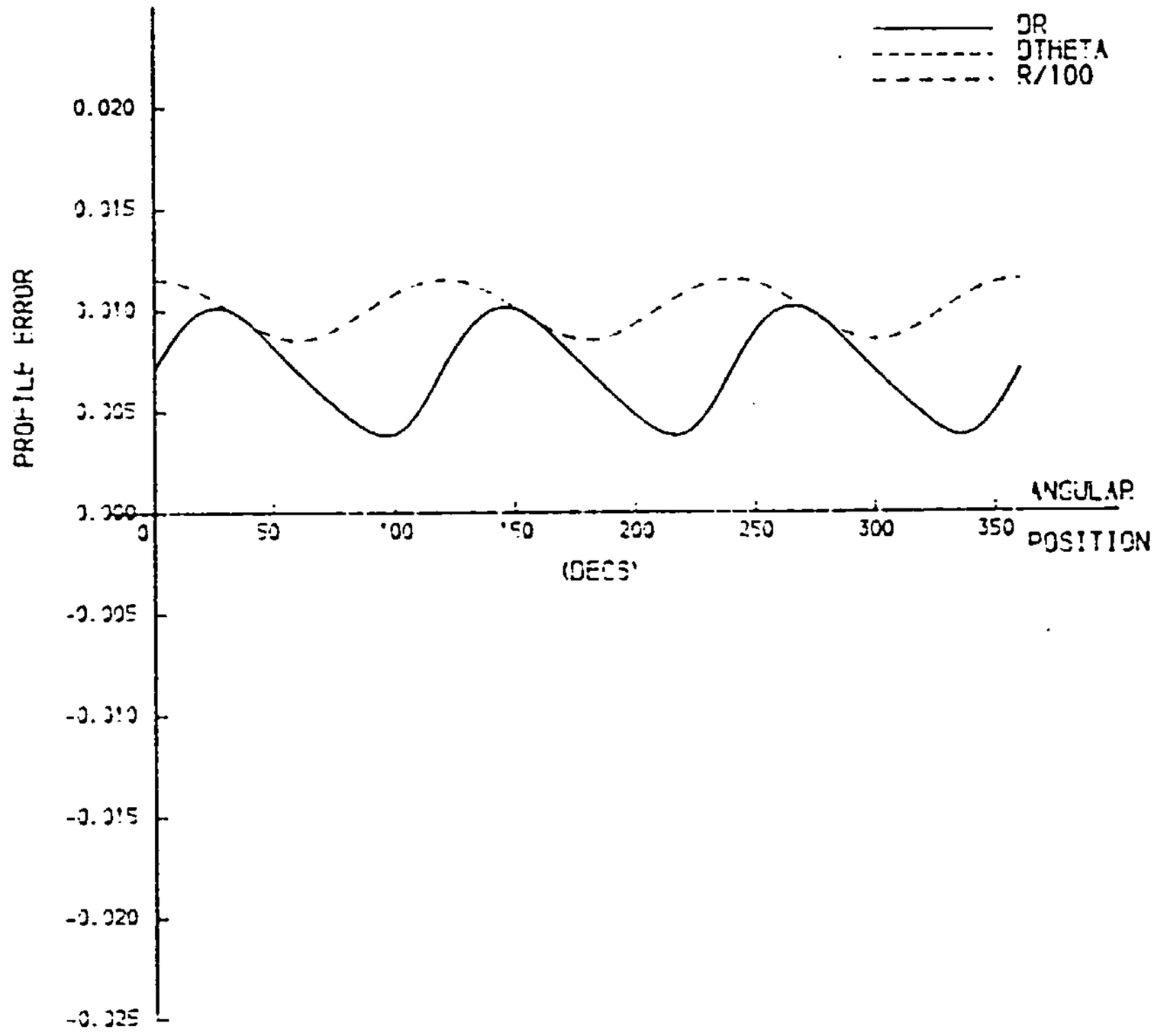

Mechanism Setting

R1 = 5.0mm
R2 = 2.5mm
R3 = 0.75mm
R4 = 40.0mm

Deviation

PL6 = 0.010mm

Profile error caused by constant deviations of individual parameters (notation of Fig.6.2)

Fig. A7.19 PL6 deviation

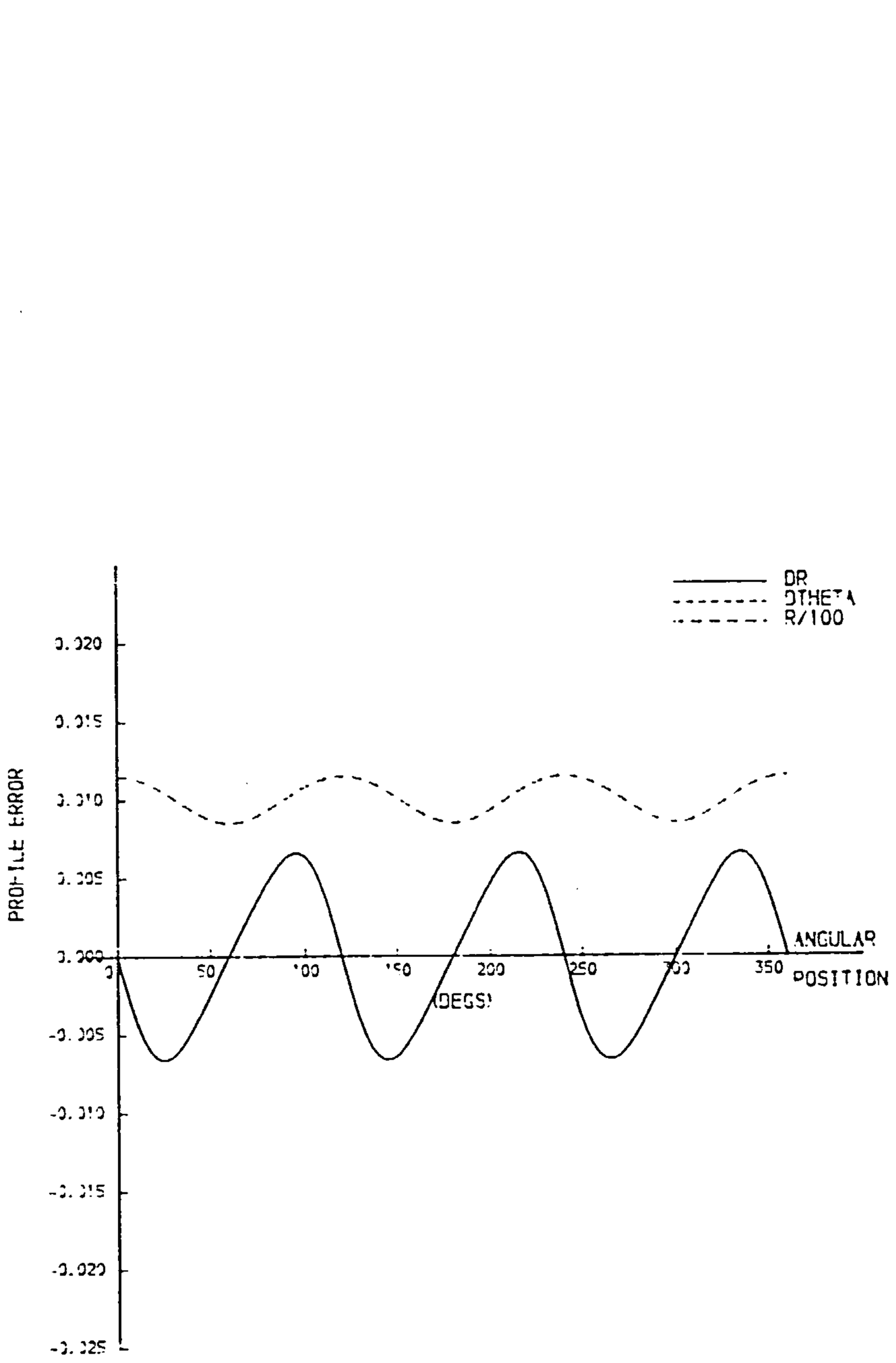

Mechanism Setting

R1 = 5.0mm
R2 = 2.5mm
R3 = 0.75mm
R4 = 40.0mm

Deviation

V4 = 0.010mm

Profile error caused by constant deviations of individual parameters (notation of Fig.6.2)

Fig. A7.21 V4 deviation

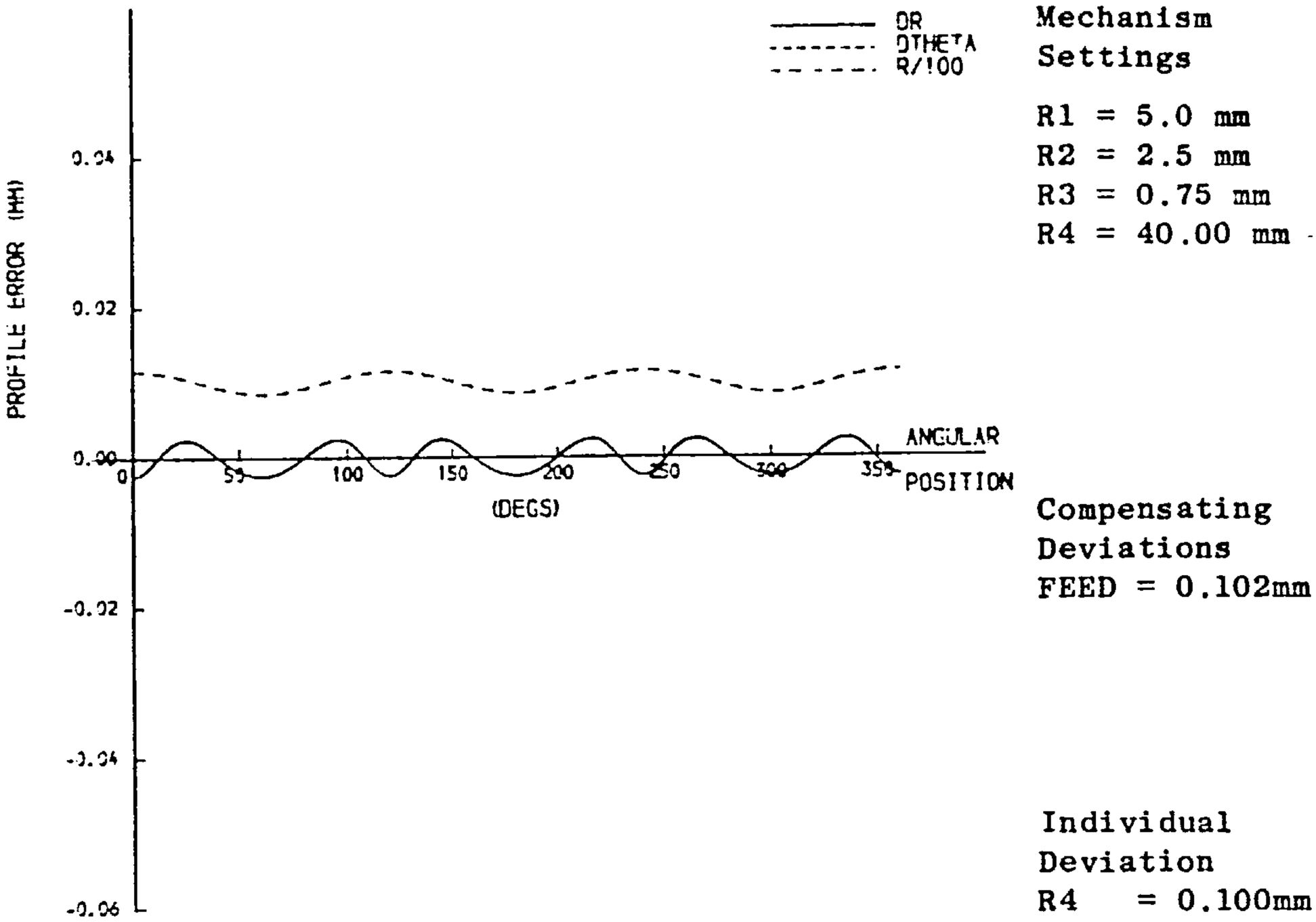

Mechanism Settings

R1 = 5.0 mm
R2 = 2.5 mm
R3 = 0.75 mm
R4 = 40.00 mm

Compensating Deviations
FEED = 0.102mm

Individual Deviation
R4 = 0.100mm

Compensation of constant deviations of individual parameters

Fig. A8.1 R4 deviation

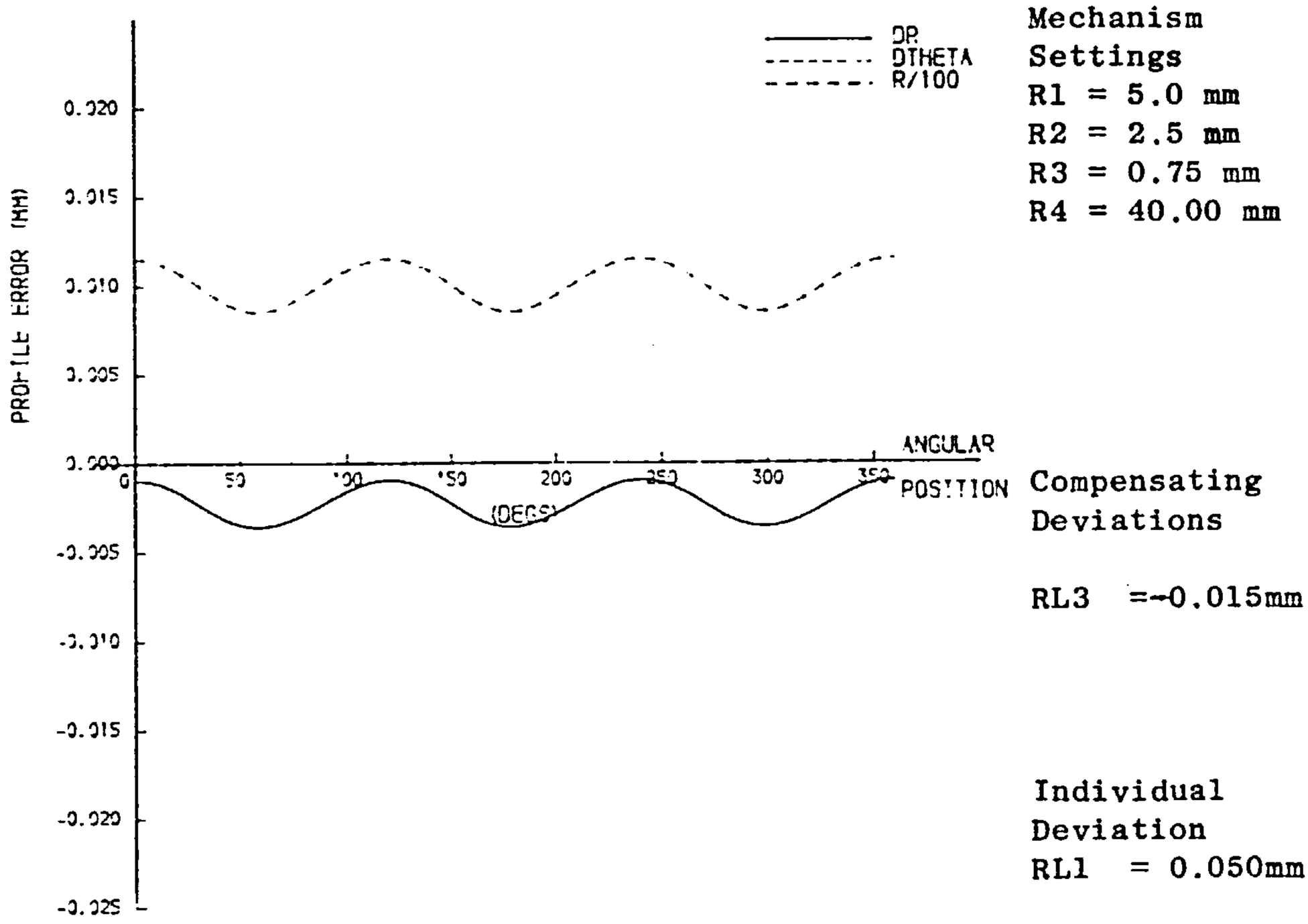

Mechanism Settings

R1 = 5.0 mm
R2 = 2.5 mm
R3 = 0.75 mm
R4 = 40.00 mm

Compensating Deviations

RL3 =-0.015mm

Individual Deviation
RL1 = 0.050mm

Compensation of constant deviations of individual parameters

Fig. A8.2 RL1 deviation

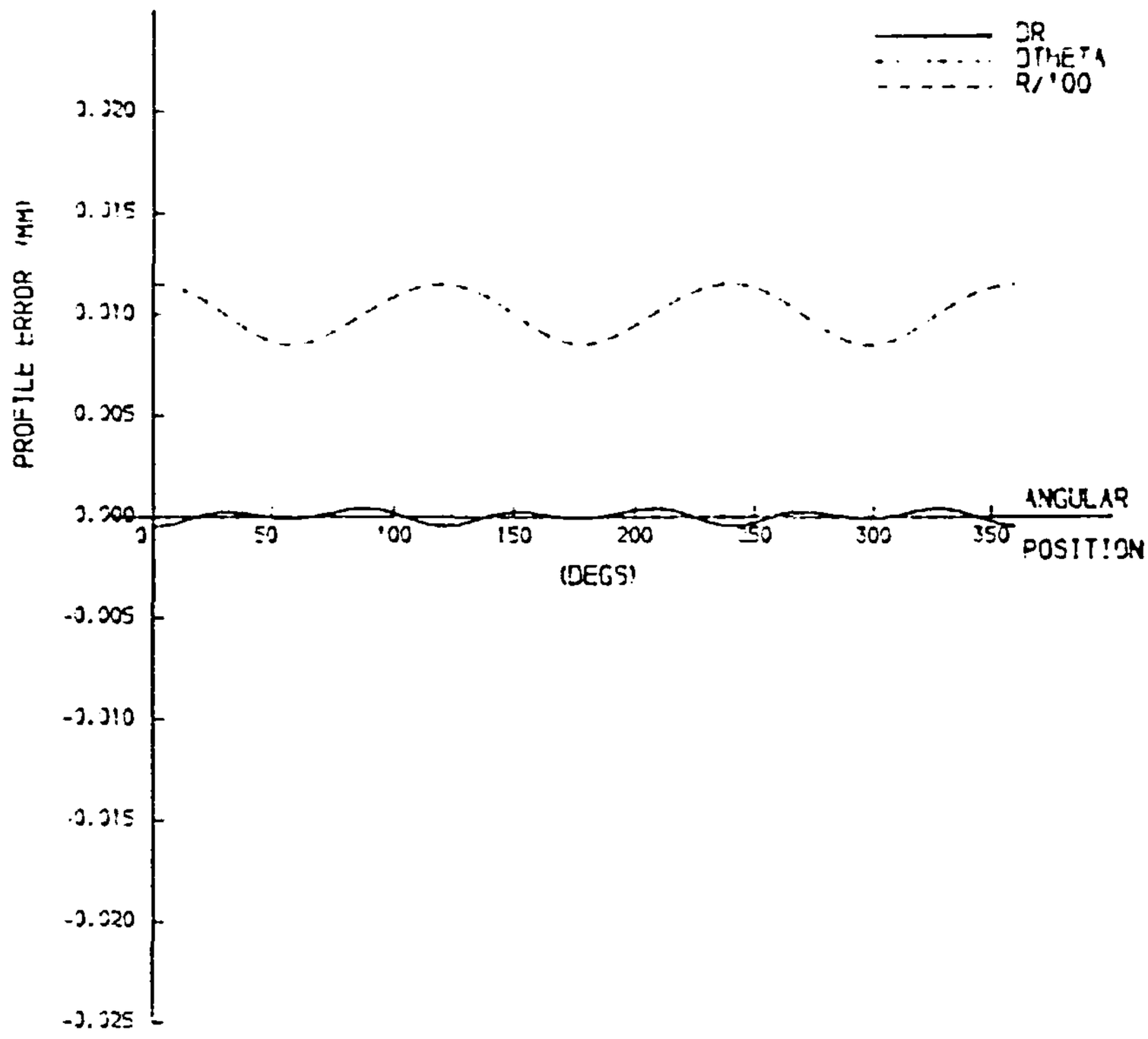

Mechanical Settings

R1 = 5.0 mm
R2 = 2.5 mm
R3 = 0.75 mm
R4 = 40.00 mm

Compensating Deviations
FEED = -0.002mm
RL3 = -0.015mm
R3 = 0.0015mm

Individual Deviation
RL1 = 0.050mm

Compensation of constant deviations of individual parameters

Fig. A8.3 RL1 deviation

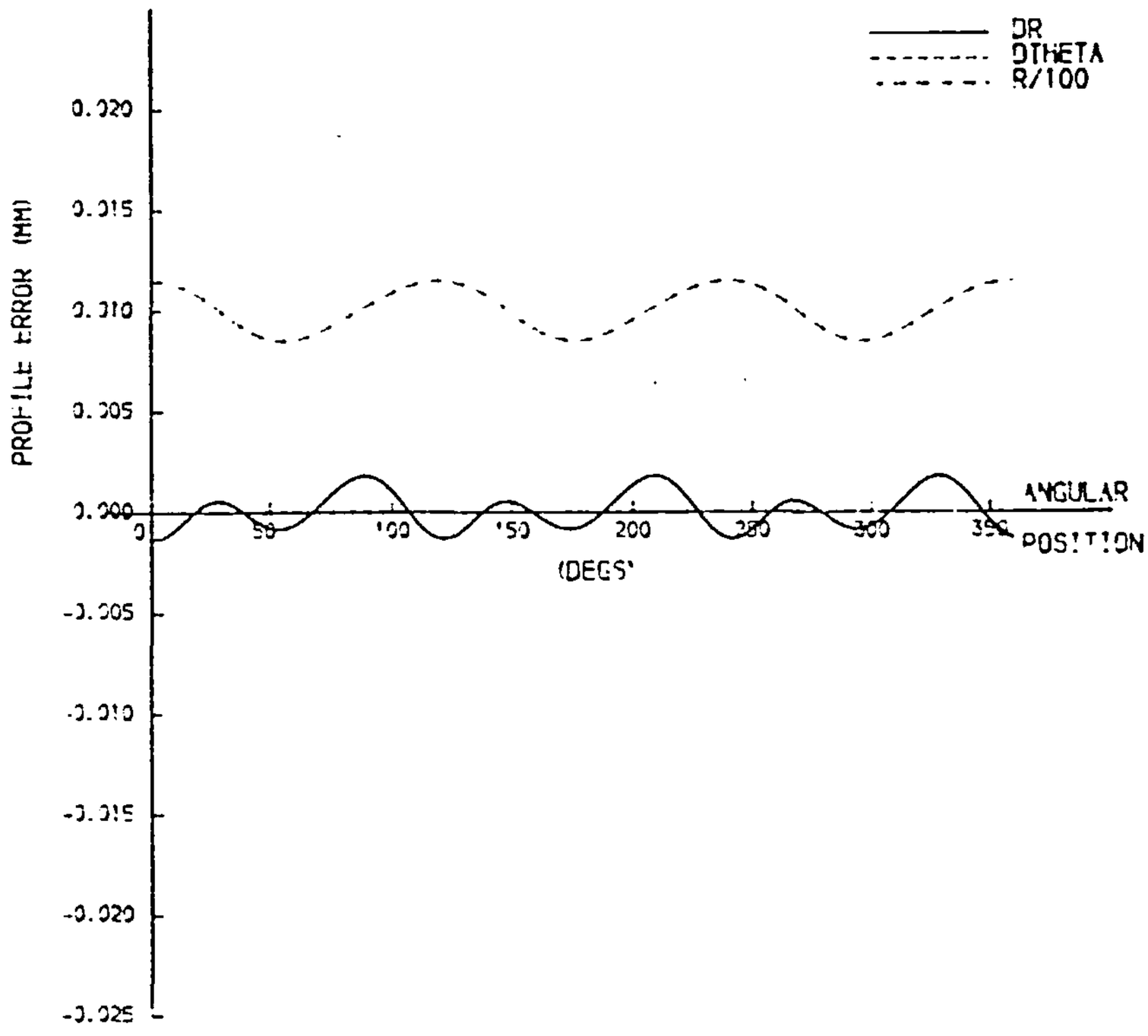

Mechanical Settings

R1 = 5.0 mm
R2 = 2.5 mm
R3 = 0.75mm
R4 = 40.00mm

Compensating Deviations
FEED = -0.008mm
RL3 = -0.030mm
R3 = 0.005 mm

Individual Deviation
RL1 = 0.100

Compensation of constant deviations of individual parameters

Fig. A8.4 RL1 deviation

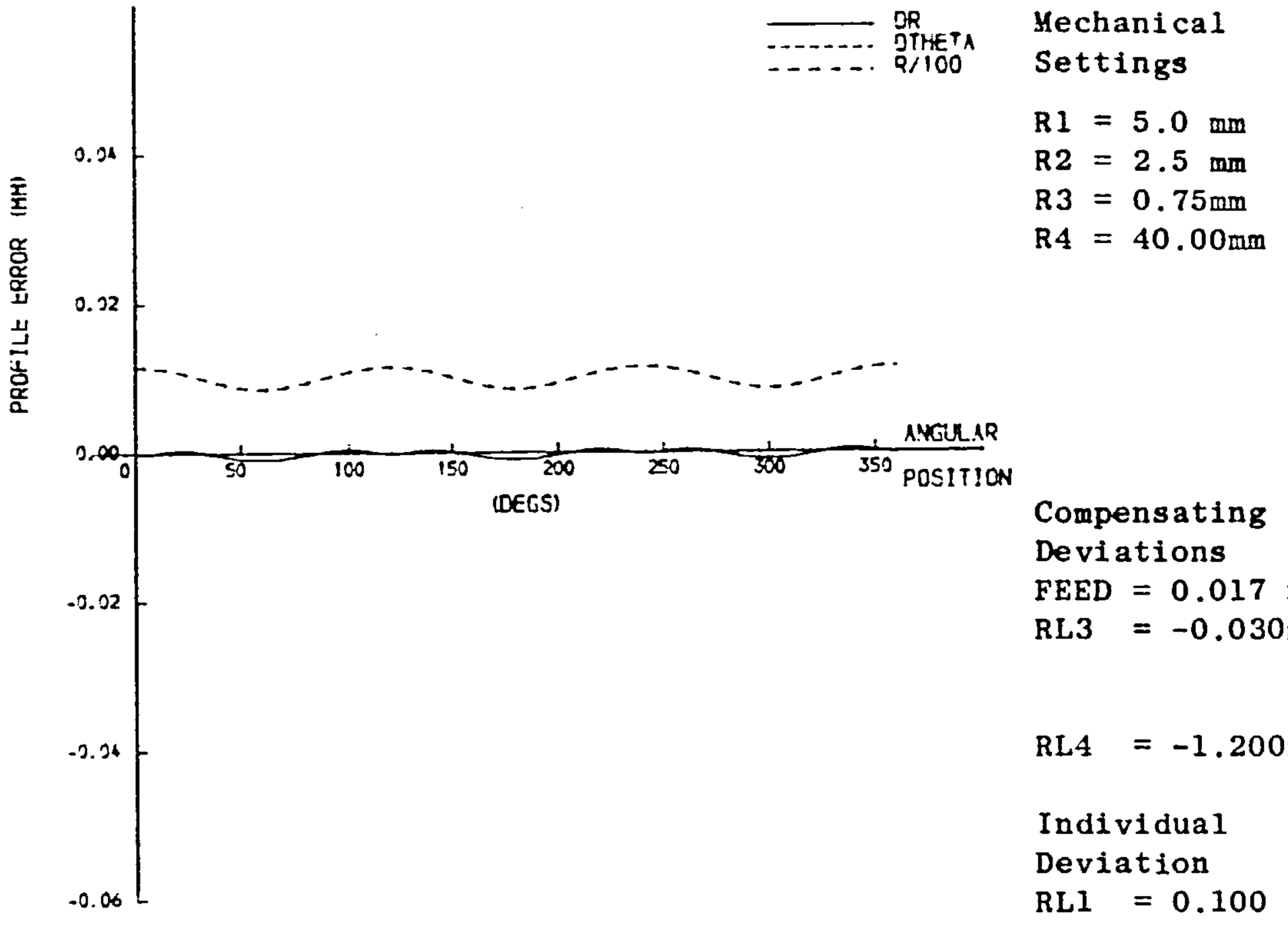

Mechanical Settings

R1 = 5.0 mm
R2 = 2.5 mm
R3 = 0.75mm
R4 = 40.00mm

Compensating Deviations

FEED = 0.017 mm
RL3 = -0.030mm

RL4 = -1.200mm

Individual Deviation

RL1 = 0.100

Compensation of constant deviations of individual parameters

Fig.A8.6 RL1 deviation

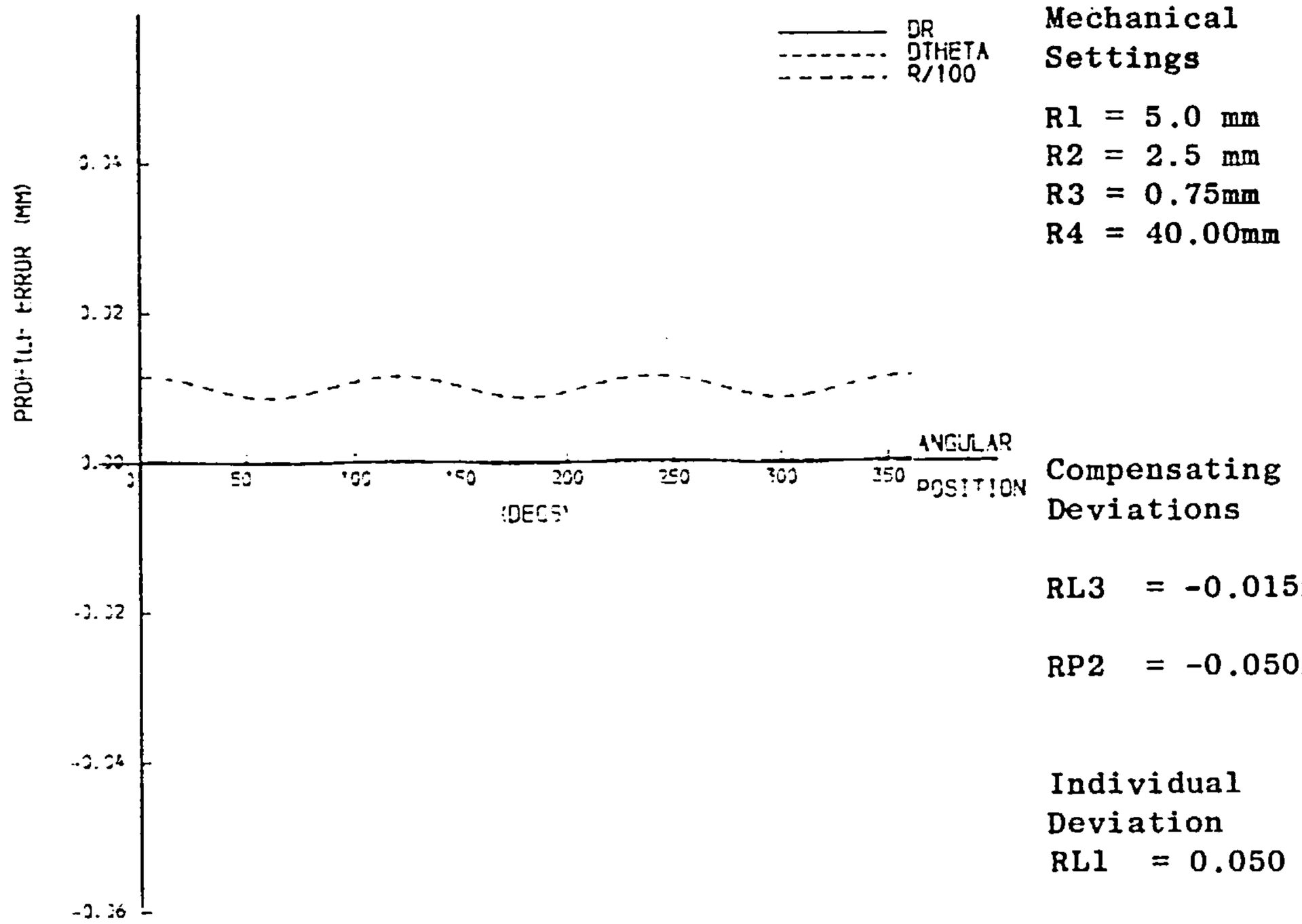

Mechanical Settings

R1 = 5.0 mm
R2 = 2.5 mm
R3 = 0.75mm
R4 = 40.00mm

Compensating Deviations

RL3 = -0.015mm

RP2 = -0.050mm

Individual Deviation

RL1 = 0.050

Compensation of constant deviations of individual parameters

Fig.A8.5 RL1 Deviation

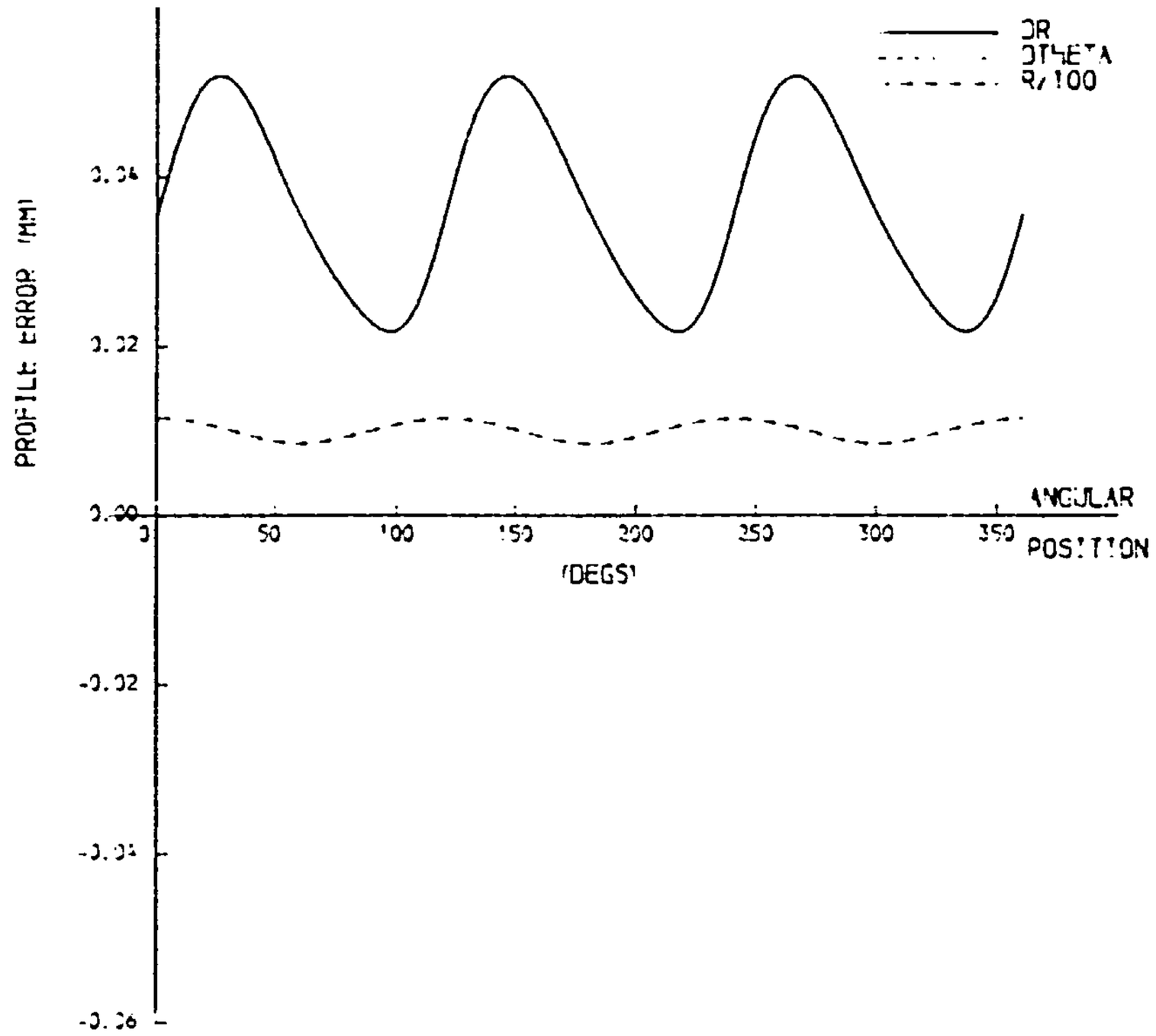

Mechanical Settings

R1 = 5.0 mm
R2 = 2.5 mm
R3 = 0.75mm
R4 = 40.00 mm

Compensating Deviations

Individual Deviation
PI = 0.050mm

Compensation of constant deviations of individual parameters

Fig.A 8.8 P1 deviation

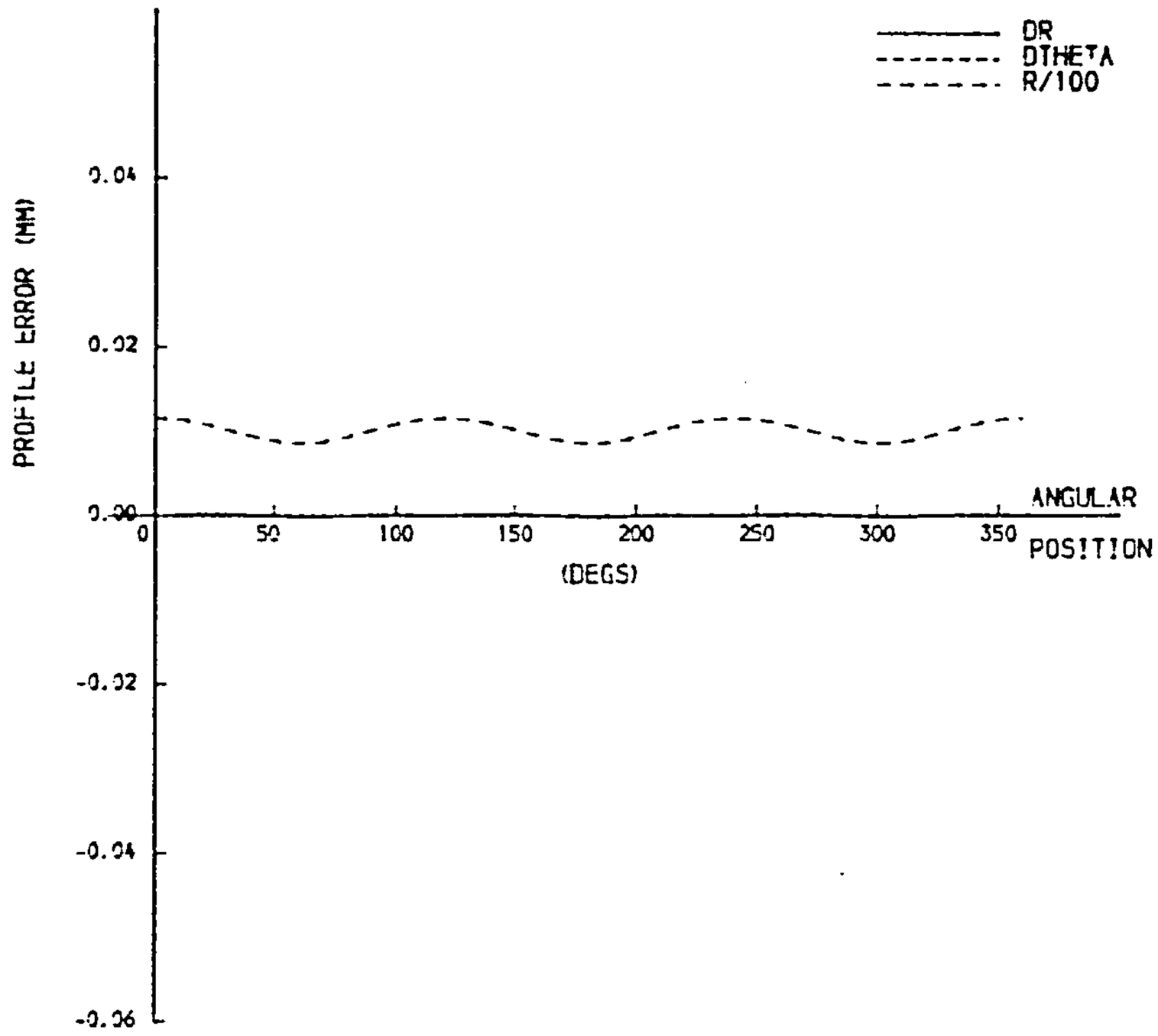

Mechanical Settings

R1 = 5.0 mm
R2 = 2.5 mm
R3 = 0.75mm
R4 = 40.00mm

Compensating Deviations

RL3 = 0.030mm
R3 = 0.001mm

Individual Deviation
V4 = 0.050

Compensation of constant deviations of individual parameters

Fig..A8.7 V4 deviation

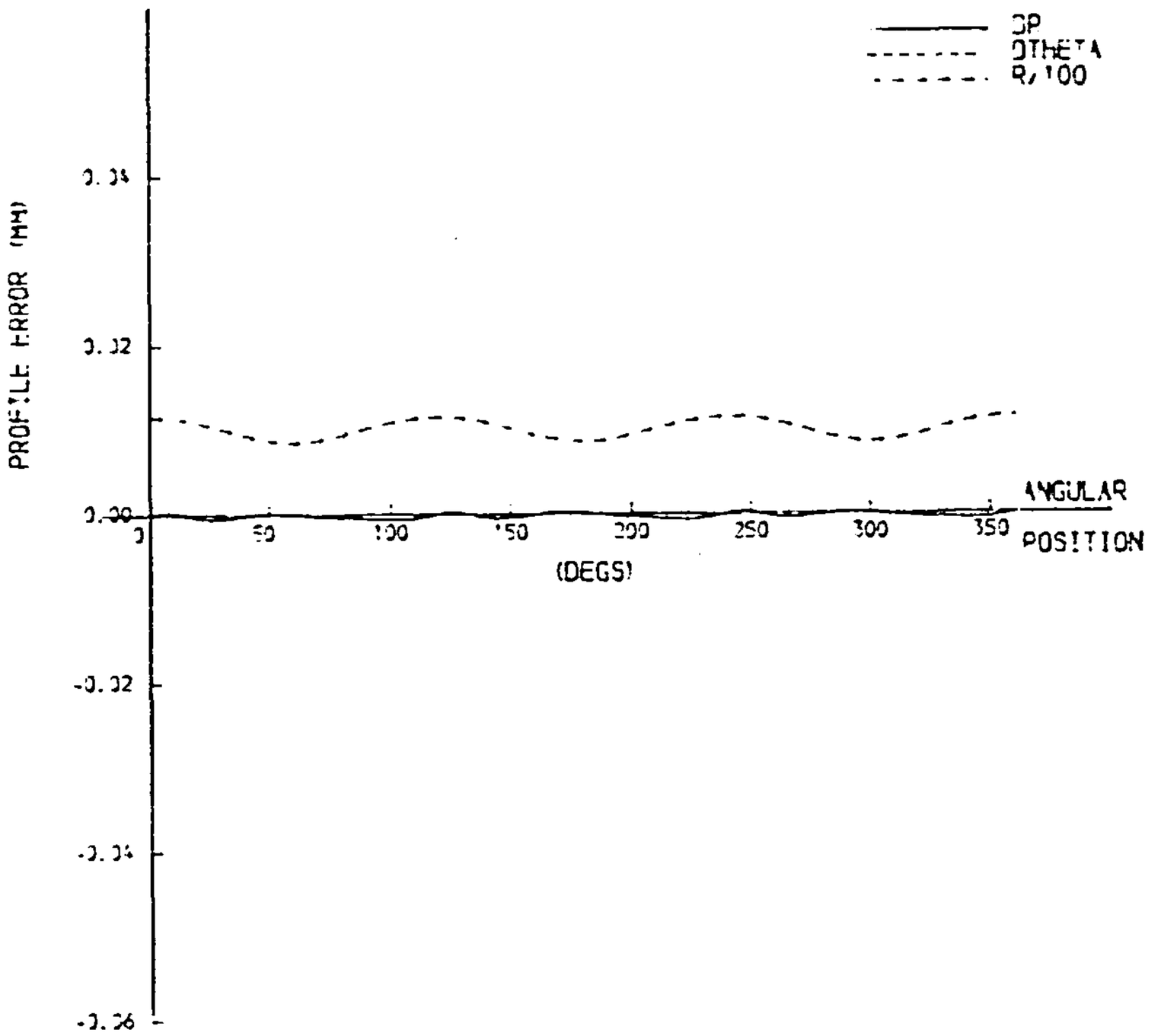

Mechanical Settings

R1 = 5.0 mm
R2 = 2.5 mm
R3 = 0.75mm
R4 = 40.00mm

Compensating Deviations
FEED = 0.035mm
RL3 = -0.014mm

Individual Deviation
P1 = 0.050mm

Compensation of constant deviations of individual parameters

Fig. A8.10 P1 deviation

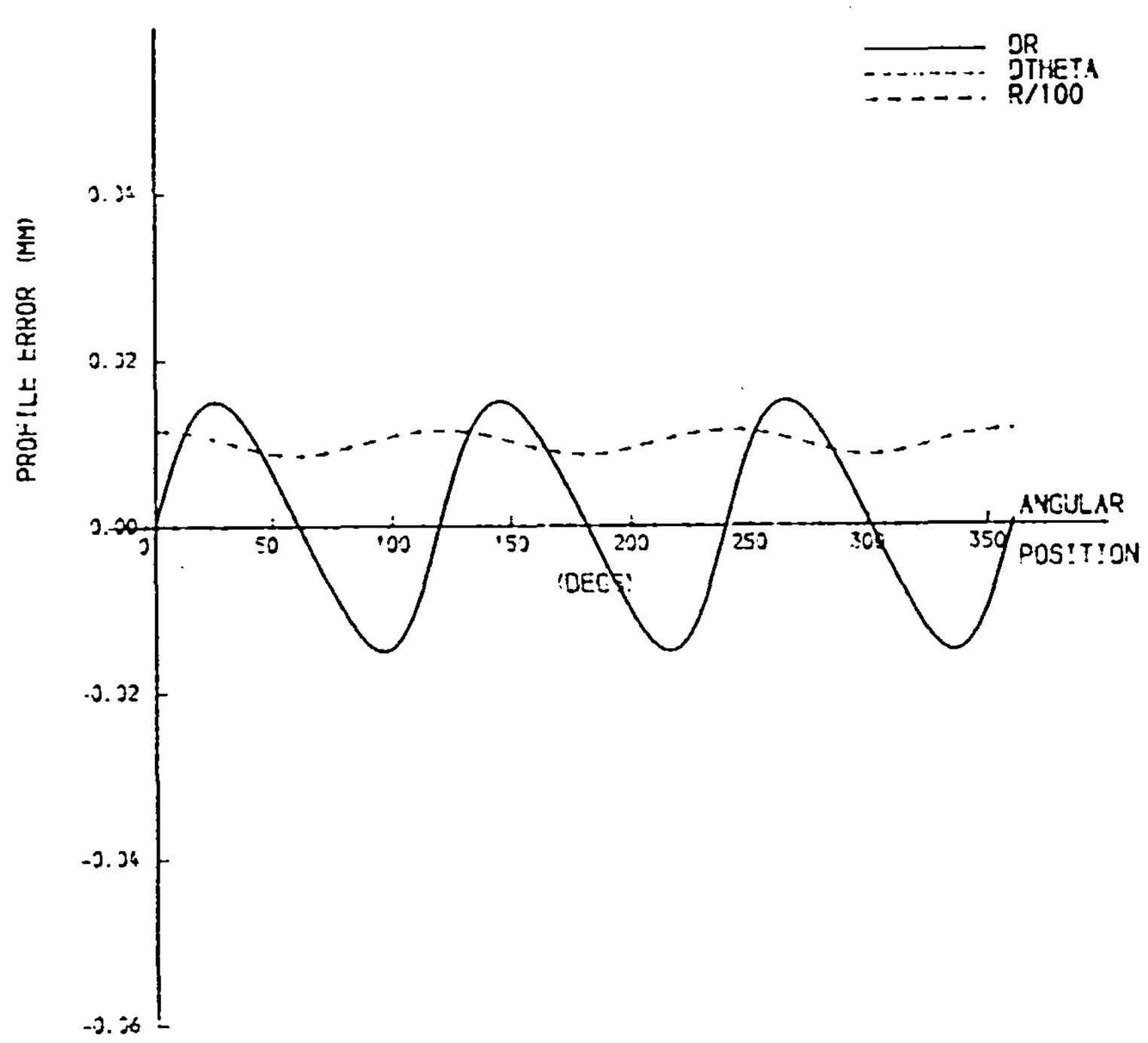

Mechanical Settings

R1 = 5.0 mm
R2 = 2.5 mm
R3 = 0.75mm
R4 = 40.00mm

Compensating Deviations
FEED = 0.035mm

Individual deviation
P1 = 0.050mm

Compensation of constant deviations of individual parameters

Fig. A8.9 P1 deviation

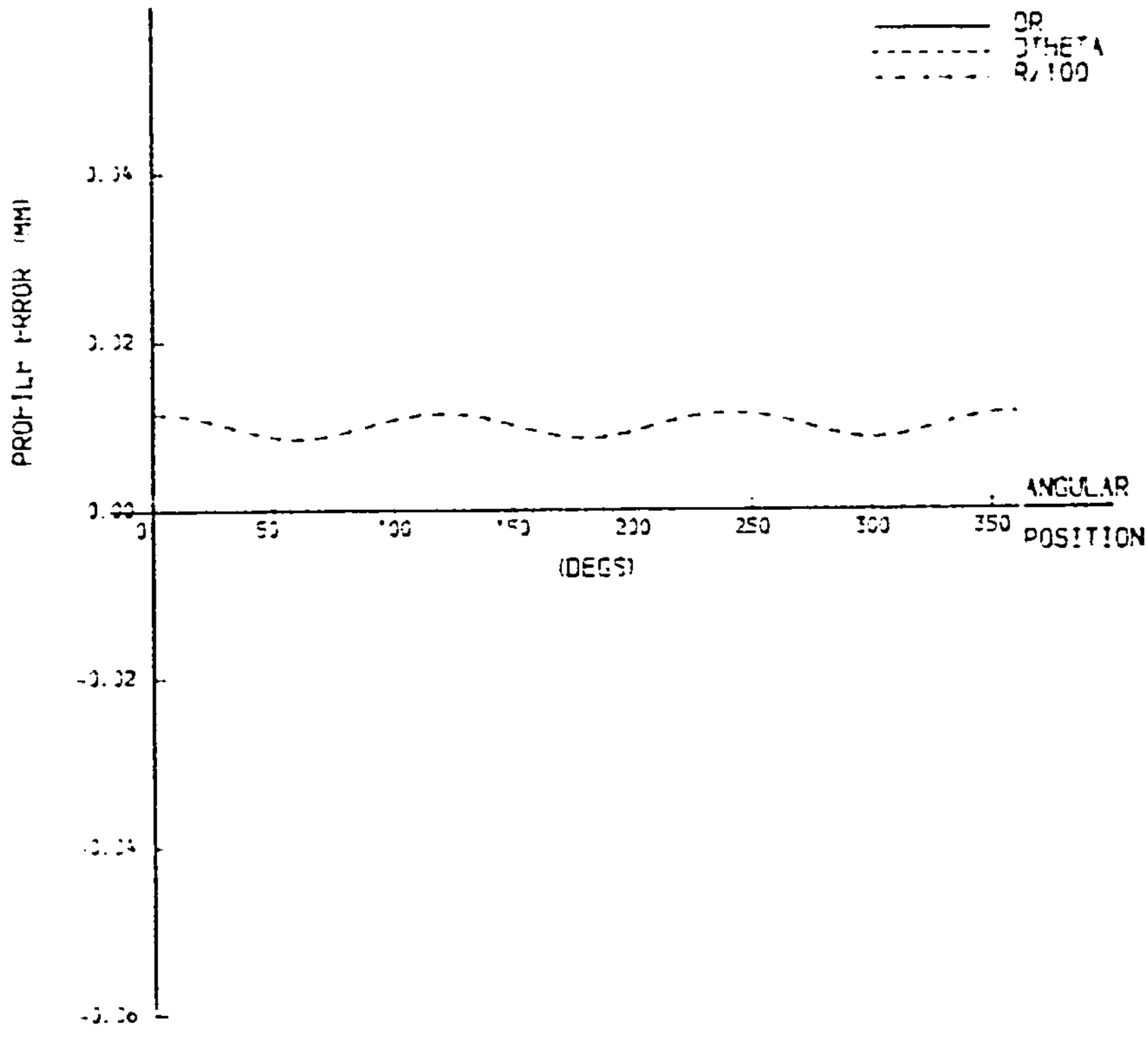

Mechanical Settings

R1 = 5.0 mm
R2 = 2.5 mm
R3 = 0.75mm
R4 = 40.00mm

Compensating Deviations

RP2 = 0.200mm

Individual Deviation

RL2 = 0.200mm

Compensation of constant deviations of individual parameters

Fig. A 8.12 RL2 deviation

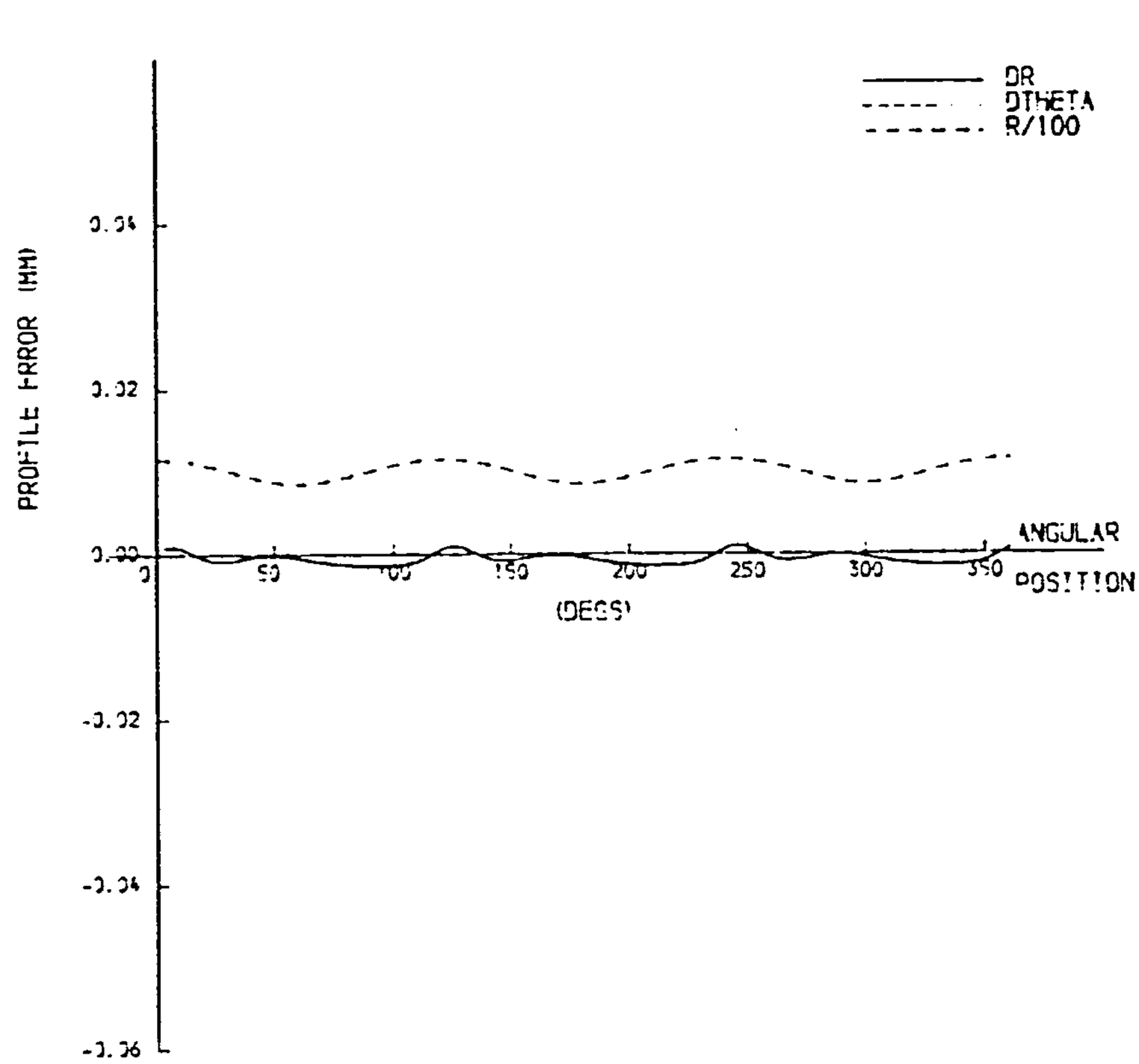

Mechanical Settings

R1 = 5.0 mm
R2 = 2.5 mm
R3 = 0.75mm
R4 = 40.00mm

Compensating Deviations

FEED = 0.070mm
RL3 =-0.027mm

Individual Deviation

P1 = 0.100mm

Compensation of constant deviations of individual parameters

Fig. A 8.11 P1 deviation

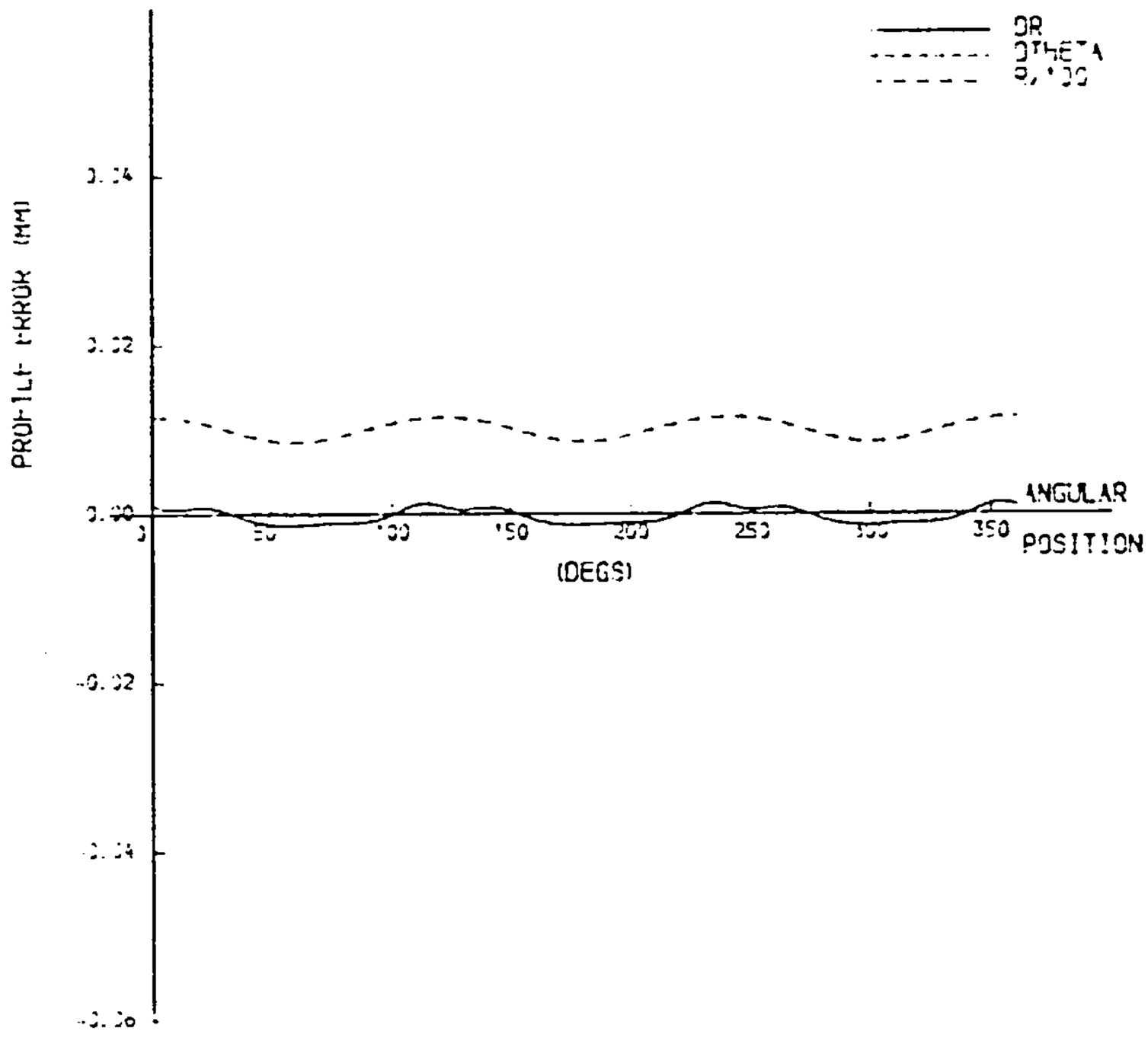

Mechanical Settings

R1 = 5.0 mm
R2 = 2.5 mm
R3 = 0.75mm
R4 = 40.00mm

Compensating Deviations

RL3 = -0.030mm

Individual Deviations

P2 = 0.050mm
P3 = 0.050mm

Compensation of constant deviations of individual parameters

Fig. A9.2 P2 + P3 deviations

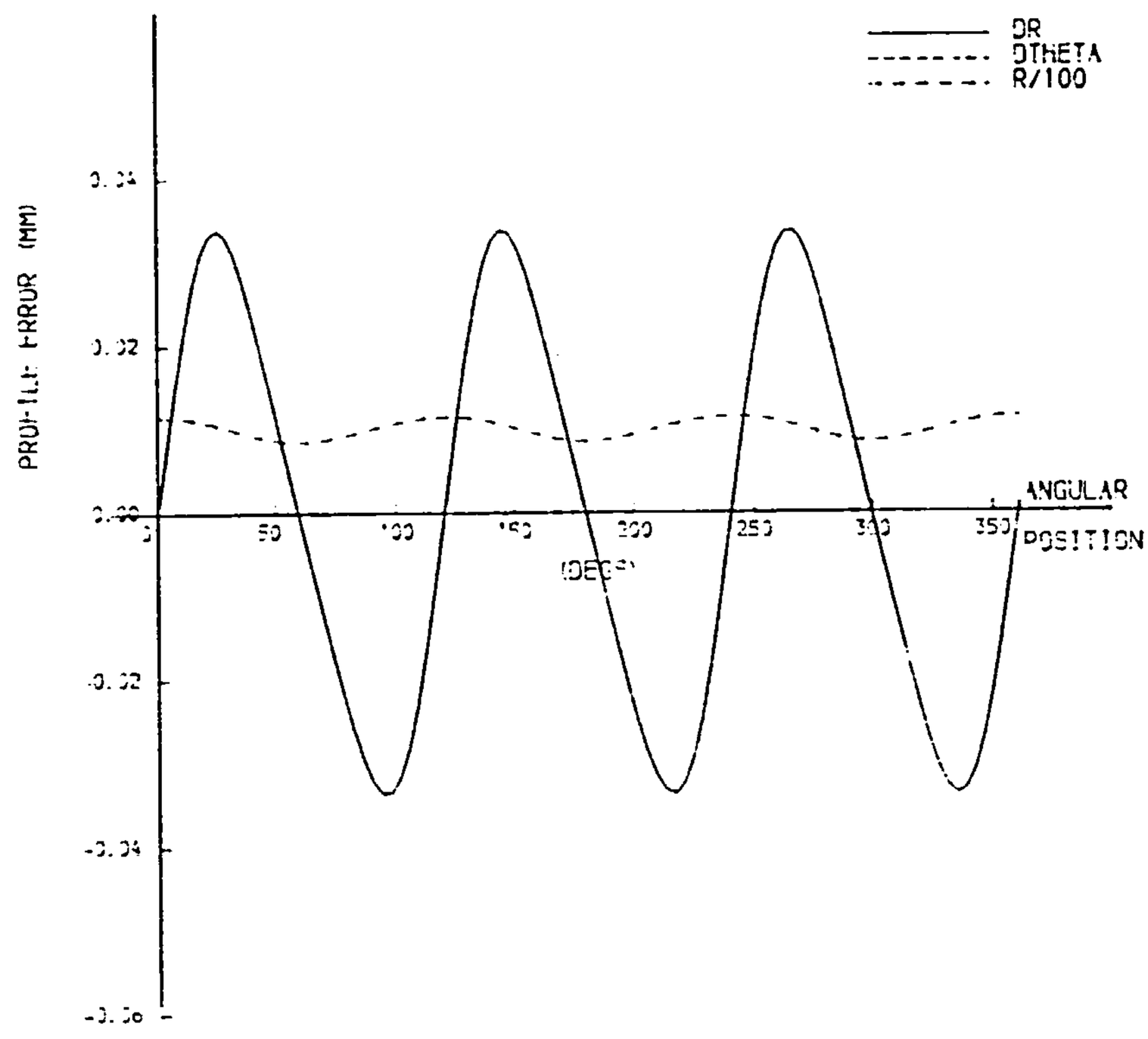

Mechanical Settings

R1 = 5.0 mm
R2 = 2.5 mm
R3 = 0.75mm
R4 = 40.00mm

Compensating Deviations

Individual Deviations

P2 = 0.050mm
P3 = 0.050mm

Compensation of constant deviations of individual parameters

Fig. A9.1 P2 + P3 deviations

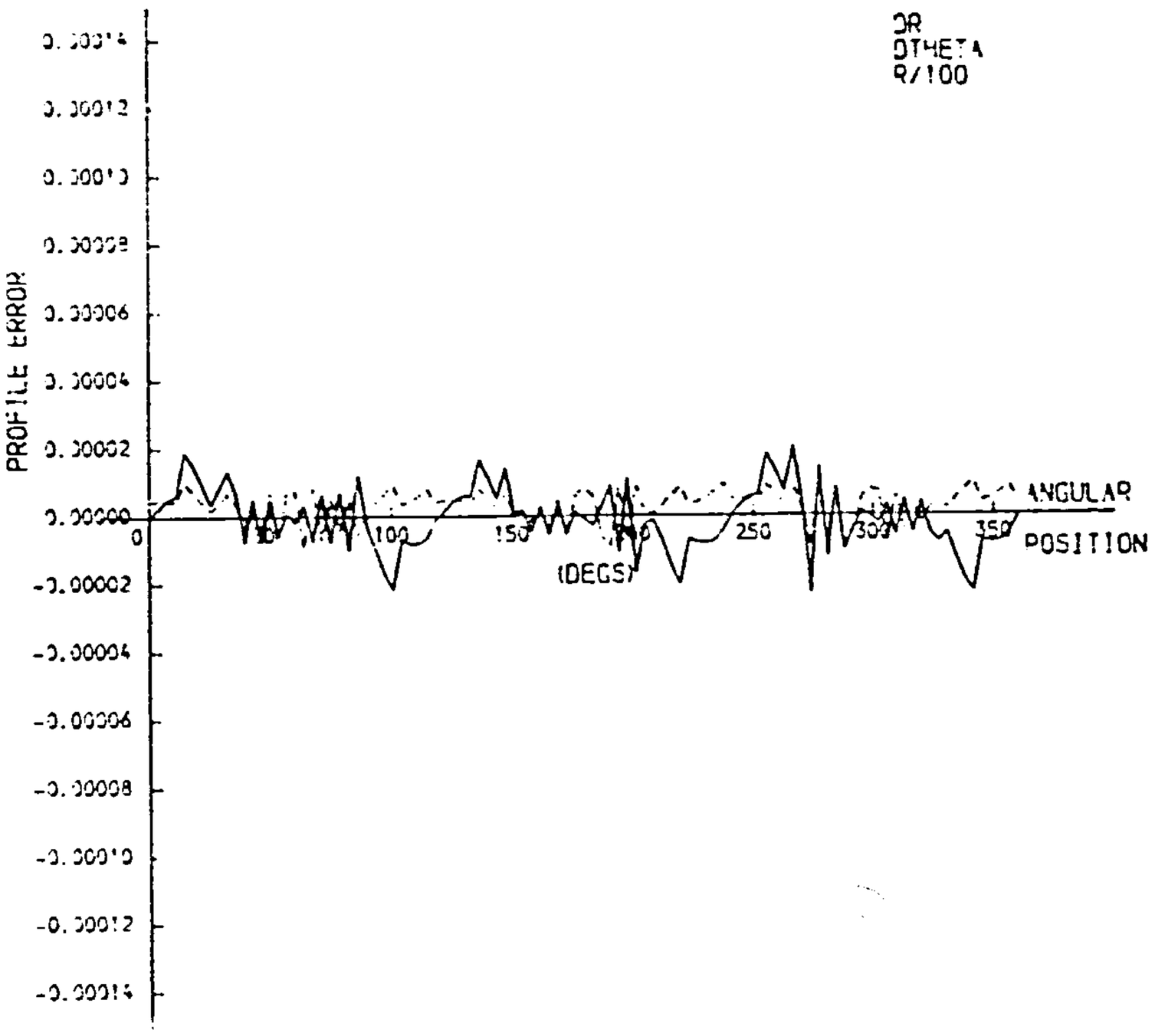

Mechanism
Setting

R1 = 5.0mm
R2 = 2.5mm
R3 = 0.75mm
R4 = 40.00mm
$\dot{\psi}_1$ = 10.0 rad/s

Profile error caused by individual parameter deviations due to deflections

Fig. A10.2 RP4 deflection

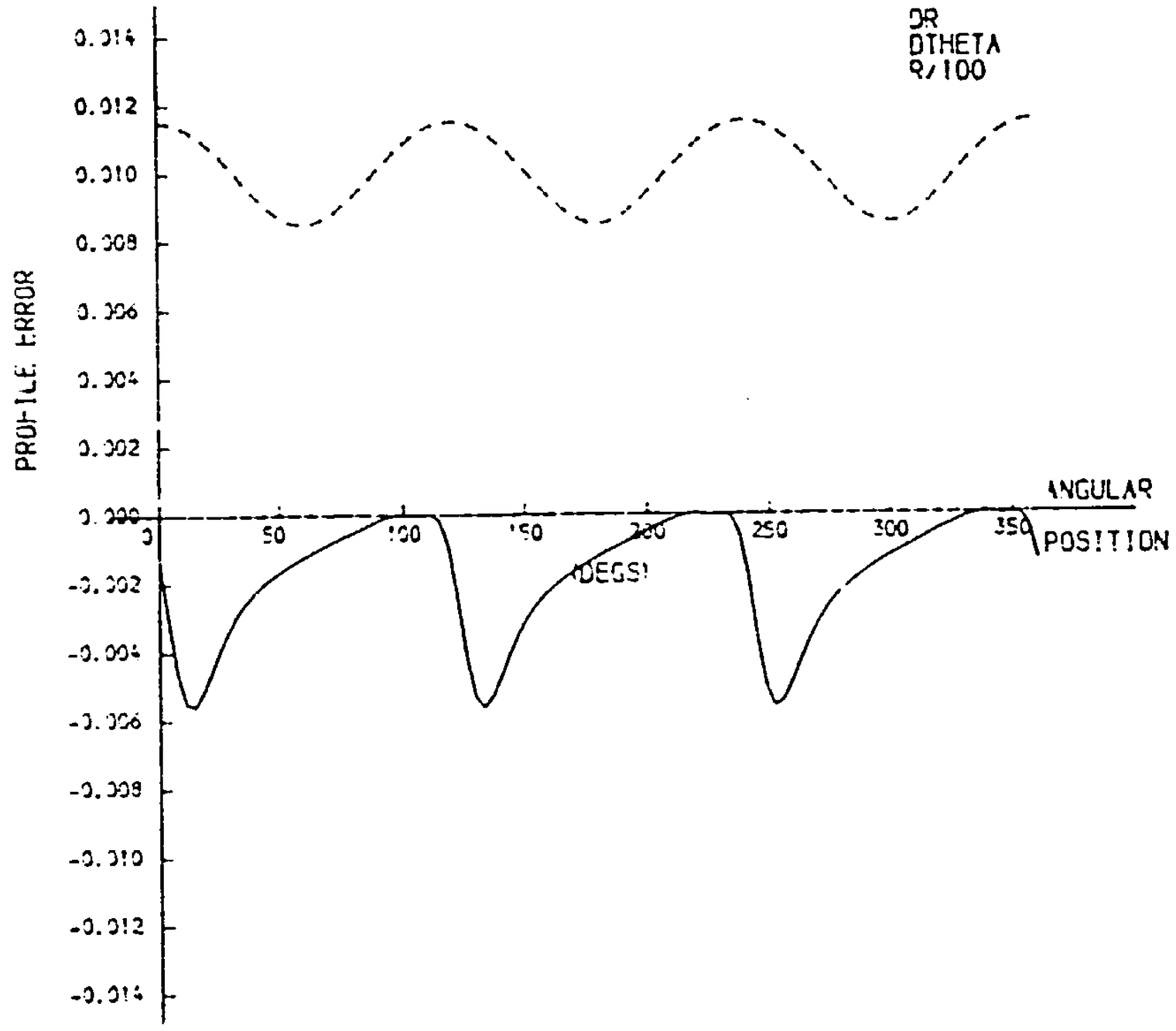

Mechanism
Setting

R1 = 5.0mm
R2 = 2.5mm
R3 = 0.75mm
R4 = 40.00mm
$\dot{\psi}_1$ = 10.0 rad/s

Profile error caused by individual parameter deviations due to deflections

Fig. A10.1 RP2 deflection

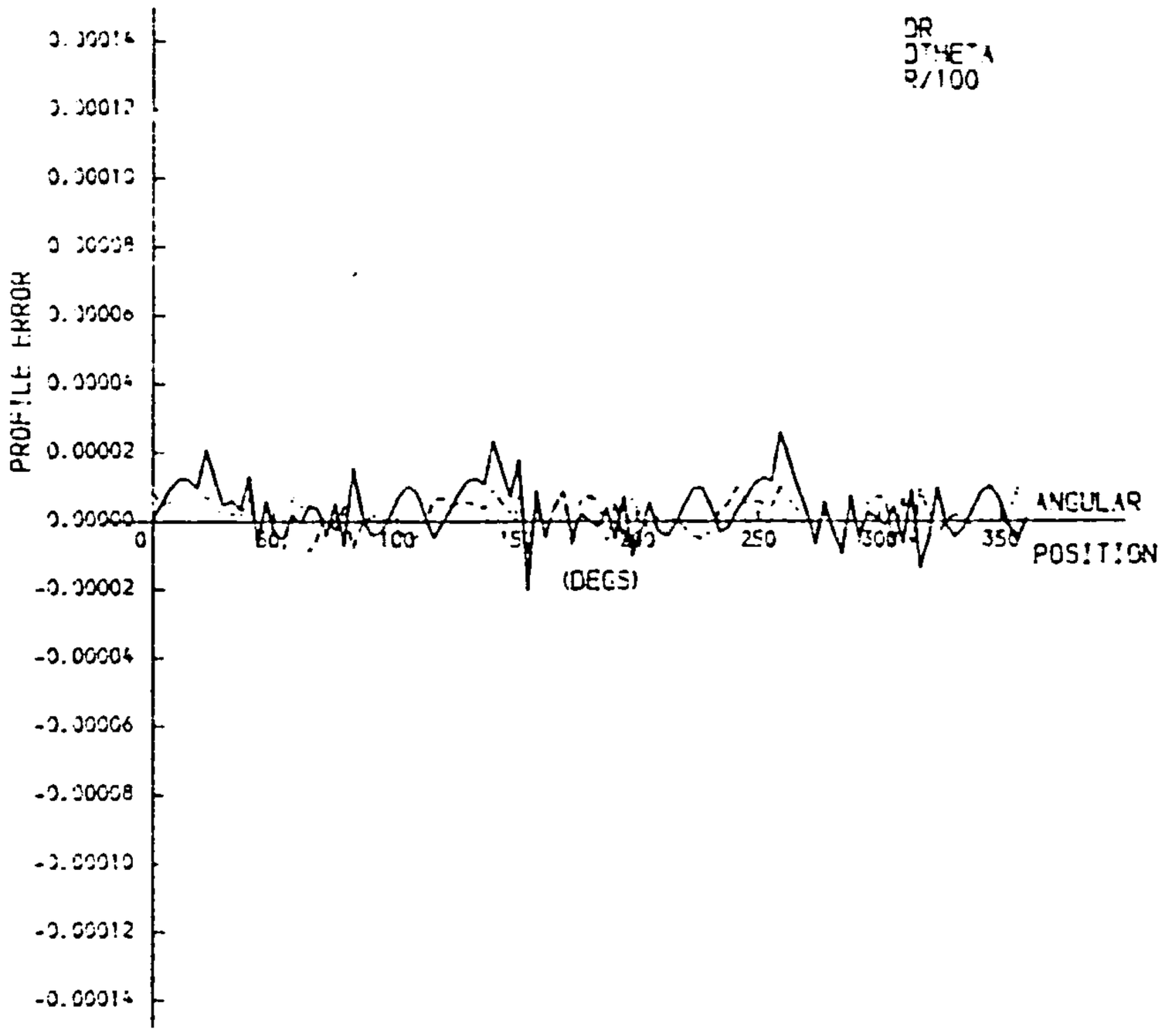

Mechanism Setting

R1 = 5.0mm
R2 = 2.5mm
R3 = 0.75mm
R4 = 40.00mm
$\dot{\psi}_1$ = 10.0 rad/s

Profile error caused by individual parameter deviations due to deflections

Fig. A10.4 RL4 deflection

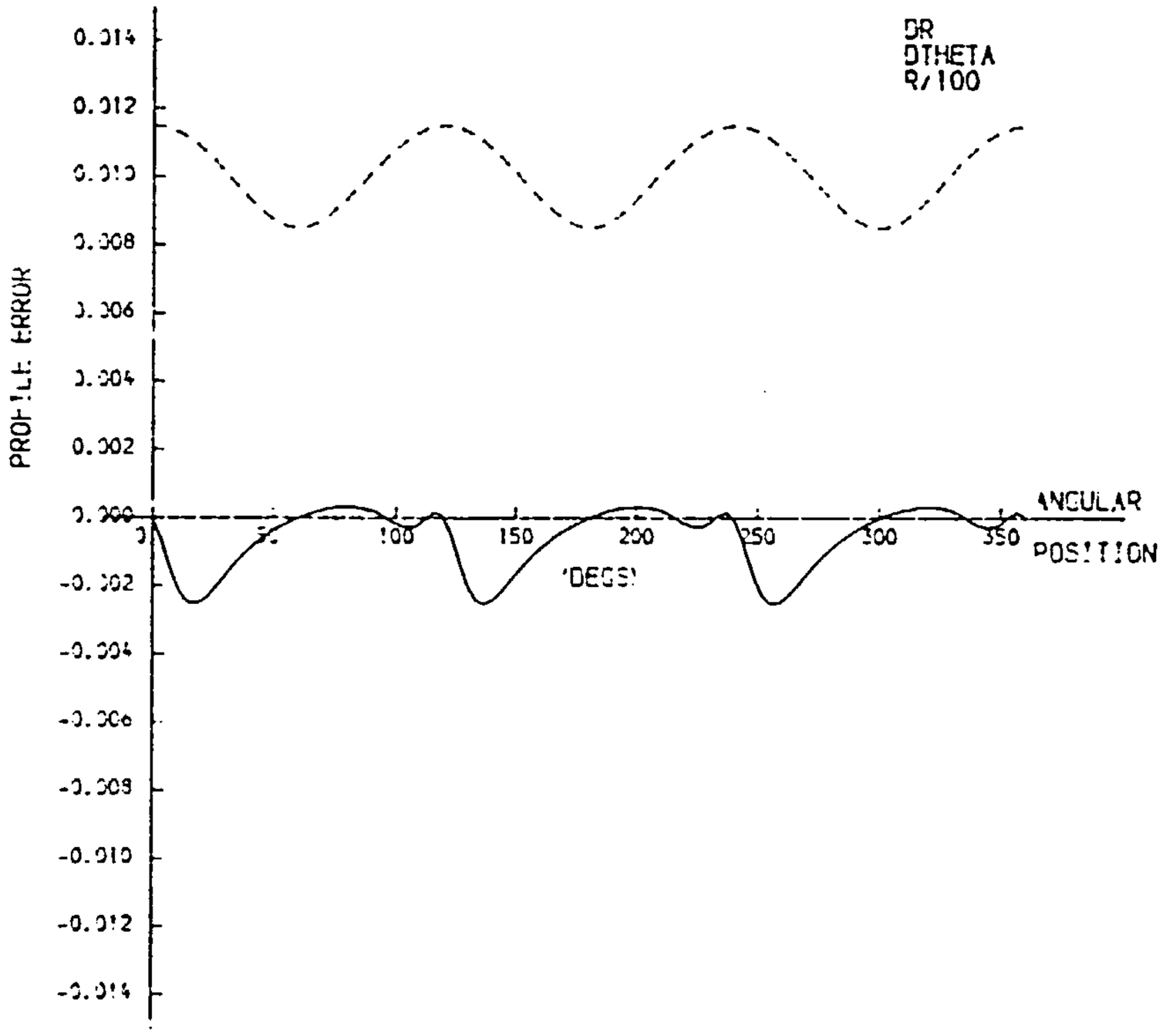

Mechanism Setting

R1 = 5.0mm
R2 = 2.5mm
R3 = 0.75mm
R4 = 40.00mm
$\dot{\psi}_1$ = 10.0 rad/s

Profile error caused by individual parameter deviations due to deflections

Fig. A10.3 RL1 deflection

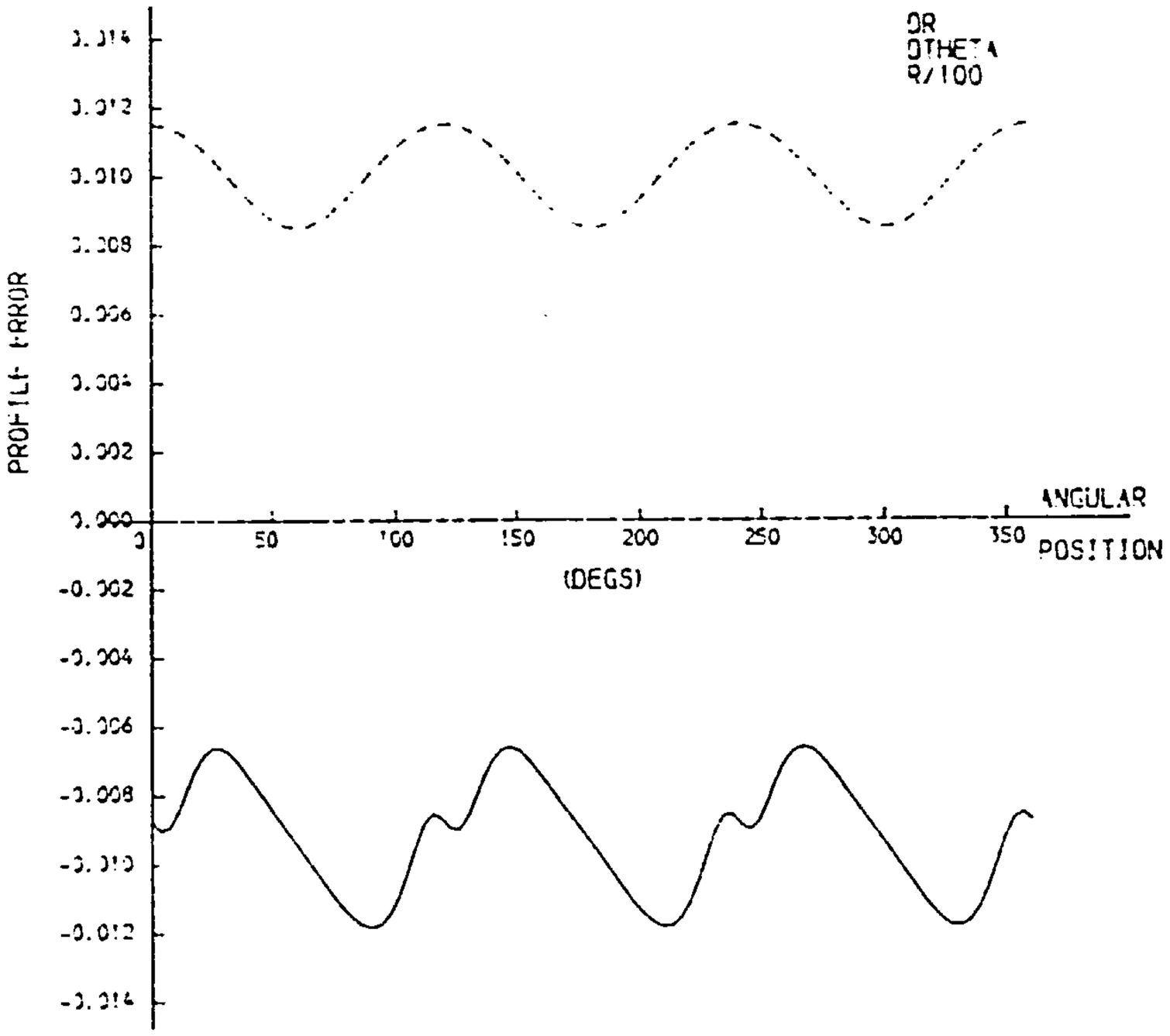

Mechanism Setting

R1 = 5.0mm
R2 = 2.5mm
R3 = 0.75mm
R4 = 40.00mm
$\dot{\psi}_1$ **= 10.0 rad/s**

Profile error caused by individual parameter deviations due to deflections

Fig. A10.6 P4 deflection

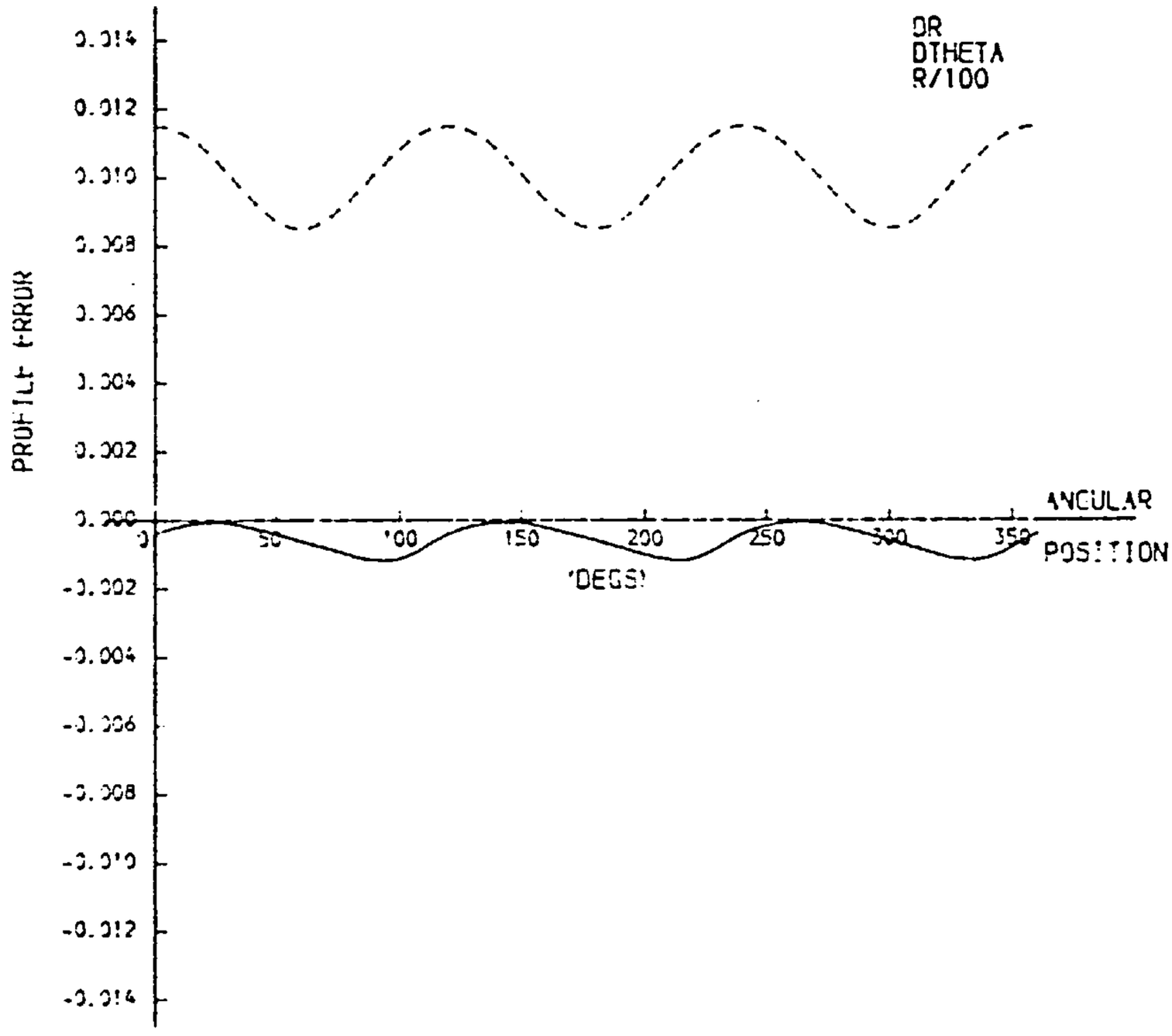

Mechanism Setting

R1 = 5.0mm
R2 = 2.5mm
R3 = 0.75mm
R4 = 40.00mm
$\dot{\psi}_1$ **= 10.0 rad/s**

Profile error caused by individual parameter deviations due to deflections

Fig. A10.5 R4 deflection

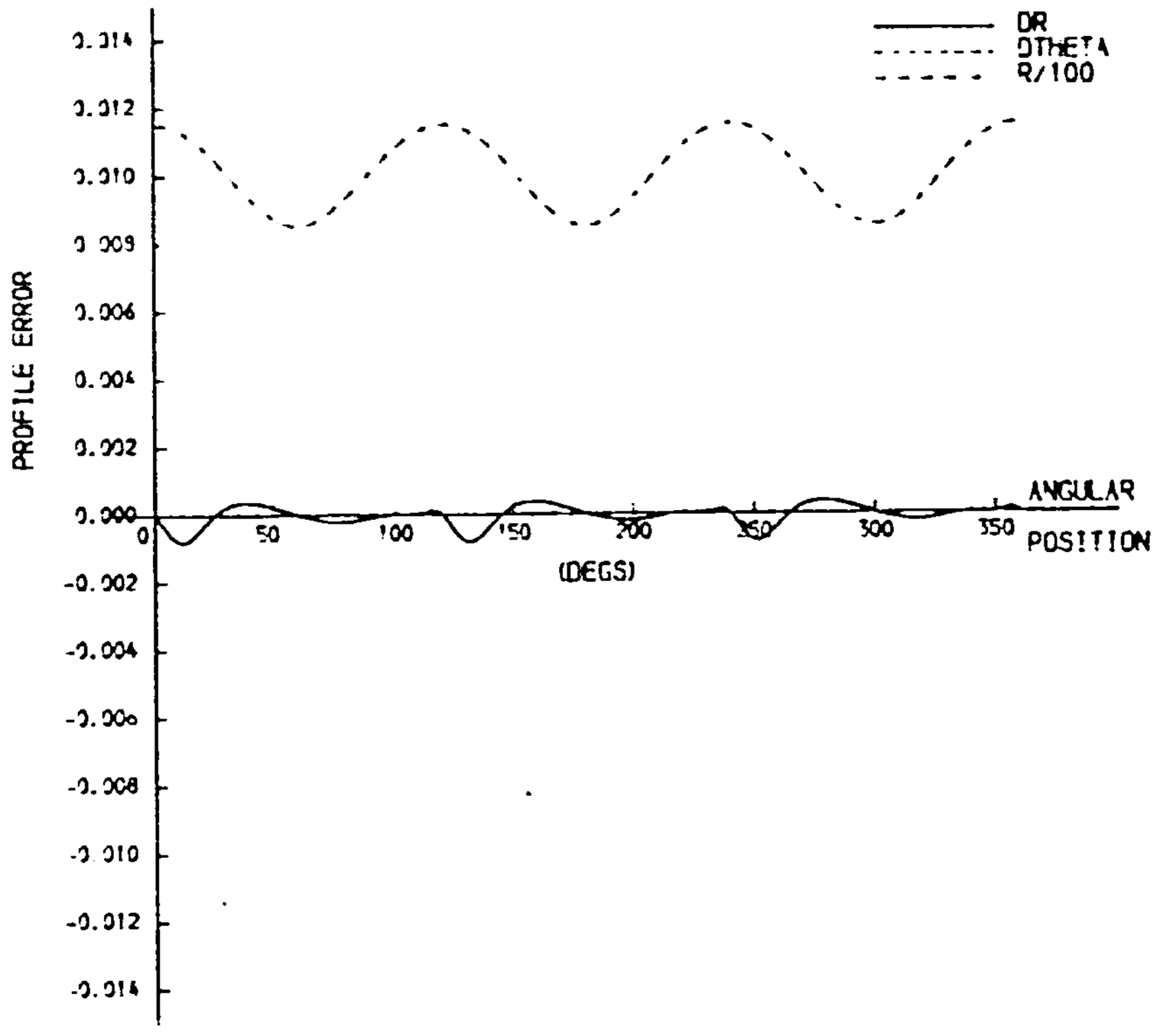

Mechanism Setting

R1 = 5.0mm
R2 = 2.5mm
R3 = 0.75mm
R4 = 40.00mm
$\dot{\psi}_1$ **= 10.0 rad/s**

Profile error caused by individual parameter deviations due to deflections

Fig. A10.8 RL3 deflection

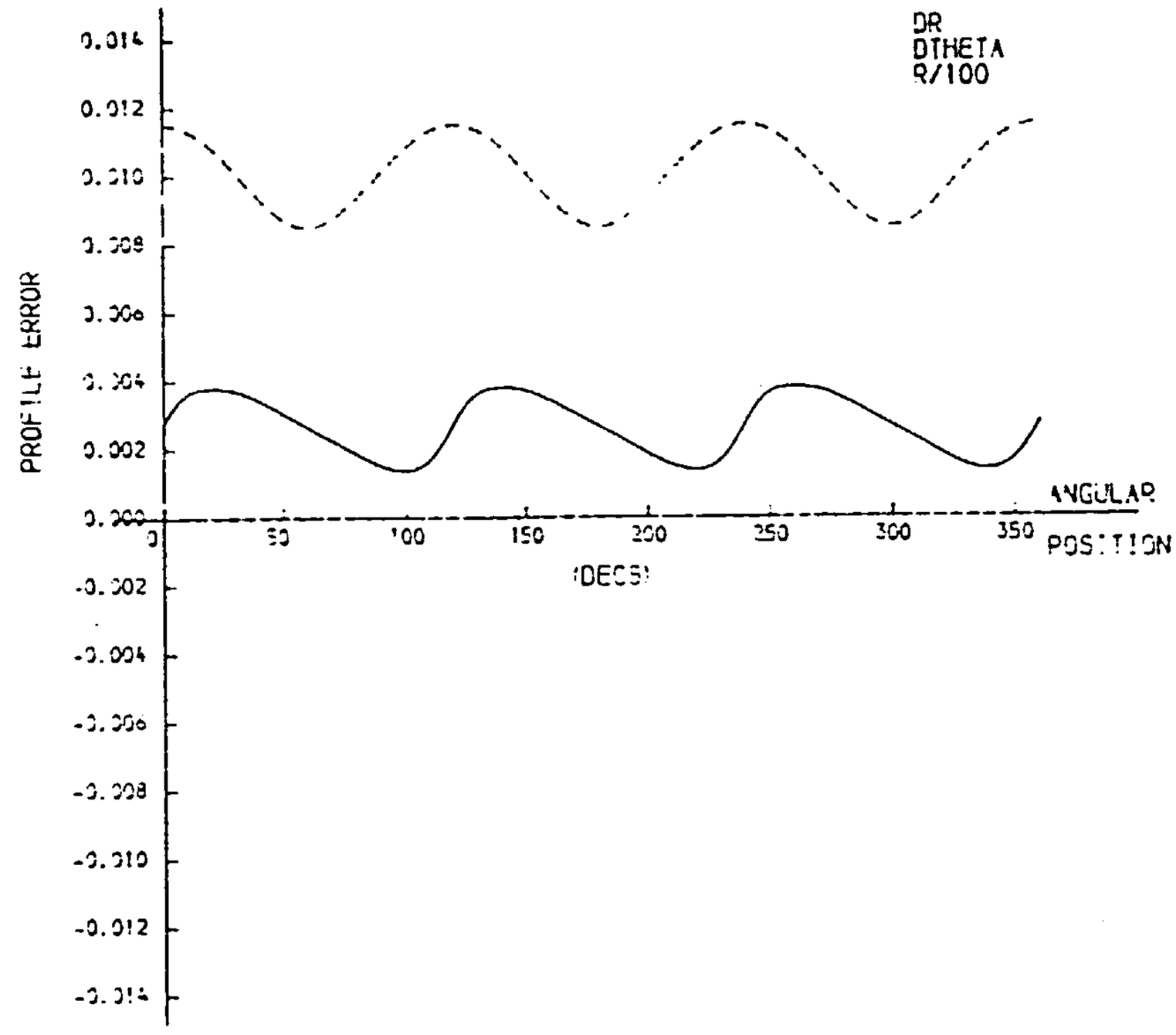

Mechanism Setting

R1 = 5.0mm
R2 = 2.5mm
R3 = 0.75mm
R4 = 40.00mm
$\dot{\psi}_1$ **= 10.0 rad/s**

Profile error caused by individual parameter deviations due to deflections

Fig. A10.7 P5 deflection

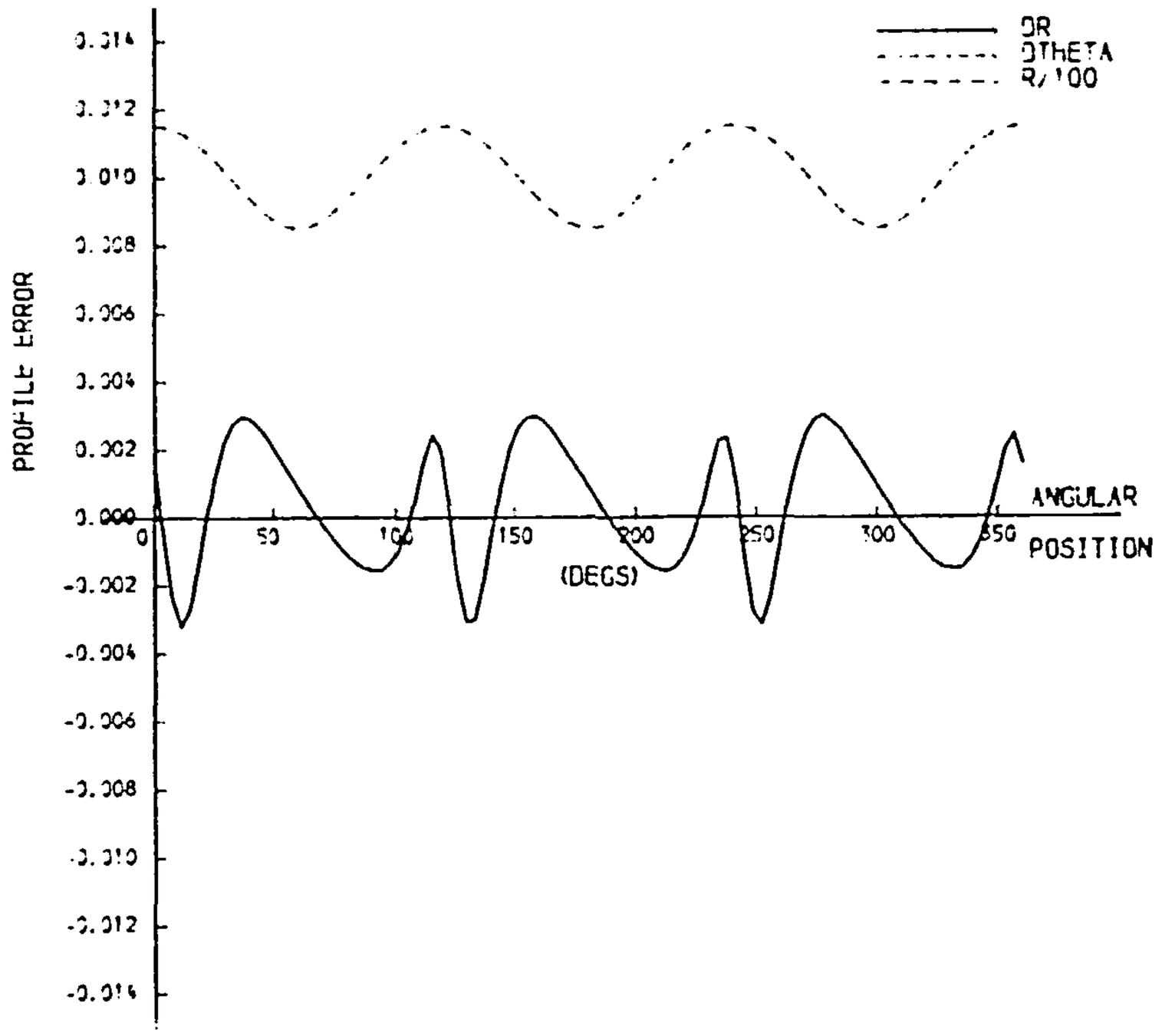

Mechanism Setting

R1 = 5.0mm
R2 = 2.5mm
R3 = 0.75mm
R4 = 40.0mm
$\dot{\psi}_1$ = 10.0 rad/s

Compensating Deviations

FEED = -0.009mm
RL3 = 0.0mm

Profile error due to mechanism deflections (and compensation of error) for various operating conditions.

Fig. A10.10

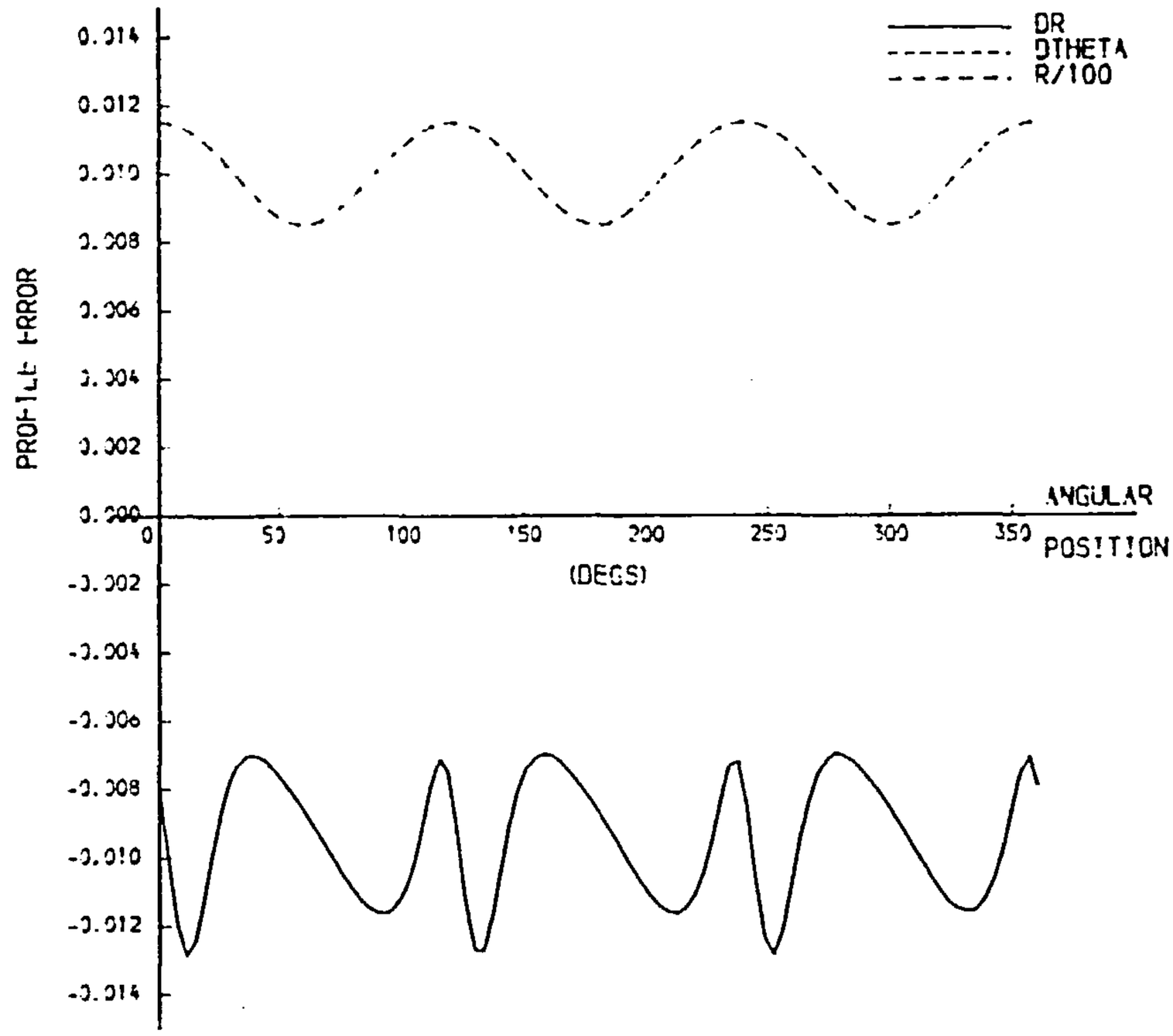

Mechanism Setting

R1 = 5.0mm
R2 = 2.5mm
R3 = 0.75mm
R4 = 40.0mm
$\dot{\psi}_1$ = 10.0 rad/s

Compensating Deviations

FEED = 0.0mm
RL3 = 0.0mm

Profile error due to mechanism deflections (and compensation of error) for various operating conditions.

Fig. A10.9

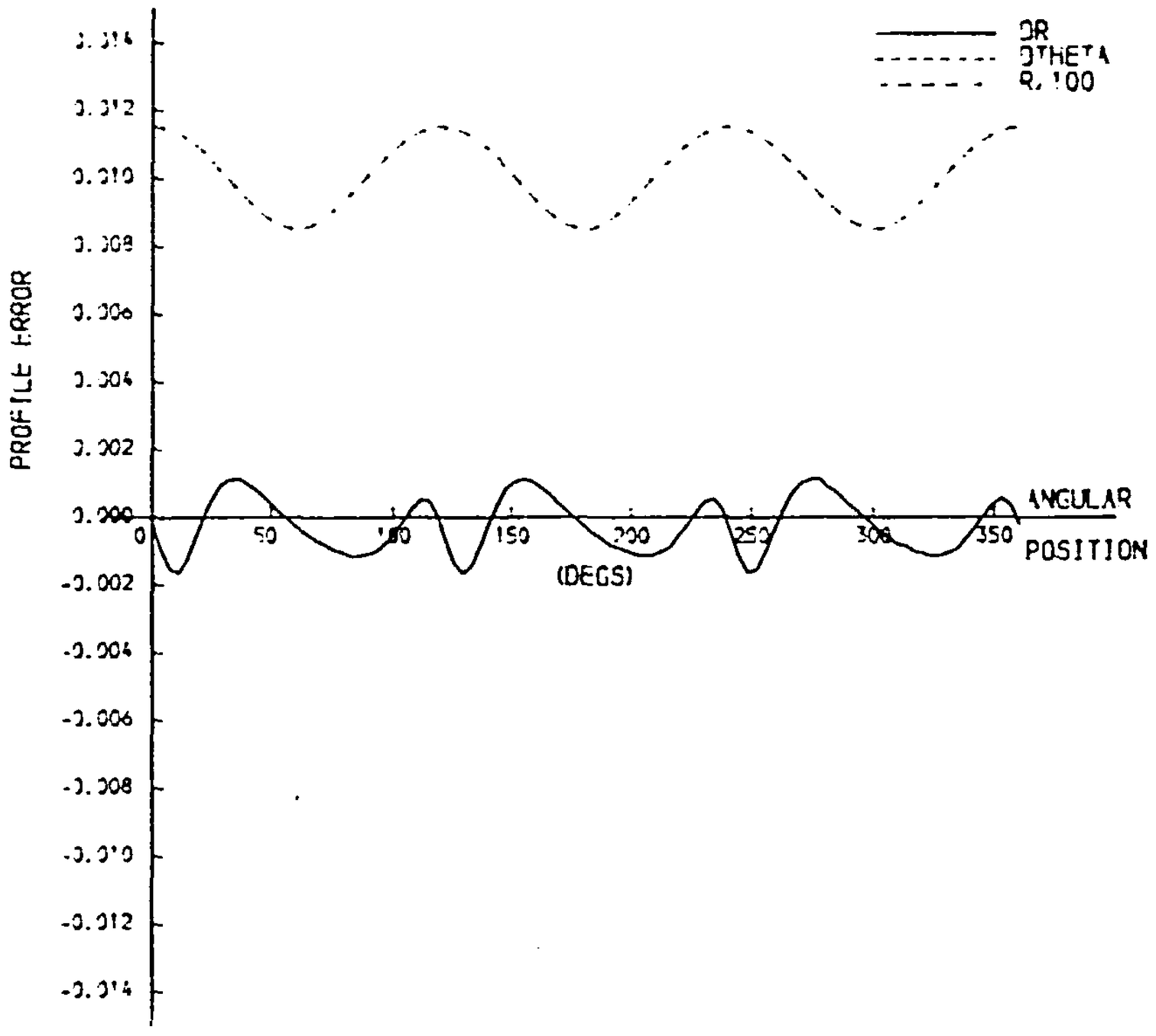

Mechanism Setting

R1 = 5.0mm
R2 = 2.5mm
R3 = 0.75mm
R4 = 40.0mm
$\dot{\psi}_1$ = 5.0 rad/s

Compensating Deviations

FEED = -0.008mm
RL3 = -0.002mm

Profile error due to mechanism deflections (and compensation of error) for various operating conditions.

Fig. A10.12

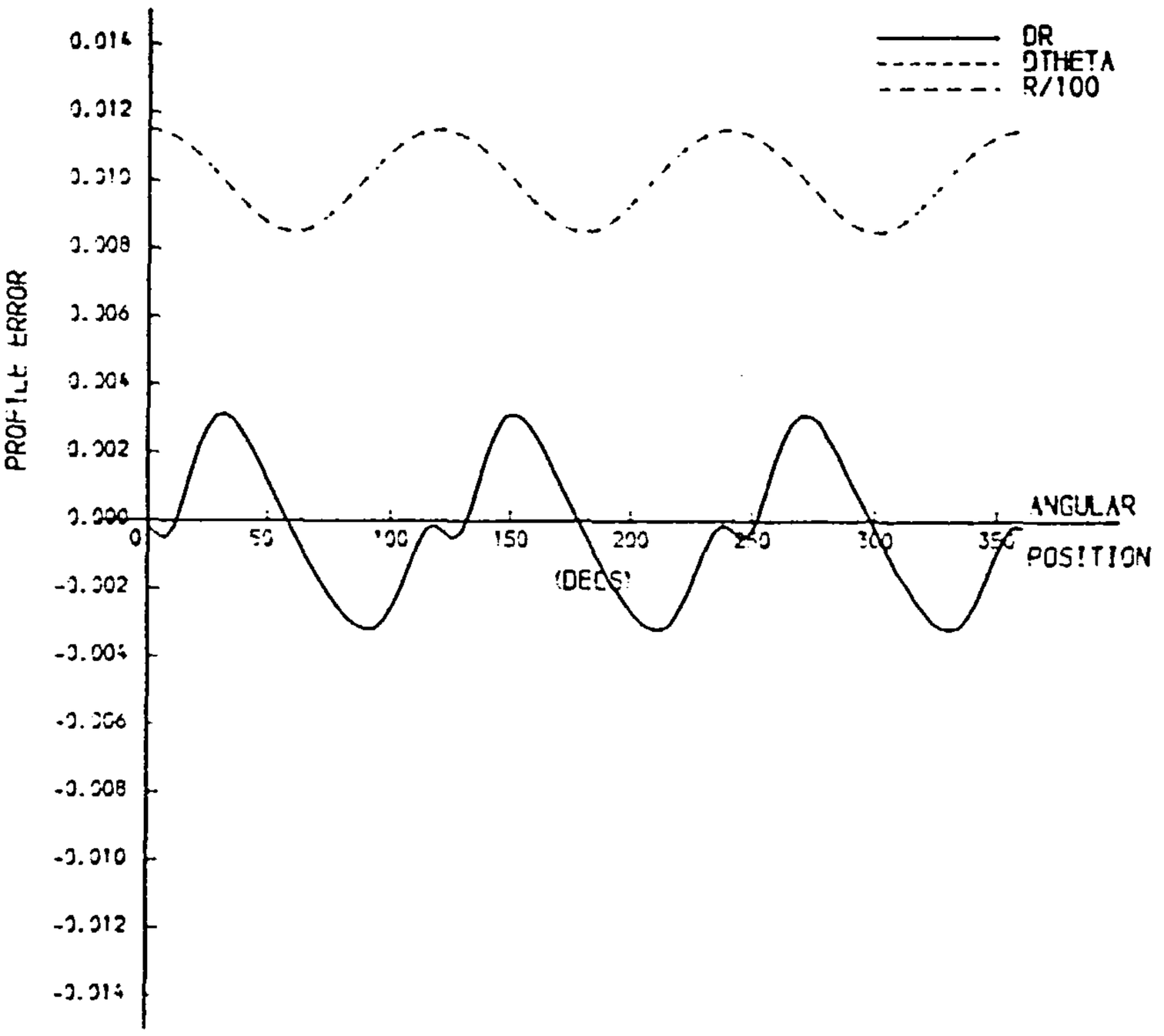

Mechanism Setting

R1 = 5.0mm
R2 = 2.5mm
R3 = 0.75mm
R4 = 40.0mm
$\dot{\psi}_1$ = 5.0 rad/s

Compensating Deviations

FEED = -0.008mm

Profile error due to mechanism deflections (and compensation of error) for various operating conditions.

Fig. A10.11

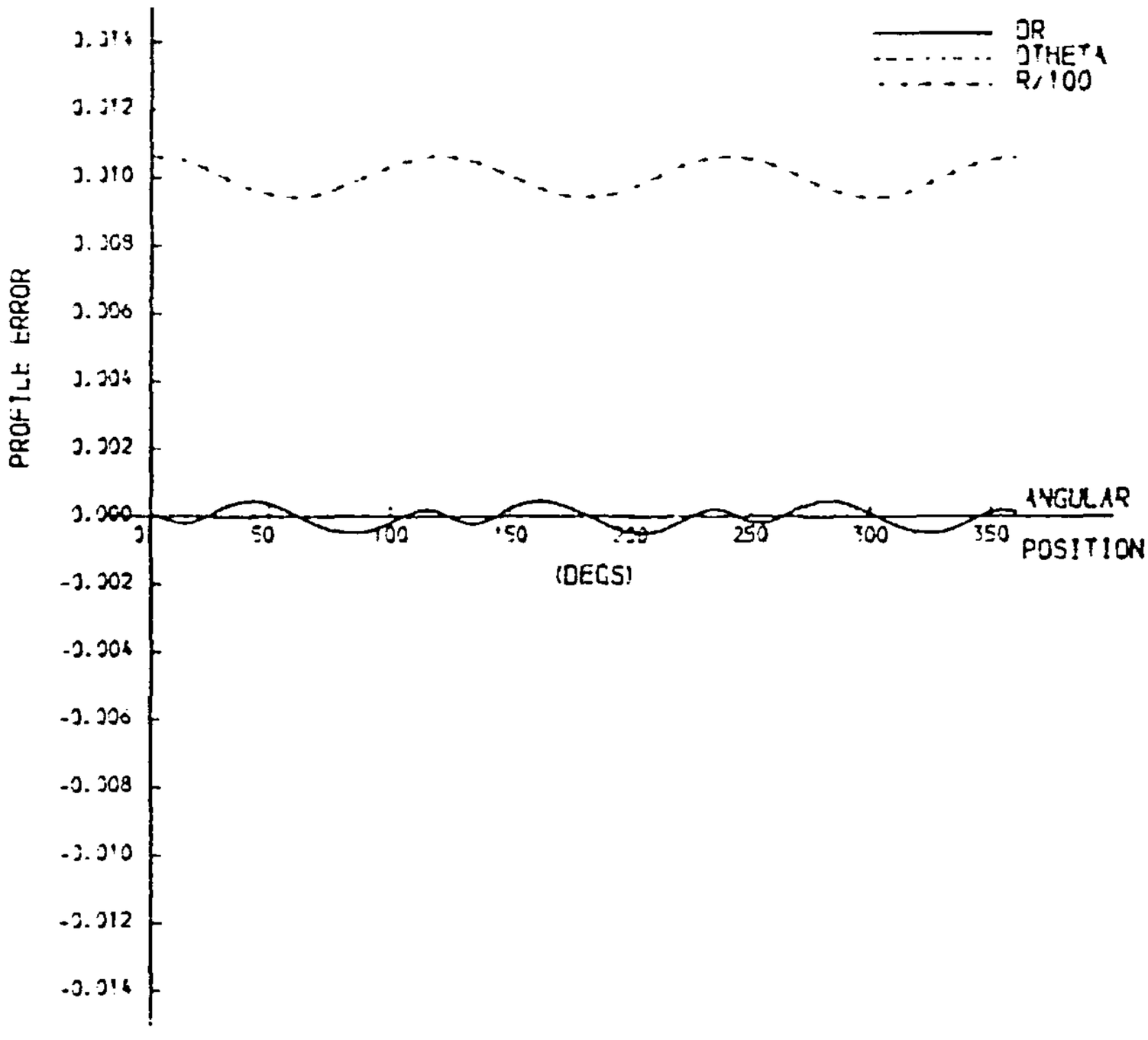

Mechanism Setting

R1 = 5.0mm
R2 = 2.5mm
R3 = 0.30mm
R4 = 40.0mm
$\dot{\psi}_1$ = 10.0 rad/s

Compensating Deviations

FEED = -0.009mm

Profile error due to mechanism deflections (and compensation of error) for various operating conditions.

Fig. A10.14

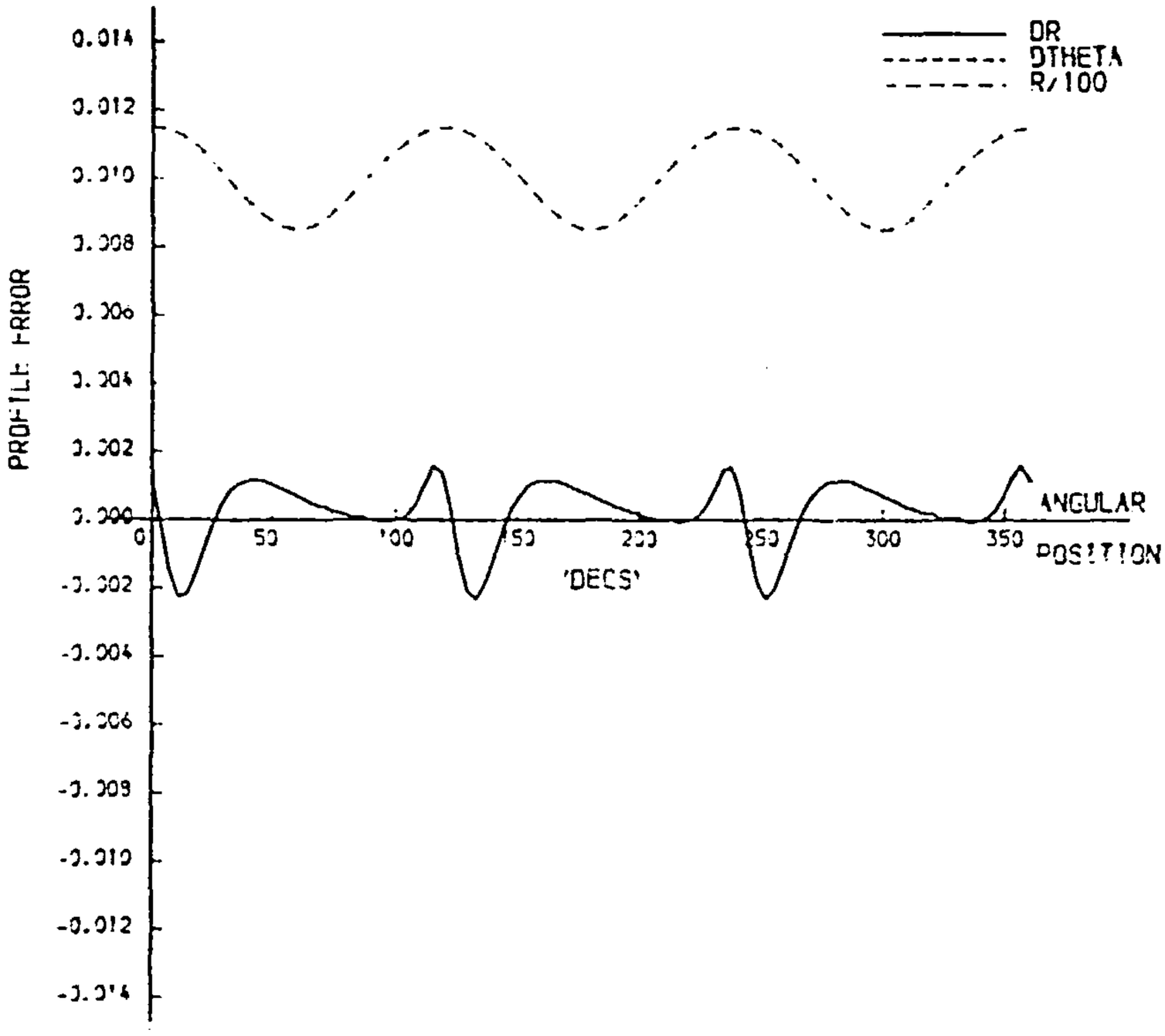

Mechanism Setting

R1 = 5.0mm
R2 = 2.5mm
R3 = 0.75mm
R4 = 20.0mm
$\dot{\psi}_1$ = 10.0 rad/s

Compensating Deviations

FEED = -0.008mm
RL3 = -0.003mm

Profile error due to mechanism deflections (and compensation of error) for various operating conditions.

Fig. A10.13

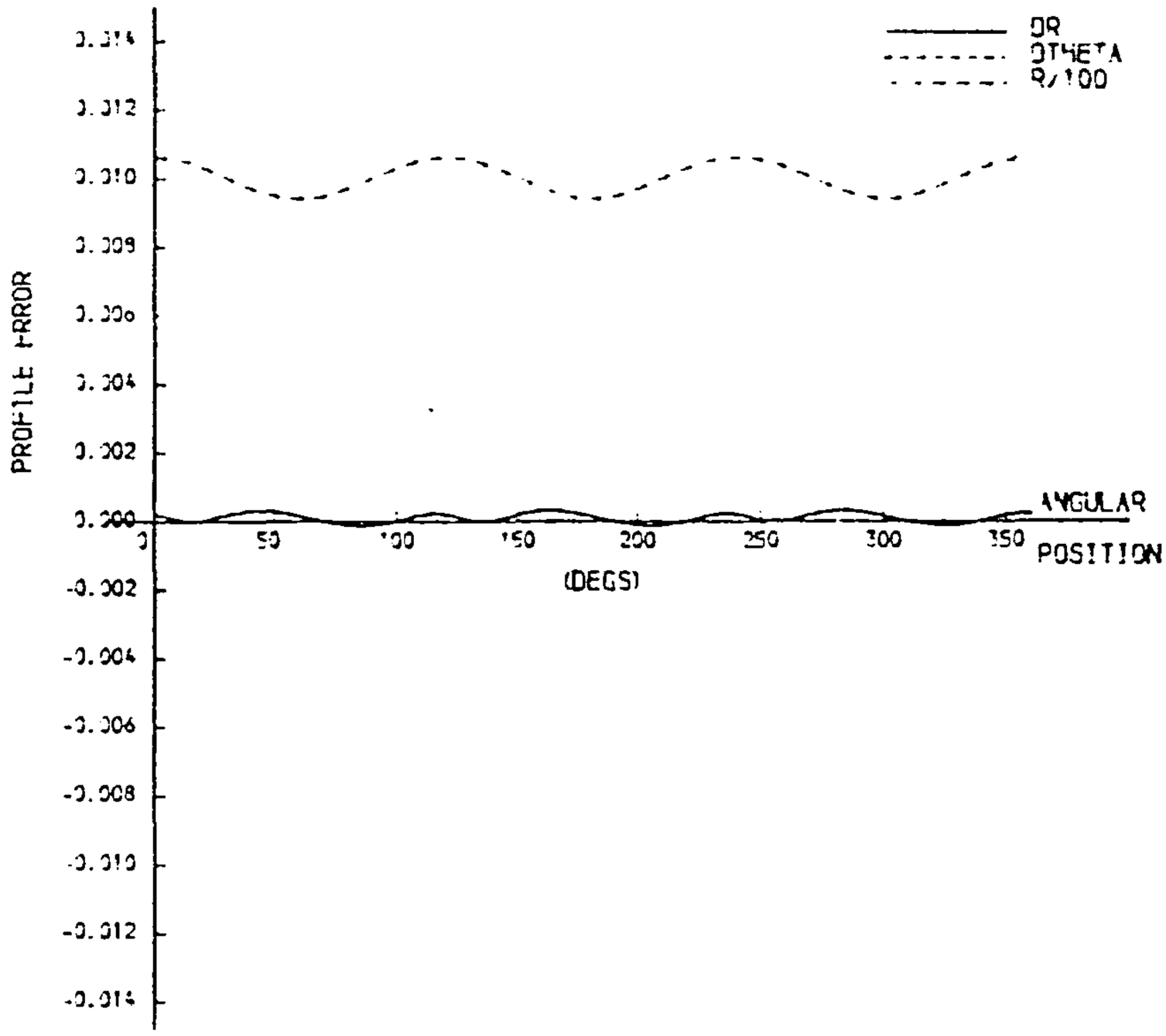

Mechanism Setting

R1 = 5.0mm
R2 = 2.5mm
R3 = 0.3mm
R4 = 20.0mm
$\dot{\psi}_1$ = 10.0 rad/s

Compensating Deviations

FEED = -0.008mm
RL3 = -0.001mm

Profile error due to mechanism deflections (and compensation of error) for various operating conditions.

Fig. A10.16

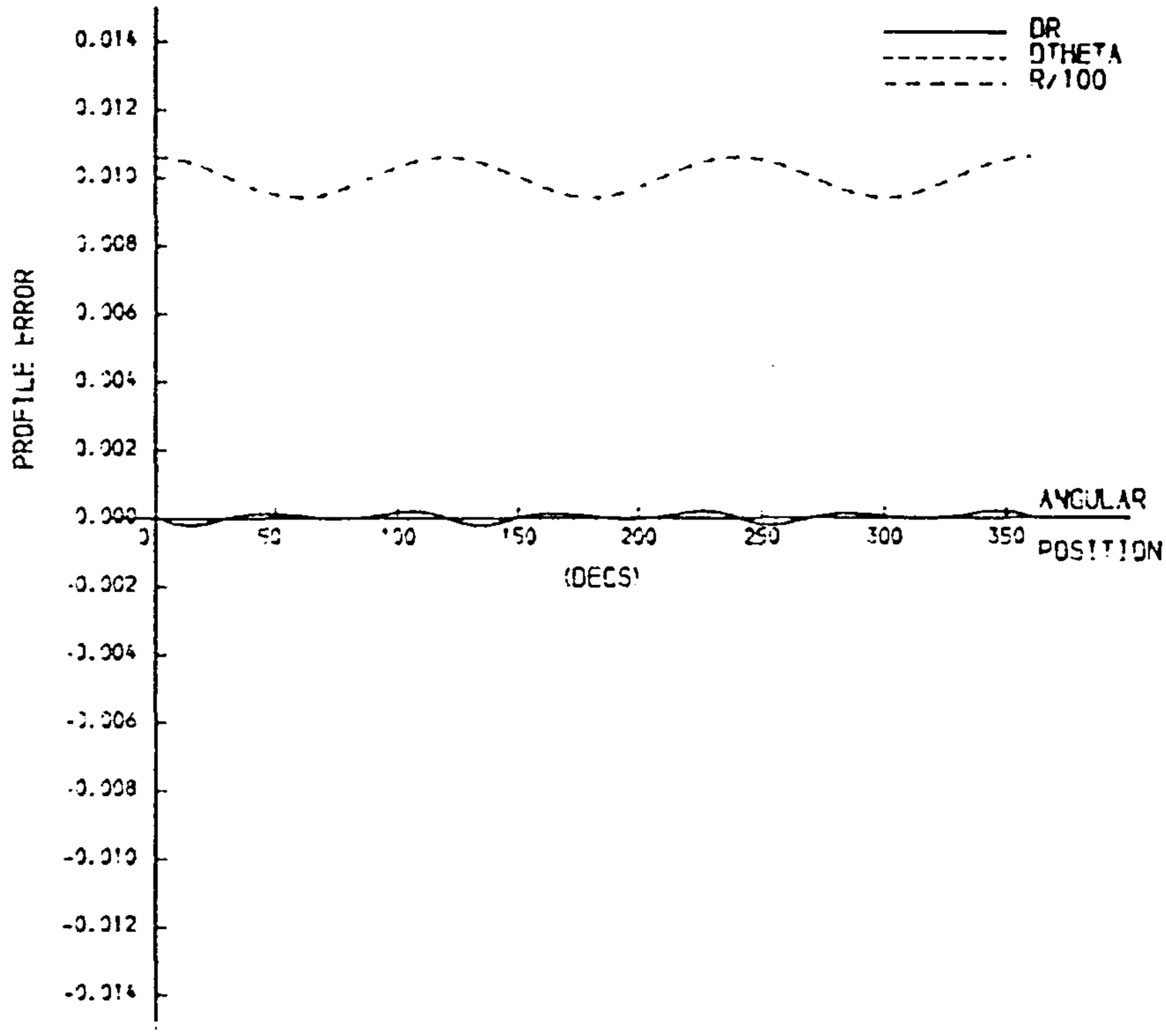

Mechanism Setting

R1 = 5.0mm
R2 = 2.5mm
R3 = 0.3mm
R4 = 40.0mm
$\dot{\psi}_1$ = 5.0 rad/s

Compensating Deviations

FEED = -0.009mm
RL3 = -0.001mm

Profile error due to mechanism deflections (and compensation of error) for various operating conditions.

Fig. A10.15

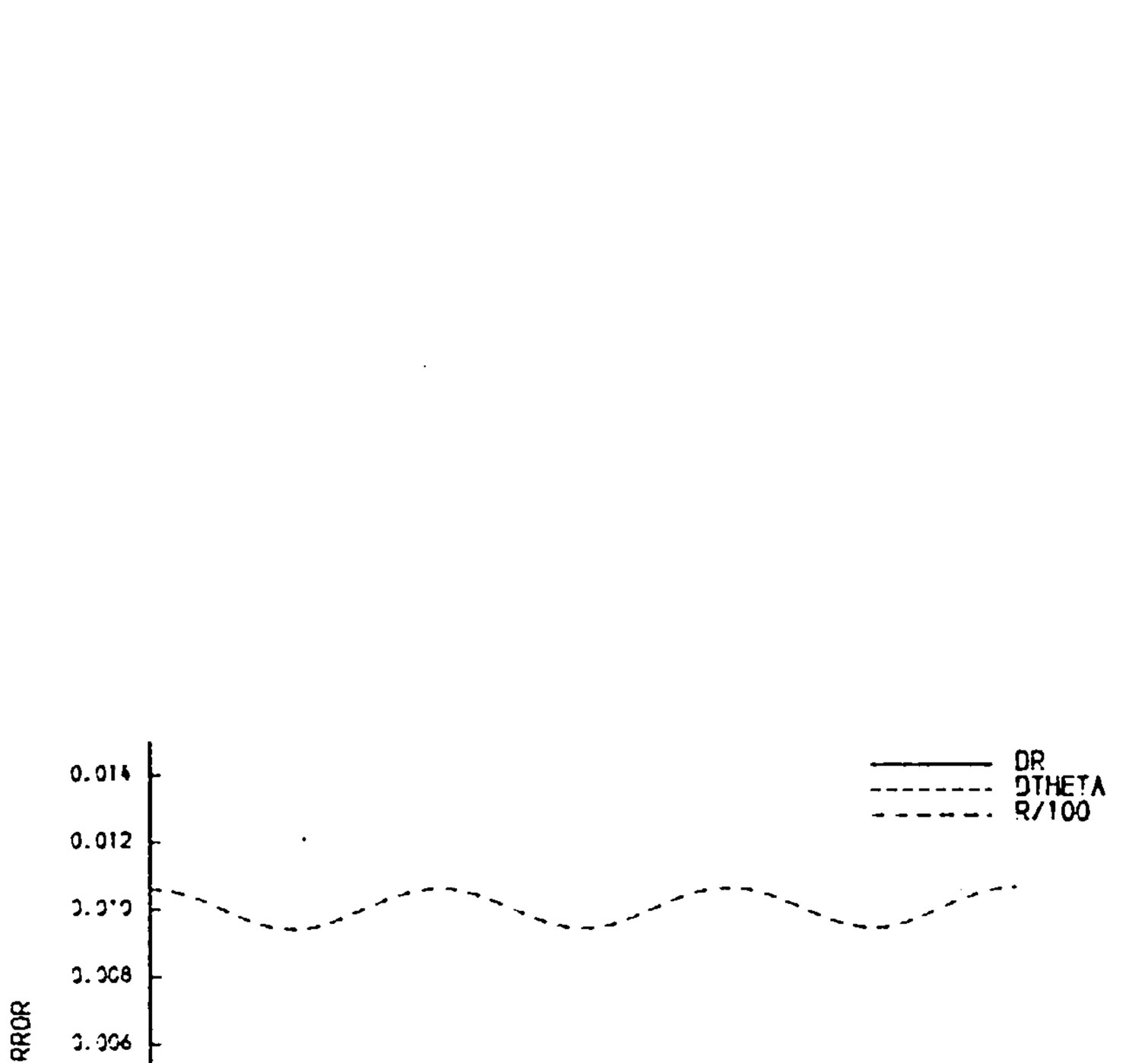

Mechanism Setting

R1 = 5.0mm
R2 = 2.5mm
R3 = 0.3mm
R4 = 20.0mm
$\dot{\psi}_1$ = 5.0 rad/s

Compensating Deviations

FEED = -0.008mm
RL3 = -0.001mm

Profile error due to mechanism deflections (and compensation of error) for various operating conditions.

Fig. A10.17

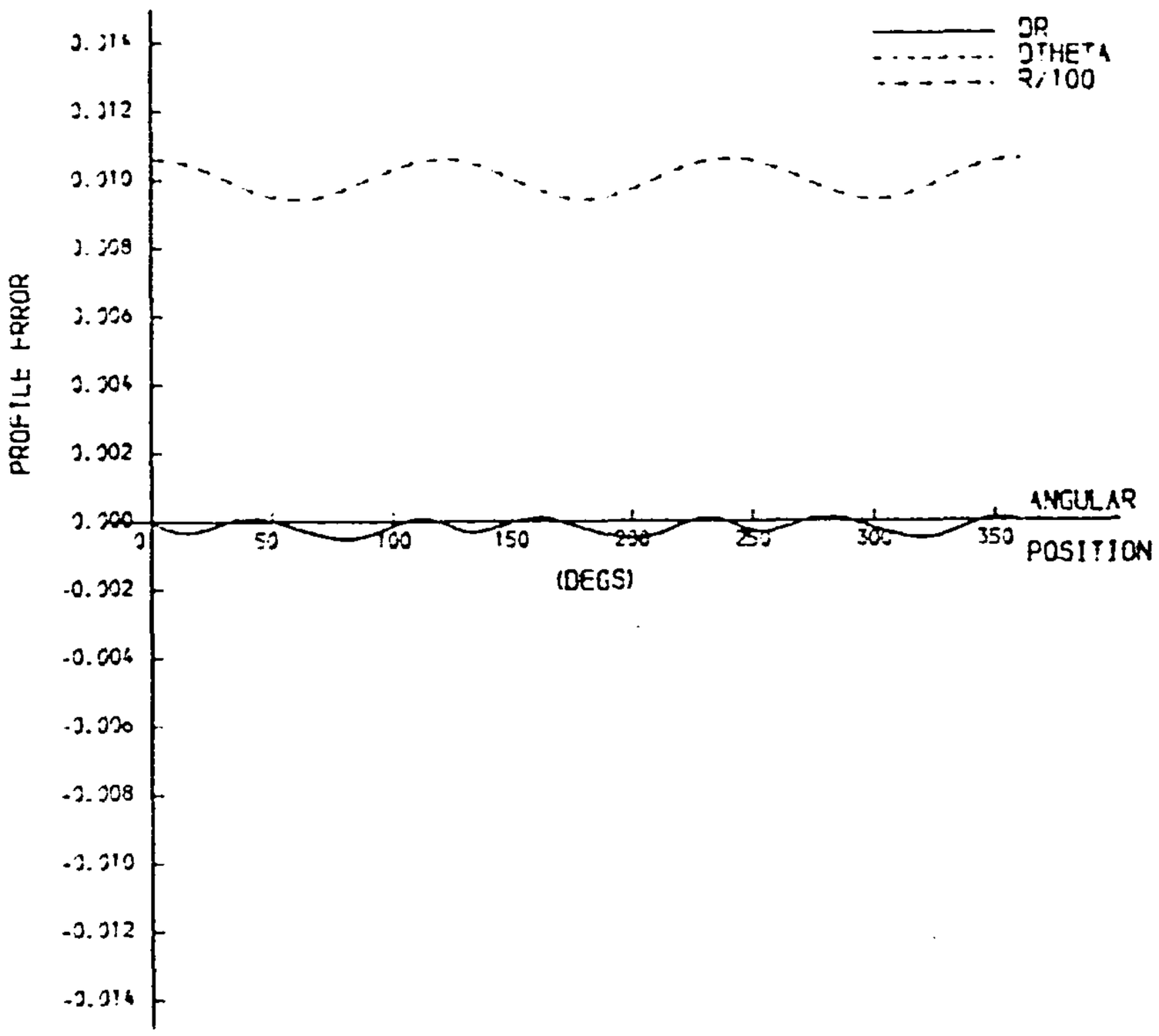

Mechanism Setting

R1 = 10.0mm
R2 = 5.0mm
R3 = 0.6mm
R4 = 40.0mm
$\dot{\psi}_1$ = 10.0 rad/s

Compensating Deviations

FEED = -0.007mm
RL3 = -0.001mm

Profile error due to mechanism deflections (and compensation of error) for various operating conditions.

Fig. A10.19

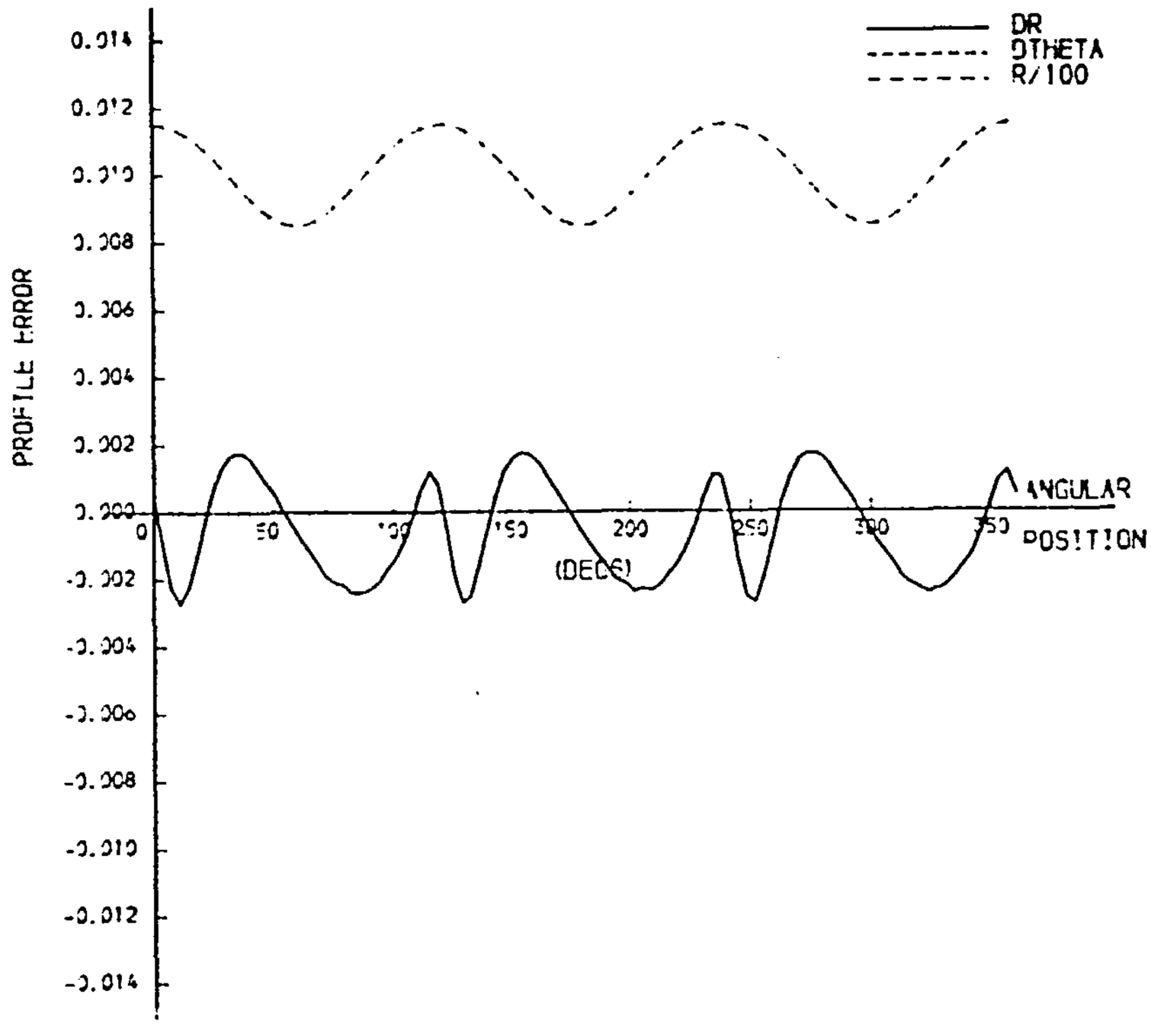

Mechanism Setting

R1 = 10.0mm
R2 = 5.0mm
R3 = 1.5mm
R4 = 40.0mm
$\dot{\psi}_1$ = 10.0 rad/s

Compensating Deviations

FEED = -0.007mm
RL3 = -0.002mm

Profile error due to mechanism deflections (and compensation of error) for various operating conditions.

Fig. A10.18

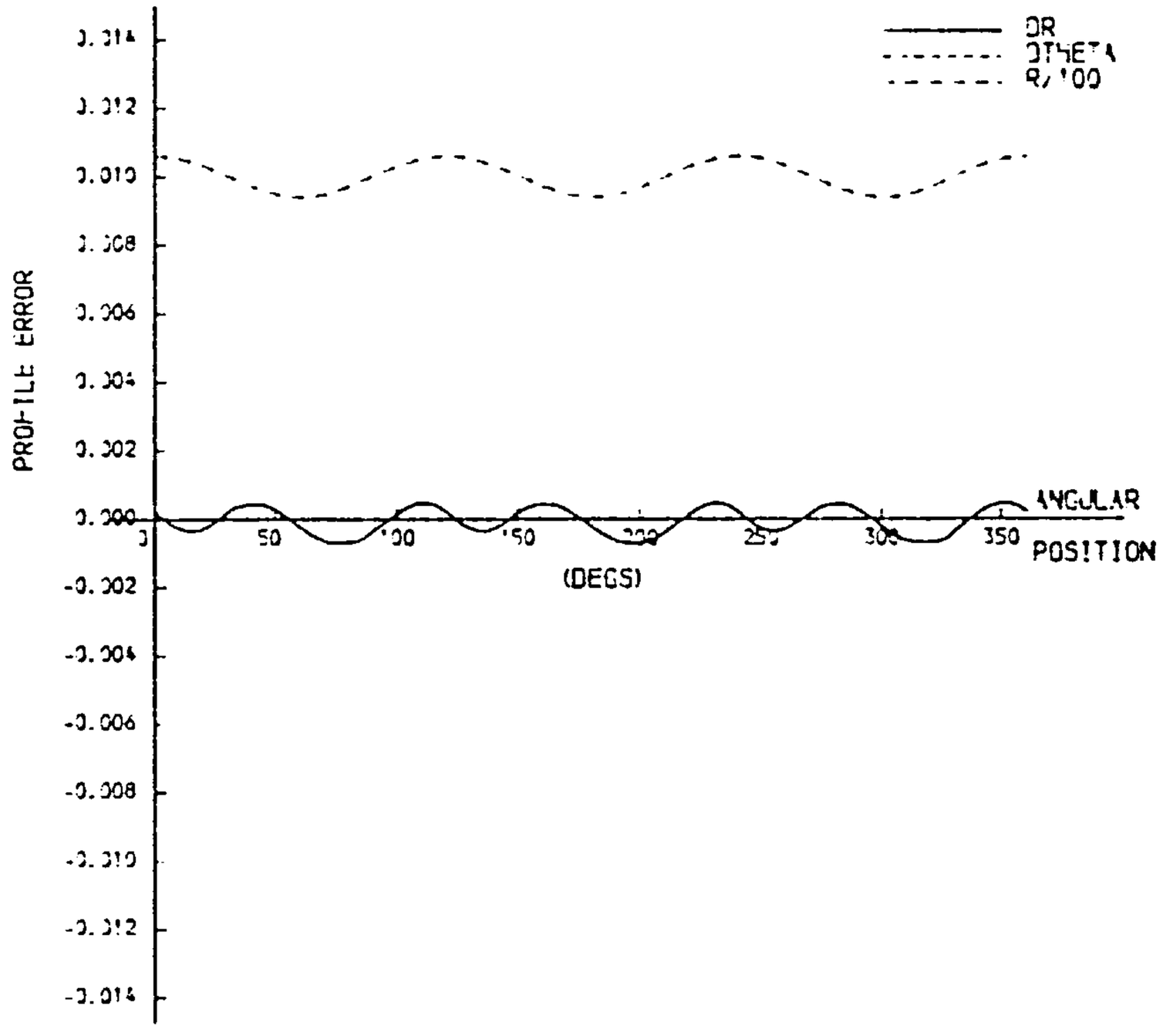

Mechanism Setting

R1 = 25.0mm
R2 = 12.5mm
R3 = 1.5mm
R4 = 40.0mm
$\dot{\psi}_1$ = 10.0 rad/s

Compensating Deviations

FEED = -0.007mm
RL3 = -0.001mm

Profile error due to mechanism deflections (and compensation of error) for various operating conditions.

Fig. A10.21

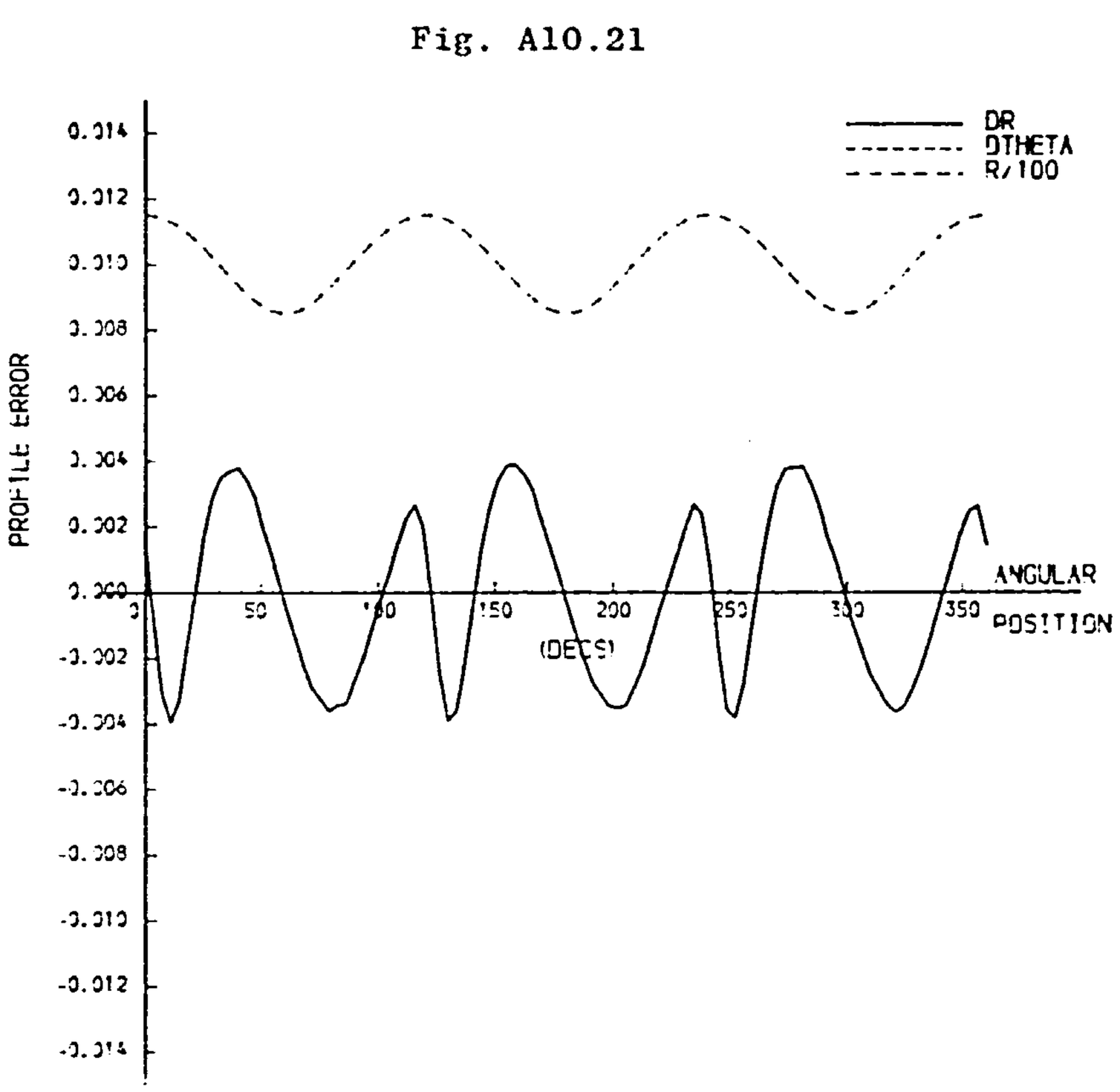

Mechanism Setting

R1 = 25.0mm
R2 = 12.5mm
R3 = 3.75mm
R4 = 40.0mm
$\dot{\psi}_1$ = 10.0 rad/s

Compensating Deviations

FEED = -0.007mm
RL3 = -0.002mm

Profile error due to mechanism deflections (and compensation of error) for various operating conditions.

Fig. A10.20

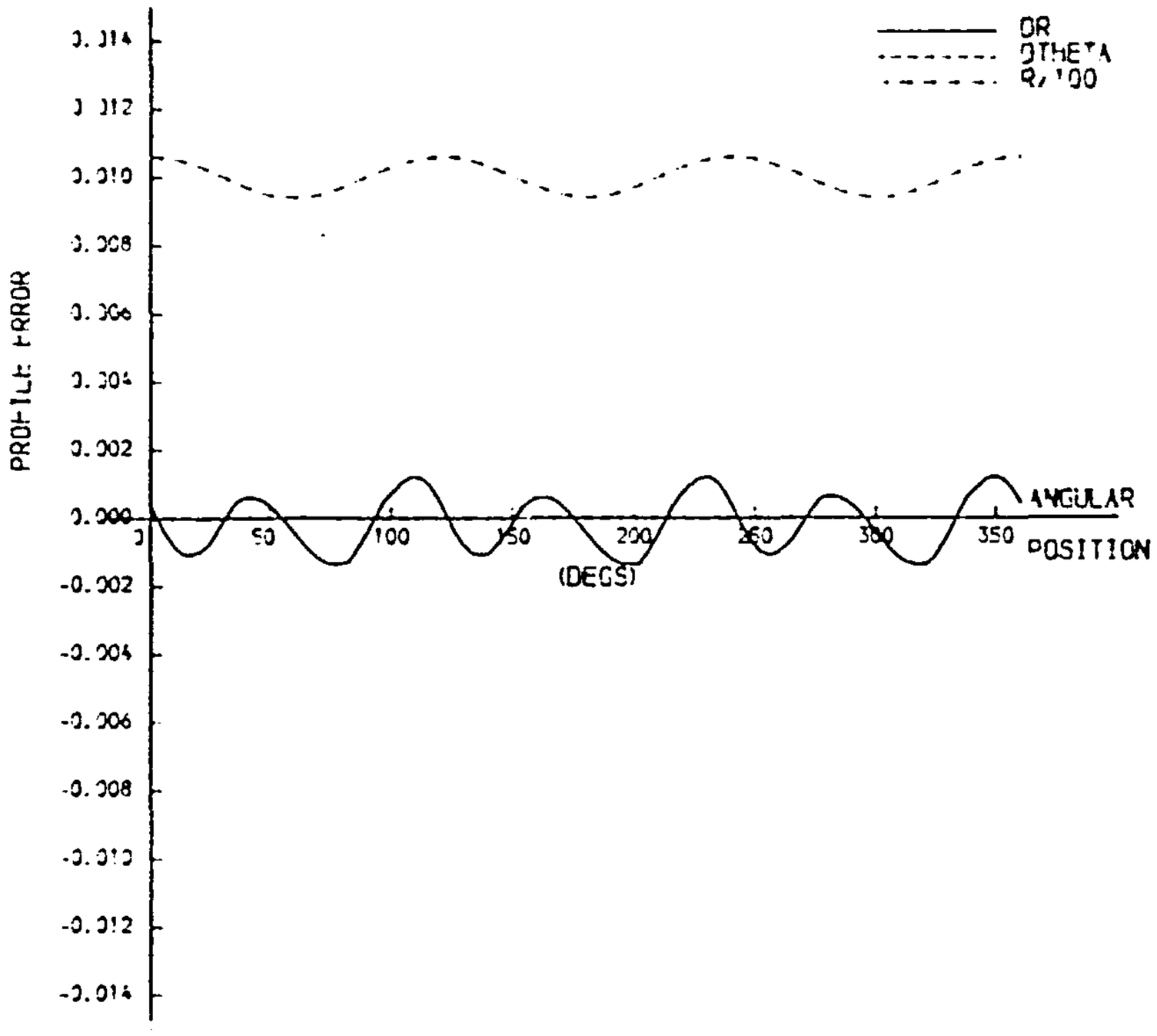

Mechanism Setting

R1 = 50.0mm
R2 = 25.0mm
R3 = 3.0mm
R4 = 40.0mm
$\dot{\psi}_1$ = 10.0 rad/s

Compensating Deviations

FEED = -0.007mm
RL3 = -0.001mm

Profile error due to mechanism deflections (and compensation of error) for various operating conditions.

Fig. A10.23

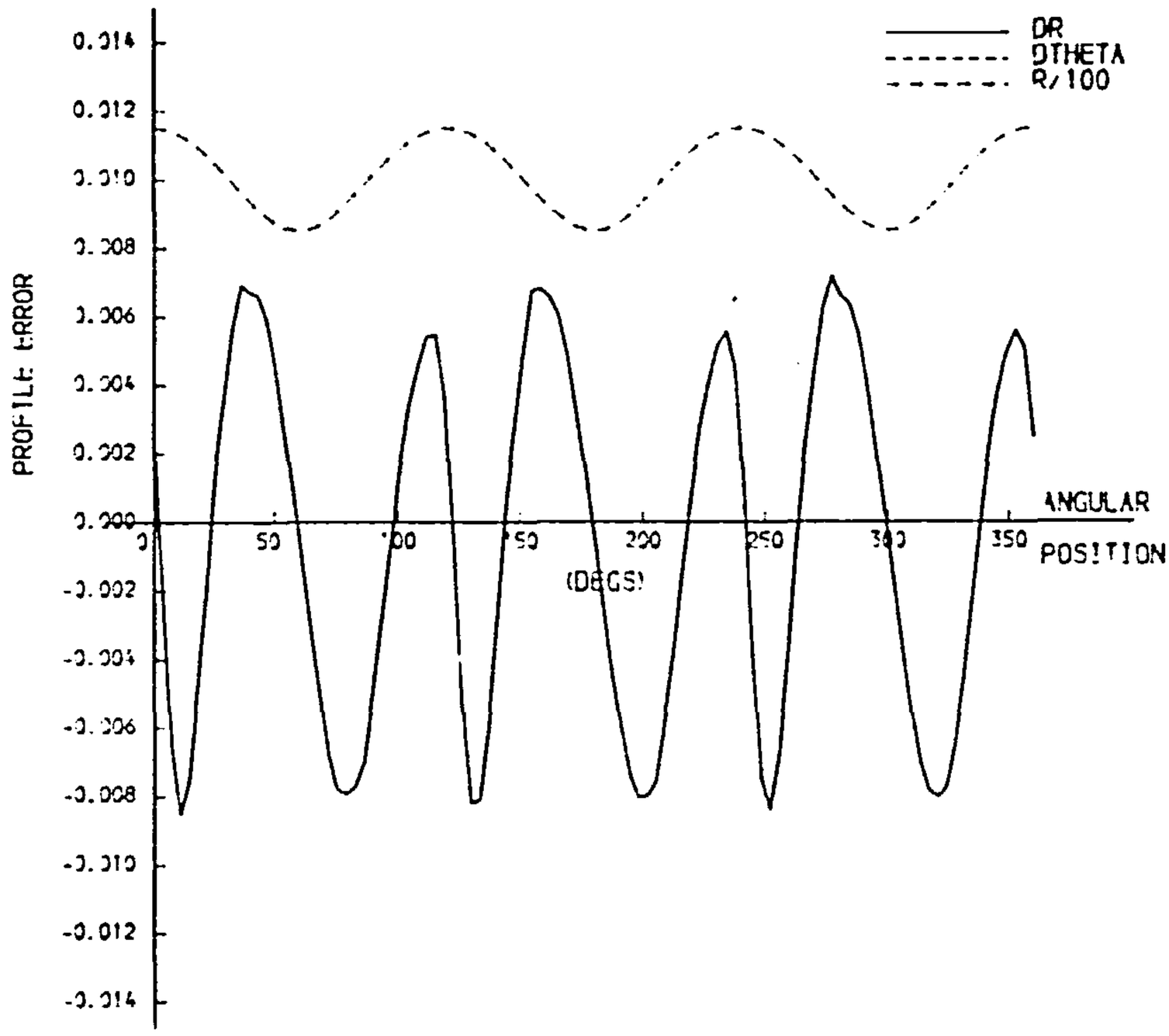

Mechanism Setting

R1 = 50.0mm
R2 = 25.0mm
R3 = 7.5mm
R4 = 40.0mm
$\dot{\psi}_1$ = 10.0 rad/s

Compensating Deviations

FEED = -0.008mm
RL3 = -0.001mm

Profile error due to mechanism deflections (and compensation of error) for various operating conditions.

Fig. A10.22

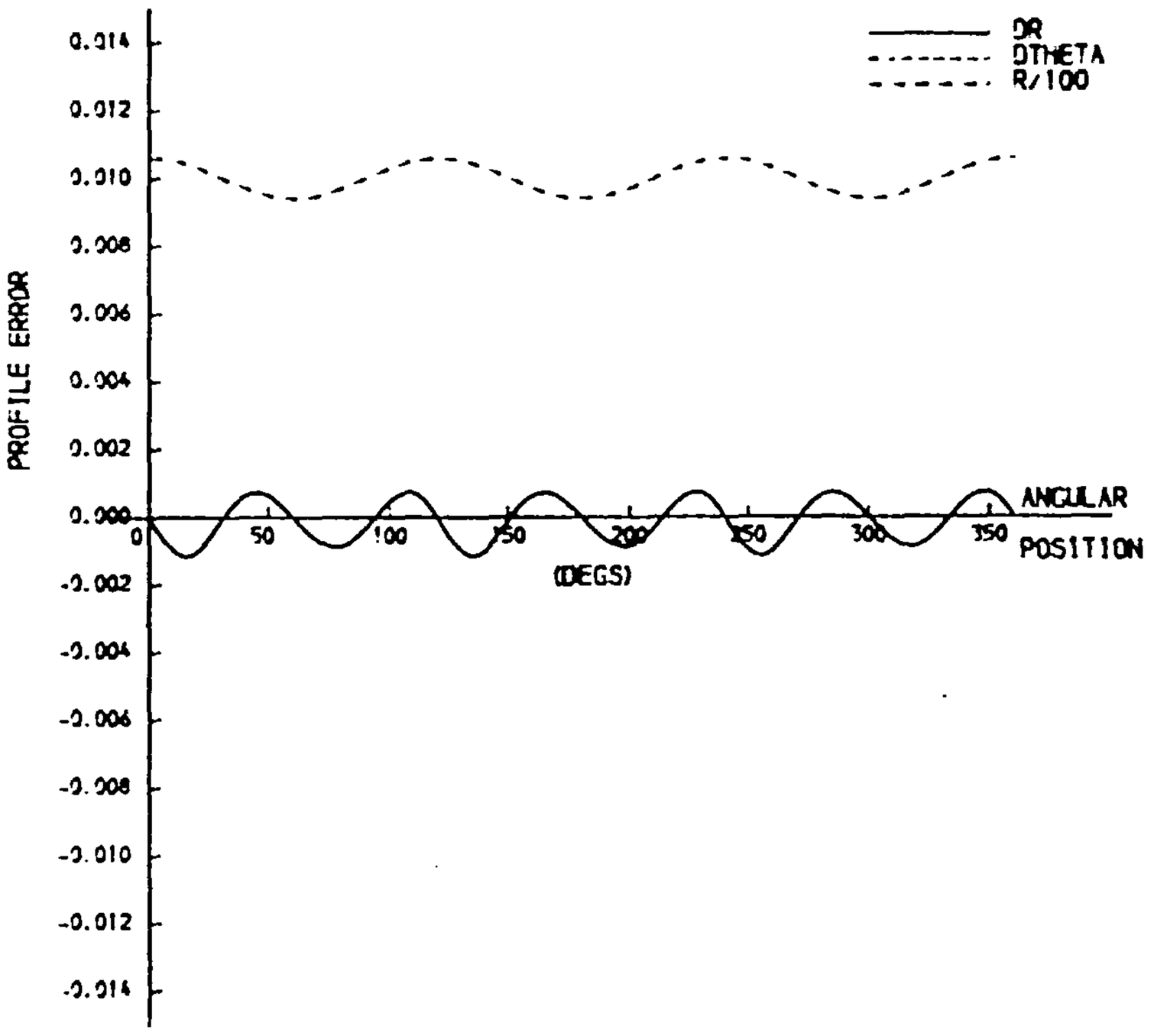

Mechanism
Setting

R1 = 50.0mm
R2 = 25.0mm
R3 = 3.0mm
R4 = 40.0mm
$\dot{\psi}_1$ = 10.0 rad/s

Profile error caused by individual parameter deviations due to deflections

Fig. A10.25 RL3 deflection

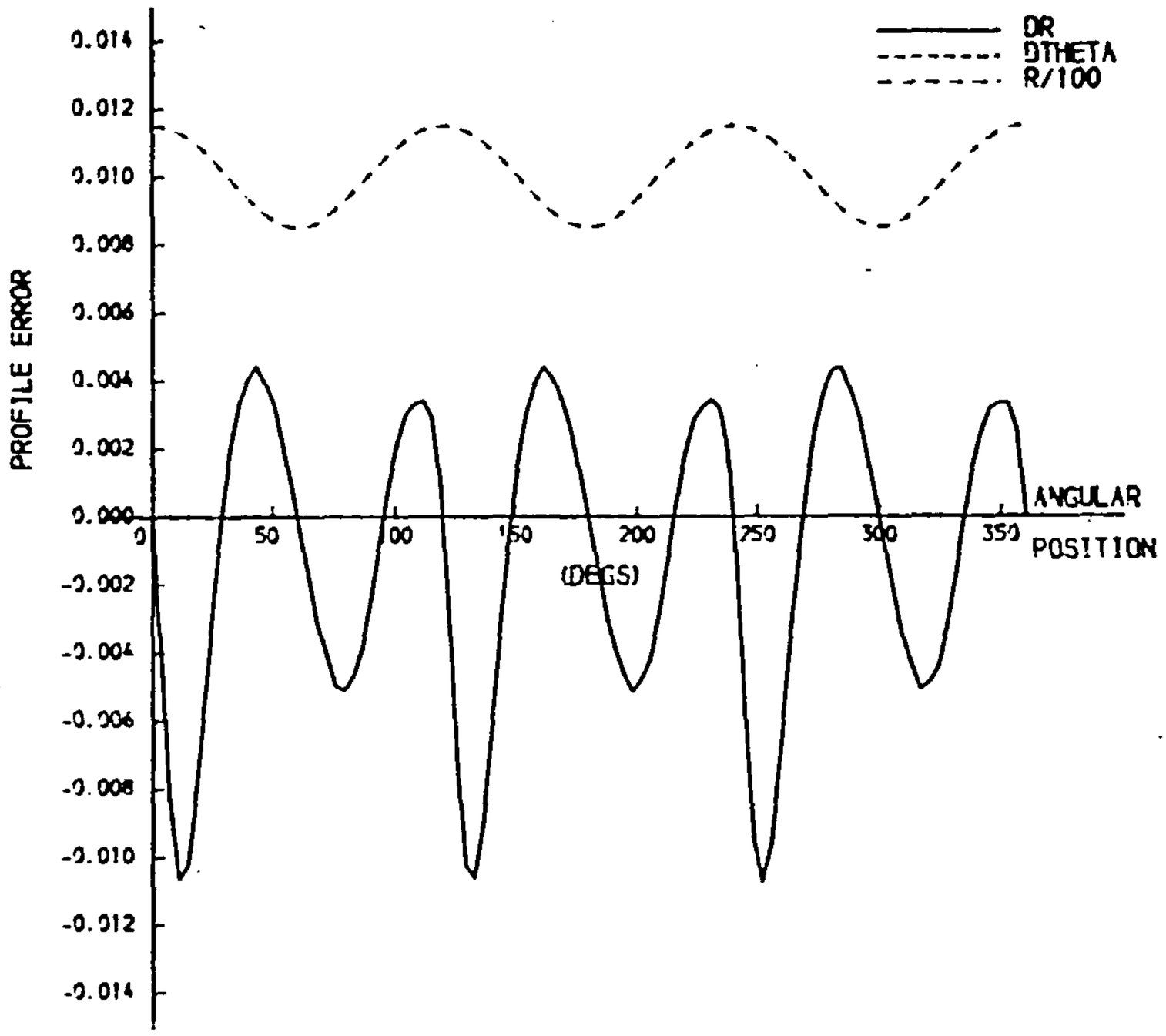

Mechanism
Setting

R1 = 50.0mm
R2 = 25.0mm
R3 = 7.5mm
R4 = 40.0mm
$\dot{\psi}_1$ = 10.0 rad/s

Profile error caused by individual parameter deviations due to deflections

Fig. A10.24 RL3 deflection

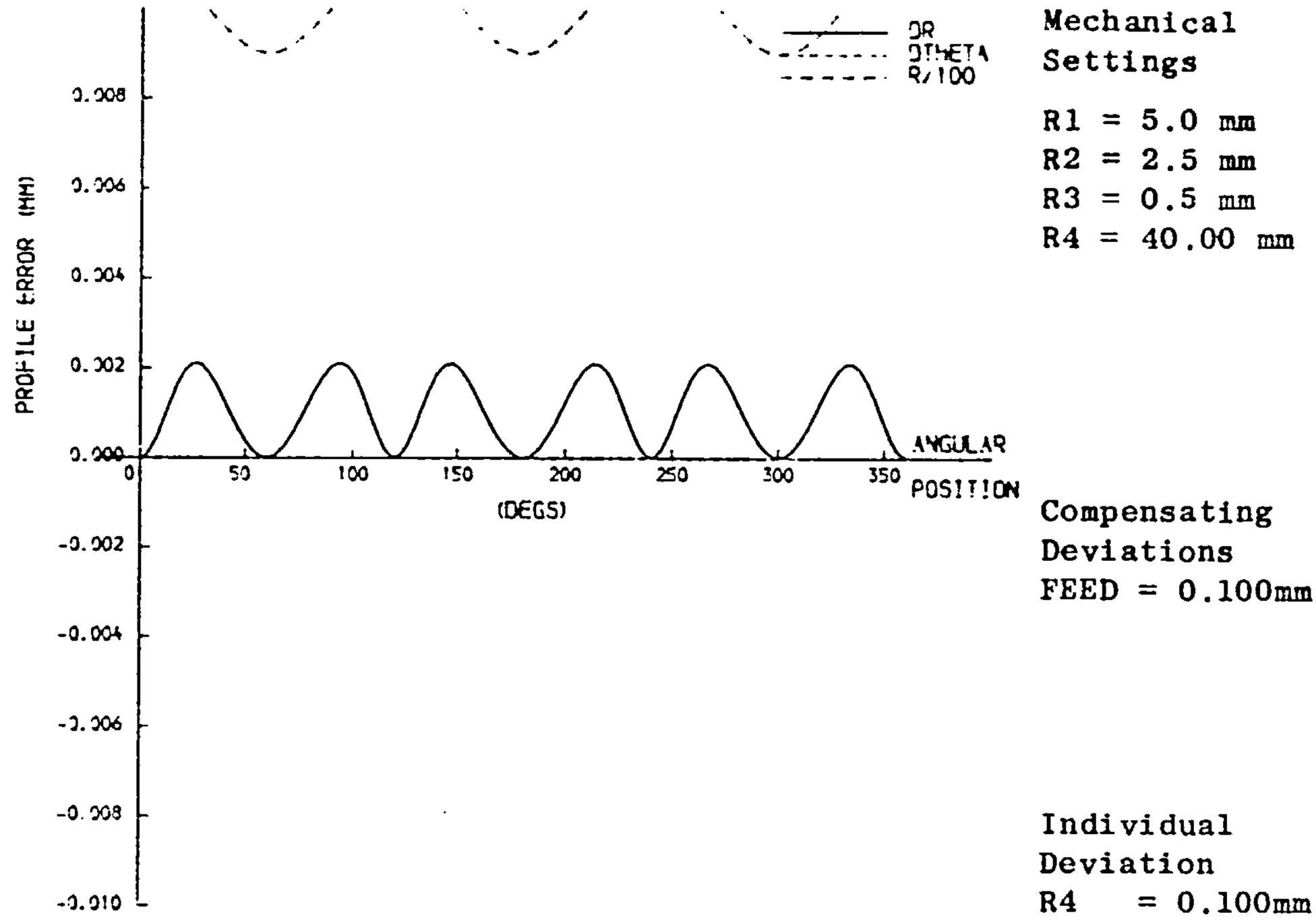

Mechanical Settings

R1 = 5.0 mm
R2 = 2.5 mm
R3 = 0.5 mm
R4 = 40.00 mm

Compensating Deviations
FEED = 0.100mm

Individual Deviation
R4 = 0.100mm

Compensation of constant deviations of individual parameters

Fig. A11.2 R4 deviation

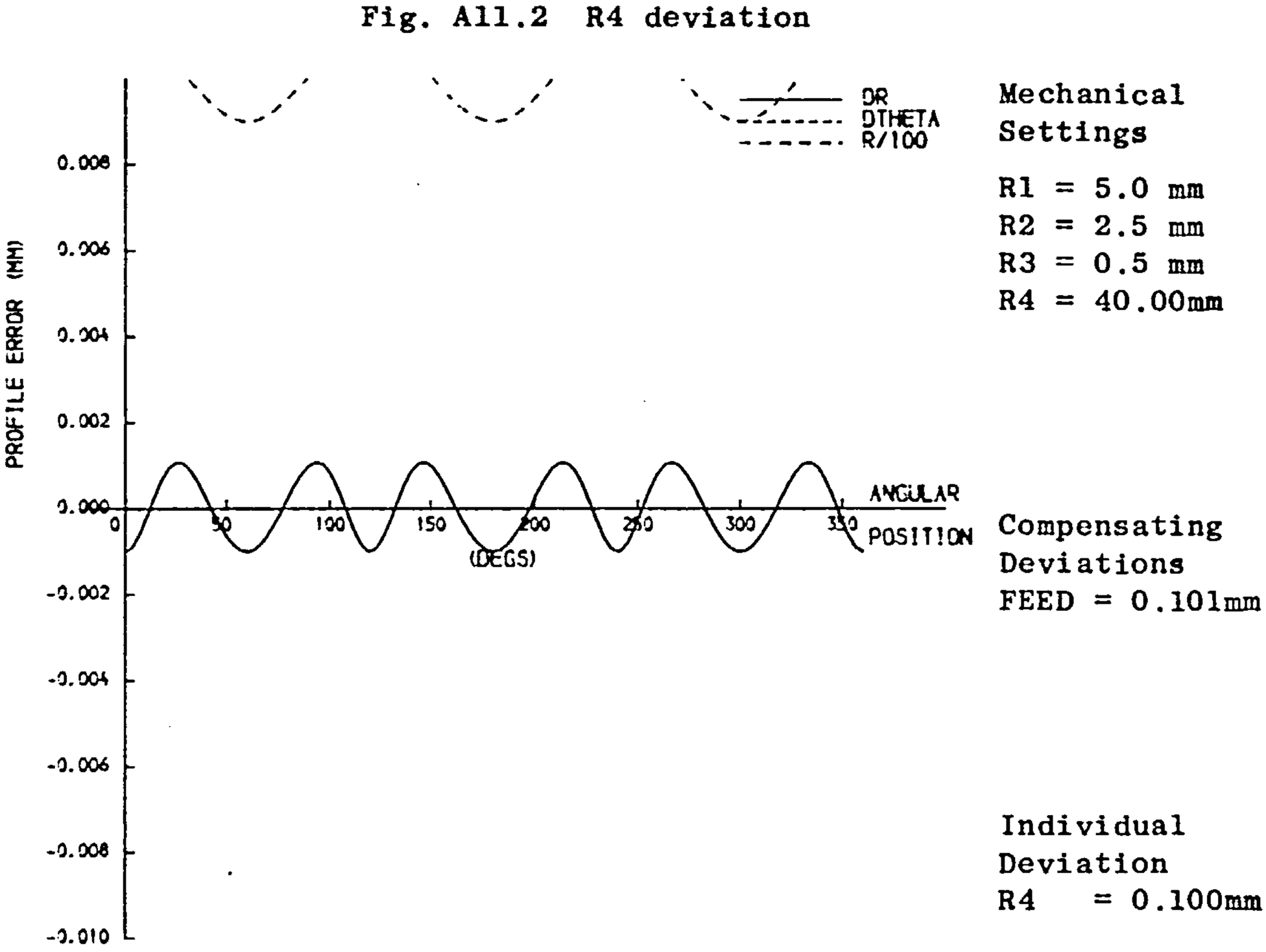

Mechanical Settings

R1 = 5.0 mm
R2 = 2.5 mm
R3 = 0.5 mm
R4 = 40.00mm

Compensating Deviations
FEED = 0.101mm

Individual Deviation
R4 = 0.100mm

Compensation of constant deviations of individual parameters

Fig. A11.1 R4 deviation

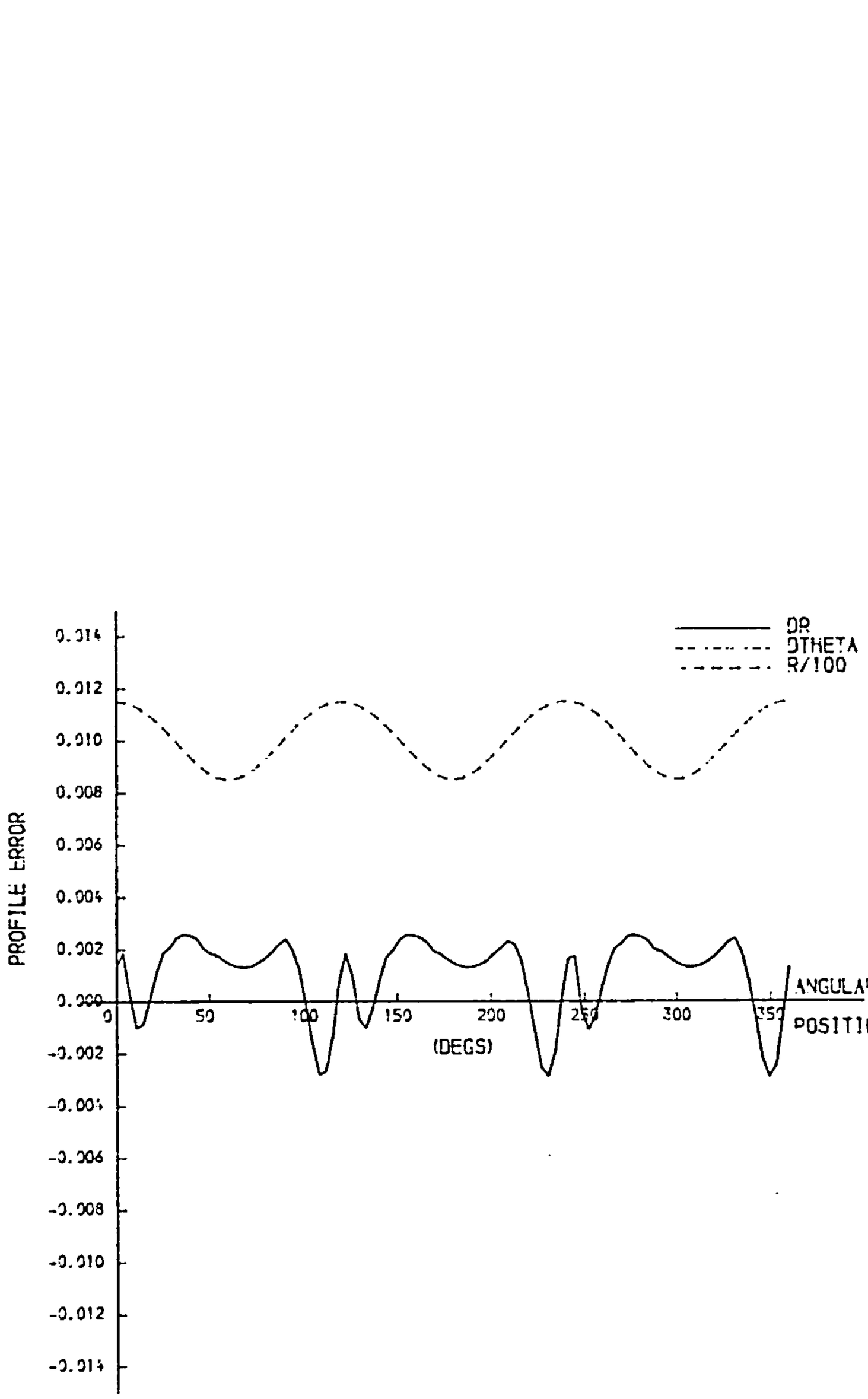

Mechanism Setting

R1 = 50.0mm
R2 = 25.0mm
R3 = 7.5mm
R4 = 40.0mm
$\dot{\psi}_1$ = 10.0 rad/s

Compensation Deviations

FEED = -0.002mm

Example of potential effect on profile error of mechanism counter-balancing (by setting gravity constant = 0).

Fig. A12.1

APPENDIX B

DYNAMIC ANALYSIS OF MECHANISM

B1. GRINDING SYSTEM

The components of force, X_{gw} and Y_{gw}, exerted by the grinding system on its supporting link (see Fig.B1.1) are given by

$$X_{gw} = -(F_{CT} \sin\psi_3 + F_{CN} \cos\psi_3 + m_{gwH} \ddot{x}_{gw}) \qquad \text{(B1.1)}$$

$$Y_{gw} = -(-F_{CT}\cos\psi_3 + F_{CN} \sin\psi_3 + m_{gwV} (\ddot{y}_{gw}+g)) \qquad \text{(B1.2)}$$

Note: the mass of the grinding system is expressed as 'effective' masses m_{gwH}, m_{gwV}, in the horizontal and vertical equilibrium equations, which include the effect of the grinding spindle transmission support links from the motor. In this way a full kinematic and dynamic analysis of the transmission links was avoided. The configuration of these links and their motion is such as to make this a reasonable approximation (see also App. C2.1).

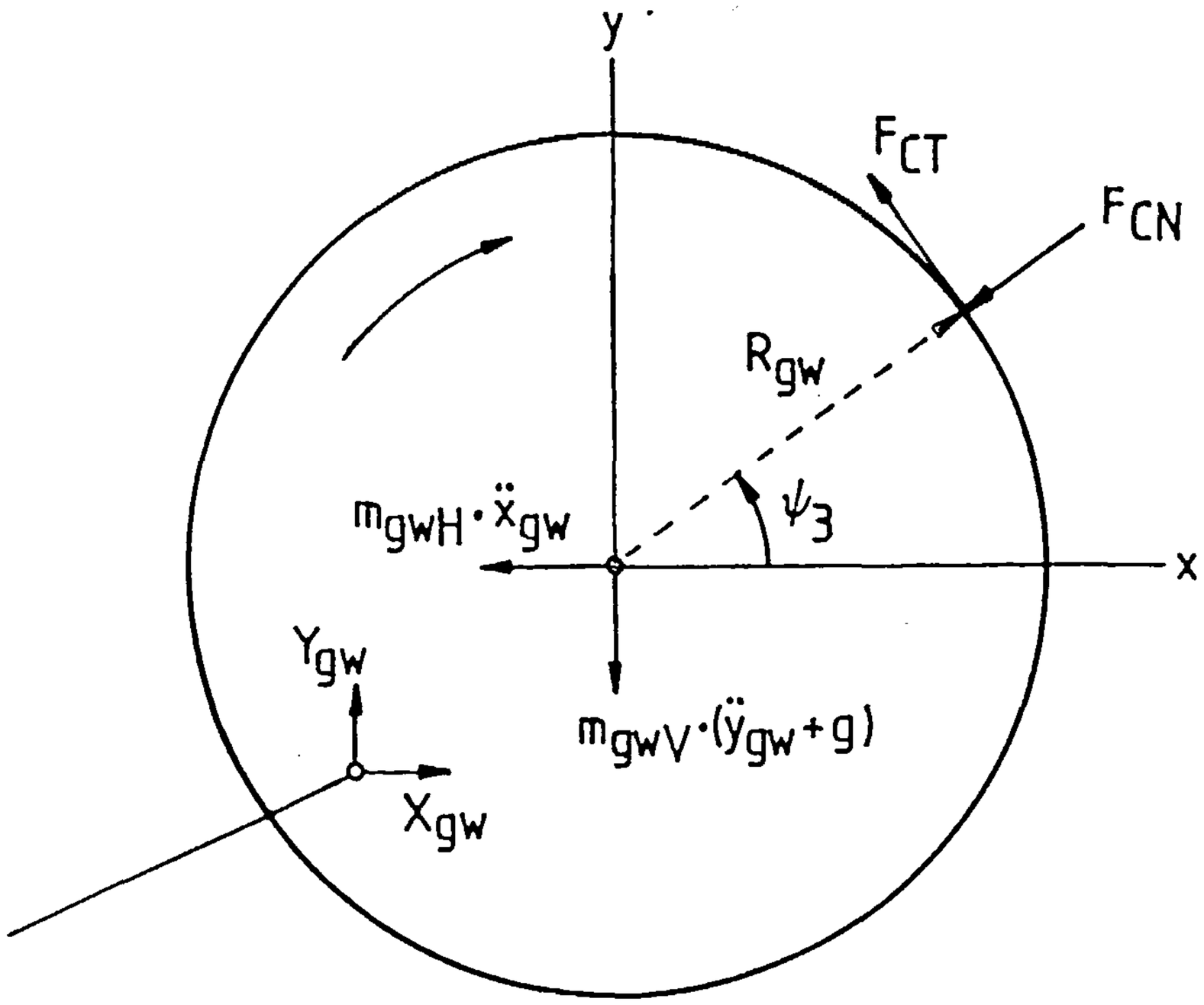

Fig. B1.1 Grinding system forces

Computer Program

Equations (B2.1) and (B2.2) are incorporated in SUBROUTINE GRIDYN called by main program MECHDYN.

B2. PANTOGRAPH

B2.1 Equilibrium Equations

With reference to the free-body diagrams and notation in Fig.B2.1, the following equilibrium equations may be written down for the respective links, (two orthogonal force equations and one moment equation per link):

Link L1

$$X_{M1} + X_{21} + X_{41} - m_1 a_{1x} = 0 \qquad \text{(B2.1)}$$

$$Y_{M1} + Y_{21} + Y_{41} - m_1(a_{1y} + g) = 0 \qquad \text{(B2.2)}$$

$$(X_{41}\ell_1 + X_{21}\ell_{J1})\sin\phi_1 - (Y_{41}\ell_1 + Y_{21}\ell_{J1} - m_1 g r_1(\cos\phi_1 + I_{1A}\alpha_1 = 0 \qquad \text{(B2.3)}$$

Link L2

$$X_{12} + X_{F2} - m_2\, a_{2x} = 0 \qquad \text{(B2.4)}$$

$$Y_{12} + Y_{F2} - m_2\,(a_{2y} + g) = 0 \qquad \text{(B2.5)}$$

$$X_{12}\ell_2 \sin\phi_2 - (Y_{12}\ell_2 - m_2\, g\, r_2)\cos\phi_2 + I_{2D}\alpha_2 = 0 \qquad \text{(B2.6)}$$

Link L3

$$X_{43} + X_{F3} - m_3\, a_{3x} = 0 \qquad \text{(B2.7)}$$

$$Y_{43} + Y_{F3} - m_3\,(a_{3y} + g) = 0 \qquad \text{(B2.8)}$$

$$X_{43}\ell_3 \sin\phi_3 - (Y_{43}\ell_3 - m_3\, g\, r_3)\cos\phi_3 + I_{3D}\alpha_3 = 0 \qquad \text{(B2.9)}$$

Link L4

$$X_{G4} + X_{34} + X_{14} - m_4\, a_{4x} = 0 \qquad \text{(B2.10)}$$

$$Y_{G4} + Y_{34} + Y_{14} - m_4(a_{4y} + g) = 0 \qquad \text{(2.11)}$$

$$(X_{14}\ell_4 + X_{34}\,\ell_{J4})\sin\phi_4 - (Y_{14}\ell_4 + Y_{34}\ell_{J4} - m_4\, g\, r_4)\cos\phi_4 + I_{4C}\alpha_4 = 0 \qquad \text{(B2.12)}$$

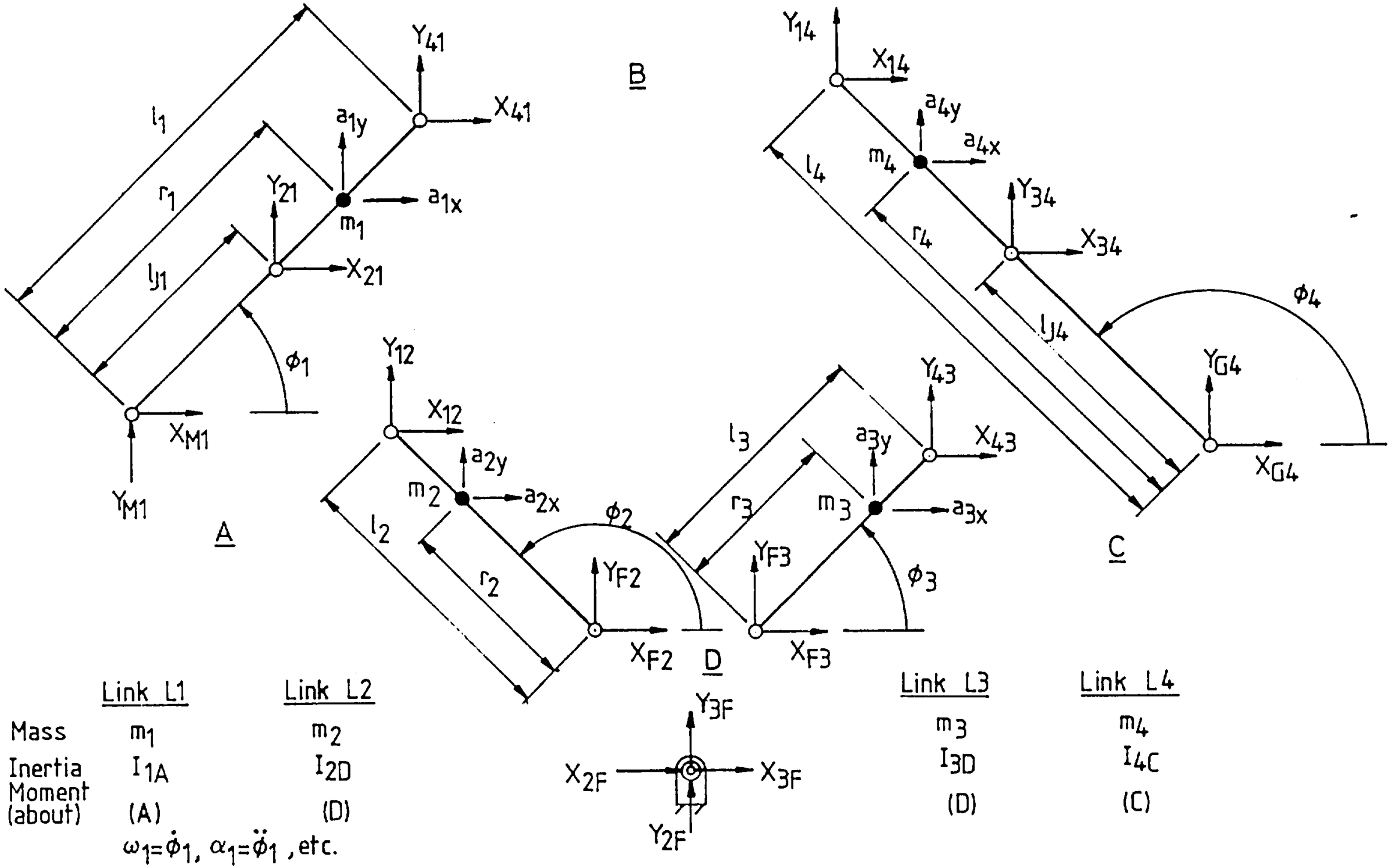

	Link L1	Link L2	Link L3	Link L4
Mass	m_1	m_2	m_3	m_4
Inertia Moment (about)	I_{1A} (A)	I_{2D} (D)	I_{3D} (D)	I_{4C} (C)

$\omega_1=\dot{\phi}_1$, $\alpha_1=\ddot{\phi}_1$, etc.

Fig. B2.1 Force and Parameter notation for Pantograph Dynamic Analysis

B2.2 Kinematic

The kinematic parameters in eqns (B2.1) to (B2.12) are deduced from the kinematic analysis of Appendix A2, which gives the motion of the linkage joints. Referring to Appendix A2 and Fig.A2.1 the angular and linear motions of the mass centres are as follows:

Angular velocities. for links L1 to L4 respectively

$$\omega_1 = \frac{v_3 - v_1}{u_3 - u_1}$$

$$\omega_2 = \frac{\dot{v}_2}{u_2 - u_4}$$

$$\omega_3 = \frac{\dot{v}_5}{u_5 - u_4}$$

$$\omega_4 = \frac{\dot{v}_3 - \dot{v}_6}{u_3 - u_6}$$

Angular accelerations

$$\alpha_1 = \frac{\ddot{v}_3 - \ddot{v}_1 + \omega_1^2 (v_3 - v_1)}{u_3 - u_1}$$

$$\alpha_2 = \frac{\ddot{v}_2 + \omega_2^2 (v_2 - v_4)}{u_2 - u_4}$$

$$\alpha_3 = \frac{\ddot{v}_5 + \omega_3^2 (v_5 - v_4)}{u_5 - u_4}$$

$$\alpha_4 = \frac{\ddot{v}_3 - \ddot{v}_6 - \omega_4^2 (v_3 - v_6)}{u_3 - u_6}$$

Linear accelerations of mass centres

$$a_{1x} = \ddot{u}_1 + (\ddot{u}_3 - \ddot{u}_1) \frac{r_1}{\ell_1}$$

$$a_{1y} = \ddot{v}_1 + (\ddot{v}_3 - \ddot{v}_1) \frac{r_1}{\ell_1}$$

$$a_{2x} = \ddot{u}_2 \frac{r_2}{\ell_2}$$

$$a_{2y} = \ddot{v}_2 \frac{r_2}{\ell_2}$$

$$a_{3x} = \ddot{u}_5 \frac{r_3}{\ell_3}$$

$$a_{3y} = \ddot{v}_5 \frac{r_3}{\ell_3}$$

$$a_{4x} = \ddot{u}_6 + (\ddot{u}_3 - \ddot{u}_6) \frac{r_4}{\ell_4}$$

$$a_{4y} = \ddot{v}_6 + (\ddot{v}_3 - \ddot{v}_6) \frac{r_4}{\ell_4}$$

B2.3 Forces

The equations (B2.1) to (B2.12) can be solved analytically to determine the forces acting at each joint. Using the abbreviations

$$\ell_{1c} = \ell_1 \cos\phi_1, \quad \ell_{1s} = \ell_1 \sin\phi_1$$

$$\ell_{J1c} = \ell_{J1} \cos\phi_1, \quad r_{1c} = r_1 \cos\phi_1$$

$$\ell_{2c} = \quad ..... \text{ etc.},$$

and noting that $X_{12} = -X_{21}$ etc, the forces may be expressed as follows:

$$X_{G4} = X_{gw} \text{ (from eqn. B1.1)} \qquad \text{(B2.13)}$$

$$Y_{G4} = Y_{gw} \text{ (from eqn. B1.2)} \qquad \text{(B2.14)}$$

$$X_{34} = \Big[(X_{G4} - m_4 a_{4x}) \ell_{4s} - (Y_{G4} - m_4 a_{4y}) \ell_{4c} - I_{4c}\alpha_4 + (I_{3D}\alpha_3 + m_3 g r_{3c}) . \left(\frac{\ell_{4c} - \ell_{J4c}}{\ell_{3c}}\right) + m_4 g (\ell_{4c} - r_{4c}) \Big] \pm \Big[\ell_{J4s} - \ell_{s4} + (\ell_{4c} - \ell_{J4c}) \frac{\ell_{3s}}{\ell_{3c}} \Big] \qquad \text{(B2.15)}$$

$$Y_{34} = \frac{X_{34}\ell_{3s} - I_{3D}\alpha_3 - m_3\ g\ r_{3c}}{\ell_{3c}} \qquad \text{(B2.16)}$$

$$X_{14} = - X_{34} - X_{G4} + m_4\ a_{4x} \qquad \text{(B2.17)}$$

$$Y_{14} = -Y_{34} - Y_{G4} + m_4\ (a_{4y} + g) \qquad \text{(B2.18)}$$

$$X_{F3} = X_{34} + m_3\ a_{3x} \qquad \text{(B2.19)}$$

$$Y_{F3} = Y_{34} + m_3\ (a_{3y} + g) \qquad \text{(B2.20)}$$

$$Y_{12} = \Big[X_{14}\ell_{1s} - Y_{14}\ell_{1c} - I_{1A}\alpha_1 - m_1\ g\ r_{1c} - (I_{2D}\alpha_2 + m_2\ g\ r_{2c})\ \frac{\ell_{J1s}}{\ell_{2s}} \Big]$$

$$\times \Big[\frac{\ell_{2s}}{\ell_{2s}\ell_{J1c} - \ell_{2c}\ \ell_{J1s}} \Big] \qquad \text{(2.21)}$$

$$X_{12} = \frac{Y_{12}\ell_{2c} - I_{2D}\alpha_2 - m_2\ g\ r_{2c}}{\ell_{2s}} \qquad \text{(B2.22)}$$

$$X_{F2} = - X_{12} + m_2\ a_{2x} \qquad \text{(B2.23)}$$

$$Y_{F2} = -Y_{12} + m_2(a_{2y} - g) \qquad \text{(B2.24)}$$

$$X_{M1} = X_{12} + X_{14} + m_1 a_{1x} \qquad \text{(B2.25)}$$

$$Y_{M1} = Y_{12} + Y_{14} + m_1(a_{1y} + g) \qquad \text{(B2.26)}$$

B2.4 Computer Program

The equations of Appendix B2 are incorporated in SUBROUTINE PANDYN which is called in the main program MECHDYN.

B3. PROFILE GENERATOR

B3.1 Equilibrium Equations

Referring to Fig.B3.1, the following equilibrium equations may be written:

Link R3

$$X_{23} + X_{43} - m_3 a_{3x} = 0 \quad \text{(B3.1)}$$

$$Y_{23} + Y_{43} - m_3 (a_{3y} + g) = 0 \quad \text{(B3.2)}$$

$$X_{43} r_3 \sin\psi_1 - (Y_{43} r_3 - m_3 g r_{g3}) \cos\psi_1 - T + I_{3A} \alpha_3 = 0 \quad \text{(B3.3)}$$

Link R4

$$X_{34} + X_{54} + X_{P4} - -m_4 a_{4x} = 0 \quad \text{(B3.4)}$$

$$Y_{34} + Y_{54} + Y_{P4} - m_4 (a_{4y} + g) = 0 \quad \text{(B3.5)}$$

$$X_{34}(x_{g4}\sin\psi_2 + y_{g4}\cos\psi_2) - Y_{34}(x_{g4}\cos\psi_2 - y_{g4}\sin\psi_2)$$

$$+ X_{54}((x_{g4} - r_{s4})\sin\psi_2 + y_{g4}\cos\psi_2)$$

$$- Y_{54}((x_{g4} - r_{s4})\cos\psi_2 - y_{g4}\sin\psi_2)$$

$$- X_{P4}((r_4 - x_{g4})\sin\psi_2 - y_{g4}\cos\psi_2)$$

$$+ Y_{P4}((r_4 - x_{g4})\cos\psi_2 + y_{g4}\sin\psi_2) + T_{54} - I_{4G}\alpha_4 = 0 \quad \text{(B3.6)}$$

Link R5

$$X_{25} + X_{45} - m_5 a_{5x} = 0 \quad \text{(B3.7)}$$

$$Y_{25} + Y_{45} - m_5 (a_{5y} + g) = 0 \quad \text{(B3.8)}$$

$$(I_{5G} + m_5 (x_{g5}^2 + y_{g5}^2))\alpha_5 + m_5 g (x_{g5}\cos\psi_5 - y_{g5}\sin\psi_5)$$

$$- T_{45} = 0 \quad \text{(B3.9)}$$

$$X_{45}\sin\psi_5 - Y_{45}\cos\psi_5 = 0 \quad \text{(B3.10)}$$

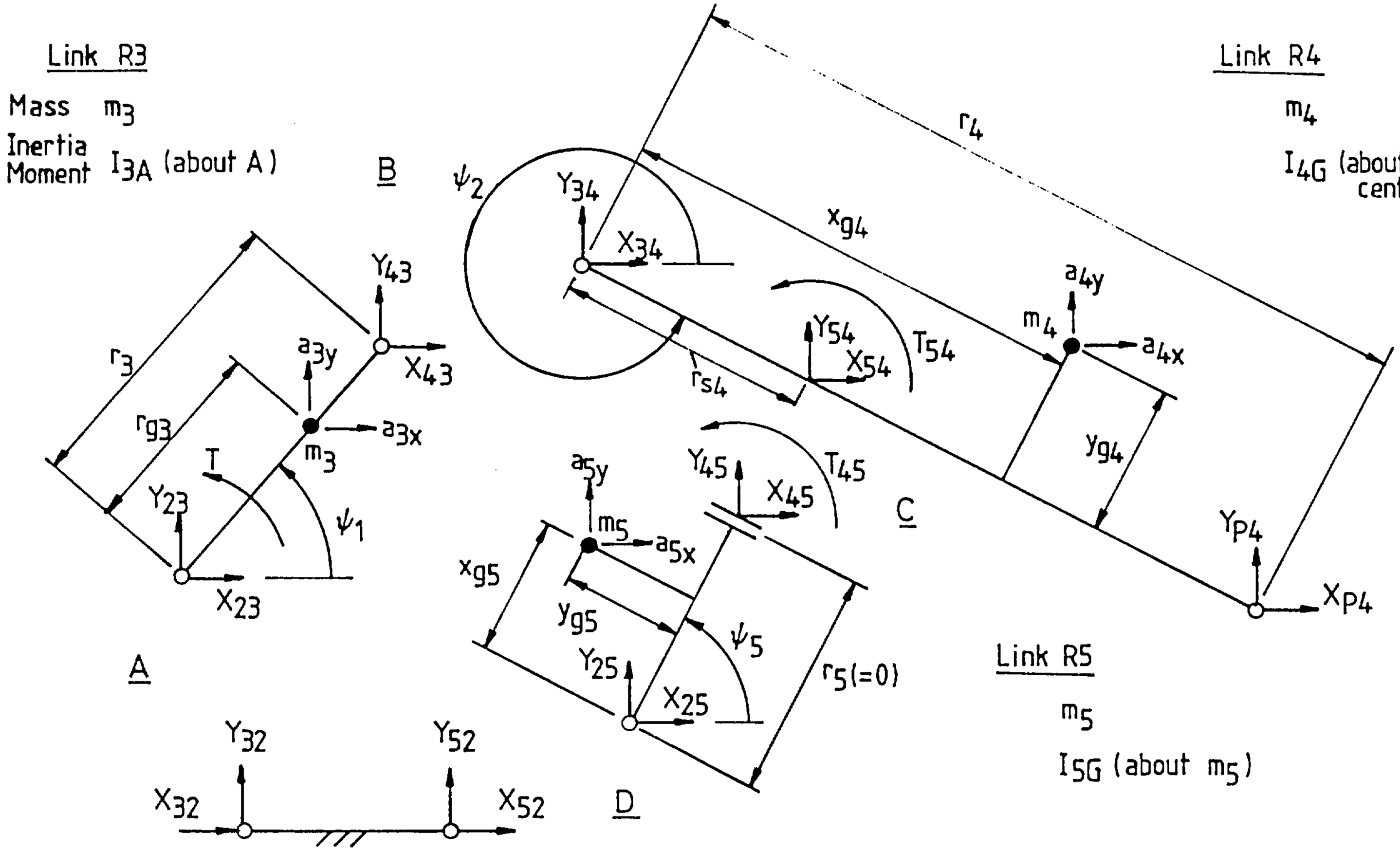

Fig. B3.1 Forces and Parameter notation for Profile Generator Dynamic Analysis.

B3.2 Kinematic

The various kinematic variables are derived from the equations of Appendix A1.

Angular velocities

$$\omega_5 = \omega_4 = \dot{\psi}_2$$

Angular acceleration

$$\alpha_5 = \alpha_4 = \ddot{\psi}_2$$

Linear accelerations of mass centres

$$a_{3x} = \ddot{x}_1 \frac{r_{g3}}{r_3}$$

$$a_{3y} = \ddot{y}_1 \frac{r_{g3}}{r_3}$$

$$a_{4x} = \ddot{x}_1 - \omega_4^2 \; r_{g4H} - \alpha_4 \; r_{g4V}$$

$$a_{4y} = \ddot{y}_1 - \omega_4^2 \; r_{g4V} + \alpha_4 \; r_{g4H}$$

where for simplification

$$\left.\begin{aligned} r_{g4H} &= x_{g4}\cos\psi_2 - y_{g4}\sin\psi_2 \\ r_{g4V} &= x_{g4}\sin\psi_2 + y_{g4}\cos\psi_2 \end{aligned}\right\} \qquad \text{(B3.11)}$$

$$a_{5x} = -\omega_5^2 \; r_{g5H} - \alpha_5 \; r_{g5V}$$

$$a_{5x} = -\omega_5^2 \; r_{g5V} + \alpha_5 \; r_{g5H}$$

where

$$\left.\begin{aligned} r_{g5H} &= x_{g5}\cos\psi_5 - y_{g5}\sin\psi_5 \\ r_{g5V} &= x_{g5}\sin\psi_5 + y_{g5}\cos\psi_5 \end{aligned}\right\} \qquad \text{(B3.12)}$$

furthermore

$$\psi_5 = \psi_2 + 90^{o}$$

therefore

$$\sin\psi_5 = \cos\psi_2$$

$$\cos\psi_5 = -\sin\psi_2$$

also $$r_{s4} = (r_2^{\,2} + r_3^{\,2} - 2r_2r_3\cos\psi_1)^{\frac{1}{2}}$$

B3.3 Forces

The equations (B3.1) to (B3.10) can be solved analytically to determine forces and couples acting on the links. After substitutions with eqns. (B3.11) and (B3.12) they may be expressed by:

$$X_{P4} = -X_{M1} \text{ (from eqn. B2.25)} \qquad \text{(B3.13)}$$

$$Y_{P4} = -Y_{M1} \text{ (from eqn. B2.26)} \qquad \text{(B3.14)}$$

$$T_{45} = (I_{5G} + m_5(x_{g5}^{\,2} + y_{g5}^{\,2}))\ \alpha_5 + m_5\ g\ r_{g5H}$$

$$X_{34} = \frac{\sin\psi_2}{r_{s4}}\Big[(X_{P4}\sin\psi_2 - Y_{P4}\cos\psi_2)r_4 + m_4(a_{4y} + g)r_{g4H}$$

$$- m_4\ a_{4x}\ r_{g4V} + I_{4G}\alpha_2 + T_{45}\Big] + m_4\ a_{4x} - X_{P4} \qquad \text{(B3.15)}$$

$$Y_{34} = -\frac{\cos\psi_2}{r_{s4}}\Big[(X_{P4}\sin\psi_2 - Y_{P4}\cos\psi_2)r_4 + m_4(a_{4y} + g)r_{g4H}$$

$$-m_4\ a_{4x}\ r_{g4V} + I_{4G}\alpha_2 + T_{45}\Big]$$

$$+ m_4(a_{4y} + g) - Y_{P4} \qquad \text{(B3.16)}$$

$$X_{54} = -X_{34} + m_4\, a_{4x} - X_{P4} \qquad \text{(B3.17)}$$

$$Y_{54} = -Y_{34} + m_4(a_{4y} + g) - Y_{P4} \qquad \text{(B3.18)}$$

$$X_{25} = X_{54} + m_5\, a_{5x} \qquad \text{(B3.19)}$$

$$Y_{25} = Y_{54} + m_5(a_{5y} + g) \qquad \text{(B3.20)}$$

$$X_{23} = X_{34} + m_3 a_{3x} \qquad \text{(B3.21)}$$

$$Y_{23} = Y_{34} + m_3\, (a_{3y} + g) \qquad \text{(B3.22)}$$

$$T = -X_{34}\, r_3 \sin\psi_1 + (Y_{34}\, r_3 + m_3\, g\, r_{g3})\cos\psi_1 \qquad \text{(B3.23)}$$

B3.4 Computer Programs

The equations of Appendix B3 are incorporated in Subroutine GENDYN called by main program MECHDYN.

B4. LISTING OF PROGRAM MECHDYN

At the end of MECHDYN a sample data file, DYNDATA, is listed.

Listing of MECHDYN at 20:15:02 on APR 4, 1987 for CCid=MCBO

```
      C
      C                          MECHDYN
      C                          *******
      C
      C       This program calculates the loads in a polygon profile
      C      grinding mechanism.
      C
      C       To run: cocatenate compiled program with +*IG+*GHOST (graph
      C               plotting library).
      C
            COMMON/G1/R1,R2,R3,R4,VP1,AP1,CMR3,CXG4,CYG4,CXG5,CYG5
            COMMON /P1/P1,P2,P3,P4,P5,P6,U4,V4,CML1,CML2,CML3,CML4
            COMMON/PD1/X2,Y2,U2,V2,U3,V3,U5,V5,U6,V6,
           +VX2,VY2,VU2,VV2,VU3,VV3,VU4,VV4,VU5,VV5,VU6,VV6,
           +AX2,AY2,AU2,AV2,AU3,AV3,AU4,AV4,AU5,AV5,AU6,AV6
            COMMON/GD2/GW4,M3,I4G,I5G,M5
            COMMON/PD2/W1,W2,W3,W4,I1A,I2D,I3D,I4C,FS
            COMMON/DYN/FX(20),FY(20),GRAV
            REAL X(121),Y(121),GX(121),GY(121),CX(121),CY(121)
            REAL XPT(21),YPT(21),PSI(21),GXPT(21),GYPT(21),CXPT(21),CYPT(21)
            REAL M3,MGWV,MGWH,I4G,I1A,I2D,I3D,I4C,I5G,M5
      C
      C     Read input data; kinematic parameters,masses,etc.
      C
            READ(5,40)R1,R2,R3,R4,RGW,VP1,AP1
         40 FORMAT(F8.4,6(/F8.4))
            READ(5,41)P1,P2,P3,P4,P5,P6,U4,V4
         41 FORMAT(F7.3,7(/F7.3))
            READ(5,42) CMR3,CXG4,CYG4,CXG5,CYG5,CML1,CML2,CML3,CML4
         42 FORMAT(F10.3,8(/F10.3))
            READ(5,45)FCT,FCN
         45 FORMAT(F10.3,/F10.3)
            READ(5,30)W1,W2,W3,W4
         30 FORMAT(F7.3,3(/F7.3))
            READ(5,35)GW4,M5,M3,MGWV,MGWH,JOINT,GRAV
         35 FORMAT(F10.4,4(/F10.4),/I2,/F10.4)
            READ(5,37)I4G,I5G,I1A,I2D,I3D,I4C
         37 FORMAT(F10.5,5(/F10.5))
            READ(5,39) FS
         39 FORMAT(F10.5)
      C
      C Output principal mechanism settings for MECHKIN use.
            WRITE(7,1010)R1,R2,R3,R4,RGW,VP1
       1010 FORMAT(6(F10.6))
            U4=R1+R4+(P5*P5+P6*P6)**0.5
            V4=0.0
            R1=U4*2.0 -R1
            R2=-R2
            R3=-R3
      C
            STGRAV=GRAV
            STOW1=W1
            STOW2=W2
            STOW3=W3
            STOW4=W4
            STOGW4=GW4
            STOM5=M5
            STOM3=M3
```

Listing of MECHDYN at 20:15:02 on APR 4, 1987 for CCid=MCBO

```
     59              STMGWV=MGWV
     60              STMGWH=MGWH
     61              STOI4G=I4G
     62              STOI5G=I5G
     63              STOI1A=I1A
     64              STOI2D=I2D
     65              STOI3D=I3D
     66              STOI4C=I4C
     67              STOFS=FS
     68             PI=4.0*ATAN(1.0)
     69      C    Forces on individual or all joints?
     70      C       IF(JOINT .NE. 20) GO TO 8
     71             DO 9 IJOINT=1,20
     72              JOINT=IJOINT
     73      C    8 CONTINUE
     74      C    Reset initial data after each step in loop.
     75              GRAV=STGRAV
     76              W1=STOW1
     77              W2=STOW2
     78              W3=STOW3
     79              W4=STOW4
     80              GW4=STOGW4
     81              M5=STOM5
     82              M3=STOM3
     83              MGWV=STMGWV
     84              MGWH=STMGWH
     85              I4G=STOI4G
     86              I5G=STOI5G
     87              I1A=STOI1A
     88              I2D=STOI2D
     89              I3D=STOI3D
     90              I4C=STOI4C
     91              FS=STOFS
     92             THETA=0.0
     93             XYMAX=0.0
     94             DO 68 II=1,3
     95             GO TO (61,62,63),II
     96      C     Effect of inertial forces only.
     97         62 STOFCN=FCN
     98             STOFCT=FCT
     99             FCN=0.0
    100             FCT=0.0
    101             GO TO 61
    102      C     Effect of cutting forces only.
    103         63 FCN=STOFCN
    104             FCT=STOFCT
    105             GRAV=0.0
    106             W1=0.0
    107             W2=0.0
    108             W3=0.0
    109             W4=0.0
    110             GW4=0.0
    111             M5=0.0
    112             M3=0.0
    113             MGWV=0.0
    114             MGWH=0.0
    115             I4G=0.0
    116             I5G=0.0
```

Listing of MECHDYN at 20:15:02 on APR 4, 1987 for CCid=NCBO

```
117             I1A=0.0
118             I2D=0.0
119             I3D=0.0
120             I4C=0.0
121              FS=0.0
122          61 IPT=0
123             IANG=15
124             DO 10 I=1,121
125         C  Swap statements if producing data for MECHKIN.
126         C       DO 10 I=1,101
127         C       THETA=2.0*PI*(I-1)/100.0
128               THETA=2.0*PI*(I-1)/360.0
129               PSI1=3.0*THETA
130               FX(12)=PSI1*180.0/PI
131         C   Calculate position, velocity, and accelerations.
132               CALL GEN(X2,Y2,VX2,VY2,AX2,AY2,PSI1)
133               CALL PANTO
134               CALL GRIND(XCP,YCP,U6,V6,VU6,VV6,RGW,VP1/3.0)
135         C   Calculate forces
136               CALL GRIDYN(MGWV,MGWH,AU6,AV6,FCT,FCN,FXG4,FYG4)
137               CALL PANDYN(FXG4,FYG4,FXM1,FYM1)
138               FXP=-FXM1
139               FYP=-FYM1
140               CALL GENDYN(FXP,FYP,FX34,FY34,AX2,AY2)
141               FX(15)=FX(13)+FX(14)
142               FY(15)=FY(13)+FY(14)
143               FX(16)=FX(12)
144               FY(16)=FY(13)*(U4-R1)-FY(2)*R2
145               FX(18)=FX(12)
146                 F5=(FX(5)*FX(5)+FY(5)*FY(5))**0.5
147                 F9=(FX(9)*FX(9)+FY(9)*FY(9))**0.5
148         C
149         C  Output forces required by MECHKIN for deflection analysis.
150                 WRITE(7,1001)FY(2),FY(4),F5,F9,FY(12),FX(19),FY(19),FY(20)
151          1001  FORMAT(8(F9.2))
152         C
153         C   Calc. & store data for graph plotting.
154               GO TO (111,112,113),II
155           111 X(I)=FX(JOINT)
156               Y(I)=FY(JOINT)
157               R=(X(I)*X(I)+Y(I)*Y(I))**0.5
158               IF(I.GT.1) GO TO 120
159               RMAX=R
160               RMIN=R
161           120 IF(R.LT.RMAX) GO TO 121
162               RMAX=R
163               RMAXPS=PSI1*180.0/PI
164           121 IF(R.GT.RMIN) GO TO 122
165               RMIN=R
166               RMINPS=PSI1*180.0/PI
167           122 IF(IANG.NE.15) GO TO 70
168               IPT=IPT+1
169               XPT(IPT)=X(I)
170               YPT(IPT)=Y(I)
171               PSI(IPT)=PSI1*180.0/PI
172               IANG=0
173            70 CONTINUE
174               IANG=IANG+1
```

Listing of MECHDYN at 20:15:02 on APR 4, 1987 for CCid=MCBO

```
175           GO TO 115
176         112 GX(I)=FX(JOINT)
177           GY(I)=FY(JOINT)
178           IF(IANG.NE.15) GO TO 71
179           IPT=IPT+1
180           GXPT(IPT)=GX(I)
181           GYPT(IPT)=GY(I)
182           PSI(IPT)=PSI1*180.0/PI
183           IANG=0
184          71 CONTINUE
185           IANG=IANG+1
186           GO TO 115
187         113 CX(I)=FX(JOINT)
188           CY(I)=FY(JOINT)
189           IF(IANG.NE.15) GO TO 72
190           IPT=IPT+1
191           CXPT(IPT)=CX(I)
192           CYPT(IPT)=CY(I)
193           PSI(IPT)=PSI1*180.0/PI
194           IANG=0
195          72 CONTINUE
196           IANG=IANG+1
197         115  IF(ABS(FX(JOINT)).LT.XYMAX) GO TO 101
198           IF(JOINT.EQ.12) GO TO 101
199           IF(JOINT.EQ.16) GO TO 101
200           IF(JOINT.EQ.18) GO TO 101
201           XYMAX=ABS(FX(JOINT))
202         101 IF(ABS(FY(JOINT)).LT.XYMAX) GO TO 102
203           XYMAX=ABS(FY(JOINT))
204         102 CONTINUE
205           RMEAN=(RMAX+RMIN)/2.0
206           RALT=(RMAX-RMIN)/2.0
207          10 CONTINUE
208          68 CONTINUE
209       C
210       C       GRAPH PLOTTING
211       C
212           CALL PSPACE(0.1,0.95,0.1,0.95)
213           IF(JOINT.EQ.12) GO TO 50
214           IF(JOINT.EQ.16) GO TO 50
215           IF(JOINT.EQ.18) GO TO 50
216           CALL MAP(-XYMAX,XYMAX,-XYMAX,XYMAX)
217           CALL PLACE(40,1)
218           CALL TYPECS('RMAX=',5)
219           CALL TYPENF(RMAX,1)
220           CALL PLACE(28,2)
221           CALL TYPECS('Y(N)',4)
222           CALL PLACE(55,16)
223           CALL TYPECS('X(N)',4)
224           GO TO 51
225         50 CALL MAP(-20.0,400.0,-XYMAX,XYMAX)
226           CALL PLACE(1,1)
227           CALL TYPECS('TORQUE',6)
228           CALL PLACE(2,2)
229           CALL TYPECS('(NM)',4)
230           CALL PLACE(54,16)
231           CALL TYPECS('ANGLE',5)
232           CALL PLACE(54,18)
```

Listing of MECHDYN at 20:15:02 on APR 4, 1987 for CCid=MCBO

```
      CALL TYPECS('(DEG)',5)
   51 CALL CTRSET(4)
      CALL CTRMAG(15)
      CALL PTPLOT(XPT,YPT,1,9,50)
      CALL PTPLOT(GXPT,GYPT,1,9,52)
      CALL PTPLOT(CXPT,CYPT,1,9,60)
      CALL PLOTNC(-0.7*XYMAX,-1.05*XYMAX,50)
      CALL PLOTNC(-0.7*XYMAX,-1.1*XYMAX,52)
      CALL PLOTNC(-0.7*XYMAX,-1.15*XYMAX,60)
      CALL CTRSET(1)
      CALL PLOTCS(-0.65*XYMAX,-1.05*XYMAX,'  TOTAL',7)
      CALL PLOTCS(-0.65*XYMAX,-1.1*XYMAX,'  INERTIA',9)
      CALL PLOTCS(-0.65*XYMAX,-1.15*XYMAX,'  GRINDING',10)
      IPSI=0
      DO 75 K=1,9,2
      CALL CTRMAG(12)
      CALL POSITN(XPT(K),YPT(K))
      CALL SPACE(1)
      CALL TYPENI(IPSI)
      IPSI=IPSI+90
   75 CONTINUE
      CALL CTRSET(1)
      IPSI=0
      DO 76 K=1,9,2
      CALL CTRMAG(12)
      CALL POSITN(GXPT(K),GYPT(K))
      CALL SPACE(1)
      CALL TYPENI(IPSI)
      IPSI=IPSI+90
   76 CONTINUE
      CALL CTRSET(1)
      IPSI=0
      DO 77 K=1,9,2
      CALL CTRMAG(12)
      CALL POSITN(CXPT(K),CYPT(K))
      CALL SPACE(1)
      CALL TYPENI(IPSI)
      IPSI=IPSI+90
   77 CONTINUE
      CALL CTRMAG(20)
      CALL CURVED(X,Y,1,121)
      CALL BROKEN(5,5,5,5)
      CALL CURVED(GX,GY,1,121)
      CALL BROKEN(5,10,5,10)
      CALL CURVED(CX,CY,1,121)
      CALL FULL
      CALL AXES
      CALL PLACE(40,34)
      CALL TYPECS('PLOT ',5)
      CALL TYPENI(JOINT)
C  Go to next joint
   9  CALL FRAME
      CALL GREND
C
C  END OF GRAPH PLOTTING
C
      STOP
      END
```

Listing of MECHDYN at 20:15:02 on APR 4, 1987 for CCid=MCB0

```
      C
      C     CALCULATION OF VELOCITIES & ACCELERATIONS IN GENERATION MECH.
      C
            SUBROUTINE GEN(X2,Y2,VX2,VY2,AX2,AY2,PSI1)
            COMMON/G1/R1,R2,R3,R4,VP1,AP1,CMR3,CXG4,CYG4,CXG5,CYG5
            COMMON/GD1/C1,S1,C2L,AX1,AY1,S2,C2,VP2,AP2
            C1=COS(PSI1)
            S1=SIN(PSI1)
            X1=R3*C1+R1
            Y1=R3*S1
      C
            C2U=R2-R3*C1
            C2L=(R2*R2+R3*R3-2.0*R2*R3*C1)**0.5
            S2U=-R3*S1
            C2=C2U/C2L
            S2=S2U/C2L
      C
            X2=R4*C2+X1
            Y2=R4*S2+Y1
            VX1=-R3*S1*VP1
            VY1=R3*C1*VP1
      C
            AX1=-R3*S1*AP1-R3*C1*VP1*VP1
            AY1=R3*C1*AP1-R3*S1*VP1*VP1
      C
            VP2=(1.0-R2*C2/C2L)*VP1
            AP2=(VP2/VP1)*AP1+R2*(S2/C2L)*VP2*VP1+R2*R2*R3*C2*(S1/C2L**3.0)
           +*VP1*VP1
            VX2=-R4*S2*VP2+VX1
            VY2=R4*C2*VP2+VY1
      C
            AX2=-R4*S2*AP2-R4*C2*VP2*VP2+AX1
            AY2=R4*C2*AP2-R4*S2*VP2*VP2+AY1
            RETURN
            END
      C
      C     CALCULATION OF FORCES IN GENERATION MECH.
      C
            SUBROUTINE GENDYN(FXP,FYP,FX34,FY34,AX2,AY2)
            COMMON/G1/R1,R2,R3,R4,VP1,AP1,CMR3,CXG4,CYG4,CXG5,CYG5
            COMMON/GD1/C1,S1,C2L,AX1,AY1,S2,C2,VP2,AP2
            COMMON/GD2/M4,M3,I4G,I5G,M5
            COMMON/DYN/FX(20),FY(20),GRAV
            REAL M4,I4G,MG,M3,I5G,M5
            RG3=CMR3*R3
            XG4=CXG4*R4
            YG4=CYG4*R4
            XG5=CXG5*R4
            YG5=CYG5*R4
            RS4=C2L
            A3GX=AX1*RG3/R3
            A3GY=AY1*RG3/R3
      C
            VP5=VP2
            AP5=AP2
      C
            S5=C2
            C5=-S2
```

Listing of MECHDYN at 20:15:02 on APR 4, 1987 for CCid=MCRO

```
      C
            XYG4V=XG4*S2+YG4*C2
            XYG4H=XG4*C2-YG4*S2
      C
            XYG5V=XG5*S5+YG5*C5
            XYG5H=XG5*C5-YG5*S5
            A4GX=AX1-XYG4H*VP2*VP2-XYG4V*AP2
            A4GY=AY1-XYG4V*VP2*VP2+XYG4H*AP2
      C
            A5GX=-XYG5H*VP5*VP5-XYG5V*AP5
            A5GY=-XYG5V*VP5*VP5+XYG5H*AP5
      C
      C     FORCES
      C
             M4=W4
      C
             T45=(I5G+M5*(XG5*XG5+YG5*YG5))*AP5+M5*GRAV*XYG5H
      C
              FX34A=(FXP*S2-FYP*C2)*R4
              FX34B=(M4*(A4GY+GRAV)*XYG4H-M4*A4GX*XYG4V)
              FX34C=I4G*AP2+T45
              FX34D=M4*A4GX-FXP
             FX34=S2/RS4*(FX34A+FX34B+FX34C)+FX34D
      C
              FY34A=M4*(A4GY+GRAV)-FYP
             FY34=-C2/RS4*(FX34A+FX34B+FX34C)+FY34A
      C
             FY54=-FY34+FY34A
             FX54=-FX34+FX34D
      C
             FY25=M5*(A5GY+GRAV)+FY54
             FX25=M5*A5GX+FX54
      C
             FX23=M3*A3GX+FX34
             FY23=M3*A3GY+FY34+M3*GRAV
      C
             TOR=-FX34*R3*S1+FY34*R3*C1+M3*RG3*GRAV*C1
             FX(4)=FXP
             FY(4)=FYP
             FX(3)=FX34
             FY(3)=FY34
             FX(2)=FX25
             FY(2)=FY25
             FX(17)=FX54
             FY(17)=FY54
             FY(18)=T45
             FX(1)=FX23
             FY(1)=FY23
             FY(12)=TOR
             FX(14)=-FX25-FX23
             FY(14)=-FY25-FY23
              FX(19)=FXP*C2 +FYP*S2
              FY(19)=FYP*C2 -FXP*S2
               FX(20)=-FX34*C2-FY34*S2
               FY(20)=-FY34*C2+FX34*S2
             RETURN
             END
      C
```

Listing of MECHDYN at 20:15:02 on APR 4, 1987 for CCid=MCBO

```
      C
      C  CALCULATION OF GRINDING CUTTING COORDINATES
      C
            SUBROUTINE GRIND(XCP,YCP,XGW,YGW,VXGW,VYGW,RGW,DTHETA)
            COMMON/GWD1/S,C
            SU=-VXGW-YGW*DTHETA
            CU=VYGW-XGW*DTHETA
            T=SU/CU
            SCL=(SU*SU+CU*CU)**0.5
            SCL=-(1.0+T*T)**0.5
            S=SU/SCL
            C=CU/SCL
            S=T/SCL
            C=1.0/SCL
            XCP=RGW*C+XGW
            YCP=RGW*S+YGW
            RETURN
            END
      C
      C
      C   CALCULATION OF GRINDING FORCES
      C
            SUBROUTINE GRIDYN(MGWV,MGWH,AXGW,AYGW,FCT,FCN,FXGW,FYGW)
            COMMON/GWD1/S,C
            COMMON/DYN/FX(20),FY(20),GRAV
            REAL MGWV,MGWH
            AYGW=AYGW
            FXGW=-(FCT*S+FCN*C+MGWH*AXGW)
            FYGW=-(-FCT*C+FCN*S+MGWV*AYGW+MGWV*GRAV)
            FX(11)=FCT
            FY(11)=FCN
            FX(10)=FXGW
            FY(10)=FYGW
            RETURN
            END
      C
      C
      C   CALCULATION OF PANTOGRAPH DISPLACEMENTS,VELOCITIES & ACCELERATIONS
      C
            SUBROUTINE PANTO
            COMMON /P1/P1,P2,P3,P4,P5,P6,U4,V4,CML1,CML2,CML3,CML4
            COMMON/PD1/U1,V1,U2,V2,U3,V3,U5,V5,U6,V6,
           +VU1,VV1,VU2,VV2,VU3,VV3,VU4,VV4,VU5,VV5,VU6,VV6,
           +AU1,AV1,AU2,AV2,AU3,AV3,AU4,AV4,AU5,AV5,AU6,AV6
            CALL CALCUV(U2,V2,U1,V1,U4,V4,P1,P4)
            U3=(P2/P1)*(U2-U1)+U2
            V3=(P2/P1)*(V2-V1)+V2
            CALL CALCUV(V5,U5,V3,-U3,V4,-U4,P3,P5)
             U5=-U5
      C   LAST LINE NEEDED AS CANNOT ASSIGN TO -VE ARGUMENT
      C  -VE'S NEEDED TO GET CORRECT SOL. OF QUADRATIC IN CALCUV
            U6=(P6/P3)*(U5-U3)+U5
            V6=(P6/P3)*(V5-V3)+V5
      C
      C    PANTOGRAPH VELOCITIES
      C
            CALL VELUV(U2,V2,U1,V1,U4,V4,VU2,VV2,VU1,VV1,0.0,0.0)
            VU3=(P2/P1)*(VU2-VU1)+VU2
```

Listing of MECHDYN at 20:15:02 on APR 4, 1987 for CCid=MCBO

```
      VV3=(P2/P1)*(VV2-VV1)+VV2
      CALL VELUV(U5,V5,U3,V3,U4,V4,VU5,VV5,VU3,VV3,0.0,0.0)
      VU6=(P6/P3)*(VU5-VU3)+VU5
      VV6=(P6/P3)*(VV5-VV3)+VV5
C
C
C  ACCELERATIONS
C
       CALL ACCUV(U2,V2,U1,V1,U4,V4,VU2,VV2,VU1,VV1,0.0,0.0,
      /AU2,AV2,AU1,AV1,0.0,0.0)
       AU3=(P2/P1)*(AU2-AU1)+AU2
       AV3=(P2/P1)*(AV2-AV1)+AV2
       CALL ACCUV(U5,V5,U3,V3,U4,V4,VU5,VV5,VU3,VV3,0.0,0.0,
      /AU5,AV5,AU3,AV3,0.0,0.0)
       AU6=(P6/P3)*(AU5-AU3)+AU5
       AV6=(P6/P3)*(AV5-AV3)+AV5
       RETURN
       END
C
       SUBROUTINE CALCUV(UA,VA,UB,VB,UC,VC,PB,PC)
       C1=(VB-VC)/(UC-UB)
       C2=0.5*(UC*UC-UB*UB+VC*VC-VB*VB+PB*PB-PC*PC)/(UC-UB)
       CA=1.0+C1*C1
       CB=2.0*(C1*C2-C1*UC-VC)
       CC=C2*C2-2.0*C2*UC+VC*VC+UC*UC-PC*PC
       VA=(-CB+(CB*CB-4.0*CA*CC)**0.5)/(2.0*CA)
C NOTE:- IS THIS NECESSARY SOL OF QUADRATIC (CB+/-)?
C
C
      UA=C1*VA+C2
      RETURN
      END
C
      SUBROUTINE VELUV(UA,VA,UB,VB,UC,VC,VUA,VVA,VUB,VVB,VUC,VVC)
       UAB=UA-UB
       VAB=VA-VB
       UCA=UC-UA
       VCA=VC-VA
C
        VVA1=UAB*VUB+VAB*VVB-UAB*VUC
        VVA2=-UAB*VCA*VVC/UCA
        VVA3=VAB-UAB*VCA/UCA
      VVA=(VVA1+VVA2)/VVA3
      VUA=-VCA*VVA/UCA+VUC+VCA*VVC/UCA
      RETURN
       END
C
C
       SUBROUTINE ACCUV(UA,VA,UB,VB,UC,VC,VUA,VVA,VUB,VVB,VUC,VVC,
      /AUA,AVA,AUB,AVB,AUC,AVC)
         UAB=UA-UB
         VAB=VA-VB
         UCA=UC-UA
         VCA=VC-VA
C
         DUAB=VUA-VUB
         DVAB=VVA-VVB
         DUCA=VUC-VUA
```

Listing of MECHDYN at 20:15:02 on APR 4, 1987 for CCid=MCBO

```
      DVCA=VVC-VVA
C
      VVA3=VAB-UAB*VCA/UCA
C
     AVA1=DUAB*VUB+UAB*AUB+DVAB*VVB+VAB*AVB-DUAB*VUC-UAB*AUC
     AVA2=DUAB*VCA*VVC/UCA+UAB*DVCA*VVC/UCA
     AVA3=UAB*VCA*AVC/UCA-UAB*VCA*VVC*DUCA/(UCA*UCA)
     AVA4=DVAB-DUAB*VCA/UCA-UAB*DVCA/UCA+UAB*VCA*DUCA/(UCA*UCA)
    AVA=(AVA1-AVA2-AVA3)/VVA3-VVA*AVA4/VVA3
C
      AUA1=(-DVCA*VVA-VCA*AVA+VCA*VVA*DUCA/UCA)/UCA
       AUA2=(+UCA*AUC+DVCA*VVC+VCA*AVC-VCA*VVC*DUCA/UCA)/UCA
     AUA=AUA1+AUA2
     RETURN
     END
C
C
C  CALCULATIONS OF PANTOGRAPH FORCES
C
      SUBROUTINE PANDYN(FXG4,FYG4,FXM1,FYM1)
      COMMON /P1/P1,P2,P3,P4,P5,P6,U4,V4,CML1,CML2,CML3,CML4
      COMMON/PD1/U1,V1,U2,V2,U3,V3,U5,V5,U6,V6,
     +VU1,VV1,VU2,VV2,VU3,VV3,VU4,VV4,VU5,VV5,VU6,VV6,
     +AU1,AV1,AU2,AV2,AU3,AV3,AU4,AV4,AU5,AV5,AU6,AV6
      COMMON/PD2/W1,W2,W3,W4,I1A,I2D,I3D,I4C,FS
      COMMON/DYN/FX(20),FY(20),GRAV
      REAL M1,M2,M3,M4,I1A,I2D,I3D,I4C,L1,L2,L3,L4,LJ1,LJ4,
     +L1C,L1S,L2C,L2S,L3C,L3S,L4C,L4S,LJ1C,LJ1S,LJ4C,LJ4S
      L1=P1+P2
      L2=P4
      L3=P5
      L4=P3+P6
      LJ1=P1
      LJ4=P6
C
      M1=W1
      M2=W2
      M3=W3
      M4=W4
C
      RG1=CML1*L1
      RG2=CML2*L2
      RG3=CML3*L3
      RG4=CML4*L4
C
      L1C=U3-U1
      L1S=V3-V1
      L2C=U2-U4
      L2S=V2-V4
      L3C=U5-U4
      L3S=V5-V4
      L4C=U3-U6
      L4S=V3-V6
C
      LJ1S=L1S*LJ1/L1
      LJ1C=L1C*LJ1/L1
      LJ4S=L4S*LJ4/L4
      LJ4C=L4C*LJ4/L4
```

Listing of MECHDYN at 20:15:02 on APR 4, 1987 for CCid=MCBO

```
      C
            RG1C=L1C*RG1/L1
            RG2C=L2C*RG2/L2
            RG3C=L3C*RG3/L3
            RG4C=L4C*RG4/L4
      C
      C   ANGULAR VELOCITIES
      C
            OME1=(VV3-VV1)/L1C
            OME2=VV2/L2C
            OME3=VV5/L3C
            OME4=(VV3-VV6)/L4C
      C
      C  ANGULAR ACCELERATIONS
      C
            ALP1=(AV3-AV1+OME1*OME1*L1S)/L1C
            ALP2=(AV2+OME2*OME2*L2S)/L2C
            ALP3=(AV5+OME3*OME3*L3S)/L3C
            ALP4=(AV3-AV6+OME4*OME4*L4S)/L4C
      C
      C  LINEAR ACCELERATIONS OF C. OF M.'S
      C
            A1X=AU1+(AU3-AU1)*RG1/L1
            A1Y=AV1+(AV3-AV1)*RG1/L1
            A2X=AU2*RG2/L2
            A2Y=AV2*RG2/L2
            A3X=AU5*RG3/L3
            A3Y=AV5*RG3/L3
            A4X=AU6+(AU3-AU6)*RG4/L4
            A4Y=AV6+(AV3-AV6)*RG4/L4
      C
      C  COUNTERBALANCING SPRING FORCES ON PANTO (NOT APPLIED
      C   TO FINAL DESIGN)
      C  (SPRING BETTWEEN J4 & J10)
      C
             DIST14=((U1-U4)*(U1-U4)+(V4-V1)*(V4-V1))**0.5
            FSX1=FS*(U4-U1)/DIST14
            FSY1=FS*(V4-V1)/DIST14
            FXG4=FXG4-FSX1
            FYG4=FYG4-FSY1
      C
      C  FORCES ON JOINTS
      C
             FX34A=(FXG4-M4*A4X)*L4S-(FYG4-M4*A4Y)*L4C-I4C*ALP4
               FX34B=(I3D*ALP3+M3*GRAV*RG3C)*(L4C-LJ4C)/L3C
           + +M4*GRAV*(L4C-RG4C)
               FX34C=+LJ4S-L4S+(L4C-LJ4C)*L3S/L3C
            FX34=(FX34A+FX34B)/FX34C
            FY34=(-I3D*ALP3+FX34*L3S-M3*GRAV*RG3C)/L3C
      C
            FX14=-(FX34+FXG4-M4*A4X)
            FY14=-(FY34+FYG4-M4*A4Y-M4*GRAV)
      C
            FXF3=FX34+M3*A3X
            FYF3=FY34+M3*A3Y+M3*GRAV
      C
              FY12A1=(-I2D*ALP2-M2*GRAV*RG2C)*LJ1S/L2S
              FY12A2=-I1A*ALP1+FX14*L1S-FY14*L1C-M1*GRAV*RG1C
```

```
Listing of MECHDYN at 20:15:02 on APR  4, 1987 for CCid=MCRO

    639              FY12A=FY12A1+FY12A2
    640              FY12B=L2S/(L2S*LJ1C-L2C*LJ1S)
    641             FY12=FY12A*FY12B
    642             FX12=(-I2D*ALP2+FY12*L2C-M2*GRAV*RG2C)/L2S
    643       C
    644             FXF2=-(FX12-M2*A2X)
    645             FYF2=-(FY12-M2*A2Y-M2*GRAV)
    646       C
    647             FXM1=FX12+FX14+M1*A1X
    648             FYM1=FY12+FY14+M1*A1Y+M1*GRAV
    649       C
    650       C  BALANCE FORCE
    651                 FXM1=FXM1-FSX1
    652                 FYM1=FYM1-FSY1
    653       C
    654               FX(9)=FX34
    655               FY(9)=FY34
    656               FX(6)=FX14
    657               FY(6)=FY14
    658               FX(8)=FXF3
    659               FY(8)=FYF3
    660               FX(5)=FX12
    661               FY(5)=FY12
    662               FX(7)=FXF2
    663               FY(7)=FYF2
    664               FX(13)=-FXF3-FXF2
    665               FY(13)=-FYF3-FYF2
    666               RETURN
    667               END
#
```

Listing of DYNDATA at 20:58:31 on APR 4, 1987 for CCid=MCBO

1	0.005	R1	nominal dimensions etc.
2	0.0025	R2	
3	0.00075	R3	
4	0.04	R4	
5	0.04	RGW	
6	9.5	VP1	
7	0.0	AP1	
8	0.075	P1	
9	0.075	P2	
10	0.075	P3	
11	0.075	P4	
12	0.075	P5	
13	0.075	P6	
14	0.153	U4	
15	0.0	V4	
16	1.0	CMR3	Positions of mass centres
17	0.028	CXG4	
18	0.0	CYG4	
19	0.0	CXG5	
20	0.0	CYG5	
21	0.44	CML1	
22	0.47	CML2	
23	0.5	CML3	
24	0.45	CML4	
25	-0.0	FCT	Cutting forces
26	0.0	FCN	"
27	2.075	W1	Masses
28	0.720	W2	
29	2.84	W3	
30	2.049	W4	
31	10.28	GW4	
32	2.30	M5	
33	7.32	M3	
34	7.045	MGWV	
35	4.49	MGWH	
36	12	JOINT	Select joint for output plot
37	9.81	GRAV	gravity const.
38	0.0338	I4G	Moments of inertia
39	0.00932	I5G	
40	0.0167	I1A	
41	0.002098	I2D	
42	0.01095	I3D	
43	0.01392	I4C	
44	0.0	FS	Balance spring force - NOT used in final design

MECHANISM SET-UP				DRIVING TORQUE (Nm)		
R1 (mm)	R3 (mm)	R4/RGW (mm)	$\dot{\psi}_1$ (rad.s^{-1})	MIN.	MAX.	PK-PK
5.0	0.75	40.0	10.0	- 1.88	0.78	2.66
5.0	0.75	40.0	5.0	-1.42	0.73	2.15
5.0	0.75	20.0	10.0	-1.21	0.42	1.63
5.0	0.3	40.0	10.0	-0.45	0.34	0.79
5.0	0.3	40.0	5.0	-0.42	0.33	0.75
5.0	0.3	20.0	10.0	-0.25	0.18	0.43
5.0	0.3	20.0	5.0	-0.23	0.18	0.41
10.0	1.5	40.0	10.0	-2.02	0.82	2.84
10.0	0.6	40.0	10.0	-0.47	0.36	0.83
25.0	3.75	40.0	10.0	-2.18	1.02	3.20
25.0	1.5	40.0	10.0	-0.56	0.45	1.01
50.0	7.5	40.0	10.0	-2.45	1.40	3.85
50.0	3.0	40.0	10.0	-0.71	0.60	1.31

DRIVING TORQUE: Positive torque given here is that torque required to drive the mechanism at constant speed <u>excluding</u> friction, and with grinding forces set to zero. This latter condition represents the worst case since grinding forces tend to reduce driving torque, variation.

Table B.5.1 Summary of driving torque variations.

B5. <u>MECHDYN</u> RESULTS - FORCES AND TORQUE IN MECHANISM

Table B5.4.1 summarises the torque variation for mechanism operating conditions in addition to that of Fig.B5.1.

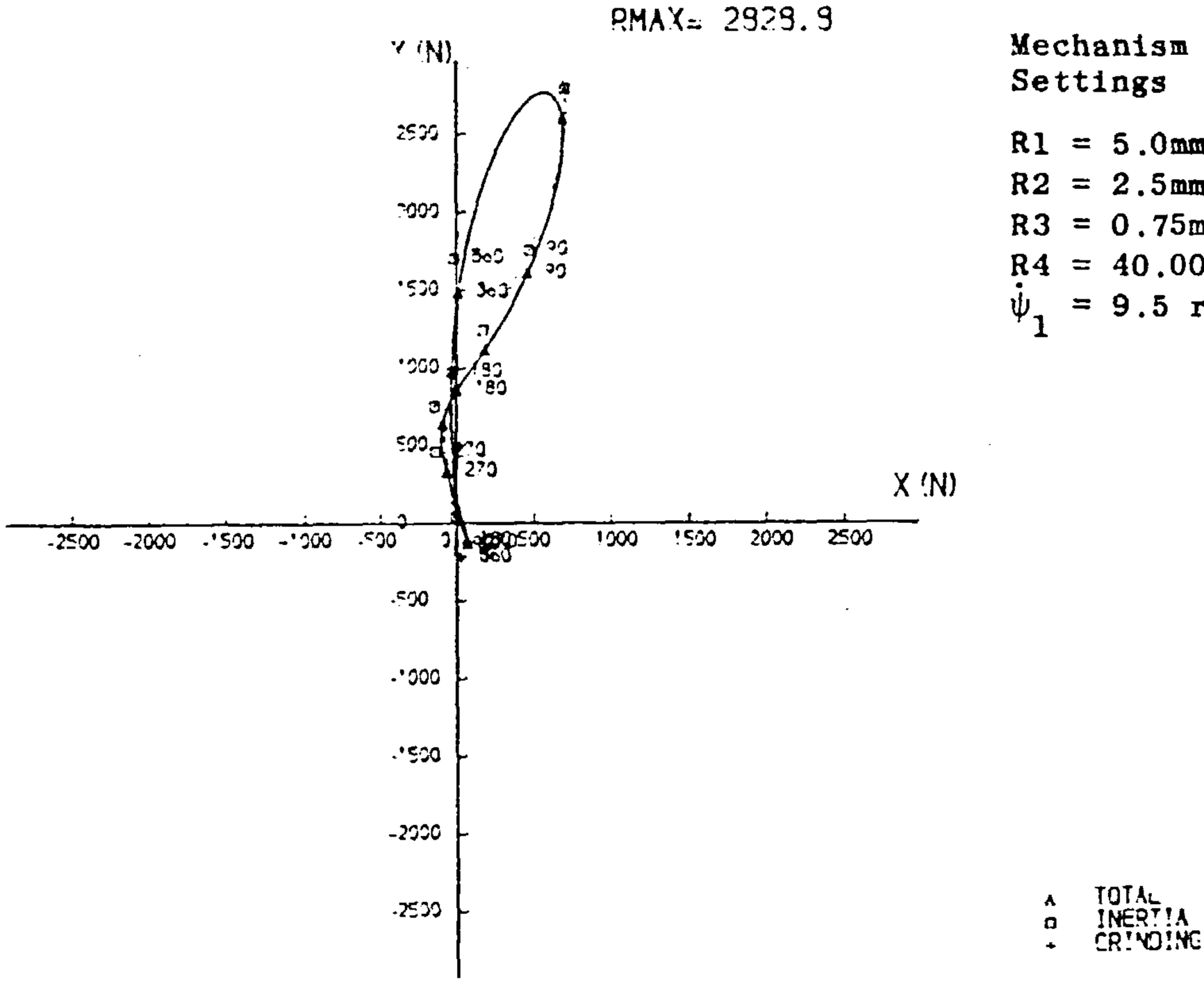

Loads in mechanism (notation of Fig.6.3)

Fig. B5.2 FY1 v FX1

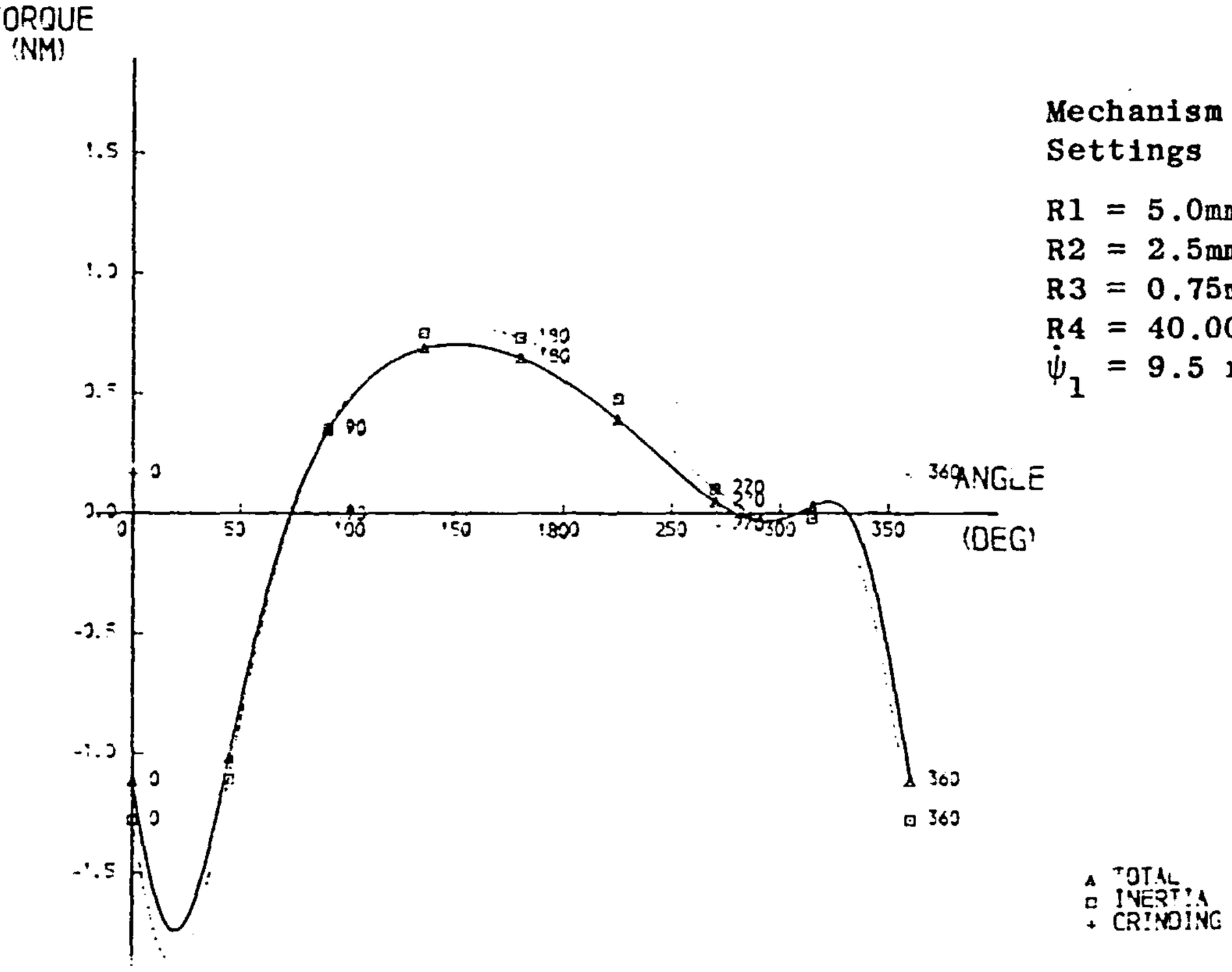

Loads in mechanism (notation of Fig.6.3)

Fig. B5.1 TOR v ψ_1

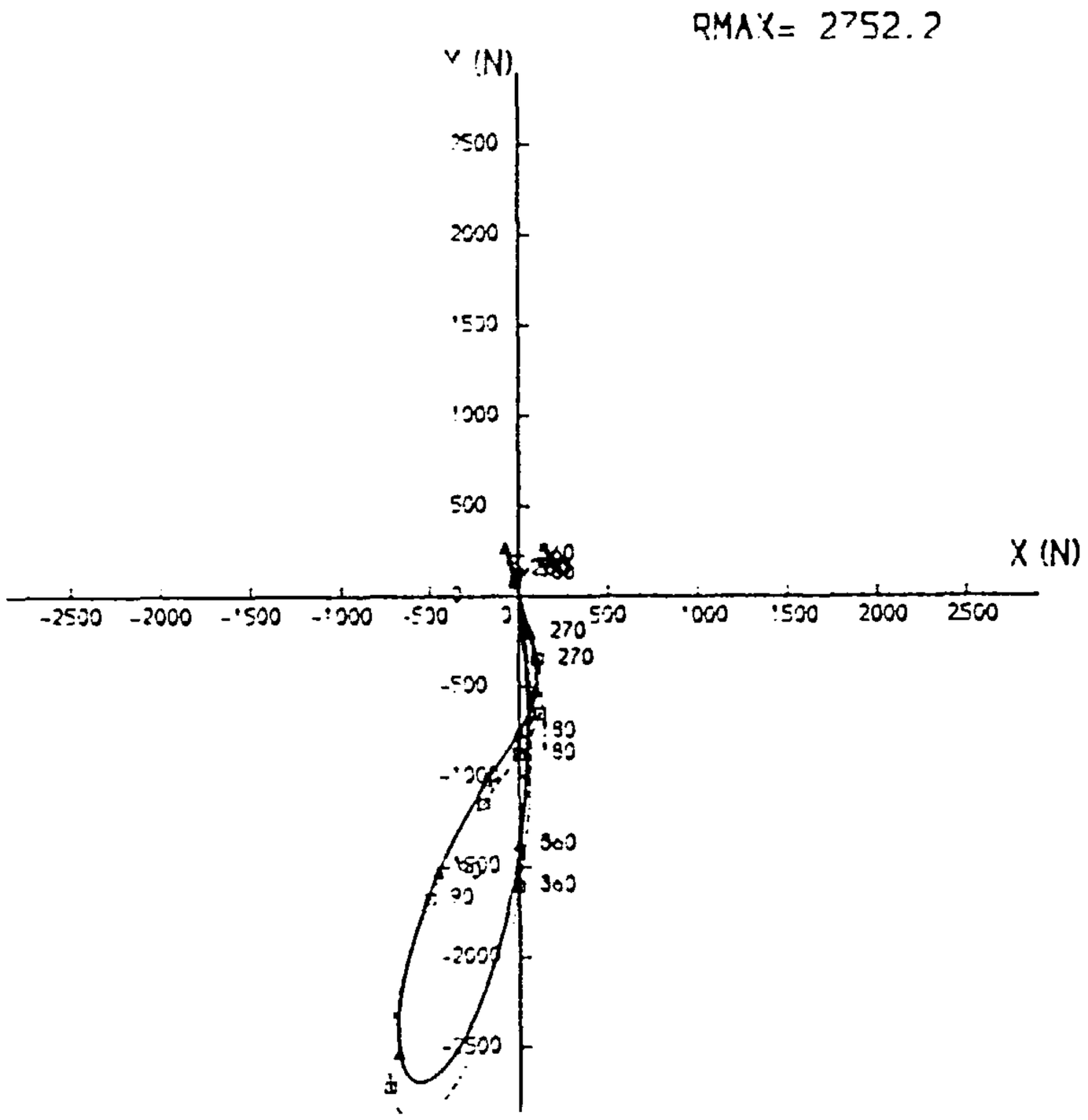

Mechanism Settings

R1 = 5.0mm
R2 = 2.5mm
R3 = 0.75mm
R4 = 40.00mm
$\dot{\psi}_1$ = 9.5 rad/s

Loads in mechanism (notation of Fig.6.3)

Fig.B5.4 $FY2_L$ v $FX2_L$

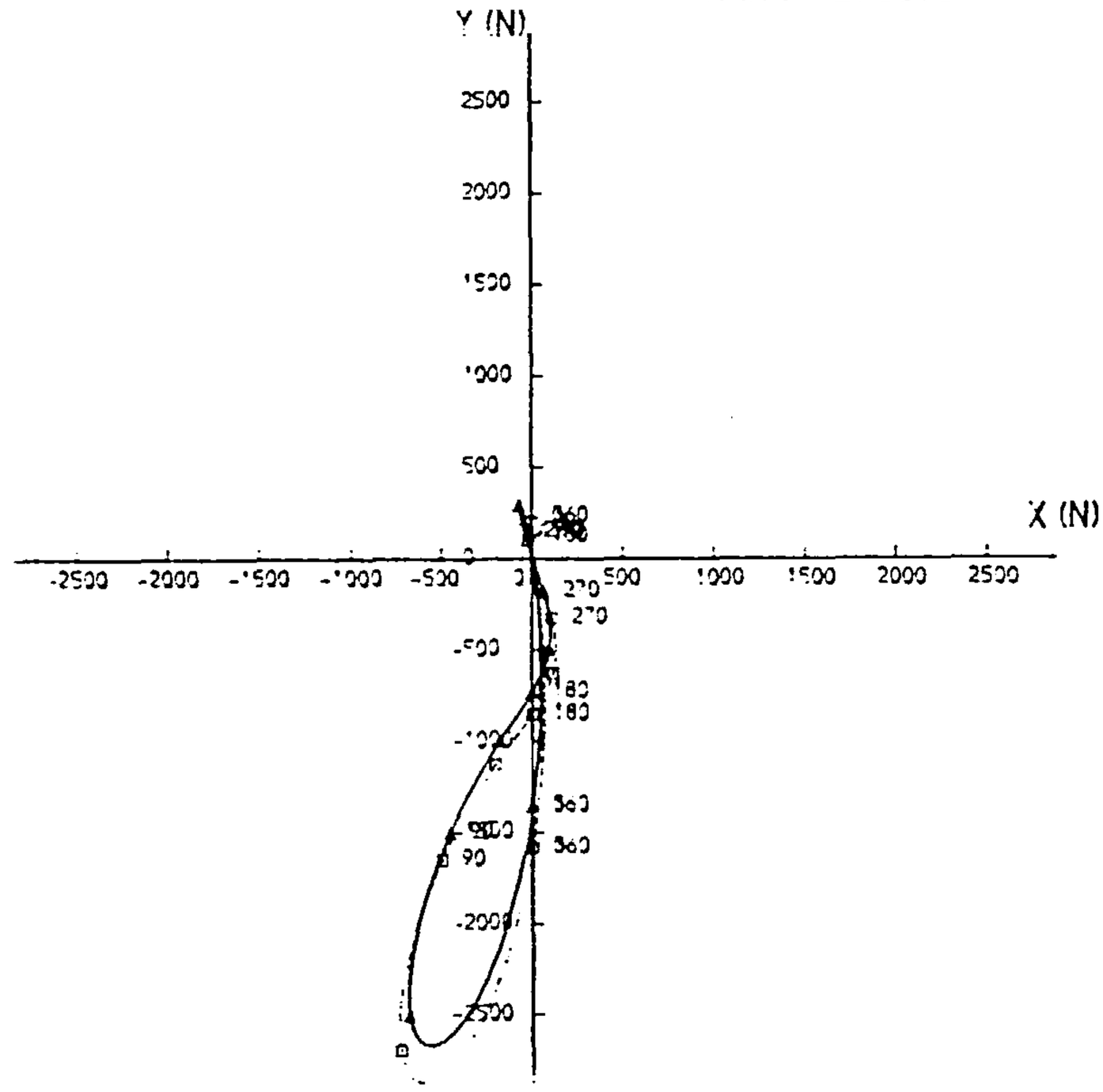

Mechanism Settings

R1 = 5.0mm
R2 = 2.5mm
R3 = 0.75mm
R4 = 40.00mm
$\dot{\psi}_1$ = 9.5 rad/s

Loads in mechanism (notation of Fig.6.3)

Fig. B5.3 $FY2_R$ v. $FX2_R$

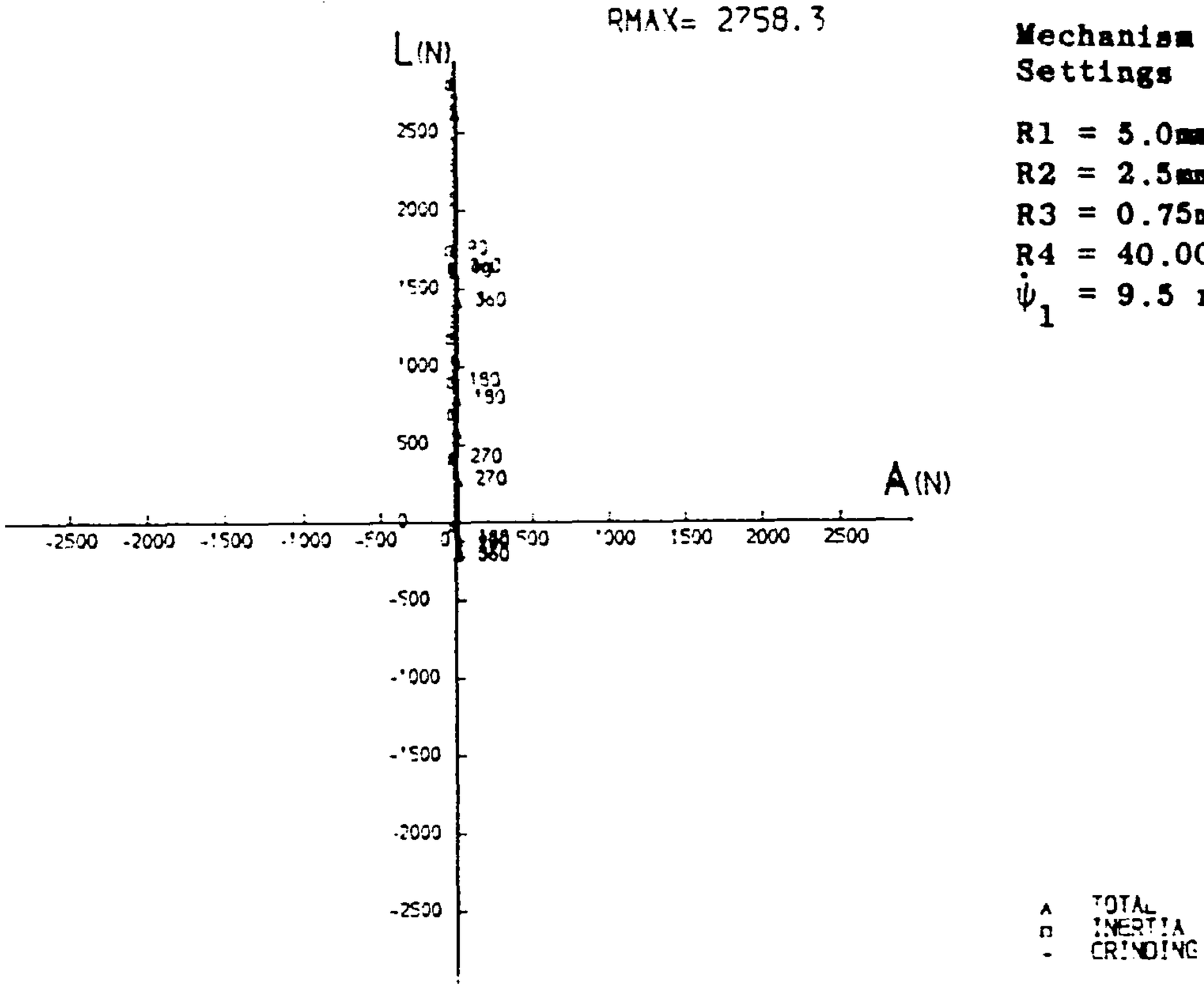

Mechanism Settings

R1 = 5.0mm
R2 = 2.5mm
R3 = 0.75mm
R4 = 40.00mm
$\dot{\psi}_1$ **= 9.5 rad/s**

Loads in mechanism (notation of Fig.6.3)

Fig. B5.6 F3L v. F3A

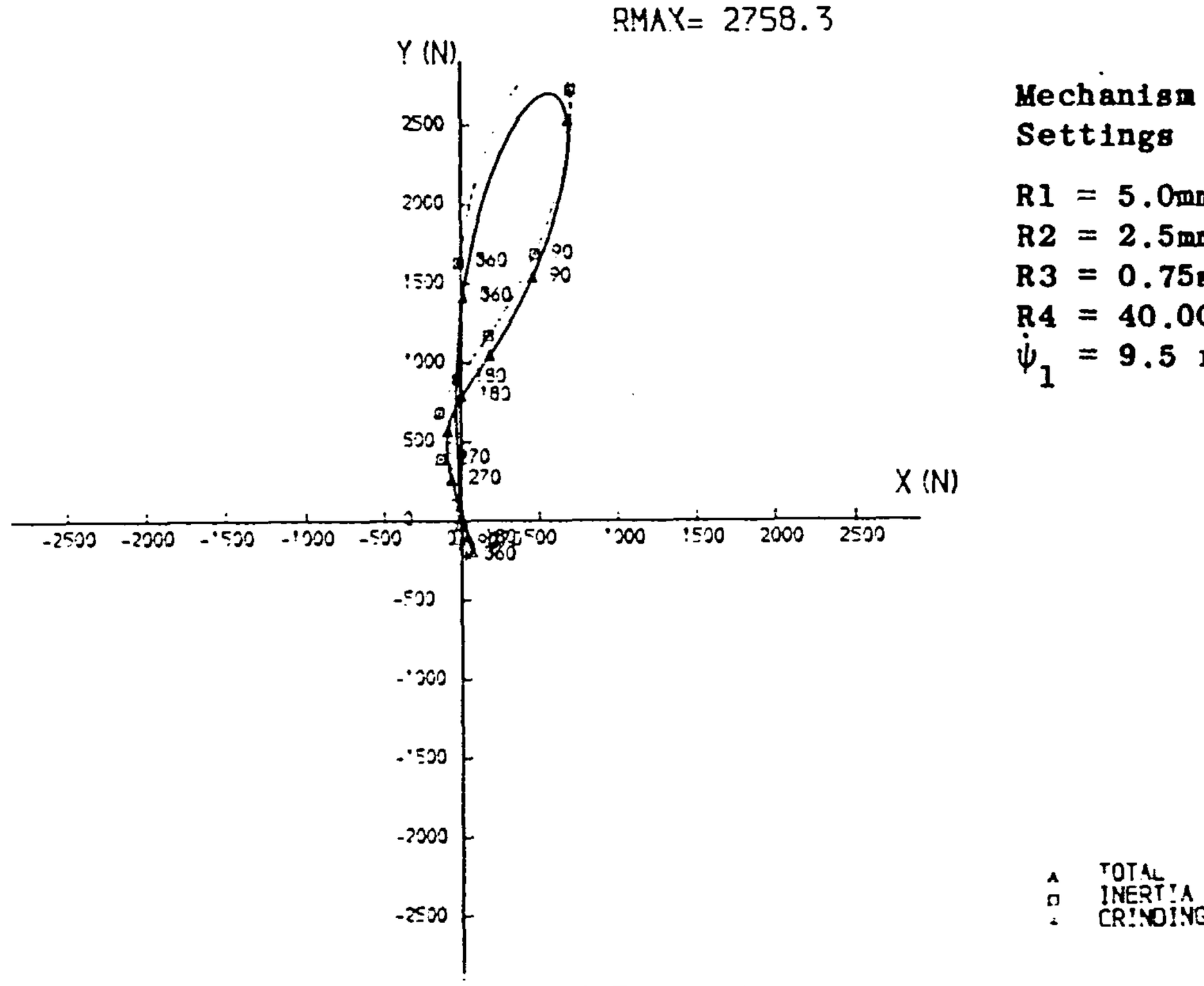

Mechanism Settings

R1 = 5.0mm
R2 = 2.5mm
R3 = 0.75mm
R4 = 40.00mm
$\dot{\psi}_1$ **= 9.5 rad/s**

Loads in mechanism (notation of Fig.6.3)

Fig. B5.5 FY3 v. FX3

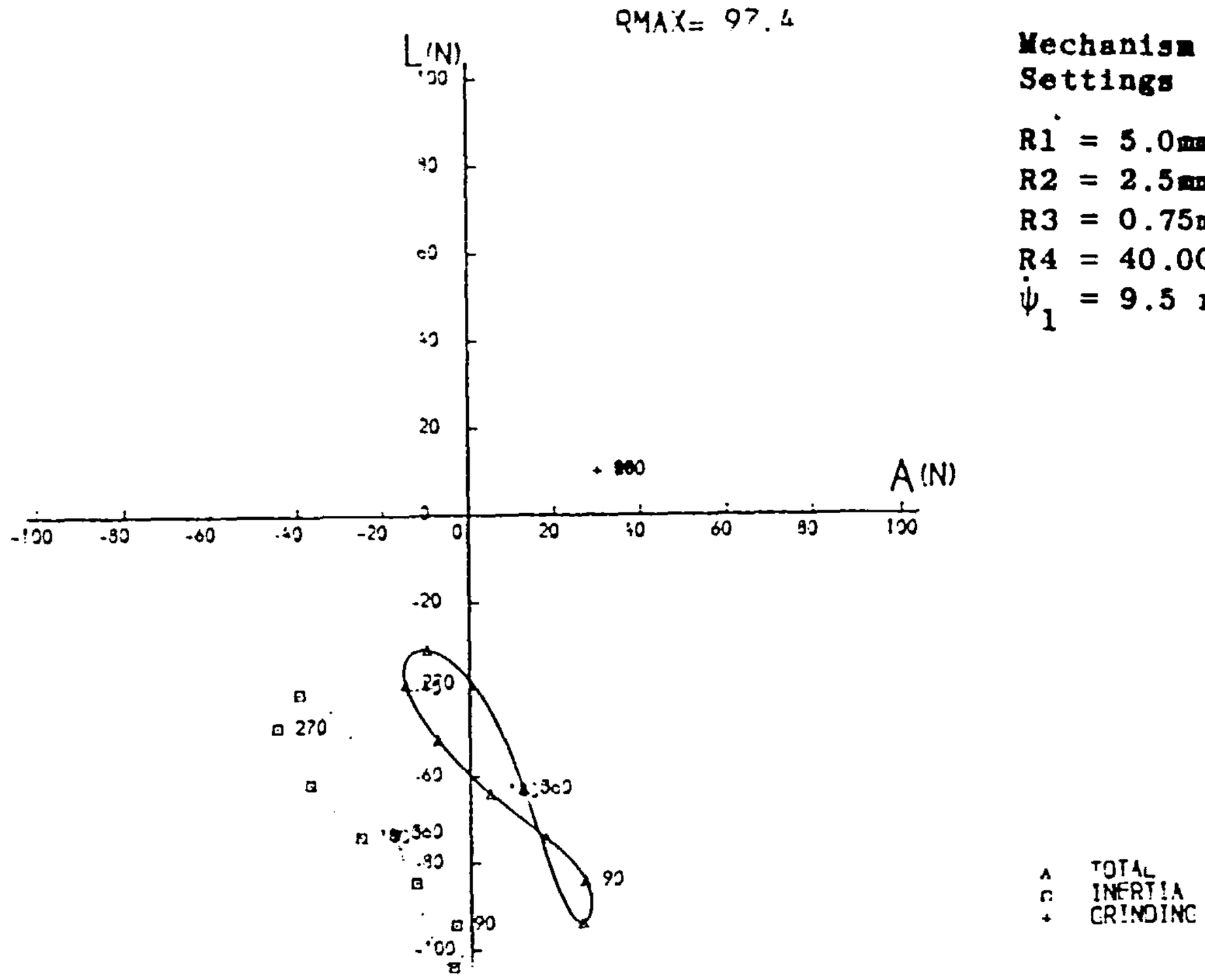

Mechanism Settings

R1 = 5.0mm
R2 = 2.5mm
R3 = 0.75mm
R4 = 40.00mm
$\dot{\psi}_1$ = 9.5 rad/s

Loads in mechanism (notation of Fig.6.3)

Fig. B5.8 F4L v. F4A

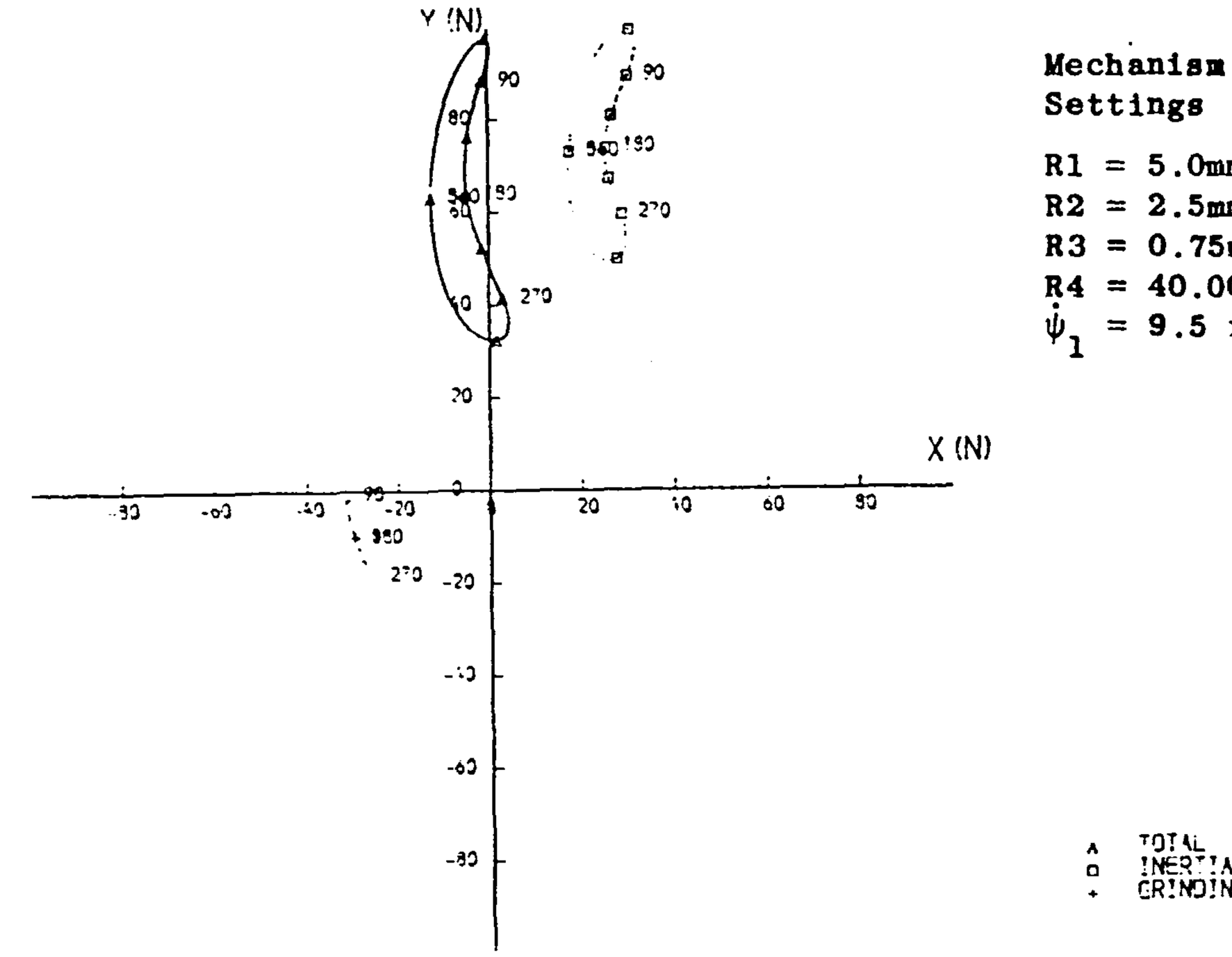

Mechanism Settings

R1 = 5.0mm
R2 = 2.5mm
R3 = 0.75mm
R4 = 40.00mm
$\dot{\psi}_1$ = 9.5 rad/s

Loads in mechanism (notation of Fig.6.3)

Fig. B5.7 FY4 v. FX4

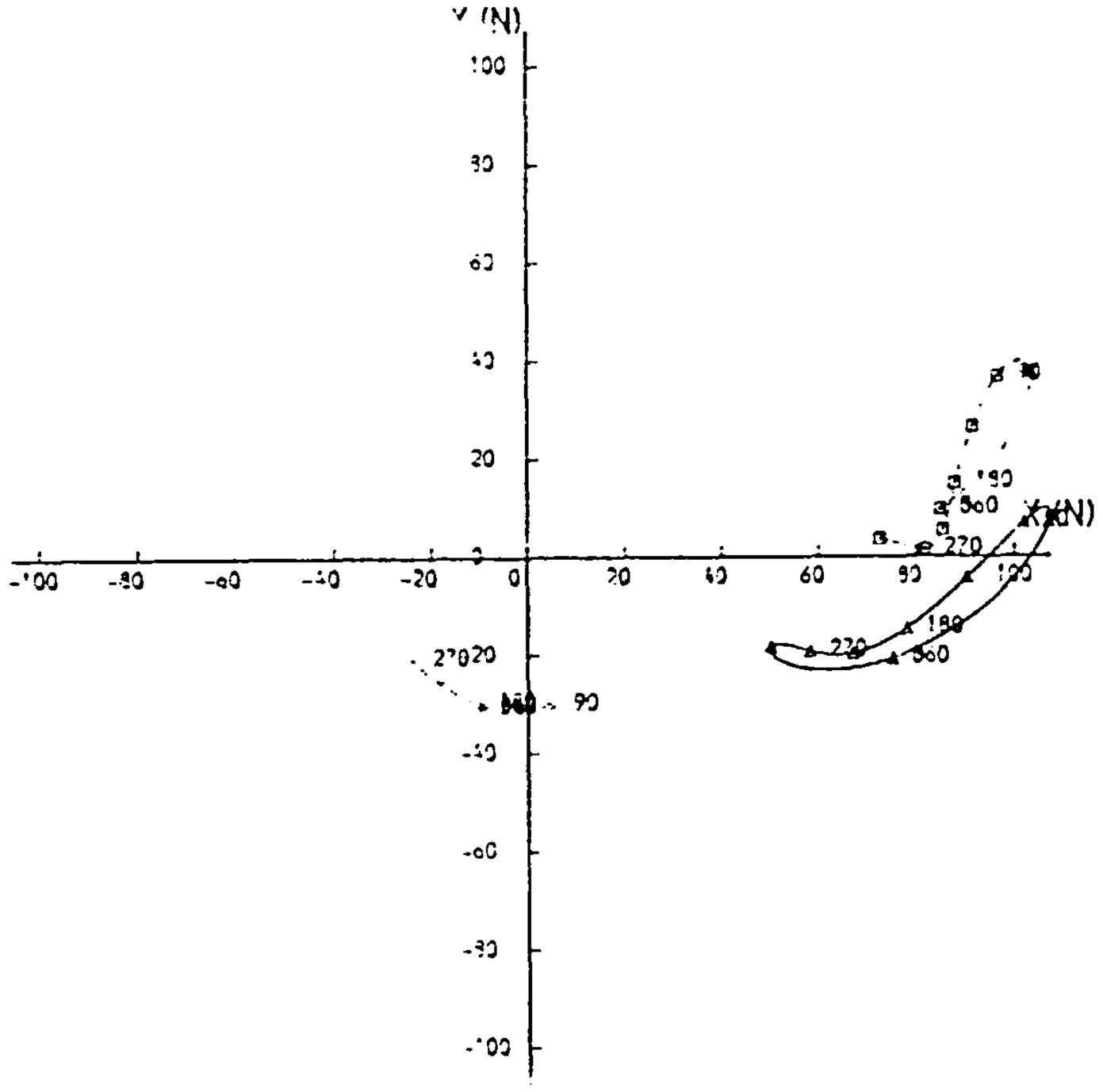

Mechanism Settings

R1 = 5.0mm
R2 = 2.5mm
R3 = 0.75mm
R4 = 40.00mm
$\dot{\psi}_1$ **= 9.5 rad/s**

Loads in mechanism (notation of Fig.6.3)

Fig. B5.10 FY6 v. FX6

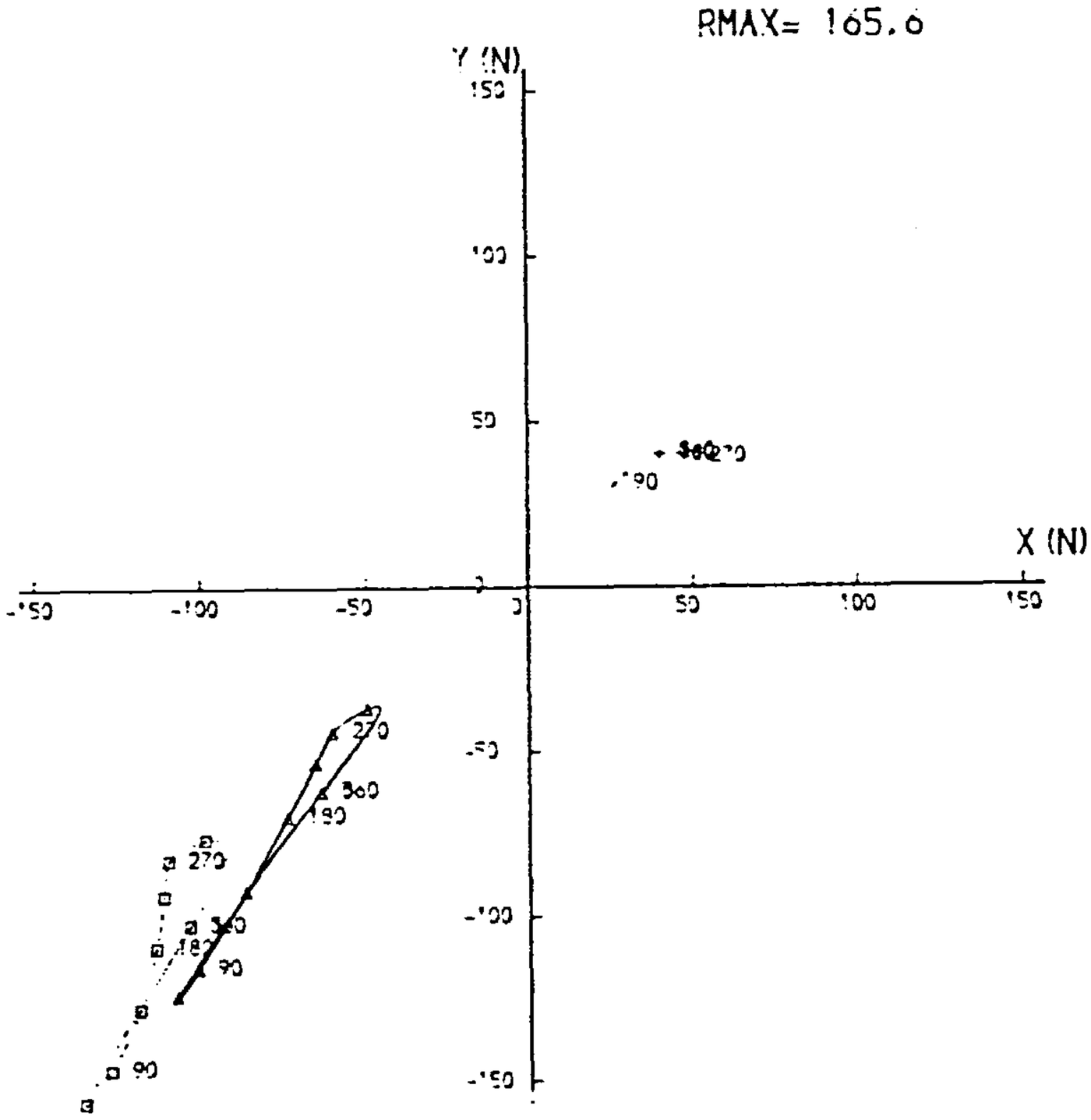

Mechanism Settings

R1 = 5.0mm
R2 = 2.5mm
R3 = 0.75mm
R4 = 40.00mm
$\dot{\psi}_1$ **= 9.5 rad/s**

Loads in mechanism (notation of Fig.6.3)

Fig. B5.9 FY5 v. FX5

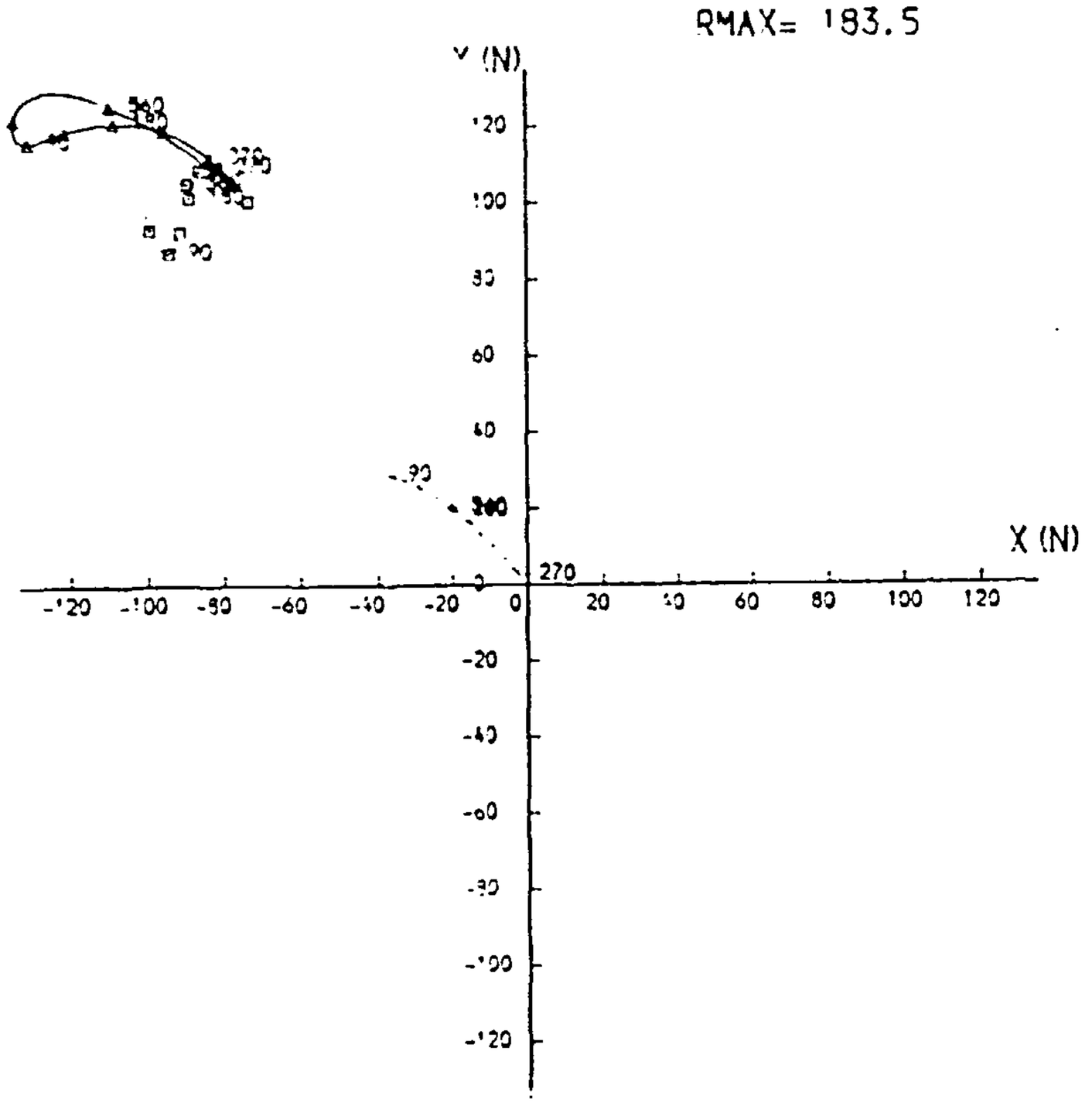

Mechanism Settings

R1 = 5.0mm
R2 = 2.5mm
R3 = 0.75mm
R4 = 40.00mm
$\dot{\psi}_1$ **= 9.5 rad/s**

Loads in mechanism (notation of Fig.6.3)

Fig. B5.12 FY8 v. FX8

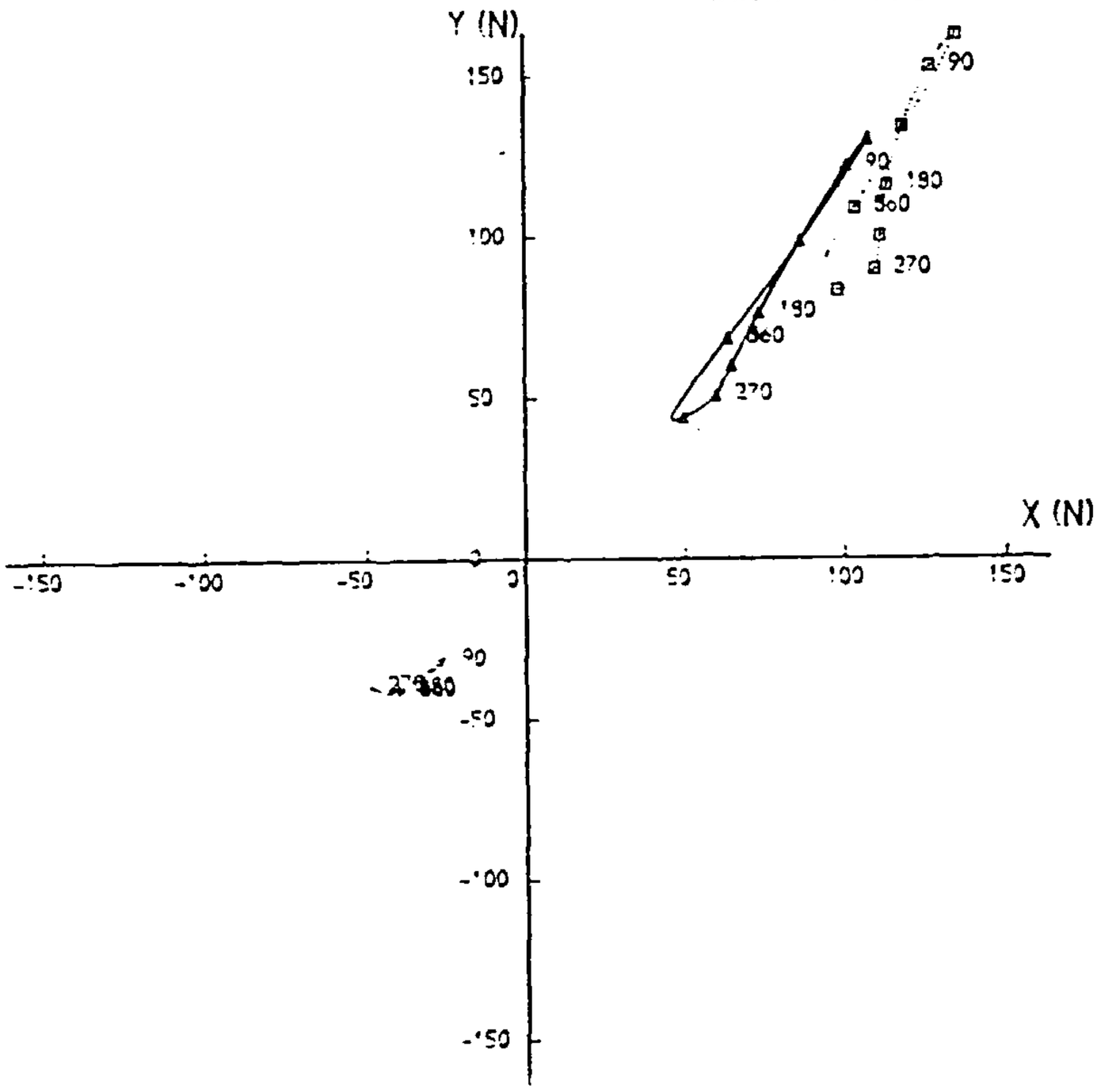

Mechanism Settings

R1 = 5.0mm
R2 = 2.5mm
R3 = 0.75mm
R4 = 40.00mm
$\dot{\psi}_1$ **= 9.5 rad/s**

Loads in mechanism (notation of Fig.6.3)

Fig. B5.11 FY7 v. FX7

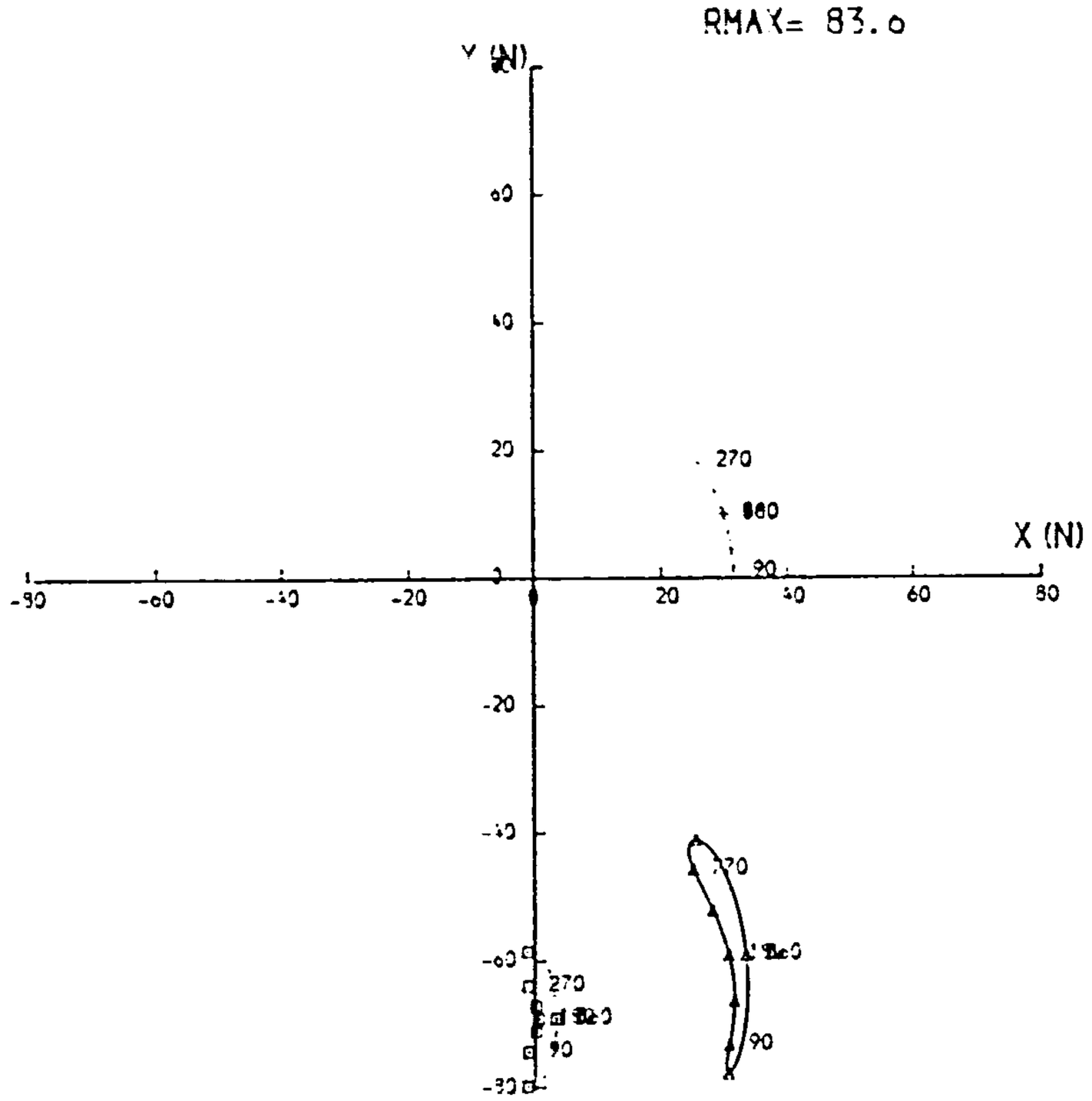

Mechanism Settings

R1 = 5.0mm
R2 = 2.5mm
R3 = 0.75mm
R4 = 40.00mm
$\dot{\psi}_1$ = 9.5 rad/s

Loads in mechanism (notation of Fig.6.3)

Fig. B5.14 FY10 v. FX10

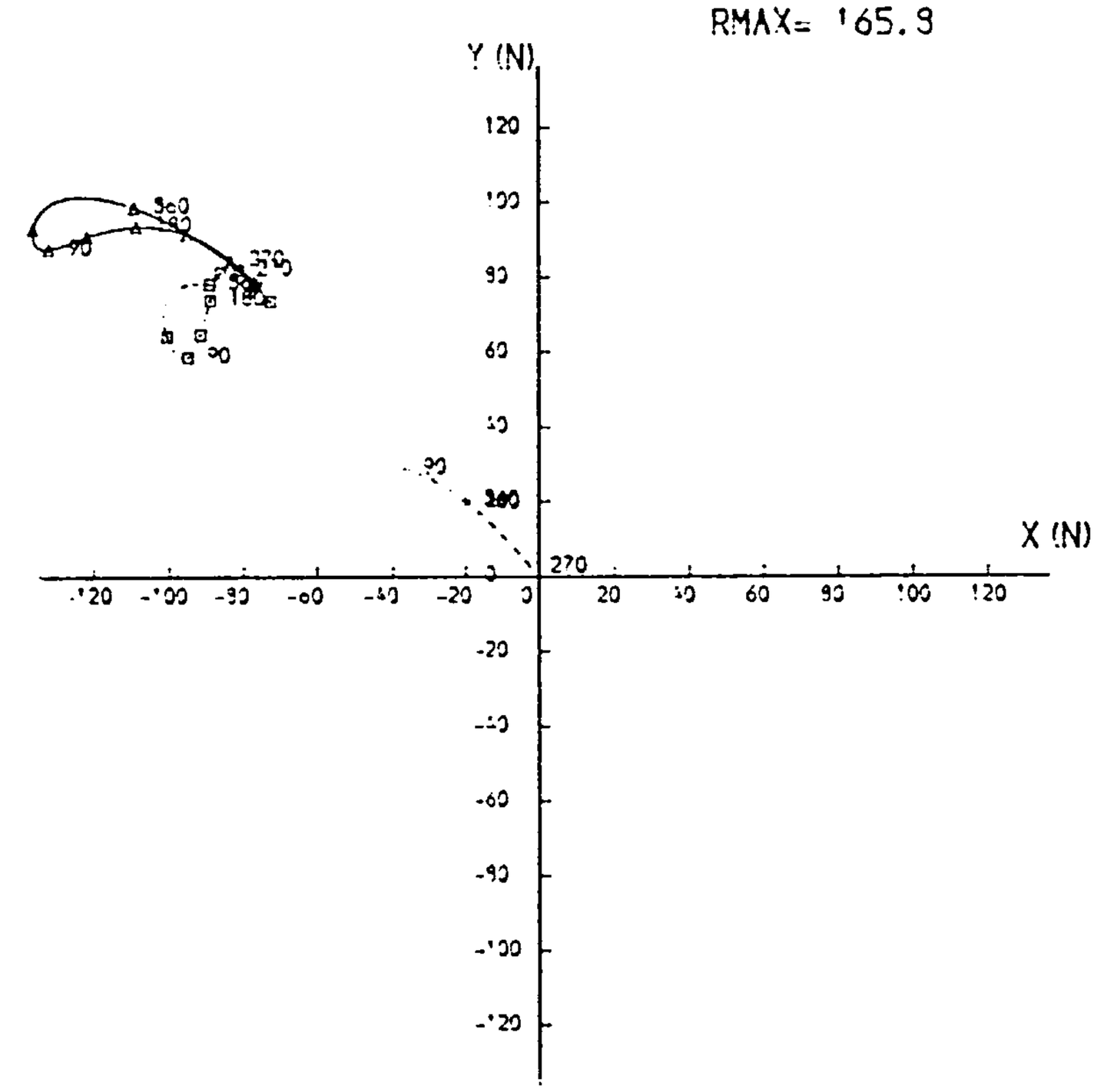

Mechanism Settings

R1 = 5.0mm
R2 = 2.5mm
R3 = 0.75mm
R4 = 40.00mm
$\dot{\psi}_1$ = 9.5 rad/s

Loads in mechanism (notation of Fig.6.3)

Fig. B5.13 FY9 v. FX9

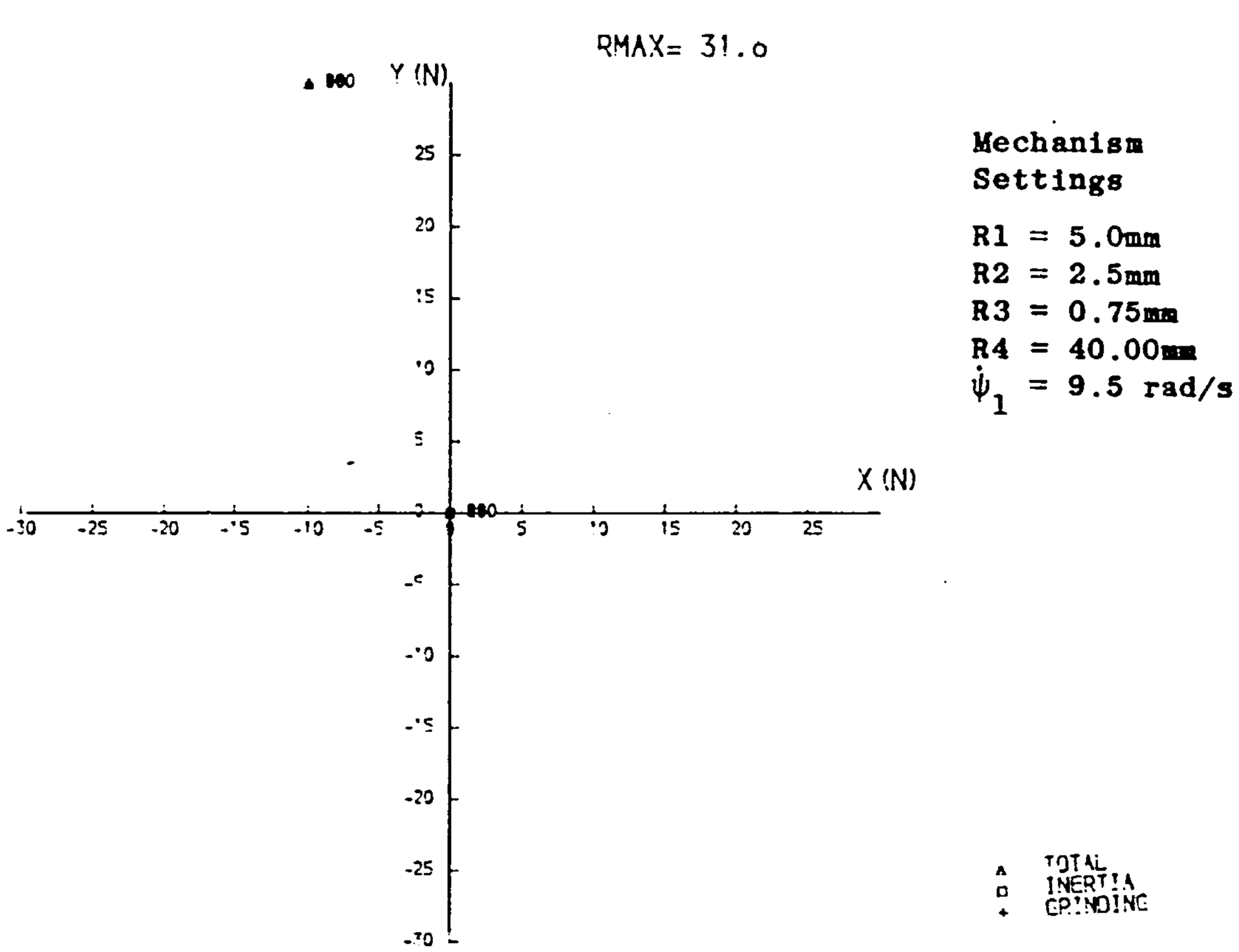

Loads in mechanism (notation of Fig.6.3)

Fig. B5.15 FY11 v. FX11

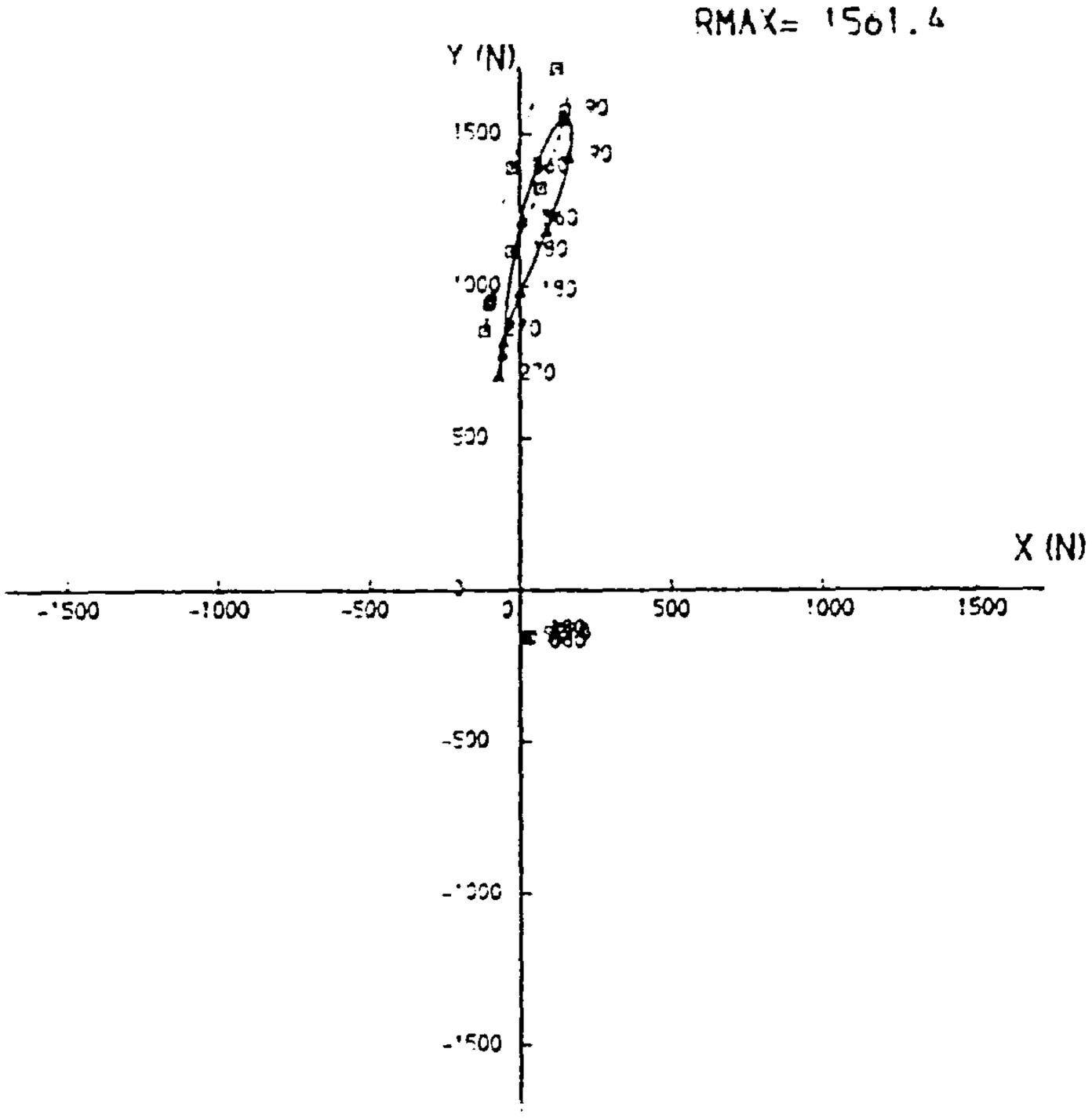

Mechanism Settings

R1 = 5.0mm
R2 = 2.5mm
R3 = 0.3 mm
R4 = 40.00mm
$\dot{\psi}_1$ = 9.5 rad/s

Loads in mechanism (notation of Fig.6.3)

Fig. B5.17 FY1 v. FX1

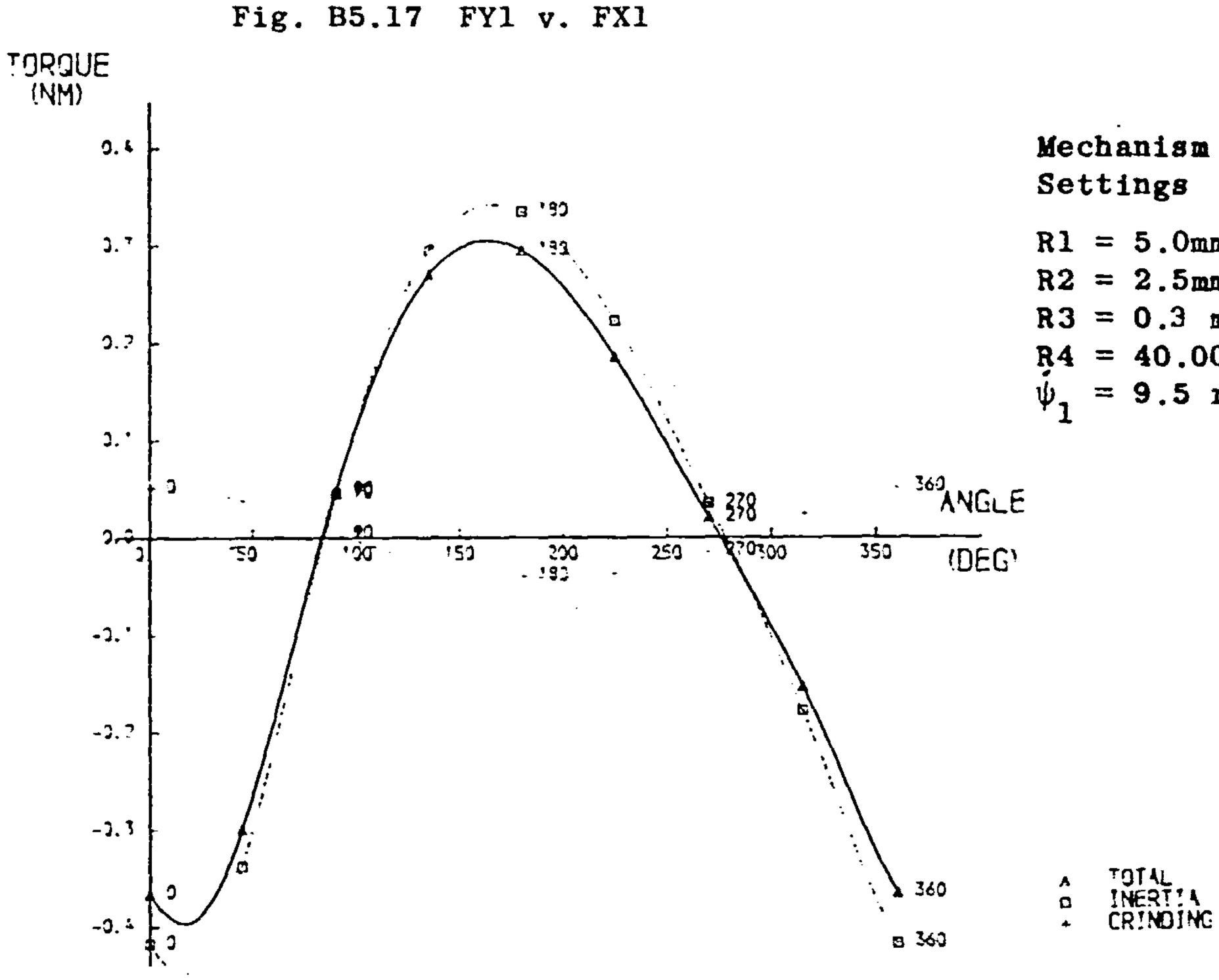

Mechanism Settings

R1 = 5.0mm
R2 = 2.5mm
R3 = 0.3 mm
R4 = 40.00mm
$\dot{\psi}_1$ = 9.5 rad/s

Loads in mechanism (notation of Fig.6.3)

Fig. B5.16 TOR v. ψ_1

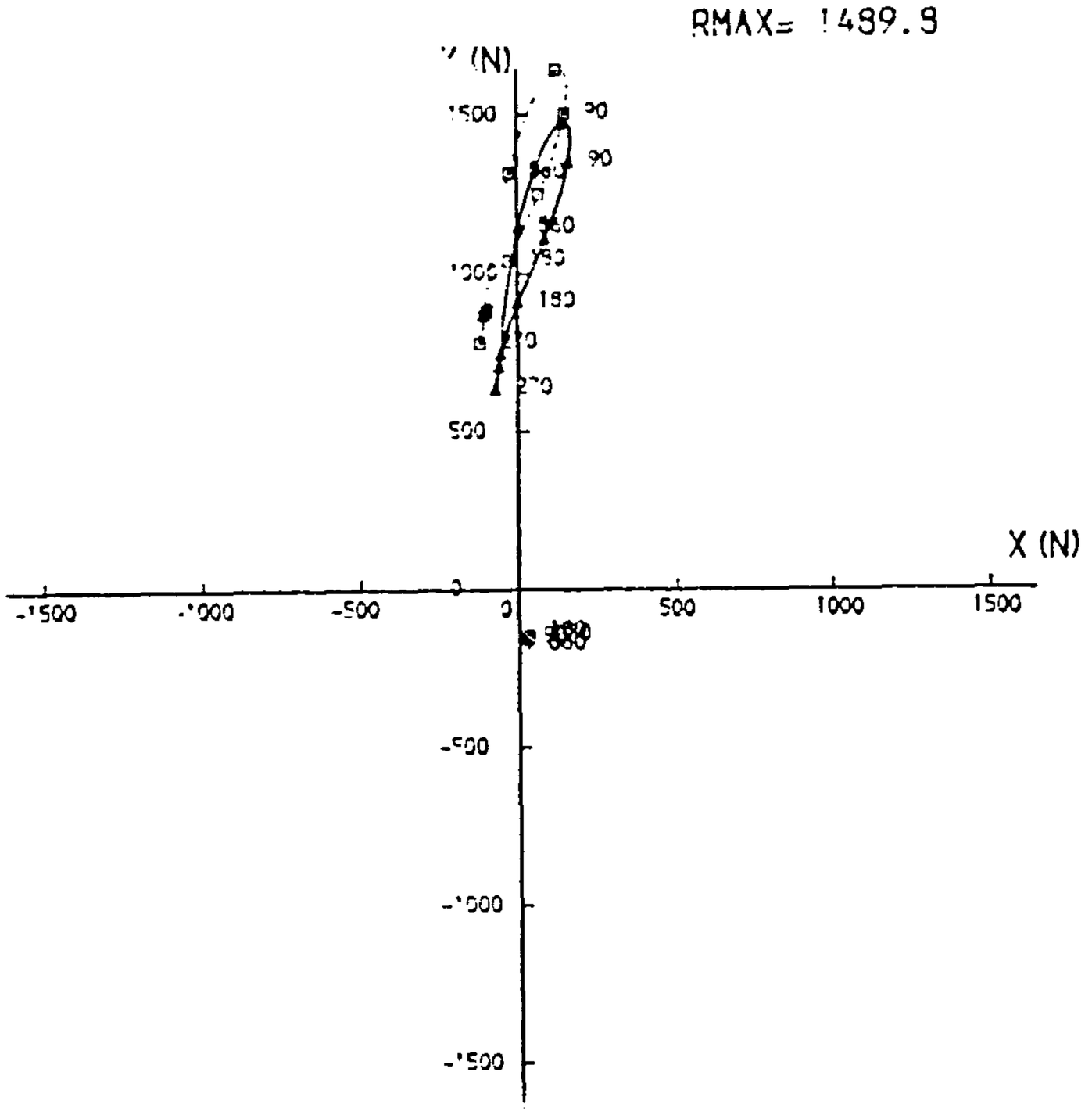

Mechanism Settings

R1 = 5.0mm
R2 = 2.5mm
R3 = 0.3 mm
R4 = 40.00mm
$\dot{\psi}_1$ = 9.5 rad/s

Loads in mechanism (notation of Fig.6.3)

Fig. B5.19 FY3 v. FX3

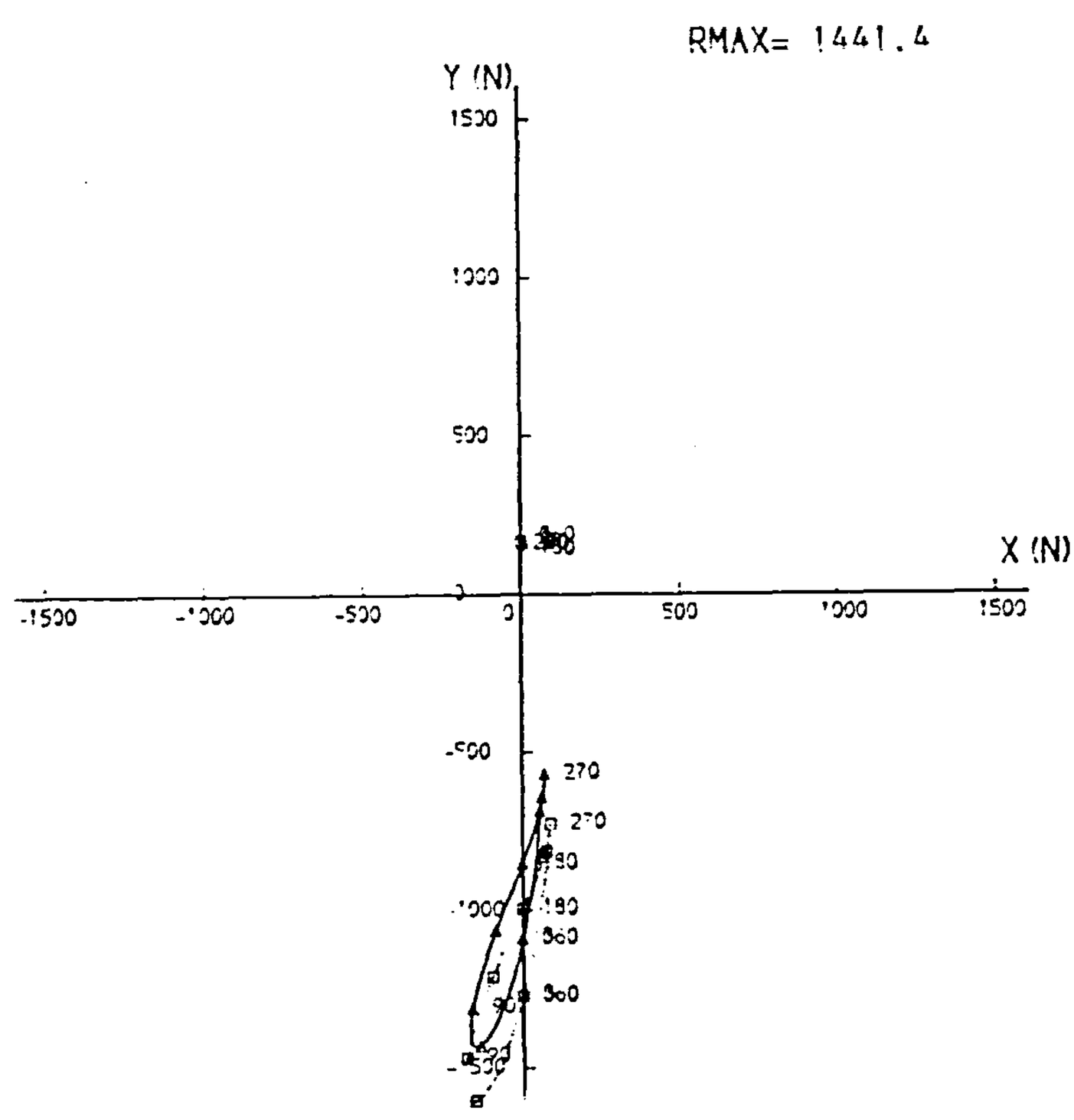

Mechanism Settings

R1 = 5.0mm
R2 = 2.5mm
R3 = 0.3 mm
R4 = 40.00mm
$\dot{\psi}_1$ = 9.5 rad/s

Loads in mechanism (notation of Fig.6.3)

Fig. B5.18 $FY2_R$ v. $FX2_R$

APPENDIX C

GENERAL DESIGN ANALYSES

C1 GRINDING FORCES

C2 MECHANISM MASSES, MOMENTS OF INERTIA, ETC.

C3 DEFLECTION ANALYSES

C4 MECHANISM TOLERANCES

C5 FRICTION IN BEARINGS

C6 SELECTION OF STEPPER MOTOR AND TIMING BELT TRANSMISSION

C1. GRINDING FORCES

The maximum grinding forces can be estimated from the power available from the motor.

The thrust, or normal force between wheel and work F_{CN} is assumed to be 1.5 to 3.0 times that of the cutting or tangential force F_{CT} and the latter is given by

$$F_C = \frac{P}{v} \quad (N)$$

where P is the available power

= motor power x efficiency (Watts)

and v is the grinding wheel surface speed (m/s).

Assuming a 0.55 Kw motor is used at 90% efficiency and for

rough grinding v = 20 m/s, then F_{CT} = 24.75 N

and for

fine grinding v = 30 m/s, then F_{CT} = 16.5 N.

In the mechanism error analysis these values became irrelevant: since grinding forces generally reduced overall forces and thus deflections, the worst case was considered to be $F_{CT} = 0$, $F_{CN} = 0$.

And in practice the grinding operating conditions may have to be modified from conventional conditions because of restrictions in work speed as discussed in Chapter 8.

Fluctuation of grinding forces.

Although the work rotational speed $\dot{\theta}$ is constant, the motion of the grinding wheel introduces an effective fluctuation in the work surface speed and, therefore, the grinding force as measured relative to the cutting point.

The variation is calculated by referring to the cycloidal generating motion as shown in Fig.3.1b of Chapter 3.

The effective work surface speed v_w is the relative velocity of the cutting point P on link r_2 to the work at that point.

At the maximum dimension of the profile $(r_1 + r_2)$ the work velocity = $(r_1 + r_2)\dot{\theta}$ and the cutting point velocity = $n\, r_2\dot{\theta}$ both in the same directions.

Thus $v_w = (r_1+r_2)\dot{\theta} - nr_2\dot{\theta} = (r_1-(n-1)r_2)\dot{\theta}$

At the minimum dimension of the profile (r_1-r_2) work and cutting point move in opposite directions.

Thus $v_w = (r_1-r_2)\dot{\theta} + nr_2\dot{\theta} = (r_1 + (n-1)r_2)\dot{\theta}$

Thus the fluctuation $v_w = \pm (n-1)r_2\dot{\theta}$

and the mean $v_w = r_1\dot{\theta}$

and the relative fluctuation = $\pm$ (n-1)e x 100%

after replacing r_2/r_1 by e.

Fluctuation in the grinding forces will be less than those of v_w. All other conditions (depth of cut, feed etc) being constant, $F_C \alpha v_w^{0.7}$; thus for an eccentricity ratio of e = 0.15,
for triangular profiles, fluctuation, in speed = $\pm$ 30%, and in force = $\pm$ 20%
and for square " " " " = $\pm$ 45%, and in force = $\pm$ 30%.

C2. MECHANISM MASSES, MOMENTS OF INERTIA ETC.

C2.1 Moving parts

The following component masses, moments of inertia, and centres of mass were calculated, for the design in Drawings 1 to 7, and used in the dynamic analysis of Appendix B. Their notation according to Figs.B1.1, B2.1 and B3.1 is given. And the general notation of Fig.B.1 is also referred to.

Grinding system.

As explained in App.B1, this is simply represented by two equivalent masses in the horizontal and vertical directions, m_{gwH} and m_{gwV} respectively, acting at the centre of the grinding wheel, joint J10.

Referring to Drawing No.7, m_{gwH} consists of the masses of the grinding spindle, wheel, and guard, and half the vertical link assembly and; m_{gwV}, those of the grinding spindle, wheel, and guard, all the vertical link, the twin pulley, and half the horizontal link assembly, giving;

m_{gwH} = 4.49 kg

m_{gwV} = 7.045 kg

Pantograph

These are summarised as follows

Link	Mass (kg)	Moment of Inertia (10^{-2} kgm^2)	Centre of mass (mm)
L1	m_1 = 2.08	I_{1A} = 1.67	r_1 = 66
L2	m_2 = 0.72	I_{2D} = 0.21	r_2 = 36
L3	m_3 = 2.84	I_{3D} = 1.10	r_3 = 38
L4	m_4 = 2.05	I_{4C} = 1.39	r_4 = 67

Calculations of these were straightforward for the regular shaped links and bearing assemblies of the pantograph.

Profile generator.

These may be summarised as

Link	Mass kg	Moment of Inertia 10^{-2} kgm^2	Centre of mass mm
R3	m_3 = 7.32*	I_{3A} = 4.30	$r_{g3} = r_3$
R4	m_4 = 10.28	I_{4G} = 3.38	x_{g4} = 1.4 y_{g4} = 0
R5	m_5 = 2.30	I_{5A} = 0.93	x_{g5} = 0 y_{g5} = 0

These were more complicated to calculate because of the irregular shape of components, see Drawing Nos. 1 and 2, and the variation of link R3 and R4 settings.

* For R3 the analysis is simplified by neglecting the mass of the shaft through joint J1, and assuming the remaining mass, of the eccentric shaft of joint J3, is always centred at joint J3, hence $r_{g3} = r_3$. Its M.o.I I_{3A} for the whole shaft, is irrelevant in the dynamic analysis as it runs at constant speed.

The variation of R4 due to the sliding joint J4 was ignored as negligible, as it is dominated by the housings of joints J3 and J2L.

R5 consists of the inner races and shafts of joints J2L and J2R.

C2.2 Total mass of attachment

The following masses for the static parts were estimated.

Motor (grinding system)	12	
Bedplate	60	
Housing of joint J1	24	
Housing of joint J2	4.7	
Pantograph base	3.2	
Stepper motor	3.5	
Static parts total	107.4	
together with Moving parts total	45.4	
	152.8	+ allowance, say 160 kg

Estimated total mass of attachment 160 kg

C3. DEFLECTION ANALYSES

C3.1 Deflections of main shafts (eccentricity link R3) assembly

A major source of deformations is the main shaft of Joint J1, the eccentricity shaft, R3, and the housing of joint J3 in link R4, and their respective bearings. A simplified sketch of this part of the assembly is shown in Fig.C3.1(a). For the purposes of further analysis of the effects of these deformations a single resultant deviation is sought at the position of joint J2, linear and revolute, bearings, signified by position E in Fig.C3.1(a) and (b). In this part of the analysis, the supports of bearings at A and B within joint J1 housing are assumed rigid; the deformation of the housing and bearings are considered later.

The deformations are related to a force P applied at position E. The bearing reactions are specified as P_A,P_B,P_C and P_D respectively, and the distances between reaction points as a, b, c and d.

Thus the reactions can be related to force P as follows:

$$P_A = P.\frac{(b+c+d)}{a}, \qquad P_C = P\frac{d}{c}$$

$$P_B = P.\frac{(a+b+c+d)}{a}, \qquad P_D = P\frac{(c+d)}{c}$$

Therefore for a = 155mm, b = 40mm, c = 70mm, d = 60 mm

$$P_A = 1.0968P, \qquad P_B = 2.0968P$$

$$P_C = 0.8571P, \qquad P_D = 1.8571P$$

The force acting at G, representing bearing forces at joint J4 is considered later, see C3.11, thus simplifying the analysis.

C3.2 Bending deflection of input/eccentric shaft of joints J1 and J3.

C3.2.1 Theory

The input shaft of joint J1 and the sliding eccentric and shaft of joint J3 are considered as one for this analysis. The largest eccentric offset is 7.5 mm which is small compared to the diameters of the load bearing shafts.

The shafts are considered as the simply-supported beam, ABCD, shown in Fig. C3.1(b).

The bending moment, M, acting at a point at distance, z, from the left-hand end at A is given by:

$$M = P_A z - P_B \langle z-a \rangle^1 - P_C \langle z-a-b \rangle^1$$

where $\langle z-x \rangle = 0$ for $z \leq x$

$= (z-x)$ for $z > x$ etc.

For a beam of constant second moment of area, I the slope

$$\phi = \frac{1}{EI} \int_o^z M \, dz + C_1$$

and displacement $y = \int_o^z \phi \, dz + C_2$

where E is the modulus of elasticity and C_1 and C_2 are constants of integration.

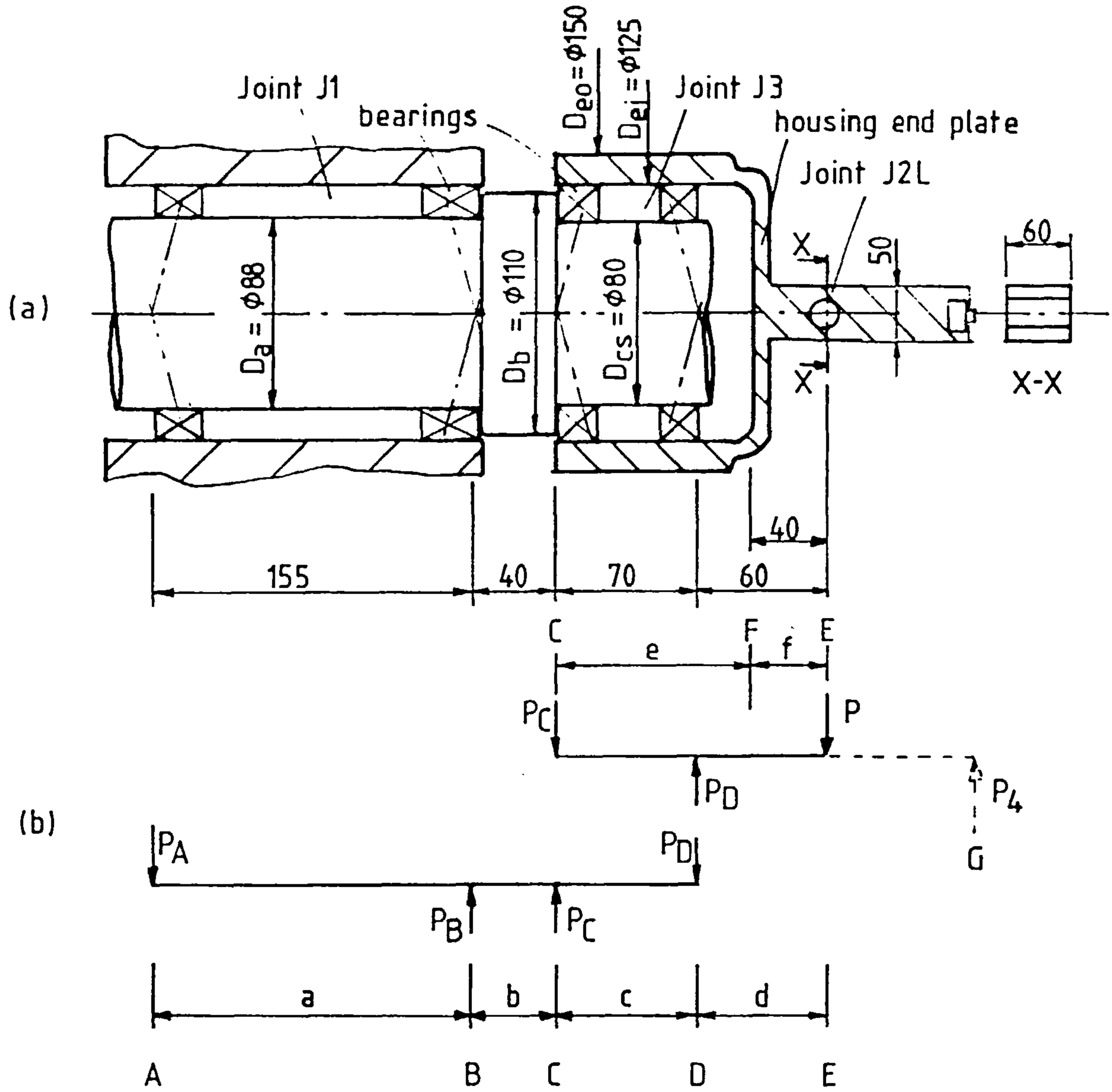

Fig.C3.1 Main shaft assembly-deflection a) sketch of assembly, b) equivalent beams - loading.

Thus

$$\phi = \frac{1}{EI}\left(\frac{P_A z^2}{2} - \frac{P_B}{2}\langle z-a\rangle^2 - \frac{P_C}{2}\langle z-a-b\rangle^2 + C_1\right)$$

and

$$y = \frac{1}{EI}\left(\frac{P_A z^3}{6} - \frac{P_B}{6}\langle z-a\rangle^3 - \frac{P_C}{6}\langle z-a-b\rangle^3 + C_1 z + C_2\right)$$

At $z = 0$, $y = 0$, and at $z = a$, $y = 0$, and thus substituting in the above equations gives

$$C_2 = 0 \quad \text{and} \quad C_1 = -\frac{P_A a^2}{6}$$

and the equations can be rewritten as

$$\phi = \frac{1}{EI}\left(\frac{P_A}{2}\left(z^2 - \frac{a^2}{3}\right) - \frac{P_B}{2}\langle z-a\rangle^2 - \frac{P_C}{2}\langle z-a-b\rangle^2\right) \qquad (1)$$

$$y = \frac{1}{EI}\left(\frac{P_A}{6}\left(z^3 - a^2 z\right) - \frac{P_B}{6}\langle z-a\rangle^3 - \frac{P_C}{6}\langle z-a-b\rangle^3\right) \qquad (2)$$

The resulting displacement, y_{El}, and slope, ϕ_{El} at position E, could be given by

$$y_{El} = y_D + \phi_D . d, \quad \text{and} \quad \phi_{El} = \phi_D$$

where y_D and ϕ_D are the displacement and slope at position D.

However, y_D and ϕ_D cannot be calculated directly from the above equations (1) and (2) since the beam is not of constant cross-section and second moment of area.

Alternative expressions can be stated as:

$$\phi_{E1} = \phi_B + \phi_{CB} + \phi_{DC} \tag{3}$$

$$y_{E1} = \phi_B.(b+c+d) + y_{CB} + \phi_{CB}.(c+d) + y_{DC} + \phi_{DC}.d \tag{4}$$

where ϕ_B is the slope at B

y_{CB} is the displacement at C relative to B,

ϕ_{CB} is the slope at C relative to B,

y_{DC} is the displacement at D relative to C,

and ϕ_{DC} is the slope at D relative to C.

Furthermore

$$y_{CB} = y'_C - y'_B - \phi'_B \cdot b \tag{5}$$

where y'_B and y'_C, the displacements at B and C, and ϕ'_B, the slope at B, are calculated from equations (1) and (2) using $I = I_b$, the second moment of area of section BC.

Similarly

$$\phi_{CB} = \phi'_C - \phi'_B \quad \text{using } I = I_b \text{ in eqn.(1)} \tag{6}$$

$$y_{DC} = y'_D - y'_C - \phi'_C.c \quad \text{using } I = I_c \text{ in eqn.(2)} \tag{7}$$

$$\phi_{DC} = \phi'_D - \phi'_C \quad \text{using } I = I_c \text{ in eqn.(1)} \tag{8}$$

and ϕ_B is directly found using $I = I_a$ in eqn.(1) (9)

C3 .2.2 Calculations

The second moment of inertia for a circular cross-section of diameter, D, is

$$I = \frac{\pi D^2}{64}$$

Therefore,

using $D = D_a = 88$ mm, $I_a = 2.944 \times 10^6$ mm^4,

$D = D_b = 110$ mm, $I_b = 7.187 \times 10^6$ mm^4,

and $D = D_c = 80$ mm, $I_c = 2.011 \times 10^6$ mm^4.

From eqns.(1) and (2), substituting values of P_A, P_B, P_C, a,b,c,d from C3.1.1

for $z = a = 155$mm $\quad \phi_B = \frac{8.784 \times 10^3}{EI}.P$ rads.

and $y_B = 0$

for $z = a+b = 195$mm $\quad \phi_C = \frac{14.784 \times 10^3}{EI}.P$ rads

and $y_C = \frac{0.4767 \times 10^6}{EI}.P$ mm

for $z = a+b+c = 265$ mm $\quad \phi_D = \frac{19.334 \times 10^3}{EI}.P$ rads

and $y_D = \frac{1.724 \times 10^6}{EI}.P$ mm

Substituting these values in eqns.(5) thro' (9) and using the appropriate values of I ($=I_a, I_b$ or I_c) and

$E = 207 \times 10^3$ N mm^{-2} for steel,

gives $y_{CB} = 0.0843 \times 10^{-6} P$ mm

$\phi_{CB} = 4.033 \times 10^{-9}$ P rads

$y_{DC} = 0.510 \times 10^{-6}$ P mm

$$\phi_{DC} = 1.093 \times 10^{-8} \text{ P rads.}$$

and $$\phi_{B} = 1.4414 \times 10^{-8} \text{ P rads}$$

and finally substituting these values in eqns.(3) and (4)

$$\phi_{E1} = 29.377 \times 10^{-9} \times \text{P radians}$$

$$y_{E1} = 4.225 \times 10^{-6} \times \text{P mm}$$

where the additional subscript, 1, indicates the slope and displacement at E due to bending of the main shaft and eccentric link only.

C3.3 Shear deflection of input-eccentric shaft of joints J1 and J3.

The shear strain, γ is given by

$\gamma = \frac{\tau}{G}$ where τ is the shear stress,

and G the modulus of rigidity.

Use the maximum shear stress which is 1.33 x $\tau_{average}$ for a circular section. If the shear strain in sections AB, BC and CD of the beam shown in Fig.C3.1.1(b) are denoted as γ_a, γ_b, γ_c respectively, the slope at position E, γ_{E1} is given by

$$\gamma_{E1} = \gamma_a$$

and the displacement at E, δ_{E1} is given by

$$\delta_{E1} = \gamma_a \times (b+c+d) + \gamma_b \times b + \gamma_c \times c$$

where $$\gamma_a = \frac{4 P_A}{\pi D_a^2} \cdot \frac{1.33}{G} = 3.006 \times 10^{-9} \text{ P radians}$$

$$\gamma_b = \frac{4(P_B - P_A)}{\pi D_b^2} \cdot \frac{1.33}{G} = 1.754 \times 10^{-9} \text{ P rads}$$

$$\gamma_c = \frac{4(P_B - P_A + P_C)}{\pi D_c^2} \cdot \frac{1.33}{G} = 6.158 \times 10^{-9} \text{ P rads}$$

Therefore

$$\gamma_{E1} = 3.01 \times 10^{-9} \text{ P rads.}$$

$$\delta_{E1} = 1.012 \times 10^{-6} \text{ P mm}$$

C3.4. Bending deflection of joint J3 housing in link R4

C3.4.1 Theory

The housing of J3 and part of link R4 up to joint J2, position E in Fig.C3 .1(a) is treated as a simply supported beam CDFE with loads P_C, P_D and P applied at C, D and E respectively, and a change in cross-section at F. (Note: the housing end plate at position F is analysed in section C3.6). The analysis is similar to that of C3.2.1.

The bending moment, M, acting at point at distance, z, from the left-hand end c, is given by

$$M = P_C z - P_D \langle z - c \rangle^1$$

and
$$\phi = \frac{1}{EI}\left(\frac{P_C}{2}(z^2 - \frac{c^2}{3}) - \frac{P_D}{2}\langle z - c\rangle^2\right) \quad (1)$$

$$y = \frac{1}{EI}\left(\frac{P_C}{6}(z^3 - c^2 z) - \frac{P_D}{6}\langle z-c\rangle^3\right) \quad (2)$$

$$\phi_{E2} = \phi_F + \phi_{EF} \quad (3)$$

$$y_{E2} = y_F + \phi_F . f + y_{EF} \quad (4)$$

where ϕ_F is the slope at F

ϕ_{EF} is the slope at E relative to F

y_F is the displacement at F

and y_{EF} is the displacement of E relative to F.

Also

$$\phi_{EF} = \phi'_E - \phi'_F \quad (5)$$

where ϕ'_E, ϕ'_F are calculated from eqn.(1) using $I = I_F$, the second moment of area of FE

$$y_{EF} = y'_E - y'_F - \phi'_F \cdot f \quad \text{using } I = I_F \text{ in eqn.(2)} \qquad (6)$$

and ϕ_F, y_F calculated directly from (1) and (2) using $I = I_E$.

C3.4.2 Calculations

For annular cross-section between C and F

$$I_E = \frac{\pi}{64}(D_{eo}^4 - D_{ei}^4)$$ where D_{eo} is the outer diameter = 150 mm

and D_{ei} is the inner diameter = 125 mm.

Therefore

$$I_E = 12.866 \times 10^6 \text{ mm}^4.$$

For rectangular cross-section between F and E

$$I_F = \frac{bh^3}{12}$$ where b is the width = 60 mm

and h is the height = 50 mm.

Therefore

$$I_F = 0.625 \times 10^6 \text{ mm}^4.$$

From eqns.(1) and (2), substituting values of P_C, P_D, c,d,e and f

for $z = e = 90$ $\quad \phi_F = \frac{2.400 \times 10^3}{EI}$ P radians

$$y_E = \frac{38.665 \times 10^3}{EI} \text{ P mm}$$

for $z = e + f = 130$ $\quad \phi_E = \frac{3.120 \times 10^3}{EI}$ P rads

$$y_E = \frac{155.99 \times 10^3}{EI} \text{ P mm}$$

From eqns.(5) and (6) using $E = 207 \times 10^{-3}$ Nmm^{-2} for steel and

$$I = I_F = 0.625 \times 10^6 \text{ mm}^4$$

$$\phi_{EF} = 5.565 \times 10^{-9} \text{ P rads.}$$

$$y_{EF} = 0.1648 \times 10^{-6} \text{ P mm}$$

and using $I = I_E = 12.866 \times 10^6$ P mm^4

$$\phi_F = 0.9012 \times 10^{-9} \text{ P rads.}$$

$$y_F = 0.0145 \times 10^{-6} \text{ P mm}$$

substituting these values in eqns.(3) and (4) gives

$$\underline{\phi_{E2} = 6.466 \times 10^{-9} \text{ P rads.}}$$

and

$$\underline{y_{E2} = 0.2154 \times 10^{-6} \text{ P mm}}$$

C3.5 Shear deflections of link R4 including housing of joint J3.

Theory as in C3.3.

If the shear strain in cross-sections CF and FE of the beam shown in Fig.C3.1 (b) are denoted by γ_e and γ_f respectively then the resulting slope at position E, γ_{E2} is given by

$$\gamma_{E2} = \gamma_e$$

and the displacement at E, δ_{E2} is given by

$$\delta_{E2} = \gamma_e \cdot f + \gamma_f \cdot f$$

where
$$\gamma_e = \frac{4}{\pi} \frac{P_C}{(D_{eo}^2 - D_{ei}^2)} \cdot \frac{133}{G} = 2.639 \times 10^{-9} \text{ P rads.}$$

$$\gamma_f = \frac{(P_D - P_C)}{bh} \cdot \frac{1.5}{G} = 6.25 \times 10^{-9} \text{ P rads.}$$

(Note for rectangular section $\tau_{max} = 1.5\ \tau_{average}$)

Therefore

$$\underline{\gamma_{E2} = 2.639 \times 10^{-9} \text{ P rads.}}$$

$$\underline{\delta_{E2} = 0.3556 \times 10^{-6} \text{ P mm.}}$$

C3..6 Twisting of housing end plate in link R4.

The plate is positioned at the change in cross-section position F in Fig. C3.1 (a) and (b).

The problem is considered as that of a 'central couple acting on a circular plate with a fixed edge' for which formulae are given by Roark & Young [41]. The notation is shown in Fig.C3.6 and applies to this section only.

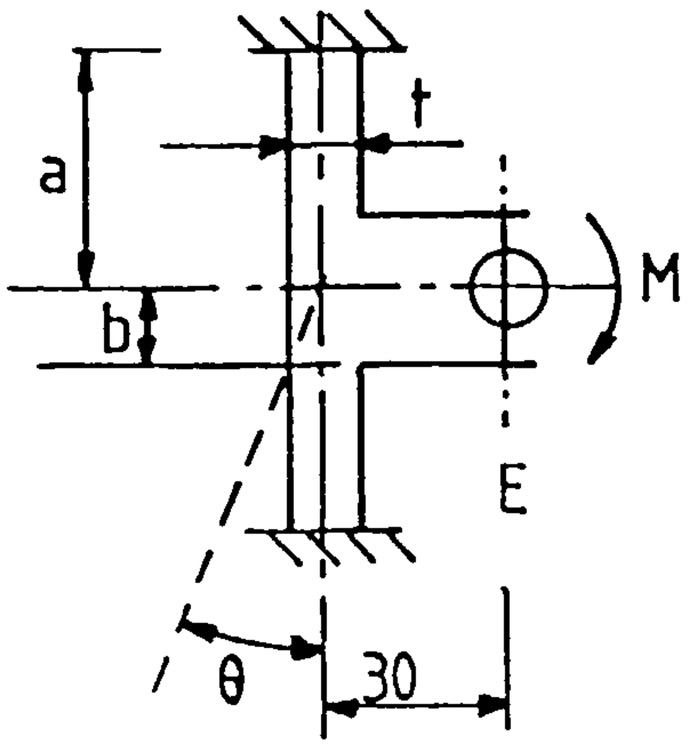

a = 62.5 mm

b = 25.0 mm

t = 10.0 mm

M = P x 30 Nmm where P is the force acting at E, in Fig.C3.1(b).

Fig.C3.6 Sketch of plate twisting under the action of a central couple, M.

The angle of twist, θ is given by

$$\theta = \frac{\alpha M}{Et^3} = \phi_{E3}, \text{ the resulting slope at position E, Fig.C3.1(b)}$$

where $\alpha = 0.167$ for $b/a = \frac{25}{62.5} = 0.4$

Thus

$$\underline{\phi_{E3} = 24.203 \times 10^{-9} \text{ P rads.}}$$

which is also the resulting slope at E, Fig.C3 .1(b).

The resulting deflection at position E, Fig.C3 .1(b),

$$\underline{\delta_{E3}} = \theta \times 30 \text{ mm} = \underline{0.7261 \times 10^{-6} . \text{ P mm}}$$

C3.7. Bearing deflections on main shaft and eccentric link.

(Taper roller bearings of joints J1 and J3).

Joint, J1, contains two taper roller bearings, (SKF designation 32018 XC) positioned at A and B as shown in Fig.C3.1 (a) and joint J3, two taper roller bearings (SKF designation 32016 XC) positioned at C and D as shown in Fig.C3.1(a).

C3.7.1 Theory

If the bearing deformations at A, B, C and D are denoted as δ_A, δ_B, δ_C and δ_D respectively the resultant deflection δ_{E4} and slope ϕ_{E4} of link R4 at position E, Fig.C.3.1. (a), are given by:

$$\delta_{E4} = \delta_A \times \frac{b+c+d}{a} + \delta_B \times \frac{a+b+c+d}{a} + \delta_C \times \frac{d}{c} + \delta_D \times \frac{c+d}{c} \quad (1)$$

$$\phi_{E4} = \frac{\delta_A}{a} + \frac{\delta_B}{a} + \frac{\delta_C}{c} + \frac{\delta_D}{c} \quad (2)$$

The bearing deformations are estimated after the method of Houghton[25] using the expression:

$$W = Z\, K_n\, (\delta_o - 0.5\, Cd)^n\, Jr_{(\varepsilon)} \quad (3)$$

where W is the radial bearing load in N

Z is the number of elements (rollers)

K_n is a deflection constant

n is an index, n = 1.11 for roller bearings

δ_o is the bearing deformation in mm

C_d is the diametral clearance (negative for preloading) in mm

$Jr_{(\varepsilon)}$ and ε are both tabulated by Houghton (Table 11.1 Ref. [25])

also given are

$$\varepsilon = 0.5\, (1 - \frac{C_d}{2\delta_o}) \quad (4)$$

$$K_n = \frac{1}{(1/K_L)^{1/n} + (1/K_L)^{1/n}}^{n} \quad (5)$$

and

$$K_L = 7.86 \times 10^4 \times \ell^{0.89} \quad (6)$$

where ℓ = element (roller) length in mm

for n = 1.11

eqns.(5) and (6) give $K_n = K_L \times (0.5)^{1.11} = 3.64 \times 10^4\, \ell^{0.89}$

eqn.(4) can be rearranged to give:

$$C_d = (2 - 4\varepsilon)\, \delta_o \quad (7)$$

Substituting for C_d in eqn.(3) and rearranging gives

$$\delta_o = \frac{1}{2\varepsilon} \left(Z \frac{W}{K_n \, Jr_\varepsilon}\right)^{1/n} \qquad (8)$$

The equations developed so far apply for ordinary roller bearings: a further correction should be made for taper roller bearings to take account of the contact angle, α, of the load bearing surfaces.

With reference to Fig.C3.7, the load acting normal to the roller $= \frac{W}{\cos\alpha}$, if this is then used in eqn.(8), replacing $W^{0.9}$ by $(W/\cos\alpha)^{0.9}$, the calculated δ_o will be the deformation also along the normal to the roller.

Assuming that the relative motion of the inner and outer races of bearing to take up the deformation is in a radial direction, then this radial deformation $\delta = \delta_o/\cos\alpha$.

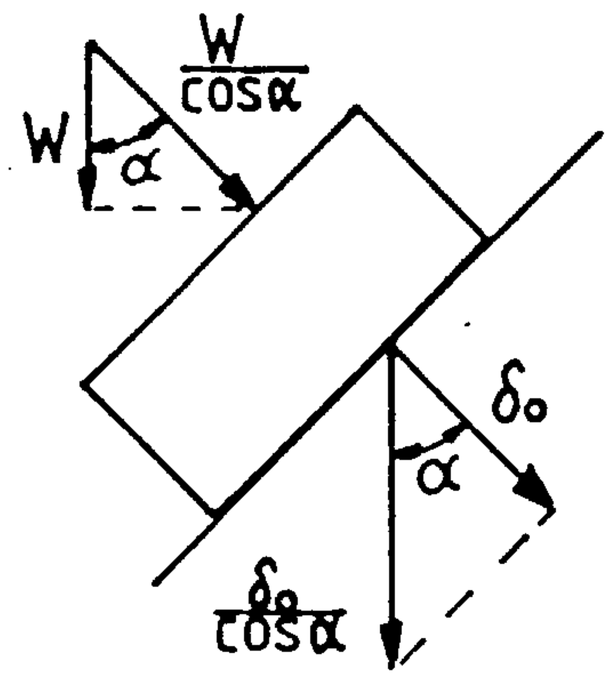

Fig.C3.7 Load directions and deformation on a taper roller.

Equation (8) can be rewritten for taper roller bearings as

$$\delta = \frac{1}{2\varepsilon} \left(\frac{W}{Z \, K_n \, Jr_{(\varepsilon)}}\right)^{0.9} \times \left(\frac{1}{\cos\alpha}\right)^{1.9} \qquad (9)$$

C3.7.2 Calculations.

For bearings of A and B, taper roller type SKF.32018 XC [26]

length of roller $\ell = 23.6$ mm, therefore $K_n = 3.73 \times 10^3 \times 23.6^{0.89}$

number of rollers $Z = 27$

contact angle $\alpha = 15$ degrees

radial load $W = P_A$ or $= P_B$, when P_A, P_B are in N.

Substituting these in eqn.(9) gives:

$$\delta_{\substack{A\\B}} = \frac{1.71 \times 10^{-7}}{\varepsilon} \left(\frac{1}{Jr_{\varepsilon}}\right)^{0.9} P_{\substack{A\\B}}^{0.9} \text{ mm}$$

$Jr_{(\varepsilon)}$ is tabulated against, ε in Houghton [25]
Thus for several values of ε, the ratio of Cd/δ_o and $\delta/P_A^{0.9}$ $(= \delta/P_B^{0.9})$ can be calculated. These results are given in Table C3.7.2.

Similarly:

For bearings at C and D of joint J3

SKF Designation : 32016 XC

$$\ell = 21.4, \quad z = 27, \quad \alpha \simeq 15^{o}, \quad W = P_C, = P_D$$

Eqn.(9) reduces to

$$\delta_{\substack{C\\D}} = \frac{1.85 \times 10^{-7}}{\varepsilon} \left(\frac{1}{Jr_{\varepsilon}}\right)^{0.9} \cdot P_{\substack{C\\D}}^{0.9}$$

which is tabulated in Table C3.7.2.

ε	Jr_{ε}	C_d/δ_o	$\delta_A/P_A^{0.9}, \delta_B/P_B^{0.9}$	$\delta_C/P_C^{0.9}$, $\delta_D/P_D^{0.9}$
0.5	0.2452	0	1.21×10^{-6}	1.31×10^{-6}
1.0	0.2523	-2.0	0.59×10^{-6}	0.64×10^{-6}
2.5	0.1075	-8.0	0.51×10^{-6}	0.55×10^{-6}
5.0	0.0544	-18.0	0.47×10^{-6}	0.51×10^{-6}

Table C3.7.2 Relationships between deformation and loads for bearings of joints J1 and J3, at various preload conditions (given by C_d/δ_o).

It can be seen from Table C3.7.2 that the deformation-load relationship varies according to the amount of preload in the bearings, signified by the ratio C_d/δ_o (a negative value indicates negative clearance, i.e. preload deformation). If the preload deformation ($-C_d$) is at least twice as large as the expected operating load deformation, δ_o, then the actual operating deformation will be at least half that expected at zero preload, $C_d/\delta_o = 0$.

Therefore assume $-Cd/\delta_o \geq 2$,(see App.C5.2.3) and choose appropriate relationships for use in further analyses as follows.

$$\delta_A = 0.59 \times 10^{-6} P_A^{0.9} \text{ mm}$$

$$\delta_B = 0.59 \times 10^{-6} P_B^{0.9} \text{ mm}$$

$$\delta_C = 0.64 \times 10^{-6} P_C^{0.9} \text{ mm}$$

$$\delta_D = 0.64 \times 10^{-6} P_D^{0.9} \text{ mm}$$

After replacing P_A, ...P_D in terms of P, from C3.1 and substituting in eqns.(1) and (2), (of C3.7.1) with the values of a,b,c,d, the resulting displacement and slope at E are given by:

$$\underline{\delta_{E4} = 5.66 \times 10^{-6} P^{0.9}} \text{ mm}$$

$$\underline{\phi_{E4} = 35.47 \times 10^{-9} P^{0.9}} \text{ radians.}$$

C3.8. Deflection of baseplate and joint J1 housing.

An estimate of the contribution of deflections of the bearing housing of joint J1 and the mechanism baseplate to the effective deflection at joint J2, can be made using elementary theory.

A simplified diagram of the problem is shown in Fig.C3.8. The beam ABE represents the main shaft assembly of Fig.C3.1.1 where A and B are the load bearing positions in joint J1, and E the application point of the external load, P, at joint J2. In this part of the analysis ABE is assumed rigid and the resultant displacement, y_{E4}, and slope, ϕ_{E4}, of the housing and baseplate at E, relative to ABE, are calculated.

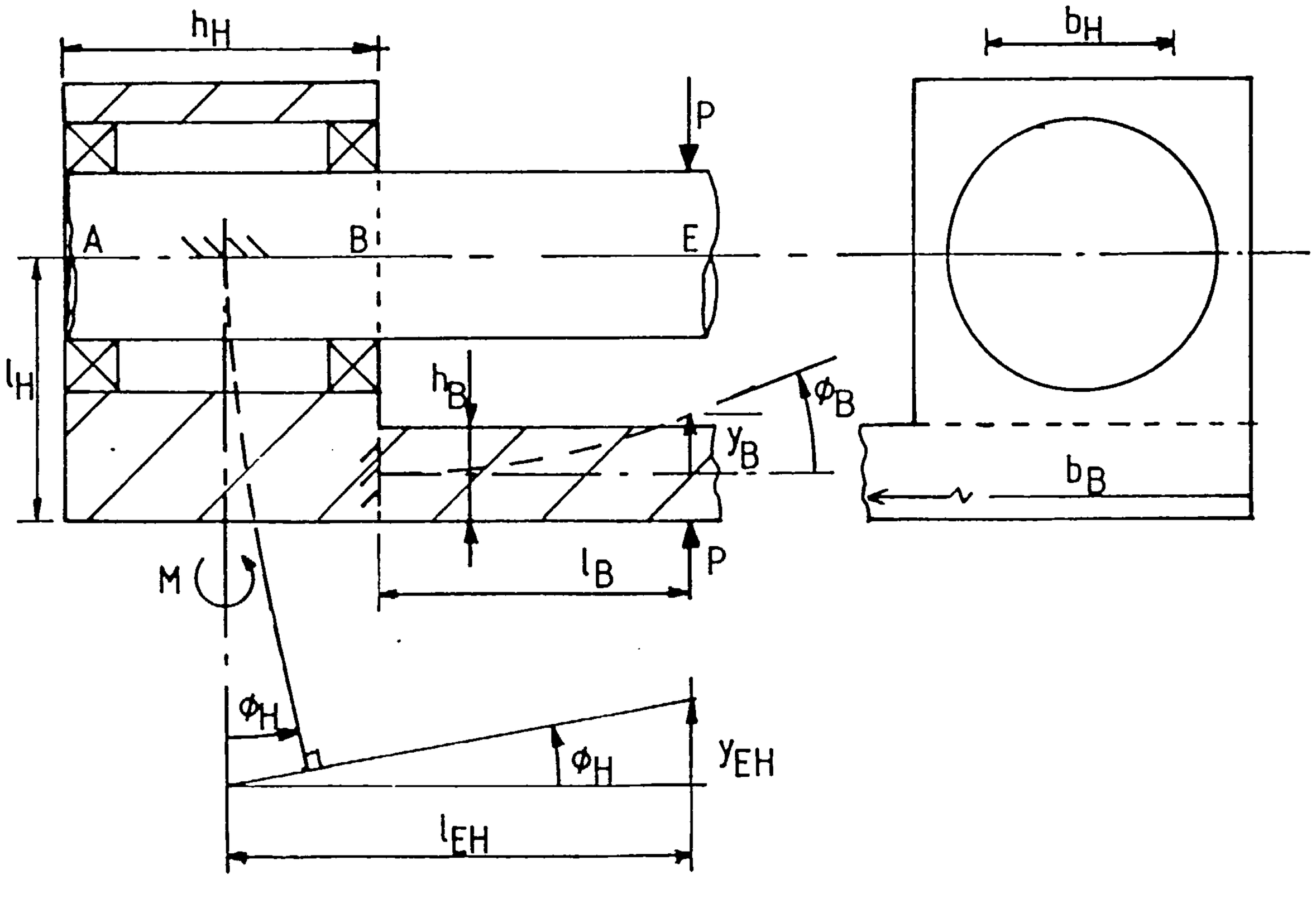

Fig. C3.8. Deflection of baseplate (bending only)

.8.1 Housing deflection.

The housing is treated as a simple cantilever of length ℓ_H, rigidly fixed on the centre line AB, midway between A and B and acted upon by a couple, M and thus constant bending moment, M along the beam. The couple $M = P.\ \ell_{EH}$ the distance of the beam from the external load P at E.

For constant bending moment, M, the slope ϕ_H is given by

$$\phi_H = \frac{M\ \ell_H}{E\ I_H}$$

where the second moment of inertia $I_H = \frac{b_H h_H^3}{12}$ for a rectangular section.

The effective width of the section b_H, is taken as less than the external width to compensate for the bearing bore.

The displacement of this beam would act horizontally and is ignored since it will not effect performance of the mechanism.

The slope ϕ_{EH} and displacement, y_{EH}, at E due to ϕ_H are given by

$$\phi_{EH} = \phi_H$$

$$y_{EH} = \phi_H \times \ell_{EH}.$$

Taking $b_H = 100$ mm, $h_H = 175$, $\ell_H = 140$ mm, $\ell_{EH} = 250$ mm, $E = 207 \times 10^3$ Nmm^{-2} for steel, gives

$$\phi_{EH} = 3.786 \times 10^{-9} \text{ P radians}$$

$$y_{EH} = 0.9465 \times 10^{-6} \text{ P mm.}$$

.8.2 Base plate deflections.

The baseplate is treated as a simple cantilever of length, ℓ_B, rigidly fixed to the housing at position B and is acted upon by an end load P at E.

The slope is given by

for bending, $\phi_B = \dfrac{P\,\ell_B^{\,2}}{2EI_B}$, shear $\gamma_B = \dfrac{1.5\,P}{AG}$

and displacement by

bending $y_B = \dfrac{P\ell_B^{\,3}}{3EI_B}$, shear $\delta_B = 1.5\,\dfrac{P\ell_B}{AG}$

where $I_B = \dfrac{b_B.\,h_B^{\,3}}{12}$, $A = b_B.\,h_B$

$= 3.64 \times 10^6$ mm^4.

Taking $\ell_B = 170$ mm, $b_B = 350$, $h_B = 50$ and $E = 208 \times 10^3$ Nmm^{-2}

$$\phi_B = 19.147 \times 10^{-9} \times P \text{ radians}$$

$$\gamma_B = 1.07 \times 10^{-9} \times P \text{ radians}$$

$$y_B = 2.170 \times 10^{-6} \ P \text{ mm}$$

$$\delta_B = 0.18 \times 10^{-6} \ P \text{ mm}$$

.8.3 Baseplate plus housing deflections at E

The resultant slope $\phi_{E5} = \phi_{EW} + \phi_B$

displacement $y_{E5} = y_{EH} + y_B + \delta_B$.

Therefore

$$\underline{\phi_{E5} = 22.93 \times 10^{-9}. \ P \text{ radians}}$$

$$\underline{y_{E5} = 3.297 \times 10^{-6}. \ P \text{ mm}}.$$

C3.9 Deflection of joint J2, radial and linear bearing assembly.

Joint J2 consists of a large diameter needle roller bearing mounted on a hollow shaft which has a linear ball bearing sliding on a solid shaft mounted across a diameter of the radial bearing. This is shown in Drawings No. 1 and No. 2 and in simple form in Fig. C.3.9.

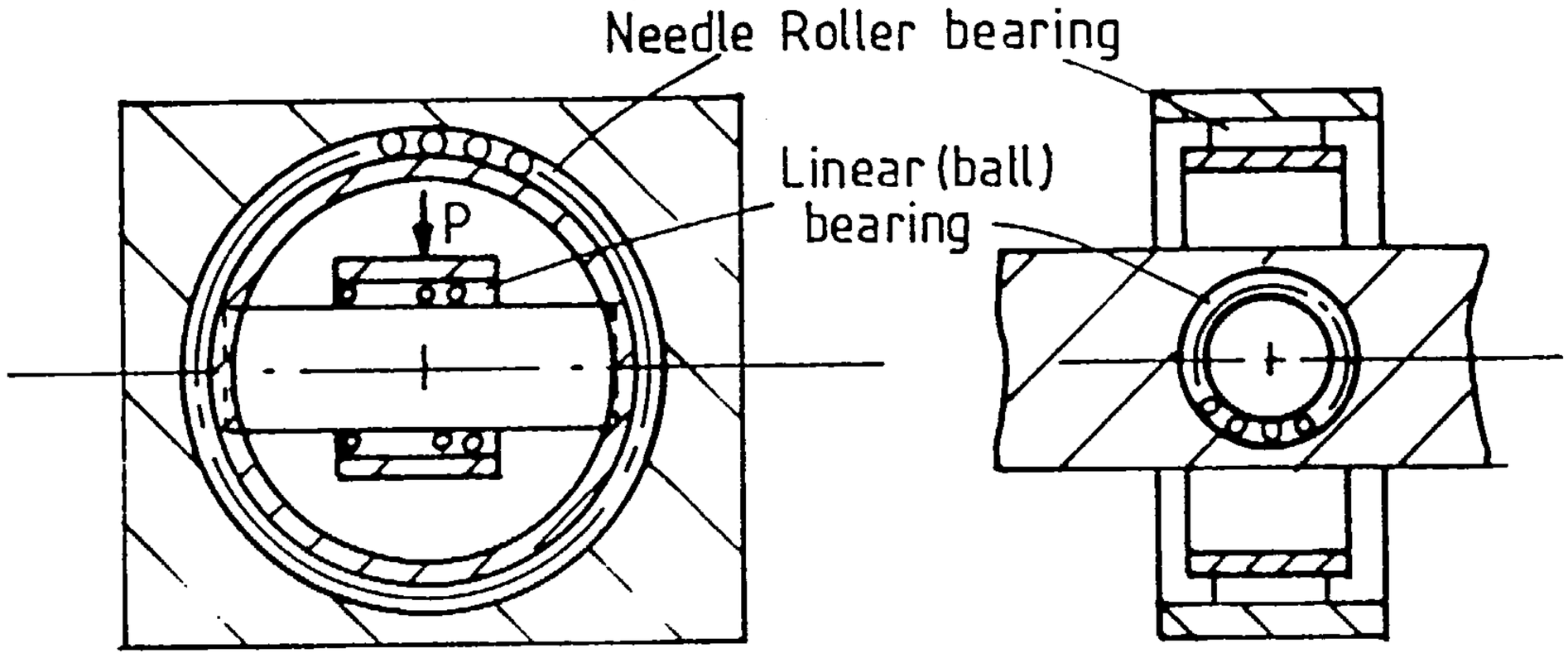

Fig. C3.9. Simplified diagram of joint J2.

The load, P, is applied at the centre of the two bearings corresponding to position E, as denoted in Figs. C3.1 . . and C3.8 in previous sections of C3.

C3.9.1. Rotary bearing displacement.

The bearing designation is from INA catalogue [28]

K145 x 153 x 26 (rollers and cage only).

length of roller ℓ = 19 mm

number of rollers z = 30

The displacement, δ_{E5}, is calculated using eqns.(6) and (8) of section C3.7 after placing, W = P to give

$$\delta_{E5} = \delta_o = \frac{1}{2\varepsilon} \left(\frac{1}{Z\ K_n\ J_{r\varepsilon}}\right)^{0.9} . P^{0.9} \text{ mm} \qquad (1)$$

where $K_n = 3.64 \times 10^4\ \ell^{0.89}$

The needle roller bearing is designed to operate with zero clearance (≡ zero preload) therefore from C3 .7 for $C_d \simeq 0$

$$\varepsilon = 0.5, \quad J_{r\varepsilon} = 0.2452$$

Inserting these values in (1) results in

$$\underline{\delta_{E5} = 1.227 \times 10^{-6}\ P^{0.9} \text{ mm.}}$$

C3.9.2 Linear bearing displacement

The bearing designation from the Rotolin catalogue [27] is ML 20-32-50. The bearing consists of several rows of ball bearings held in a cage, which allows both rotary and linear movement between the inner and outer sleeves or races. The balls, of necessity, do not run in grooves.

Again, the deflection can be estimated using eqn.(8) of C3.7 . from Houghton [25]

However, in this case for point contact of ball bearings

$$K_n = \left[\frac{1}{\left(\frac{1}{K_{pi}}\right)^{1/1.5} + \left(\frac{1}{K_{po}}\right)^{1/15}} \right]^{1.5} \qquad (1)$$

where $$K_{pi,o} = 2.15 \times 10^5 \; \Sigma_{\rho i,o}^{-0.5} \; \lambda^{-1.5} \qquad (2)$$

where $$\Sigma_{\rho 1} = \frac{2}{r_b} + \frac{1}{r_i}, \quad \Sigma_{\rho o} = \frac{2}{r_b} - \frac{1}{r_o} \qquad (3)$$

and r_b = radius of balls

r_i = radius of inner sleeve, or shaft, contact surface

r_o = radius of outer sleeve, contact surface.

λ is tabulated in Houghton [25] against a function of ρ

$$F(\rho)_{1,o} = \frac{1/r_i}{\Sigma_{\rho i}} \text{ and } \frac{1/r_o}{\Sigma_{\rho o}}$$

For Rotolin bearing ML20 - 32 - 50

Ball radius = 1.19 mm = r_b

Shaft radius = 10 mm = r_i

Outer sleeve radius = 12.38 mm = r_o

Number of balls = 105 (in several rows, but does not affect formula).

Therefore

$\Sigma_{\rho i} = 1.78 \text{ mm}^{-1}$

$\Sigma_{\rho o} = 1.60 \text{ mm}^{-1}$

$F(\rho)_1 = 0.056, \quad F(\rho)_o = 0.050$

from Table 8.1 *of* Houghton, $\lambda = 0.998$ *for both cases therefore take*

$\lambda = 1.0,$

$K_{pi} = 1.612 \times 10^5$

$K_{po} = 1.70 \times 10^5$

Thus $K_n = 5.85 \times 10^4$ from eqn.(1).

From eqn.(8), C3 7

displacement $\delta = \frac{1.49 \times 10^{-5}}{\varepsilon} \left(\frac{1}{J_{r\varepsilon}}\right)^{0.67} p^{0.67}$

Table C3.9.2. shows $\delta/p^{0.67}$ for several values of ε

Table C3.9.2 Displacement-load relationships at various preloads for joint J2 linear bearing

ε	$J_{r\varepsilon}$ *	C_d/δ_o	$\delta_o/p^{0.67}$ $(mm/N^{0.67})$
0.5	0.2288	0	8.0×10^{-5}
0.6	0.2417	-0.4	6.4×10^{-5}
0.7	0.2505	-0.8	5.4×10^{-5}
0.8	0.2559	-1.2	4.6×10^{-5}
1.0	0.2546	-2.0	3.7×10^{-5}

* $J_{r\varepsilon}$ for ball bearings.

According to the Rotolin catalogue the bearings should be mounted with a preload interference $(-C_d) = 0.002$ to 0.012 mm.

After some trial calculations, using the relationship in Table C3.9.2, the ratio $-C_d/\delta_o$ was not likely to be 0.4 for the high loadings that would be encountered, for machining small workpieces. Thus the safest relationship to choose for displacement due to J2 linear bearing is

$$\delta_{E6} = 80.0 \times 10^{-6} \; p^{0.67} \text{ mm.}$$

C3 .9.3. Deflection of shaft of linear bearing.

The shaft is shown in Fig.C3.9 and is seen to be supported at each end by the ring carrying the inner race of the needle roller bearing. The shaft is treated as a simple supported beam loaded at the centre by P. Elementary theory gives the displacement as

$$y = \frac{P\,\ell^3}{48EI} \text{ in bending,} \quad \delta = \frac{P\,\ell}{4AG} \text{ in shear}$$

$$I = \pi d^4/64, \quad A = \pi d^2/4$$

where length of the shaft, ℓ = 130 mm

diameter of the shaft d = 20 mm

modulus of elasticity $E = 207 \times 10^{3}$ Nmm^{-2}

Thus $y = 28.15 \times 10^{-6} P$, $\delta = 1.29 \times 10^{-6} P$

Therefore the displacement at, E, due to bending and shear of the linear bearing shaft

$$y_{E6} = 29.44 \times 10^{-6} \times P \text{ mm.}$$

C3 .10 Combined deflections of mechanism (as seen at the centre of joint J2, or position E in Figs.C3.1, C3.6, C3.8 and C3.9).

For a force, P, acting perpendicular to link R4, through linear bearing, J2, most deflections will act in the direction of P, since the components rotate with P or are axi-symmetrical. These can be taken as contributing to RP2 type errors as defined in Chapter 6. The baseplate and J1 bearing housing are not axi-symmetrical and will always deflect vertically (if deflection horizontally is assumed negligible due to shape) and should therefore be considered as contributing to RL1 or RL2 type errors (as defined in Chapter 6) depending where the base is fixed on the parent machine.

The total deflection at E, contributing to RP2 type deviation, ΔRP2 and corresponding slope ΦRP2 are given by

$$-\Delta RP2 = y_{E1} + \delta_{E1} + y_{E2} + \delta_{E2} + \delta_{E3} + y_{E6} + \delta_{E4} + \delta_{E5} + \delta_{E6}$$

$$-\Phi RP2 = \phi_{E1} + \gamma_{E1} + \phi_{E2} + \gamma_{E2} + \phi_{E3} + \phi_{E4}$$

and, deflection at E, contributing to RL1 errors, ΔRL1, øRL1 are

$$-\Delta RL1 = y_{E5}$$

$$-\Phi RL1 = \phi_{E5}$$

Summary of deflection (in mm, radians) due to load, P, acting at position E (Joint J2):

$y_{E1} = 4.225 \times 10^{-6}$ P, $\phi_{E1} = 29.4 \times 10^{-9}$ P - bending main shaft C3.2
$\delta_{E1} = 1.012 \times 10^{-6}$ P, $\gamma_{E1} = 3.01 \times 10^{-9}$ P - shear " " C3.3
$y_{E2} = 0.215 \times 10^{-6}$ P, $\phi_{E2} = 6.47 \times 10^{-9}$ P - bending J3 housing C3.4
$\delta_{E2} = 0.356 \times 10^{-6}$ P, $\gamma_{E2} = 2.64 \times 10^{-9}$ P - shear " " C3.5
$\delta_{E3} = 0.726 \times 10^{-6}$ P, $\phi_{E3} = 24.2 \times 10^{-9}$ P - twisting J3 endplate C3.6
$y_{E6} = 29.44 \times 10^{-6}$ P shear + bending J2 shaft C3.9.3
$\delta_{E4} = 5.66 \times 10^{-6} P^{0.9}$, $\phi_{E4} = 35.5 \times 10^{-9} P^{0.9}$ bearings J1 & J3 C3.7
$\delta_{E5} = 1.23 \times 10^{-6} P^{0.9}$ rotary bearing J2 C3.9.1
$\delta_{E6} = 80.0 \times 10^{-6} P^{0.67}$ linear bearing J2 C3.9.2.
$y_{E5} = 3.30 \times 10^{-6}$ P, $\phi_{E5} = 22.9 \times 10^{-9}$ P bending baseplate etc. C3.8.

Thus after replacing P by F_{3L} of general rotation, see Fig.6.2

$$\frac{\Delta RP2 = -(35.97 \times 10^{-6} F_{3L} + 6.89 \times 10^{-6} F_{3L}^{0.9} + 80.0 \times 10^{-6} F_{3L}^{0.67}) \text{ mm}}{\Phi RP2 = -(65.72 \times 10^{-9} F_{3L} + 35.5 \times 10^{-9} F_{3L}^{0.9}) \text{ radians}}$$

and similarly by replacing P by FY2 (see Fig.6.2)

$$\frac{\Delta RL1 = 3.30 \times 10^{-6} \text{ FY2 mm}}{\Phi RL2 = 22.9 \times 10^{-9} \text{ FY2 radians}}$$

C3.11 The force applied at joint J4 will also cause deflections at joint J2. Position of the force is denoted by G in Fig.C3.1..

The deflections are calculated using the same analysis as in section C3.1 -C3.8 (J2 bearing calculations do not apply).

$$\frac{-\Delta RP4 = \Delta RP2/4 = -11.84 \times 10^{-6} F_{4L} - 8.15 \times 10^{-6} F_{4L}^{0.9} \text{ mm}}{\Phi RP4 = \Phi RP2/4 = -171.2 \times 10^{-9} F_{4L} - 56.5 \times 10^{-9} F_{4L}^{0.9} \text{ rads.}}$$

$$\frac{\Delta RL1/4 = -5.14 \times 10^{-6} F_{4L} \text{ mm}}{\Phi RL1/4 = -42.2 \times 10^{-9} F_{4L} \text{ rads}}$$

where F_{4L} is the lateral force on R4 at joint J4

and $\Delta RL1/4$ is the deflection of RL1 due to F_{4L} etc.

C3 .12 Deflection of slider link R4 connection to pantograph, at joint J4 (causing RL4 type errors).

The joint, J4, of link R4 will deflect not only due to the direct load applied at J4, G in Fig.C3.1, but also due to the resultant slope at joint J2, of the main eccentric shaft, baseplate and joint J3 housing of link R4.

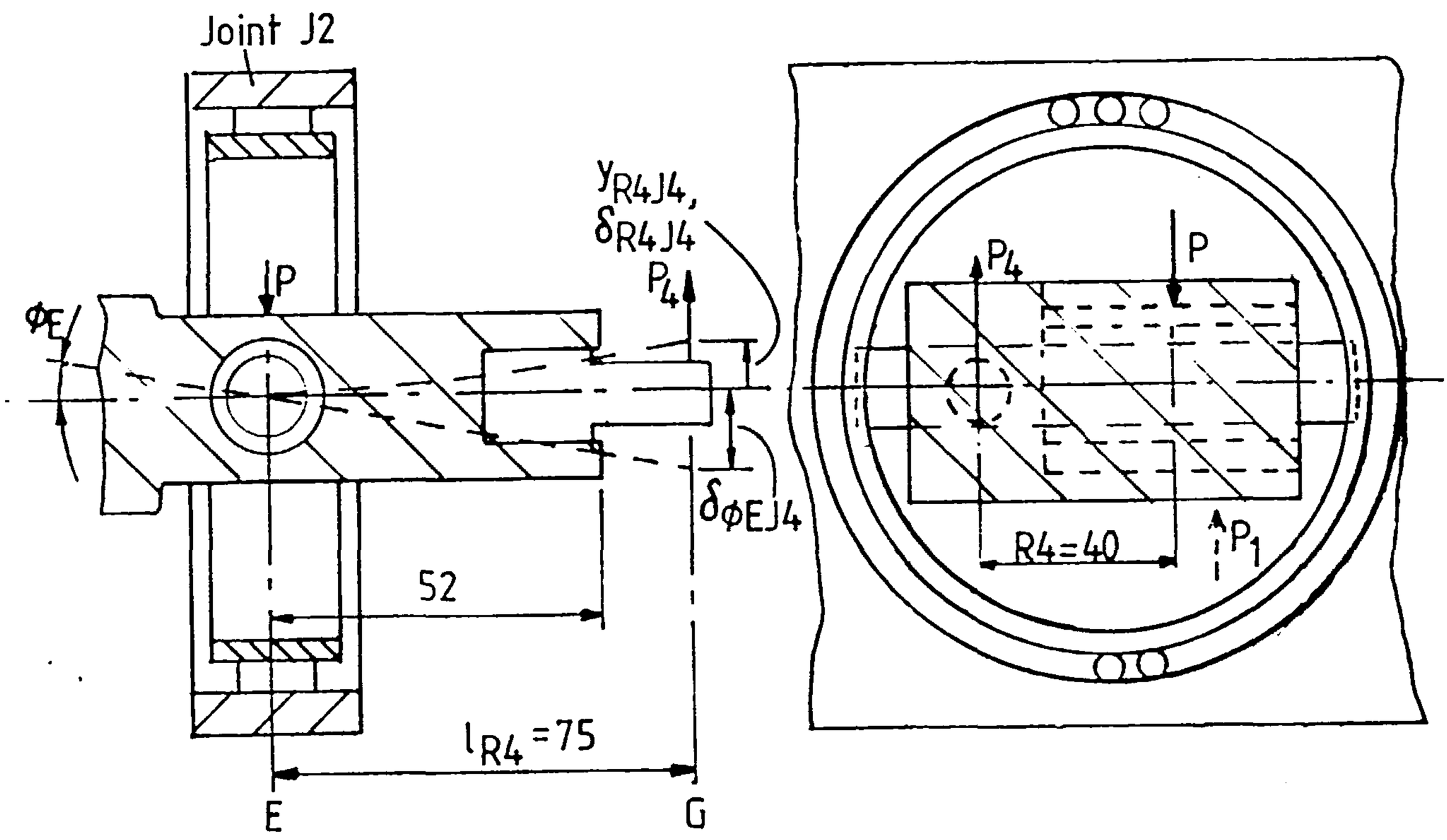

Fig. C3.12 Sketch of slider link, R4, and deflections.

The slider link R4 is shown in Fig.C3.12 with the deflection system superimposed. The slider assembly is shown in more detail in Drawing Nos. 1,2 and 5.

The displacement due to slope ϕ_E of main shaft, $\delta_{\phi E\ J4} = \phi_E . \ell_{R4}$

where ℓ_{R4}, the coplanar distance between joints J4 and J2 = 75 mm.

From C3.10 $\quad \phi_E = 65.72 \times 10^{-9} P + 35.47 \times 10^{-9} P^{0.9}$

and C3.11 $\quad -(171.2 \times 10^{-9} P_4 + 56.5 \times 10^{-9} P_4^{0.9})$ radians

thus $\quad \delta_{E\phi J4} = 4.93 \times 10^{-6} P + 2.66 \times 10^{-6} P^{0.9}$

$\quad -(12.84 \times 10^{-6} P_4 + 4.24 \times 10^{-6} P_4^{0.9})$ mm

The displacement , y_{R4J4} and δ_{R4J4} of link R4, due to bending and shear respectively between J4 and J2,is approximated by treating as a cantilever of length, 75 mm, fixed at E,or J2,but of two differenct cross-sections.

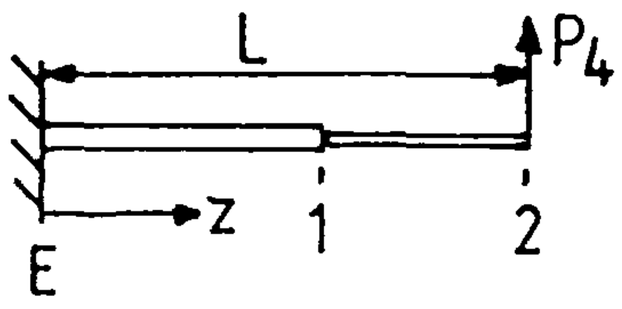

$$y_1 = \frac{P_4}{EI_1}\left(\frac{LZ^2}{2} - \frac{Z^3}{6}\right), \quad y_2 = \frac{P_4}{3EI_2}(L-Z)$$

$$\phi_1 = \frac{P_4}{EI_1}\left(LZ - \frac{Z^2}{2}\right),$$

$I_1 = 3.1 \times 10^5$ mm^4, $\quad Z = 52$

$I_2 = 1.0 \times 10^4$ mm, $(L-Z) = 23$

$y_{R4J4} = y_1 + \phi_1 (L-Z) + y_2 = 4.09 \times 10^{-6} P_4$ mm

Displacement due to shear

$$\delta = \frac{P.Z}{A_1 G} + \frac{P(L-Z)}{A_2 G} \qquad A_1 \quad 1.05 \times 10^3, \quad A_2 = 400 \text{ mm}^2$$

$\delta_{R4J4} = 1.338 \times 10^{-6} P_4$

Using general notation of Fig.6.3, and putting $P = F_{3L}$ and $P_4 = -F_{4L}$

$$\Delta_{RL4} = \delta_{E\phi J4} - y_{R4J4} - \delta_{R4J4}$$

$$\Delta_{RL4} = \underline{18.27 \times 10^{-6} F_{4L} + 4.24 \times 10^{-6} F_{4L}^{0.9}}$$
$$\underline{+ 4.93 \times 10^{-6} F_{3L} + 2.66 \times 10^{-6} F_{3L}^{0.9}} \quad \text{mm}$$

Similarly, deflections in axial direction of R4 are given by

$$y_{R4} = 7.95 \times 10^{-6} F_{4A} \text{ mm}, \quad \delta_{R4} = 1.338 \times 10^{-6} F_{4A} \text{ mm}$$

$$\underline{\Delta_{R4} = 22.13 \times 10^{-6} F_{4A} + 4.24 \times 10^{-6} F_{4A}^{0.9} \text{ mm}}$$

where F_{4A} is the axial force on R4 at joint J4.

C3.13 Simplifying assumptions of the pantograph deflection analysis.

The pantograph layout is shown in Drawing No.6. The linkages are arranged to minimise the co-planar distances between planes of motion of each link. However there will be out-of-plane forces producing couples on links. Figures C3 .15, - .16, -.17, -.18 and -.19 show free body diagrams of the links with the loads resolved into two forces and two couples, acting at each joint in directions parallel and perpendicular (orthogonal) to the axis of each link.

The ensu ing analysis derives formulae expressing the deflections, (due to bending, tension, shear, and torsion of links and bearing deformations) in the same orthogonal directions.

Assumptions for parameter allocation.

Two major approximations are made to simplify the calculation of deflections and their allocation to kinematic parameters for the computer analysis. They are both based on the approximation that the distortion of the pantograph geometry during motion is sufficiently small to be ignored and therefore links L2 and L3 remain perpendicular to each other and to links L1 and L4 respectively. Also the forces on links L2 and L3 must always be aligned axially with the links. Thus the simplifications are

1) the component forces on links L1 and L4 can be expressed in terms of the direct forces on links L3 and L3 (the differences due to link inertias are assumed to average out).
2) the deflections of links L1 and L4 (to parameters P1, P2, PL2, P3, P6 and PL6) can also be expressed in terms of deviations to links L2 and L3 only (that is P4 and P5 deviations).

Thus all the pantograph deflections are approximated by two formulae expressing deviations of P4 and P5 in terms of the forces on L2 and L3, F_5 and F_9. In the subsequent formulae of Apps. C3.15 - .19, the allocations are given in parentheses.

Simplifying assumptions in derivation of formulae.

Some assumptions also need to be made concerning the calculation of the couples acting at the joints since the problem is statically

indeterminate. For instance the couples acting on link L1 at joints J4, J5 and J6 will depend on the relative stiffnesses of these joints and the links to which they connect L1. For the layout of Drawing No.6 the stiffnesses are difficult to assess.

The analysis can be simplified and the design improved if one of the joints is deliberately made much stiffer than the others in order to provide all the resistance to overturning. In this way the calculation of a single couple at the stiffened joint becomes statically determinate, and the other joints are assumed to be subjected to direct forces only.

Of the various choices, joint J6 has been chosen in the analysis, and its redesign using a double row (or even, taper roller bearings) is suggested. Furthermore, if the joint at J4 connecting the pantograph to the generating mechanism link R4 is also fitted with a self-aligning bearing, either needle roller or plain (SKF supply preloaded self-aligning plain bearings), this will enhance the basis for the single couple assumption: any misalignment due to the deflecting slope of the generating mechanism main shaft will not be able to induce a couple at J4. Various other assumptions are made throughout the analysis when selecting basic bending and shearing formulae etc.

C3.14. Pantograph bearings deflection formulae.

.14.1 Bearing deflections in joints J9 and J8.

The bearings are SKF Taper roller designation 32009 XC.

The analysis is similar to that of section C3.1.7.

$$\delta = \frac{1}{2\varepsilon} \left(\frac{W}{ZK_n J_{r\varepsilon}} \right)^{0.9} \cos\alpha^{-1.9} \text{ mm}$$

where W = load in Newtons

Z = number of rollers = 23

ℓ = length of roller = 14.00 mm

$K_n = 3.64 \times 10^4 \ \ell^{0.89} = 3.812 \times 10^5$

α = contact angle = 14.1 degrees

ε, $J_{r\varepsilon}$ are tabulated by Houghton[25] against C_d/δ_o

$$\frac{\delta}{W^{0.9}} = \frac{2.99 \times 10^{-7}}{\varepsilon} \left(\frac{1}{J_{r\varepsilon}}\right)^{0.9}$$

Since expected deformations are relatively small, of order of 0.1 μm, and expected preload will be at least 10 x greater, use $C_d/\delta_o = -10$ which gives

$$\delta = 0.85 \times 10^{-6} \; W^{0.9} \text{ mm}$$

.14.2 Bearing deflections in joints J4, J5, J6.

These are needle roller bearings to INA designation RNA 4904 or (J6) RNA 6904 - same formula per row. Again use formulae of C3 7 length,

ℓ = 11.8 mm, thus $K_n = 3.274 \times 10^5$, α = 0 degrees

Z = 19.

For zero clearance and preload, use $\delta = 2.71 \times 10^{-6} \; W^{0.9}$ mm

for interference ≧ 2x deflection, use $\delta = 1.32 \times 10^{-6} \; W^{0.9}$ mm.

.14.3 Bearing deflection in joint J7.

Needle roller bearing RNA 4906, ℓ = 11.8, Z = 26

for zero clearance $\delta = 2.05 \times 10^{-6} \; W^{0.9}$

for interference ≧ 2x deflection $\delta = 1.0 \times 10^{-6} \; W^{0.9}$

C3.15. Deflection of pantograph link L4 assembly, and allocation to P4 and P5 type errors.

Figure C3.15 shows the forces and couples resolved in the directions of links L2 and L3 (or P4 and P5).

.15.1 Bending of rectangular section link L4 only, in-plane of operation.

Treat as simply supported beam, with deflection y_{5L4} at centre (joint J9) in direction of P5.

$$y_{5L4} = \frac{F_9 . \ell^3}{48EI}$$ where length ℓ = 150 mm.

inertia $I = 20 \times 50^3/12 = 2.08 \times 10^5$ mm^4

$E = 207 \times 10^3$ Nmm^{-2}

$\therefore$ $y_{5L4} = 1.63 \times 10^{-6} . F_9$ mm (Allocate as; - P5 error).

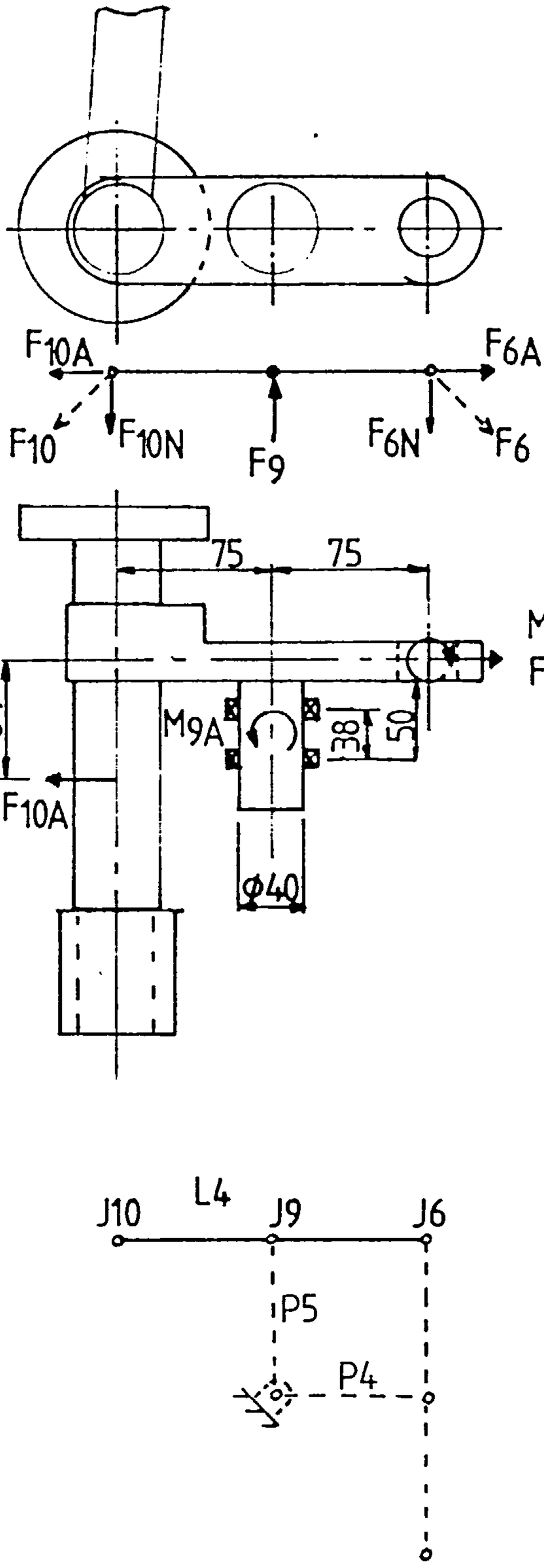

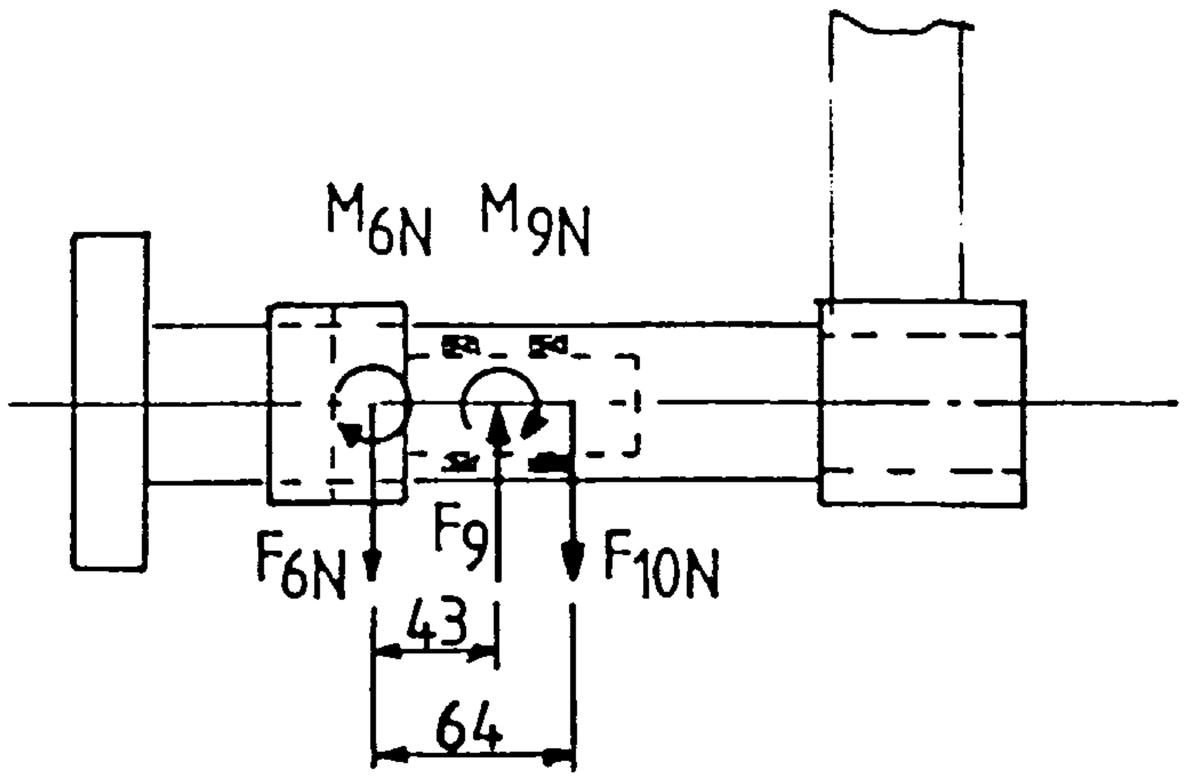

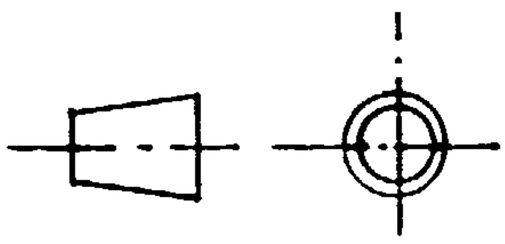

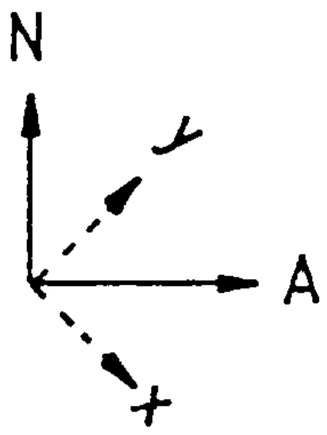

Fig. C3.15 Forces and Couples acting on LINK L4

.15.2 Bending of P6 part of L4 in plane perpendicular to P5, due to couple of $F_{10A} = F_{10A}.64$ Nmm. This will cause effective displacement of J10 (grinding wheel) in axial direction of link due to slope of P6 and overhang of grinding wheel.

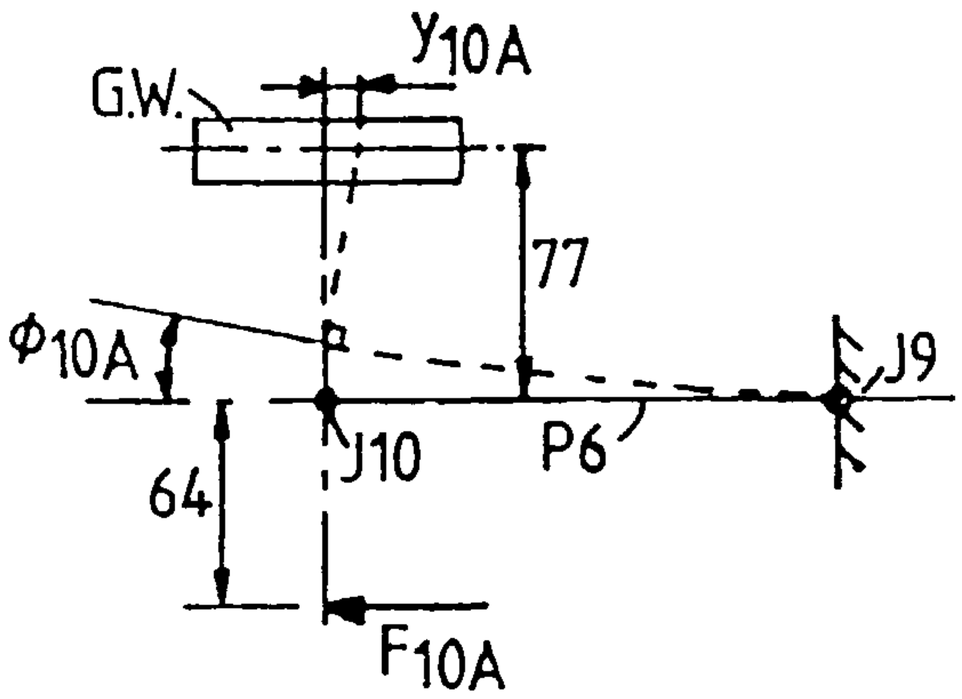

$$\phi_{10A} = \frac{M\ell}{EI}$$

$$y_{10A} = \phi_{10A} \cdot 77$$

$\ell = 75$ mm

$I = 3.33 \times 10^{4}$ mm^4

$E = 207 \times 10^{3}$ Nmm^2

$M = 64.F_{10A}$

$F_{10A} \simeq 0.5\ F_9$

$$\phi_{10A} = 6.96 \times 10^{-7}\ F_{10A} \text{ rads}$$

$$\underline{y_{10A} = 26.8 \times 10^{-6}\ F_9 \text{ (x 0.5, + P4 error)}}$$

.15.3 Uni-axial deflection of L4 due to forces F_{10A} F_{6A}.

Mean value $(F_{10a} + F_{6A})/2 \simeq F9/2$

$$\therefore \quad \delta_{AL4} = \frac{F_9 \times 0.5 \times \ell}{h.b.E}, \quad \ell = 150 \text{ mm}, \ h = 50, \quad b = 20$$

$$\underline{\delta_{AL4} = 0.36 \times 10^{-6}.\ F_9 \text{ mm} \quad (\text{x } 0.5, - \text{ P4 error})}$$

.15.4 Twisting of P6 part of L4 due to couple $F_{10N}.64$.

Assume fixed at J9.

Angle of twist $\theta_{L4} = \frac{M\ell}{GI_p}$, $M = F_{10N} \times 64$ Nmm

where ℓ = length P6 = 75 mm

G = torsion modulus = 80×10^{3} Nmm^2

I_p = polar moment of area = $\frac{bh^3}{12} + \frac{b^3h}{12} = 2.42 \times 10^{5}$ mm^4.

Deflection of J10 at grinding wheel, y_{ML4}, in direction of P5

$$= \theta_{L4} \times \text{overhang} = \theta_{L4} \times 77$$

Thus after replacing $F_{10N} = 0.5\ F_9$

$$\theta_{L4} = 48.0 \times 10^{-9} \times F_9 \text{ rads}$$

$$\underline{y_{ML4} = 3.70 \times 10^{-6} \times F_9 \text{ mm}} \qquad (\times 0.5 = + \text{P5 error}).$$

.15.5 Shear deflection of L4 in P5 direction

$$\delta_s = \frac{F_9 . \ell}{2Gbh}, \quad \ell = 150 \text{ mm}, \ b = 20, \ h = 50, \ G = 80 \times 10^3$$

$$\underline{\delta_{5L4} = 0.94 \times 10^{-6} F_9} \qquad (- \text{P5 error})$$

.15.6 Deflection of shaft of joint J9 of link L4 due to bending in direction of P5.

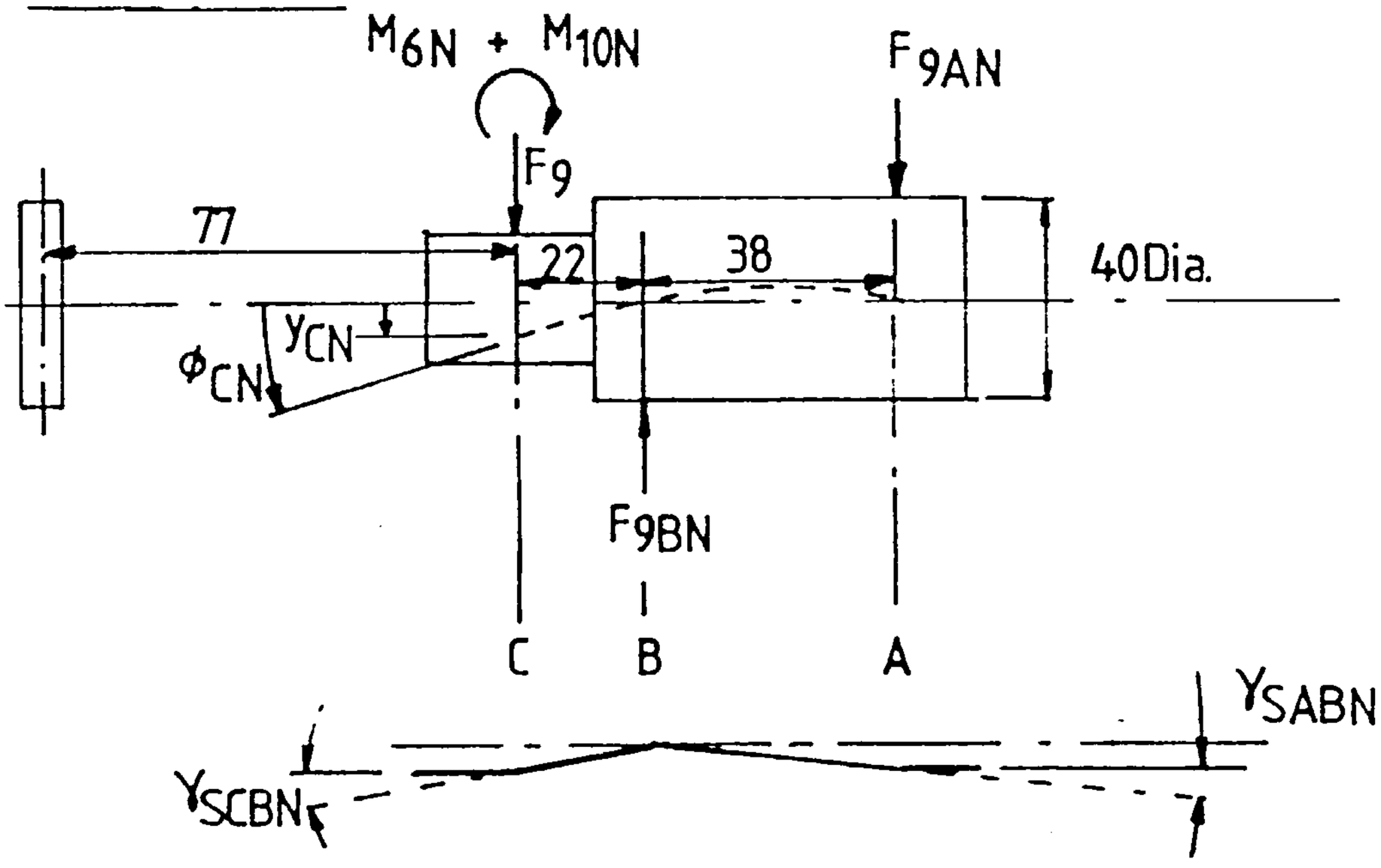

$$M_{10N} = F_{10N} \times 64, \quad M_{6N} = F_{4N} \times 55$$

$$I = \pi D^4/64 = 1.26 \times 10^5 \text{ mm}^4$$

$$F_{9AN} \times 38 = F_9 \times 22 - F_{10N} \times 64 - F_{4N} \times 55$$

If $F_{10N} = F_9/2 \simeq F_{4N}$, $F_{9AN} = -0.987 \times F_9$

$$F_{9BN} \times 38 = F_9 \times 60 - F_{10N} \times 64 - F_{4N} \times 55$$

$$\therefore \quad F_{9BN} = 0.013 \times F_9$$

$$y_{CN} = \frac{F_9}{EI}\left[- \frac{0.987}{6} (60^3 - 60 \times 38^2) - \frac{0.013}{6} \times 22^3 \right]$$

$$= -0.817 \times 10^{-6} F_9 \text{ mm}$$

$$\phi_{CN} = \frac{F_9}{EI}\left[- \frac{0.263}{2} (60^2 - \frac{38^2}{3}) - \frac{0.737}{2} \times 22^2 \right]$$

$$= -59.1 \times 10^{-9} F_9 \text{ rads.}$$

Effective deflection at grinding wheel = $2y_{CN} + \phi_{CN} \times 77$

$$= \underline{y_{s9N} = -6.18 \times 10^{-6} F_9 \text{ mm}} \quad (\times 0.5, -P_5 \text{ error})$$

$$\phi_{s9N} = -59.1 \times 10^{-9} F_9 \text{ rads.}$$

.15.7 Shear of shaft of J9 in L4

$$\gamma_s = \frac{\tau}{G} = \frac{F}{\pi d^2/4.G} = 13.2 \times 10^{-9} F \text{ rads}$$

$$\gamma_{sABN} = F_{9AN} \times 13.27 \times 10^{-9} \qquad \gamma_{sCBN} = F_9 \times 13.27 \times 10^{-9} \text{ rads}$$

$\therefore$ $\gamma_{sABN} = -13.1 \times 10^{-4} F_9$ rads

$$\gamma_{CN} = \gamma_{sCBN} + \gamma_{sABN} = 0.17 \times 10^{-9} F_9 \text{ rads}$$

$$\delta_{CN} = \gamma_{CN} \times 22 = 0.004 \times 10^{-6} F_9 \text{ mm}$$

Effective displacement at grinding wheel J10, $\delta_{s9N} = \gamma_{sABN} \times 77+2 \times \delta_{CN}$

$\underline{\delta_{s9N} = -1.0 \times 10^{-6} F_9 \text{ mm}}$, $\gamma_{s9N} = -13.1 \times 10^{-9} F_9$ rads .(x0.5,-P5 error).

.15.8 Similarly, for deflections of shaft of J9, in plane perpendicular to P5

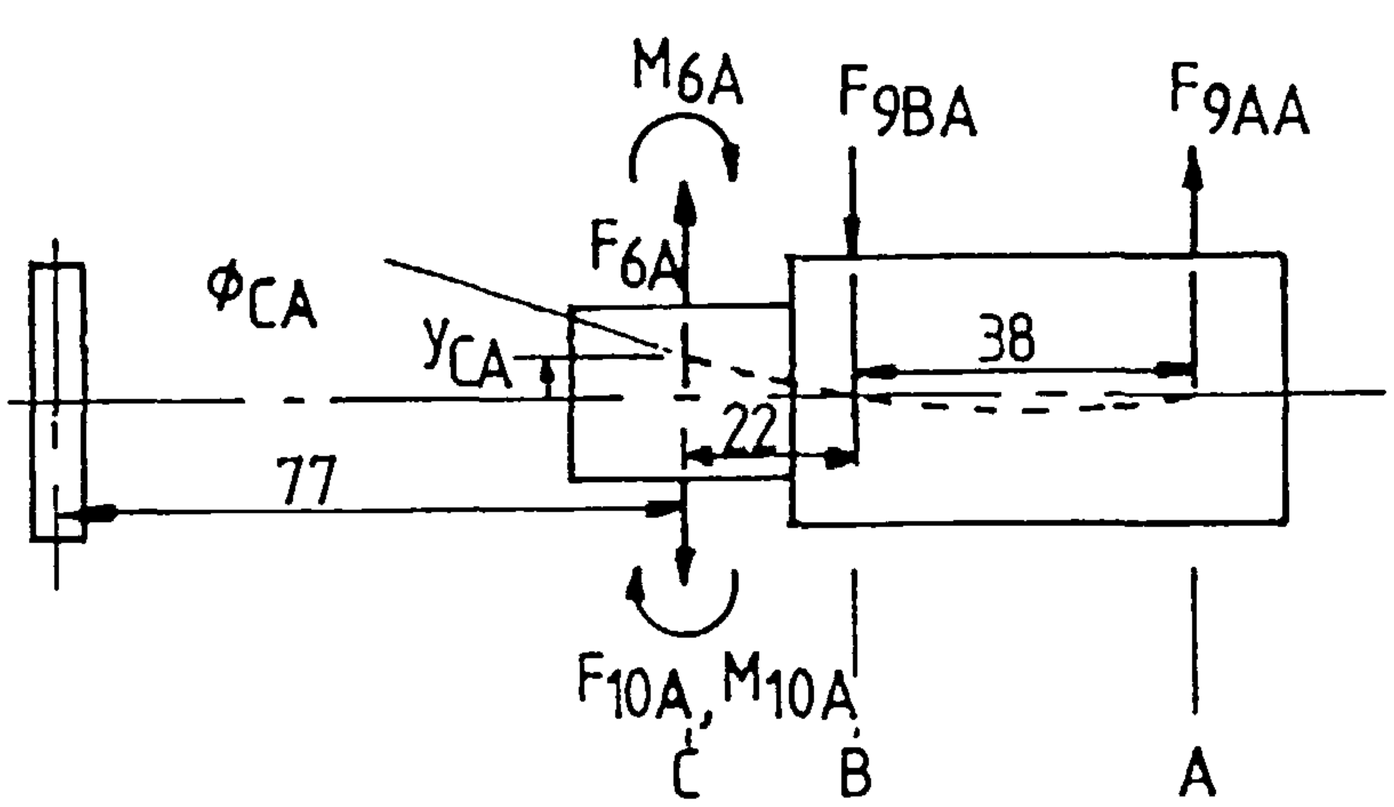

$$M_{10A} = F_{10A}.64, \quad M_{6A} = F_{4A} \times 55$$

Take moments about A, $F_{9BA} \times 38 = F_{4A} \times 55 + F_{10A} \times 64$.

Assume $F_{6A} \simeq F_{10A} \simeq 0.5\, F_9 \simeq F_{4A}$

$$\therefore \quad F_{9BA} = 1.57\, F_9$$

Similarly moments about B, $F_{9AA} \times 38 = F_{4A} \times 55 + F_{10A} \times 64$

$$\therefore \quad F_{9AA} = 1.57 \times F_9$$

$$y = \frac{1}{EI}\left[\frac{F_{9AA}}{6}(z^3 - za^2) - \frac{F_{9BA}}{6}\langle z-a\rangle^3\right]$$

$$\phi = \frac{1}{EI}\left[\frac{F_{9AA}}{2}\left(z^2 - \frac{a^2}{3}\right) - \frac{F_{9BA}}{2}\langle z-a\rangle^2\right]$$

At centre line of link L4, position C, $z = 60$, $a = 38$, $F_{9AA} = F_{9BA} = 1.57\, F_9$

$$y_{CA} = 1.9 \times 10^{-6}\, F_9 \text{ mm}$$

$$\phi_{CA} = 79.0 \times 10^{-9}\, F_9 \text{ rads.}$$

Effective deflection at grinding wheel $= + \phi_{CA} \times 77$

$$= \underline{y_{s9A} = 6.08 \times 10^{-6}\, F_9 \text{ mm} \quad (\times 0.5, + \text{P4 error})}$$

$$\phi_{s9A} = \phi_{CA} = 79.0 \times 10^{-9}\, F_9 \text{ rads.}$$

.15.9 Shear deflections

$$\gamma_s = 13.27 \times 10^{-9}\, F \text{ rads. from section (.6)}$$

$$\gamma_{AB} = 13.27 \times 10^{-9}\, F_9 \times 1.57 = 20.8 \times 10^{-9}\, F_9$$

At grinding wheel

$$\underline{\delta_{s9A}} = \gamma_{AB} \times 77 = \underline{1.6 \times 10^{-6}\, F_9 \text{ mm} \quad (0.5, \text{ P4 error})}$$

$$\gamma_{s9A} = 20.8 \times 10^{-9}\, F_9 \text{ rads.}$$

.15.10 Deflection due to bearings of joint J9 in direction of P5.

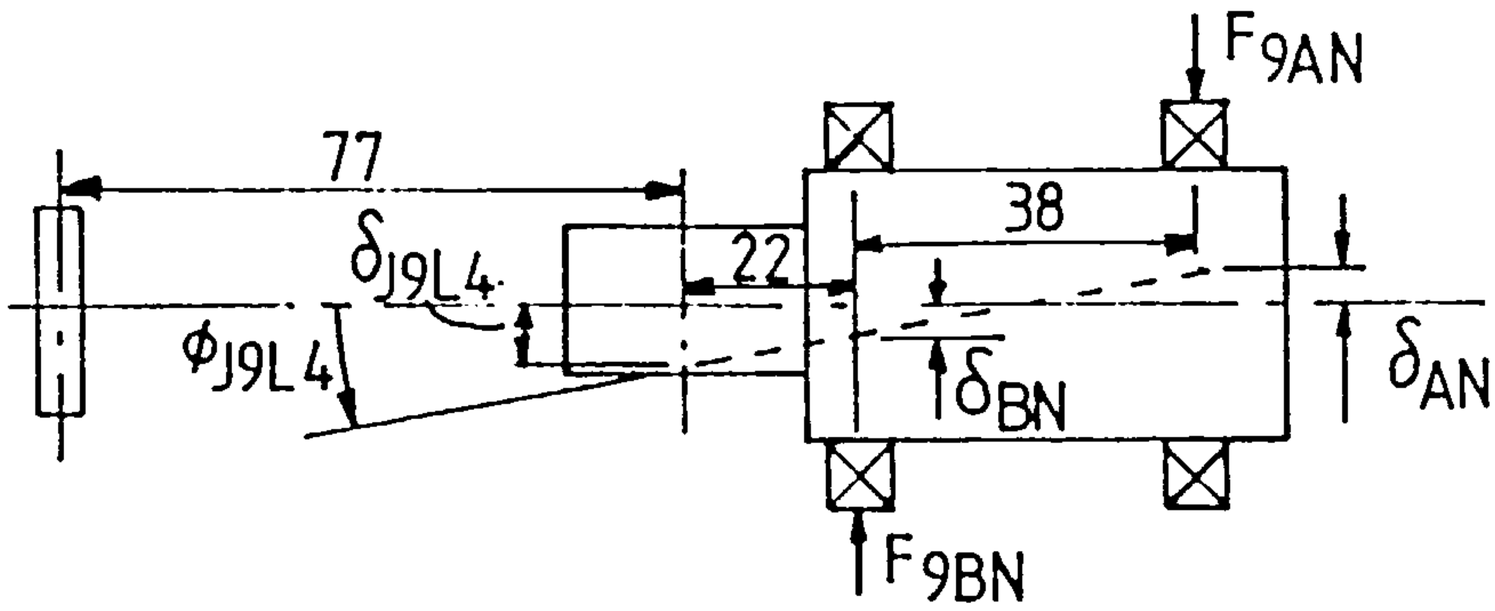

where $F_{9AN} = - 0.987 \times F_9$

$F_{9BN} = 0.013 \times F_9$

Deflection of link L4 at J9

$$\delta_{J9L4} = \delta_{BN} \cdot \frac{22 + 38}{38} + \delta_{AN} \frac{22}{38}$$

From C3.14.1

$\delta = 0.85 + 10^{-6} W^{0.9}$

$\delta_{AN} = 0.85 \times 10^{-6} \times (0.987 \times F_9)^{0.9} = 0.840 \times 10^{-6} F_9^{0.9}$ mm

$\delta_{BN} = -0.85 \times 10^{-6} \times (0.013 \times F_9)^{0.9} = -0.017 \times 10^{-6} F_9^{0.9}$ mm

$\delta_{J9L4} = 0.4595 \times 10^{-6} F_9^{0.9}$

slope, $\phi_{J9L4} = (\delta_{BN} + \delta_{AN})/38 = 21.6 \times 10^{-9} F_9^{0.9}$ radians.

Effective error at grinding wheel J10, $\delta_{J9N} = 2 \times \delta_{J9L4} + \phi_{J9L4} \times 77$

$\delta_{J9N} = 2.59 \times 10^{-6} F_9^{0.9}$ mm (x0.5, P5 error)

$\phi_{J9N} = 21.6 \times 10^{-9} F_9^{0.9}$ rads.

.15.11 Deflection of bearings of J9 in direction of P4.

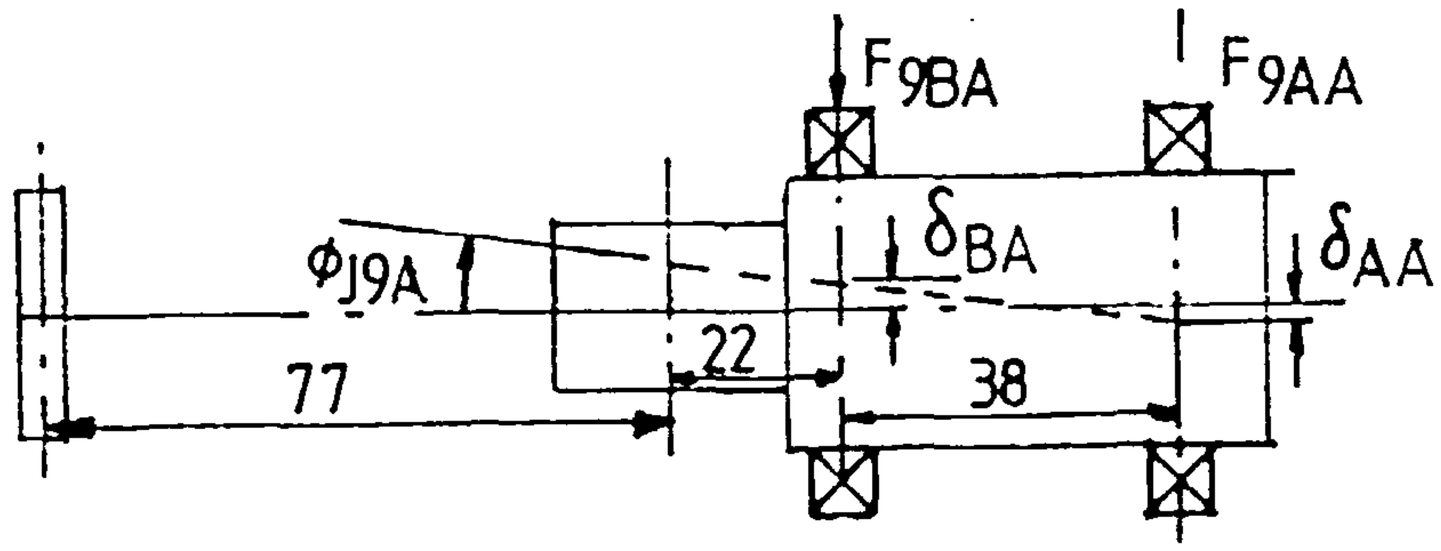

$$F_{9AA} = F_{9BA} = 1.57 \times F_9$$

$$\delta_{J9A} = \delta_{BA}\,(22 + 38)/38 + \delta_{AA}\,22/38$$

$$\delta_{BA} = -1.36 \times 10^{-6}\, F_9^{0.9}, \quad \delta_{AA} = -1.36 \times 10^{-6}\, F_9^{0.9}$$

slope $\phi_{J9A} = (\delta_{AA} + \delta_{BA})/38 = -71.5 \times 10^{-9}\, F_9^{0.9}$

At grinding wheel, $\underline{\delta_{J9A}} = \phi_{J9A} \times 77 = \underline{-5.51 \times 10^{-6}\, F_9^{0.9}}$ mm (x0.5, -P4 error)

.15.12 Twisting of P3 part of L4 due to moments applied at joint J6 in plane normal to P4.

Moment $M_{6N} \simeq F_{4N} \times 55 = F_9 \times 27.5$

Assume as cantilever fixed at joint J9 of link L4.

Polar moment of inertia, $I_p = (20 \times 50^3 + 50 \times 20^3)/12 = 2.42 \times 10^5$ mm^4

Angle of twist at J6

$$\theta_{L46} = \frac{M\ell}{GI_p} = \frac{F_9 \times 27.5 \times 75}{80 \times 10^3 \times 2.42 \times 10^5}$$

$$= 106.7 \times 10^{-9}\, F_9 \text{ radians.}$$

This will rotate link L1, to give an effective deflection at joint

J4 = θ_{L46} x (coplanar distance = 55)

$$= \underline{\delta_{J4L4} = 5.87 \times 10^{-6}\, F_9 \text{ mm}} \text{ (x0.5, -P5 error).}$$

Joint J5 is in same plane as J6 therefore no effect.

.15.13 Bending of P3 part of L4 due to moment applied at joint J6 in plane normal to P5.

Assume as cantilever fixed at joint J9 of link L4

Second moment of inertia I, = 50 x $20^3/12$ = 3.33 x 10^4 mm^4

slope at J6, $\phi_{6A} = \frac{M\ell}{EI}$, ℓ = 75, M = M_{6A} = F_9 x 27.5

= 299.0 x 10^{-9} F_9 rads.

Effective deflection occurring at joint J4 =

y_{J4L4} = ϕ_{6A} x 55

= 16.44 x 10^{-6} F_9 mm (x0.5, -P4 error).

C3.16 Deflections of pantograph link L3 (See Fig.C3.16 for forces etc.)

.16.1 Axial compression of link L3

Cross-section area at joint J9 and J8

= (80-68) x 45 = 540.0 mm^2

Cross-section area at midpoint of link

= 65 x 45 = 2925.0 mm^2.

Assume cross-section changes linearly with length, then average cross-section = (2925.0 + 540.0)/2

= 1732.5 mm^2

Axial deflection in direction of (-P5)

$\delta_{5L3} = \frac{F_8 \times \ell}{1732.5 \times E}$ length, ℓ = 75 mm, E = 207 x 10^3 Nmm^2

= 0.209 x 10^{-6} F_8 mm (-P5 error).

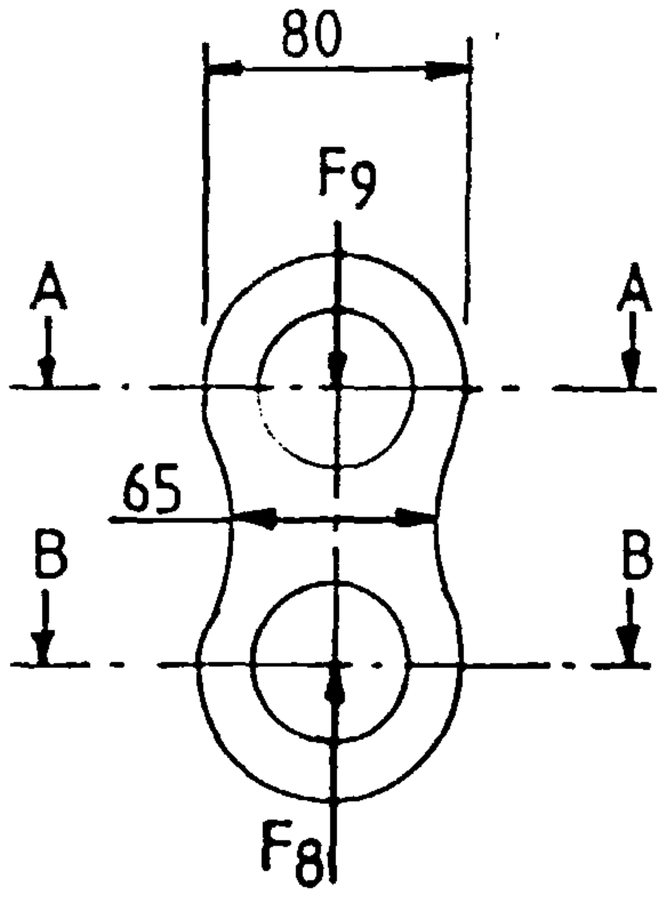

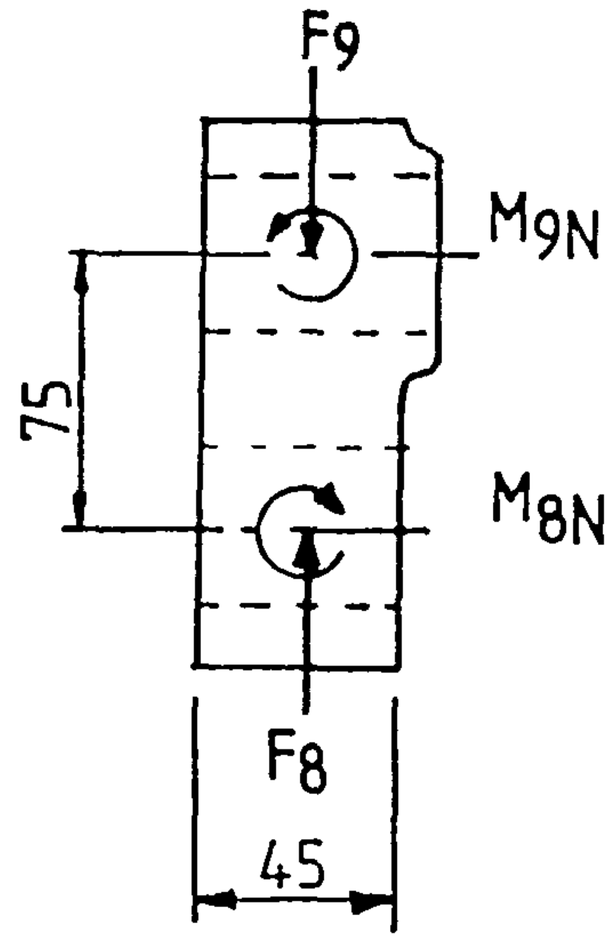

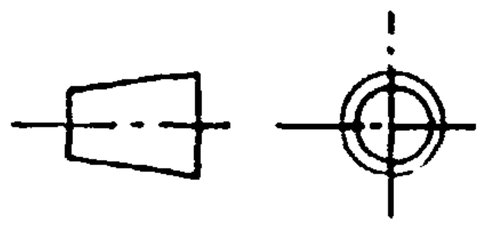

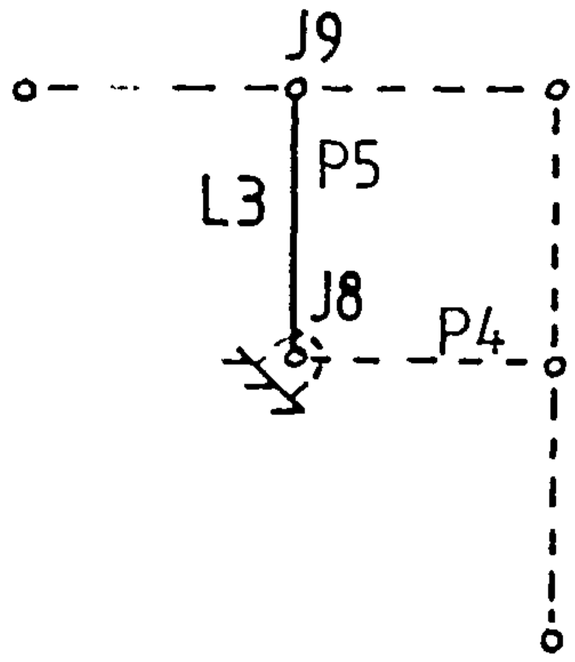

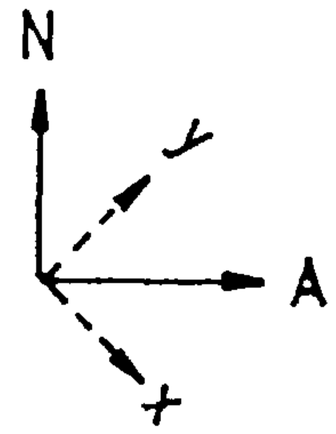

Fig. C3.16 Forces and Couples acting on LINK L3

.16.2 Torsion of link L3

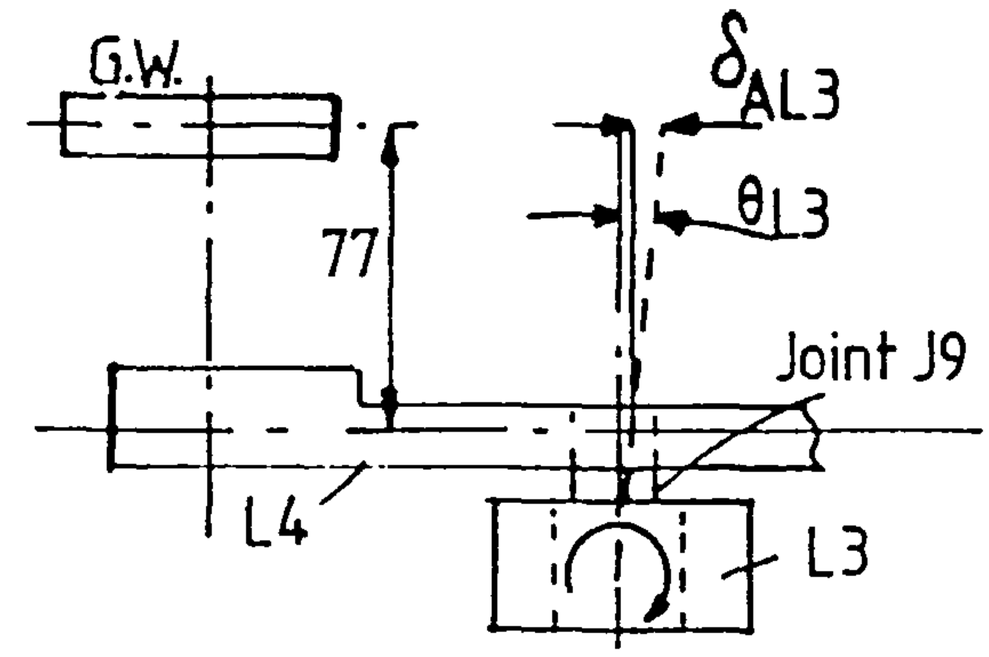

$$M_{9A} = M_{10A} + M_{6A}$$

$$M_{10A} = F_{10A} \times 64 = F_9 \times 32$$

$$M_{6A} = F_{4A} \times 55 = F_9 \times 27.5$$

$$\theta_{L3} = \frac{M_{9A}\,\ell}{G\,I_p},$$

Length ℓ = 75mm, rigidity modulus $G = 80 \times 10^3$ Nmm^{-2}

At joints, $I_p = (80^3 - 68^3) \times 45/12 + (80-68) \times 45^3/12 = 8.32 \times 10^5$ mm^4

At midlink, $I_p = 65^3 \times 45/12 + 65 \times 45^3/12 = 15.20 \times 10^5$ mm^4

As approximation take $I_p = (8.32 + 15.20 + 8.32)/3 \times 10^5 \simeq 10 \times 10^5$ mm^4.

Angle of twist $\theta_{L3} = 55.78 \times 10^{-9} F_9$ radians.

Effective deflection w.r.t grinding wheel, $\delta_{AL3} = \theta_{L3} \times 77$

$$\underline{\delta_{AL3} = 4.30 \times 10^{-6} F_9 \text{ mm (x0.5, P4 error)}}$$

.16.3 Bending of link L3 in plane perpendicular to P4, due to couple M_{9N}

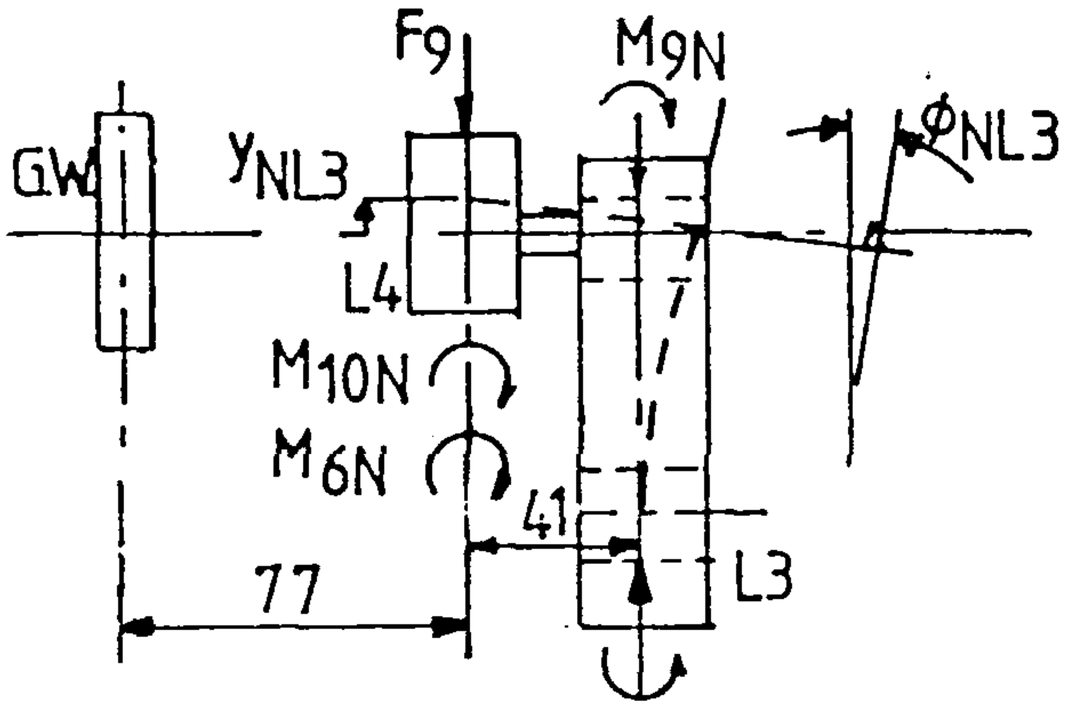

$$M_{9N} = M_{10N} - F_9 \times 41 + M_{6N}$$

$$= F_9 \times 32 - F_9 \times 41 + F_9 \times 27.5$$

$$= F_9 \times 18.5 \text{ Nm}$$

$$\phi = \frac{M\ell}{EI}, \quad \ell = 75$$

I at joints = $(80-68) \times 45^3/12 = 0.911 \times 10^5$ mm^4

at midlink = $65 \times 45^3/12 = 4.936 \times 10^5$ mm^4

Assume thickness varies from 12 to 65 linearly

$\therefore$ I varies linearly, and take average value

$$I = 2.92 \times 10^{5} \text{ mm}^4$$

$$\phi_{NL3} = 22.95 \times 10^{-9} F_9 \text{ rads.}$$

$$y_{NL3} = \phi_{NL3} \times 41 = 0.941 \times 10^{-6} F_9 \text{ mm}$$

Effective displacement at grinding wheel ($= 2y_{NL3} + \phi_{NL3} \times 77$)

$$\underline{y_{NL43} = 3.65 \times 10^{-6} F_9} \quad (\times 0.5, \text{ P5 error}).$$

.16.4 Deformation of bearings of joint J8 in direction P5.

Assume reactions same as for J9, see C3.15.10

$\therefore$ effective displacement of grinding wheel also identical

$$\delta_{J8N} = \delta_{J9N}, \quad \phi_{J8N} = \phi_{J9N}$$

$\therefore$ $$\underline{\delta_{J8N} = 2.59 \times 10^{-6} F_9^{0.9} \text{ mm}} \quad (\times 0.5, \text{ P5 error})$$

$$\phi_{J8N} = 21.6 \times 10^{-9} F_9^{0.9} \text{ radians.}$$

.16.5 Deformation of bearings of joint J8 in direction P4

$$\delta_{J8A} = \delta_{J9A}, \quad \phi_{J8A} = \phi_{J9A} \quad \text{see C3.15.11.}$$

$\therefore$ $$\underline{\delta_{J8A} = -5.51 \times 10^{-6} F_9^{0.9}} \quad (\times 0.5, -\text{P4 error})$$

$$\phi_{J8A} = -71.5 \times 10^{-9} F_9^{0.9}$$

C3.17 Deflections of link L1

The application of forces is shown in Fig. C3.17.

.17.1 Bending in plane of operation, in direction of P4.

For simply supported beam, deflection at centre;

$$y_{4L1} = \frac{F_5 \ell^3}{48EI}, \qquad \ell = 150 \text{ mm}$$

$$I = 20 \times 35^3/12 = 7.146 \times 10^4 \text{ mm}^4$$

$$E = 207 \times 10^3 \text{ Nmm}^{-2} \text{ for steel}$$

thus $$\underline{y_{4L1} = 4.75 \times 10^{-6} . F_5 \text{ mm}} \text{ (-P4 error).}$$

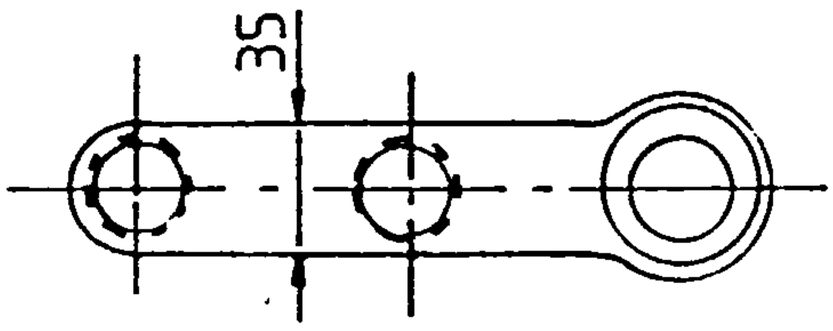

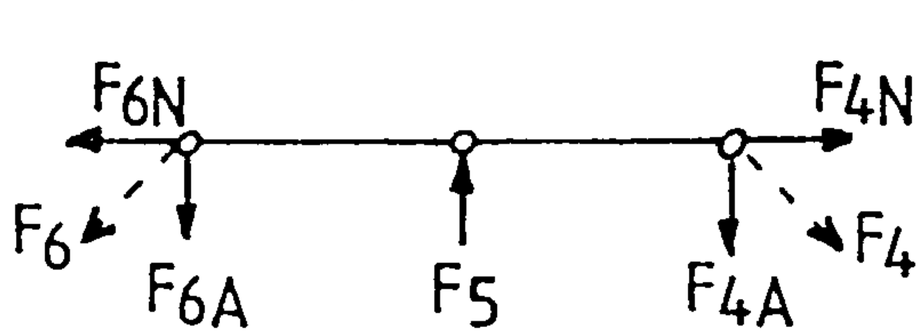

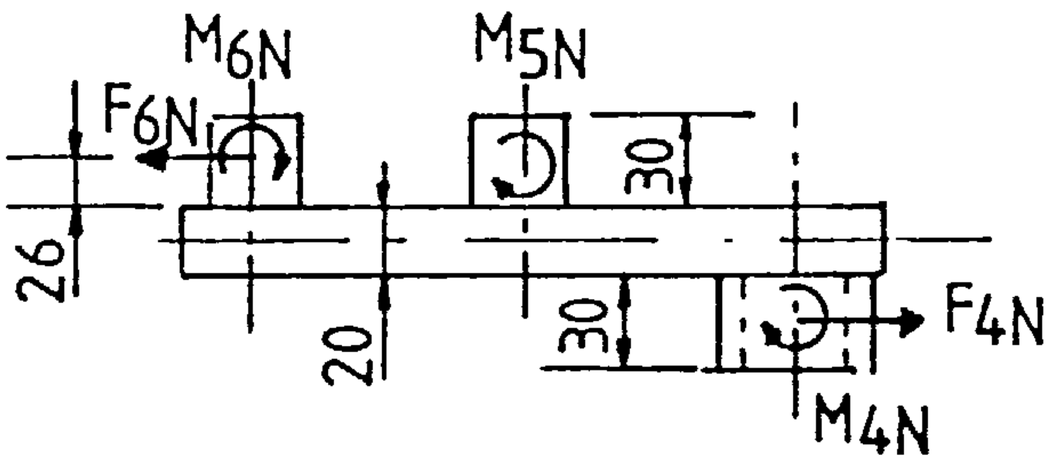

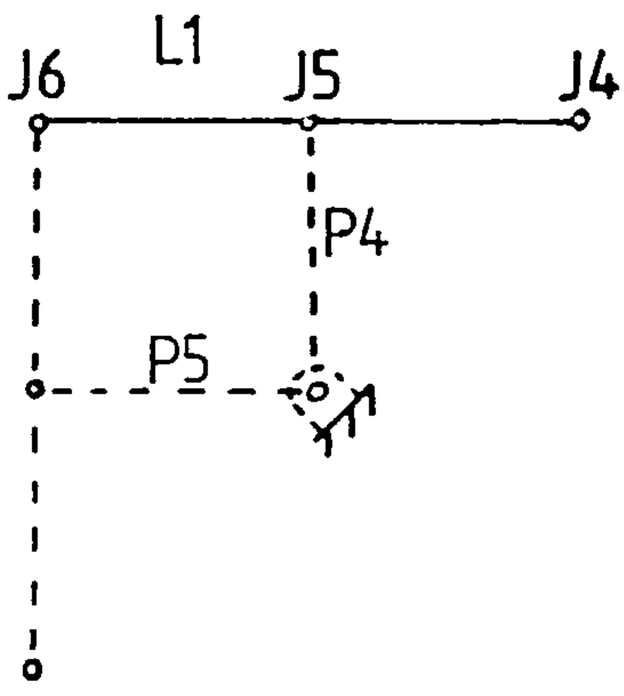

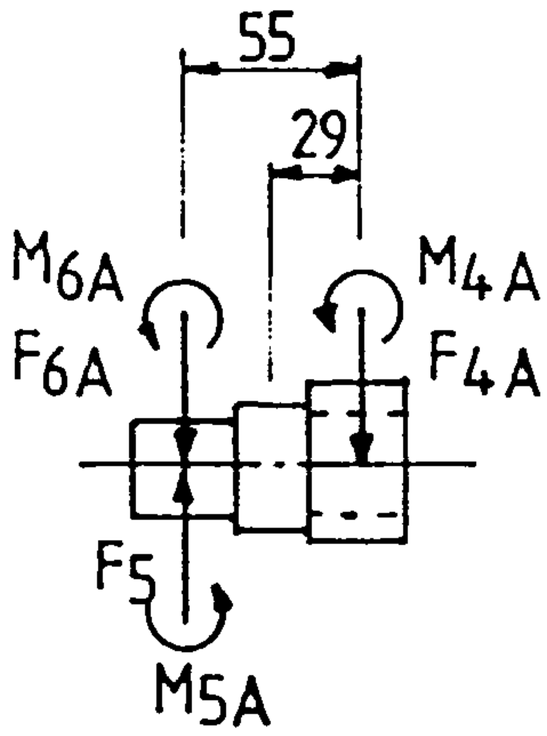

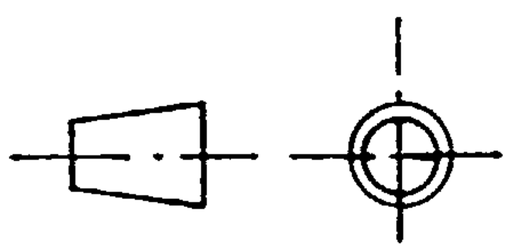

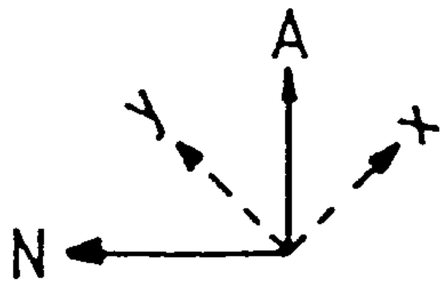

Fig. C3.17 Forces and Couples acting on LINK L1

.17.2 Shear of link L1 in direction of P4

For simply-supported beam, shear deflection at centre

$$\delta_{4L1} = \frac{1.5F_5}{2AG} \cdot \ell$$

ℓ = 75 mm

A = 20 x 35 = 700 mm^2

G = 80×10^3 N mm^{-2}

thus $\delta_{4L1} = 1.0 \times 10^{-6} F_5$ mm (-P4 error)

.17.3 Axial tension in direction of P5

mean force = $(F_{6N} + F_{4N})/2 \simeq F_5/2$

extension $\delta_{AL1} = \frac{F_5/2.\ell}{b.h.E}$ where ℓ = 150 mm

b = 20 mm

h = 35 mm

$\delta_{AL1} = 0.52 \times 10^{-6} F_5$ mm (x0.5, -P5 error).

.17.4 Twisting due to overhang of forces.

Angle of twist $\theta_{5L1} = \frac{M\ell}{GI_p}$, at joint J5 relative to J6

where $M = F_{4N}.29 + F_5.26 = 40.5 F_5$

ℓ = 75 mm, G = 80×10^3 N mm^{-2}

$I_p = \frac{bh^3}{12} + \frac{hb^3}{12}$, b = 20 mm, h = 35 mm

$I_p = 9.48 \times 10^4$ mm^4

$\theta_{5L1} = 400.5 \times 10^{-9} F_5$ radians.

$\therefore$ Deflection at joint J5 relative to J6, $y_{5L1} = \theta_{5L1} \times 26$

$y_{5L1} = 10.4 \times 10^{-6} F_5$ mm.

Similarly the angle of twist of J4 relative to J5, θ_{4L1} is found by putting $M = F_{4N}.29 = 14.5 F_5$ in formula

$\theta_{4L1} = 143.4 \times 10^{-9} F_5$ rads.

the deflection of J4 relative to J6,

$$y_{4L1} = -(\theta_{5L1} + \theta_{4L1}) \times 29$$

$$y_{4L1} = -15.77 \times 10^{-6} F_5 \text{ mm}$$

(total P4 error due to twisting = $-y_{5L1} + y_{4L1}/2$

$$y_{ML1} = -18.29 \times 10^{-6} F_5 \text{ mm} \quad (+ \text{P4 error}).$$

.17.5 Bending of link L1, in plane perpendicular to P4 direction.

Assume as cantilever fixed at J6, acted upon by moment

$$M = F_{4N} \times 29 \quad = F_5 \times 14.5$$

slope at J_4, $\phi_{NL1} = \frac{M\ell}{EI}$, $\ell = 150$ mm,

$$I = 35 \times 20^3/12 = 2.33 \times 10^4 \text{ mm}^4$$

$$= 450.3 \times 10^{-9}. F_5 \text{ radians.}$$

Deflection of J4, in direction of P5, $y_{NL1} = \phi_{NL1} \times 29$

$$y_{NL1} = 13.06 \times 10^{-6} F_5 \text{ mm (x0.5, -P5 error).}$$

.17.6 Bending of bearing shaft for joint J6.

Assume cantilever fixed at link centreline subject to forces F_{6N}, F_{6A} and couples M_{6N}, M_{6A} acting at centre of bearing, see Fig.C3.17.

Using slope $\phi = \frac{1}{EI}\left(M\ell + \frac{F\ell^2}{2} \right)$, deflection $y = \frac{1}{EI}\left(\frac{M\ell^2}{2} + \frac{F\ell^3}{3}\right)$

$$\ell = 26, \quad I = 1.92 \times 10^4 \text{ mm}^4$$

$$M_N = -M_{6N} = -F_{4N} \times 55 = -F_5 \times 27.5, \quad F_{6N} \simeq F_5/2$$

$$M_A = +M_{6A} = +F_{4A} \times 55 = +F_5 \times 27.5, \quad F_{6A} \simeq F_5/2$$

$$\phi_{6N} = -137.4 \times 10^{-9} F_5 \text{ rads.}$$

$$y_{6N} = -1.60 \times 10^{-6} F_5 \text{ mm (x0.5, -P5 error)}$$

$$\phi_{6A} = 222.0 \times 10^{-9} \text{ rads.}$$

$$y_{6A} = 3.08 \times 10^{-6} \text{ mm} \quad (\text{x0.5, -P4 error})$$

(y_{6N}, y_{6A} etc. - included in deflections in next Section,.17.7)

.17.7 Shear of bearing shaft for J6.

slope $\gamma_F = \frac{1.33F}{AG}$ $\quad \gamma_M = \frac{-1.33M}{AG\ell_B}$ $\quad \ell_B$ = distance between bearing reaction = 13mm

$\delta_F = \frac{1.33F\ell}{AG}$ $\quad _M = \frac{-1.33M/2}{AG}$ $\quad$ A = cross-section area = 491. mm^2

ℓ = 26 mm

$F = F_5/2, \quad M = -F_5 \times 27.5$

$\gamma_F = 16.93 \times 10^{-9} F_5, \quad \gamma_M = -71.63 \times 10^{-9} F_5$

$\delta_F = 0.44 \times 10^{-6} F_5, \quad \delta_M = -0.47 \times 10^{-6} F_5$

$\gamma_{6N} = \gamma_F + \gamma_M = -54.7 \times 10^{-9} F_5$ rads.

$\delta_{6N} = \delta_F + \delta_M = -0.03 \times 10^{-6} F_5$ mm (x0.5, -P5 error)

$\gamma_{6A} = \gamma_F - \gamma_M = 88.6 \times 10^{-9} F_5$ rads.

$\delta_{6A} = \delta_F - \delta_M = 0.91 \times 10^{-6} F_5$ mm (x0.5, -P4 error)

If it is assumed J6 shaft fixed, and calculate relative deflections at other joints.

Deflection of J5, due to deflection of J6 shaft

$$\underline{y_{56A}} = -(\gamma_{6A} + \phi_{6A}) \times 26 + (y_{6A} + \delta_{6A})$$

$$= -8.07 \times 10^{-6} F_5 \text{ mm} + 3.99 \times 10^{-6} F_5$$

$$= \underline{-4.08 \times 10^{-6} F_5 \text{mm}} \quad (+ \text{P4 error})$$

Deflection of J4, due to deflection of J6 shaft in P4 direction.

$$\underline{y_{46A}} = (\gamma_{6A} + \phi_{6A}) \times 29 + y_{6A} + \delta_{6A}$$

$$= \underline{13.0 \times 10^{-6} F_5 \text{ mm}} \quad (x0.5, -P4 \text{ error})$$

Deflection of J4, due to deflection of J6 shaft in P5 direction

$$\underline{y_{46N}} = (\gamma_{6N} + \phi_{6N}) \times 26 + y_{6N} + \delta_{6N}$$

$$= \underline{-6.62 \times 10^{-6} F_5 \text{ mm}} \quad (x0.5, + \text{P5 error})$$

y_{56N} has no effect.

.17.8 Bending and shear of shaft of joint J5 on L1.

Similar to that for shaft of J6 but with assumed zero moment

$$\phi = \frac{F_5 \ell^2}{2EI} \quad , \quad y = \frac{F_5 \ell^3}{3EI} \quad \text{bending}$$

$$\gamma = 1.33 \frac{F_5}{AG} \quad , \quad \delta = 1.33 \frac{F_5 \ell}{AG}$$

$$I = 1.92 \times 10^4 \text{ mm}^4$$

$$A = 491.9 \text{ mm}^2$$

$$\ell = 26 \text{ mm}$$

slopes unimportant as assumed not to affect any other kinematic position.

Therefore only calculate deflection due to F_5 in direction P4.

$$\underline{y_{5A} = 1.47 \times 10^{-6} F_5 \text{ mm}} \quad \text{(-P4 error)}$$

$$\underline{\delta_{5A} = 0.88 \times 10^{-6} F_5 \text{ mm}} \quad \text{(-P4 error)}.$$

.17.9 Bending and shear of joint J4 housing on link L1.

Again assume slope is unimportant and moments zero

$\therefore$ bending and shear due to direct loads F_{4N}, F_{4A} only.

$$I = \frac{\pi}{64} (50^4 - 37^4) = 2.15 \times 10^5 \text{ mm}^4$$

$$A = \frac{\pi}{4} (50^2 - 37^2) = 888.3 \text{ mm}^2$$

$$F_{4N} \simeq F_{4A} \simeq 0.5 F_5, \quad \ell = 29 \text{ mm}$$

Bending deflection $\underline{y_{4N} = y_{4A}} = \underline{0.18 \times 10^{-6} \text{ mm}}$

Shear deflection $\underline{\delta_{4N} = \delta_{4A}} = \underline{0.55 \times 10^{-6} \text{ mm}}$

(y_{4N}, δ_{4N}; x 0.5, - P5 error)

(y_{4A}, δ_{4A}; x 0.5, - P4 error)

.17.10 Bearing deflection in joint J6.

Bearing subjected to couples M_{6N}, M_{6A}, as assumed before, sec.C3.17.1, as well as direct loads F_{6N}, F_{6A}.

$M_{6N} \simeq M_{6A} \simeq F_5 \times 27.5$. If use single RNA4904 needle bearing, length of roller 11.8 mm:- Difficult to estimate load distribution. Better to use double bearing RNA6094 or use preloaded taper rollers.

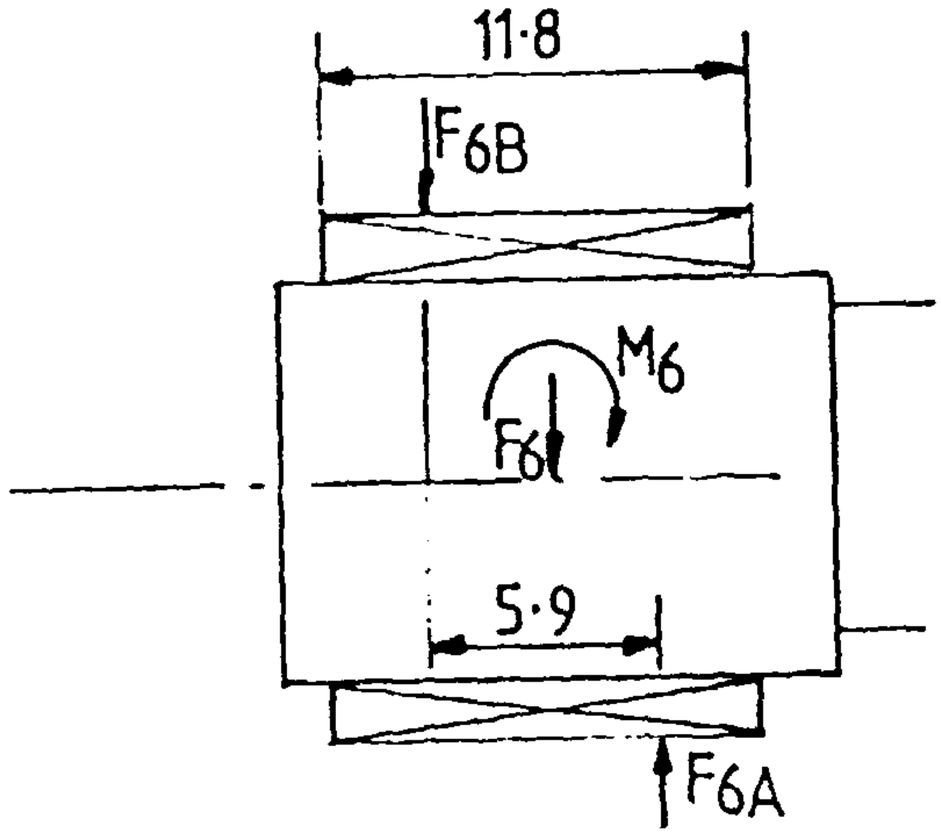

First assume single bearing as in Drawing No.6.

$\therefore$ Reactions A, B = M/5.9

$= F_5 \times 4.58$

$F_{6N} \simeq F_{6A} \simeq F_{5A} \times 0.5$

$\therefore \quad F_{6AA} = F_{6BN} = (4.58 + 0.25)F_5 = 4.83\ F_5,\ \delta = 11.2 \times 10^{-6} F_5^{0.9}$

$F_{6BA} = F_{6AN} = (4.58 - 0.25)F_5 = 4.33\ F_5,\ \delta = 10.13 \times 10^{-6} F_5^{0.9}$

(from C3.14.2, $\delta = 2.71 \times 10^{-6}\ W^{0.9}$, (assuming even load on roller)

$$\phi = \left(\frac{11.2 + 10.13}{59}\right) 10^{-6} F_5^{0.9} = 3616. \times 10^{-9} F_5^{0.9}$$ Too large!

Need to increase reaction distances in joint J6. Now assume double row bearing RNA6909 in J6

distance between centres of bearings → 13mm

$F_{6AA} = F_{6BN} = 2.37\ F_5,\ \delta_{6AA} = \delta_{6BN} = 5.89 \times 10^{-6}\ F_5^{0.9}$

$F_{6BA} = F_{6AN} = 1.87\ F_5,\ \delta_{6BA} = \delta_{6AN} = 4.75 \times 10^{-6}\ F_5^{0.9}$

$$\phi_{6N} = \phi_{6A} = \frac{(\delta_{6AA} + \delta_{6BA})}{13} = 818.5 \times 10^{-9}\ F_5^{0.9}$$

$\underline{\delta_{6A}} = (\delta_{6AA} - \delta_{6BA})/2 = \underline{0.57 \times 10^{-6}\ F_5^{0.9}}$ (x0.5, -P4 error)

$\underline{\delta_{6N}} = (\delta_{6AN} - \delta_{6BN})/2 = \underline{0.57 \times 10^{-6}\ F_5^{0.9}}$ (x0.5, -P5 error)

Effective deflection of J4 due to slope ϕ_{6N}

$$\underline{\delta_{J46N}} = \phi_{6N} \times 55 = \underline{45.0 \times 10^{-6} F_5^{0.9}} \quad (\times 0.5, -P5 \text{ error})$$

Effective deflection at J4 due to slope ϕ_{6A}

$$\underline{\delta_{J46A}} = \phi_{6A} \times 55 = \underline{45.0 \times 10^{-6} F_5^{0.9}} \quad (\times 0.5, -P4 \text{ error})$$

.17.11 Bearing deflection in joint J4.

Assume moments M_{4N}, M_{4A} negligible (sec. C3.13); only direct loads $F_{4N}, \simeq F_{5A} \simeq 0.5 F_5$.

From C3.14.2 for needle roller in joint J4,

$$\underline{\delta_{J4N}} = 2.71 \times 10^{-6} F_{4N}^{0.9} = \underline{1.36 \times 10^{-6} F_5^{0.9}} \quad (\times 0.5, -P5 \text{ error})$$

also $$\underline{\delta_{J4A}} = 1.36 \times 10^{-6} F_5^{0.9} \quad (\times 0.5, -P4 \text{ error})$$

C3.18 Deflections of link L2. (see Fig.C3.18 for forces etc.)

The moments on the link are assumed to equal zero, (see C3.13), therefore only direct loads $F_5 \simeq F_7$ considered.

.18.1 Axial tension/compression of link L2

$$\delta_{AL2} = \frac{F_5 \ell}{AE} \quad \text{where length } \ell = 75 \text{ mm}$$

thickness = 20 mm, width = 50 at J5, 60 at J7,

$\therefore$ take mean area $A = 20 \times 55 = 1.1 \times 10^3 \text{ mm}^2$

$\therefore$ $\underline{\delta_{AL2} = 0.33 \times 10^{-6} F_5 \text{ mm}}$ (- P4 error).

.18.2 Deformation of bearings at joints J5 and J7 in link L2.

From C3.14

for J5 take $\underline{\delta_{J5} = 2.71 \times 10^{-6} F_5^{0.9}}$ mm (-P4 error)

and for J7 take $\underline{\delta_{J7} = 2.05 \times 10^{-6} F_5^{0.9}}$ mm (-P4 error).

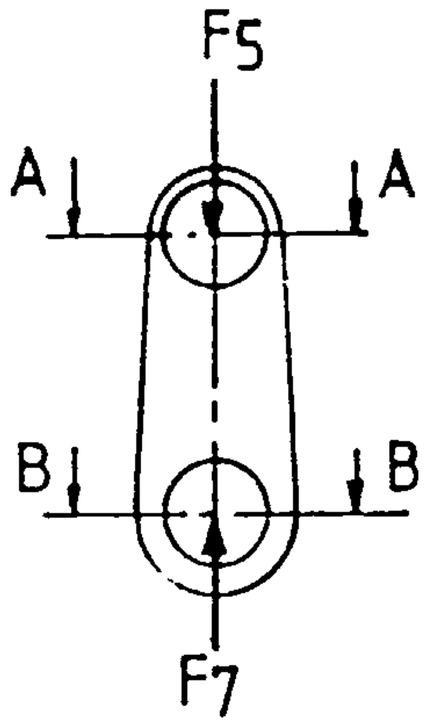

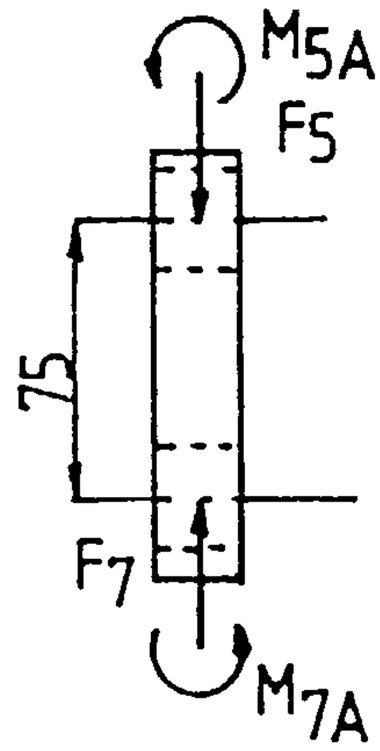

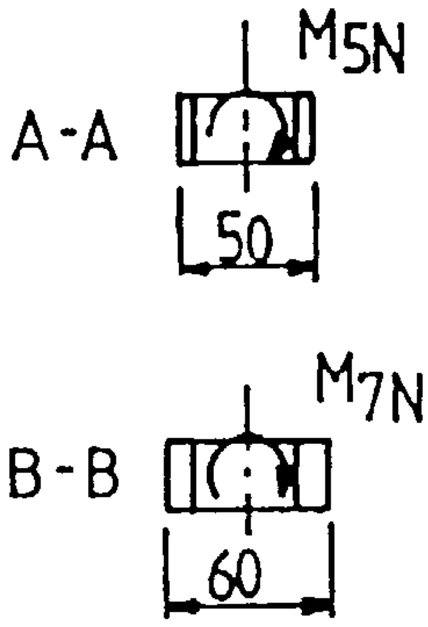

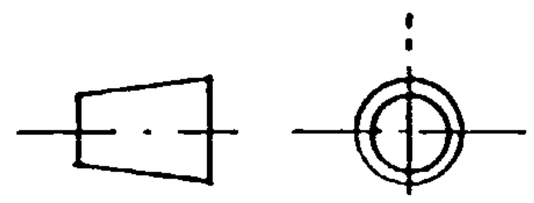

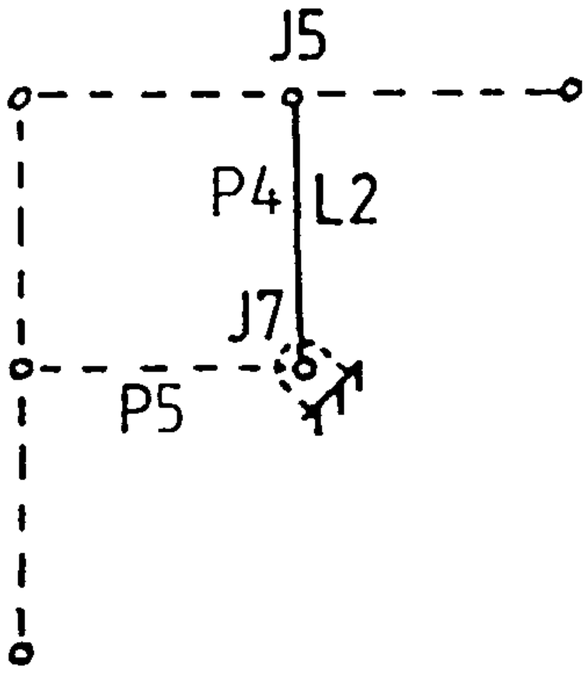

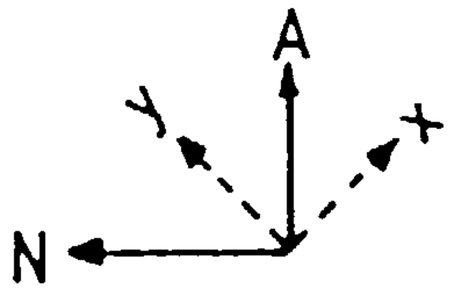

Fig. C3.18 Forces and Couples acting on LINK L2

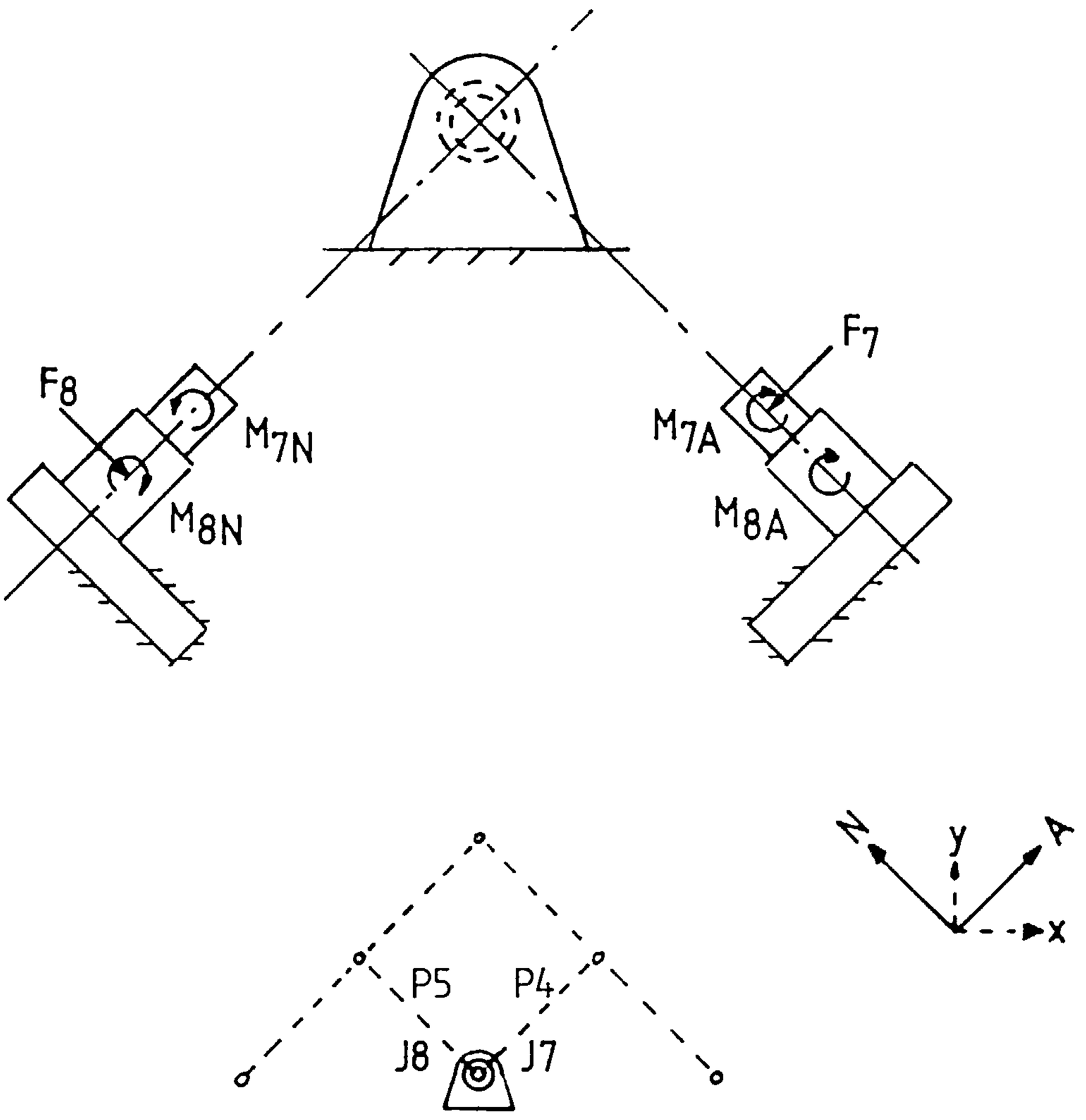

Fig. C3.19 Forces and Couples acting on Pantograph pivot.

C3.19 Deflection of fulcrum shaft of joints J7 and J8.

See Fig. C3.19.

.19.1 Joint J8 bears the load transmitted from link L3. These consist of direct force $F_8 \simeq F_9$, and couples M_{9N}, M_{9A} to resist overturning out of plane. The resultant bearing reactions have already been calculated in C3.15 for joint J9.

Joint J7 bears only the direct load $F_7 \simeq F_5$.

$F_{8AN} = F_{9AN} = -0.987\ F_9$, $F_{8BN} = +0.013\ F_9$

$F_{8AA} = F_{9AA} = 1.57\ F_9$, $F_{8BA} = 1.57\ F_9$

.19.2 Bending and shear of fulcrum shaft in direction of P5

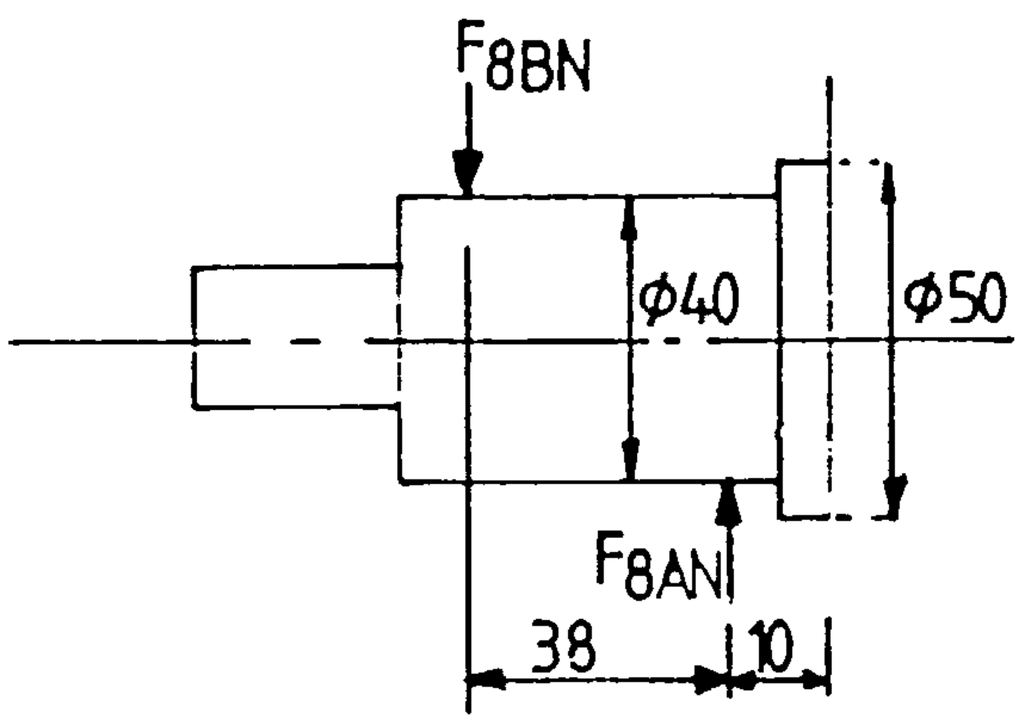

Virtually all load taken at bearing A

$$\text{slope } \phi_{8AN} = \frac{F_{8AN}\ell^2}{2EI}, \quad \ell = 10, \quad F_{8AN} = 0.987\ F_9$$

$$I = \pi 50^4/64 = 3.9 \times 10^5\ \text{mm}^4$$

$$\phi_{8AN} = 0.78 \times 10^{-9}\ F_9$$

$$y_{8AN} = 0.005 \times 10^{-6}\ F_9$$

this is negligible compared to other deflections. Shear strain even more so. ∴ ignore.

.19.3 Bending deflection of fulcrum shaft in direction of P4.

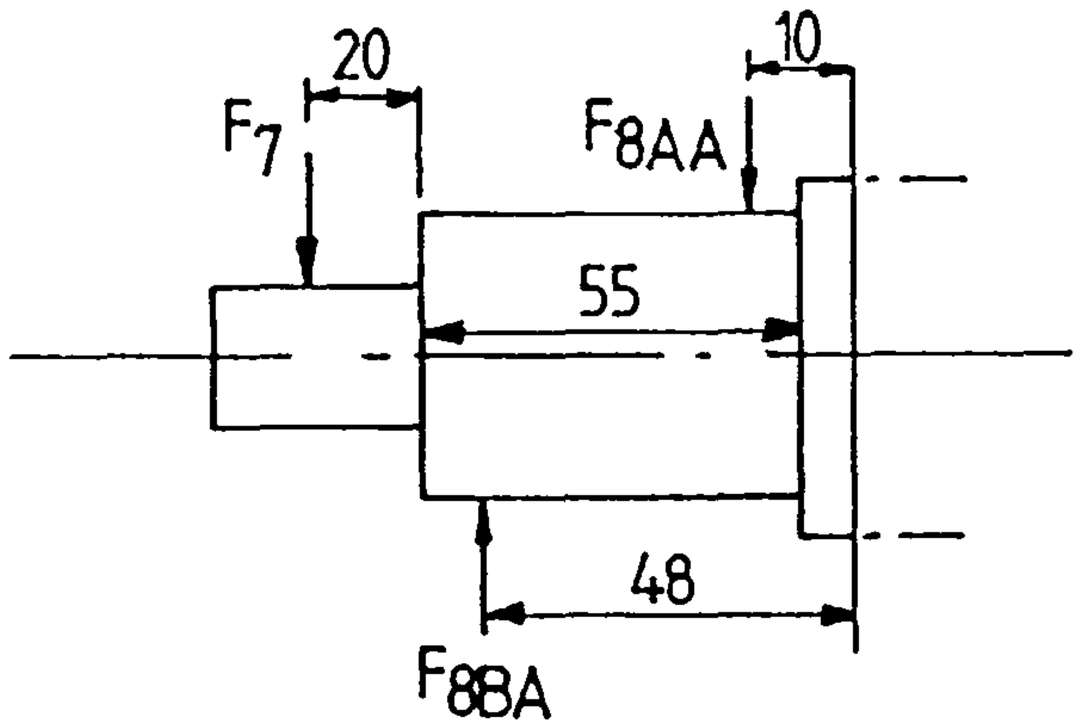

$$\phi_z = \frac{P}{EI}\left(Lz - \frac{z^2}{2}\right), \quad y_z = \frac{P}{EI}\left(\frac{Lz^2}{2} - \frac{z^3}{6}\right)$$

For F_{8AA}, $\phi_{AA} = -1.22 \times 10^{-9} F_9$

F_{8BA}, $\phi_{BA} = 69.5 \times 10^{-9} F_9$

$\delta_{BA} = 2.23 \times 10^{-6} F_9$

slope at centre of J8

$z = 29$ $\phi_{A8} = 58.6 \times 10^{-4} F_9$

$y_{A8} = 0.97 \times 10^{-6} F_9$

deflection at J7 due to F_{8A}, $6_{78} = 4.1 \times 10^{-6} F_9$

$(= (\phi_{AA} + \phi_{BA}) . 27 + \delta_{BA}))$

bending deflection at centre of J8 due to F_7

$y_{87} = -1.66 \times 10^{-6} F_9$

$\phi_{87} = -105.9 \times 10^{-9} F_9$

Deflection at centre of J7 due to F_7

at z = 55 $\quad y_{55} = -3.29 \times 10^{-6} F_7$

for dia.40, $\quad \phi_{55} = -100.4 \times 10^{-9} F_7$

for dia.30, z = 55 to 75 $\quad \ell = 20$

$$y_{75} = -0.32 \times 10^{-6} F_7 \text{ mm}$$

Thus total deflection at J7

assume $F_9 \simeq F_7$

$$y_{7A} = y_{78} + y_{55} + \phi_{55} \times 20 + y_{75}$$

$$\underline{y_{7A} = -1.52 \times 10^{-6} F_9 \text{ mm}} \quad (+ \text{P4 error}).$$

Total bending deflection at J8

$$y_{8A} = y_{A8} + y_{87}$$

$$y_{8A} = -0.69 \times 10^{-6} F_9 \text{ mm} \quad \text{no P4 error}$$

$$\phi_{8A} = -47.3 \times 10^{-9} F_9 \text{ radians}$$

only error due to grinding wheel overhang of 77mm at J10

$$\underline{y_{108A}} = \phi_{8A} + 77 = \underline{-3.6 \times 10^{-6} F_9 \text{ mm}} \quad (\times 0.5, + \text{P4 error}).$$

.19.4 Shear deflection of fulcrum shaft of J7 and J8 in P4 direction.

$$\gamma = \frac{1.33F}{AG} \qquad \delta = \frac{1.33F\ell}{AG}$$

At bearing A, $F = 1.57 F_9$

$$\gamma_{8AA} = -13.3 \times 10^{-9} F_9, \quad \delta_{8AA} = -0.13 \times 10^{-6} F_9$$

B relative to A

$$\gamma_{BA} = 1.33\left(\frac{F_{8BA} - F_7}{AG}\right) = 4.83 \times 10^{-9} F_9$$

$$\delta_{BA} = 0.184 \times 10^{-6} F_9$$

Shear deflection at centre of J8

$$\delta_{8A} = \delta_{BA}/2 + \delta_{8AA}$$

$$= -0.04 \times 10^{-6} F_9 \qquad \text{no effect on P4}$$

$$\gamma_{8A} = \gamma_{BA} = 4.83 \times 10^{-9} F_9 \text{ rads.}$$

at grinding wheel $\underline{\delta_{10\ 8A}} = \gamma_{8A} \times 77 = \underline{2.93 \times 10^{-6} F_9}$ rads

(x0.5, + P4 error)

at change in section $F = -F_7$

$z = 55$

$$\delta_{55} = \delta_{BA} + \delta_{8AA} = \frac{1.33 F_9 \ell}{AG} \qquad \ell = 7 \qquad A = \pi 40^2/4$$

$$= 0.005 \times 10^{-6} F_9$$

at centre of J7,

$$\delta_{7A} = \delta_{55} - \frac{1.33 F_9 \ell}{AG} \qquad \ell = 20 \qquad A = \pi 30^2/4$$

$\delta_{7A} = -0.47 \times 10^{-6} F_9$ mm (+ P4 error)

$$\gamma_{7A} = -1.33 \frac{F_9}{AG}$$

$= 23.52 \times 10^{-9} F_9$ rads. no effect.

C3.20 Deflections summary for pantograph

	P5 errors		P4 errors	
Link L4 - (Sec.C3 .15)				
C3.15.1	y_{5L4}	$1.63 F_9 \times 10^{-6}$	C3.15.2 y_{10A}	$26.8 \times 0.5 F_9 \times 10^{-6}$
.4	y_{ML4}	$3.70 \times 0.5 F_9$"	.3 δ_{AL4}	$-.36 \times 0.5 F_9$ "
.5	δ_{5L4}	$-.94 F_9$ "	.8 y_{s9A}	$6.08 \times 0.5 F_9$ "
.6	y_{s9N}	$6.18 \times 0.5 F_9$ "	.9 δ_{s9A}	$1.6 \times 0.5 F_9$ "

P5 errors

C3.15.7 δ_{s9N} 1.0 x 0.5 F_9 x 10^{-6}

.10 δ_{J9N} 2.59 x 0.5 $F_9^{0.9}$ "

.12 δ_{J4L4} 5.87 x 0.5 F_9 "

$\Sigma = (5.80F_9 = 1.30\ F_9^{0.9}).10^{-6}$

P4 errors

C3.15.11 δ_{J9A} 5.51 x 0.5 $F_9^{0.9}$ x 10^{-6}

.13 y_{J4L4} -16.44 x 0.5 F_9 "

$\Sigma = (8.84\ F_9 + 2.76\ F_9^{0.9}).10^{-6}$

Link L3 (sec C3.16)

C3.16.1 δ_{5L3} - .209 F_9 10^{-6}

.3 y_{NL43} 3.65 x 0.5 F_9 10^{-6}

.4 δ_{J8N} 2.59 x 0.5 $F_9^{0.9}$ "

$\Sigma = (1.616\ F_9 + 1.30\ F_9^{0.9}) x10^{-6}$

C3.16.2 δ_{AL3} 4.30 x 0.5 F_9 x 10^{-6}

.5 δ_{J8A} 5.51 x 0.5 $F_9^{0.9}$ "

$\Sigma = (2.15\ F_9 + 2.76\ F_9^{0.9})$ x10^{-6}

Link L1 (sec. C3.17)

C3.17.3 δ_{AL1} - 0.52 F_5 x10^{-6}

.5 y_{NL1} -13.06 x 0.5 F_5 "

.6&.7 y_{46N} - 6.62 x 0.5 F_5 "

.9 y_{4N} - 0.18 x 0.5 F_5 "

.9 δ_{4N} - 0.55 x 0.5 F_5 "

.10 δ_{6N} - 0.57 x 0.5 $F_5^{0.9}$ "

.10 δ_{J46N} -45.0 x 0.5 $F_5^{0.9}$ "

.11 δ_{J4N} -1.36 x 0.5 $F_5^{0.9}$ "

$\Sigma = (-10.725\ F_5 - 23.47\ F_5^{0.9}) \times 10^{-6}$

C3.17.1 y_{4L1} - 4.75 F_5 x 10^{-6}

.2 δ_{4L1} - 1.0 F_5 "

.4 y_{ML1} - 18.29 F_5 "

.6 &.7 y_{56A} - 4.08 F_5 "

.6 &.7 y_{46A} - 13.0 x 0.5 F_5 "

.8 y_{5A} - 1.47 F_5 "

.8 δ_{5A} - 0.88 F_5 "

.9 y_{4A} - 0.18 x 0.5 F_5 "

.9 δ_{4A} - 0.55 x 0.5 F_5 "

.10 δ_{6A} - 0.57 x 0.5 $F_5^{0.9}$ "

.10 δ_{J46A} - 45.0 x 0.5 $F_5^{0.9}$ "

.11 δ_{J4A} - 1.36 x 0.5 $F_5^{0.9}$ "

$\Sigma = (-37.34\ F_5 - 23.47\ F_5^{0.9}) \times 10^{-6}$

Link L2(Sec.C3.18)

P5 error			P4 error	
C3.18.1	δ_{AL2}	- 0.33	F_5	x 10^{-6}
.2	δ_{J5}	- 2.71	$F_5^{0.9}$	"
.2	δ_{J7}	- 2.05	$F_5^{0.9}$	"
Σ =		$(-0.33\ F_5 - 4.76\ F_5^{0.9})\ \times 10^{-6}$		

Fulcrum shaft J7, &J8 (Sec.C3.19)

C3.19.3	y_{7A}	- 1.52	F_9	x 10^{-6}
.3	y_{108A}	- 3.6 x 0.5	F_9	"
.4	δ_{108A}	2.93 x 0.5	F_9	"
.4	δ_{7A}	- 0.47 x	F_9	"
Σ =		$-\ 2.32 \times F_9 \times 10^{-6}$		

Total deviation to P4 and P5 from all links

$\Delta P5 = (-3.309\ F_9 - 20.87\ F_9^{0.9})10^{-6}$ $\Delta P4 = (-29.0\ F_5 - 22.71\ F_5^{0.9})10^{-6}$

Note: these final summations assume that F_5 is replaced by F_9 for all $\Delta P5$ calculations and F_9 is replaced by F_5 for all $\Delta P4$ calculations, based on approximations of App.C3.13.

C3.21 Summary of allocation of mechanism deflections to kinematic parameters for use in computer program MECHKIN.

Multiply all by x10^{-6}

		Source
Δ_{RP2}	$= -(35.97 \times E_{3L} + 6.89 \times E_{3L}^{0.9} + 80.0 \times E_{3L}^{0.67})$	C3.10
Δ_{RP4}	$= +11.84 \times F_{4L} + 8.15 \times F_{4L}^{0.9}$	C3.11
Δ_{RL1}	$= 3.30 \times F_{Y2} + 5.14 \times F_{Y4}$	C3.10

		Source
Δ_{RL4}	$= 18.27\ F_{4L} + 4.24\ F_{4L}^{0.9}$	C3.12
	$+ 4.92\ F_{3L} + 2.66\ F_{3L}^{0.9}$	
Δ_{R4}	$= 22.13\ F_{4A} + 4.24\ F_{4A}^{0.9}$	C3.12
Δ_{P4}	$= -29.0\ F_{5} - 22.71\ F_{5}^{0.9}$	C3.19
Δ_{P5}	$= -3.31\ F_{9} - 20.87\ F_{9}^{0.9}$	C3.19
Δ_{RL3}	$= -921.0 \times R3 \times TOR$	C6.7

C4. MECHANISM TOLERANCES

C4.1 Because of the profile's general insensitivity to mechanism tolerances, only a few of the most relevant are quoted. Stepper motor drive system tolerances are analysed in Appendix C6.

Bearings

The tolerances of particular concern for mechanism accuracy are the bearing radial run outs. These vary depending on the type and precision class of bearing as follows.

Type Bearing Designation (Joint Location in Notation of Fig.6.1)	Precision Class	Radial run-out(μm) 0	P6	P5
	Ring			
SKF Taper roller 32018XC (Joint J1)	Outer	40	20	11
	Inner	25	13	6
SKF Taper roller 32016XC (Joint J3)	Outer	40	20	11
	Inner	20	10	5
SKF Taper roller 32008XC (Joints J8 & J9)	Outer	25	13	8
	Inner	15	10	5
INA Needle roller RNA4904RS and (Joints J4,J5,J6) RNA6904RS	Outer	20	10	7
RNA4906 (Joint J7)	Outer	20	10	7
	Inner (spacer)	13	8	4

For grinding spindle run-out of bearings to outside of housing assume ISO tolerance grades IT7 (30 μm) or IT8 (46μm). The needle roller and linear ball bearings of joint J2 are assumed unrestricted.

Linkages

Assume those of profile generator unrestricted and therefore to IT7/IT8, say.

	ISO tolerances	IT6	IT7	IT8	(μm)
Joint centre distances for pantograph links (Parameters P1 to P6)	= 75 mm	19	30	46	

C4.2 Calculation of single equivalent pantograph tolerance

$$\delta P1^* = \pm(\delta P1^2+\delta P2^2+\delta P5^2+(2x\delta P4)^2 + (2x\delta P5)^2 +\delta P6^2)^{\frac{1}{2}} \qquad (C4.1)$$

Assuming PL2 and PL6 tolerances included in P2 and P6 and noting P4 and P5 have twice as effective a tolerance as P1.

Each individual tolerances δP1 etc.

$$= \pm \tfrac{1}{2} ((\text{centre distance tol})^2 + (\text{bearing run out})^2)^{\frac{1}{2}} \qquad (C4.2)$$

Using various combinations of centre distance tolerances and bearing classes the following equivalent tolerances of parameter P1 arise

Centre dist. Tol. grade	Bearing Class	Equivalent P1 tolerance μm	Approximate Profile error after compensation
IT8	0	± 98	~ ± 1μm
IT7	0	± 75	
IT6	0	± 62	
		± 50	~ ± 0.5 μm
IT6	P6	± 44	
IT6	P5	± 39	

The last column indicates the maximum profile error which may occur for worst mechanism setting, for P1 deviations of 100μm and 50μm. (see Sec.6.8.2)

Table C4.1 Pantograph tolerance summary

C.5 FRICTION IN BEARINGS

C.5.1 Calculation of bearing friction in needle roller bearing of revolute joint J2.

C5.1.1 Formulae

The calculations are made using formulae given in INA Catalogue 304GB (INA Bearing Company Ltd.) [28]

Friction torque M_R is given by the following:

$$M_R = M_o + M_1 \qquad \text{(C5.1)}$$

where M_o is load independent friction torque

M_1 is load dependent friction torque

and $$M_o = f_o\ (\nu\ n)^{2/3}\ d_M^3\ .\ 10^{-6}\ \text{Nmm for } \nu n \geq 2000 \qquad \text{(C5.2)}$$

or $$= f_o . 160 . d_M^3\ .\ 10^{-6}\ \text{Nmm for } \nu n < 2000$$

$$M_1 = f_1\ .\ F_R\ .\ \frac{d_M}{2}\ \text{Nmm} \qquad \text{(C5.3)}$$

f_o = bearing factor for idling = 0.1 to 1.0 for grease lubrication

f_1 = bearing factor for loading = 0.00015 to 0.0003

F_R = radial load in N

d_M = mean bearing diameter in mm

n = bearing speed in min^{-1}

ν = kinematic viscosity in $mm^2.s^{-1}$ (of base oil in grease lubrication.)

Designation of bearing to be used is NA4826 (INA) for which inner and outer diameters are d = 130 and D = 165 respectively

$\therefore$ Assume d_M = (d + D)/2 = 147.5 mm

Bearing speed, n

This bearing oscillates and its speed varies from 0 to $\pm\ n_{max}$ (maximum velocity)

where n_{max} is determined by the geometry of the profile generating linkages R2, R3 and R4 and joints J1, J2 and J3.

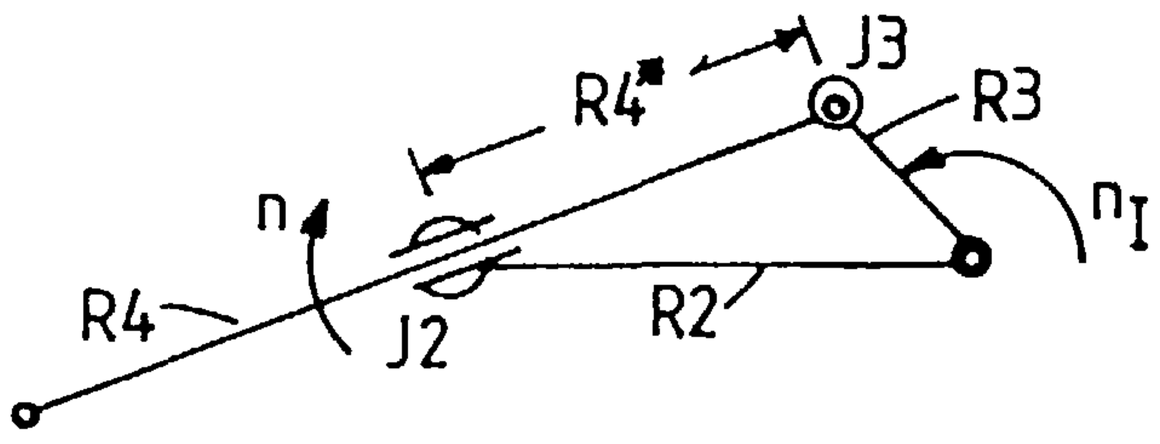

The velocity does not change when the required size of workpiece is changed since R3, R2, R4* all change in proportion.

$\therefore$ Speed is only affected by change in the required eccentricity, e, which is determined by R3.

If n_I is the constant driving speed of the mechanism then n_{max} is given by:

$$n_{max} = n_I \cdot \frac{R3}{R4^*_{min}}$$

where $R4^*_{min} = R2 - R3$

also $R3 = e.R1$ where R1 ≡ mean radius of profile.

$R2 = 0.5 .R1$

$$\therefore \quad n_{max} = n_I \cdot \frac{e}{(0.5-e)}$$

Design speed is n_I = 10 rad/sec 95 r.p.m.

$\therefore$ for 'e' = 0.06, n_{max} = 13.0 min^{-1}

e = 0.15, n_{max} = 40.7 min^{-1}

Viscosity 'ν'

This can be determined from Figure 31 of INA catalogue 304GB.

The minimum required value of 'ν' is dependent on the velocity of the bearing. The figure indicates that viscosity increases as the velocity ratio $\frac{400,000}{n.d_M}$ increases, which would indicate $\nu = \infty$ for n = 0 (which is minimum velocity of oscillating bearing. However 'ν' will be estimated using n_{max} from before. In practice the optimum viscosity can be chosen during prototype testing. And it is probable that the indicated viscosity could be reduced because of the very low loads for the size of bearing.

(C/P > 38, where C is the nominal dynamic capacity (= 118000 N for bearing NA4826)and P is the operating load ≃ 3100 N max. and in most cases is much less).

For e = 0.06, n_{max} = 13.9 min^{-1}, $\frac{400,000}{n.d_M}$ = 209.

Although off the scale of graph, by extrapolation $\nu \simeq 300$ $mm^2 s^{-1}$

e = 0.15, n_{max} = 40.7 min^{-1}, $\frac{400,000}{n.d_M}$ = 67 → $\nu \simeq 140$ $mm^2 s^{-1}$

Radial load, F_R

F_R varies considerably, depending on operating conditions.

In general 'F_R' decreases as workpiece size increases, and also as eccentricity of profile decreases.

The highest load, F_R, considered, is that for a workpiece of nominal radius, 5 mm, (R1), and eccentricity e = 0.15 (R3 = 0.75 mm) which gives rise to a maximum load of ≃ 3100 N (see Fig. 5.3)

This assumes that there is zero preload on the bearing, which is the intended operating condition. (see also C3.9.1)

In practice, from INA catalogue, the variation in operating clearance, for 'less-than-normal' specification is 30 μm to 60 μm or for normal specification 60 μm to 90 μm.

C5.1.2 Load independent friction torque, M_o

For e = 0.06

Using $\nu = 300\ mm^2 s^{-1}$ $n = 13.0\ min^{-1}$ in eqn.(C5.2)

$$\nu n = 3900$$

$$\therefore \quad M_o = f_o\ (3900)^{2/3} \cdot 147.5^3\ 10^{-6}\ Nmm$$

$$= f_o \times .795 \cdot 10^3\ Nmm = f_o \times .795\ Nm$$

and for e = 0.15, $\nu = 140$, n = 40.7 → $\nu n = 5698$

$$M_o = f_o \times 1.024 \times 10^3\ Nmm = f_o \times 1.024\ Nm$$

However if the same ν is used for both, and $\nu = 300\ mm^2 s^{-1}$, the minimum for e = 0.06 is also used for e = 0.15 then for e = 0.15, ν = 300, n = 40.7 → νn = 12210.

$$M_o = f_o \times 1.7 \times 10^3\ Nmm. \qquad = f_o \times 1.7\ Nm$$

The value of f_o is largely dependent on the quality and quantity of grease used.

∴ calculate extreme values of M_o for f_o = 0.1 and f_o = 1.0.

Also include M_o values if νn is reduced to limiting value of 2000 (by using lower than normal viscosity or reducing operating speeds).

The various possible values of load independent friction torque M_o are summarised in Table C5.1.2.

Eccentricity e	Max. Speed n r.p.m	Viscosity ν mm^2s^{-1}	νn	Friction Factor f_o	Friction Torque M_o Nm	Torque on Link R3 M_{R3} Nm	Joint Reaction Force, F_o for R1=5mm N
0.06	13.0	300	3900	0.1	0.08	0.01	34
0.06	13.0	300	3900	1.0	0.80	0.1	340
0.06	-	-	2000	0.1	0.05	0.007	24
0.15	40.7	140	5698	0.1	0.102	0.04	54
.15	40.7	140	5698	1.0	1.02	0.44	534
.15	40.7	300	12210	0.1	0.17	0.07	94
.15	40.7	300	12210	1.0	1.7	0.73	974
.15	-	-	2000	0.1	0.05	0.02	26

Table C5.1.2 Load independent friction torque in Joint J2.

M_{R3} is resulting torque on drive link R3 = $M_o \times \frac{R3}{R4*} = M_o(\frac{e}{0.5 - e})$

(at n_{max})

F_o is reaction of joints J1, J2 and J3 = $\frac{M_o}{(0.5-e)R1} = \frac{M_{R3}}{e.R1}$

The joint reaction forces are worst for smallest workpieces with largest eccentricity.

Max loads (without friction) for e = 0.06 R1 = 5 mm is 1640 N

" " " e = 0.15 R1 = 5 mm is 3100 N

If f_o is 1.0 the load independent friction could be significant, approx. 20% of friction-free load for normal ν values.

However, if f_o = 0.1 can be achieved and also lower values of viscosity be acceptable then friction reaction loads would be < 2% of friction free loads.

C5.1.3 Load dependent friction torque, M_l

Depends only on bearing load, F_R which varies for each operational setting of the mechanism.

For example: R1 = 5mm, e = 0.15

$F_R \simeq$ 3100 which is the worst case considered. (see C5.1.1)

From eqn.(C5.3):

$$M_l = f_l \times 3100 \times 147.5 \times 0.5 \quad \text{Nmm}$$

for $f_l = 0.00015$ $M_l = 34.3$ Nmm = 0.03 Nm

$f_l = 0.0003$ $M_l = 68.6$ Nmm = 0.07 Nm

The reaction force F_l at J1 $= \dfrac{M_l}{(0.5-e)R1} = \dfrac{M_l}{(0.35)x5}$

$$= \frac{68.6}{(0.35 \times 5)} = 39N, \quad f_l = 0.0003$$

or $= 19.5N$, $f_l = 0.00015$

i.e. Friction dependent load is approximately 1% of total load.

C5.1.4 Conclusions

Load dependent friction is always relatively small ~ 1% and can be considered insignificant and ignored.

Load independent friction can be varied considerably by choice of lubricant quality, quantity and viscosity. It should be possible to achieve conditions where this also can be considered to have negligible effects, especially as it will reach maximum values at maximum velocity and therefore does not coincide with the maximum inertia loads which occur when the angular velocity of R4 is zero.

C5.2 Calculation of friction torque in the taper roller bearings of joints J1 and J3.

C5.2.1 Formulae

The calculations are made using formulae given by SKF Bearing Catalogue 300011E/GB66611 (SKF(U.K.) Ltd.).

Friction torque is given by the following:

$$M = M_o + M, \qquad \text{(C5.4)}$$

where M_o is load independent friction torque

M_1 is load dependent friction torque

and $M_o = f_o \times 10^{-7} (\nu n)^{2/3} d_m^{\,3}$ (Nmm) for $\nu n \geq 2000$

or $M_o = 160 \times 10^{-7} f_o d_m^{\,3}$ (Nmm) for $\nu n < 2000$ } (C5.5)

$$M_1 = f_1 g_1 Po\, d_m \text{ (Nmm)} \qquad \text{(C5.6)}$$

where

f_o = bearing factor = 3 to 4 for grease lubrication

f_1 = bearing factor = 0.0004 to 0.0005

$g_1 Po = 2\ Y\ F_a$ unless $g_1 Po < F_R$ in which case put $g_1 Po = F_R$.

where Y = 1.4 from bearing tables

F_a = axial load

F_R = radial load

d_m = mean bearing diameter

n = bearing speed r/min

ν = kinematic viscosity in $mm^2 s^{-1}$ (of base oil for grease lubrication).

The designation of the bearings of joint J1 (bearings A and B) is 32018 X C

and for joint J3 (bearings C and D) - 32016X C

For A and B $d_m = (d + D)/2$ where d = 90 mm and D = 140 mm are the inner and outer diameters respectively.

$$\therefore \quad {}_{AB}d_m = \frac{90 + 140}{2} = \underline{115 \text{ mm}}$$

For C and D, d = 80, D = 125

$$\therefore \quad {}_{CD}d_m = \underline{102.5 \text{ mm}}$$

Bearing speed, n is constant and the same for all four bearings and is 10 rad/s = 95 r/min.

Viscosity, ν

The minimum value necessary at operating temperature is determined from Diagram 2, Page 111 of SKF catalogue.

for $d_m = 115$ mm $n = 95$ r/min ν_{min} 90 mm^2/s

for $d_m = 102.5$mm $n = 95$ r/min ν_{min} 100 mm^2/s.

$\therefore$ use 100 min^2/s for both joints.

(Note also that a $\nu = 300$ mm^2/s may be needed for joint J2 needle roller bearing thus a higher value might be used in J1 and J3 if the same grease is specified for all joints. Operating viscosity will then depend on temperature of each joint which would need to be measured experimentally).

C5.2.2 Load independent torque, M_o

Using $\nu = 100$ mm^2/s, $n = 95$ r/min.

gives $\nu n = 9500$

Therefore for J1 bearing A and B from eqn.(C5.6)

using $f_o = 3$, $M_{A,B^o} = 0.20$ Nm per bearing

and using $f_o = 4$, $M_{A,Bo} = 0.27$ Nm per bearing.

Similarly for joint J3, bearings C and D

$M_{C,D^o} = 0.14$ Nm for $f_o = 3$ per bearing

$= 0.19$ Nm for $f_o = 4$ per bearing.

C5.2.3 Preloading of Bearings

The reactions in the bearings of J1 and J3 to the overhang loads on the main shaft in the plane of joint J2 are determined in Appendix C3.1.

If the overhang load is denoted by P and the radial reaction loads on bearings A,B and C,D of J1 and J3 as P_A, P_B, P_C, P_D respectively then

$P_A = 1.1\ P$ $P_C = 0.86\ P$

$P_B = 2.1\ P$ $P_D = 1.86\ P$

The worst case considered is for a workpiece nominal diameter of 10mm and eccentricity of e = 0.15, which results in a load P ≃ 3100 N. This gives reaction forces of:-

$$P_A = 3410N, \quad P_B = 6510\ N, \quad P_C = 2666\ N, \quad P_D = 5766\ N.$$

Calculation of bearing preloads

As in Appendix C3.7 it was originally decided to adopt a load/deflection formuli for these bearings of;deflection

$$\delta = 0.55 \times 10^{-6}\ P_{A,B}^{0.9}\ \text{mm for A and B} \qquad \text{(C5.7)}$$

and $$\delta = 0.6 \times 10^{-6}\ P_{C,D}^{0.9}\ \text{mm for C and D} \qquad \text{(C5.8)}$$

These formuli required an assumption that the preload deformation or interference $- CD > 2.0\delta$

For bearings A and B the maximum δ_o's from eqn.(C5.7) are

$$\delta_A = 0.8\ \mu m, \quad \delta_B = 1.5\ \mu m$$

For bearings C and D the maximum δ_o's from eqn.(C5.8) are

$$\delta_C = 0.7\ \mu m, \quad \delta_D = 1.5\ \mu m.$$

In both cases to justify the assumed deflection formuli the radial preload deformation $- C_D > 3\ \mu m$.

The preload is distributed uniformly amongst the rollers and the resulting radial preload is given by rearrangement of eqn.(9),App.C3.7.1, for evenly distributed bearing load:-

$$F_R = (C_D \cos\alpha)^{1.11}\ \ell\omega^{0.89}\ Z \cos\alpha\ \ 3.7 \times 10^4\ N \qquad \text{(C5.9)}$$

where α = contact angle of taper roller ≃ 15^o

C_D = negative clearance = 3×10^{-3} mm

Z = number of rollers in the bearing = 27

$\ell\omega$ = roller length = 23.7 mm for A and B, 21.4 mm for C and D.

$\therefore$ For A and B, $F_R = (3 \times 10^{-3} \times \cos 15^o)^{1.11}\ 23.7^{0.89} \times 27 \times \cos 15^o \times 3.7 \times 10^4$ N.

$= 24.6 \times 10^3$ N. per bearing

Similarly for C and D,

$$_{p}F_{R} = 22.5 \times 10^{3} \text{ N per bearing.}$$

Resulting axial preloads $_{p}F_{A} = {}_{p}F_{R} \cdot \tan\alpha$

$\therefore$ for A and B $_{p}F_{A} = 6.6 \times 10^{3}$ N per bearing

for C and D $_{p}F_{A} = 6.0 \times 10^{3}$ N per bearing.

Contribution of operating load and preloads to bearing friction, M_1.

Once the bearings are preloaded, the application of the operating load will have a negligible effect on the total distributed load on the bearing, as long as the deflection does not result in any clearance occurring in the bearing. In other words, the total radial load, F_R, remains equal to the preload, $_{p}F_{R}$.

This can be quickly checked by looking at the deformation and loads on two rollers in a bearing, which are directly aligned with the operating load direction but on opposite sides of the bearing.From the previous section it can be seen that one roller will have its deformation changed from C_D = 3 μm (preload) to $C_D + \delta_o$ = 4.5 μm (preload + operating deformation) and the opposite roller will have its deformation reduced from C_D = 3 μm (preload) to $C_D + \delta_o$ = 1.5μm (preload - operating deformation).

Since load α (deformation)$^{1/0.9}$ the load on the first bearing will increase to $(1.5)^{1/0.9} = 1.57$ of its individual preload, whilst the load on its opposite will decrease to $(0.5)^{1/0.9} = 0.46$ of its initial preload. Therefore the total load on these two rollers

(1.57 + 0.46) x preload

2.03 x Preload

i.e. 1.015 per roller and virtually unchanged.

Thus the bearing friction M_1 will be determined by the bearing preloads.

C5.2.4 Load dependent torque M_1

From C5.2.1 it can be seen that since $F_R > 2.8\ F_A$ that $g_1 P_o = F_R$ should be used and that $F_R = {}_{p}F_{R}$.

For joint J1 bearings A and B from eqn.(C5.6) using F_R

$$_{A,B}M_1 = f_1 \times 24600 \times 115 \times 10^{-3} \text{ Nm} = 2.81 \times 10^3 \times f_1 \text{ Nm}$$

and for joint J3 bearings C and D

$$_{C,D}M_1 = f_1 \times 22500 \times 102.5 \times 10^{-3} \text{ Nm} = 2.31 \times 10^3 \times f_1 \text{ Nm}$$

if $f_1 = 0.0004$ $_{A,B}M_1 = 1.12$ Nm per bearing

$_{C,D}M_1 = 0.92$ Nm per bearing

if $f_1 = 0.0005$ $_{A,B}M_1 = 1.41$ Nm per bearing

$_{C,D}M_1 = 1.16$ Nm per bearing.

These values are relatively high compared to other sources of friction and the total torque required will be particularly sensitive to the setting of the preloads on bearings of joints J1 and J3. Therefore, the resolution of the method of preload application should be checked.

C5.2.5 Bearing preload setting accuracy.

In practice the preload is applied axially by adjustment of bearing locknuts and lockwashers as shown in Drawing No.1, items 15, 16.

The SKF designations of the locknuts are KM16 and KM18 and of the lockwashers, MB16 and MB17 for joints J3 and J1 respectively. On each joint, the locknuts have 4 circumferential slots which are used in conjunction with 19 locating tabs on the lockwashers to provide a total of 4 x 19 = 76 radial locations of the locknut.

One full turn of the locknut produces an axial movement equal to the thread pitch which is 2mm.

Therefore the resolution of axial preload displacement is $2 \div 76$ mm 26×10^{-3} mm or 26 μm.

The two bearings in each joint are adjusted back to back by a single locknut and therefore the adjustment resolution of axial preload deformation per bearing = 13 μm.

This value is based on the assumption that all preloaded elements of the bearing assembly except the bearings themselves are relatively very stiff. Any deformation of the shaft or distance pieces would reduce the preload deformation applied to the bearing, thus 13 μm represents the maximum value of the resolution.

The equivalent resolution of the radial preload deformation = 13 x tan 15^{o} = 3.5 μm per bearing. To satisfy the assumptions for the load deflection formulae of the previous section, the radial preload deflection > 3 μm.

If the locknut is locked in the nearest location to this value, then the actual preload deformation will be = $(3 \pm \frac{3.5}{2})$ μm that is between 1.25 and 4.75 μm.

These would result in preloads between

9.3×10^{3} N and 41.0×10^{3} N for A and B

8.5×10^{3} N and 37.5×10^{3} N for C and D.

In turn, these would result in friction loads, M_1 per bearing of:

$_{A,B}M_1$ = 0.43 Nm to 1.89 Nm for f_1 = 0.0004

$_{C,D}M_1$ = 0.35 Nm to 1.54 Nm for f_1 = 0.0004

or

$_{A,B}M_1$ = 0.53 Nm to 2.36 Nm for f_1 = 0.0005

$_{C,D}M_1$ = 0.44 Nm to 1.92 Nm for f_1 = 0.0005

Thus, in practice, the actual preload may be either insufficient to satisfy load-deflection assumptions or at the other extreme cause too high a friction torque.

C5.2.6 Alternative preloading method using springs.

C5.2.6.1 Reassessment of preload requirement

Requirements of preload: (see also Sec.7.3.1)

(1) To satisfy assumption in bearing deflection calculations that negative clearance - C_D > 2 x δ_o the bearing deflection under external load.

(2) To provide a level of friction torque which is greater than the -ve friction-free torque reversals of the mechanism in order to avoid backlash in the mechanism drive system.

Other factors for consideration:-

Effect on choice of stepper motor. (See also App.C6)

(torque > 2 x load-dependent friction torque for start-up).

Previous calculation for the worst case (App. C5.2.4) estimate a total load-dependent friction torque for both bearing pairs of 2 x (1.41 + 1.16) Nm = 5.14 Nm, and a total load-independent friction torque of 2 x (0.27 + 0.19) = 0.92 Nm and thus a total friction torque $M = M_o + M_1 = 6.06$ Nm.

This is much greater than the maximum friction-free operating torque reversal of -2.45 Nm (Table B5.1).

The stepper motor and transmission would need to supply > 2 x 5.14 > 10.28 Nm for start-up.

A drive system providing > 10.28 Nm is still powerful compared to the basic friction free torque requirements (50 x greater in some settings).

Also, providing a motor of this capacity will require rearrangement, and enlargement of the mechanism assembly to accommodate its size. Whereas a motor transmission which would provide up to 9 Nm can be fitted without extensive rearrangement or enlargement of the rest of the layout.

Compromise by reducing preload to provide < 9 ÷ 2 Nm load dependent friction torque (≡ < 9 Nm start-up torque).

Only 1.5 Nm load-dependent torque is required to satisfy requirement (2) above, since load-independent provides approximately 1 Nm.

Therefore choose load-dependent friction torque of 3 Nm and thus 6 Nm static friction for start-up, this allows 50% safety margin for a 9 Nm drive system and will result in about 4 Nm total friction torque at operating speed, and maximum friction plus operating torque of 5.5 Nm.

Load-dependent friction torque is proportional to the bearing preloads for J1 and J3.

The radial preloads required to give 5.14 Nm friction torque are given as 24,600 N and 22,500 N for J1 and J3 respectively in App.C5.2.3.

Reducing these to provide 3 Nm, if both pairs are reduced in proportion, will require preloads:

$$\text{for J1 of } 24{,}600 \times \frac{3}{5.14} = 14{,}358 \text{ N}$$

$$\text{and for J3 of } 22{,}500 \times \frac{3}{5.14} = 13{,}132 \text{ N}$$

Conclusion

Set J1 radial preload at nominally=14,500 N
and thus axial preload = 3,885 N
and J3 radial preload at nominally = 13,000 N
and thus axial preload = 3,483 N

Reducing preloads to this level will result in < 7% increased profile error for the worst case settings.

C5.2.6.2 Choice of springs

Ordinary Belleville washers do not have suitable internal and external diameter combinations. However, ball bearing disc springs manufactured by Bauer Springs Ltd. come in suitable sizes, although their stiffnesses are very low and will require many springs layered in parallel. They also have a non-linear softening stiffness giving low effective stiffness at deflected positions. There is sufficient room in J1 housing but not in J3. But approximately 1600 N axial preload could be set in J3 without redesigning the rest of the assembly.

Preloading of J3 (using available space between bearings without redesigning surrounding assembly as shown in Drawing No.1).

From Bauer design data.[43]	Outside dia.	Inside dia.
Bearings	125	80
Springs	124*	90.5*

* In pressed flat state.

Spring thickness 1.25 mm

Spring deflection 1.00 mm

Unloaded height = 3.00 mm

Preloaded height = 2.00 mm

Use 8 springs in two stacks of 4 mounted back to back. Therefore each stack has deflection of 1 mm giving total of 2mm, and

a Preloaded height = 11 mm = Inner spacer length.

Preload per spring at 1mm deflection

= 406 N

$\therefore$ Total = 4 x 406 = 1624 N = axial preload

equivalent radial preload = $\frac{1624}{\tan 15^{o}}$ = 6061 N

Resulting friction torque from eqn.(C5.6)

for f_1 of 0.0004 M_1 = 0.25 Nm per bearing

and for f_1 of 0.0005 M_1 = 0.31 Nm.

Remaining torque required, must be supplied from joint J1 bearings.

Preloading of J1

	Outside dia.	Inside dia.
Bearing	140	90
Spring	139	101

Spring thickness = 1.25 mm

Spring unloaded height = 3.25 mm.

To achieve required M_1 of 3 Nm, joint J1 needs to supply

3 - 0.5 = 2.5 Nm (f_1 = 0.0004); this requires an axial preload of 7280N.

Deflection of 1.25 mm gives ~ 412.5 N.

Use two stacks of 18 parallel springs each in series with 2.5 mm deflection.

Preloaded total height = 46.5 mm

Unloaded height = 49 mm

Required difference between outer and inner spacers = 2.5 mm.

Total preload = 7425 N

Equivalent radial preload = 27710 N

Friction torque

f_1 of 0.0004 = 1.27 Nm per bearing

f_1 of 0.0005 = 1.60 Nm

Total friction torque

for f_1 = 0.0004 J1 = 3.04 Nm

f_1 = 0.0005 = 3.82 Nm

Check preload deflections.

For J1 $_{pre}F_R$ = 27710 N

from eqn.(C5.9) in section C5.2.3

$C_D \simeq 3.2$ µm

$\therefore$ satisfies $C_D/\delta_D > 2$ for all operating conditions.

For J3 $_{pre}F_R$ = 6061 N

and $C_D \simeq 0.9$ µm.

Gives $C_D/_D = \frac{0.9}{1.5} = 0.6$ for worst case on bearing D

$\frac{0.9}{0.7} = 1.3$ for worst case on bearing C

This will increase deformations of C and D by ~ 50% and affect total deflection in RP2 direction by ~ 1.6% and overall profile error by < 1% in worst case only. Therefore satisfactory compromise achieved.

Finally check bearing load rating.

Equivalent bearing load for J1 = 26,700 N dynamic

Basic capacity C = 143,000N

$\therefore$ C/P ratio = 5.35

From SKF Cat.[42] this gives life for 90% of bearings of ~ 130,000 hrs. ∴ no problem.
(≡ 27,000 hrs. for 99% reliability).

Bearing	TORQUE (Nm)					
	Load-Independent M_o		Load Dependent M_1		Total $(M_o + M_1)$	
	$f_o = 3$	$f_o = 4$	$f_1 = 0.0004$	$f_1 = 0.0005$	Min.	Max.
J1 A	0.20	0.27	1.23	1.54	1.43	1.81
J1 B	0.20	0.27	1.27	1.60	1.47	1.87
J3 C	0.14	0.19	0.25	0.31	0.39	0.50
J3 D	0.14	0.19	0.25	0.31	0.39	0.50
Totals	0.68	0.92	3.04	3.82	3.72	4.74

Table C5.2.1 Summary of friction torque generated in the taper roller bearings of joints J1 and J3.

Comments.

In practice, the factors f_o and f_1 will depend on operating conditions. Experimental tests to measure actual operating friction would enable a more precise setting of these values.

If necessary preloading springs could be redesigned in light of tests. Also the optimum grease viscosity could be determined.

C5.2.7 Effect of friction torque acting at joint J3 on link R4 upon forces at joints J2 and J3.

The friction torque M_{J3} at J3 (≃ 1 Nm max, see Table C5.2.1) must be resisted by reaction forces on R4 at J2 and J3.

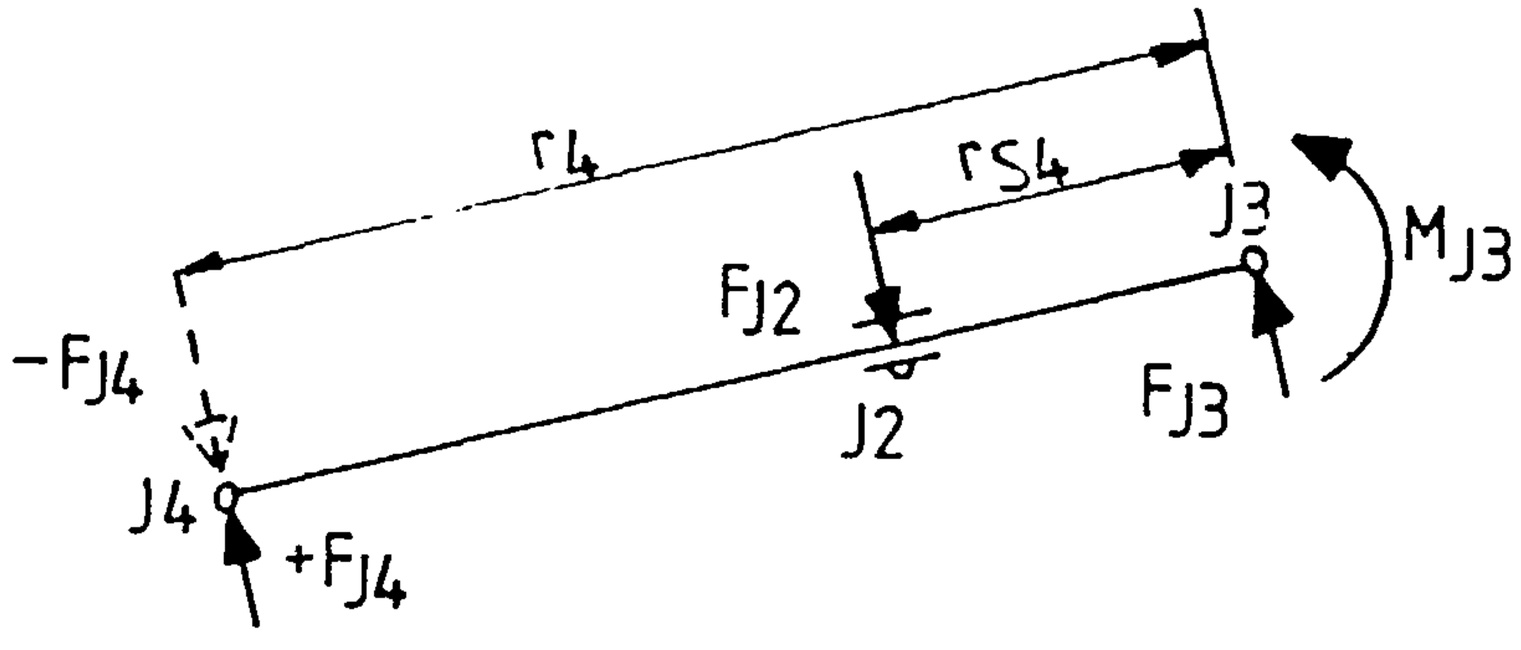

$$F_2 = -\frac{M_{J3}}{RS4} + F_{J4}\,\frac{R4}{RS4}$$

$$F_3 = F_2 - F_4$$

Fig. C5.2. Friction forces at joints.

The maximum $+F_2$ (when $M_{J3} = 0$) occurs when F_4 is positive as shown in Fig.C5.2, and the additional inclusion of M_{J3} due to friction, will reduce the maximum positive value of F_2.

For maximum $-F_2$ (when $M_{J3} = 0$) occurring when F_4 is negative as shown., the inclusion of M_{J3} will increase maximum negative value of F_2.

For RS4 ≃ 2.5 mm the change in force will be 400 N. This effectively shifts the mean value by 400 N. However, since the +ve value is highest and is reduced, the actual max. force occurring is reduced, and thus the variation in deflections should reduce due to non-linearity effects; although backlash may occur more often in J2.

C5.3 Friction due to felt seals in bearing housings of joints J1 and J3.

Friction will be caused by the pressure of the seals which rub on the bearing shafts; however this pressure can be set virtually to zero and thus very low friction. A more likely source of friction is therefore due to shearing of the grease layer between the seal and shaft surfaces. However this would be difficult to calculate accurately since the shear force in the layer is inversely proportional to the gap size and therefore would tend to infinity for zero nominal gap, which is unlikely.

Perhaps the best estimate could be made using a coefficient of friction and a radial sealing pressure. Since this will depend very much on tolerances of components and their fit, the best method would be by experimentation.

However, assume seal friction to be relatively low and at most to be similar to M_o for bearings which result in approximately 0.2 Nm per bearing. Only <u>three</u> seals and one of those, on J1, is rubbing on much smaller diameter (ø50mm) than the other one on J1 (ø125mm) and the one on J3 (ø120mm).

$\therefore$ assume total torque

$$\tfrac{1}{2} \times 0.2 + 0.2 + 0.2 = 0.5 \text{ Nm}.$$

If this is added to the bearing friction torques it gives a maximum of 8.0 Nm which is only likely in very few cases.

C6. SELECTION OF STEPPER MOTOR AND TIMING BELT TRANSMISSION.

C6.1 Torque requirements (to drive eccentricity link R3).

(a) Non-friction torque (inertia, gravity, grinding).

The maximum required is obtained from Table B.5.1, for machining a workpiece of radius 50mm and eccentricity 7.5 mm and is 1.40 Nm.

(b) Dynamic friction torque.

The worst cases are for:

(i)	Main shaft bearings (J1 and J3)	4.7 Nm from Table C5.2.1
(ii)	Revolute roller J2 (Needle roller bearing)	0.7 Nm from Table C5.1.1
(iii)	Felt seals on main shaft	0.5 Nm, see Sec. C5.3

Maximum total dynamic friction torque is 5.9 Nm.
(Assuming all other sources of friction are negligible).

(c) Static friction torque (starting torque).

The torque required to start rotation can generally be taken as twice the value of load-dependent friction.

Although operating loads are lowest at start-up, the load-dependent friction in the main shaft bearings J1 and J3 is due to preload, cf. C5.2.

From Table C5.2.1 the maximum load dependent torque is 3.8 Nm. Therefore take the starting torque as 2 x3.8 Nm = 7.6 Nm.

(d) Acceleration torque.

The motor and transmission must supply sufficient torque in addition to that required above, in (a), (b) and (c), in order to accelerate the mechanism up to operating speed in reasonable time, cf. C6.5. This time is not of particular importance since position synchronisation will be achieved after reaching operating speed, cf. Sec.7.5.3, and therefore there is no requirement to match the workpiece acceleration time on the parent lathe.

(e) Summary of torque requirements.

(i) Maximum required at normal operating speed from (a) and (b) above = 1.4 + 5.9 = 7.3 Nm.

(ii) Maximum required at start-up from (a) and (c) above = 1.4 + 7.6 = 9.0 Nm.

(The value of 1.4 Nm has been included here since although inertia torques will be zero, gravity torque will still be appreciable).

(iii) Maximum required immediately after start-up from (a) and (c) above = 1.4 + 3.8 = 5.2 Nm.

(iv) A drive has been chosen, below, to provide 9.3 Nm (to satisfy (ii) above) thus the torque available for acceleration varies from 4.1 Nm immediately after start-up to 2.0 Nm at normal operating speed.

C6.2 SPECIFICATION OF STEPPER MOTOR.

A suitable stepper motor is manufactured by Berger Lahr GmbH [29] which when used together with a 3:1 transmission will supply sufficient torque to satisfy the requirements set out above.

Motor designation : Berger Lahr RDM 5913/50

Maximum torque available at 270 r.p.m. is 3.1 Nm (using constant current mode of operation). Thus with 3:1 (speed of motor:speed of mechanism) transmission, the torque available to drive the mechanism = 9.3 Nm. at 90 r.p.m.

This motor is a 5phase stepper motor with a step angle of 0.72 deg. giving 500 full steps per revolution.

Step angle accuracy = ± 3 min of arc maximum systematic deviation, from a nominal position, which can occur in a full rotor revolution.

Magnetic stiffness (approximately linear relationship between torque and deviation from nominal step position)

= 2.6 Nm/degree.

Rotor inertia = 1.8×10^{-4} kgm^2 (negligible compared to mechanism inertia, see App. C6.4).

C6.3 DESIGN OF TIMING BELT TRANSMISSION

C6.3.1 The design procedure is that set out in the Uniroyal PowerGrip design manual. [44]

1. Maximum power transmitted.

   = stepper motor max. torque x speed

   = 3.1 Nm x 30 rads/sec.

   = 93 Watts.

2. Design power = 93 x service factor

   Service factor selected from design manual = 1.5

   ∴ Design power = 139.5 Watts.

3. Select appropriate timing belt tooth pitch as pitch "L" (3/8 in. or ~ 9.5 mm).

4. Select pulley diameters.

   Drive ratio = 3:1

   ∴ Select small pulley 16L (dia.= 48.51 mm)

   " large pulley 48L (dia.= 145.53 mm)

5. Select pulley centre distance.

   (i) Radius of main bearing housing = 90 mm

   (ii) Radius of stepper motor = 45 mm

   (iii) Space for brackets etc. = 15 mm

   Minimum centre distance (i + ii + iii) = 150 mm.

   ∴ Choose centre distance = 164 mm

   and thus belt code 255L.

6. Select belt width

   Optimum width factor = $\frac{\text{Design Power}}{\text{Power capacity of belt.}}$

   Power capacity of belt with small pulley 16L = 190 Watts.

   ∴ Optimum width factor = $\frac{139.5}{190}$ = 0.73

   ∴ Select belt code L100, width = 25 mm.

   (Width factor = 1 which is > 0.73).

Summary of timing belt transmission selection:

Timing belt 255 L 100, width 25 mm

Small pulley 16L, diameter 48.51 mm

Large pulley 48L, diameter 145.53 mm

Pulley centre distance = 164 mm.

The belt design has standard PowerGrip trapezoidal tooth form. This transmission is shown in the layout drawings Nos. 1, 2 and 3.

C6.3.2 An alternative PowerGrip HTD system could be selected which has a curvilinear tooth form, which is a more recent design with higher torque and power capacity.

Summary of alternative PowerGrip HTD transmission selection.

Timing belt	635 - 5M - 25, width 25 mm
Small pulley	P30 - 5M - 25, diameter 47.75 mm
Large pulley	P90 - 5M - 25, diameter 143.24 mm.

This is the nearest equivalent in actual size to the PowerGrip standard belt system. However because of the improved power capacity a belt width of 9mm would suffice using the PowerGrip HTD belts.

This belt design is NOT shown in the layout drawings.

A final design would be best with the PowerGrip HTD belts. The stiffness of the belts is of more importance because of its effect on accuracy than the power capacity. Thus the 25 mm belt width could still be most appropriate.

C6.4 MOMENT OF INERTIA OF MECHANISM AS SEEN AT THE MAIN INPUT SHAFT OF R3 AT JOINT J3, BY DRIVE SYSTEM.

This consists of a constant component for the main input/eccentricity shaft, R3, and a varying component for the rest of the mechanism as its geometry changes. The former can be calculated simply from the shaft dimensions and is done in section C2.1, giving a value for constant inertia of 0.043 kg m^2.

The latter component can be calculated using the dynamic analysis program MECHDYN, see App. B. By putting in a value of constant acceleration and zero velocity the instantaneous inertia at any point is given by:

$$\frac{\text{Torque}}{\text{Acceleration}}$$

(Note: Other data such as gravity-constant, and cutting forces were set to zero so that only inertia induced torque was calculated by the program. Also this will not include the constant 0.043 kgm^2 above as this was not used in the program.)

Some peak values of the varying inertia component are shown in the Table C6.4.1. for various mechanism set-ups. The peak inertia only occurs for a small part of each rotation, with much smaller values elsewhere.

Mechanism Set-Up			Peak Value of Varying Inertia Component ($kg\ m^2$)
R1 (mm)	R3 (mm)	R4/RGW (mm)	
5.0	0.75	40	0.012
5.0	0.3	40	0.0012
10.0	1.5	40	0.01
10.0	0.6	40	0.001
25.0	3.75	40	0.012
25.0	1.5	40	0.001
50.0	7.5	40	0.0095
50.0	3.0	40	0.001

Table C6.4.1. Peak values of varying inertia component at various mechanism settings.

C6.4.2 Summary

Total mechanism inertia:- design value for stepper motor design.

The maximum inertia for the worst case would be 0.043 + 0.012 =.055kgm^2. However, as this only applied for part of each cycle and only at worst set-up, take design inertia of mechanism as 0.05 kgm^2.

C6.5 APPROXIMATE ESTIMATE OF ACCELERATION TIME.

From App.C6.1(e), assume 2Nm torque is available to accelerate the mechanism.

$$\text{Acceleration} = \frac{\text{Torque}}{\text{Moment of Inertia}}$$

This assumes the Moment of Inertia is constant, which is a fair approximation, since the variations due to mechanism geometry changing are relatively small compared to the large constant inertia moment of the main input shaft. This is shown in section C6.4 where the appropriate value of Moment of Inertia is determined as ~ 0.05 kgm^2.

Therefore Acceleration = $\frac{2}{0.05}$ rads.sec^{-2}

= 40 rad.sec^{-2}.

Final speed required is approx. 10 rad.sec^{-1}.

Therefore time to accelerate = $\frac{\text{Operating speed}}{\text{Acceleration}}$

= $\frac{10}{40}$ secs.

= 0.25 seconds.

Rotation required to achieve operating speed

= 0.5 x Acceleration x (time)^2

= 0.5 x 40 x 0.25^2 = 1.25 radians = 71.6 degrees,

which is equivalent to = 24 degrees of workpiece rotation.
This represents the slowest possible acceleration but is reasonable. In practice acceleration should be much greater than that based on the above assumptions.

C6.6 ESTIMATE OF MECHANISM DEVIATION DUE TO MANUFACTURE TOLERANCES OF DRIVE SYSTEM COMPONENTS.

C6.6.1 The dimensional errors of the drive system components will combine on assembly to produce an error in the angular position of the main input shaft. For small errors this is equivalent to lateral error of the eccentricity link and is designated as RL3 in the computer analysis of error sensitivity by program MECHKIN.

The maximum systematic angle deviation, or cumulative error, is the largest deviation that can occur during a full rotation.

C6.6.2 Sources of error that contribute.

(i) Berger Lahr stepper motor RDM 5913/50.

From C6.2 the maximum systematic angular deviation tolerance = $\pm$ 3 min = $\pm$ 0.00087 rads.
Divide by drive ratio 3:1 to give equivalent angular deviation tolerance at mechanism input shaft = 0.00029 rads = T_1.

(ii) Small pulley (dia. 48.51 mm, on stepper motor shaft)
(Tolerance data from reference [44])
(a) Maximum cumulative pitch error = $\pm$ 0.089 mm.

Divide by pitch radius and drive ratio to give <u>equivalent angular deviation</u> tolerance at input shaft

$$= \pm 0.089 \times \frac{2}{48.51} \times \frac{1}{3} = \pm 0.00122 \text{ rads.} = T_2$$

(b) Allowable pulley eccentricity of outside diameter to bore

= 0.1 mm total indicator reading

= $\pm$ 0.05 mm effective radius error.

Divide by pitch radius and drive ratio to give <u>equivalent angular error</u> at mechanism input shaft

$$= \pm 0.05 \times \frac{2}{48.51} \times \frac{1}{3} = \pm 0.00069 \text{ rads.} = T_3$$

(iii) Large pulley (Dia. 145.53 mm on mechanism input shaft).

Tolerance data from reference [44]

(a) Maximum cumulative pitch error = $\pm$ 0.127 mm

Equivalent angular error = $\pm 0.127 \times \frac{2}{145.53}$

$= \pm$ 0.00175 rads. = T_4.

(b) Eccentricity of outside diameter to bore

= 0.1 mm total indicator reading = $\pm$ 0.05 mm radially.

Equivalent angular error = $\pm 0.05 \times \frac{2}{145.53}$

$= \pm$ 0.00069 rads. = T_5.

(iv) Trantorque extra-precision lock bushes, c.f. Ref. [34]

Eccentricity of mounted components (pulleys) with shafts

= 0.025 mm total indicator reading

= $\pm$ 0.0125 mm radial.

(a) In small pulley, equivalent angular error at mechanism input shaft

$$= \pm 0.0125 \times \frac{2}{48.51} \times \frac{1}{3} \text{ rads.}$$

$= \pm$ 0.00017 rads. = T_6.

(b) In large pulley, equivalent angular error

$$= \pm 0.0125 \times \frac{2}{145.53}$$

$= \pm$ 0.00017 rads. = T_7.

(v) Timing belt, length 635 mm (Based on equivalent pulley diameter = 635 ÷ π = 202 mm).

Cumulative pitch accuracy $\pm$ 0.076 mm

Equivalent angular error (÷ by large pulley rad.) = $\frac{0.076}{148.53}$ x 2=0.00102 rads. = T_8.

Summary of contributing tolerances (in radians);

(i) Motor		$T_1 = \pm$ 0.00029
(ii) Small pulley	a)	$T_2 = \pm$ 0.00122
	b)	$T_3 = \pm$ 0.00069
(iii) Large pulley	a)	$T_4 = \pm$ 0.00175
	b)	$T_5 = \pm$ 0.00069
(iv) Lock bushes	a)	$T_6 = \pm$ 0.00017
	b)	$T_7 = \pm$ 0.00017
(v) Timing belt		$T_8 = \pm$ 0.00120

C6.6.3 Statistical summation.

The worst case mechanism input tolerance, T, will occur if all the above components are aligned in worst directions and is given by:

$$T = \pm \quad (T_1^2 + T_2^2 + T_3^2 + T_4^2 + T_5^2 + T_6^2 + T_7^2 + T_8^2)^{\frac{1}{2}}$$

$$= \pm 0.00259 \text{ radians.}$$

In practice,components will be randomly assembled and will be unlikely to align to give so high a mechanism input angle tolerance.

To analyse the effects of component alignment would be cumbersome and is not done here. Instead a qualitative assessment, cf. Sec.8.2.4, should be made when interpreting the resulting profile errors from those tabulated below in Table C6.6.4

C6.6.4 Equivalent eccentricity link lateral error, RL3.

Using the worst case angular deviation tolerance 0.00259 rads. from above, equivalent linkage errors, RL3, are given by:-

$$\text{Lateral error, RL3} = \frac{\text{Eccentricity length, R3, [mm]} \times 0.00259\ \text{mm}}{\text{[rads]}}$$

These values are tabulated for a range of mechanism set-ups used often in the design analysis.

Mechanism Set-up		Equivalent Link error
R1	R3	RL3
mm	mm	μm
5.0	0.75	± 1.94
	0.3	± 0.78
10.00	1.5	± 3.89
	0.6	± 1.55
25.0	3.75	± 9.71
	1.5	± 3.89
50.0	7.5	±19.43
	3.0	± 7.77

Table C6.6.4. Stepper motor and transmission assembly tolerances expressed as equivalent mechanism eccentricity link lateral tolerance, RL3.

C6.7 MECHANISM DEVIATION DUE TO DYNAMIC DEFORMATION OF DRIVE SYSTEM.

It is assumed here that the main source of mechanism input deviation is due to the magnetic flexibility of the stepper motor and the elastic deformation of the timing belt. All other deformations, such as that of the motor shaft and bearings and also the pulleys are assumed negligible: in the former case, quick calculations check this out and in the latter case the design of the timing belts is such that the load distribution on the pulley is spread evenly over many teeth, such that the load on individual teeth is very small.

C6.7.1 Stepper motor deflection.

The stepper motor torque is related approximately linearly to the angular deviation of the rotor from the nominal position at any instant, due to the magnetic 'stiffness' characteristics.

For the RDM 5913/50 this is specified as

2.6 Nm per degree ≡ 149.0 Nm per radian (see C6.2)

Therefore the angular deviation of the motor

= (motor torque)/stiffness

resulting in a mechanism input shaft angular deviation

$$= \frac{\text{(mechanism torque)}}{\text{(drive ratio)}^2 \text{ x stiffness}} = \text{(mechanism torque)} \times \frac{1}{9} \times \frac{1}{149.0} \text{ rads.}$$

$$= \text{(mechanism torque)} \times 7.46 \times 10^{-4} \text{ rads.}$$

C6.7.2 Timing belt deflection.

According to manufacturers the extension of a timing belt, optimally designed from their catalogue, [44] should be 1/20 x the extension rate at failure, which is 3% to 4%.

Therefore for properly designed belt assume extension rate

= 0.04/20 = 0.002.

For the PowerGrip HTD timing belt 635-5M-25 (c.f. C6.3.2), the width is 25mm. However the optimum width based on the design torque of 9.3 Nm, is 9 mm for which the 0.002 extension rate would apply.

Therefore modify the extension rate accordingly to give extension rate = $0.002 \times \frac{9}{25} \times \frac{\text{torque (Nm)}}{9.3}$ for a 25 mm belt and torques other than 9.3Nm.

The centre distance of pulleys = 164 mm,
therefore assume actual belt elongation

$$= 0.002 \times \frac{9}{25} \times \frac{\text{(torque)}}{9.3} \times 164 = 0.0127 \times \text{(torque Nm) mm}$$

Divide by radius of mechanism input shaft pulley to give angular deviation

$$= 0.0127 \times \frac{2}{145.53} \times \text{torque, radians}$$

$$= \text{torque} \times 1.75 \times 10^{-4}\text{, radians.}$$

Summary.

Total Angular deviation of mechanism input due to mechanism torque variation causing

(i) stepper motor deviation (= Torque x 0.000746 rads,)
and (ii) timing belt elongation (= Torque x 0.000175 rads,)
= Torque x 0.000921 rads,
where torque is expressed in Nm.

C6.7.3 Equivalent eccentricity link lateral error, RL3.

The angular deviation of the input shaft of the mechanism is effectively equivalent to lateral deviation, RL3, of the eccentricity shaft, for small errors, of the order arising here.

The equivalent lateral error, RL3 has been tabulated in Table C6.7.3, for various mechanism operational settings, used elsewhere in the design analysis.

Lateral error RL3

= Eccentricity length, R3(mm) x Torque(Nm) x 0.000921 mm.

Mechanism Set-up				Torque Variation	Angular input deviation	Equivalent linkage deviation, RL3
R1 (mm)	R3 (mm)	R4 (mm)	$\dot{\psi}_1$ ($Rad.s^{-1}$)	(Nm)	(10^{-3}rads)	(10^{-3} mm)
5.0	0.75	40.0	10.0	2.76	2.54	1.91
5.0	0.75	40.0	5.0	2.15	1.98	1.49
5.0	0.75	20.0	10.0	1.63	1.50	1.13
5.0	0.3	40.0	10.0	0.79	0.73	0.22
5.0	0.3	40.0	5.0	0.75	0.69	0.21
5.0	0.3	20.0	10.0	0.43	0.40	0.12
5.0	0.3	20.0	5.0	0.41	0.38	0.11
10.0	1.5	40.0	10.0	2.84	2.62	3.93
10.0	0.6	40.0	10.0	0.83	0.76	0.46
25.0	3.75	40.0	10.0	3.20	2.95	11.06
25.0	1.5	40.0	10.0	1.01	0.93	1.40
50.0	7.5	40.0	10.0	3.85	3.55	26.63
50.0	3.0	40.0	10.0	1.31	1.21	3.63

Table C6.7.3. Stepper motor and transmission dynamic deviations expressed as equivalent mechanism eccentricity link lateral deviation, RL3.

APPENDIX D

STUDY OF POLYGONAL CONNECTIONS

D1. COMPUTER PROGRAM TO CALCULATE SHEAR STRESSES

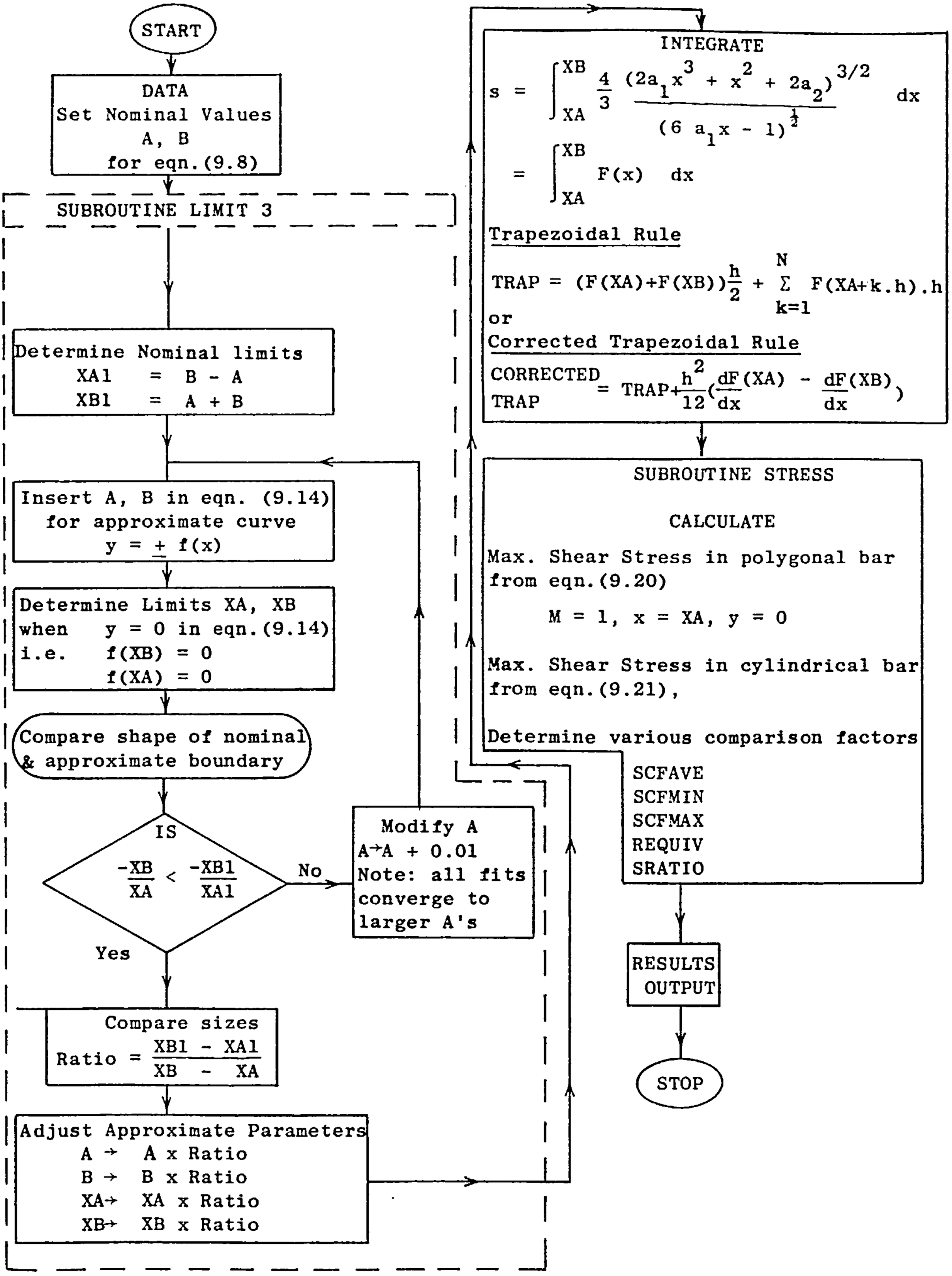

Fig.D1.1 Flowchart for program STRESS

Listing of STRESS at 21:16:48 on APR 4, 1987 for CCid=MCB0

```
      C   MAXIMUM SHEAR STRESS OF HYPOTROCHOIDAL BAR IN TORSION
      C   ---------------------------------------------------
      C
      C       THIS PROGRAM CALCULATES THE MAX. SHEAR STRESS IN THE HYPOTROCHOIDAL
      C     SECTION BAR AND COMPARES WITH THOSE OF A CIRCULAR SECTION
      C
      C Define Functions for later use
            YTOP(X)=2.*D*X**3+X**2+2.*E
            YBOT(X)=6*D*X-1.0
            F(X)=(4./3.)*SQRT(YTOP(X)**3/YBOT(X))
            FPRIME(X)=4.*(3.*D*X**2+X)*F(X)-4.*D*F(X)**3
            Y(X)=YTOP(X)**3/YBOT(X)
             B1=0.0
             NU=100
           WRITE(6,700)
        700 FORMAT(1X,'  RAVE    ECC.    TAU    SCFAVE  SCFMIN',
           1'  SCFMAX  REQUIV  SRATIO')
            DO 30 J=1,11
            A=1.0
      C  Set eccentricity
            B=B1+0.03*J
            ECC=B
            RAVE=A
            RMIN=A-B
            RMAX=A+B
      C  Fit approximate to exact curve
            CALL LIMIT3(A,B,XA,XB)
            CALL LIMIT(A,B,XA,XB)
      C  Coefficients of approximate curve
            C=A**4+A**2*B**2-2.*B**4
            D=-(A**2*B)/C
            E=-(A**6-3.*A**4*B**2+3.*A**2*B**4-B**4-B**6)/(2.*C)
      C Numerical Integration
            N=NU
            H=(XB-XA)/FLOAT(N)
            NM1=N-1
            TRAP=(F(XA)+F(XB))/2.
            DO 1 I=1,NM1
      C Trapezium rule
          1 TRAP=TRAP+F(XA+FLOAT(I)*H)
            TRAP=TRAP*H
      C Corrected trapezium rule
            CORTRP=TRAP+H*H*(FPRIME(XA)-FPRIME(XB))/12.
      C Calculate stresses etc.
            CALL STRESS(XA,XB,D,CORTRP,TAU,SCFAVE,SCFMIN,SCFMAX,REQUIV)
             SRATIO=RMAX/REQUIV
      C  Output data
            WRITE(6,710)RAVE,ECC,TAU,SCFAVE,SCFMIN,SCFMAX,REQUIV,SRATIO
        710 FORMAT(8F8.3)
        620 FORMAT(2F5.3,I5)
         30 CONTINUE
            STOP
            END
      C
      C  LIMIT3 adjusts coefficients of approx. to fit exact curve
            SUBROUTINE LIMIT3(A,B,XA,XB)
            YTOP(X)=2.*D*X**3+X**2+2.*E
            YBOT(X)=6*D*X-1.0
```

Listing of STRESS at 21:16:48 on APR 4, 1987 for CCid=MCB0

```
      Y(X)=YTOP(X)/YBOT(X)
      XA1=B-A
      XB1=A+B
   52 C=A**4+A**2*B**2-2.*B**4
      D=-(A**2*B)/C
      E=-(A**6-3.*A**4*B**2+3.*A**2*B**4-B**4-B**6)/(2.*C)
      XB=A+B
      XA=B-A
      XA2=XA
      XB2=XB
C Find limits of curve on x-axis (i.e. when y=0)
   21 IF(Y(XB).LT.0.001) GO TO 24
      XB=XB+0.001
      IF(XB.GT.(1.2*XB2)) GO TO 49
      GO TO 21
   24 XB=XB-0.001
      IF(XB.LT.(0.9*XB2)) GO TO 49
      IF(Y(XB).LT.0.001) GO TO 24
   25 IF(Y(XA).LT.0.001) GO TO 27
      XA=XA-0.001
      IF(XA.LT.(1.2*XA2)) GO TO 49
      GO TO 25
   27 XA=XA+0.001
      IF(XA.GT.(0.9*XA2)) GO TO 49
      IF(Y(XA).LT.0.001) GO TO 27
C  Adjust SHAPE of approx. to fit exact curve
      IF((-XB/XA).LT.(-XB1/XA1)) GO TO 51
   49 A=A+0.001
      GO TO 52
C Ajust SIZE to fit
   51 RATIO=(XB1-XA1)/(XB-XA)
      XB=XB*RATIO
      XA=XA*RATIO
      A=A*RATIO
      B=B*RATIO
   40 RETURN
      END
C
C LIMIT rechecks limits of adjusted curve;
      SUBROUTINE LIMIT(A,B,XA,XB)
      YTOP(X)=2.*D*X**3+X**2+2.*E
      YBOT(X)=6*D*X-1.0
      Y(X)=YTOP(X)/YBOT(X)
      IF(A.EQ.0.0)GO TO 40
      C=A**4+A**2*B**2-2.*B**4
      D=-(A**2*B)/C
      E=-(A**6-3.*A**4*B**2+3.*A**2*B**4-B**4-B**6)/(2.*C)
      XB=A+B
      XA=B-A
   21 IF(Y(XB).LT.0.001) GO TO 24
      XB=XB+0.001
      GO TO 21
   24 XB=XB-0.001
      IF(Y(XB).LT.0.001) GO TO 24
   25 IF(Y(XA).LT.0.001) GO TO 27
      XA=XA-0.001
      GO TO 25
   27 XA=XA+0.001
```

Listing of STRESS at 21:16:48 on APR 4, 1987 for CCid=MCBO

```
117           IF(Y(XA).LT.0.001) GO TO 27
118        40 RETURN
119           END
120      C
121      C  Calculation of stresses & concentration factors;
122           SUBROUTINE STRESS(XA,XB,D,CORTRP,TAU,SCFAVE,SCFMIN,SCFMAX,REQUIV)
123           PI=3.1415927
124           TAU=-(XA+3.0*D*XA**2)/CORTRP
125           TAURAV=2.0/PI
126           TAURXA=-2.0/(PI*XA**3)
127           TAURXB=2.0/(PI*XB**3)
128           REQUIV=(2.0/(PI*TAU))**(1.0/3.0)
129           SCFAVE=TAU/TAURAV
130           SCFMIN=TAU/TAURXA
131           SCFMAX=TAU/TAURXB
132           RETURN
133           END
```

D3. PRESSURE ANGLE OF POLYGONAL PROFILES

The pressure angle, or contact angle, at a point on the profile is defined as the acute angle ø between the respective tangents to the profile and a circumference at that point as depicted in Fig.D3.1

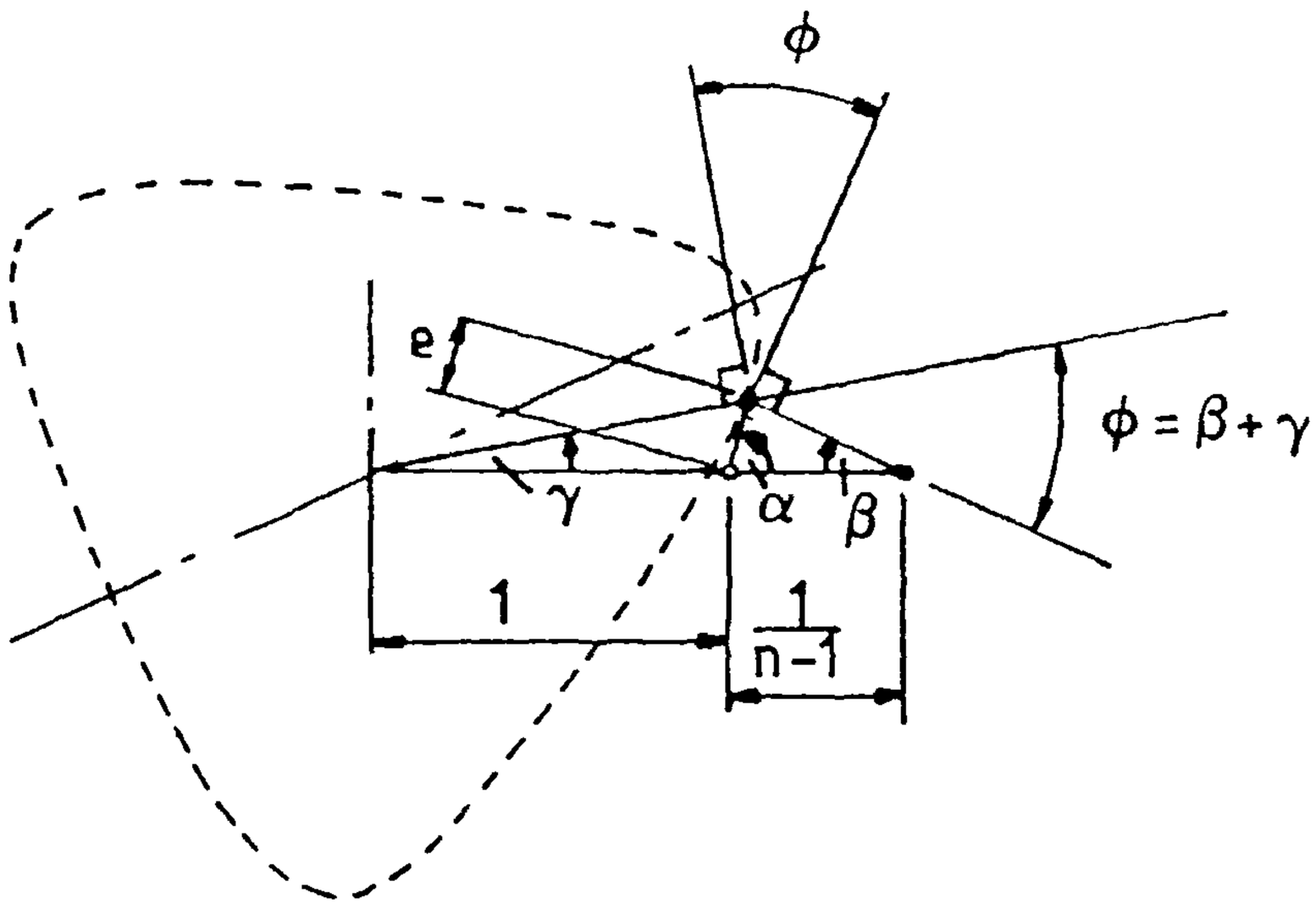

Fig.D3.1 Profile pressure angle ø.

The pressure angle can be derived from the parameters of the linkage mechanism which generate the profile (as originally shown in Fig.3.5) Adopting the rotation of Fig.D3.1 it can be seen that ø = $\beta+\gamma$, where β and γ are the angles with the horizontal of the curve normal and of a

radial vector from the profile centre to the point, respectively. If the angle of the eccentric link e is designated by α, and the number of sides by n, then the following trigonometric expressions can be deduced;

$$\tan\gamma = \frac{e\sin\alpha}{1 + e\cos\alpha} \qquad \text{(D3.1)}$$

$$\tan\beta = \frac{e\sin\alpha}{\frac{1}{n-1} - e\cos\alpha} \qquad \text{(D3.2)}$$

Substituting eqns.(D3.1) and (D3.2) in the elementary relationship

$$\tan(\beta+\gamma) = \frac{\tan\beta + \tan\gamma}{(1 - \tan\beta\tan\gamma)}$$

and rearranging gives

$$\tan\phi = \frac{ne\ \sin\alpha}{1-\ (n-2)e\ \cos\alpha\ -(n-1)e^2} \qquad \text{(D3.3)}$$

The maximum pressure angle $\hat{\phi}$ occurs when $\tan\phi$ is a maximum, that is when

$$\frac{d\ (\tan\phi)}{d\alpha} = 0.$$

Differentiating eqn.(D3.3) and equating to zero results in the following expression for α when $\phi = \hat{\phi}$,

$$\cos\alpha = \frac{(n-2)e}{1-(n-1)e^2} \qquad \text{(D3.4)}$$

Substituting $\sin\alpha = (1-\cos^2\alpha)^{\frac{1}{2}}$ and eqn.(D3.4) in eqn.(D3.3) gives

$$\tan\hat{\phi} = \frac{ne}{(1+(n-1)^2\ e^4\ -(n^2-2n+2)e^2)^{\frac{1}{2}}} \qquad \text{(D3.5)}$$

Similarly the values of γ and β when $\phi = \hat{\phi}$ are given by

$$\tan\gamma = \frac{e}{1-e^2}\ (1+(n-1)^2e^4\ -(n^2-2n+2)e^2)^{\frac{1}{2}} \qquad \text{(D3.6)}$$

and

$$\tan\beta = \frac{(n-1)e(1+(n-1)^2e^4\ -(n^2-2n+2)e^2)^{\frac{1}{2}}}{1\ -\ (n^2-2n+1)\ e^2} \qquad \text{(D3.7)}$$

The maximum pressure angle ϕ for 'triangular' and 'square' profiles of various eccentricities calculated from eqn.(D3.5) are tabulated in Table D3.1.

Eccentricity ratio e	n = 3		n = 4	
	$\tan\hat{\phi}$	$\hat{\phi}$	$\tan\hat{\phi}$	$\hat{\phi}$
0.06	0.182	10.29^{o}	0.244	13.74^{o}
0.1	0.308	17.10^{o}	0.421	22.85^{o}
0.15	0.477	25.51^{o}	0.680	34.20^{o}
0.2	0.668	33.75^{o}	1.021	45.58^{o}
0.25	0.894	41.81^{o}	1.56	57.36^{o}

Table D3.1 Pressure angles for 'triangular' (n=3) and 'square' (n=4) profiles vs. eccentricity ratio, e.

Note that eqn.(D3.5) can be approximated for small eccentricities by

$$\tan\hat{\phi} \approx ne \qquad \text{(D3.8)}$$